

## Structural Response of Reinforced Concrete Frames Subjected to Explosions

*Master of Science Thesis in the Master's Programme Structural Engineering and Building Technology*

JOANNA KLOREK  
ANNA SANDBERG

Department of Civil and Environmental Engineering  
Division of Structural Engineering  
Concrete Structures  
CHALMERS UNIVERSITY OF TECHNOLOGY  
Göteborg, Sweden 2013  
Master's Thesis 2013:87



MASTER'S THESIS 2013:87

# Structural Response of Reinforced Concrete Frames Subjected to Explosions

*Master of Science Thesis in the Master's Programme Structural Engineering and  
Building Technology*

JOANNA KLOREK

ANNA SANDBERG

Department of Civil and Environmental Engineering  
*Division of Structural Engineering  
Concrete Structures*

CHALMERS UNIVERSITY OF TECHNOLOGY

Göteborg, Sweden 2013

## Structural Response of Reinforced Concrete Frames Subjected to Explosions

*Master of Science Thesis in the Master's Programme Structural Engineering and Building Technology*

JOANNA KLOREK  
ANNA SANDBERG

© JOANNA KLOREK & ANNA SANDBERG, 2013

Examensarbete / Institutionen för bygg- och miljöteknik,  
Chalmers tekniska högskola 2013:87

Department of Civil and Environmental Engineering  
Division of Structural Engineering  
Concrete Structures  
Chalmers University of Technology  
SE-412 96 Göteborg  
Sweden  
Telephone: + 46 (0)31-772 1000

Cover:

Illustration of the initial local and general global structural response of a 2D frame subjected to an explosion where  $t_2 > t_1$ .

Chalmers Reproservice  
Göteborg, Sweden

Structural Response of Reinforced Concrete Frames Subjected to Explosions  
*Master of Science Thesis in the Master's Programme Structural Engineering and Building Technology*

JOANNA KLOREK

ANNA SANDBERG

Department of Civil and Environmental Engineering

Division of Structural Engineering

Concrete Structures

Chalmers University of Technology

ABSTRACT

The knowledge of the response of reinforced concrete structures subjected to explosions and impulse load is limited. The design methodology is often simplified and there is a great need for further investigations within this subject. This Master's Thesis is a continuation of several previous Master's Theses and part of a long time project carried out as collaboration between Chalmers, the Swedish Civil Contingencies Agency (MSB) and Reinertsen.

A parametric beam study is carried out in order to investigate the important parameters for impulse loaded structures. Depending on how the effective depth is interpreted in Eurocode 2, CEN (2004), the deformation capacity of the structure will differ, which is investigated. It is proved that for most cases it can be considered conservative to neglect the top reinforcement and to calculate the effective depth as the distance between the top of the beam to the centre of gravity of the bottom reinforcement.

The main focus of this report is on structures composed of a few members, such as frame structures, which are investigated both in 2D and 3D finite element (FE) analysis, considered to present the reality in a sufficient degree. The analysed structures with infinite number of degrees of freedom are transformed into single degree of freedom (SDOF) systems in order to simplify the analysis. The SDOF system is created in Matlab R2013a and checked using hand calculation methods and more detailed numerical methods based on the central difference method.

The 2D analysis focuses on the response models of the structures. Both the local model of the front column of the frame and the global model of the whole frame has proved to have trilinear response models. This results in that the first sway of the structure have a higher magnitude than the following sways for the elasto-plastic case. It is also proved that the interaction between the local and global model may increase the total plastic deformation of the frame.

In the 3D analysis a comparison is done between applying the impulse load directly on the front column of the frame, and applying the load on the wall and transferring it to the column by the reaction forces of the wall. A parametric study is done in order to investigate the influence of the walls structural properties. It is proven that applying the load directly on the column is conservative compared to the 3D FE analysis. However, the relative properties of the wall and column have a large influence on the results.

Key words: Explosion impulse load, reinforced concrete, SDOF, frame structure, elastic, elasto-plastic, 3D analysis, finite element analysis, dynamic

Strukturell respons för ramar i armerad betong utsatta för explosioner  
Examensarbete inom Structural Engineering and Building Technology

JOANNA KLOREK

ANNA SANDBERG

Institutionen för bygg- och miljöteknik

Avdelningen för konstruktionsteknik

Betongbyggnad

Chalmers tekniska högskola

## SAMMANFATTNING

Kunskapen om hur armerade betongkonstruktioner reagerar på explosions-last är begränsad. Design-metodiken förenklas ofta och det finns ett stort behov av vidare efterforskningar inom området. Detta examensarbete är en fortsättning på flera tidigare examensarbeten samtidigt som det är en del av ett större samarbete mellan Chalmers, Myndigheten för Samhällsskydd och beredskap (MSB) och Reinertsen.

En parametrisk studie har utförts för att undersöka vilka som är de viktigaste parametrarna för konstruktioner utsatta för impulslast. Beroende på hur den effektiva höjden tolkas erhålls olika plastiska rotationskapaciteter från Eurocode 2, vilket också undersöks. Studien visar att det för de flesta studerade fall kan anses konservativt att försumma topp-armeringen samt att beräkna den effektiva höjden som avståndet mellan botten-armeringen och toppen på balken.

Examensarbetets huvudfokus ligger på sammansatta konstruktioner, så som ramverk, vilka undersöks i både 2D och 3D finita element (FE) analyser vilka anses representera verkligheten i tillräcklig utsträckning. De analyserade strukturerna, som har oändligt många frihetsgrader, förenklas till enfrihetsgradssystem (SDOF-system). SDOF-systemen programmeras i Matlab R2013a och kontrolleras med enkla handberäkningar samt mer detaljerade numeriska metoder baserade på centrala differens-metoden.

2D-analysen fokuserar på strukturernas respons-modeller. Både den lokala modellen av den främre pelaren samt den globala modellen av hela ramen har uppvisat tri-linjärt beteende. Detta har, för det elasto-plastiska fallet, visat sig resultera i en högre första deformations-topp jämfört med de efter-följande. Det har även visat sig att interaktionen mellan den lokala och globala modellen kan öka ramens plastiska deformation.

I 3D-analysen görs en jämförelse mellan att applicera impulslasten direkt på ramens främre pelare och att applicera den på väggen som får föra lasten vidare till pelaren genom reaktionskrafter. En parametrisk studie utförs för att undersöka hur väggens styvhet och resistans påverkar resultaten. Studien visar att det är konservativt att applicera lasten direkt på pelaren jämfört med 3D FE analysen. Vidare har de relativa egenskaperna mellan väggen och pelaren stor påverkan på resultaten.

Nyckelord: Explosion, impulslast, armerad betong, enfrihetsgradssystem, ramverk, elastisk, elasto-plastisk, 3D-analys, finit element analys, dynamisk

# Contents

ABSTRACT	I
SAMMANFATTNING	II
CONTENTS	III
PREFACE	IX
NOTATIONS	X
1 INTRODUCTION	1
1.1 Background	1
1.2 Method	1
1.3 Limitations	1
1.4 Aim	2
1.5 Outline of report	2
2 BACKGROUND THEORY	4
2.1 References	4
2.2 Explosions	4
2.2.1 Definition of explosion	4
2.2.2 Idealized shock wave	4
2.2.3 Strain rate due to a shock wave	5
2.2.4 Blast load	6
2.2.5 Wave propagation	7
2.3 Material response due to static load	9
2.3.1 Concrete	9
2.3.2 Reinforcement	10
2.4 Structural response due to static load	11
2.4.1 Orientation	11
2.4.2 Linear elastic model	11
2.4.3 Ideal plastic model	13
2.4.4 Elasto-plastic model	14
2.5 Plastic hinges and plastic rotation capacity	15
2.5.1 Theory of plastic hinges	15
2.5.2 Definition of plastic rotation capacity	18
2.5.3 Calculation method for plastic rotation capacity	20
2.6 Structural response of statically indeterminate structures	22
2.7 Structural response due to impulse load	23
2.7.1 Difference between impulse and static load	23
2.7.2 Force and Pressure	24
2.7.3 Momentum, impulse and impulse intensity	24
2.7.4 External work and energy	25
2.7.5 Internal work and corresponding deformation	27
2.7.6 Modification factors for impulse loads other than characteristic	30

2.7.7	Essential parameters for impulse loaded structures	34
2.8	Equivalent static load	35
2.8.1	Introduction	35
2.8.2	Elastic model	35
2.8.3	Plastic model	35
2.8.4	Elasto-plastic model	35
2.9	Transformation into SDOF system	36
2.9.1	Introduction to SDOF system concept	36
2.9.2	Equation of motion	37
2.9.3	Differential equation for equation of motion	38
3	PARAMETRIC BEAM STUDY	42
3.1	Introduction	42
3.2	Different interpretations of $x/d$	43
3.2.1	Case 1	43
3.2.2	Case 2	44
3.2.3	Case 3	45
3.3	Geometry and properties of the beam	45
3.3.1	Introduction	45
3.3.2	Parameters studied	46
3.4	Results and comparisons	47
3.4.1	Orientation	47
3.4.2	Resistance versus deformation capacity for Case 1	48
3.4.3	Rotation capacity, internal work and resistance for Case 1	51
3.4.4	Comparison of Case A and Case B	56
3.4.5	Different interpretation of $d$ for Case 2	60
3.5	Concluding remarks	63
4	STRUCTURAL RESPONSE OF A 2D FRAME	64
4.1	Introduction and method	64
4.2	Geometry and properties of the studied frame	64
4.3	Reflected impulse load	66
4.4	Adaption of frame into SDOF system	67
4.4.1	Introduction	67
4.4.2	Local SDOF model	68
4.4.3	Global SDOF model	72
4.4.4	Combination of the global and local SDOF model	75
4.5	Modelling in ADINA	76
4.6	Results of the elastic model	78
4.6.1	Local elastic model	78
4.6.2	Global elastic model	79
4.6.3	Combination of the local and global elastic model	80
4.7	Results of the elasto-plastic model	83
4.7.1	Local elasto-plastic model	83



4.7.2	Global elasto-plastic model	102
4.7.3	Combination of the local and global elasto-plastic model	115
4.8	Concluding remarks	117
5	STRUCTURAL RESPONSE OF A 3D FRAME	119
5.1	Introduction and method	119
5.2	Geometry and properties	119
5.3	Adaptation into SDOF system	121
5.3.1	SDOF model of the wall	121
5.3.2	SDOF model of the front column	122
5.4	Application of impulse load	123
5.4.1	Introduction	123
5.4.2	Direct application of load	124
5.4.3	Delayed application of load	125
5.5	Modelling in ADINA	131
5.5.1	Introduction	131
5.5.2	2D model	131
5.5.3	3D model	132
5.6	Results and comparison	134
5.6.1	Elastic model	134
5.6.2	Elasto-plastic model	151
5.6.3	Comparison of elastic and elasto-plastic model	161
5.7	Parametric study	163
5.7.1	Orientation	163
5.7.2	Elastic model	163
5.7.3	Elasto-plastic model	175
5.8	Concluding remarks	185
6	CONCLUSIONS	187
6.1	Final comments	187
6.1.1	Parametric beam study	187
6.1.2	Structural response of a 2D frame	187
6.1.3	Structural response of a 3D frame	188
6.2	Further investigations	188
7	REFERENCES	190
APPENDIX A HAND CALCULATIONS		192
A.1	Introduction	192
A.2	Deformations	192
A.3	Stiffness and moment of inertia	192
A.4	Moment resistance	193
A.4.1	Main concept	193

A.4.2	Section without top reinforcement	194
A.4.3	Section with top reinforcement	195
A.5	Maximum deformation capacity	196
A.6	Internal and external work	197
A.7	Equivalent static load	198
APPENDIX B ADDITIONAL GRAPHS FOR PARAMETRIC BEAM STUDY		199
B.1	Introduction	199
B.1.1	Case 1	199
B.1.2	Case 2	199
B.2	Resistance versus deformation for Case 1	200
B.3	Plastic rotation capacity for Case 1	203
B.4	Internal work for Case 1	205
B.5	Internal resistance for Case 1	206
B.6	Maximum plastic deformation for Case 1	208
B.7	Sections with and without top reinforcement for Case 1	209
B.8	Resistance versus deformation for Case 2	215
B.9	Plastic rotation capacity for Case 2	221
B.10	Internal work for Case 2	222
B.11	Internal resistance for Case 2	224
B.12	Maximum plastic deformation for Case 2	225
B.13	Sections with and without top reinforcement for Case 2	227
APPENDIX C TRILINEAR STRUCTURAL RESPONSE MODELS		232
C.1	Introduction	232
C.2	Ultimate moments and resistances for the local frame model	232
C.3	Structure subjected to impulse load	234
C.4	Structure subjected to a static load	237
APPENDIX D CENTRAL DIFFERENCE METHOD		240
D.1	Introduction	240
D.2	Calculation method	240
D.3	Response models	241
D.3.1	Introduction	241
D.3.2	Elastic response model	242
D.3.3	Bilinear elasto-plastic response model	242
D.3.4	Trilinear elasto-plastic response model	243

APPENDIX E	HAND CALCULATIONS FOR 2D FRAME	246
E.1	Input data	246
E.2	Global and local elastic frame models	249
E.2.1	Deformation	249
E.3	Local elasto-plastic frame model	251
E.3.1	Deformation	251
E.3.2	Plastic deformation capacity	253
APPENDIX F	STUDY OF 3D STRUCTURE	255
F.1	Input data	255
F.1.1	Wall	255
F.1.2	Front Column	257
F.2	Plastic deformation capacity of the front column	259
F.3	Hand calculations of the dynamic reaction from the wall	261
F.4	Verification of the SDOF models	262
F.4.1	Elastic model	262
F.4.2	Elasto-plastic model	265
F.5	Support reactions in 3D FE analysis	266
F.5.1	Elastic response	266
F.5.2	Elasto-plastic response	270
APPENDIX G	PARAMETRIC STUDY OF 3D STRUCTURE	275
G.1	Orientation	275
G.2	Verification of SDOF model	275
G.2.1	Elastic response	275
G.2.2	Elasto-plastic response	280
G.3	Comparison of deformation in SDOF and 3D FE analysis	281
G.3.1	Elastic response	281
G.3.2	Elasto-plastic response	286
G.4	Reaction loads	288
G.4.1	Elastic response	288
G.4.2	Elasto-plastic response	295
G.5	Comparison of delayed load in SDOF and 3D FE analysis	303
G.5.1	Elastic response	303
G.5.2	Elasto-plastic response	304
APPENDIX H	INDATA FILES FOR ADINA	306
H.1	2D Frame with elasto-plastic material model	306
H.2	3D Frame with elasto-plastic material model	308



## Preface

In this study, impulse loaded reinforced concrete structures have been investigated with focus on frame structures. The work has been carried out between January and June 2013. The project was carried out at Reinertsen Sverige AB in Gothenburg and in collaboration with the Department of Civil and Environmental Engineering, Division of Structural Engineering, Concrete Structures, Chalmers University of Technology, Sweden. The project has been carried out with Ph.D. Morgan Johansson as supervisor and Senior Lecturer Joosef Leppänen as examiner.

We would especially like to thank Morgan Johansson for his commitment to the work carried out in this Master's Thesis. His engagement to the subject has made the analyses very interesting and motivating to perform. We also want to show our gratitude to our examiner at the Department of Structural Engineering, Joosef Leppänen, for cheering on the project and giving helpful feedback.

Moreover, we want to express our gratitude to the staff at Reinertsen Sverige AB in Gothenburg for welcoming us to their office. Sebastian Andersson and Mattias Carlsson at Reinertsen Sverige AB have especially been very helpful throughout the project.

Finally, we want to thank each other for all the hard work, learning outcomes and fun times during the work with this project.

Gothenburg June 2013

Joanna Klorek

Anna Sandberg

# Notations

## Roman upper case letters

$A$	Area
$A_s$	Area of reinforcement
$B$	Roof span
$E$	Young's modulus
$E_c$	Young's modulus for concrete
$E_s$	Young's modulus for steel
$E_k$	Kinetic energy
$F$	External force
$F'$	Impulse load acting on the wall length $w$
$F_c$	Force in concrete
$F_k$	Characteristic pressure load
$F_s$	Force in steel
$I$	Impulse, moment of inertia
$I_k$	Characteristic impulse
$L$	Length
$L_0$	Distance from plastic hinge to zero moment section
$M$	Moment
$M_{cr}$	Cracking moment
$M_{rd}$	Ultimate moment capacity
$M_{yd}$	Moment capacity when yielding starts
$P$	Pressure
$P_0$	Ambient air pressure
$P_{peak}$	Peak pressure load
$P_s^+$	Unreflected pressure load, positive phase
$R$	Internal resisting force, support reaction
$R_m$	Maximum internal resisting force
$R_{mf}$	Ultimate resistance at the support
$R_{ms}$	Ultimate resistance in the field
$T$	Natural period
$V_{rd}$	Shear force
$W$	Amount of energy
$W_e$	External energy
$W_{el}$	Elastic section modulus

$W_i$	Internal energy
$W_k$	Kinetic energy
$W_{pl}$	Plastic section modulus
$Q$	Equivalent static load

### **Roman lower case letters**

$a$	Acceleration, distance, length of middle line for slab
$b$	Width of cross-section
$c$	Damping
$c$	Distance from the edge of the beam to the centre of reinforcement
$c_1$	Concrete cover
$d$	Effective depth of cross-section
$f$	Frequency
$f_{cc}$	Concrete compressive strength
$f_{cd}$	Design value of concrete compressive strength
$f_{su}$	Ultimate reinforcement strength
$f_{sy}$	Yield stress for reinforcement
$f_{yd}$	Characteristic value of yield stress
$f_{yk}$	Design value of yield stress
$h$	Height of cross-section
$i$	Impulse intensity
$k$	Stiffness
$k_\lambda$	Multiplying factor for allowed rotation capacity
$l_{pl}$	Extension length of plastic hinge
$m$	Mass
$n$	Total number
$p$	Momentum
$q$	Distributed load
$q_{cr}$	Distributed crack load
$q_{rd}$	Distributed load when ultimate capacity is reached
$q_{yd}$	Distributed load when yielding starts
$r$	Detonation distance, radius of curvature

$s$	Column spacing, reinforcement bar spacing
$t$	Time
$t_a$	Arrival time
$t_1$	Load duration
$t_{el}$	Time when maximum $u_{el}$ is reached in elasto-plastic model
$t_{max}$	Time for which $u_{max}$ is reached
$t_{peak}$	Time for which pressure load reaches maximum value $P_{peak}$
$u$	Displacement
$\dot{u}$	Velocity
$\ddot{u}$	Acceleration
$u_{el}$	Elastic deformation
$u_{ep}$	Elasto-plastic deformation
$u_{ep,el}$	Elastic part of elasto-plastic deformation
$u_{ep,pl}$	Plastic part of elasto-plastic deformation
$u_{max}$	Maximum deformation
$u_{pl}$	Plastic deformation
$u_{rd}$	Ultimate plastic deformation
$u_{res}$	Residual plastic deformation
$u_s$	Displacement of system point
$u_{sum}$	Sum of global and local deformation
$w$	Length of slab, length of wall section
$v$	Velocity
$x$	Length coordinate
$x$	Height of compression zone
$x_{cg}$	Distance to centre of gravity
$x_u$	Height of compression zone in ULS
$z$	Coordinate from neutral axis, internal lever arm for reinforcement

### **Greek upper case letters**

$\Delta$	Incremental
$\Lambda$	Ratio between the reflected pressure and a shock wave



### Greek lower case letters

$\alpha$	Deformation relation factor
$\alpha$	Ratio between Young's modulus for steel and concrete
$\delta_{el}$	Displacement error for elastic response
$\delta_{pl}$	Displacement error for plastic response
$\varepsilon$	Strain
$\varepsilon_c$	Concrete strain
$\varepsilon_{cc}$	Concrete compressive strain
$\varepsilon_{ct}$	Concrete tensile strain
$\varepsilon_{cu}$	Ultimate concrete strain
$\varepsilon_{pl}$	Plastic strain
$\varepsilon_{pl,acc}$	Accumulated plastic strain
$\varepsilon_s$	Reinforcement strain
$\varepsilon_{sh}$	Reinforcement strain at hardening
$\varepsilon_{s,f_{su}}$	Reinforcement strain at the ultimate tensile stress $f_{su}$
$\varepsilon_{su}$	Ultimate reinforcement strain
$\varepsilon_{sy}$	Reinforcement strain when yielding begins
$\phi$	Bar diameter
$\gamma$	Heat capacity ratio
$\gamma_I$	Impulse load factor
$\gamma_F$	Pressure load factor
$\gamma_{Rm}$	Ratio between $R_m$ of beam with and without top reinforcement
$\gamma_{u_{rd}}$	Ratio between $u_{rd}$ of beam with and without top reinforcement
$\gamma_{W_i}$	Ratio between $W_i$ of beam with and without top reinforcement
$\kappa$	Transformation factor
$\kappa_F$	Transformation factor for the external load
$\kappa_k$	Transformation factor for the internal force
$\kappa_m$	Transformation factor for the mass
$\kappa_{mF}$	Transformation factor for the mass and the external load
$\lambda$	Wave length, shear slenderness

$\theta_{pl}$	Plastic rotation capacity
$\theta_{pl.rev}$	Plastic rotation capacity with regard to shear slenderness $\lambda$
$\rho$	Density, reinforcement amount
$\sigma$	Stress
$\sigma_c$	Concrete stress
$\sigma_{cc}$	Concrete compressive stress
$\sigma_{ct}$	Concrete tensile stress
$\sigma_s$	Reinforcement stress
$\sigma_y$	Yield stress
$\omega$	Angular frequency

## Index

+	Indicates positive phase
$0$	Initial position
$1,2,3,4$	Numbering
$I, II, III$	Indicate state I (uncracked), II (cracked), III (plastic)
$a$	Indicates indata to FE program (ADINA)
$b$	Bilinear
$ba$	Indicates back column
$c$	Indicates column
$cr$	Cracking, indicates critical value
$d$	Indicates decreased value
$dyn$	Dynamic
$e$	Equivalent
$el$	Elastic
$ep$	Elasto-plastic
$f$	Indicates span
$fr$	Indicates front column
$gl$	Global
$i$	Indicates increased value
$k$	Characteristic
$l$	Local

<i>mod</i>	Indicates modified value
<i>pl</i>	Plastic
<i>r</i>	Indicates roof
<i>s</i>	Indicates support
<i>sta</i>	Static
<i>t</i>	At time <i>t</i> , trilinear
<i>tot</i>	Total
<i>u</i>	Indicates ultimate value, indicates unchanged value
<i>w</i>	Indicates wall
<i>x</i>	Vertical direction
<i>y</i>	Horizontal direction, yielding



# 1 Introduction

## 1.1 Background

Explosions can be both accidental and intentional. The accidental explosions are typically occurring in the processing industry or in tunnels while intentional explosions can be connected to military or terrorist activity.

An explosion can be characterized as an instantaneous expansion of matter resulting in high pressure and temperature that propagates away from the centre of detonation. The result is a load that might differ considerably from the type of static or quasi-static loads normally used for design of structures. Due to the fact that the knowledge of the response of the structures in these situations is limited and the designing methodology often is simplified, there is a great need for further investigations within this subject.

The response of reinforced concrete structures due to explosive load has been studied in a long time project performed by Chalmers in collaboration with the Swedish Civil Contingencies Agency (MSB) and Reinertsen. This Master's Thesis carries on the studies as a continuation of five previous Master's Theses carried out by Nyström (2006), Ek and Mattsson (2009), Augustusson and Härenstam (2010), Andersson and Karlsson (2012) and Carlsson and Kristensson (2012).

## 1.2 Method

In order to get a deeper knowledge about the response of concrete structures with regard to explosive loading a literature study is carried out. In order to simplify the analysis the analysed structures with infinite degrees of freedom are transformed into single degree of freedom (SDOF) systems. The SDOF systems are adapted to consider the local and global response of the frame structure. The SDOF system is created in Matlab R2013a and analysed using simplified hand calculation methods and a more detailed numerical method based on the central difference method. The FE program ADINA (2011) is used to create models in 2D and 3D which is considered to present the reality in sufficient degree.

## 1.3 Limitations

The material studied is reinforced concrete without taking the effects of temperature, creep or shrinkage into consideration. However, the methodology with some adjustments could be used for other materials.

The material response models are approximated with elastic and elasto-plastic material response models. These models have proved to give satisfying results in previous studies. For the elasto-plastic model, plastic transformation factors are used, which is a simplification.

The Master's Thesis investigates the early response of impulse loaded structures. The impulse loads studied are induced by shock waves in air from an explosion and it is mainly the displacement that is studied. The influence of ground shock waves, bomb fragments and secondary effects from collapsing structures will be neglected.

The effect of strain hardening and increasing the resistance of the structure due to high strain rates is also neglected.

## 1.4 Aim

The aim of this Master's Thesis is to further investigate the response of reinforced concrete structures subjected to explosions. This is based on the previous Master's Theses and the intention is to provide a more comprehensive understanding of the subject. The main focus of this report is on structures composed of a few members, such as a frame structure which is investigated both in 2D and 3D analysis.

Since the capacity of an impulse loaded structure depends on its ability to develop internal work, a parametric study is carried out in order to investigate the important parameters for impulse loaded structures. Depending on how the neutral axis is interpreted in Eurocode 2, the plastic deformation capacity of the structure will differ. This is investigated in order to find the most appropriate way of performing the calculations.

The aim of the 2D analysis is to further investigate the SDOF models of a frame proposed in Johansson (2013) for the elastic case as well as the elasto-plastic. The focus for the elasto-plastic case is on the response models of the structures. The relationship between the resistance of the structure and the deformation is investigated with the aim to evaluate whether an SDOF system is appropriate for such cases. An intention is also to find a combination of the two SDOF models in order to provide a more realistic response.

In the 3D analysis a comparison is carried out between applying the impulse load directly on the front column of the frame, and applying the load on the wall and transferring it to the column by the reaction forces of the wall. The aim of the study is to investigate how realistic the direct application of the load, proposed in Johansson (2013), is and if there are alternative ways of calculating the load in the SDOF model. A parametric study is done in order to investigate the differences for when the stiffness and resistance of the wall is varied.

## 1.5 Outline of report

This report is divided into five chapters starting with Chapter 1, Introduction. Chapter 2, Background theory, covers the theoretical background of explosions and impulse load as well as the material and structural response models of structures subjected to both static and impulse load. The chapter also includes the theory of plasticity and plastic hinges. Finally, the concept of equivalent static load and transformation into a SDOF system is described.

In Chapter 3, Parametric beam study, the important parameters for impulse loaded beams are investigated. A study is carried out in order to find an appropriate interpretation of the effective depth,  $d$ , for calculating the plastic deformation capacity in Eurocode 2. It is also examined whether the top reinforcement should be neglected or not in the hand calculations.

Chapter 4, Structural response of a 2D frame, describes a simplified SDOF model of a frame consisting of a local and global model used for the front column and the whole frame, respectively. Both the elastic and elasto-plastic models are investigated with

focus on the structural response models. The SDOF calculations are compared with FE analyses.

Chapter 5, Structural response of a 3D frame, focuses on the front wall and front column of the frame. A comparison is done between applying the impulse load directly on the front column of the frame, and applying the load on the wall and transferring it to the column by the reaction forces from the wall. Finally, a parametric study is carried out in order to investigate the effects of varying the stiffness and resistance of the wall.

The results are presented and discussed in each chapter followed by a main concluding discussion at the end of the report, Chapter 6. References can be found in Chapter 7. In the appendices further background theory, hand calculations and additional graphs are presented. Appendix C discusses trilinear response models which are essential for this Master's Thesis.

## 2 Background theory

### 2.1 References

The main information presented in Chapter 2 is based on Johansson and Laine (2012a) and several figures are also taken from this reference. Some general information about the theory of plastic hinges and plastic rotation capacity are based on Engström (2011). Eurocode 2, CEN (2004), is used to present the calculation method for plastic rotation capacity.

### 2.2 Explosions

#### 2.2.1 Definition of explosion

An explosion is an instantaneous release of energy which creates a fast increase in pressure, see Figure 2.1. The explosion is an exothermal reaction which is over within a few microseconds. From the explosion a wave front, called a shock wave, is formed and spreads spherically. The temperature and pressure decreases with increasing distance from the centre of detonation. After a few milliseconds the whole process is over and then the pressure returns to atmospheric pressure.

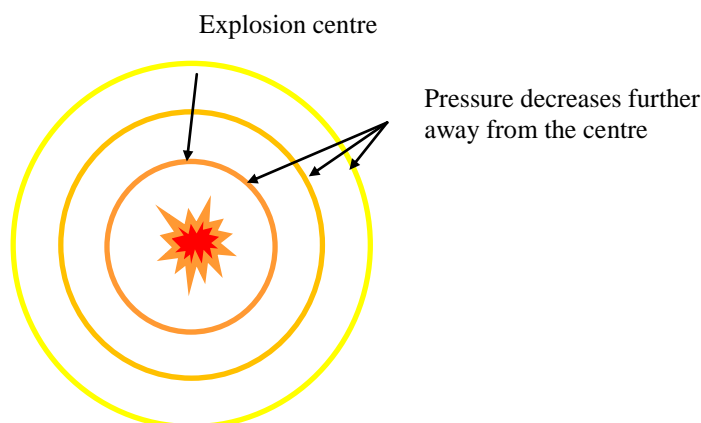


Figure 2.1 The energy spreads outwards from the source of the explosion.

The magnitude of the explosion is measured in the released energy, Joule. However, it also depends on the density of the explosive and the speed of ignition. Another, more applicable, way of measuring the magnitude of explosions is the effect that is obtained from the detonation of 1 kg TNT, corresponding to about 4.6 MJ.

#### 2.2.2 Idealized shock wave

An idealized shock wave has both a positive and a negative phase, see Figure 2.2. The shock wave forces the air to move as it spreads and it will create a lack of air behind it, causing partial vacuum or negative pressure. At the time of arrival,  $t_a$ , there is an instantaneous increase in pressure followed by the positive and negative phase. The negative phase is normally neglected and the positive phase is considered to be critical.



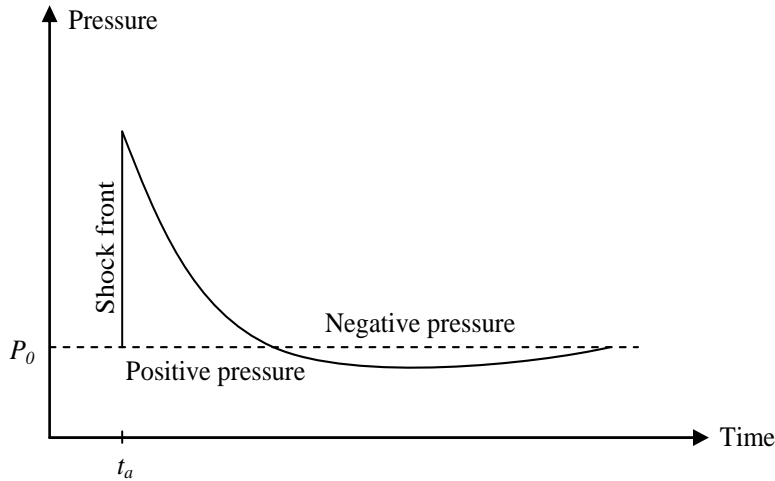


Figure 2.2 Idealised shock wave from an explosion showing the positive and negative phase.

A simplification of the shock wave is often made to make it easier to describe the load that the wave will give rise to. Usually, the negative phase is neglected and the pressure is assumed to be linear as illustrated in Figure 2.3.

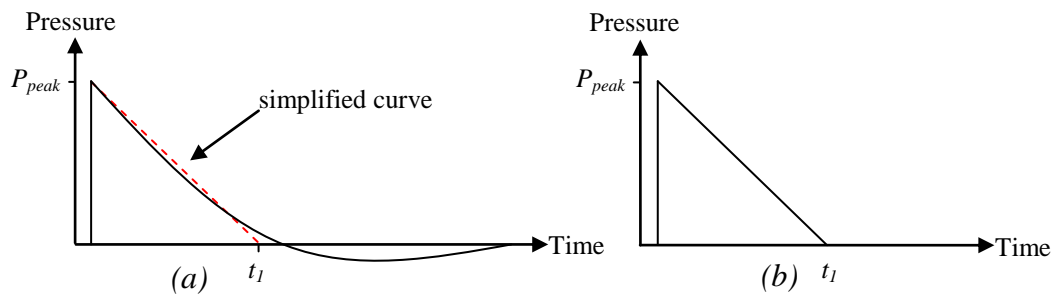


Figure 2.3 (a) Idealised shock wave indicating the simplified curve. (b) Simplified shock wave.

### 2.2.3 Strain rate due to a shock wave

The load intensity applied on a structure subjected to an explosion results in a strain rate of the structure. A comparison of the strain rates obtained in a structure due to different loads is shown in Figure 2.4. The strain rate due to a static load is used as a reference and is therefore shown as 1.

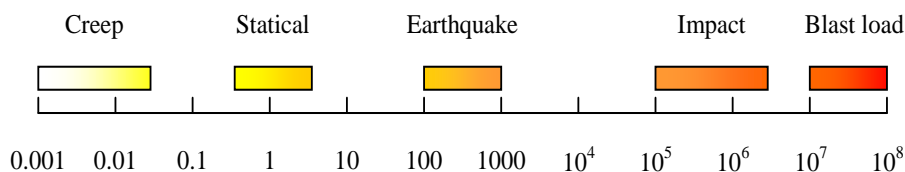


Figure 2.4 Comparison of strain rate between different types of loading where the static load is the reference load.

The load due to an explosion is characterized by a very high load magnitude acting during a very short period of time. An explosion load is shown as an impact or blast

load in Figure 2.4 and the strain rate due to an explosion load can be up to 100 million times larger than a static load.

The difference in strain rate demands different structural designs depending on which type of load the structure is subjected to. It is important to consider the fact that high strain rates influences the input material parameter of the structure. However this effect is not further discussed in this Master's Thesis.

## 2.2.4 Blast load

There are several things affecting the load from an explosion, such as the energy content, the surroundings and the complexity of the target. The distance between the explosion and the target as well as the position of the target has a large influence on the size of the load.

The shock wave can hit a building in several different ways and the distribution of pressure over time will differ depending on how it is reflected. For example, the angle between the structure and the explosion will matter, but most important is if the wave is reflected or not.

Reflection occurs when a shock wave hits a building as illustrated in Figure 2.5. The size of the pressure depends on the magnitude of the explosion, the angle of which the explosion hits the structure as well as the distance between the structure and the explosion. When a shock wave hits the building perpendicular to the surface it is called a normal reflection and this type of reflection results in the highest pressure.

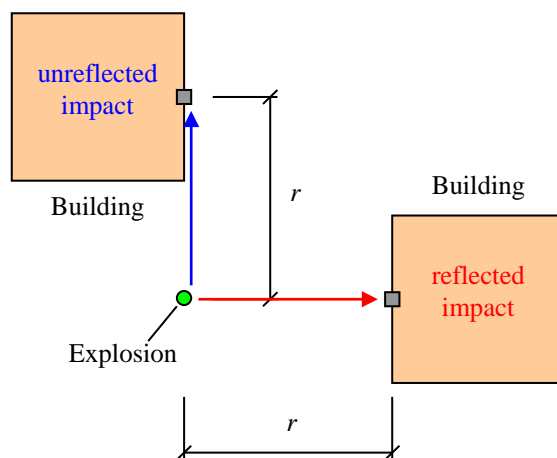


Figure 2.5 Reflected and unreflected shock wave.

The difference in pressure between a reflected and an unreflected shock wave is at least two times but can be up to 20 times. The ratio between the reflected pressure and the shock wave,  $A$ , can be described as

$$A = \frac{(3\gamma - 1)P_s^+ + 4\gamma P_0}{(\gamma - 1)P_s^+ + 2\gamma P_0} \quad (2.1)$$

where the heat capacity ratio,  $\gamma$ , varies with the pressure. For a pressure lower than 1000 kPa the heat capacity ratio can be put as 1.4.

The shock wave hits the different parts of the building at slightly different times, something that is often neglected since the difference in time is very small. The loading will also differ at different parts of the building, which can be dealt with in several ways. Either the worst load case is chosen for every part of the building, the load size closest to the explosion, or the load can be divided into different parts with different magnitudes.

In a city environment, the complexity of the structures gives rise to several different phenomena such as diffraction and reflection. Diffraction is a decrease in pressure which occurs after a shock wave has hit an irregularity of a building and spread behind it. When a shock wave reaches the irregularity of the structure an air vortex is created and the pressure on the back side of the structure will decrease.

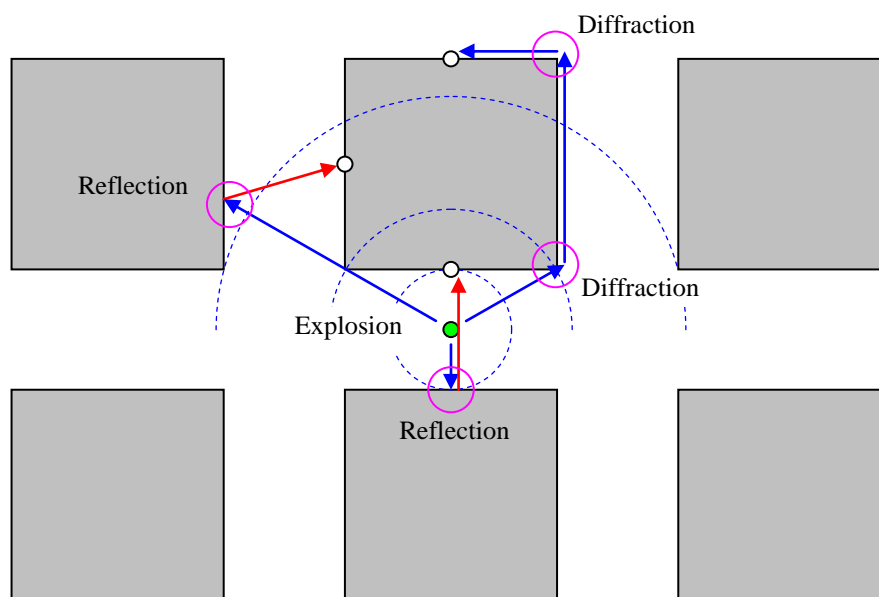


Figure 2.6 Graphical presentation of shock wave phenomena due to an explosion.

### 2.2.5 Wave propagation

An impulse load which hits a body starts a mechanical wave that travels through the body and affects the different parts of the structure gradually with time. The effect of an explosion will therefore not always be active in the whole structure at the same time. This phenomenon occurs for all types of loads, but for impulse loads in particular it is noticeable due to the fact that it happens so fast.

Figure 2.7 shows a three meter high and five meter deep concrete structure exposed to an explosion. The longitudinal wave propagation in concrete is about 3500 m/s why the rear wall isn't affected by the load until about 1.4 milliseconds from the time the front wall is affected.

In the figure it can be seen that after one millisecond the rear wall is not affected by the load. However, after two milliseconds the rear wall has begun to react to the loading.

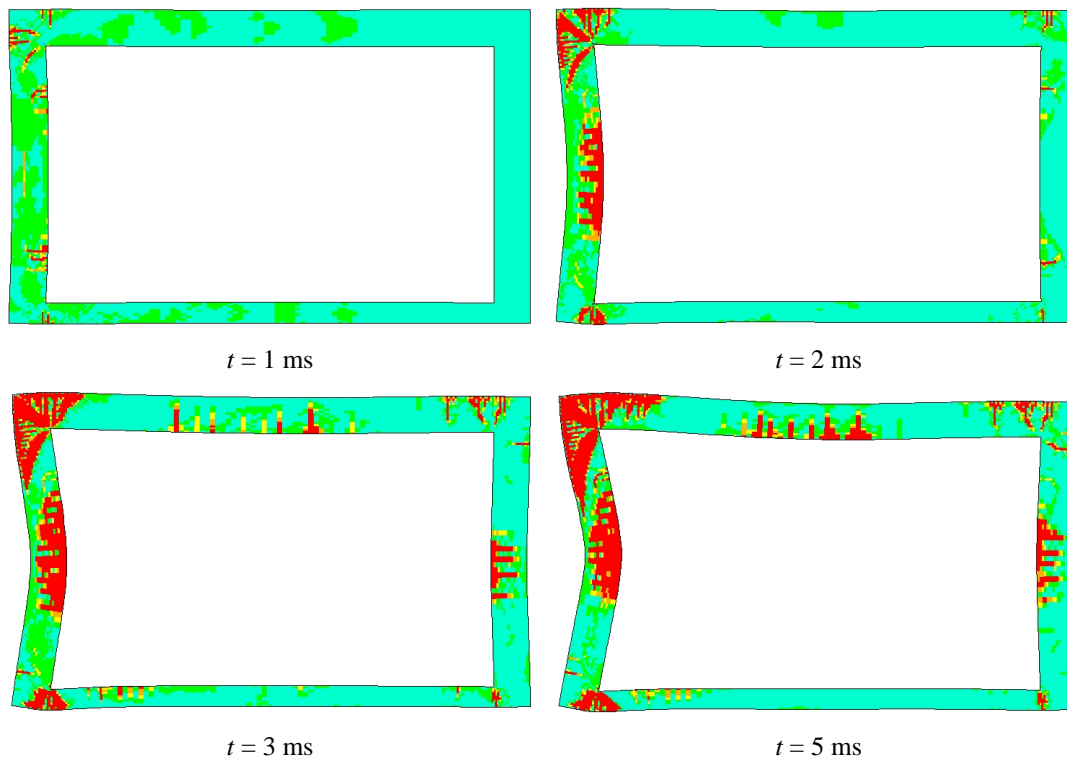


*Figure 2.7 Response of a shelter subjected to an impulse load acting on the left wall. The deformations are enhanced 20 times and the dark colour marks fully developed cracks. From Johansson and Laine (2012a).*

There are different types of mechanical waves which all need a medium to propagate through. The longitudinal waves, also called pressure waves, travels parallel to the direction of the energy. These are stronger and faster than the other mechanical waves and they are able to travel through all types of mediums. Mechanical waves that travel perpendicular to the direction of energy are called transverse or shear waves. These can only travel through solids. Surface waves travel in elliptical patterns such as ripples on a water surface.

An illustration of a material at rest, a pressure wave and shear wave are shown in Figure 2.8.

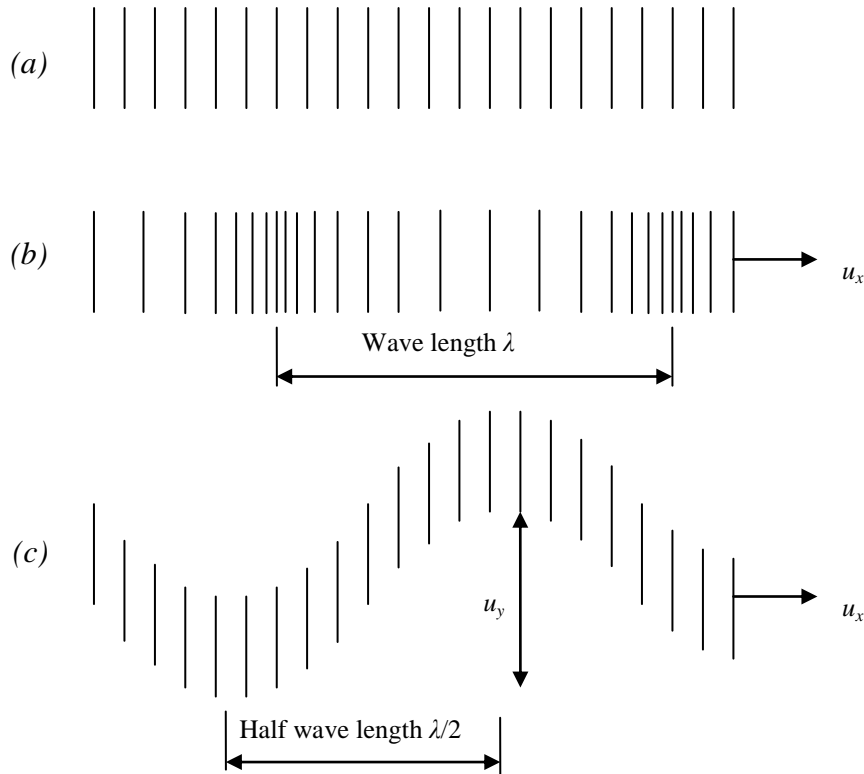


Figure 2.8 Waves propagating through a body for: (a) material at rest; (b) pressure wave; (c) shear wave.

Normally, a wave propagates as a combination of all waves but it's the type and direction of load that decides which wave type will be dominant. If a beam, for example, is axially loaded the dominant wave type will be a pressure wave and if it is loaded perpendicularly to its longitudinal axis, the dominant wave type will be a shear wave.

## 2.3 Material response due to static load

### 2.3.1 Concrete

The stress-strain relationship for concrete is presented in Figure 2.9. The material behaviour is close to linear at the very beginning of loading, after which it becomes non-linear. As can be seen in the figure, the concrete strength is much higher for compression compared to tension.

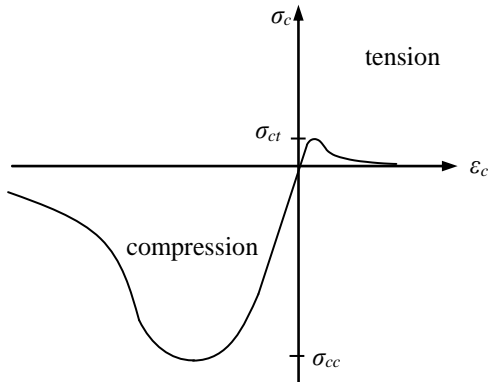


Figure 2.9 Stress-strain relationship for concrete.

### 2.3.2 Reinforcement

The structural response of reinforcement is presented in Figure 2.10a where  $f_{sy}$  is the yield strength,  $f_{su}$  is the ultimate tensile strength,  $\epsilon_{sy}$  is the strain at which the reinforcement start to yield,  $\epsilon_{sh}$  is the strain at which steel hardening begins,  $\epsilon_{s,f_{su}}$  is the strain at the ultimate tensile stress  $f_{su}$  and  $\epsilon_{su}$  is the ultimate strain. The point when the stresses reach the yielding value,  $f_{sy}$ , is followed by a plastic plateau, after which strain hardening begins.

A simplification of this response, according to Eurocode 2, involves two alternatives shown in Figure 2.10b. The first alternative is characterised by a horizontal top branch with no strain limit, which is appropriate for hot rolled steel. The other alternative, with an inclined top branch and with a certain strain limit, is recommended for cold worked steel.

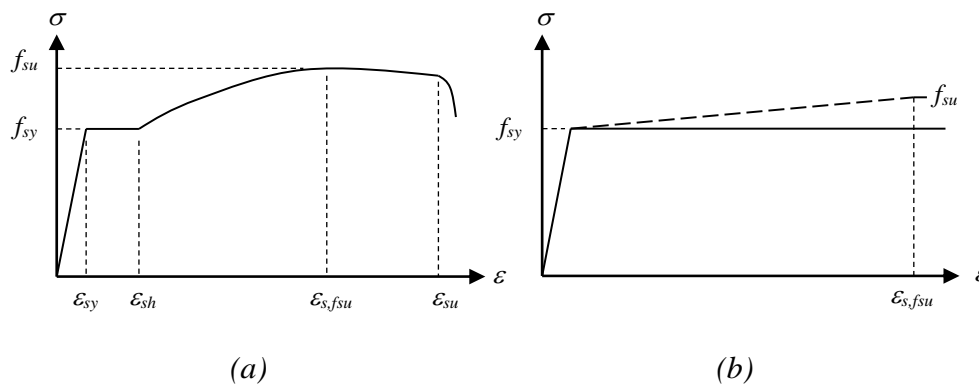


Figure 2.10 (a) Stress-strain relationship for a hot-rolled reinforcement bar and (b) idealized bilinear model according to Eurocode 2.

The ductility of reinforcement has an important influence on the plastic rotation capacity and plastic deformation capacity, further described in Section 2.5. As these parameters are essential for impulse loaded structures, it is worth to mention the classification of reinforcement steel according to Eurocode 2, see Table 2.1.

Table 2.1 Classification of reinforcing steel according to Eurocode 2. The notations  $f_{su}$ ,  $f_{sy}$  and  $\varepsilon_{s,fsu}$  are illustrated in Figure 2.10.

Class	$f_{yk}$ [MPa]	$f_{su} / f_{sy}$ [-]	$\varepsilon_{s,fsu}$ [%]
A	400 - 600	$\geq 1,05$	$\geq 2,5$
B	400 - 600	$\geq 1,08$	$\geq 5,0$
C	400 - 600	$\geq 1,15$ $< 1,35$	$\geq 7,5$

## 2.4 Structural response due to static load

### 2.4.1 Orientation

Reinforced concrete structures subjected to loading involve both linear and nonlinear behavior and depend on the material response for both the reinforcement and the concrete. The typical response of a reinforced concrete section, subjected to increasing load, is presented in Figure 2.11. The section shows linear behavior as long as it is uncracked (state I). After the first crack has occurred, the stiffness decreases but the response is still linear (state II). When the concrete in the compression zone has started to show nonlinear behavior or the reinforcement has started to yield, the response of the section becomes plastic (state III).

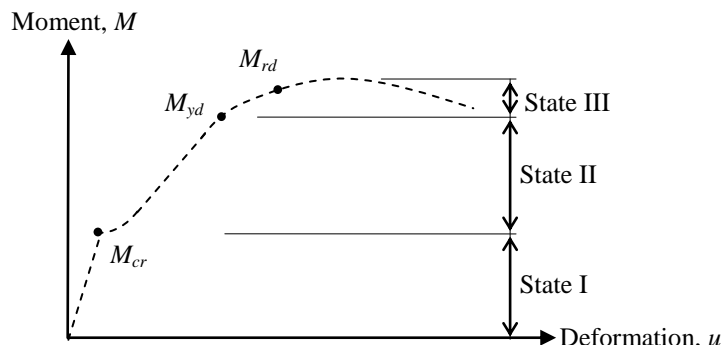


Figure 2.11 Typical response of a reinforced concrete section.

This non-linear behavior makes the analyses of concrete structures complicated and induces a need of introducing simplifications. Thus, the typical reinforced concrete response is often approximated to a linear relationship. Models simulating the response of the reinforced concrete, which are used in this Master's Thesis, are further described in Sections 2.4.2 and 2.4.4. Despite that these models present the real structural behavior in a simplified way, their correctness is assumed to be sufficient to understand the differences in response of investigated structure.

### 2.4.2 Linear elastic model

The simplest model is linear elastic which is characterized by unlimited elastic deformations and constant stiffness. The stiffness can be chosen as either the stiffness

in state I or state II, i.e. for an uncracked or a cracked section, respectively. This is illustrated in Figure 2.12. The behaviour simulated by this model corresponds best to the response of a reinforced concrete structure subjected to limited loads, before state III is reached.

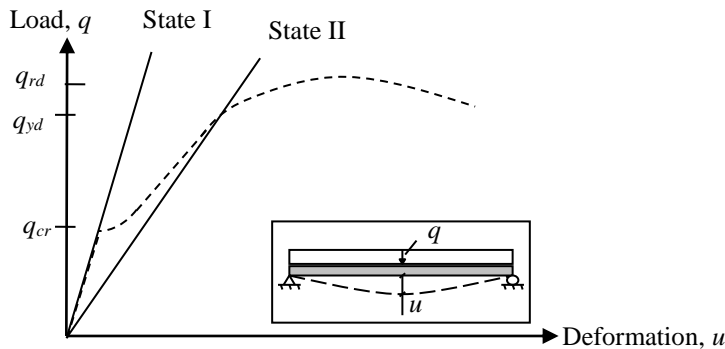


Figure 2.12 Typical response for a reinforced concrete structure marked with a dashed line and assumed linear elastic response marked with continuous lines for stiffness of state I and state II.

If the stiffness of state II is used, the influence of the uncracked part is neglected. Nyström (2006) has investigated models where the uncracked stiffness is taken into consideration with the conclusion that the uncracked part does not have a significant influence on the response of the structure why it is neglected in this Master's Thesis.

However, the elastic model with stiffness in state I can be useful when dealing with pre tensioned structures for which the value of cracking resistance is significantly increased compared to reinforced concrete and thus state I is extended.

The linear elastic model agrees with the response of steel before reaching its yield strength  $f_{sy}$ , see Figure 2.10a. Linear elastic material is described by Hooke's law and presented in Figure 2.13a.

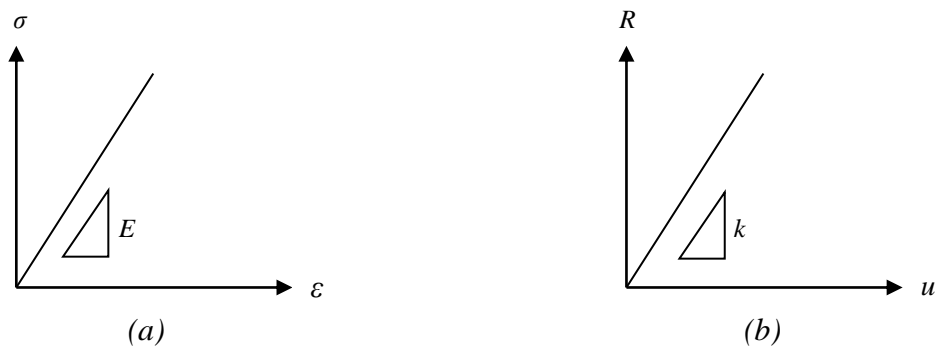


Figure 2.13 Linear elastic response for: (a) material; (b) structure.

By following Hooke's law, a relation for the linear elastic response of the concrete structure is established, Figure 2.13b. The elastic displacement  $u$  increases proportionally with increasing the internal resisting force  $R$  while the structural stiffness  $k$  remains constant. This can be described as

$$R = k \cdot u \quad (2.2)$$



The structure or material returns to its initial shape after removal of the load. This means that there will be no remaining deformation after the load is removed.

### 2.4.3 Ideal plastic model

The behaviour described by the ideal plastic model corresponds to the response in ultimate limit state, state III, when the yielding strength of the material or the ultimate load capacity of the structure is reached. A comparison of this model to the typical response of a reinforced concrete structure is presented in Figure 2.14 where  $u_{pl}$  is the plastic deformation.

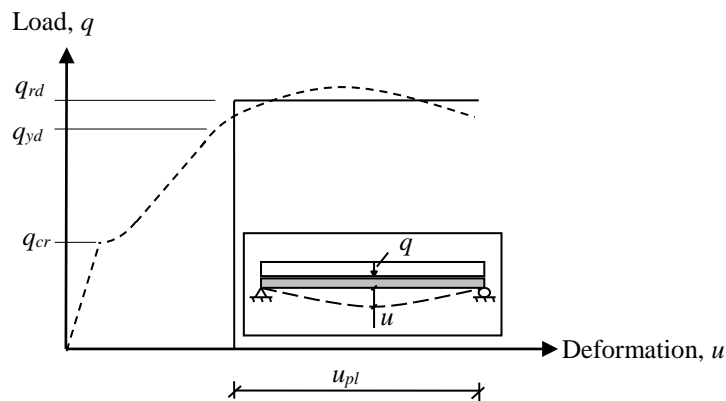


Figure 2.14 Typical response for a reinforced concrete structure marked with a dashed line and assumed plastic response marked with a continuous line.

The response of the ideally plastic material is presented in Figure 2.15a. The deformations are equal to zero until the stresses reach the material yield strength. After that, the plastic deformation develops without increasing the stresses. The model for the structure is established in Figure 2.15b.

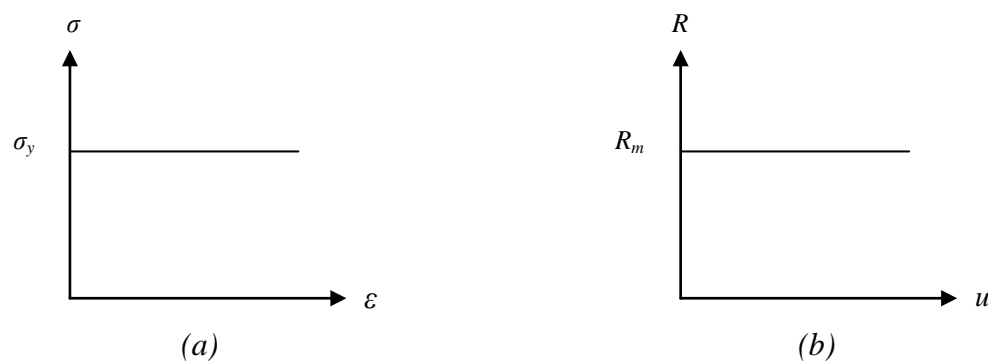


Figure 2.15 Ideal plastic response for: (a) material; (b) structure.

The structural model can be described as

$$\begin{aligned} R &= F & \text{for } F < R_m & \text{ and } u = 0 \\ R &= R_m & \text{for } F \geq R_m & \text{ and } u \geq 0 \end{aligned} \quad (2.3)$$

where  $F$  is the external load and  $R_m$  is the maximum internal force. This model assumes that the region of the structure where the plastic capacity has been reached

has an ideally plastic behavior. This results in the formation of a plastic hinge. The plastic deformation remains after removal of the load.

In an ideal plastic model the plastic deformation capacity is unlimited. However it must be remembered that this is not the case in reality and a concrete structure has limited plastic deformability. In order to assure that a plastic hinge can develop it is necessary to provide the structure with a sufficient plastic rotation capacity. The subject of plastic rotation capacity is discussed in Section 2.5.

#### 2.4.4 Elasto-plastic model

The elasto-plastic behavior combines linear elastic and ideal plastic response. It is characterized by elastic behavior with a constant stiffness that corresponds to the stiffness in state II and elastic deformations up to the material yielding strength or the ultimate load capacity of the structure. After exceeding this value the plastic state with plastic deformation is reached. A comparison of this model to the typical behavior of a reinforced concrete structure is presented in Figure 2.16, where  $u_{ep,el}$  is the elastic deformation and  $u_{ep,pl}$  is the plastic deformation.

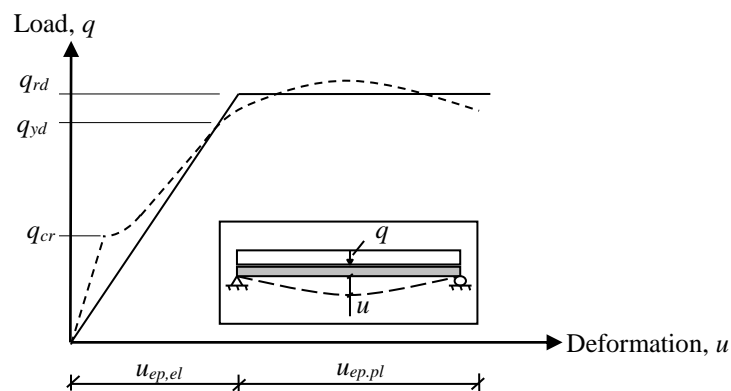


Figure 2.16 Typical response for a simply supported beam of reinforced concrete marked with a dashed line and assumed elasto-plastic response marked with a continuous line.

If the structure is unloaded in the plastic stage the response will be parallel to the inclination in the elastic stage governed by the elastic stiffness in state II, Figure 2.17. If the structure is loaded again, the deformations will follow the elastic response up to the yield strength and after reaching this value the deformations will continue from the value reached in the previous loading cycle.

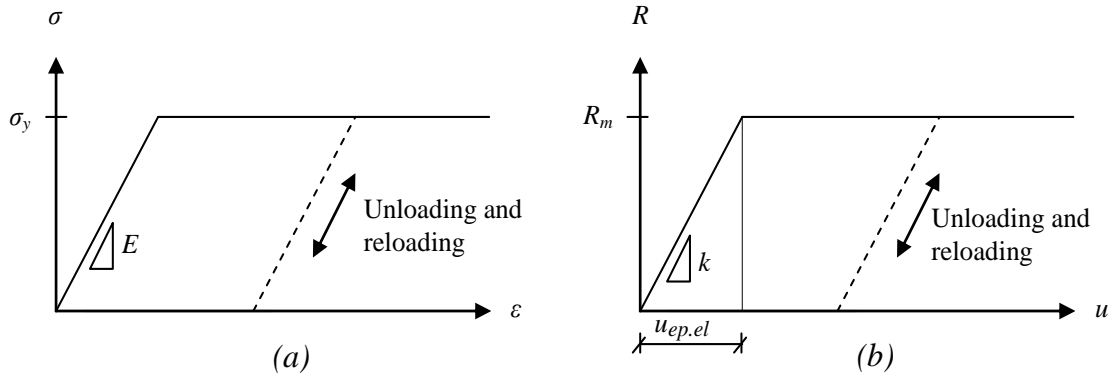


Figure 2.17 Elasto-plastic response for: (a) material; (b) structure.

Depending on if the external load  $F$  has reached the maximum internal force  $R_m$  the elasto-plastic relationship can be expressed as

$$\begin{aligned}
 R &= k \cdot u & \text{for } F < R_m & \text{ and } u \leq u_{ep,el} \\
 R &= R_m & \text{for } F \geq R_m & \text{ and } u > u_{ep,el}
 \end{aligned}
 \tag{2.4}$$

where  $u_{ep,el}$  is the elastic deformation in the elasto-plastic response model.

This model is the more realistic than the elastic and ideally plastic models presented in Section 2.4.2 and 2.4.3, respectively.

## 2.5 Plastic hinges and plastic rotation capacity

### 2.5.1 Theory of plastic hinges

At the stage when a section has reached its moment capacity,  $M_{rd}$ , and shows an ideally plastic behaviour, the deformation capacity is unlimited. If a section with such properties develops in a beam, it will deform much more than the neighbouring regions, which still shows elastic response. This plastic section will connect the regions with elastic response and the shape of the beam will differ. As this region, with such a large curvature, is comparatively small, it can be assumed that the developing deformation will concentrate only in this plastic section, i.e. plastic hinge. The regions with plastic behaviour as well the corresponding curvature and the model assumed in the calculation methodology for a simply supported beam and a beam with fixed edges is presented in Figure 2.18.

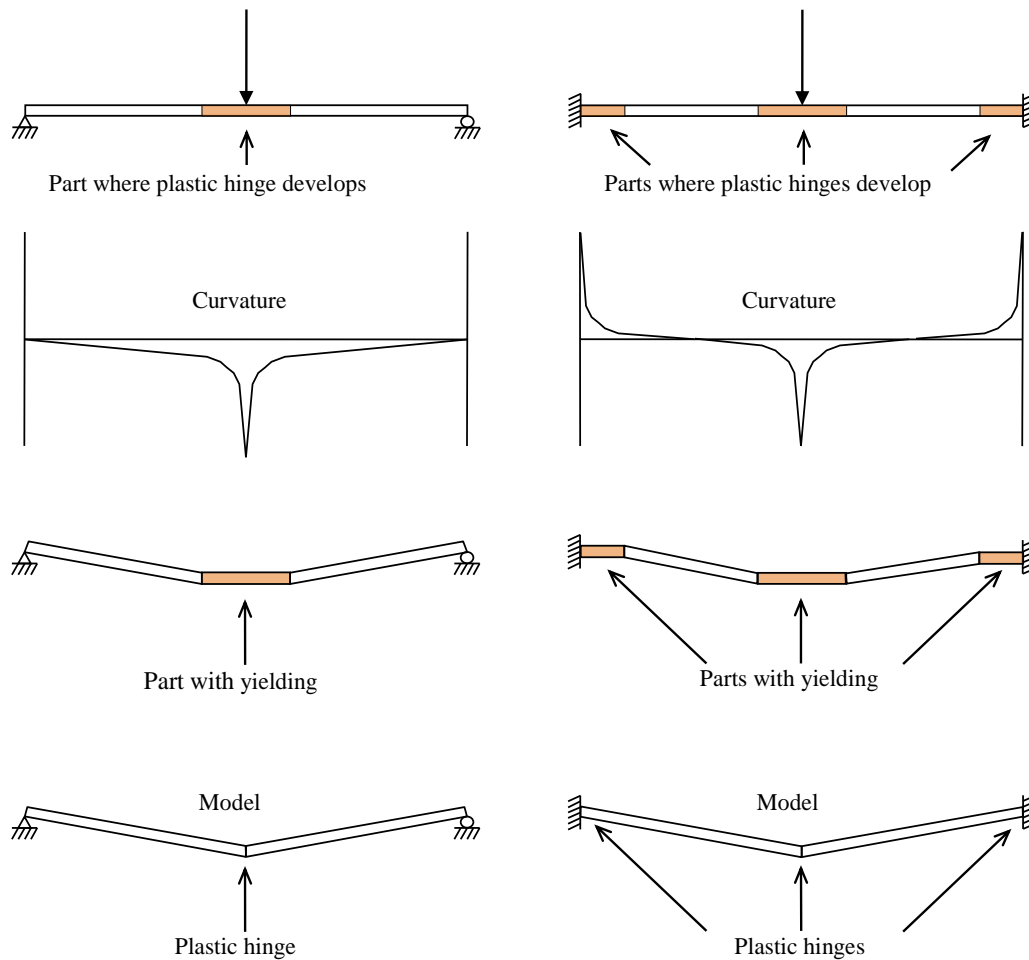


Figure 2.18. Plastic hinges and corresponding curvature for a: (a) simply supported beam; (b) fixed beam, Nyström (2006).

When the load is further increased, more than one plastic hinge can develop, depending on the support conditions. In case of static loading, failure of the structure occurs when the collapse mechanism is created. However, this is not the case for the structures subjected to dynamic loading. For such type of loading collapse of the structure occurs when the plastic rotation capacity is reached.

For a statically determinate structure such as a simply supported beam, only one plastic hinge is formed, which is the condition for the collapse mechanism to be created. The continuous beams and the beams fully restrained at the supports are more redundant. The structures which are  $n$ -order indeterminate can develop  $n + 1$  plastic hinges.

Thus, for example, a beam which is fully fixed at one edge and simply supported at the other develops plastic hinges in the span as well as at the fixed support. When it is subjected to a uniformly distributed load the yielding starts at the fixed support. If the load is further increased, a plastic hinge develops at this section. Since the moment cannot increase further in this section, it can be assumed that the restraint at this support corresponds to a simply supported boundary condition. Thus, the studied beam can be considered as simply supported, loaded with a constant moment, i.e. the plastic moment, at the fixed support. The formation of a plastic hinge at the fixed

support, however, has not triggered the collapse mechanism yet. There is still capacity left in the span section and the load can be increased until yielding starts in the span and the plastic hinge is formed there as well, at which time a collapse mechanism is created. The calculation of the moment at the fixed support and in the span in ultimate limit state, when the collapse mechanism is formed, is presented in Section 2.6.

The formation of plastic hinges for a continuous beam, together with its extension length  $l_{pl}$  and its development of plastic rotation  $\theta_{pl}$ , is schematically presented in Figure 2.19. A continuous beam with an increasing load  $q$  is illustrated in Figure 2.19a. In Figure 2.19b, the deformed shape of the studied beam, before yielding is reached in any section, is illustrated. As the load increases the first plastic hinge develops at the intermediate support, Figure 2.19c. The rotation  $\theta_{pl}$  continues to develop until two additional plastic hinges are formed in the span sections and the collapse mechanism is created, Figure 2.19d.

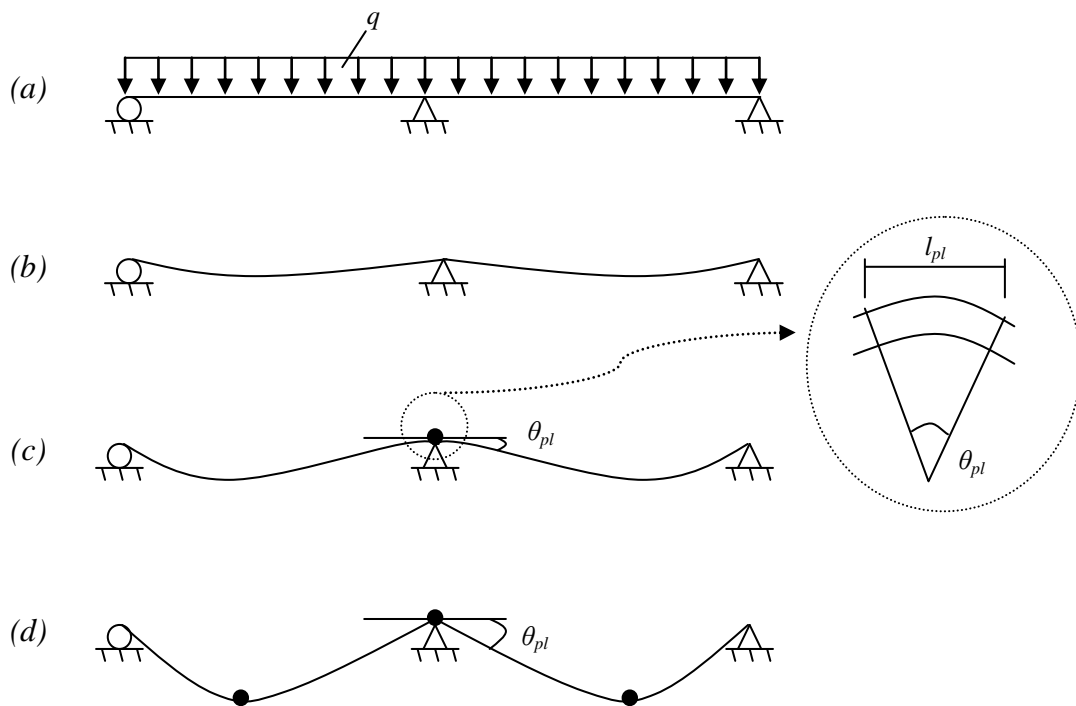


Figure 2.19 Formation of plastic hinges and development of plastic rotation for a continuous beam loaded with an increasing load  $q$ . The extension length of the plastic hinge,  $l_{pl}$ , is schematically presented.

According to Engström (2011) two types of plastic hinges can be distinguished, single and double. A single plastic hinge is formed at the fixed support, Figure 2.20a. A double plastic hinge develops in the span (Figure 2.20b) or at the support section in a continuous beam, Figure 2.20c.

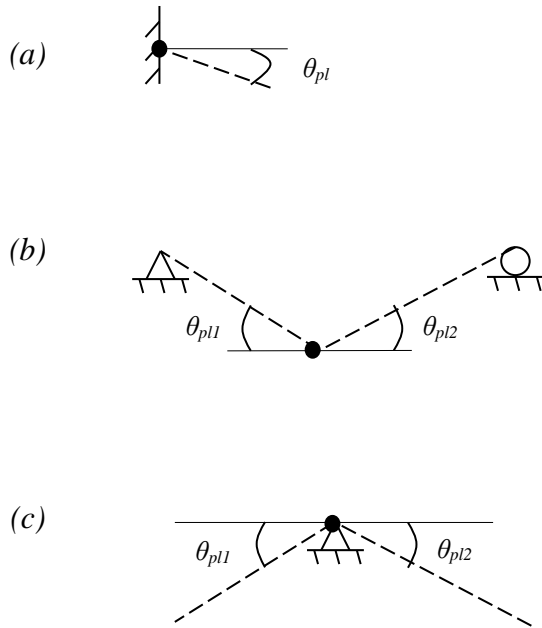


Figure 2.20 (a) Single plastic hinge at fixed support; (b) double plastic hinge in the span; (c) double plastic hinge in the section above the support of the continuous beam, Engström (2011).

## 2.5.2 Definition of plastic rotation capacity

When analysing an impulse loaded structure with a plastic or an elasto-plastic model, not only the ultimate resistance should be checked but also the ultimate deformation. The deformation is estimated by using the concept of plastic rotation,  $\theta_{pl}$ , schematically shown in Figure 2.21. Plastic rotation describes the increasing curvature of the section, due to the development of plastic deformations, which begins when the moment capacity of the section has been reached and continues until the section collapses.

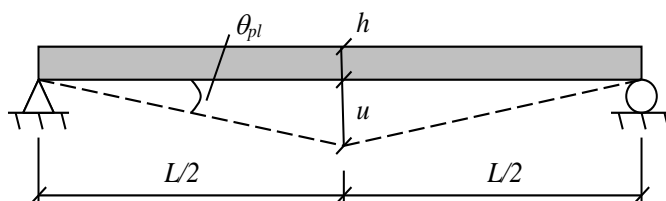


Figure 2.21 Plastic rotation and deflection for the plastic model.

In the moment curvature diagram, presented in Figure 2.22, the plastic rotation begins when the curvature reaches the value of  $(1/r)_y$  and develops until its ultimate magnitude  $(1/r)_u$  is reached.

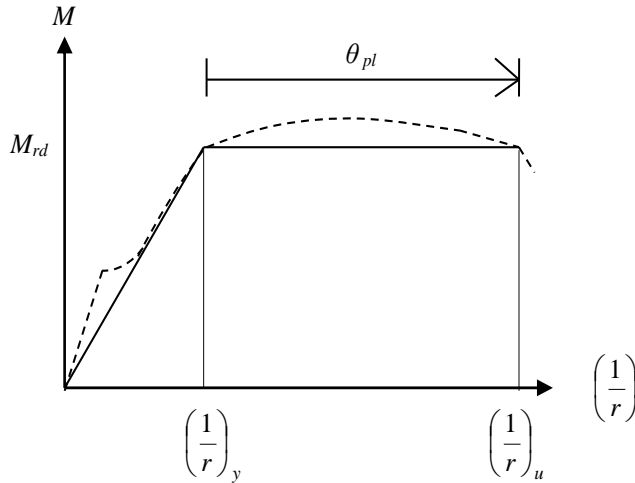


Figure 2.22 A moment curvature diagram. The plastic rotation begins at the first yielding (at curvature  $(1/r)_y$ ) and continues until the collapse mechanism develops (at curvature  $(1/r)_u$ ).

In order to calculate the plastic rotation,  $\theta_{pl}$ , an integration of the curvature over the extension length  $l_{pl}$  is done, according to equation (2.5). The extension length of a plastic hinge is schematically presented in Figure 2.19c.

$$\theta_{pl} = \int_{l_{pl}} \left( \left( \frac{1}{r} \right) - \left( \frac{1}{r} \right)_y \right) dx \quad (2.5)$$

The definition of the curvature, which is the inclination in the strain distribution diagram, Figure 2.23, can be calculated as

$$\frac{1}{r} = \frac{\varepsilon_{cc}}{x_u} = \frac{\varepsilon_s}{d - x_u} \quad (2.6)$$

where  $\varepsilon_{cc}$ , is the concrete strain at the compressed edge of the section,  $\varepsilon_s$  is the steel strain in state III,  $x_u$  is the height of the compression zone in ultimate limit state and  $d$  is the effective depth.

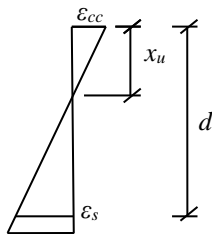


Figure 2.23 The strain distribution diagram, where the curvature of the section is its inclination.

When dealing with plastic rotation capacity it is good to recall how the magnitude of the compressive concrete zone  $x$  to the effective depth  $d$  influences the strain distribution in the loaded section. The steel strain for the cross section can be calculated as

$$\varepsilon_s = \frac{d-x}{x} \varepsilon_{cu} \quad (2.7)$$

If the ratio of  $x_1$  to  $d$  is too large, the steel strain will not reach its maximum value when the section reaches its capacity, see Figure 2.24a. In the compressed zone of the concrete the failure will be brittle and caused by crushing of the concrete. In this case, the area of the steel bars should be decreased in order to utilize the yielding strength of the steel. Another solution could be to increase the height of the section or to increase the compressive strength of the concrete. This would provide a lower ratio of  $x_2$  to  $d$  and a more effective use of the steel strength which secures plastic response. This is presented in Figure 2.24b.

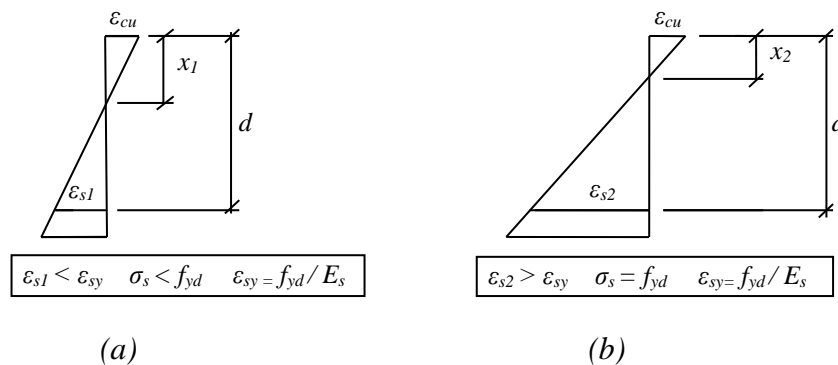


Figure 2.24 Strain and stress values for a reinforced concrete section reaching its capacity. (a) For a high value of the compressive zone  $x_1$  in relation to the effective depth  $d$ , the steel stresses are lower than the yielding strength. (b) For lower ratios of  $x_2$  to  $d$ , the stresses reach the yielding strength.

### 2.5.3 Calculation method for plastic rotation capacity

There are several calculation methods for plastic rotation capacity, established by different authorities. The parametric beam study in Chapter 3 is conducted according to the recommendations found in Eurocode 2, CEN (2004), which are briefly described in the following paragraphs. A more detailed description can be found in Section A.5.

The base for methodology in Eurocode 2 is the graph illustrated in Figure 2.25, where the plastic rotation capacity is a function of the compressed concrete zone  $x$  to the effective depth  $d$ , with consideration to the reinforcement ductility and the concrete strength class.



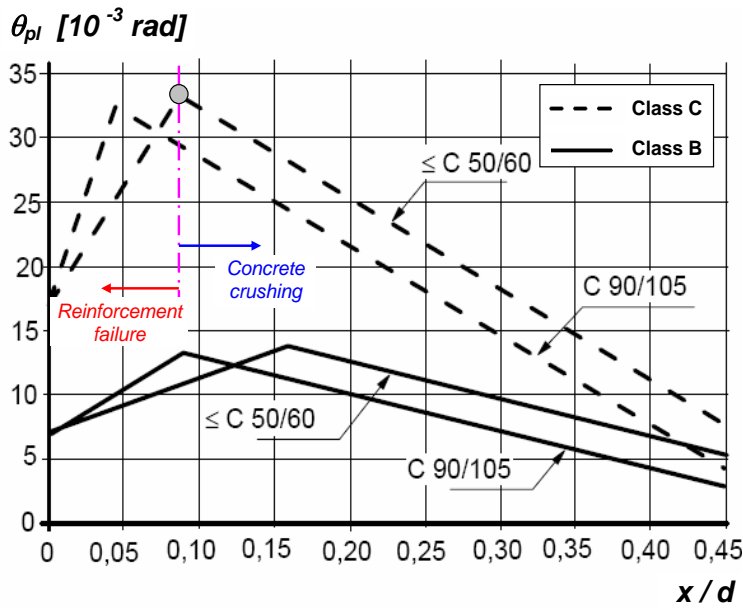


Figure 2.25 Graph for plastic rotation capacity from Eurocode 2, CEN (2004).

The plastic rotation capacity,  $\theta_{pl}$ , obtained from the graph should be multiplied with a factor  $k$  calculated as

$$k_{\lambda} = \sqrt{\frac{\lambda}{3}} \quad (2.8)$$

where

$$\lambda = \frac{L_0}{d} \quad (2.9)$$

and  $L_0$  is the distance between the plastic hinge and the section where the moment is zero. Thus, the revised plastic rotation capacity is

$$\theta_{rd} = k_{\lambda} \cdot \theta_{pl} \quad (2.10)$$

According to the graph for plastic rotation capacity, failure of the section is caused by either crushing of the concrete or by rupture of the reinforcement. In the interval with small values of  $x/d$ , where the rotation capacity is limited by the ultimate steel strain, the rotation capacity increases with increasing ratio of  $x/d$  and failure is caused by rupture of the reinforcement. For larger values of  $x/d$ , where the rotation capacity is limited by the ultimate concrete strain, failure occurs due to crushing of the concrete. According to Engström (2011) this simple method gives conservative results. Moreover, it was developed for statically loaded structures but is also applicable for impulse loading.

## 2.6 Structural response of statically indeterminate structures

In this section, a short description of the non-linear response of statically indeterminate structures is given. The description is based on the beam which is simply supported at one edge and fixed at the other, illustrated in Figure 2.26. It is assumed that the section at the support is provided with more reinforcement than the section in the span. Thus, the stiffness  $EI_s$  is larger than  $EI_f$ .

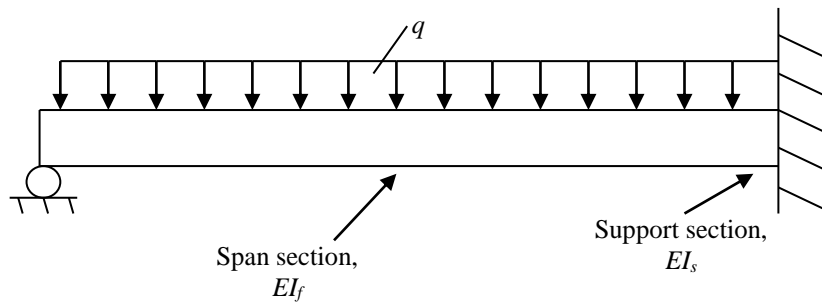


Figure 2.26 The studied beam is simply supported at one edge and fixed at the other, for which the response and changes in moment distribution due to an increase of load is studied.

During the uncracked stage, the beam shows linear structural response. The moment distribution increases in proportion to the increase of the load and corresponds to line 1 in Figure 2.27a. When the load is further increased, cracking begins at the fixed support since the moment is higher there. The section at this support cracks, and the stiffness  $EI_s$  decreases. As a consequence, the moment is attracted to the stiffer regions in the span section since they are still uncracked. The moment diagram, for that stage, is defined as line 2 in Figure 2.27a. Further increase of the load results in cracking of the span sections.

When both the sections in the span and at the fixed support are cracked, the moment is attracted to the stiffer regions at the fixed support, as it is provided with higher stiffness. The moment distribution at that stage is defined as line 3 in Figure 2.27. Now yielding starts at the fixed support, before the design load is reached and the first plastic hinge is formed. This corresponds to a moment distribution shown as line 4 in Figure 2.27b.

However, there is still capacity left as the section in the span has not reached its ultimate moment resistance yet. The load can be further increased up to the point when the ultimate capacity of the critical section in the span is reached after which a plastic hinge is created in the span and a collapse mechanism forms. The moment distribution is defined as line 5 in Figure 2.27b. From this point the load cannot be further increased. Local failure occurs, in the plastic region, as a result of either concrete crushing or reinforcement rupture.

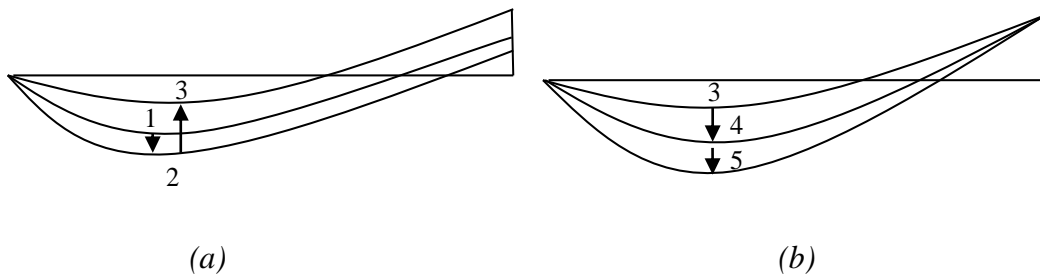


Figure 2.27 The changes in the moment distribution for a span of a continuous beam, due to an increase of load: (a) stages 1-3; (b) stages 3-5.

## 2.7 Structural response due to impulse load

### 2.7.1 Difference between impulse and static load

An explosion leads to an impulse load which can contain a maximum pressure that is many times larger than an equivalent static load. In addition to the large difference in load magnitude, the duration of the impulse load is significantly shorter than a constant static load, see Figure 2.28. These are the reasons for the considerable difference in the structural responses that may be obtained due to impulse load and static load, respectively. Thus, the calculation methodology for the impulse loaded structures, used in this Master's Thesis, involves dynamic analysis based on the equivalent single degree of freedom (SDOF) system, described in Section 2.9.

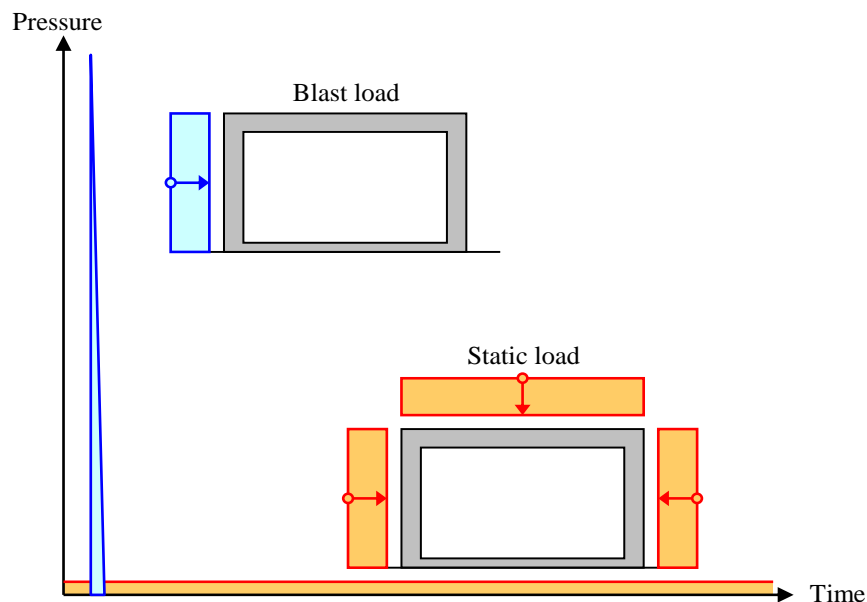


Figure 2.28 Comparison of the duration and magnitude of a blast load and equivalent static load acting on a civil defence shelter (Johansson and Laine (2012a)).

Impulse loaded structures are normally provided with an equal reinforcement amount on both edges of the cross section. This is essential due to the fact that when a

structure subjected to an impulse load sways back and forward, the compressed edge becomes tensioned and tensioned edge compressed.

In order to provide knowledge about the response of structures subjected to impulse load, it is essential to introduce some basic dynamic concepts. The most important concepts are presented in the following sections.

### 2.7.2 Force and Pressure

The force  $F$  is defined, according to Newton's second law, as the correlation between the mass  $m$  and the acceleration  $a$  as

$$F = ma \quad (2.11)$$

The definition of pressure,  $P$ , which is used to describe the magnitude of the shock waves, is

$$P = \frac{F}{A} \quad (2.12)$$

where  $P$  is the pressure and  $A$  is the area subjected to the force  $F$ .

### 2.7.3 Momentum, impulse and impulse intensity

The momentum,  $p$ , for a body with the mass  $m$  and the velocity  $v$  is expressed as

$$p = mv \quad (2.13)$$

The change in momentum for a body with an initial velocity  $v_0$  caused by the force  $F$  within the time interval from  $t_0$  to  $t_1$  can be expressed as

$$m \cdot v_1 = m \cdot v_0 + \int_{t_0}^{t_1} F(t) dt \quad (2.14)$$

The impulse  $I$  transmitted to the body is generated from the force  $F$

$$I = \int_{t_0}^{t_1} F(t) dt \quad (2.15)$$

The impulse intensity is the integral of the pressure-time-curve as illustrated in Figure 2.29 and it is expressed as

$$i = \int_{t_0}^{t_1} P(t) dt \quad (2.16)$$

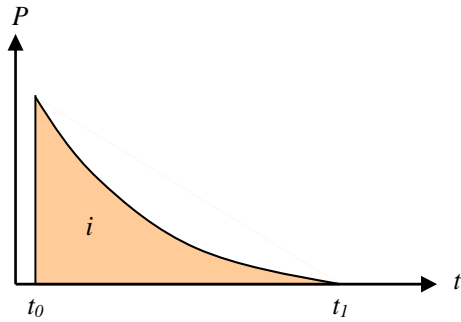


Figure 2.29 The impulse intensity.

The correlation of the pressure, which describes the magnitude of the shock wave, to the total impulse  $I$  acting on the area  $A$  can also be recognized as

$$I = i \cdot A = A \int_{t_0}^{t_1} P(t) dt \quad (2.17)$$

When discussing the concepts of pressure and impulse, two types of dynamic loading are worth mentioning. Figure 2.30a presents the ideal impulse load described by the concept of characteristic impulse  $I_k$  which is an infinite high pressure, acting during an infinite small time interval. In this case, the force instantaneously increases and decreases. Figure 2.30b illustrates a pressure load defined by a characteristic pressure load  $F_k$  which is a shock wave acting during an infinite long time with constant magnitude.

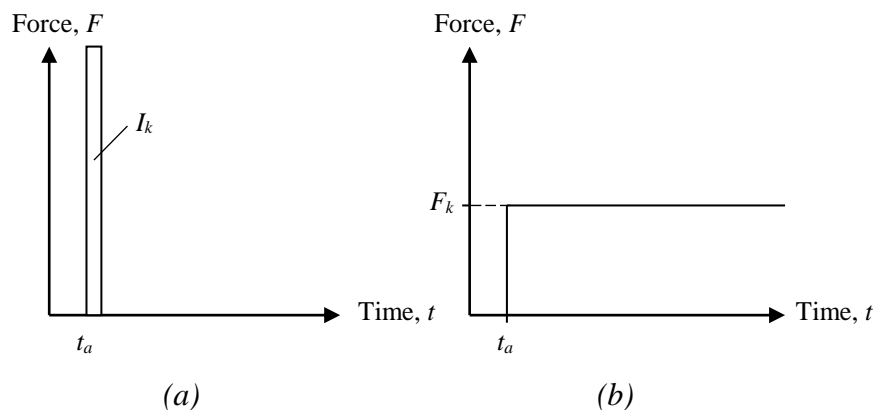


Figure 2.30 Two cases of dynamic loading: (a) ideal impulse load; (b) pressure load.

## 2.7.4 External work and energy

Work is a parameter that describes the transfer of energy based on the law of energy conservation. It can be represented by potential or kinetic energy and it can be classified as external and internal work.

The external work,  $W_e$ , is the work done by the external force, i.e. impulse load due to an explosion acting on the structure. The internal work,  $W_i$ , is a result of the action of the internal resistance of the structure. The measure of the structural response due to external work is a resulting deformation and is further discussed in Section 2.7.5.

According to the law of energy conservation, no energy disappears. If a certain force acts on the structure, the work done by this force is converted into kinetic or potential energy within the structure. Thus, the work done by the force acting on the body is equal to the increase in kinetic energy of this body, causing its movement or deformation. This is valid only when there is no friction or other forces causing energy losses. According to the law of energy conservation, the work equilibrium, where the kinetic energy should be balanced by the internal energy  $W_i$ , is

$$W_e = W_i + W_k \quad (2.18)$$

The definition of the external work, for impulse loaded structures, involves the concepts of impulse and kinetic energy transferred into the structure. The action of the impulse  $I$  on the body with mass  $m$  and velocity  $v$  can be described as

$$I = mv \quad (2.19)$$

The kinetic energy  $E_k$  that is transferred by the impulse to the structure is defined as

$$E_k = \frac{m \cdot v^2}{2} \quad (2.20)$$

This equation is most appropriate to use when the impulse  $I$  corresponds to the characteristic impulse  $I_k$ . If this is the case, the external energy can be assumed to be equal to the kinetic energy. The internal work done by the structure when the kinetic energy is transferred into potential energy within the structure can be disregarded. If the impulse is prolonged in time, the structure has time to develop the resistance and absorb the energy. This means that the external work done by the impulse will be smaller than in case of a characteristic impulse. This is illustrated in Figure 2.31.

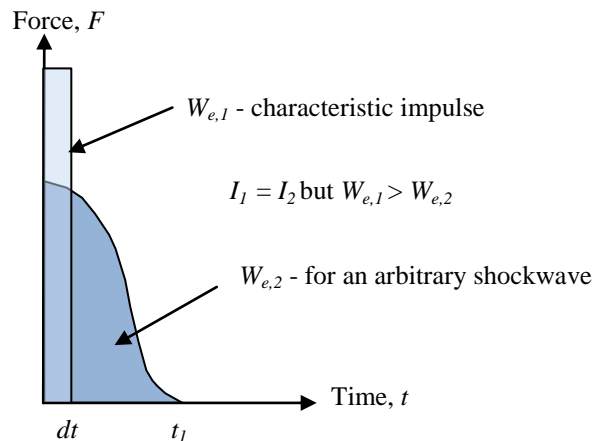


Figure 2.31 External work for a characteristic impulse and an impulse prolonged in time. Both impulses have the same magnitude.

Thus, by inserting equation (2.19) into (2.20), the external work can be presented as the result of the characteristic impulse acting on the mass  $m$ , calculated as

$$W_e = E_k = \frac{I_k^2}{2m} \quad (2.21)$$

The concept of internal energy for different response models is further described in Section 2.7.5, where also the calculation method is explained for deformations of impulse loaded structure.

## 2.7.5 Internal work and corresponding deformation

### 2.7.5.1 Introduction

One of the most important concerns when dealing with structures subjected to impulse load is the ability of the structure to deform due to assimilation of the kinetic energy resulting from the dynamic load. The energy equilibrium, equation (2.18), is the base for the calculation methodology for impulse loaded structures. The kinetic energy, which represents the external energy,  $W_e$ , should be balanced by the internal energy,  $W_i$ . By involving this condition, the resulting deformation can be assessed, Johansson and Laine (2012a). This deformation is of the minimum magnitude that assures that the structure is able to take care of the evolved energy, when the impulse affects the structure, without local failure or collapse. As the response of the structure subjected to the increasing load is nonlinear, approximate models simulating the structural behaviour are introduced. Sections 2.7.5.2 to 2.7.5.4 presents the resulting deformation for structures subjected to characteristic impulse load for elastic, plastic and elasto-plastic response models, respectively. Section 2.7.6 presents how the calculation should be modified for impulse loads other than characteristic.

### 2.7.5.2 Elastic response

In case of the elastic response, the magnitude of the internal work,  $W_i$ , presented in Figure 2.32 where  $u_{el}$  corresponds to the elastic deformation in the elastic response model, can analytically be described as

$$W_i = \frac{R(u_{el}) \cdot u_{el}}{2} = \frac{k u_{el}^2}{2} \quad (2.22)$$

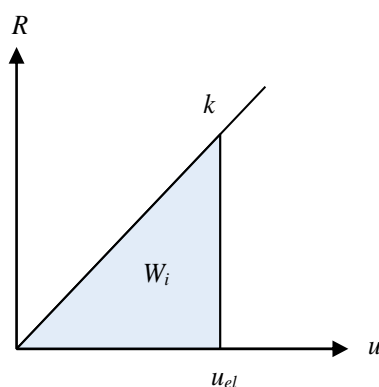


Figure 2.32 Resistance-displacement relation for a structure with elastic response.

The work equilibrium and the resulting elastic deformation, which is schematically presented in Figure 2.33, is calculated as

$$W_e = W_i \rightarrow \frac{I_k^2}{2m} = \frac{k u_{el}^2}{2} \rightarrow u_{el} = \frac{I_k}{m\omega} \quad (2.23)$$

where  $\omega$  is angular frequency which can be described as

$$\omega = \sqrt{\frac{k}{m}} \quad (2.24)$$

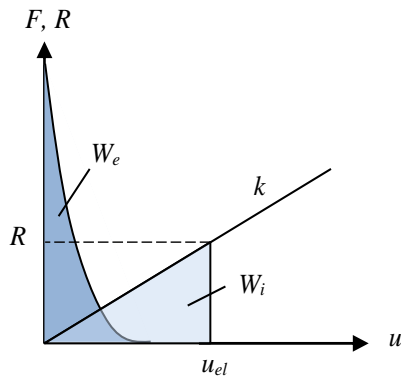


Figure 2.33 Work equilibrium for the elastic response.

### 2.7.5.3 Plastic response

The internal work,  $W_i$ , shown in Figure 2.34, where  $u_{pl}$  corresponds to the plastic deformation in the plastic response model, is calculated as

$$W_i = R_m(u_{pl}) \cdot u_{pl} = R_m u_{pl} \quad (2.25)$$

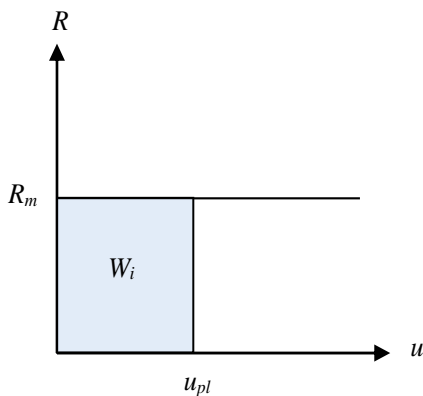


Figure 2.34 Resistance-displacement relation for a structure with plastic response.

The work equilibrium and the resulting plastic displacement presented in Figure 2.35 can be calculated as

$$W_e = W_i \rightarrow \frac{I_k^2}{2m} = R_m u_{pl} \rightarrow u_{pl} = \frac{I_k^2}{2mR_m} \quad (2.26)$$



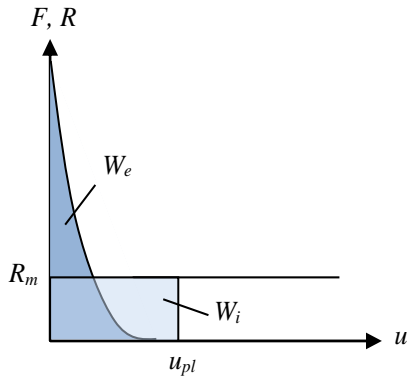


Figure 2.35 Work equilibrium for the plastic response.

### 2.7.5.4 Elasto-plastic response

The internal work shown in Figure 2.36, where  $u_{ep,el}$  corresponds to the elastic and  $u_{ep,pl}$  to the plastic deformation in the elasto-plastic response model, is calculated as

$$W_i = \frac{R_m}{2} (u_{ep,el} + 2u_{ep,pl}) \quad (2.27)$$

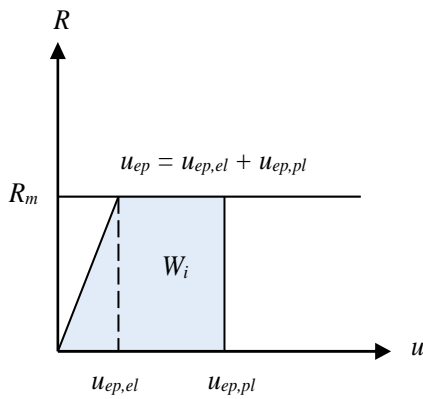


Figure 2.36 Resistance-displacement relation for a structure with elasto-plastic response.

The work equilibrium and resulting plastic displacement presented in Figure 2.37 can be calculated as

$$W_e = W_i \rightarrow \frac{I_k^2}{2m} = \frac{R_m}{2} (u_{ep,el} + 2u_{ep,pl}) \rightarrow u_{ep,pl} = \frac{I_k^2}{2mR_m} - \frac{u_{ep,el}}{2} \rightarrow u_{pl} = \frac{u_{ep,el}}{2} \quad (2.28)$$

Together with the elastic part the total deformation the elasto-plastic deformation can be calculated as

$$u_{ep} = u_{ep,el} + u_{ep,pl} = u_{pl} + \frac{u_{ep,el}}{2} = \frac{R_m}{2k} + \frac{I_k^2}{2mR_m} \quad (2.29)$$

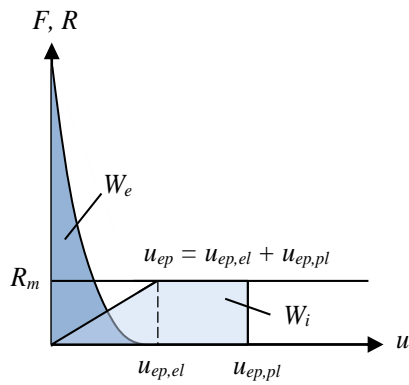


Figure 2.37 Work equilibrium for the elasto-plastic response.

## 2.7.6 Modification factors for impulse loads other than characteristic

### 2.7.6.1 Orientation

The definitions of deformation due to impulse load presented in Section 2.7.5 are established with regard to a characteristic impulse load. For impulse loads that are not considered as characteristic, the equations deliver results on the safe side since the resulting deformation is overestimated. In order to modify the result, the impulse load factor  $\gamma_I$  and pressure load factor  $\gamma_F$ , should be used together with the damage curves, according to Johansson and Laine (2012a).

A random impulse load with maximum load  $F_I$  and impulse  $I_I$  is presented in Figure 2.38.

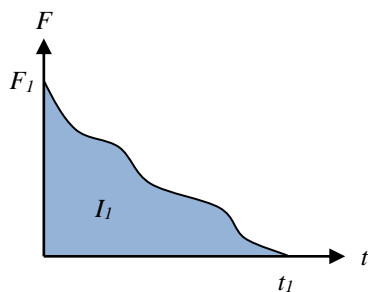


Figure 2.38 A random impulse load.

### 2.7.6.2 Elastic model

For the elastic response,  $\gamma_I$  describes the relation of the impulse  $I_I$  to the corresponding characteristic impulse load  $I_k$  in equation (2.30). The notation  $\gamma_F$  describes the relation of the maximum load  $F_I$  to the corresponding characteristic pressure load  $F_k$  in equation (2.31).

$$\gamma_I = \frac{I_I}{I_k} \quad (2.30)$$

$$\gamma_F = \frac{F_l}{F_k} \quad (2.31)$$

By involving the ratio of periodicity  $T$  to the duration of the load  $t_l$  and a type of load according to Figure 2.39, the correct value of modification factor is established from Table 2.2. The frequency  $f$  and periodicity  $T$  are calculated as

$$f = \frac{\omega}{2\pi} \quad (2.32)$$

$$T = \frac{1}{f} \quad (2.33)$$

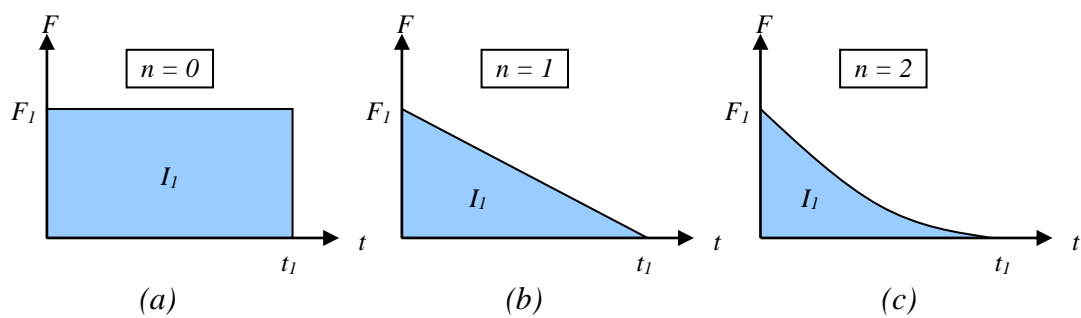


Figure 2.39 Type of impulse loads used in the estimation of the correct value of deformation where the factor  $n$  describes how the load decreases, Johansson and Laine (2012a).

Table 2.2 The correlation of error  $\delta_{el}$ , the ratio  $T/t_1$ , impulse load factor  $\gamma_I$  and pressure load factor  $\gamma_F$ , for the load types according to Figure 2.39. From Johansson and Laine (2012a).

$\delta_{el}$	$\gamma_I$	$\frac{T}{t_1} = \pi \cdot \frac{\gamma_F}{\gamma_I}$	$\frac{T}{t_1} = \frac{\pi}{2} \cdot \frac{\gamma_F}{\gamma_I}$	$\frac{T}{t_1} = \frac{\pi}{3} \cdot \frac{\gamma_F}{\gamma_I}$
[%]	[-]	$n = 0$	$n = 1$	$n = 2$
1	1,01	12,89	10,60	8,84
2	1,02	9,22	7,45	6,13
3	1,03	7,51	6,10	5,00
4	1,04	6,52	5,33	4,35
5	1,05	5,86	4,75	3,90
10	1,10	4,20	3,41	2,78
15	1,15	3,48	2,82	2,29
20	1,20	3,06	2,47	1,98
25	1,25	2,78	2,23	1,77
50	1,50	2,10	1,56	1,18
75	1,75	1,80	1,23	0,91
100	2,00	1,57	1,02	0,74

If  $\gamma_I = 1$ , the studied impulse corresponds to a characteristic impulse. The notation  $\delta_{el}$  indicates how much the deformation calculated from equation (2.23) is overestimated. In order to get the correct value of deformation, the magnitude of the studied impulse is increased with  $\delta_{el}$  when it is inserted into equation (2.23). For example, for a ratio of  $T/t_1 = 4.75$  and a type of load corresponding to  $n = 1$ ,  $\delta_{el} = 5\%$  and  $\gamma_I = 1.05$ . Thus, the value of the impulse  $I_k$  inserted into equation (2.23) is  $I_I/1.05$ .

### 2.7.6.3 Plastic model

For the plastic response, similarly as for the elastic,  $\gamma_I$  describes the relation of the random impulse  $I_I$  to the corresponding characteristic impulse load  $I_k$ , see equation (2.34). The notation  $\gamma_F$  describes the relation of the random load  $F_I$  to the internal resistance  $R$ , equation (2.35).

$$\gamma_I = \frac{I_I}{I_k} \tag{2.34}$$

$$\gamma_F = \frac{F_1}{R} \quad (2.35)$$

By using the correlation between  $F_1$  and  $R$  together with the type of load, according to Figure 2.39, the error in the estimation of the deformation when using equation (2.26) for the random impulse load,  $\delta_{pl}$ , can be calculated.

*Table 2.3 The correlation of the estimation error  $\delta_{pl}$ , the impulse load factor  $\gamma_I$  and the pressure load factor  $\gamma_F$ , for the load types according to Figure 2.39. From Johansson and Laine (2012a).*

$\delta_{pl}$ [%]	$\gamma_I$ [-]	$\gamma_F = \frac{F_1}{R}$ $n = 0$	$\gamma_F = \frac{F_1}{R}$ $n = 1$	$\gamma_F = \frac{F_1}{R}$ $n = 2$
1	1,005	100	-	-
2	1,010	52	70	77
3	1,015	35	46	52
4	1,020	27	35	39
5	1,025	21	29	32
10	1,049	11	15	17
15	1,072	7,7	10	12
20	1,095	6,0	8,0	9,0
25	1,118	5,0	6,7	7,5
50	1,225	3,0	4,0	4,5
75	1,323	2,3	3,1	3,5
100	1,414	2,0	2,7	3,0

The correct value of the deformation is obtained by modifying the value of  $I_k$  inserted in equation (2.26). For example, for an impulse load corresponding to  $n = 1$  and  $\gamma_F = 10$ , an error estimation of  $\delta_{pl} = 15\%$  and an impulse load factor of  $\gamma_I = 1.072$  is obtained according to Table 2.3. This means that the deformation for this impulse load is overestimated with 15% when equation (2.26) is used, why the impulse  $I_k$  inserted in this equation should be decreased. Thus when  $I_k$  is inserted in equation (2.26) it is modified to  $I_k = I_I / 1.072$  for the correct plastic deformation to be obtained.

### 2.7.7 Essential parameters for impulse loaded structures

Besides the mass of the structure, which decreases the effect of the impulse load, the most important parameter of the structure is its ability to absorb the external energy. When a shock wave hits a structure the external energy is transferred into internal energy of the beam in form of potential and kinetic energy due to deformations. The structure will resist the impact when its maximum internal work  $W_i$  reaches the value of the external work  $W_e$ . In such case, the maximum allowable deformation is obtained. Figure 2.40 presents a combination of these two parameters which results in a certain deformation  $u_{tot}$ .

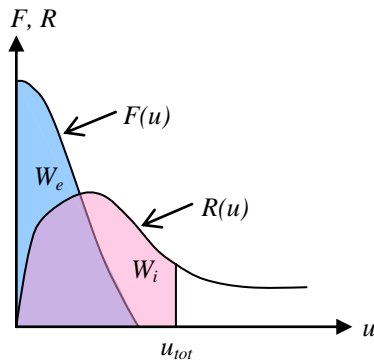


Figure 2.40 Combination of the external work  $W_e$  resulting from the external force  $F(u)$  and the internal work  $W_i$  done by the internal force  $R(u)$ .

In general, the response of a structure with high stiffness is characterised by small deformations and high resisting force while for a structure with low stiffness, the case is the opposite. The capacity of the structure to absorb energy is a combination of its ability to deform and its maximum resistance. Thus, for explosion load a high resistance combined with a small deformation is not always beneficial, Johansson and Laine (2012a). For an impact load, the internal work  $W_{i,1}$  needed to balance the external load, can be less than the internal work  $W_{i,2}$  for a structure with low stiffness. This is illustrated in Figure 2.41.

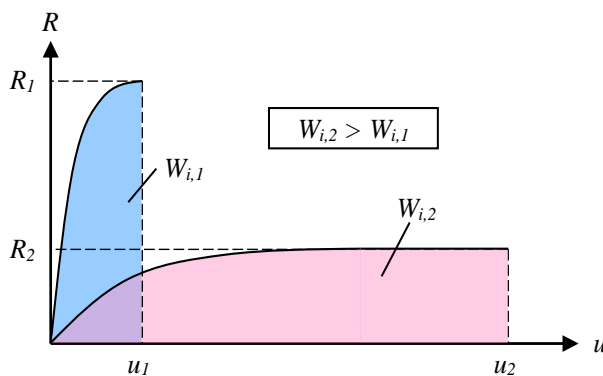


Figure 2.41 Comparison of a structure with high stiffness, high resistance and low deformation ability with a structure provided with low stiffness, low resistance and large plastic deformation ability.

A ductile material behaviour, with high plastic rotation capacities, is desired for structures subjected to impulse loading. For the statically loaded structures, on the other hand, it is preferred to obtain a high strength and small deformation through high load capacity and high stiffness.

## 2.8 Equivalent static load

### 2.8.1 Introduction

To make further simplifications when dealing with the assessments of the impulse loaded structures, the dynamic load can be transferred into an equivalent static load. Johansson and Laine (2012a) have presented this procedure based on the assumption that the acting impulse load  $I_k$  involves the same amount of transferred energy as the work done by the static load  $Q$ . The equivalent static load for the elastic, plastic and elasto-plastic model is presented in the following sections.

### 2.8.2 Elastic model

In case of an elastic response model, the work done by the external force  $Q$  is

$$W_e = \frac{Qu_{el}}{2} \quad (2.36)$$

and by comparing this to the work done by the characteristic impulse load  $I_k$ , the equivalent static load resulting in the elastic deformation is established as

$$\frac{Qu_{el}}{2} = \frac{I_k^2}{2m} \rightarrow \frac{QI_k}{2m\omega} = \frac{I_k^2}{2m} \rightarrow Q = I_k\omega \quad (2.37)$$

### 2.8.3 Plastic model

For the plastic response the work done by the external force  $Q$  is

$$W_e = Qu_{pl} \quad (2.38)$$

Following the same procedure as in case of the elastic response the equivalent static load  $Q$  is

$$Qu_{pl} = \frac{I_k^2}{2m} \rightarrow Q \frac{I_k}{2mR_m} = \frac{I_k^2}{2m} \rightarrow Q = R_m \quad (2.39)$$

### 2.8.4 Elasto-plastic model

For the elasto-plastic response the equivalent static load  $Q$  corresponds, similarly as in the case of plastic response, to the ultimate resistance  $R_m$ , which is established by the stiffness  $k$  for the elastic phase and the deformation  $u_{ep,el}$  for the elastic phase, see Figure 2.36.

$$Q = R_m \quad (2.40)$$

where  $R_m = ku_{ep,el}$

## 2.9 Transformation into SDOF system

### 2.9.1 Introduction to SDOF system concept

Deformable structures have an infinite number of degrees of freedom. However, the system can be discretized into an arrangement with a finite number of degrees of freedom. By simplifying the system it can be transformed into a system with a single degree of freedom, i.e. SDOF.

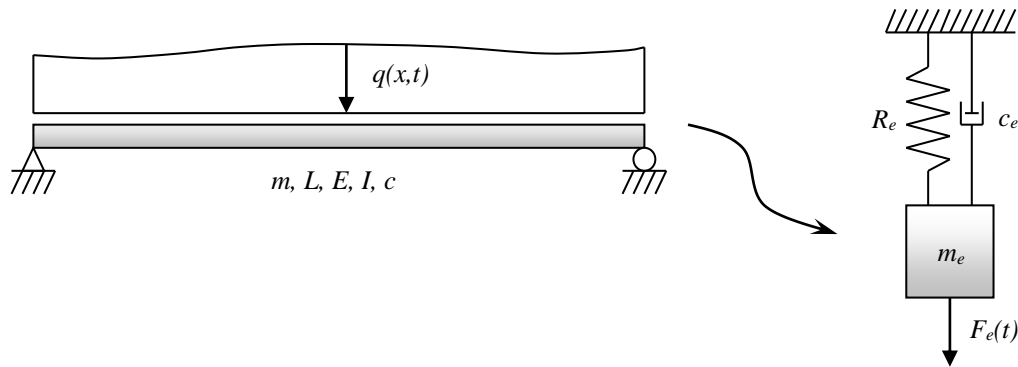


Figure 2.42 Transformation of the beam into a SDOF system.

In the SDOF system, equivalent quantities for mass as well as internal and external load are used. The quantities are written without an index  $e$  for the untransformed body and with an index  $e$  for the equivalent body of the SDOF system. The transformation is done using transformation factors,  $\kappa$ , which depend on both the applied load and the deflected shape of the structure. Transformation factors are further described in Section 2.9.3.

The SDOF system is one-dimensional and can therefore only move in one direction while the real structure is three dimensional and can move in three directions.

To be able to transform a structural system into a SDOF system a deflection shape has to be assumed. A structure has an infinite number of bending modes, but when creating a SDOF system the deflection shape is based on a static case similar to the first bending mode.

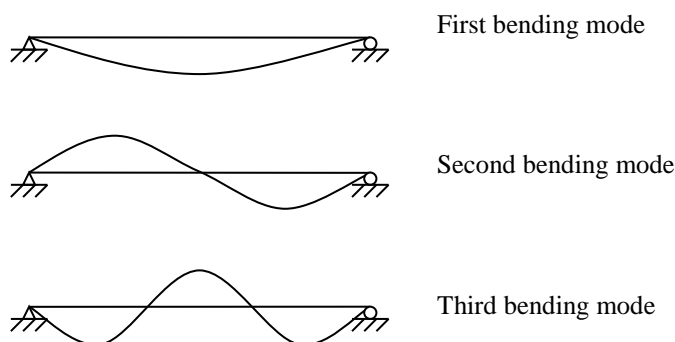


Figure 2.43 The three first bending modes.

A condition for using a SDOF system is that a uniform change of deformation is assumed, meaning that a change in displacement for every part of the beam is proportional to all other parts.



Based on this a SDOF system can describe the behaviour of the structure in any point. For a simply supported beam or a cantilever beam the chosen point is often the one with maximum deflection. For a beam fixed at one edge and simply supported at the other the chosen point is often in the middle. The chosen point represented by the SDOF system is called the system point.

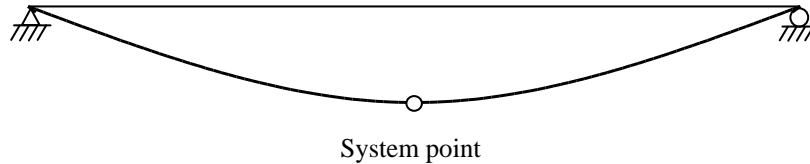


Figure 2.44 System point in the middle of a simply supported beam.

### 2.9.2 Equation of motion

Bearing in mind Newton's second law, equation (2.11), it can be noticed that the body with mass  $m$  and acceleration  $a$ , as in Figure 2.45a, is subjected to a system of forces which results in the following equilibrium

$$F(t) - (R_{sta} + R_{dyn}) = ma \quad (2.41)$$

where  $F(t)$  is the external force and  $R_{dyn}$  and  $R_{sta}$  describes the dynamic respective static internal resistance of the body.

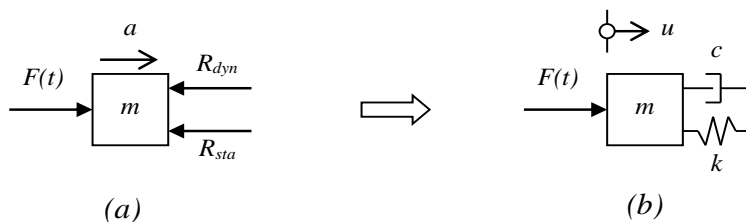


Figure 2.45 (a) Forces acting on the rigid body; (b) Forced damped SDOF system.

As presented in Figure 2.45b, this can also be described in form of a SDOF system with a damper and a spring. Thus the internal static resistance,  $R_{sta}$ , of the body can be expressed as the correlation between the spring stiffness  $k$  and the displacement  $u$

$$R_{sta} = ku \quad (2.42)$$

and the internal dynamic resistance can be expressed as the damping  $c$  times the velocity of the body  $\dot{u}$

$$R_{dyn} = c\dot{u} \quad (2.43)$$

By combining the forces with force equilibrium the equation of motion is obtained as

$$m\ddot{u} + c\dot{u} + ku = F(t) \quad (2.44)$$

where  $\ddot{u}$  is acceleration.

### 2.9.3 Differential equation for equation of motion

It has been shown in Section 2.9.2 that the equation of motion for a structure can be written as

$$m\ddot{u} + c\dot{u} + ku = F(t) \quad (2.45)$$

where  $m$  is the untransformed body mass,  $\ddot{u}$  is the acceleration,  $c$  is the damping,  $\dot{u}$  is the velocity,  $k$  is the stiffness,  $u$  the displacement and  $F(t)$  the external force acting on the untransformed body. However, for structures subjected to impulse loading the damping is usually not important and is therefore often neglected in these calculations.

For the case of one degree of freedom, the damping is neglected and therefore the equation of motion can be written as

$$m\ddot{u} + R = F(t) \quad (2.46)$$

where  $R$  is the internal force

$$R = ku \quad (2.47)$$

Transformation factors are used to transform the quantities of the original structure to a SDOF system. These are defined as

$$\kappa_m = \frac{m_e}{m} \quad (2.48)$$

$$\kappa_K = \frac{R_e}{R} \quad (2.49)$$

$$\kappa_F = \frac{F_e(t)}{F(t)} \quad (2.50)$$

Based on conservation of kinetic energy and by assuming that the mass is constant per meter, the transformation factor  $\kappa_m$  can be written as

$$\kappa_m = \frac{1}{L} \int_{x=0}^{x=L} \frac{u(x)^2}{u_s^2} dx \quad (2.51)$$

The conservation of applied load for a uniformly distributed load  $q(x) = q$  gives a transformation factor  $\kappa_F$  described as

$$\kappa_F = \frac{1}{L} \int_{x=0}^{x=L} \frac{u(x)}{u_s} dx \quad (2.52)$$

For further information about the transformation factors the reader is referred to Johansson and Laine (2012a). Inserting the transformation factors into the equation of motion gives

$$\kappa_m m \ddot{u} + \kappa_K R = \kappa_F F(t) \quad (2.53)$$

Dividing by  $\kappa_F$  the equation can be written as

$$\frac{\kappa_m}{\kappa_F} m \ddot{u} + \frac{\kappa_K}{\kappa_F} R = F(t) \quad (2.54)$$

According to Biggs (1964)

$$\kappa_K = \kappa_F \quad (2.55)$$

A new transformation factor  $\kappa_{mF}$  is introduced

$$\kappa_{mF} = \frac{\kappa_m}{\kappa_F} \quad (2.56)$$

Now, the equation of motion for a SDOF system can be written as

$$\kappa_{mF} m \ddot{u} + R = F(t) \quad (2.57)$$

This shows that it is only the body mass that is affected by a factor  $\kappa_{mF}$  in order to transform the structure into a SDOF system.

Transformation factors for different structural elements with different boundary conditions and loading cases are presented in Table 2.4, Table 2.5 and Table 2.6.

Table 2.4 Transformation factors for a beam subjected to a point load. From Johansson and Laine (2012a).

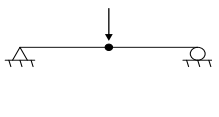
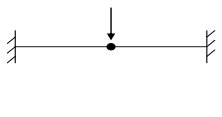
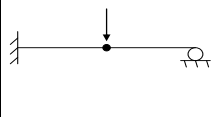

	Point load on beam element			
				
	Elastic deformation curve			
$K_M$	0.486	0.371	0.445	0.236
$K_F$	1.000	1.000	1.000	1.000
$K_{MF}$	0.486	0.371	0.446	0.236
	Plastic deformation curve			
$K_M$	0.333	0.333	0.333	0.333
$K_F$	1.000	1.000	1.000	1.000
$K_{MF}$	0.333	0.333	0.333	0.333

Table 2.5 Transformation factors for a beam subjected to a uniformly distributed load. From Johansson and Laine (2012a).

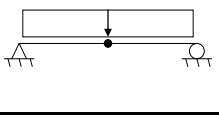
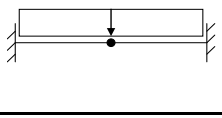
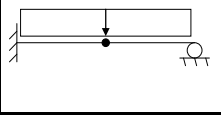
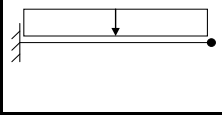
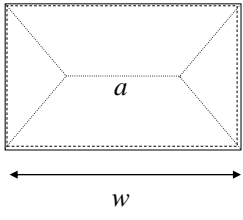
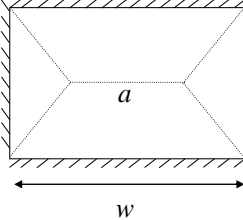
	Uniformly distributed load on beam element			
				
	Elastic deformation curve			
$K_M$	0.504	0.406	0.483	0.257
$K_F$	0.640	0.533	0.600	0.400
$K_{MF}$	0.788	0.762	0.805	0.642
	Plastic deformation curve			
$K_M$	0.333	0.333	0.333	0.333
$K_F$	0.500	0.500	0.500	0.500
$K_{MF}$	0.667	0.667	0.667	0.667

Table 2.6 Transformation factors for a plate subjected to a uniformly distributed load, based on Augustsson and Härenstam (2010).

Uniformly distributed load on slab element		
		
	Elastic deformation curve	
$\kappa_M$	0.250	
$\kappa_F$	$4/\pi^2$	
$\kappa_{MF}$	0.617	
	Plastic deformation curve	
$\kappa_M$	$(1+a/w)/6$	$(1+a/w)/6$
$\kappa_F$	$(1+a/2w)/3$	$(1+a/2w)/3$
$\kappa_{MF}$	$(1+a/w)/(2+a/w)$	$(1+a/w)/(2+a/w)$

### 3 Parametric beam study

#### 3.1 Introduction

This section is a continuation of the researches presented in the previous Master's Theses, Andersson and Karlsson (2012) and Carlsson and Kristensson (2012), where two different reinforced concrete beams, subjected to impulse loading, were analysed. The analyses were based on the method presented in Johansson and Laine (2012a) which allows for a simple and straight forward assessment of the deformation of impulse loaded structures on the basis of the energy equilibrium condition, see Section 2.7.5. In this method only the reinforcement at the bottom edge of the beam is considered while the reinforcement at the top is disregarded. However, in Carlsson and Kristensson (2012), it is pointed out that there might be some incompatibilities for this routine when not considering the top reinforcement. In order to get an idea of how much this simplification influences the results and to provide a better understanding for the assumptions in this method, a parametric study of the beams is carried out. The beam dimensions and the parameters that are assumed to have the greatest influence on its response are varied. The results in form of internal resistance, maximum plastic deflection and internal work are compared. The importance of those parameters for the impulse loaded structures is discussed in Section 2.7.7. The equations used in these calculations are stated in Appendix A. The numerical results can be found in Andersson and Karlsson (2012) and Carlsson and Kristensson (2012).

The other issue studied in this chapter concerns the methodology for calculation of plastic rotation capacity recommended in Eurocode 2, which is presented in Section 2.5.3. The fact that Eurocode 2 does not clearly specify how the effective depth,  $d$ , and the width of the compression zone,  $x$ , should be considered, leads to some uncertainty. Impulse loaded structures should be provided with reinforcement bars at both edges as mentioned in Section 2.7.1. In case of a low reinforcement amount, the neutral axis can be positioned above the top reinforcement layer which then becomes in tension, see Figure 3.1. In such a case it is not obvious how the effective depth should be calculated.

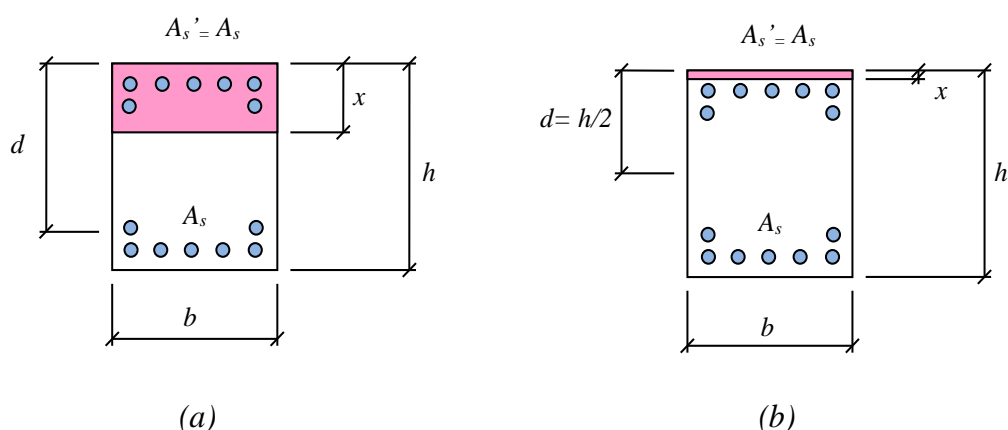


Figure 3.1 Alternative assumption of effective depth used in this parametric beam study. Neutral axis is located: (a) below top reinforcement layer; (b) above top reinforcement layer.

Moreover, in Eurocode 2 it is not specified for what type of section the plastic rotation capacity graph (Figure 2.25) has been established. For example, it is not clear if the

section is provided with top reinforcement or not. Thus, for the conducted parametric study of the beam a few alternatives, described in Section 3.2, have been controlled. Moreover, according to Eurocode 2, the contribution to the moment capacity of the compressive reinforcement can only be taken into account if stirrups with minimum allowable spacing are provided, which is assumed in this parametric study.

In the Swedish code *Betonghandboken*, the method for calculating the plastic rotation capacity is established for a section with reinforcement at both edges of the beam while in BK 25 a section with only reinforcement at the bottom is considered. A further description as well as comparisons and an evaluation of these methods are presented in Johansson and Laine (2012a).

## **3.2 Different interpretations of $x/d$**

### **3.2.1 Case 1**

For a section where the neutral axis is located below the top reinforcement level, as shown in Figure 3.2a, the effective depth  $d$  is taken as the distance from the centre of gravity of the bottom reinforcement to the top edge of the beam. The height of the compressive zone,  $x$ , is calculated with consideration to the top reinforcement, which results in a smaller value of  $x$  compared to when neglecting the top reinforcement.

At the beginning of the analysis it is unknown how the top reinforcement will contribute to the response of the beam, i.e. whether it will be in tension or in compression. When the neutral axis is above the top reinforcement there are different ways of interpreting  $d$ . For Case 1,  $d$  is calculated as shown in Figure 3.2 regardless of whether the top reinforcement is in tension or not. In short, a constant value of  $d$  is used independently on the position of the neutral axis.

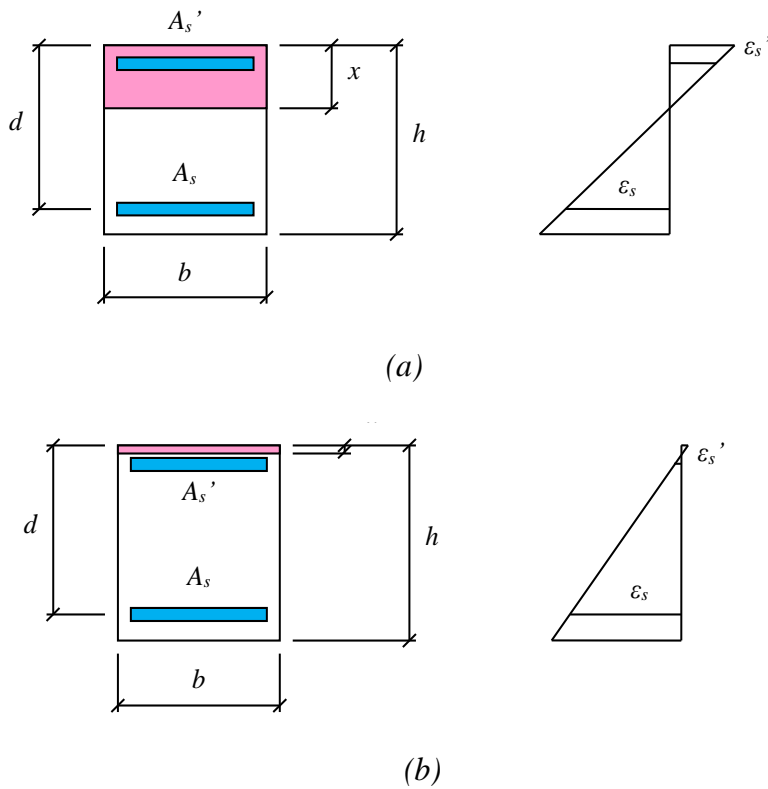


Figure 3.2 Assumption of effective depth for Case 1. Neutral axis is located: (a) below top reinforcement layer; (b) above.

### 3.2.2 Case 2

Another alternative of calculating the effective depth  $d$ , for a case when the top reinforcement is in tension, is established with regard to the reinforcement amount and its distance from the top edge. If the reinforcement amount is the same at the top and bottom of the beam, its centre of gravity will coincide with the centre of gravity of the uncracked section, see Figure 3.3.

For Case 2,  $d$  is calculated with regard to the location of the neutral axis. If the top reinforcement is still compressed,  $d$  is assumed to be as in Case 1 (see Figure 3.2a). If not,  $d$  is established with regard to the reinforcement amount at both edges, Figure 3.3.

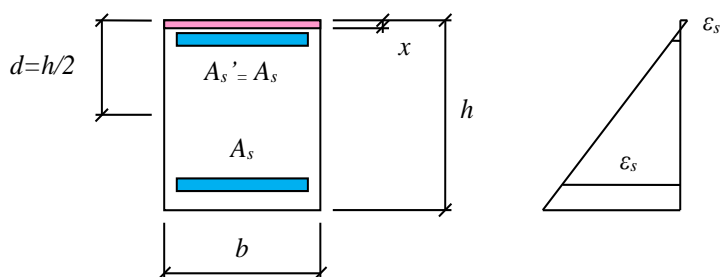


Figure 3.3 Assumption of effective depth for Case 2 when the neutral axis is located above the top reinforcement layer.



### 3.2.3 Case 3

A third way of interpreting  $d$  when the top reinforcement is in tension is by considering the magnitude of the force acting in the reinforcement as shown in Figure 3.4. However, this case would result in a more complex definition of  $d$  and is not investigated in this parametric study.

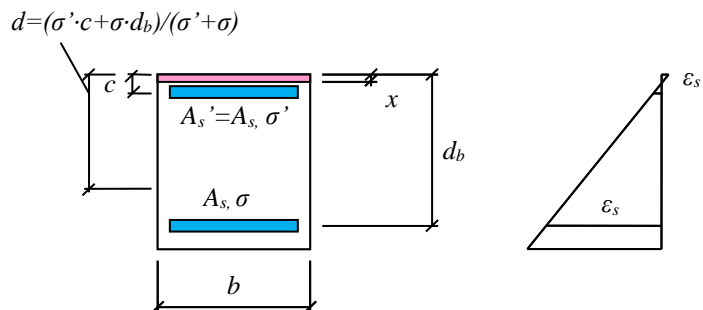


Figure 3.4 Assumption of effective depth for Case 3 when the neutral axis is located above the top reinforcement layer.

## 3.3 Geometry and properties of the beam

### 3.3.1 Introduction

The analysis carried out in this section is based on the dimensions which were used in the previous Master's Thesis Andersson and Karlsson (2012) and Carlsson and Kristensson (2012). However, for these two beams the reinforcement amount, height of the section and concrete cover differ. In this study the properties used by Andersson and Karlsson (2012) for a 400 mm thick beam are applied to the 200 mm thick beam used by Carlsson and Kristensson (2012) and vice versa. Additionally a beam with a height of 300 mm is analysed.

All geometric data are presented in Figure 3.5. It is to be noticed that the parameter  $c$  is the distance from the edge of the beam to the centre of the reinforcement. All calculations are done for a width  $b$  of 1 m. The parameters varied are further described in Section 3.3.2.

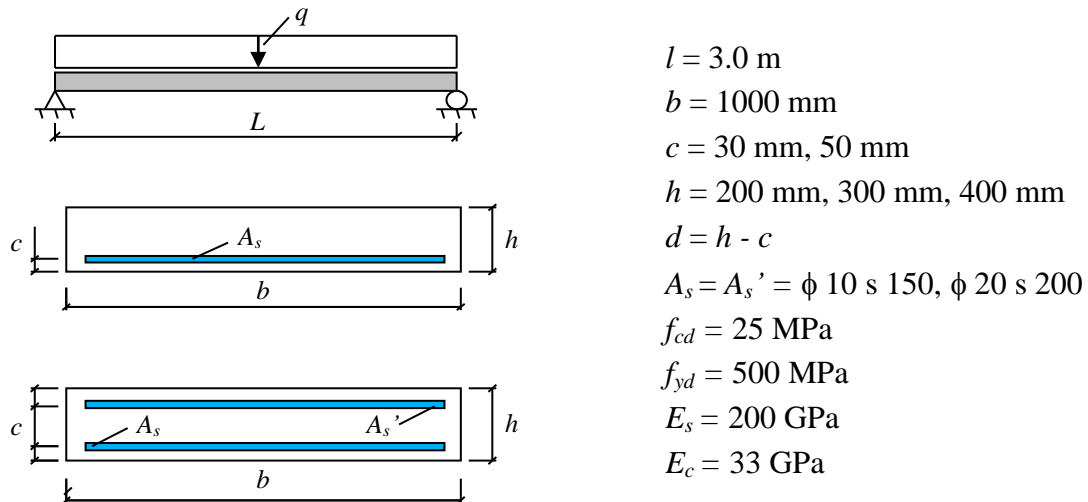


Figure 3.5 Dimensions and material properties used in the analysis.

The considered cross sections has been analysed for only one reinforcement layer and for the same amount of reinforcement at both edges, which is recommended for structures subjected to explosions explained in Section 2.7.1. According to Eurocode 2, the contribution to the moment capacity of the compressive reinforcement can only be taken into account if stirrups with minimum allowable spacing are provided. In this study it is assumed that such stirrups are provided.

### 3.3.2 Parameters studied

In this parametric beam study three different cases are analysed according to Table 3.1. Moreover, the effective depth  $d$  is defined according to Case 1 and Case 2 in Section 3.2.1 and Section 3.2.2, respectively. As an addition, the sectional height  $h$  and reinforcement amount  $A_s$  is varied according to Table 3.2.

Table 3.1 Concrete cover and reinforcement for Case A, B and C.

Case	Concrete cover, $c$ [mm]	Reinforcement
Case A	50	Top and bottom reinforcement.
Case B	50	No top reinforcement.
Case C	30	Top and bottom reinforcement.

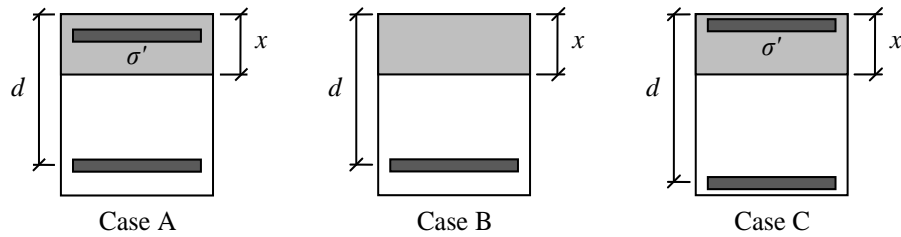


Figure 3.6 Three different sections analysed with the effective depth  $d$  according to Case 1.

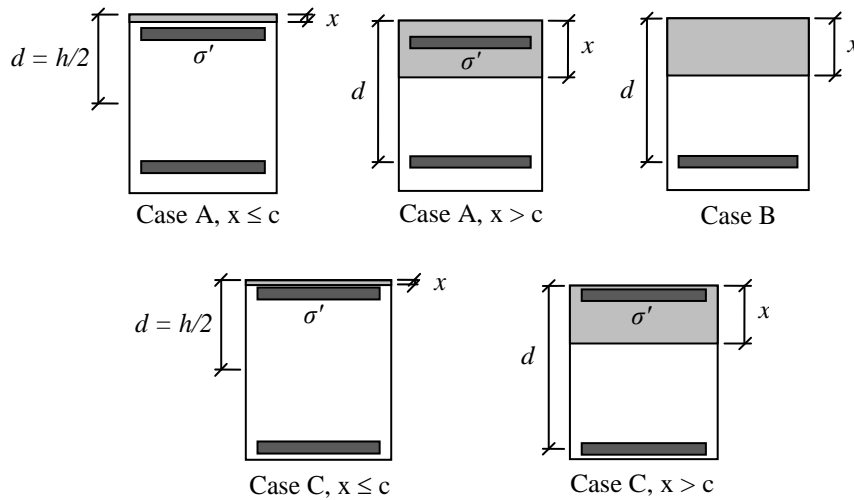


Figure 3.7 Three different sections analysed with the effective depth  $d$  according to Case 2.

Table 3.2 Cross-sections used in the parametric beam study.

Height, $h$ [mm]	Reinforcement bar diameter, $\phi$ [mm]	Spacing, $s$ [mm]
200	10	150
200	20	200
300	10	150
300	20	200
400	10	150
400	20	200

## 3.4 Results and comparisons

### 3.4.1 Orientation

In the first stage of the study, Section 3.4.2, the relation between internal resistance and increasing deformation is compared for sections of Case A, Case B and Case C with parameters according to Table 3.1.

In the next part of the study, Section 3.4.3, Case A and B are in focus. For each studied height, the dependency of the reinforcement amount of the internal work, internal resistance and plastic deformation capacity is obtained and evaluated.

The last part of the research, Section 3.4.4, aims in assessing the magnitude of difference when neglecting the top reinforcement. Thus, the internal work, internal resistance and plastic deformation capacity is presented as a ratio of Case A to B.

In all these three sections,  $d$  is calculated according to Case 1 in Section 3.2.1. The results obtained from changing the interpretation of  $d$  to Case 2, according to Section 3.2.2, are shown in Section 3.4.5. A selected amount of the obtained graphs are shown and discussed. The additional results from the parametric study can be found in Appendix B.

The internal work, internal resistance, plastic deformation capacity and plastic rotation capacity is plotted against the reinforcement amount,  $\rho$ , calculated according to equation (3.1). It is important to keep in mind that the reinforcement amount is always calculated with  $d$  according to Case 1, even for the graphs presenting Case 2.

$$\rho = \frac{A_s}{b \cdot d} \quad (3.1)$$

### 3.4.2 Resistance versus deformation capacity for Case 1

Due to that the plastic rotation capacity has a large influence on the maximum deflection, the position in the plastic rotation capacity graph from Eurocode 2 for Case A, B and C is presented next to the internal resistance graph, see Figure 3.8 to Figure 3.11. The resistance-deformation relation has been established only for the elasto-plastic model as it reflects the behaviour of the beam in the most realistic way. The results for how the resistance varies with the deformation for a height of 200 mm and 400 mm are presented here. The graphs for a 300 mm beam and for Case 2 can be found in Section B.2 and B.8, respectively.

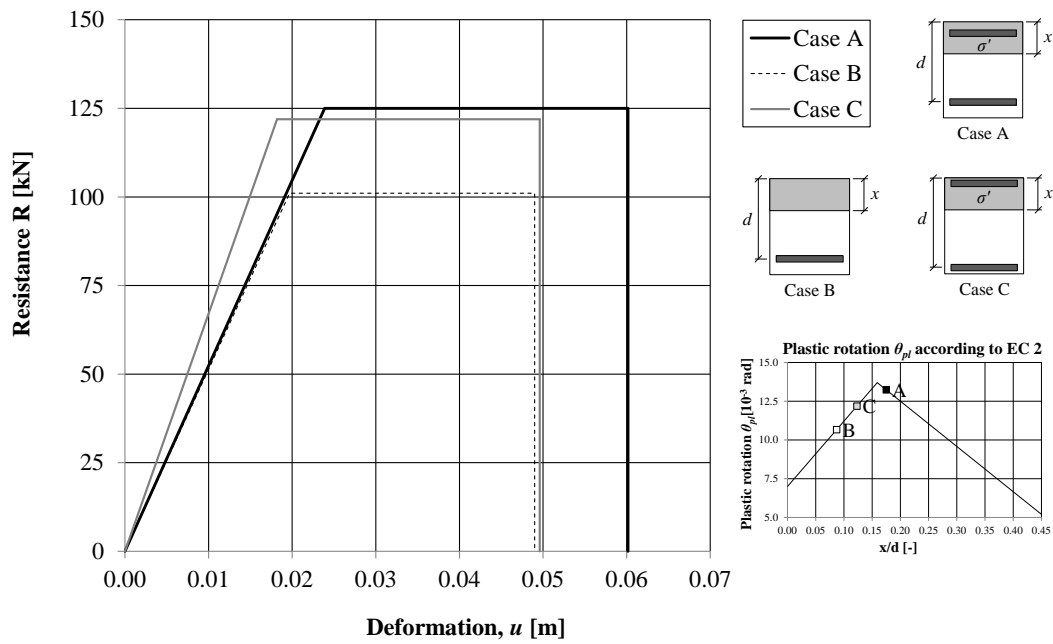


Figure 3.8 Internal resistance, ultimate deflection and position in the plastic rotation capacity graph (Eurocode 2) for a section with a height of 200 mm and reinforcement  $\phi 10$  s 150.

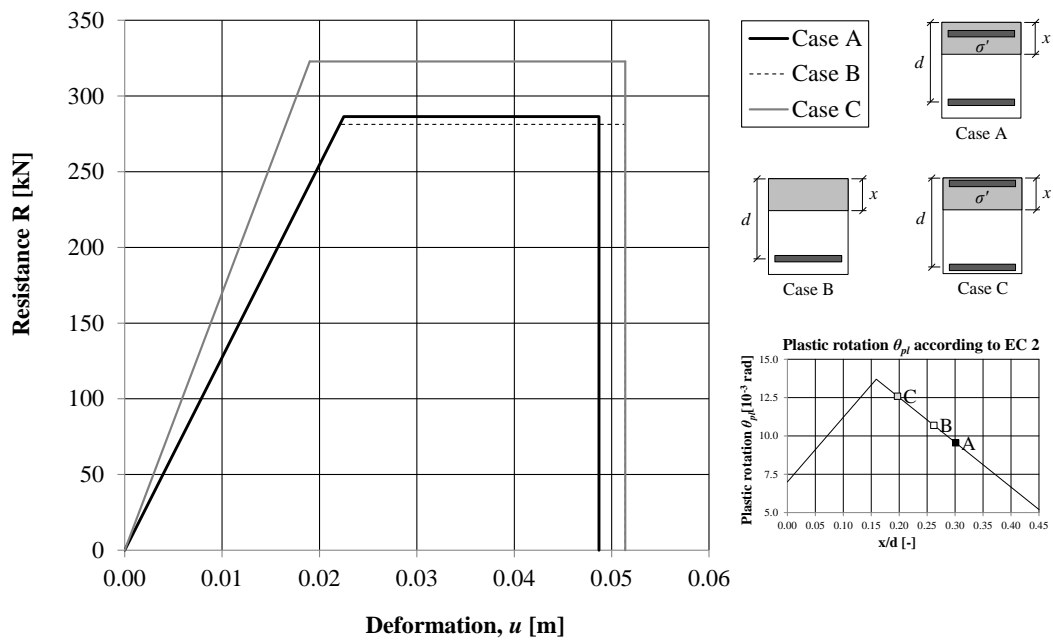


Figure 3.9 Internal resistance, ultimate deflection and position in the plastic rotation capacity graph (Eurocode 2) for a section with a height of 200 mm and reinforcement  $\phi 20$  s 200.

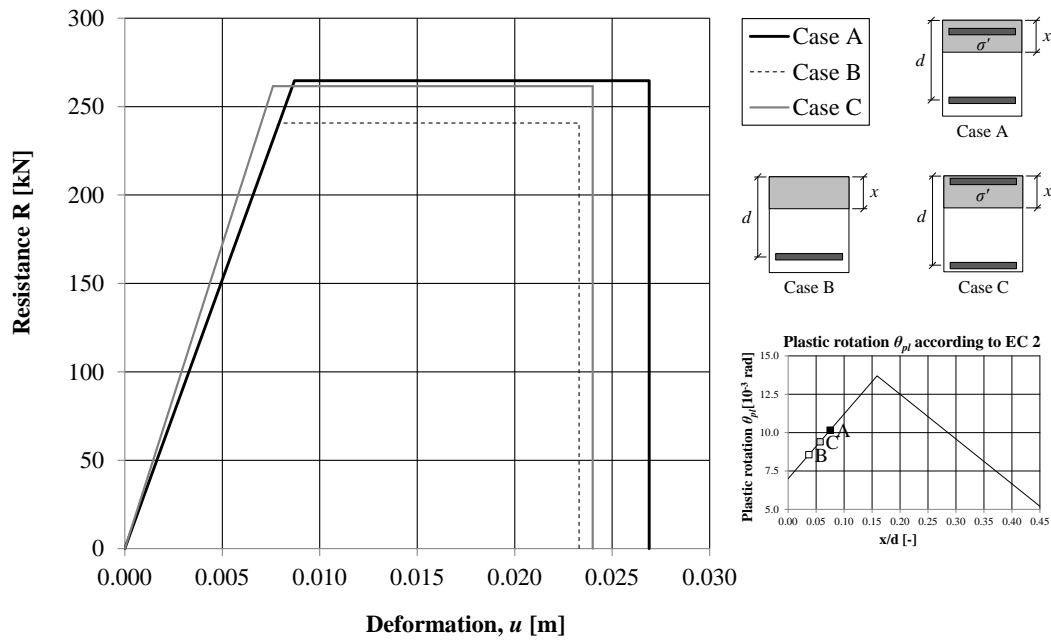


Figure 3.10 Internal resistance, ultimate deflection and position in the plastic rotation graph capacity (Eurocode 2) for a section with a height of 400 mm and reinforcement  $\phi 10$  s 150.

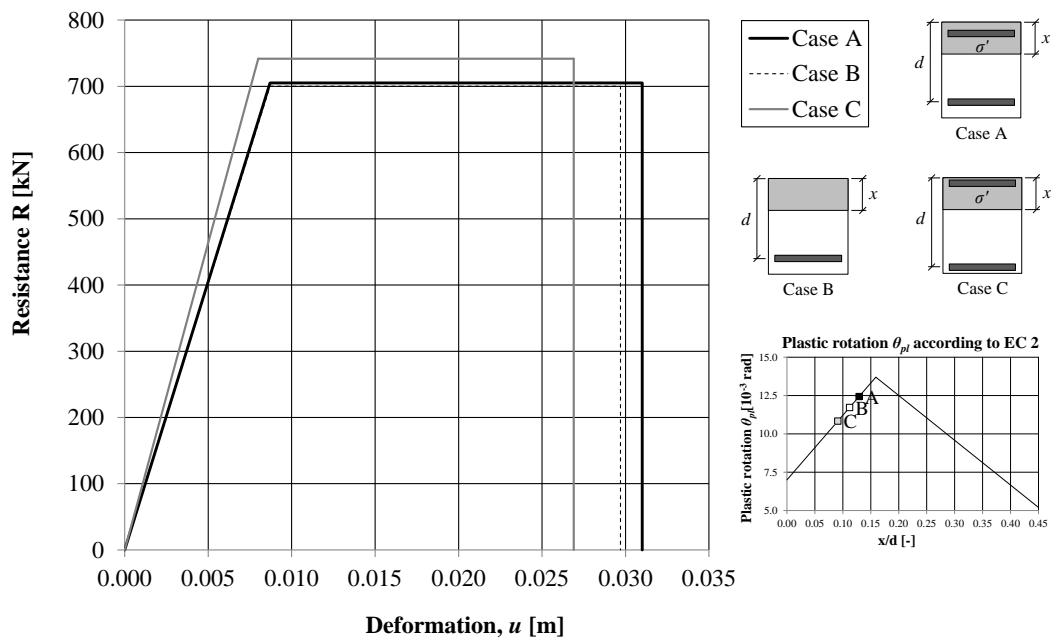


Figure 3.11 Internal resistance, ultimate deflection and position in the plastic rotation capacity graph (Eurocode 2) for a section with a height of 400 mm and reinforcement  $\phi 20$  s 200.

For the cases with low amount of reinforcement (Figure 3.8 and Figure 3.10) the top reinforcement is yielding in Case A which will affect the resistance beneficially. It follows that the resistance of the beam without top reinforcement (Case B) is up to 20 % lower than for Case A. For Case C, with a distance of 30 mm between the reinforcement and concrete edge, the top reinforcement is not yielding and therefore has a lower resistance in comparison to Case A, despite the increase in effective

depth. In the cases studied here the rotation capacity, and therefore the total deflection capacity, is highest for Case A and lowest for Case B.

For sections with high amount of reinforcement (Figure 3.9 and Figure 3.11) it appears that disregarding the top reinforcement only slightly decreases the internal resistance. Introducing thinner concrete cover affects the resistance beneficially since it increases the effective depth. If neglecting the top reinforcement when calculating the deformation, errors can occur as the height of the neutral axis is influenced. Therefore the size of the plastic rotation capacity is affected. Due to the shape of the plastic rotation capacity curve from Eurocode 2, Figure 2.25, the deformation can be both underestimated and overestimated.

For both the higher and lower reinforcement amounts investigated, the largest difference in maximum resistance is for the thinnest section of 200 mm. The simplification introduced by Johansson and Laine (2012a) gives lower values of resistance which can be considered to be on the safe side, i.e. conservative. However, due to the shape of the plastic rotation graph from Eurocode 2, Figure 2.25, it is more complicated to predict if the maximum deformation will be over- or underestimated and it is recommended to be careful with simplifications here.

For the cases studied, a small reinforcement amount assures a more ductile behaviour of the section and larger deformation. However, this is not a general conclusion since the difference depends on the position in the plastic rotation capacity graph, Figure 2.25. Yielding of the top reinforcement, independently of the height of the cross section, occurs for the investigated cases with  $c = 50$  mm and lower amounts of reinforcement. This assures a higher resistance as the strength of the steel is fully utilized. Decreasing the concrete cover to 30 mm increases the effective depth and also results in a higher resistance. However, it lowers the chances of the top reinforcement yielding why it is not always beneficial.

### **3.4.3 Rotation capacity, internal work and resistance for Case 1**

This part of the study considers only Case A and B. The behaviour of the two types of sections is analysed for different reinforcement amounts and for heights of 200 mm, 300 mm and 400 mm. The response in form of plastic rotation capacity, internal work and internal resistance is compiled and compared. A compilation of all the results can be found in Section B.3, B.4 and B.5, respectively.

In order to visualize what a certain reinforcement amount implies, a short compilation of different reinforcement dimensions and spacing is presented in Table 3.3. The reinforcement amounts used in this rapport are underlined.

Table 3.3 Values of reinforcement amount for different sectional heights, reinforcement dimensions and spacing. The distance between the reinforcement and the concrete edge,  $c$ , is 50 mm.

Height, $h$ [mm]	Reinforcement amount, $\rho$ [%]				
	Spacing of 150 mm		Spacing of 200 mm		
	Diameter of reinforcement bar, $\phi$ [mm]				
	10	12	16	20	25
200	<u>0.35</u>	0.50	0.89	<u>1.40</u>	2.18
300	<u>0.21</u>	0.30	0.54	<u>0.84</u>	1.31
400	<u>0.15</u>	0.22	0.38	<u>0.60</u>	0.93

The response of the section can clearly be followed by studying the changes in plastic rotation capacity  $\theta_{pl}$  when varying the reinforcement amount, Figure 3.12 and Figure 3.13. The calculation of plastic rotation capacity is based on the recommendations found in Eurocode 2 which is described in Section 2.5.3. It is worth to mention that the graph of the plastic rotation capacity in Eurocode 2 (Figure 2.25) does not provide exact values and the user has to approximate the values, which can lead to different interpretations. The equations used in these calculations are stated in Appendix A and the numerical results can be found in Andersson and Karlsson (2012) and Carlsson and Kristensson (2012).

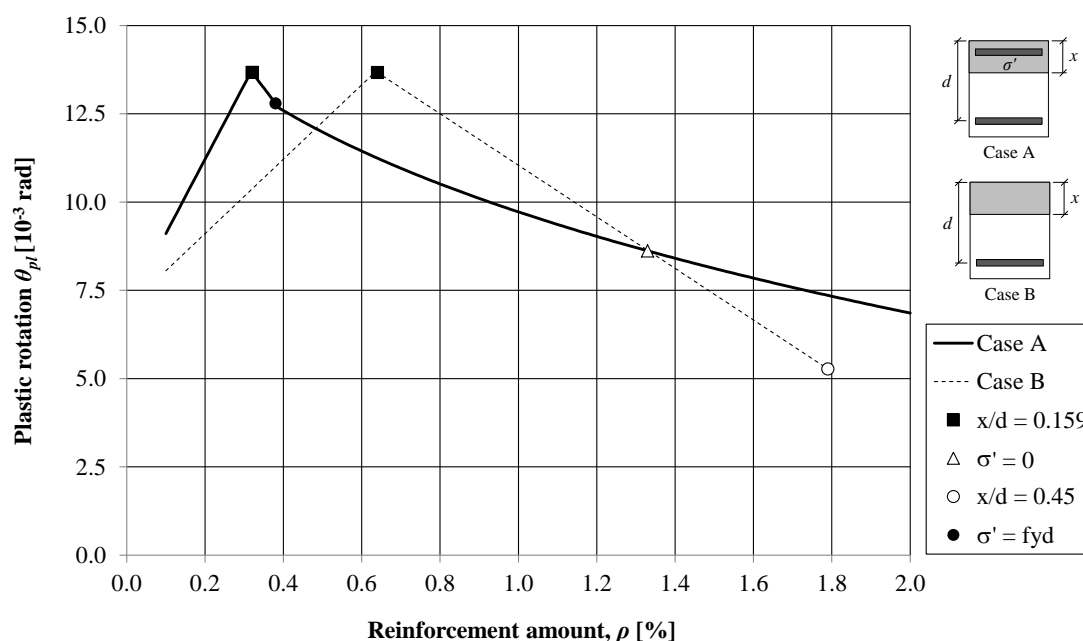


Figure 3.12 Plastic rotation capacity  $\theta_{pl}$  vs. reinforcement amount  $\rho$  for a section with a height of 200 mm (Case 1).



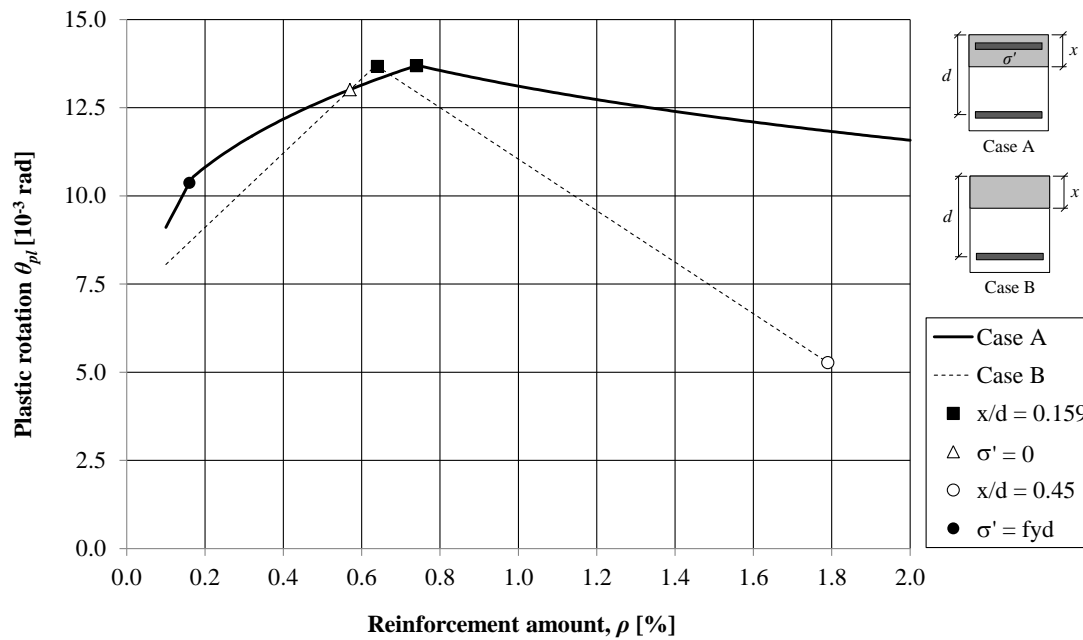


Figure 3.13 Plastic rotation capacity  $\theta_{pl}$  vs. reinforcement amount  $\rho$  for a section with a height of 400 mm (Case 1).

The maximum value of the plastic rotation capacity, which corresponds to  $x/d = 0.159$ , can clearly be spotted as a sharp deviation in the graphs. There is a clear connection between the graph of the maximum deformation and plastic rotation capacity. Simultaneously with increasing the reinforcement amount, the concrete compressive zone is increasing. At the point when the reinforcement amount is increased so much that the yielding stops, when  $\sigma' = f_{yd}$ , a sharp change of inclination in the graph can be noticed. Further increase in reinforcement amount leads to progressive lowering of the neutral axis to the point when it reaches the centre of the top reinforcement which at that specific point becomes compressed, when  $\sigma' = 0$ . This is a unique situation that corresponds to a case with no top reinforcement, and at this point the graphs will overlap. Further increase in reinforcement amount leads to a decrease in the rotation capacity which follows from the plastic rotation capacity function established in Eurocode 2. When the reinforcement amount reaches a value corresponding to the limiting ratio  $x/d$  no further development of plastic rotation capacity can be established. That is clearly marked with the point at the end of curve B where the ratio  $x/d = 0.45$  and after this point there is no information given in Eurocode 2.

Focusing on Case A in Figure 3.12, it can be noticed that for the lowest amount of reinforcement, the top reinforcement is in tension due to that the neutral axis is located above it, and it is yielding. The section with top reinforcement, Case A, reaches the maximum plastic rotation value faster than section without top reinforcement, Case B. The reason for this is that the height of the compressive concrete zone is increased when the top reinforcement is introduced.

The internal energy capacity of a structure can be calculated as the area under the resistance-deformation graph, according to equation (3.2). The internal energy is therefore depending on both the internal resistance  $R$  and the total deformation  $u$ .

$$W_i = \int R(u) du \quad (3.2)$$

For very high amounts of reinforcement, Case A shows a higher internal energy, which is beneficial for impulse loaded structures, see Figure 3.14 and Figure 3.15. However it should be noticed that the reinforcement amount, for the impulse loaded structures, should not exceed a maximum recommended value. Different authorities indicate different limits, depending on the proposed calculation methodology. According to Fortifikationsverket (2011) the maximum amount of reinforcement should be limited to 0.5 % while MSB (2009) considers 1.1 % to still be sufficient to assure a ductile behaviour of the structure. Eurocode 2, on the other hand, does not provide any information for  $x/d > 0.45$ .

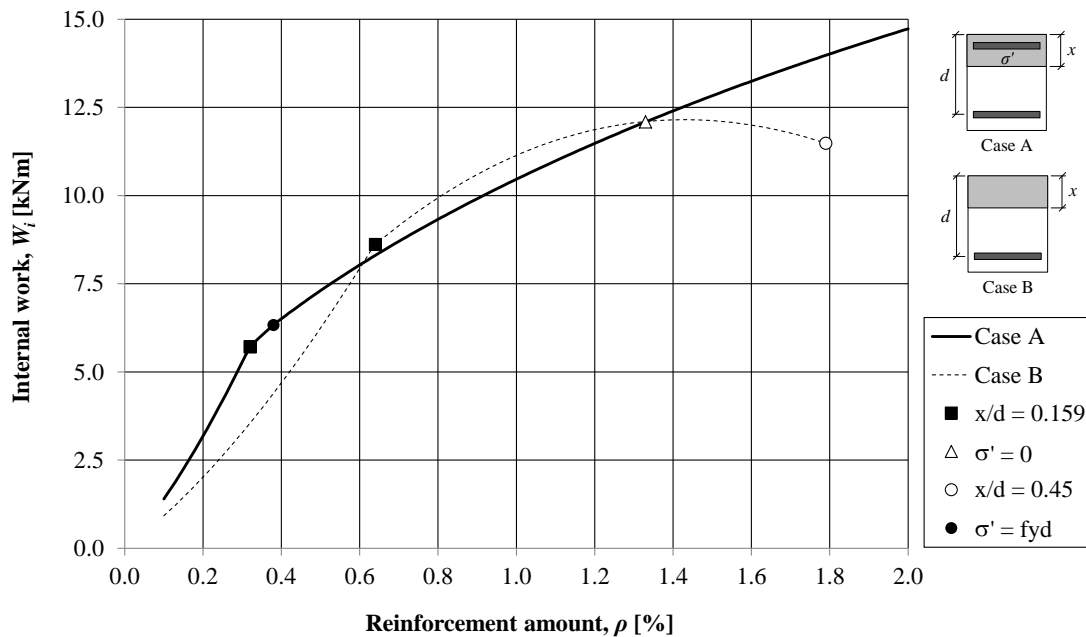


Figure 3.14 Internal work vs. reinforcement amount  $\rho$  for a section with a height of 200 mm (Case 1).

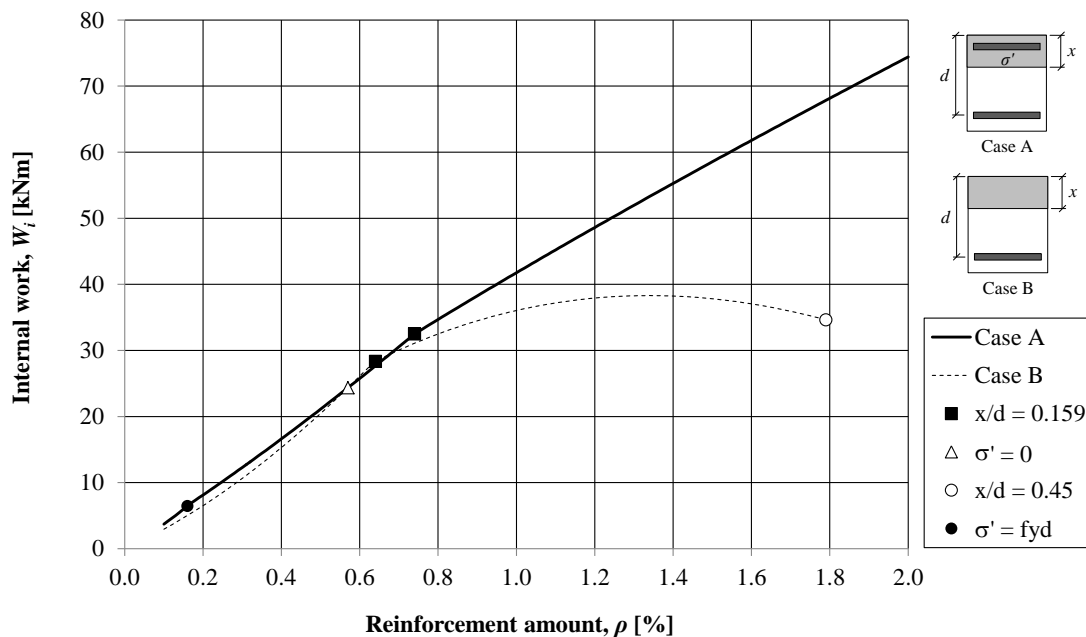


Figure 3.15 Internal work vs. reinforcement amount  $\rho$  for a section with a height of 400 mm (Case 1).

For Case B with a height of 400 mm the increase of the internal work starts to stagnate after around 0.8 % amount of reinforcement, which can be noticed in Figure 3.15. This happens due to that the maximum deformation decreases (Figure 3.13) and the maximum resistance increases (Figure 3.17) simultaneously creating a total internal work which is more or less constant with the reinforcement amount.

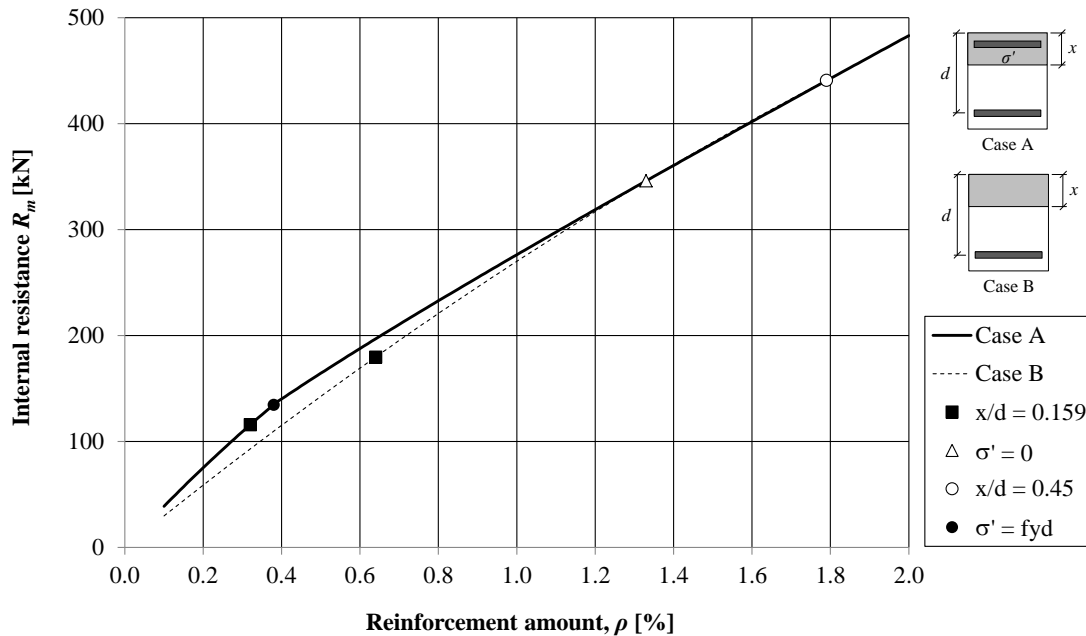


Figure 3.16 Internal resistance vs. reinforcement amount  $\rho$  for a section with a height of 200 mm (Case 1).

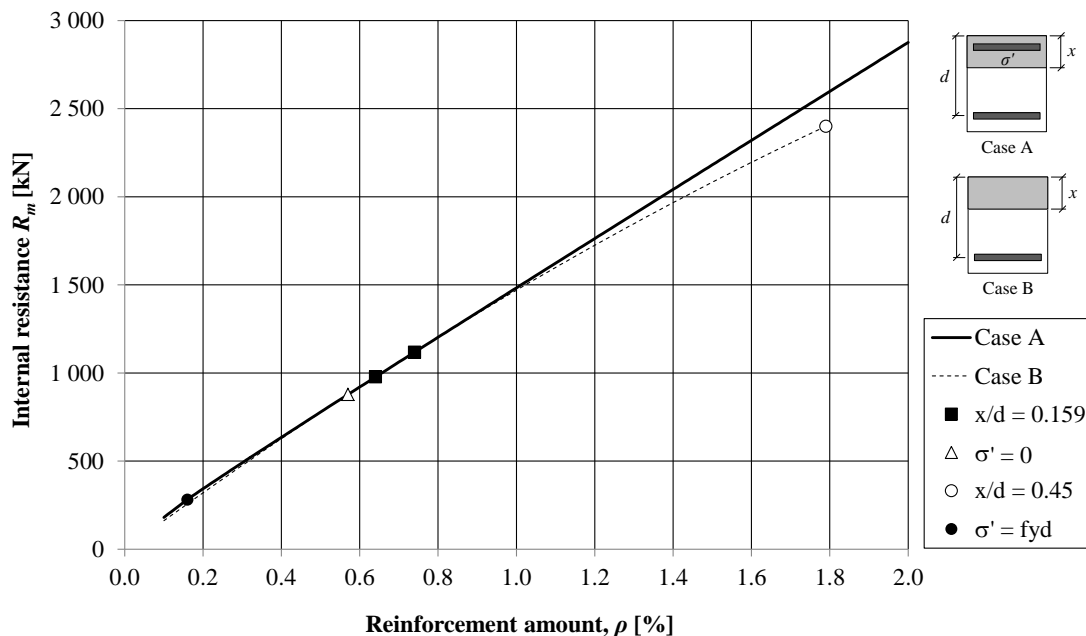


Figure 3.17 Internal resistance vs. reinforcement amount  $\rho$  for a section with a height of 400 mm (Case 1).

For Case A with a height of 400 mm, the maximum resistance is increasing with higher amount of reinforcement (Figure 3.17) and the maximum deformation is

decreasing with a lower rate than for the case with top reinforcement (Figure 3.13), resulting in higher values of the internal work (Figure 3.15). This is due to that the height of the compression zone increases slower for the case with top reinforcement, which makes the maximum deformation decrease slower.

### 3.4.4 Comparison of Case A and Case B

A comparison between Case A and B, which is plotted in Figure 3.18 to Figure 3.23, is presented as a function of  $\gamma$  and varies with the reinforcement amount. The value of  $\gamma$  has been established for the internal resistance (equation (3.3)), ultimate plastic deformation (equation (3.4)) as well as internal work (equation (3.5)). For each of those parameters,  $\gamma$  is a ratio of the case with top reinforcement (Case A) to the case without top reinforcement (Case B). The effective depth is always calculated according to Case 1.

$$\gamma_{R_m} = \frac{R_{m.A}}{R_{m.B}} \quad (3.3)$$

where  $R_{m.A}$  is the internal resistance for Case A and  $R_{m.B}$  is the internal resistance for Case B.

$$\gamma_{u_{rd}} = \frac{u_{rd.A}}{u_{rd.B}} \quad (3.4)$$

where  $u_{rd.A}$  is the ultimate plastic rotation for Case A and  $u_{rd.B}$  is the ultimate plastic rotation for Case B.

$$\gamma_{W_i} = \frac{W_{i.A}}{W_{i.B}} \quad (3.5)$$

where  $W_{i.A}$  is the internal work for Case A and  $W_{i.B}$  is the internal work for Case B.

The parameters that change the inclination of the curves can be followed with varying reinforcement amount in the different graphs. Therefore, for Case A, the reinforcement amounts at which the top reinforcement stops to yield or becomes compressed can be distinguished. For Case B, the points corresponding to the upper and lower limits of the plastic rotation capacity can be found.

In Figure 3.18 and Figure 3.19 there is a sharp deviation of the resistance at the point where the reinforcement stops to yield (when  $\sigma' = f_{yd}$ ). In another point of the curve (when  $\sigma' = 0$ ) the maximum resistance for both cases is equal. At that point the neutral axis is positioned close to the top reinforcement, hence removing its positive effect and making the case similar to a case without top reinforcement.

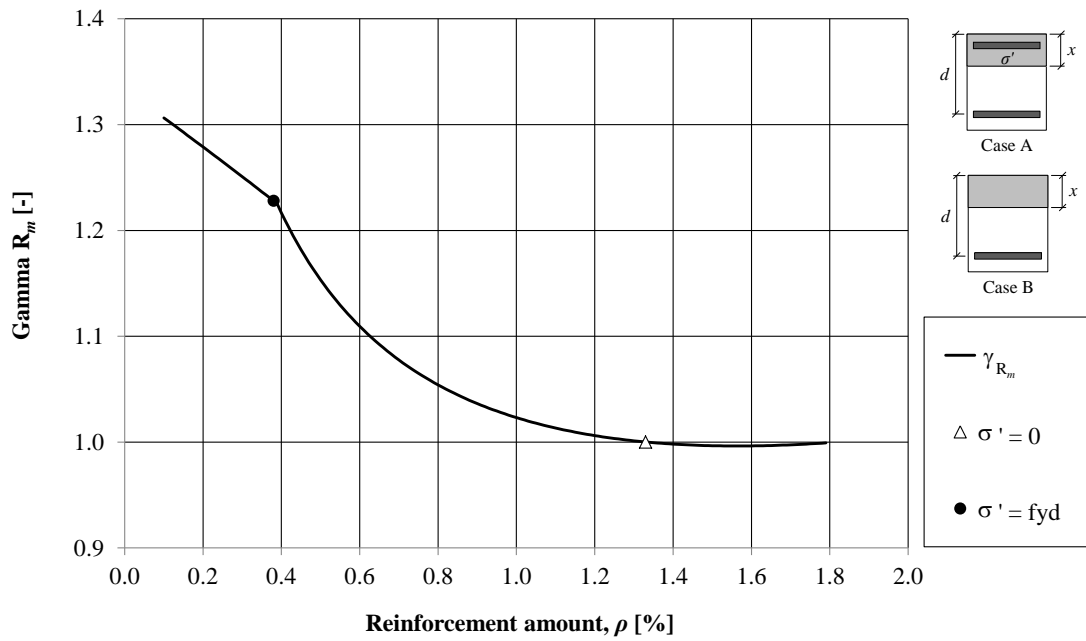


Figure 3.18 Ratio of internal resistance,  $\gamma_{R_m}$ , vs. reinforcement amount  $\rho$ . Section with a height of 200 mm (Case 1).

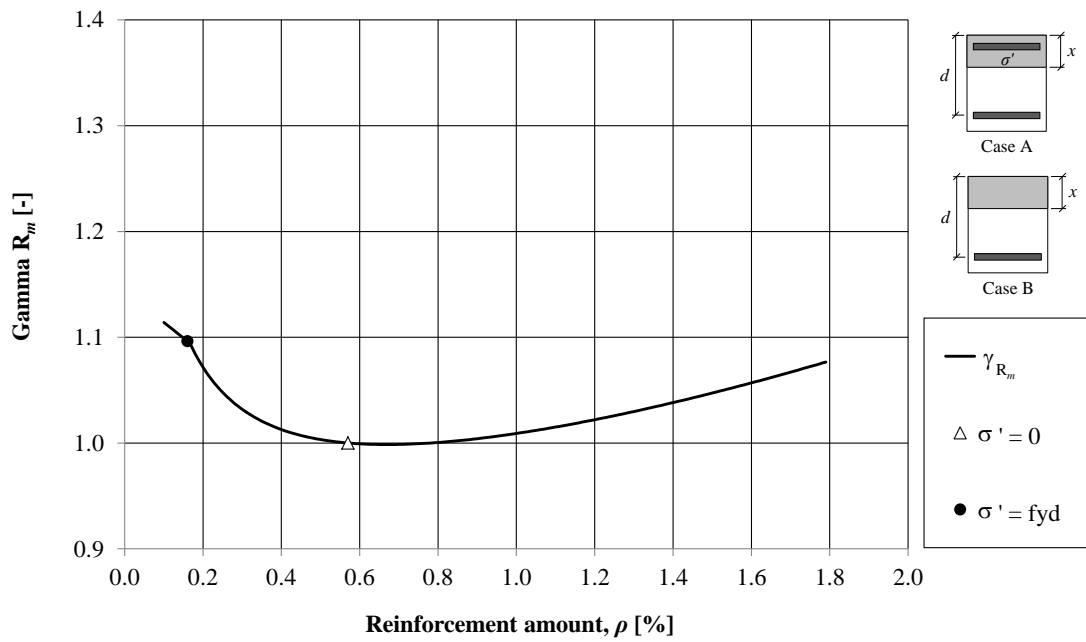


Figure 3.19 Ratio of internal resistance,  $\gamma_{R_m}$ , vs. reinforcement amount  $\rho$ . Section with a height of 400 mm (Case 1).

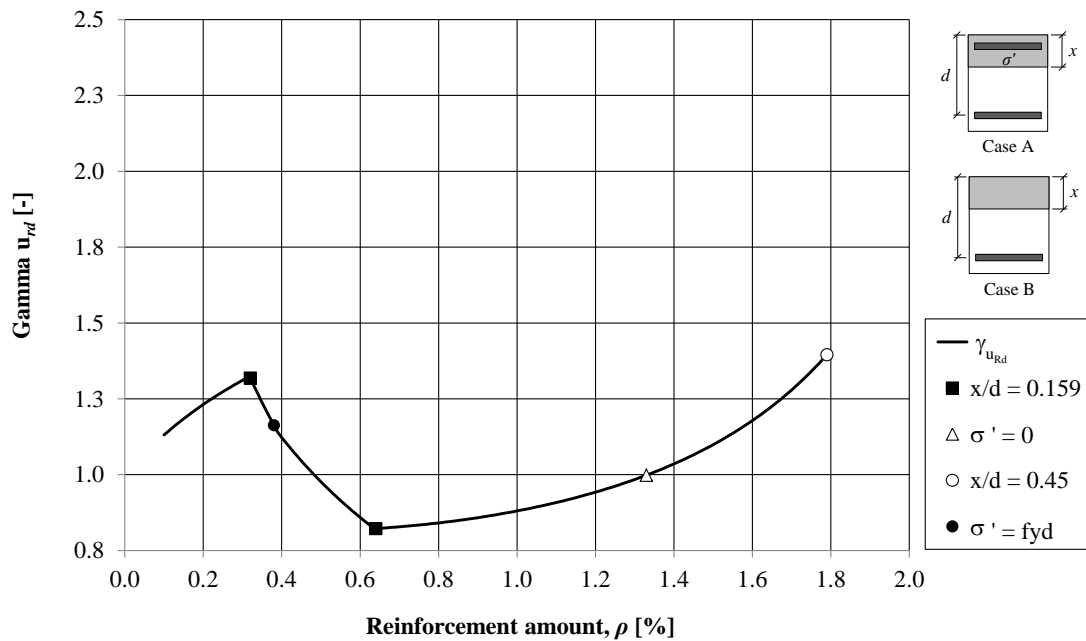


Figure 3.20 Ratio of ultimate plastic deformation,  $\gamma_{u_{Rd}}$ , vs. reinforcement amount  $\rho$ . Section with a height of 200 mm (Case 1).

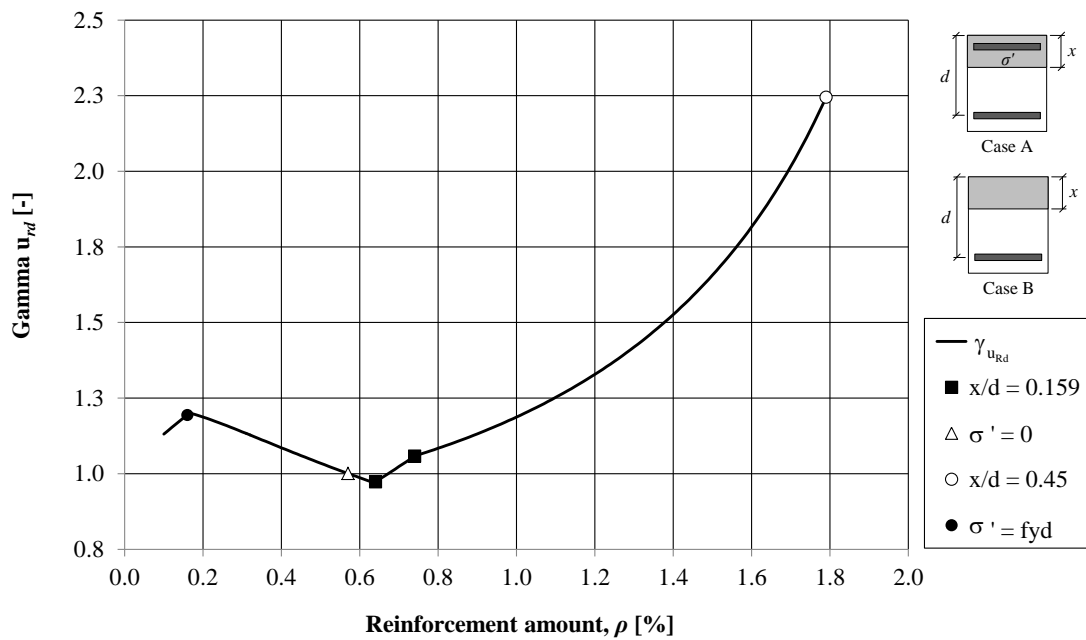


Figure 3.21 Ratio of ultimate plastic deformation,  $\gamma_{u_{Rd}}$ , vs. reinforcement amount  $\rho$ . Section with height of 400 mm (Case 1).

Figure 3.22 and Figure 3.23 indicate that there is a large benefit when introducing the top reinforcement in the calculations. The magnitude of the internal work can be increased up to 60 % in the cases studied when introducing the top reinforcement. This is evidently resulting from the larger difference in the ultimate plastic rotation and internal resistance, comparing Figure 3.18 to Figure 3.21.

For an interval when  $\gamma_{wi} < 1$  the internal work is higher for Case B than for Case A. This is when the section without top reinforcement reaches its maximum plastic rotation capacity at  $x/d = 0.159$  and therefore reaches a higher maximum deformation

than in Case A. When increasing the height of the section, the size of this interval decreases.

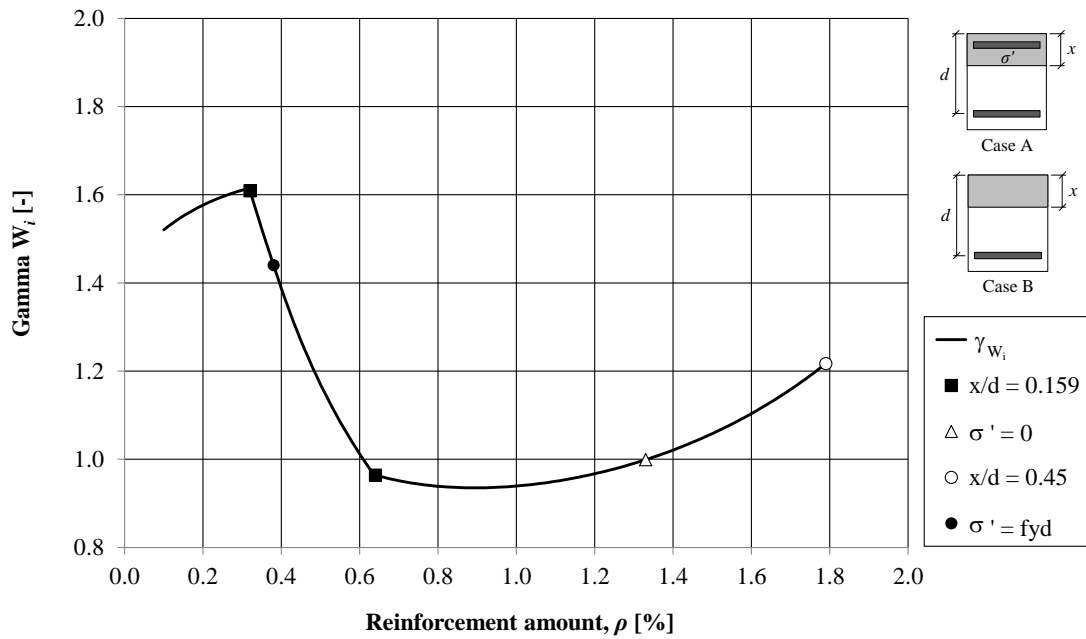


Figure 3.22 Ratio of internal work,  $\gamma_{w_i}$ , vs. reinforcement amount  $\rho$ . Section height is 200 mm (Case 1).

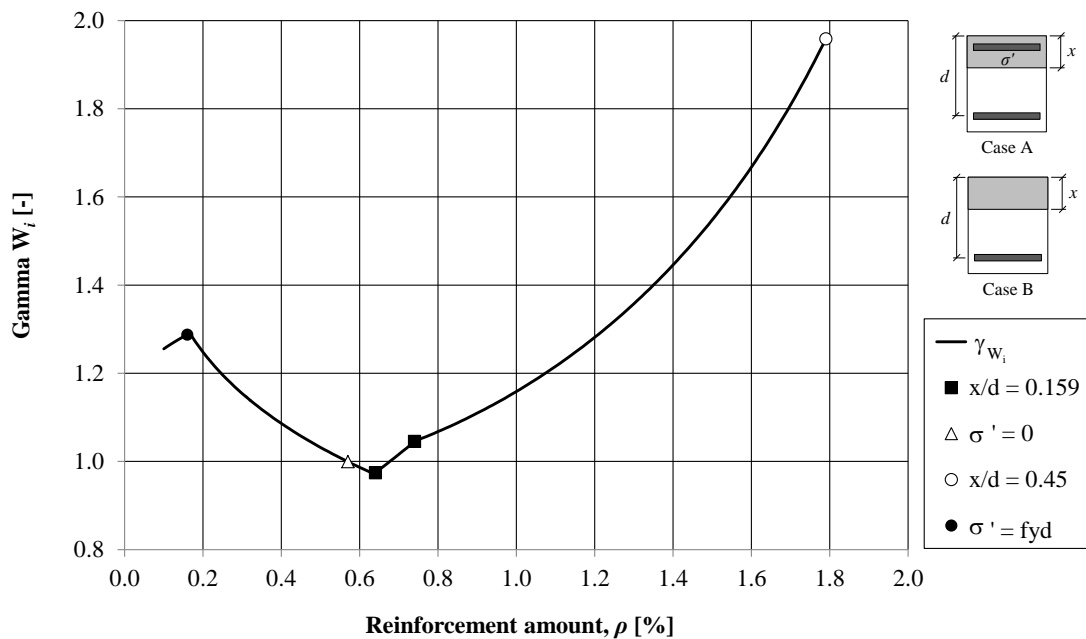


Figure 3.23 Ratio of internal work,  $\gamma_{w_i}$ , vs. reinforcement amount  $\rho$ . Section height is 400 mm (Case 1).

Again, the top of the rotation capacity curve can be spotted as a sudden change in the graph (Figure 3.22). For the 400 mm case, the point where the top reinforcement stops yielding also results in a sudden change in the graph (Figure 3.23). At this point the difference between the cases goes from increasing to decreasing.

### 3.4.5 Different interpretation of $d$ for Case 2

There are different ways of interpreting the rotation capacity curve in Eurocode 2 and here Case 2, according to Section 3.2.2, is investigated. A compilation of all the results can be found in Appendix A. It is important to notice that the amount of reinforcement on the horizontal axis is still calculated with  $d$  from Case 1 in order to be able to compare the graphs.

To understand the changes in the internal work it is preferred to analyse the development of the maximum plastic deformation, see Figure 3.24. For Case A, the sharp deviation at the interval 1.03 - 1.35 % can be noticed. This corresponds to the state when the effective depth  $d$  is transferred from being the average distance from the top of the beam to the centre of gravity of the top and bottom reinforcement, to being the distance from the top to the bottom reinforcement only. The end of the first part of the curve for Case A, marked with the round white point, corresponds to the stage when the considered section, where  $x \leq c$ , reaches the ratio  $x/d = 0.45$ , which is the upper limit of the function established in Eurocode 2. Attaining this value for Case B means no further development of plastic rotation. However, for Case A, which is designed depending on the location of the neutral axis, reaching this point means a continuation of plastic rotation development from the beginning but with a new effective depth and with  $x > c$ . Thus, at the triangular point the curve A becomes identical to the graph for Case 1.

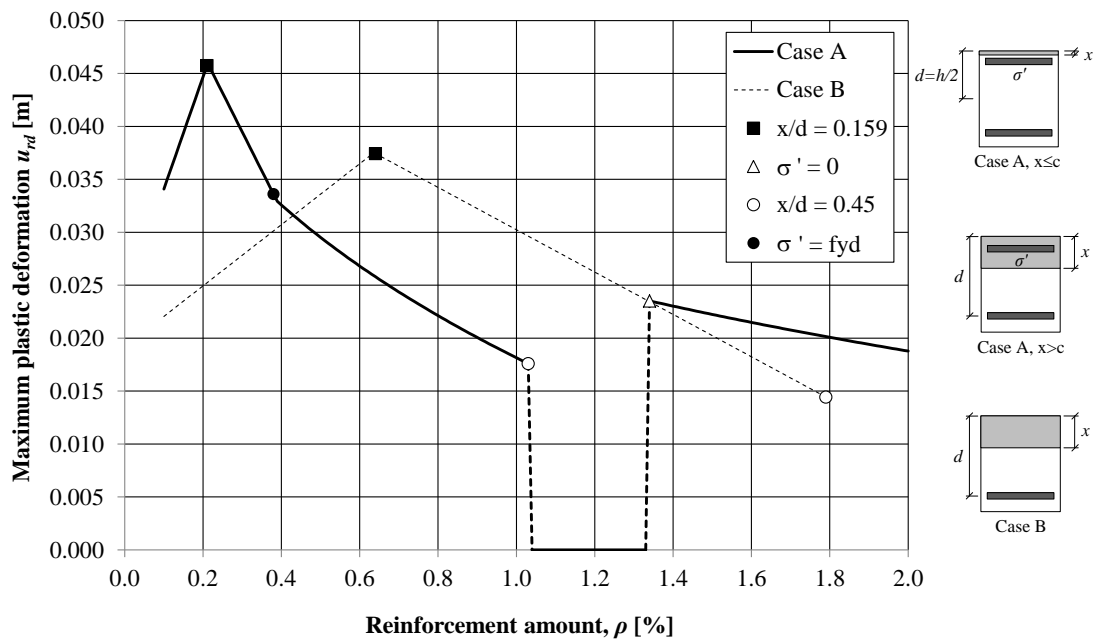


Figure 3.24 Maximum plastic deformation vs. reinforcement amount for a section with a height of 200 mm (Case 2).

Bearing this in mind, it is easy to analyse the changes in the internal energy, presented in Figure 3.25. Here, after reaching the ultimate value of  $x/d$  in the first part of the curve for Case A, the line does not drop to zero but continues, at a somewhat lower level, with a certain inclination until it comes back on track again (at 1.35 %). This interval corresponds to the elastic part of the elasto-plastic response model. Here, the plastic rotation capacity is considered to be zero, hence only the elastic response is left.



Before the sharp deviation, at 1.03 %, the difference between the cases with and without top reinforcement is larger than for Case 1. This is due to that  $d$  is smaller for low amounts of reinforcement and therefore  $x/d$  becomes larger. The plastic rotation capacity and maximum deformation reaches a higher value, increasing the internal energy before the neutral axis passes below the top reinforcement.

The internal work relations are shown in Figure 3.25 and Figure 3.26, and the corresponding ratios are shown in Figure 3.27 and Figure 3.28.

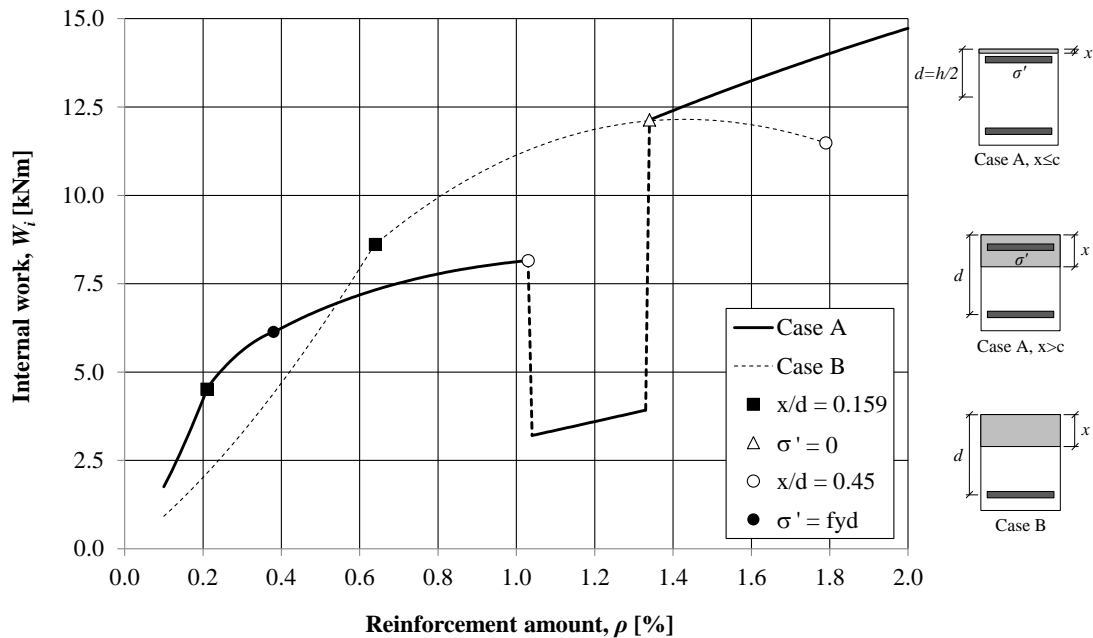


Figure 3.25 Internal work vs. reinforcement amount for a section with a height of 200 mm (Case 2).

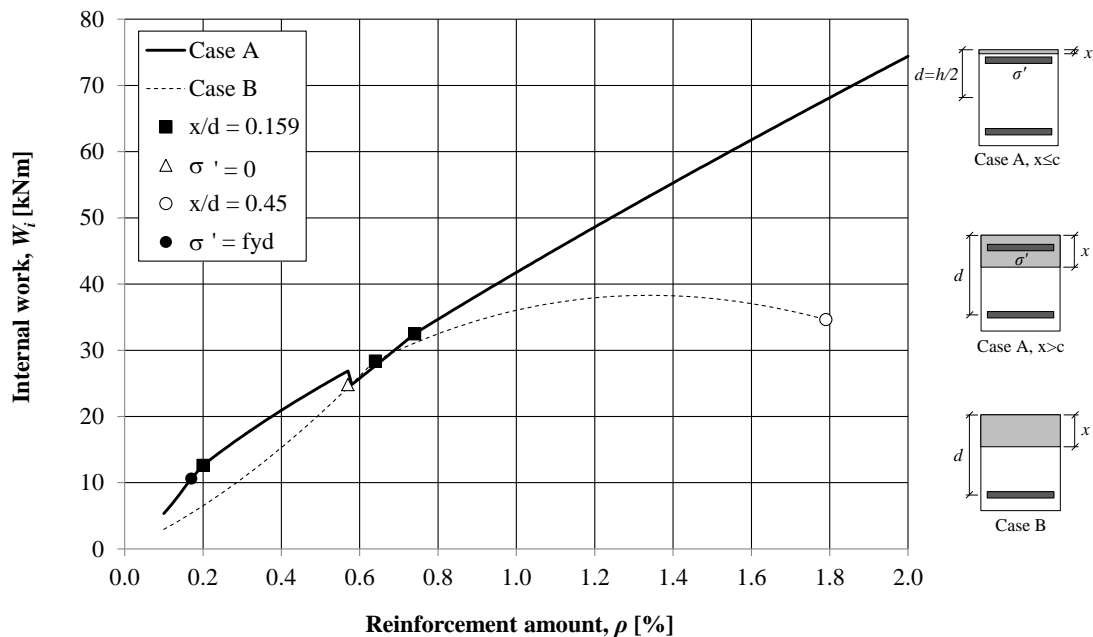


Figure 3.26 Internal work vs. reinforcement amount for a section with a height of 400 mm (Case 2).

The largest difference in a jump in the graphs, when the transformation of  $d$  occurs, is for the thinnest section. For this section, similarly as for Case 1, there is a significant interval for which the internal work is larger for Case B, comparing Figure 3.25 and Figure 3.26. The differences between Case A and B decreases with increasing height of beam.

The development of internal resistance for considered height is the same as in Case 1 and the graphs are presented in Section B.11.

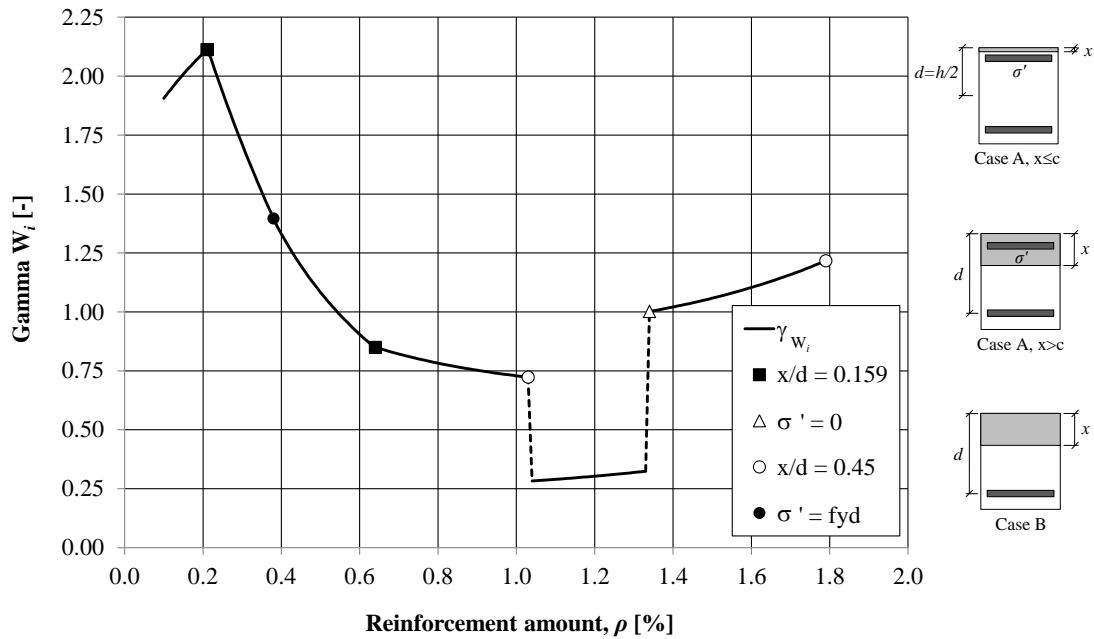


Figure 3.27 Ratio of internal work,  $\gamma_{w_i}$ , vs. reinforcement amount  $\rho$ . Section height is 200 mm (Case 2).

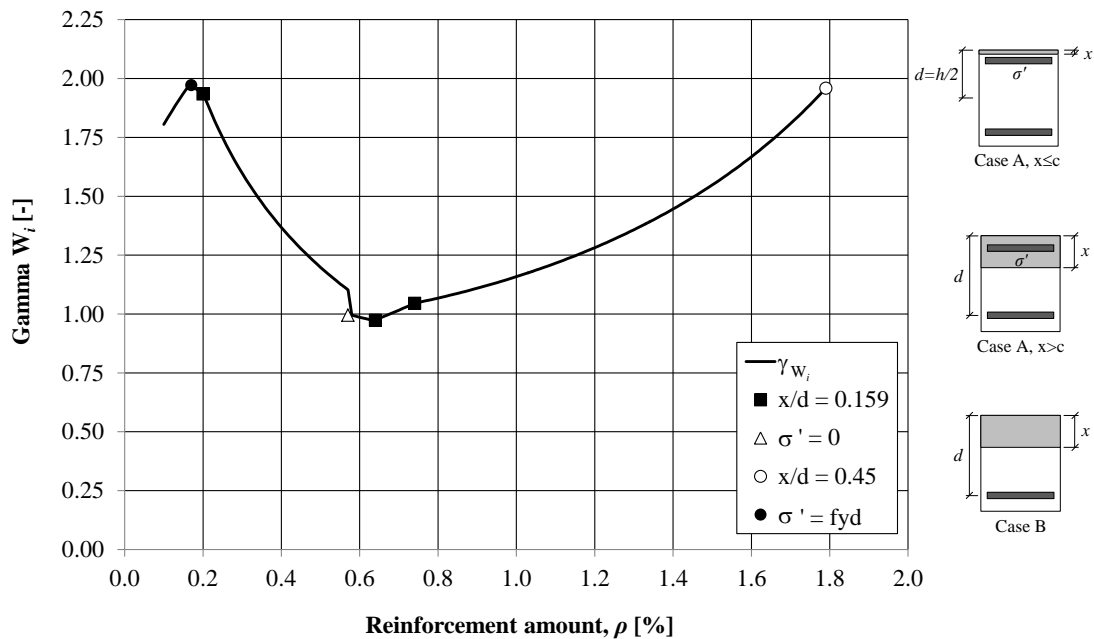


Figure 3.28 Ratio of internal work,  $\gamma_{w_i}$ , vs. reinforcement amount  $\rho$ . Section height is 400 mm (Case 2).

### 3.5 Concluding remarks

When considering a statically loaded structure the maximum resistance is the critical parameter and here it is always on the safe side to disregard the top reinforcement. However, for an impulse loaded structure, the critical parameter is the internal work, which makes it more complicated. In this study the answer should be given to if the top reinforcement should be neglected or not, and how the effective depth  $d$  should be considered. It is obvious that omitting the top reinforcement and calculating  $d$  according to Case 1, presented in Section 3.2, is the simplest method for designing an impulse loaded structure. In most cases it can be considered conservative to neglect the top reinforcement. However, for a certain interval the internal energy will be higher for a case without top reinforcement than for a case with top reinforcement due to the plastic rotation capacity curve from Eurocode 2. Within these intervals the conservative way would be to consider the top reinforcement. Some concern should also be given to the yielding of the top reinforcement. If the ultimate strain of the top reinforcement has not been reached, it would be correct to disregard it as it does not influence the internal resistance in a significant way.

Since interpreting  $d$  according to Case 2 provides higher values of the internal energy in certain intervals, from where the cases are identical, it can be considered conservative to follow Case 1. For the thinnest section it seems reasonable to use the effective depth defined as Case 2, up to the point when the top reinforcement stops to yield. For the other studied heights it is rational to use  $d$  defined as Case 2 up to the point when the top reinforcement becomes compressed. However such interpretation of effective depth would make the calculation methodology, presented in Johansson and Laine (2012a), more complicated to implement.

These are the reasons why it is not recommended to define  $d$  to depend on the position of the neutral axis. Moreover, it is preferred not to introduce the top reinforcement in the calculations in order to keep the calculations as simple as possible. The design procedures for civil defence shelters define the minimum allowable height of the roof and outer wall structure to be 350 mm (Swedish shelter regulations, MSB (2009)). In such case, the differences in the considered concepts are much smaller than for a structure with a height of 200 mm. There is also upper limit for the reinforcement amount of 1.1 %. The difference in the results for the studied methods was largest for the highest reinforcement amounts, which is not the standard solution for reinforced concrete structures.

The studies in this report have been performed considering steel of Class B, on the curve for concrete  $\leq$  C50/60. If another curve had been considered, i.e. Class C, the size as well as the relationships between the different cases of maximum deflection would have been different. The curve chosen for the plastic rotation capacity has a large influence on the maximum deformation and the internal energy. However, the aim of the work has been to study the fundamental differences and therefore reinforcement of Class B has been chosen as an example.

Finally, Betonghandboken presents a different method of receiving the plastic rotation capacity where the equation for  $\theta_{pl}$  considers the compressive reinforcement. However, this contribution can only be taken into account if there are stirrups to prevent the compressive reinforcement from breaking.

## 4 Structural response of a 2D frame

### 4.1 Introduction and method

The aim of this study is to investigate and evaluate the reliability of the simplified SDOF calculations for a frame structure subjected to impulse load. This is a continuation of the researches conducted in the previous Master's Theses, where a simply supported beam and a slab were studied. The calculation methodology is based on Johansson (2013). In this chapter a 2D analysis is performed. A 3D analysis of the structure, where two different concepts of applying the load on the structure is investigated, is found in Chapter 5.

The calculation methodology is based on the principles of the SDOF system, see Section 2.9, adapted with regard to the properties of a frame. The SDOF system is solved by the use of Matlab R2013a. The results from the SDOF model are compared to the results obtained in FE analyses, conducted in ADINA (2011). It is assumed that the response obtained in ADINA simulates, in the most appropriate way, the real behaviour of the structure subjected to impulse load. The analyses are conducted for both elastic and elasto-plastic models.

### 4.2 Geometry and properties of the studied frame

The analysed frame structure is presented in Figure 4.1. In this section a 2D-analysis is performed, and the response of a 1.0 meter strip of the wall and roof section is studied.

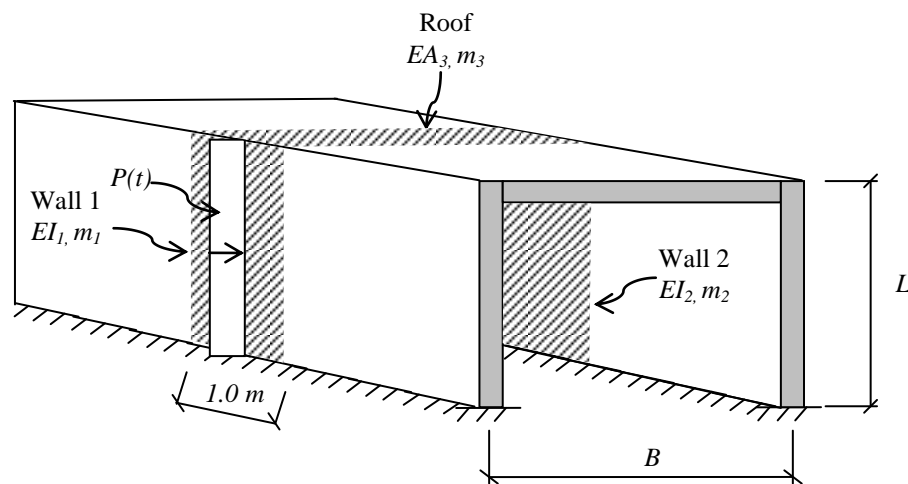


Figure 4.1 3D-illustration of the frame structure.

The reinforced concrete frame has dimensions according to Figure 4.2a. The walls supporting the roof beam are fully fixed at the base and simply supported at the connection with the roof beam. The dimensions of the considered cross section for the wall as well for the roof beam are presented in Figure 4.2b and the material properties in Table 4.1. Other parameters which are introduced in SDOF or in ADINA are presented in the sections describing particular method. The studied 1.0 meter strip of the front and back wall is, for simplicity, called for front and back column, respectively.

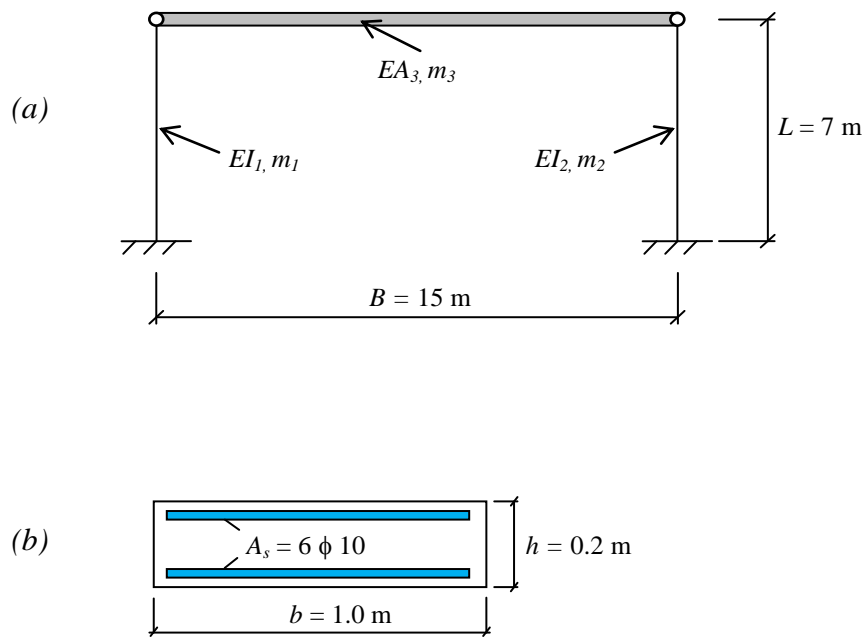


Figure 4.2 (a) Dimensions of the studied frame. (b) Dimensions of the considered cross section for the wall and for the roof beam.

Table 4.1 Material properties of the frame.

Part	$E_c$ [GPa]	$f_{cd}$ [MPa]	$E_s$ [GPa]	$f_{yd}$ [MPa]
Front column (1)	33	25	200	500
Back column (2)	33	25	200	500
Roof beam (3)	33	25	200	500

In order to simplify the SDOF analysis, the roof beam is assumed to be much stiffer than the supporting columns. Moreover, it is connected to the columns with hinges. Only the case when the impulse load,  $P(t)$ , acts from the side on the front column is considered, Figure 4.3. Thus, when the structure is subjected to the chosen impulse, the roof beam is only displaced horizontally and remains undeformed, see Figure 4.3.

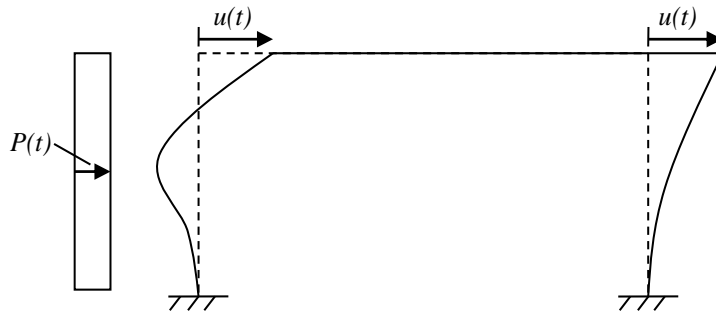


Figure 4.3 Deformed shape of the frame structure subjected to the impulse at a certain time  $t$ .

When assuming the properties of the structural parts of the frame, reinforcement of Class B is the preliminary choice. This is based on the regulations in Eurocode 2 which allows reinforcement of Class B to be used when an ability to deform plastically and develop plastic hinges is required. In Section 4.7.1.4 a comparison of the plastic rotation capacity of the front column provided with reinforcement of Class B and Class C is done.

### 4.3 Reflected impulse load

The load is applied on the front column as a reflected impulse load, see Figure 4.4.



Figure 4.4 Application of impulse load on the frame.

The shape and magnitude of the chosen impulse load, as well as its duration, is assumed to be according to Figure 4.5 and Table 4.2. This load corresponds to about 500 kg TNT at 50 meters distance.

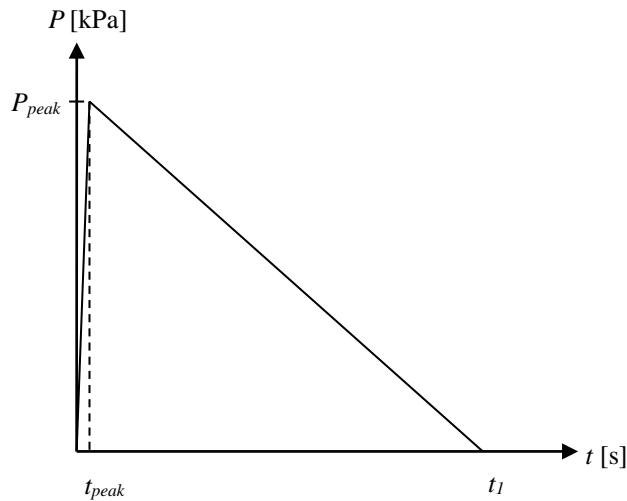


Figure 4.5 Properties of the chosen impulse load.

Table 4.2 Parameters for the chosen load.

$P_{peak}$ [kPa]	$t_{peak}$ [s]	$t_1$ [s]
60	0.00025	0.25

The first branch, in the pressure-time curve is assumed to be inclined. The time for which the pressure reaches its maximum value,  $t_{peak}$ , is 1/100 of the duration of the impulse  $t_1$ . This assumption is made since ADINA does not manage to find the solution for a case with a completely vertical branch, which can also be used to symbolise the development of the impulse load.

## 4.4 Adaption of frame into SDOF system

### 4.4.1 Introduction

In order to describe the structural behaviour due to an impulse load, the studied frame is analysed with regard to its local and global response. The concept of dividing the SDOF system into a global and local model is based on Johansson (2013).

The analysis of the local response is made for the front column, as it is not only the most exposed element but it is also provided with a relatively low mass compared with the whole structure. Thus, the initial behaviour of the front column is critical for the frame structure, which makes it important for the study.

In the global analysis the whole frame is considered as a structure. This means that not only the front column withstands the impact but also the roof beam contributes with its mass and the back column contributes with its mass and its stiffness.

A description of the central difference method as well as the calculations of the response models used for the elastic and elasto-plastic cases are described in Appendix D. The parameters used in the following sections can be found in Section E.1.

## 4.4.2 Local SDOF model

### 4.4.2.1 Orientation

In the local SDOF model only the response of the front column, with mass  $m_l$  and stiffness  $EI_l$ , is considered. The boundary conditions of the local model are presented in Figure 4.6 where the top of the column is assumed to be restrained in the horizontal direction. This assumption is based on the fact that at the beginning of the loading, the horizontal displacement at the top of the frame is very small and can be disregarded, Johansson (2013). Further theoretical explanations behind the structural behaviour of the model can be found in Appendix C.

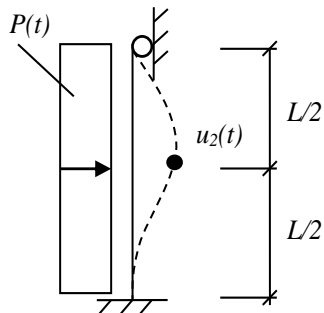


Figure 4.6 Local response model for the front column of the frame. The deformation,  $u_2$ , is measured in the middle of the column.

### 4.4.2.2 Elastic response

When using the elastic response model, Figure 4.7, in this study of the local behaviour, the stiffness for state II,  $k_l$ , is used. With the assumed boundary conditions of the local model and moment of inertia for the cracked section  $I_{II}$ , the stiffness in state II is calculated as

$$k_l = \frac{192 \cdot E_c \cdot I_{II}}{L^3} \quad (4.1)$$

where  $I_{II}$  is the moment of inertia calculated according to equation (E.4) and  $E_c$  can be found in Table 4.1.

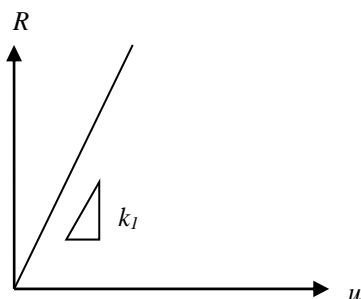


Figure 4.7 Elastic response model.



#### 4.4.2.3 Elasto-plastic response

The elasto-plastic response of the local front column follows a trilinear model as shown in Figure 4.8. This phenomenon is due to the fact that the structure has the ability to develop two plastic hinges, one at the fixed support and one in the span.

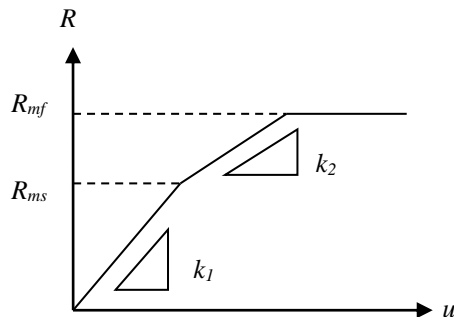


Figure 4.8 Trilinear, elasto-plastic model.

The inclination of the first branch in the elasto-plastic response model is obtained according to equation (4.1) and corresponds to the stiffness in state II for a structure with one fixed edge and one simply supported. The first point of deviation in Figure 4.8 describes that the ultimate resistance at the fixed support,  $R_{ms}$ , is reached.  $R_{ms}$  is calculated as

$$R_{ms} = \frac{8 \cdot M_{rd}}{L} \quad (4.2)$$

where  $M_{rd}$  is the moment capacity of the section calculated according to equation (E.12).

Reaching the point  $R_{ms}$  is followed by a significant decrease in stiffness due to a change in boundary conditions. When the maximum capacity of the fixed support is reached, the plastic hinge starts to develop, Figure 4.9b. Due to the plastic hinge the restraint at the fixed support does not prevent rotation any longer and the structure changes boundary conditions from fully restrained at one support and simply supported at the opposite one, to simply supported at both edges, as shown in Figure 4.9c.

Now, the stiffness is changed to  $k_2$  considering the new simply supported boundary conditions, and calculated as

$$k_2 = \frac{384 \cdot E_c \cdot I_{II}}{5 \cdot L^3} \quad (4.3)$$

where  $I_{II}$  is calculated according to equation (E.4) and  $E_c$  can be found in Table 4.1.

The ultimate capacity of the column is reached when the maximum resistance at the critical section in the span,  $R_{mf}$ , is developed according to equation (4.4).  $R_{mf}$  is the ultimate resistance of the section when a plastic hinge is developed in the field as illustrated in Figure 4.9d.

$$R_{mf} = \frac{12 \cdot M_{rd}}{L} \quad (4.4)$$

where  $M_{rd}$  is calculated according to equation (E.12).

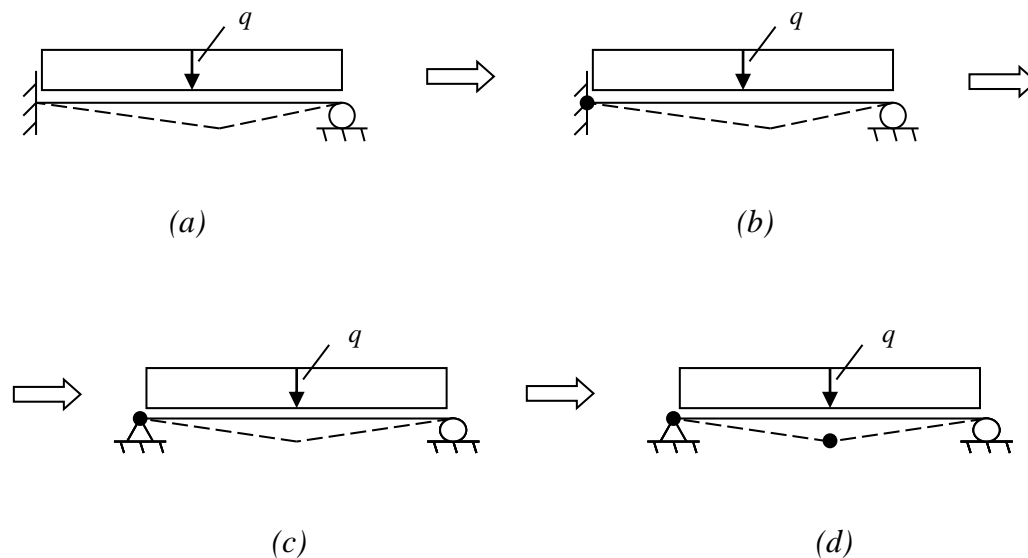


Figure 4.9 (a) Boundary conditions of the studied structure. (b) Formation of plastic hinge when the maximum capacity is reached at the fixed support. (c) Transformation of boundary condition from fixed to simply supported. (d) Formation of plastic hinge in span. The plastic hinges are marked with black points.

To simplify the calculations, a bilinear elasto-plastic response model can be considered, as shown in Figure 4.10. The results obtained, by employing this response model in the SDOF system shows to be significantly different comparing to the results obtained in the FE analysis. This problem is further described in Section 4.7.1.

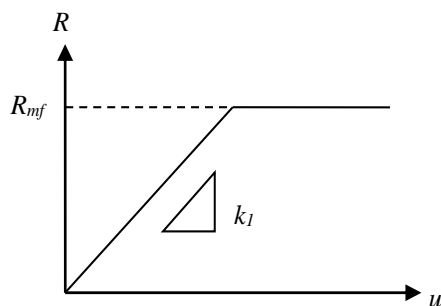


Figure 4.10 Bilinear, elasto-plastic model introduced in the study of the local response.

#### 4.4.2.4 SDOF system

For the local response, when transforming it into an SDOF system, the system point is chosen to be located in the mid span of the front column, see Figure 4.11a. The resistance of this section is used in the structural response model. However, it is worth to mention that this position of the system point does not match the point where the maximum moment and thus maximum deformation is obtained, Figure 4.11b.

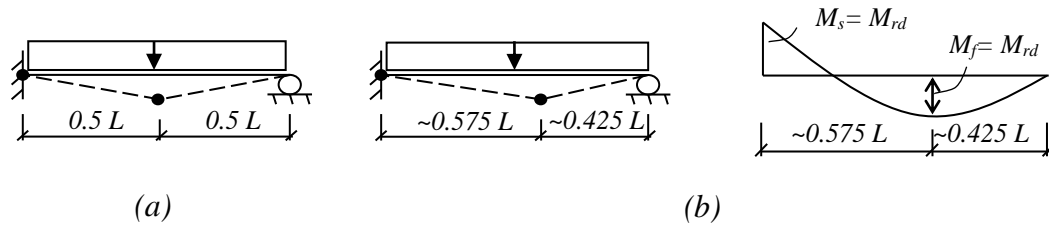


Figure 4.11 (a) Assumed deformation and location of system point for the SDOF system. (b) Deformation and location of the plastic hinges as well as moment distribution in ultimate limit state.

The equation of motion with the appropriate transformation factors for the local response is

$$\kappa_m m_1 \ddot{u} + \kappa_K R(u) = \kappa_F P(t) \quad (4.5)$$

When dividing equation (4.5) by  $\kappa_F$  and introducing  $\kappa_k = \kappa_F$  according to Section 2.9 as well as introducing  $\kappa_{mF}$  as

$$\kappa_{mF} = \frac{\kappa_m}{\kappa_F} \quad (4.6)$$

the equation of motion for this local SDOF system can now be written as

$$\kappa_{mF} m_1 \ddot{u} + R(u) = P(t) \quad (4.7)$$

The input data for the equation of motion for the elastic, bilinear elasto-plastic and trilinear elasto-plastic structural response is presented in Table 4.3, Table 4.4 and Table 4.5, respectively. The calculations of these parameters can be found in Section E.1 and the resistance  $R(u)$  in Section D.3.

Table 4.3 Mass, stiffness and transformation factors used for the elastic model.

Part	$\kappa_{mF}$ [-]	$m$ [kg]	$I = I_{II}$ [ $10^{-4} \text{ m}^4$ ]	$k_I$ [kN/m]
Front column (1)	0.805	3 360	0.54	1 007.6

Table 4.4 Mass, stiffness and transformation factors used for the elasto-plastic bilinear model.

Part	$\kappa_{mF}$ [-]	$m$ [kg]	$I_{II}$ [ $10^{-4} \text{ m}^4$ ]	$k_1$ [kN/m]	$M_{rd}$ [kNm]	$R_{mf}$ [kN]
Front column (1)	0.607	3 360	0.54	1 007.6	37.8	64.9

Table 4.5 Mass, stiffness and transformation factors used for the elasto-plastic trilinear model.

Part	$\kappa_{mF}$ [-]	$m$ [kg]	$I_{II}$ [ $10^{-4} \text{ m}^4$ ]	$k_1$ [kN/m]	$k_2$ [kN/m]	$M_{rd}$ [kNm]	$R_{ms}$ [kN]	$R_{mf}$ [kN]
Front column (1)	0.607	3 360	0.54	1 007.6	403.0	37.8	43.3	64.9

### 4.4.3 Global SDOF model

#### 4.4.3.1 Orientation

The global response is simulated according to the model in Figure 4.12a, and it is described by the response of a cantilever. The stiffness of this cantilever,  $EI$ , as well as its mass,  $m$ , is a combination of both the front and back column. The contribution from the roof beam to the model is its concentrated mass,  $m_3$ , at the top of the cantilever. All together, the global response is the sum of the response of the front column directly exposed to an impulse load and the back column loaded with the force transferred by the roof beam, Figure 4.12b.

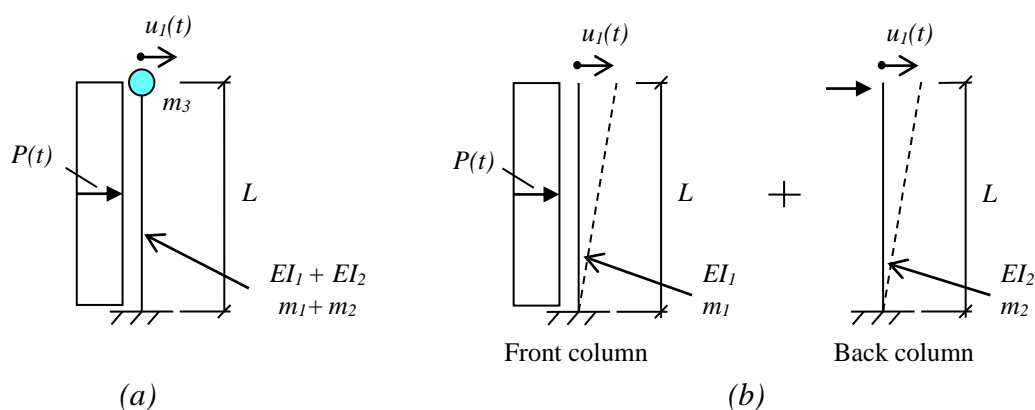


Figure 4.12 (a) Assumed model for the simulation of the global response and its deformation  $u_1$ . (b) This model is the sum of the response of the front and back column, according to Johansson (2013).

#### 4.4.3.2 Elastic response

When the elastic response model is considered, the stiffness for the front column,  $k_{I,fr}$ , and back column,  $k_{I,ba}$ , is described according to equation (4.8) and equation (4.9), respectively and corresponds to the stiffness in state II.

$$k_{I,fr} = \frac{8 \cdot E_c \cdot I_{II}}{L^3} \quad (4.8)$$

$$k_{I,ba} = \frac{3 \cdot E_c \cdot I_{II}}{L^3} \quad (4.9)$$

where  $I_{II}$  is the moment of inertia of the cracked section calculated according to equation (E.4) and  $E_c$  can be found in Table 4.1.

#### 4.4.3.3 Elasto-plastic response

In this Master's Thesis an attempt has been made to implement the SDOF system for a frame simulated with an elasto-plastic model, but the response of the studied structure has been proven to be more complicated than expected.

The static structural response model of the elasto-plastic global model has in the FE analysis shown a trilinear behaviour due to the two plastic hinges that can be developed at the fixed support and at the back. However, when this static structural response model is used in the SDOF calculations for the considered load, the response is still elastic, while the FE analysis shows some plastic deformations. The results, investigations and discussion of this behaviour can be found in Section 0

For simplicity, the elastic structural response model is used for the elasto-plastic global model since they show the same response for the considered load.

#### 4.4.3.4 SDOF system

When transforming the structure into a SDOF system it should be noticed that the deformation  $u$  is the same for the front column, roof beam as well as for the back column, see Figure 4.13. The system point for which the deformation is calculated by using a SDOF system is located at the free edge for both columns and in the centre of the concentrated mass for the roof beam.

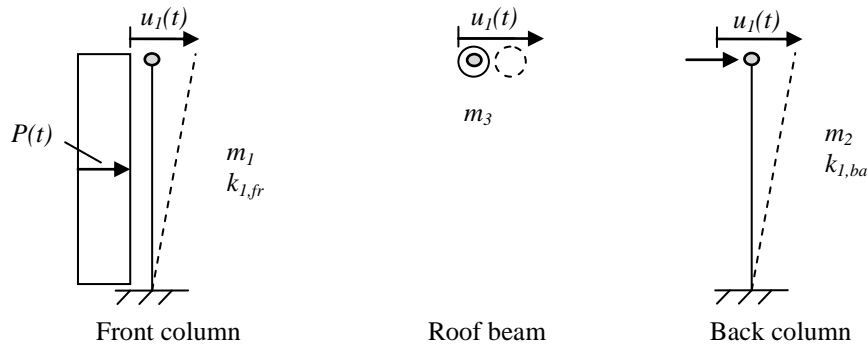


Figure 4.13 Position of the system point which is represented by the grey point. Deformation in the system point is the same for all members in the frame structure.

In the global analysis, each member of the frame contributes, in a certain degree, to the total response of the structure. Thus, the equation of motion can be described as the sum of the contributions from each part of the frame adapted by using the appropriate transformation factors. The equation of motion for the global model can be expressed as

$$\sum_{i=1}^n (\kappa_m m)_i \ddot{u} + \sum_{i=1}^n (\kappa_k k)_i u = \sum_{i=1}^n (\kappa_F P(t)) \quad (4.10)$$

where  $n$  is the number of the members in the structure.

When the model and the assumptions for the SDOF system are made, the transformations factors can be introduced. The transformations factors, together with the input data for the mass and stiffness used in the SDOF calculations for the elastic response are presented in Table 4.6. The calculations of these parameters can be found in Section E.1. The transformation factor for the mass of the roof beam is 1.000, but the transformation factors for the stiffness and force are put to zero since the roof beam is connected with hinges to the columns and does not restrain the movement of the frame in any way.

Table 4.6 Mass, stiffness and transformation factors used for the elastic model.

Part	$\kappa_m$ [-]	$m$ [kg]	$\kappa_k = \kappa_F$ [-]	$I = I_{II}$ [ $10^{-4} \text{ m}^4$ ]	$k_I$ [kN/m]
Front column (1)	0.257	3 360	0.400	0.54	41.9
Back column (2)	0.236	3 360	1.000	0.54	15.7
Roof beam (3)	1.000	7 200	0	0.54	0

#### 4.4.4 Combination of the global and local SDOF model

So far, the calculation method for the resulting deformation has been introduced separately for the local, initial, response and for the global response. For the local response the system point is located in the mid span of the front column and the deformation at the top of the column is neglected. For the global response, the system point is placed at the top of the column, where the biggest deformation is obtained. In order to obtain the actual deformation in the middle of the front column, a combination of the two models is made in this point.

For statically loaded structures, the magnitude of deformation in each point of the structure can be calculated. Recalling from the elementary case, the deformation at the free edge of a cantilever,  $u_1$ , shown in Figure 4.14, is described as

$$u_1 = \frac{qL^4}{8EI} \quad (4.11)$$

The deformation  $\alpha u_1$  at the distance  $a$  from the fixed edge is described as

$$\alpha u_1 = \frac{qa^2L^2}{24EI} \left( 6 - \frac{4a}{L} + \frac{a^2}{L^2} \right) \quad (4.12)$$

When the distance  $a$  is equal to  $L/2$ , the deformation can be further expressed as

$$\alpha u_1 = \frac{17qL^4}{384EI} \quad (4.13)$$

By a comparison of the deformations at the free edge and in the middle of the column, the factor  $\alpha$ , describing the relation of those two deformations is received as

$$\alpha = \frac{17}{48} \quad (4.14)$$

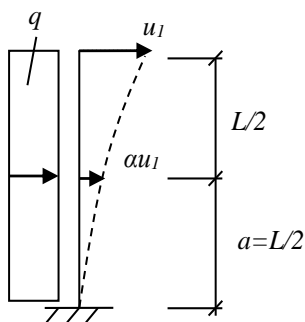


Figure 4.14 The deformation in the middle of the column is a factor  $\alpha$  times the deformation at the free edge.

The deformation in the middle of the column in the frame structure,  $u_{2,tot}(t)$ , can be described as the sum of the local deformation  $u_2(t)$  and the deformation, for the same point, in the global model,  $\alpha u_1(t)$ . This concept is presented in the Figure 4.15 and can be expressed as

$$u_{2,tot}(t) = u_2(t) + \alpha u_1(t) \quad (4.15)$$

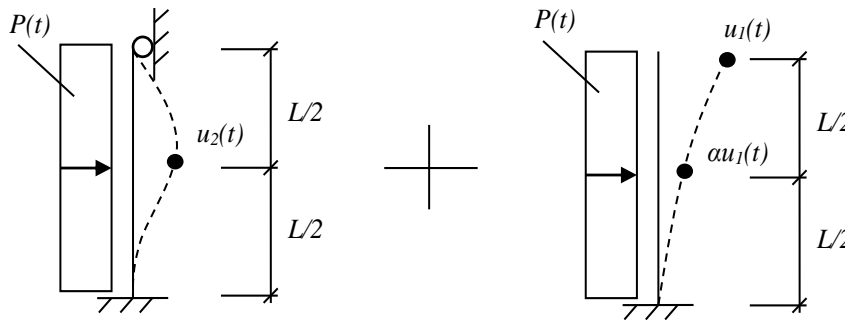


Figure 4.15 The total deformation in the middle of the front column for the frame can be approximated as the sum of the deformation of the local response and the global response in that point.

## 4.5 Modelling in ADINA

The FEM-analyses are conducted in the program ADINA (2011). When choosing the methods of modelling in this program, the recommendations from previous Master's Theses are followed. This subject is not studied in depth in this Master's Thesis, as the main focus is to adapt the SDOF system to the response of the frame structure. The input files for the elasto-plastic frame model is presented in Section H.1.

When performing the dynamic analyses, two methods with two integration schemes are available. One is implicit, where Newmarks's constant-average-acceleration method with  $\delta=0.5$  and  $\alpha=0.25$ , is used. The other method is an explicit method, which is a special case of Newmark's method for which  $\delta=0.5$  and  $\alpha=0$ . The solution for this method is stable and delivers reliable results only when a sufficiently small time step is provided. This means that the chosen time step should not be larger than a certain critical time step, according to Bathe (1996). One example, for which this method is used, is the central difference method, explained in Appendix D. This method is beneficial to use for the central difference method as the explosion pressure increases almost instantaneously, within a very short time span, which provides very short time steps. Moreover the central difference method works well when the lumped mass is introduced (Bathe (1996)), which fits the principles of the SDOF system method. Carlsson and Kristensson (2012) have proved that the dynamic analysis which employs the implicit method provides results in agreement with the results obtained from the hand calculations. The explicit method, on the other hand, delivers a solution which differs in both magnitude and frequency. These are the reasons which govern the implicit method in the FE analysis and explicit method in the SDOF system.

For both models, local and global, 2D beam elements with three integration points along the height of the cross section are used, Figure 4.16.



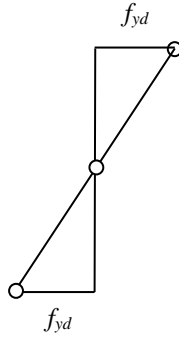


Figure 4.16. Stress distribution in ADINA for three integration points according to Augustsson and Härenstam (2010).

In order to simulate different behaviour of reinforced concrete and assure more comprehensive understanding of such a complex material, two material models are studied in ADINA. The first model is an elastic isotropic material model, which simulates the response before the yielding strength of the material is reached. The second model is an elasto-plastic bilinear material model.

The input parameters for the elastic and elasto-plastic material model is equivalent to Young's modulus,  $E_{II}$ , which is calculated as

$$E_{II} = \frac{I_{II}}{I_{I,a}} E_I = \frac{0.54 \cdot 10^{-4}}{0.64 \cdot 10^{-4}} \cdot 33 = 2.70 \text{ GPa} \quad (4.16)$$

where  $I_{II}$  is the moment of inertia for the cracked section presented in Table 4.3 and  $I_{I,a}$  is the moment of inertia for the uncracked section calculated according to Section E.1.  $E_I$  is Young's modulus in the state I which can be found in Table 4.1.

Moreover, for the elasto-plastic material model a yield limit must be introduced. In case of 2D beam elements with three integration points, where the stress varies linearly across the section, the fictional yield stress is calculated according to Figure 4.16 as

$$f_{yd} = \frac{M_{rd}}{W_{el}} = \frac{37.8 \cdot 10^3}{(1.0 \cdot 0.2^2) / 6} = 5.68 \text{ MPa} \quad (4.17)$$

where  $M_{rd}$  is the moment capacity of the section found in Table 4.4 and calculated according in Section E.1 and  $W_{el}$  is elastic section modulus.

When discussing the elasto-plastic material model, it is worth to mention that ADINA has difficulty to find a solution for the same time step size as used for the elastic material model. Thus, for the elasto-plastic analysis it is reasonable to increase the number of time steps.

Modelling with elasto-plastic material makes the analysis more complicated and demanding. However, by implementing this model, the results, in good agreement with the real behaviour of concrete structures, are obtained.

For the local response, the beam with restrains according to Figure 4.6 is modelled. The number of elements is chosen as 30. For the global analysis a model of the frame structure where all members are divided into 30 elements is used. For the frame

model, the connections between the columns and the roof beams are modelled as rigid links. Rigid links provide a restraint between the master node (node at the top of the column) and slave node (node at the edge of the roof beam). When the structure is subjected to loading, the nodes are displaced. The slave node translates so that its distance to the master node is constant. The rotation of the slave node is the same as the rotation of the master node, according to ADINA manual. In general, the introduction of rigid links, where only translations are allowed, provided a connection that corresponds to the restrains for a simply supported element.

## 4.6 Results of the elastic model

### 4.6.1 Local elastic model

The local elastic front column with corresponding material model is shown in Figure 4.17. The results obtained from the SDOF calculations, hand calculations and the analysis in ADINA agrees well which can be seen in Figure 4.18. Thus it can be stated that the methodology proposed in Johansson (2013) for the local elastic response is reliable. The hand calculations can be found in Section E.2.

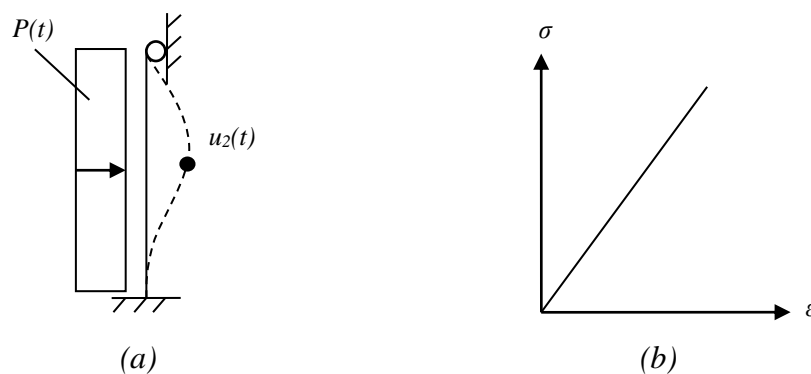


Figure 4.17 Illustration of: (a) the local SDOF and FE model as well as the deformation  $u_2(t)$ ; (b) the elastic material response model.

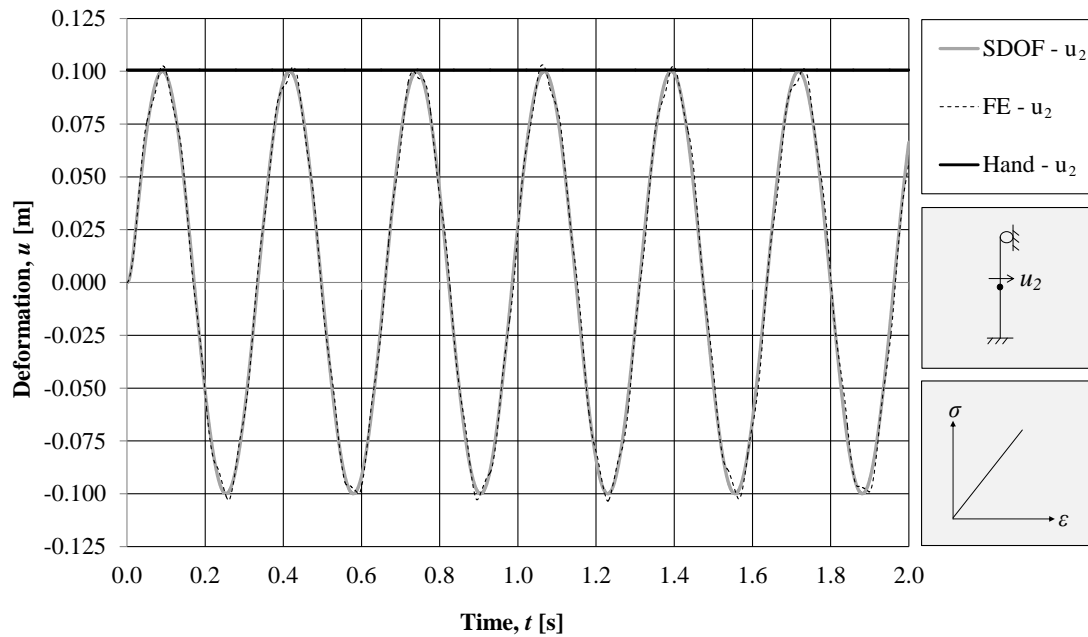


Figure 4.18 The deformations obtained in the local analysis of the frame subjected to an impulse load of 60 kPa and 0.025 s. Both the material and the structural response are elastic.

It can be noticed that the SDOF system provides a smooth curve which is not fully the case for the curve from the FE analysis. The reason for the unevenness in the FE analysis is the fact that ADINA considers several bending modes. The SDOF system, on the other hand, only uses the first bending mode, see Section 2.9.1.

The hand calculations, which can be found in Section E.2, give a very close estimation of the maximum deformations obtained in the SDOF and FE calculations. This implies that the load can be seen as a characteristic impulse load for this structure. The  $\gamma_I$ -value is equal to 1.0, meaning that the hand calculations do not need to be modified.

## 4.6.2 Global elastic model

The global SDOF model and the elastic material response model are shown in Figure 4.19. The elastic deformations of the global model obtained with the SDOF model, the FE analysis and the hand calculations can be seen in Figure 4.20. The hand calculations can be found in Section E.2.

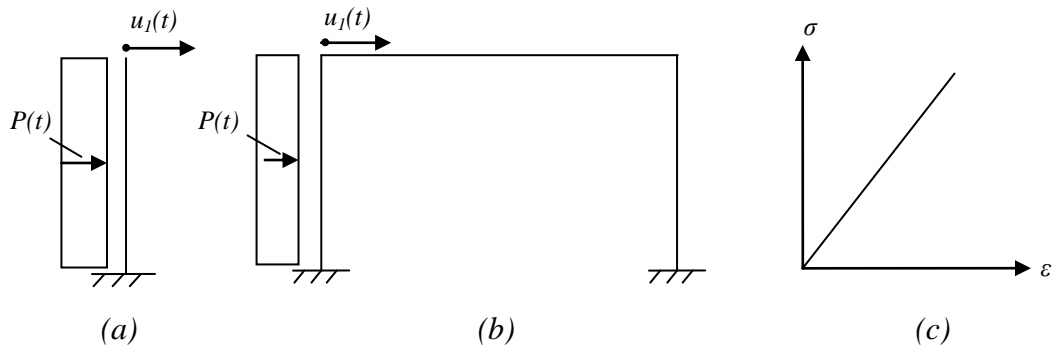


Figure 4.19 An illustration of: (a) the global SDOF model and the deformation  $u_1(t)$ ; (b) the global FE model and the deformation  $u_1(t)$ ; (c) the elastic material response model.

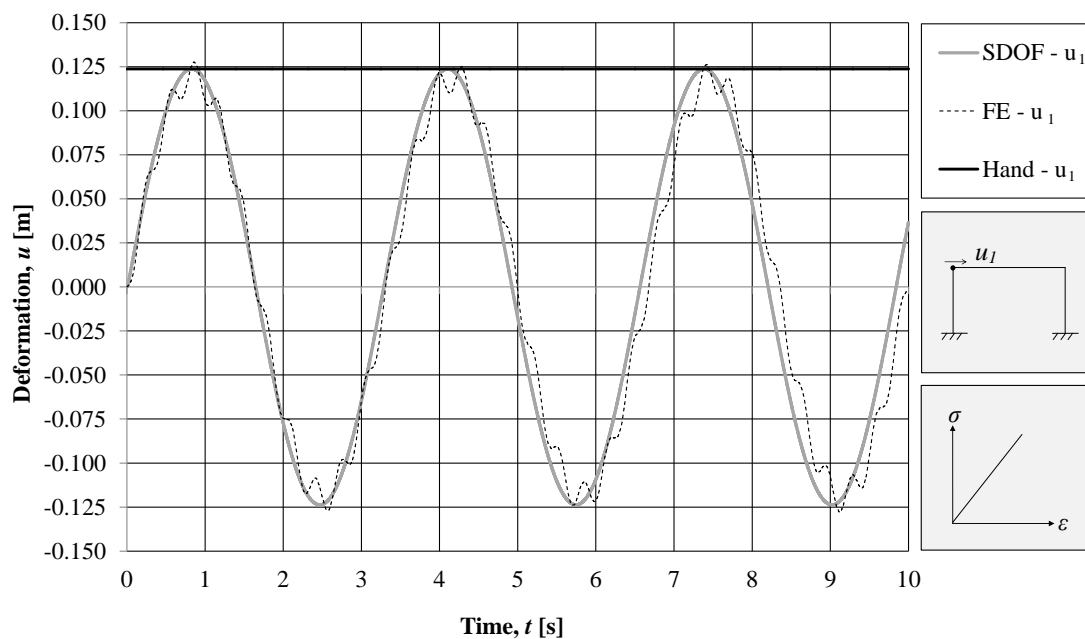


Figure 4.20 The deformations obtained in the global analysis of the frame subjected to an impulse load of 60 kPa and 0.025 s. Both the material and the structural response models are elastic.

The magnitude of the deformations agrees well for the FE model, the SDOF model and the hand calculations. Since the hand calculation agrees well, the load can be seen as a characteristic impulse load for this structure. It can be noticed that the SDOF solution shows a slightly higher frequency than the FE analysis. The unevenness in the FE analysis is due to that ADINA considers several bending modes while the SDOF model considers only first one.

### 4.6.3 Combination of the local and global elastic model

When comparing the local and global elastic models, Figure 4.21, some differences can be found. The frequency for the local model is about ten times larger than for the global model. This means that for each sway of the whole frame, the front column manages to sway ten times. This is a consequence of the higher mass and lower

stiffness of the global model. In Section E.2.1 the calculations of the frequency for both cases can be found.

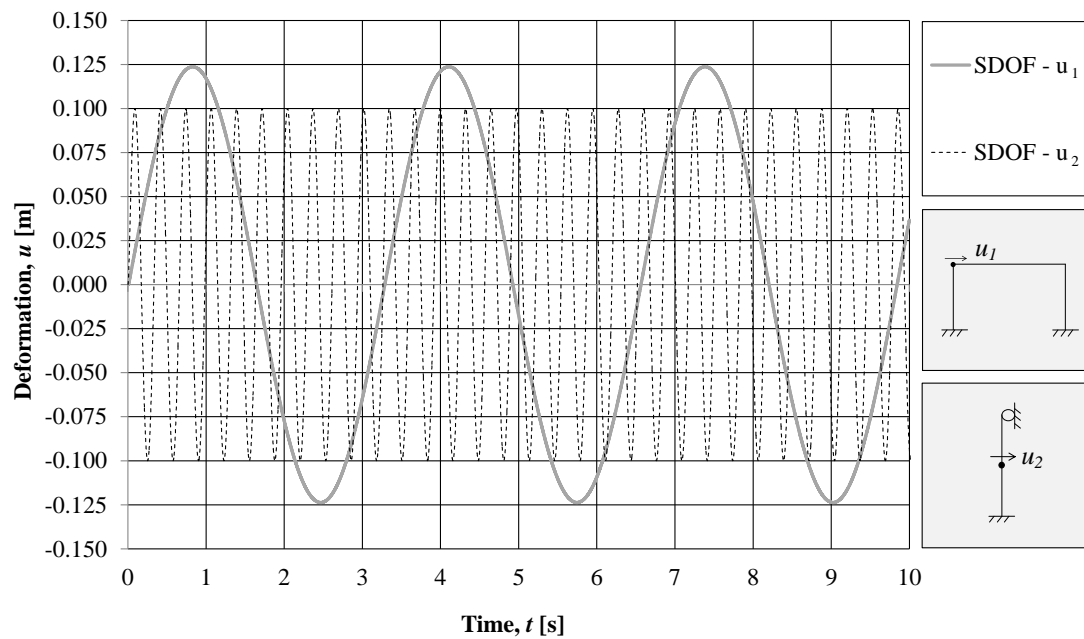


*Figure 4.21 The local and global deformations obtained from the SDOF models when the frame is subjected to an impulse load of 60 kPa and 0.025 s. Both the material and the structural response models are elastic.*

The local model aims to simulate the response in the initial stage of the loading when the displacement of the top of the column is relatively small, which can be seen in Figure 4.21. Thus, the support at the top of the local model can be seen as simply supported and the simplification of the local model should be realistic.

The response in the middle of the front column when combining the global and local SDOF model is presented in Figure 4.22. The combination of the SDOF models is carried out according to Section 4.4.4. The corresponding deformation obtained in the FE analysis is shown in Figure 4.23.

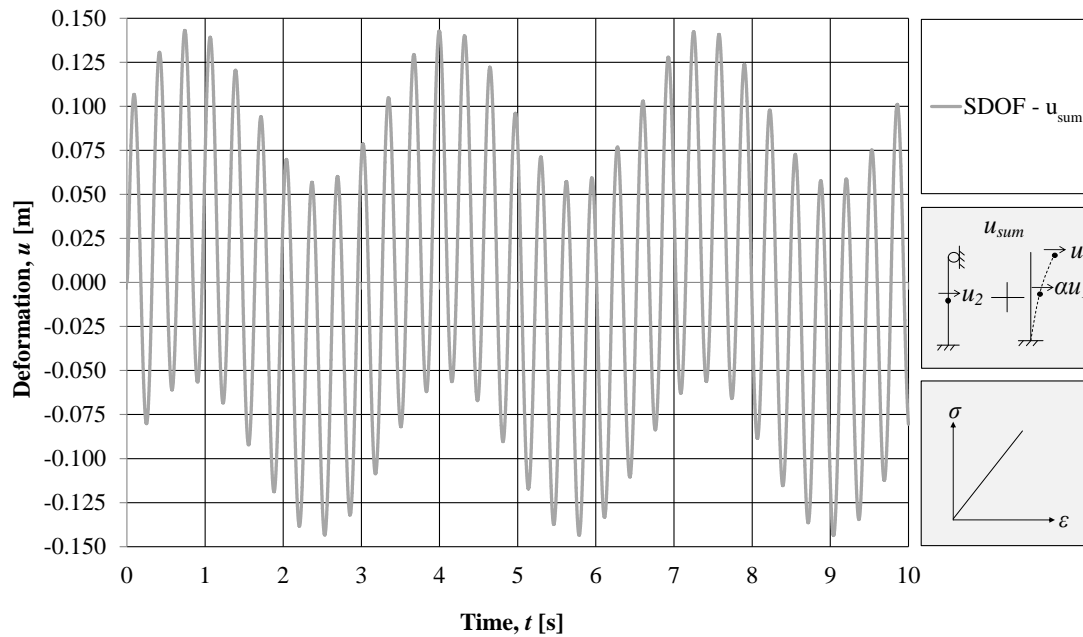


Figure 4.22 A combination of the local and global deformations due to an impulse load of 60 kPa and duration of 0.025 s. Both the material and the structural response models are elastic.

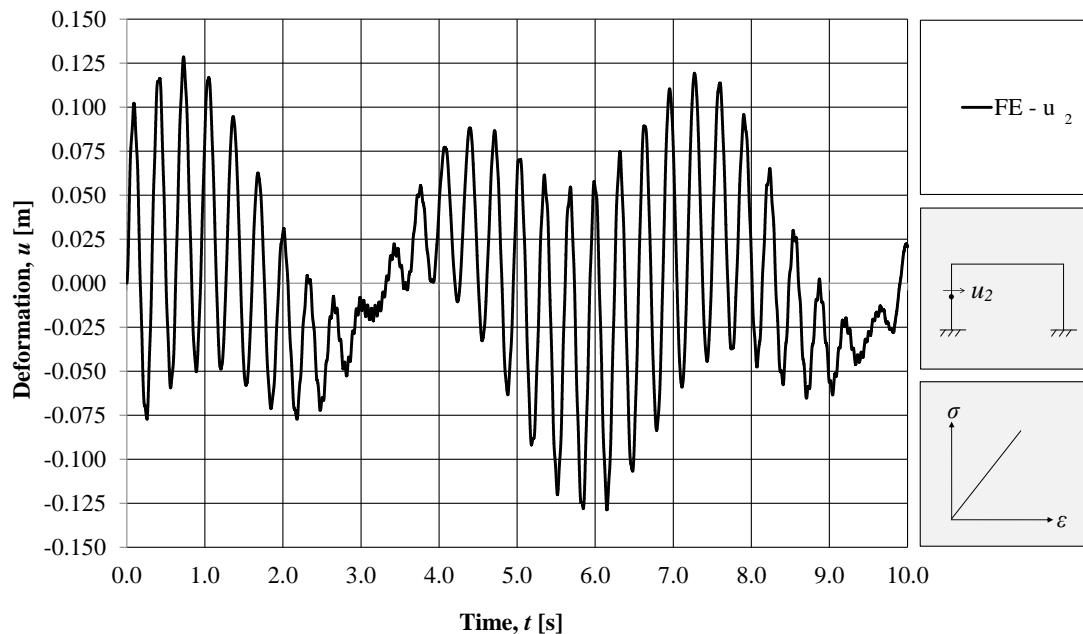


Figure 4.23 The deformations,  $u_2$ , obtained in the FE analysis for the considered impulse load of 60 kPa and duration of 0.025 s. Both the material and the structural response models are elastic.

When comparing the results obtained by implementing these two methods, Figure 4.24, the magnitude of the deformation as well as the frequency seems to agree quite well. The SDOF model provides results on the safe side and the combined SDOF method presented in Section 4.4.4 seems to give an approximate estimation of the behaviour in the middle of the front column. However, a significant difference in deformation magnitude is obvious at certain intervals. The difference can for example

easily be spotted between 2 and 5 seconds where the FE model shows a decrease in magnitude while the SDOF model does not. It seems that the FE structure possesses some damping which decreases the magnitude of the deformation at certain intervals. This phenomenon is not investigated further in this Master's Thesis since it is assumed not to be critical for the structure.

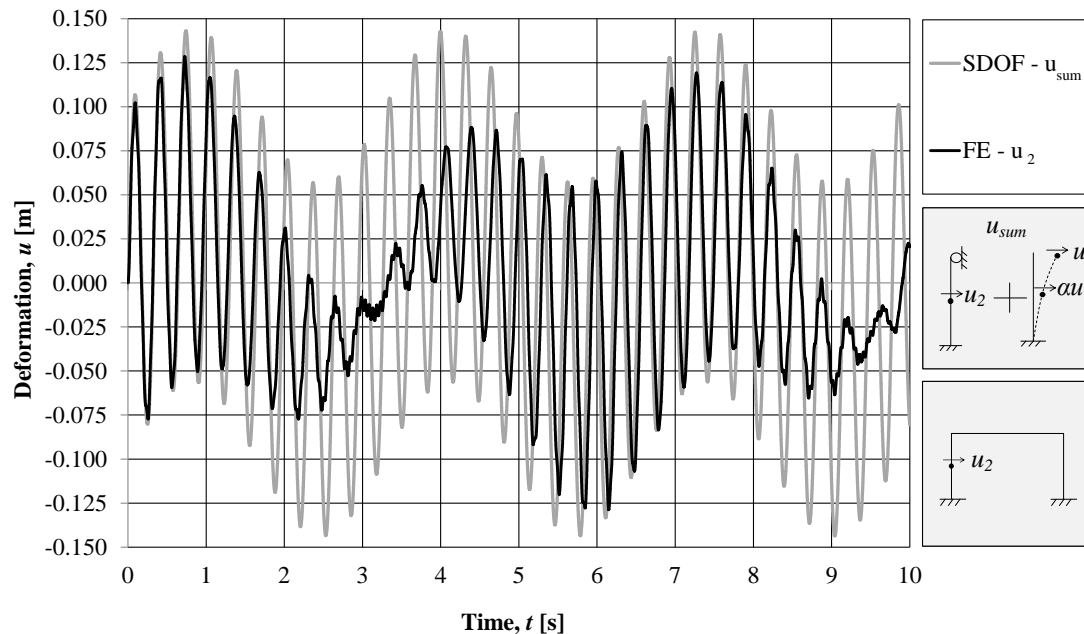


Figure 4.24 The deformations obtained from the SDOF system and FE modelling in the global analysis for the middle of the front column. Both the material response and structural response are elastic.

## 4.7 Results of the elasto-plastic model

### 4.7.1 Local elasto-plastic model

#### 4.7.1.1 Response of the structure

The elasto-plastic model, shown in Figure 4.25, proved to be more complicated than the elastic model. The development of the deformation over time for the impulse loaded front column obtained in the FE analysis and SDOF system is presented in Figure 4.26. The hand calculations can be performed in different ways and are further described in Section 4.7.1.2.

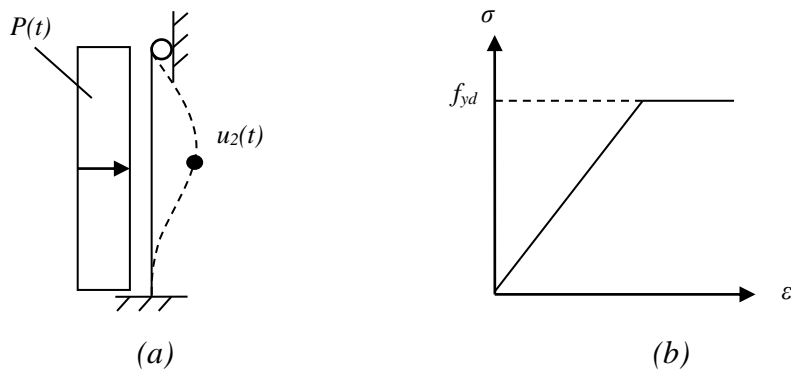


Figure 4.25 Illustration of (a) the local SDOF model and the deformation  $u_2(t)$ , and (b) the elasto-plastic material response model.

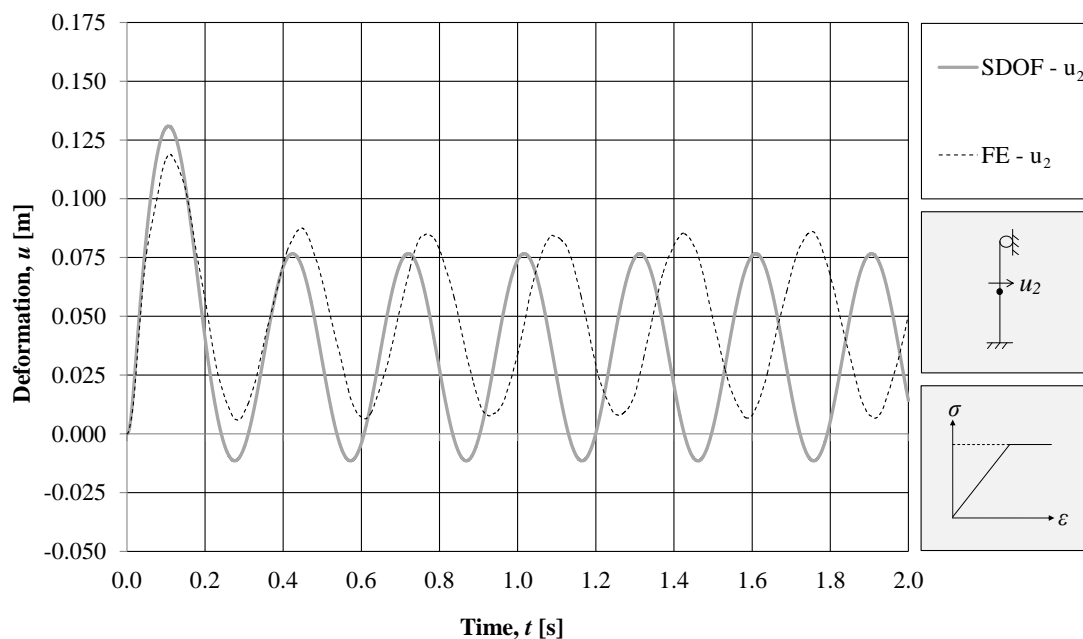


Figure 4.26 The deformations obtained in the local analysis of the frame subjected to an impulse load of 60 kPa and 0.025 s. Both the material and the structural response are elasto-plastic.

The studied front column shows elastic response at the beginning of the loading. After the yield strength has been reached the deformation becomes plastic until the structure starts to sway back again. The following oscillations are elastic but since the column has gained some plastic deformation, the structure will oscillate elastically at a higher position in the graph.

The overall shape of the deformation curve is the same in the FE analysis as in the SDOF calculations. However, some differences in magnitude of deformation and frequency are obvious. The reason for the differences may lie in the choice of transformation factors in the SDOF model. For both the plastic and elastic part of the SDOF response model, plastic transformation factors have been used. A solution to this problem could be to vary the transformation factors in time with transformation factors obtained from the FE analysis, proposed by Andersson and Karlsson (2012). This has however not been evaluated in this Master's Thesis.

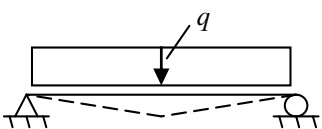
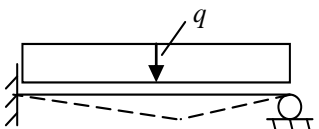
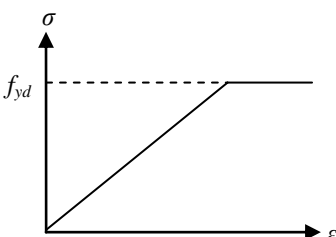
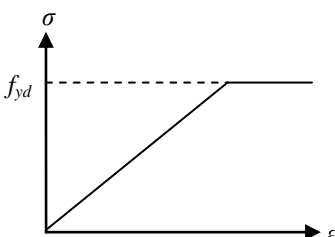
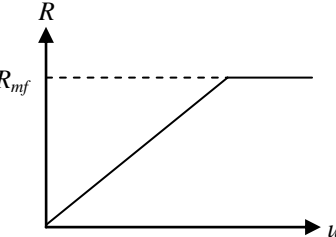
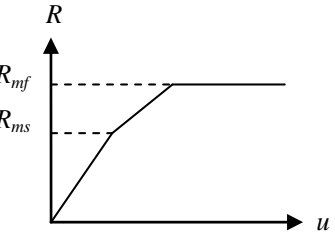


The most evident difference comparing the response of the studied front column to the response of a simply supported beam is the higher magnitude of deformation at the first peak.

This study has shown that the structural and material response models do not always have the same shape. To use the same shape is correct for studies of simply supported beams where both the structural and material models are bilinear. However, for the studied column, with one fixed edge and one simply supported, the material model is bilinear while the structural response model has been proven to be trilinear. This is due to the fact that the local front column can develop two plastic hinges, one at the fixed support and one in the span.

A compilation of the material response models and the structural response models for the two types of beams are presented in Table 4.7. In order to understand the theory of plasticity and plastic hinges, the reader is referred to Section 2.5.

*Table 4.7 A summary of the material response models and structural response models for a simply supported beam and a beam with one edge fully fixed and the other simply supported.*

Support conditions		
Material response model		
Structural response model		

The structural response model of the front column subjected to the considered impulse load is presented in Figure 4.27. The development of resistance over time is illustrated in Figure 4.28 where the stiffness and plastic hinges are described in Table 4.8. The resistance follows the arrows until the end of the line where they start to oscillate elastically. The response model used for the SDOF model is programmed in Matlab according to Appendix D with the corresponding response model described in

Section D.3.4. The concept of impulse loaded structures with a trilinear response model is described in Section C.3.

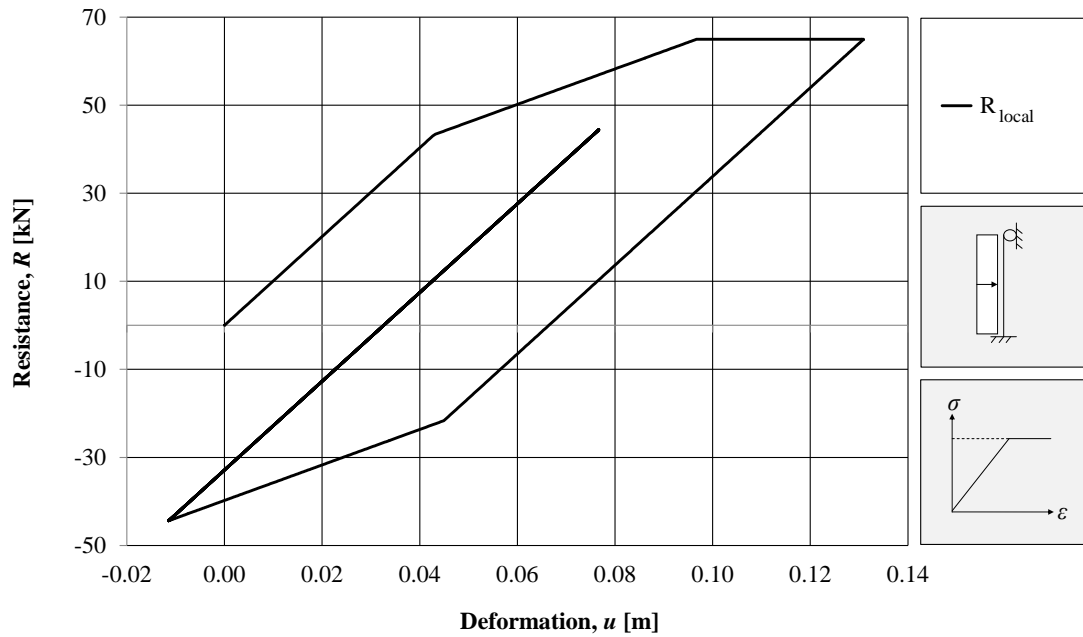


Figure 4.27 Structural response of the local frame model subjected to an impulse load of 60 kPa and 0.025 s in the SDOF analysis. Both the material and the structural response are elasto-plastic.

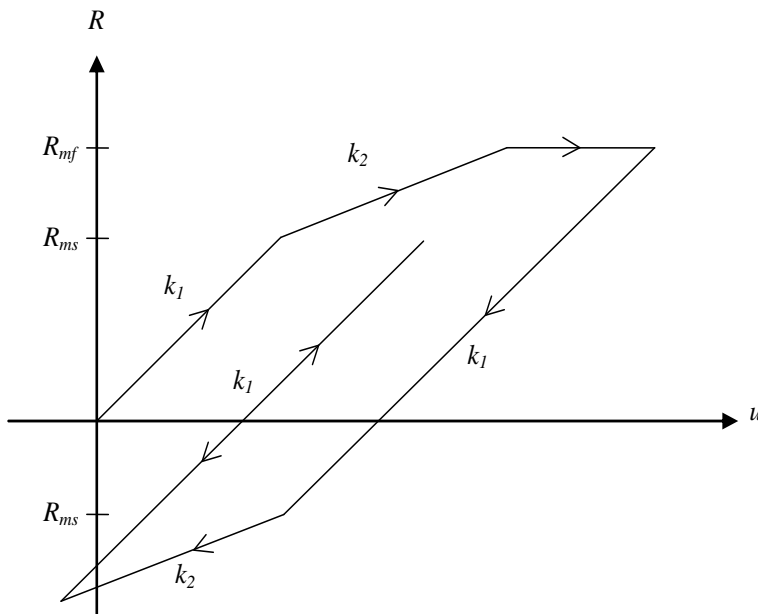


Figure 4.28 Illustration of the response of the local frame model. The arrows indicate the development of resistance and deformation,  $R(u)$ , over time. When the end of the line is reached the deformation starts to oscillate elastically.

Table 4.8 Description of the notations in Figure 4.28.

Notation	Description
$k_1$	Stiffness of the local front column with one fixed edge and one simply supported.
$R_{ms}$	Plastic hinge formed at fixed support. Stiffness of beam is changed to $k_2$ .
$k_2$	Stiffness for a simply supported beam.
$R_{mf}$	Plastic hinge formed in the span. Ultimate resistance is reached.

The studied front column is a statically indeterminate structure since it develops two plastic hinges in ultimate limit state. Each change of inclination in the structural response curve corresponds to reaching the maximum resistance at a certain critical section, as described in Section 4.4.2.3. The first change of stiffness simulates developing maximum capacity at the fixed support. For the studied structure this happens at a value of 43.3 kN. The second hinge occurs in the span and ultimate resistance for the whole structure is reached at 65 kN, see Figure 4.27.

After both the fixed support and the span have yielded, the deformation increases further while the resistance is constant. An increase in deformation after reaching the maximum resistance is possible since the structure has a certain plastic rotation capacity. When the structure starts to sway back, before reaching the ultimate plastic deformation, the structure has a stiffness corresponding to  $k_1$ . After a certain point, yielding at the fixed support occurs in the opposite direction and the stiffness changes to  $k_2$ . At the point where the structure switches direction of swinging again, at a resistance of -38 kN, the structure begins to oscillate back and forth, following this line with a stiffness of  $k_1$ .

#### 4.7.1.2 Hand calculations

Due to the trilinear response model of the local front column, there are different ways of performing the hand calculations. The main concept of estimating the deformations are described in Section A.2.

The elasto-plastic estimation of the deformation  $u_{ep}$  can be calculated according to equation (4.18).

$$u_{ep} = u_{ep,el} + u_{ep,pl} = \frac{R_m}{2k} + \frac{I_k^2}{2mR_m} \quad (4.18)$$

where  $I_k$  is the characteristic impulse load,  $m$  and  $k$  is the mass and stiffness and  $R_m$  is the resistance.

However, this equation is created for a bilinear case and therefore the stiffness has to be estimated for the trilinear case. Two extreme cases are created according to Figure 4.29 where the stiffness is taken as the stiffness for a beam with one fixed edge

and one simply supported  $k_1$ , as well as the stiffness,  $k_3$ . The stiffness that would give the correct results should lie in between these values.

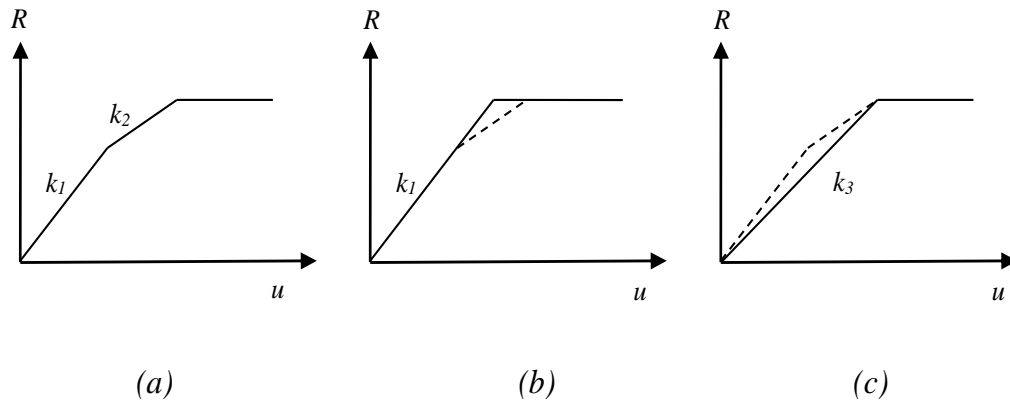


Figure 4.29 (a) Stiffness of the elasto-plastic local front column. (b) Simplified bilinear case with stiffness  $k_1$  (continuous line). (c) Simplified bilinear case with stiffness  $k_3$  (continuous line).

The non-modified values of the hand calculations together with the SDOF calculations and FE analysis in are shown in Figure 4.30. The hand calculations can be found in Section E.3.1. Since the true value should lie in between the lines it can be seen that the estimation correspond well with the SDOF calculations and is on the safe side of the FE analyses.

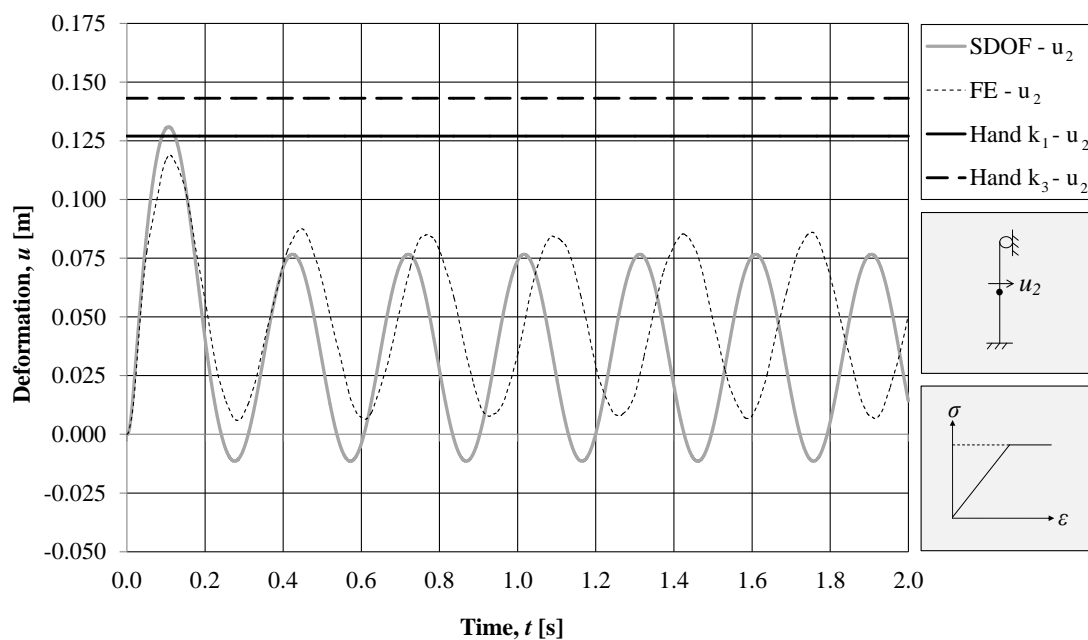


Figure 4.30 The deformations obtained in the local analysis, in the middle of the column, for the elasto-plastic case.

#### 4.7.1.3 Comparison of bilinear and trilinear response models

The true structural behaviour of the studied front column follows a trilinear response model. However, since a trilinear response model is more complicated than a bilinear,

a comparison is done in order to investigate the differences in the obtained deformation. All calculations in this comparison are carried out in Matlab R2013a and the SDOF models and response models are created according to Section E.3.

The bilinear model is created with a stiffness identical to the stiffness before any plastic hinge is formed,  $k_1$ . The ultimate resistance is the same as for the trilinear model,  $R_{mf}$ . The conceptual deformations and corresponding response models for the bilinear and trilinear case can be seen in Figure 4.31.

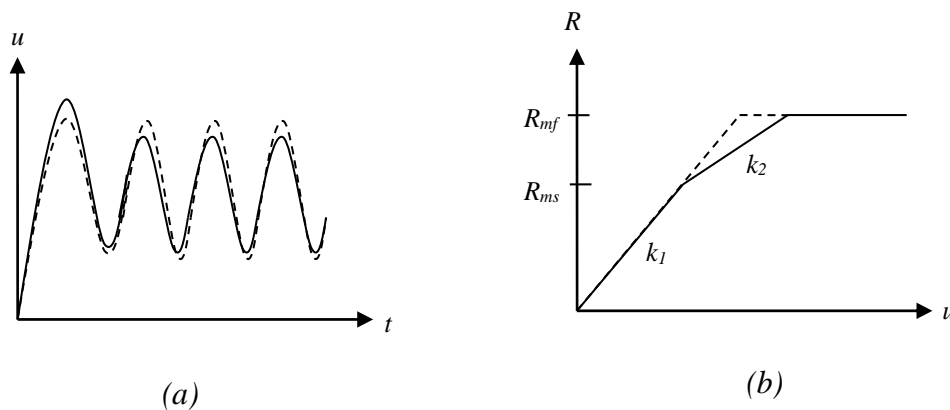


Figure 4.31 (a) Deformation for trilinear (continuous line) and bilinear (dashed line) response. (b) Trilinear and bilinear (dashed line) response models.

In order to further understand the behaviour of the two models, Figure 4.32 and Figure 4.33 shows the considered response models and resulting development of deformations in time for the two cases. The numbered points in the resistance-deformation curve corresponds to the same numbers in the deformation graph and the areas  $W_1$ ,  $W_2$ ,  $W_3$  and  $W_4$  refer to the work done when reaching the corresponding points. The areas  $W_1$  and  $W_2$  as well as  $W_3$  and  $W_4$  are equal, meaning that the internal work of the two pairs equalise each other.

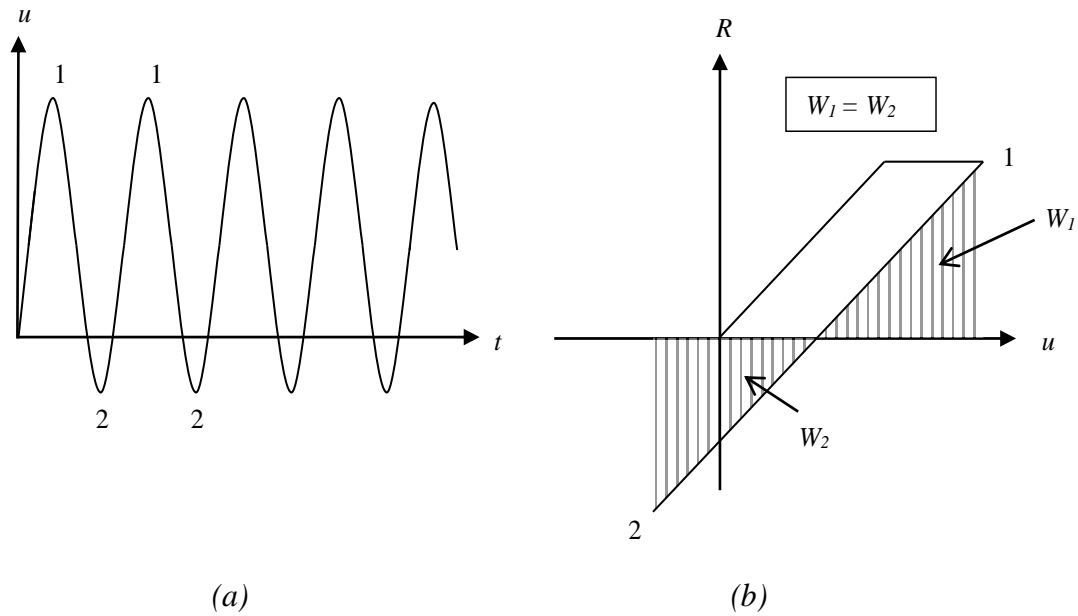


Figure 4.32 (a) Deformation in time; (b) Structural response for a bilinear response model. The numbered points on the resistance-deformation curve corresponds to the same numbers in the deformation graph.

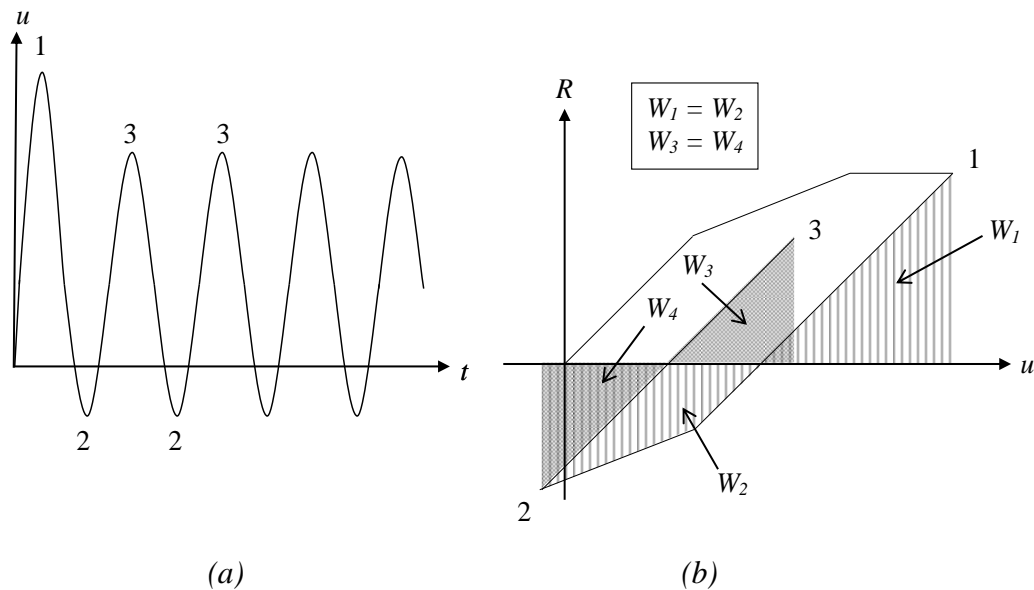


Figure 4.33 (a) Deformation in time; (b) Structural response for a trilinear response model. The numbered points on the resistance-deformation curve corresponds to the same numbers in the deformation graph.

The biggest difference between assuming a bilinear response model instead of a trilinear one is that the trilinear model results in a higher maximum deformation followed by elastic sways with a lower magnitude than the first one, see Figure 4.33a. In order to investigate how the deformation-time curve changes depending on the magnitude of the impulse load, and therefore the position in the resistance-deformation curve, a study is carried out for three different impulse loads shown in

Table 4.9. The position reached in the resistance-deformation curve for each load is marked with a black point in Figure 4.34.

Table 4.9 Loads investigated in order to compare bilinear and trilinear response models.

Magnitude, $P$ [kPa]	Duration, $t_I$ [s]
20	0.025
40	0.025
60	0.025

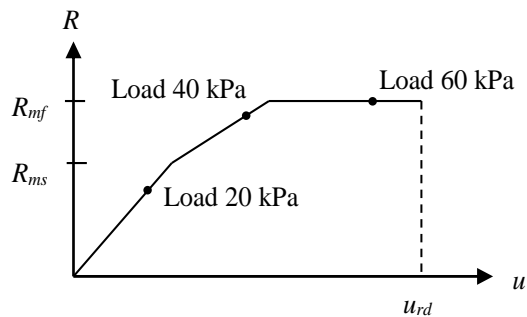


Figure 4.34 The maximum deformation in the resistance-deformation curve for the three different impulse magnitudes.

The resulting deformation for the three loads as well as the resistance-deformation curves obtained in the SDOF system, when employing the trilinear model are presented in Figure 4.35 and Figure 4.36, respectively. It can be noticed that the first deformation peak is higher than the following only for the two largest loads. The reason for this is explained in the following paragraphs.

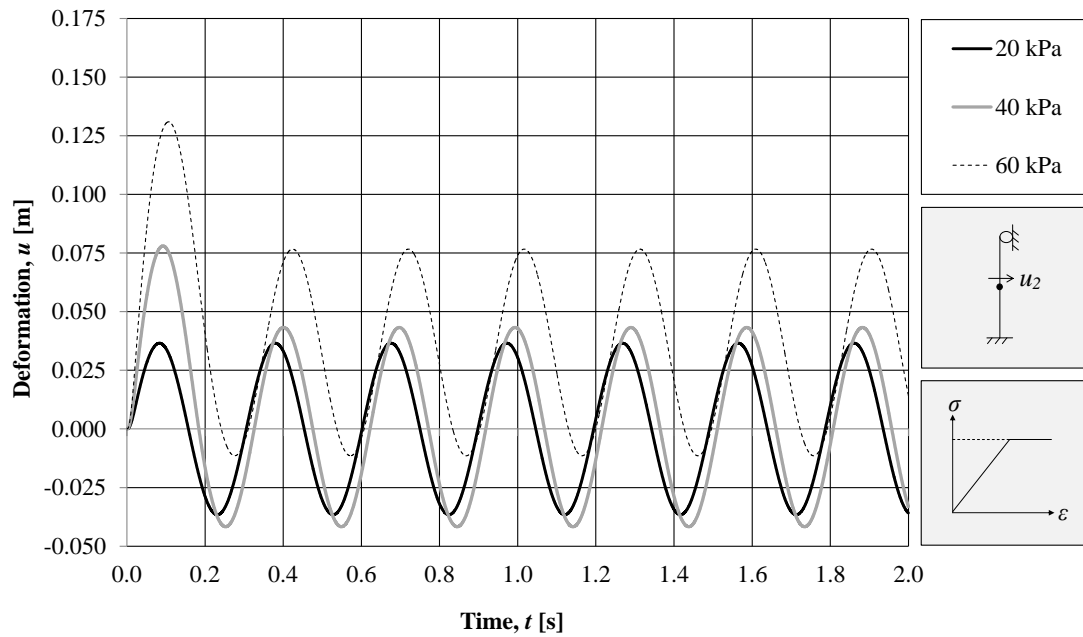


Figure 4.35 The deformations obtained for the three loads when the response model is trilinear.

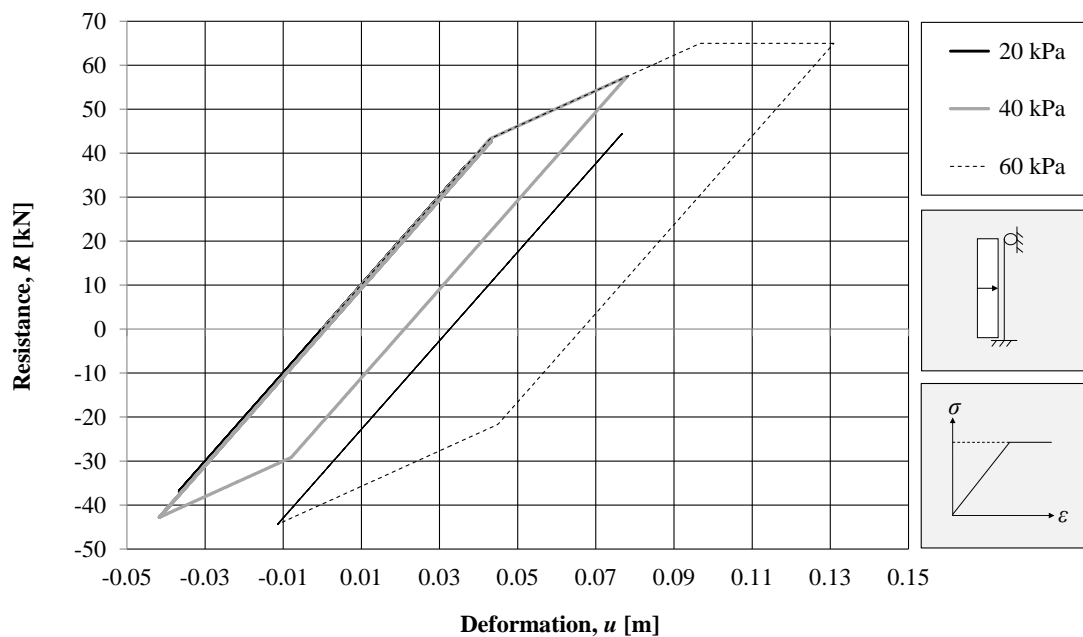


Figure 4.36 The resistance-deformation curves for the three loads when the response model is trilinear.

When the local column is subjected to an impulse load with a magnitude of 20 kPa and duration of 0.025 s, the deformations are completely elastic. In this stage the inclination of the first branch in the trilinear model coincides with the bilinear model, meaning that the stiffness, magnitude of deformation and frequency is equal for these two cases. This is illustrated in Figure 4.37 where the work is the same for both models and the area under the resistance curve for the trilinear model,  $W_t$ , coincides



with the area for the bilinear model,  $W_b$ . Also, the deformation in the bilinear model  $u_b$  is equal to deformation in the trilinear model  $u_t$ .

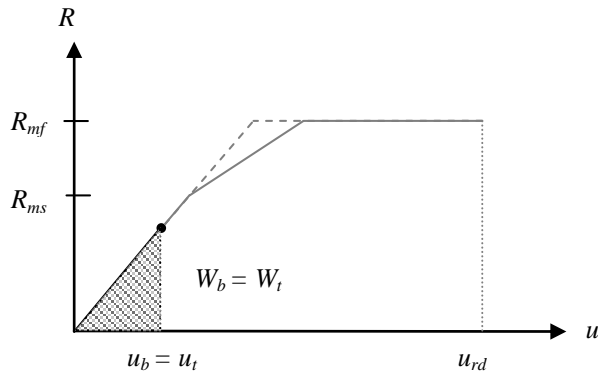


Figure 4.37 A comparison of a bilinear and trilinear response model for an impulse load with a magnitude of 20 kPa and duration of 0.025 s.

Thus, the shape of deformation in time and the resistance-deformation curve is the same for both models, see Figure 4.38 and Figure 4.39.

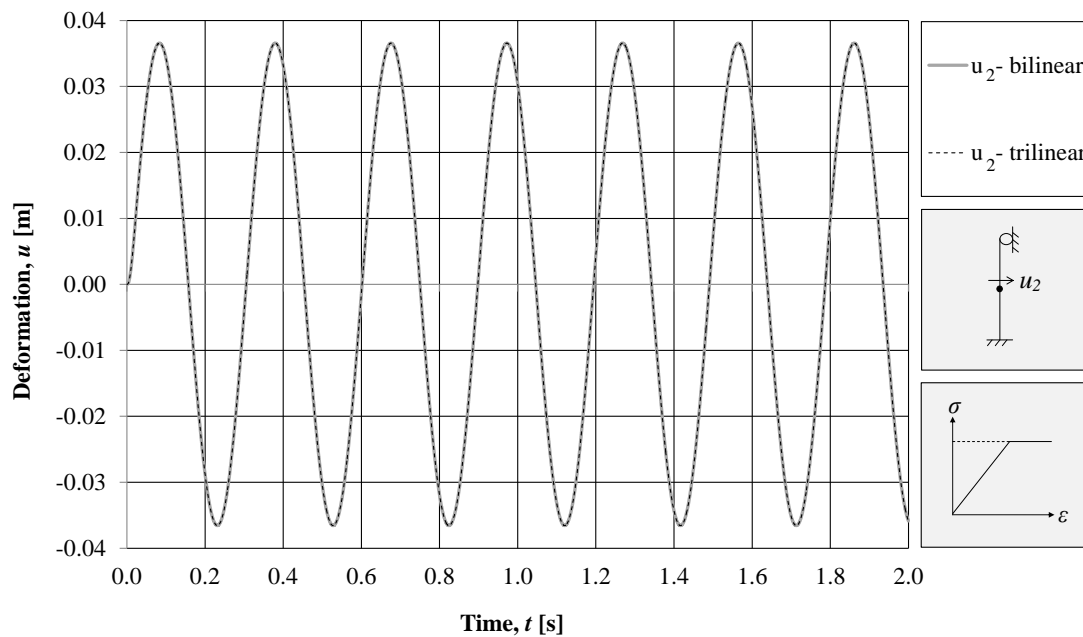


Figure 4.38 Comparison of deformation obtained by employing a trilinear and bilinear model for an impulse load of 20 kPa and duration of 0.025 s.

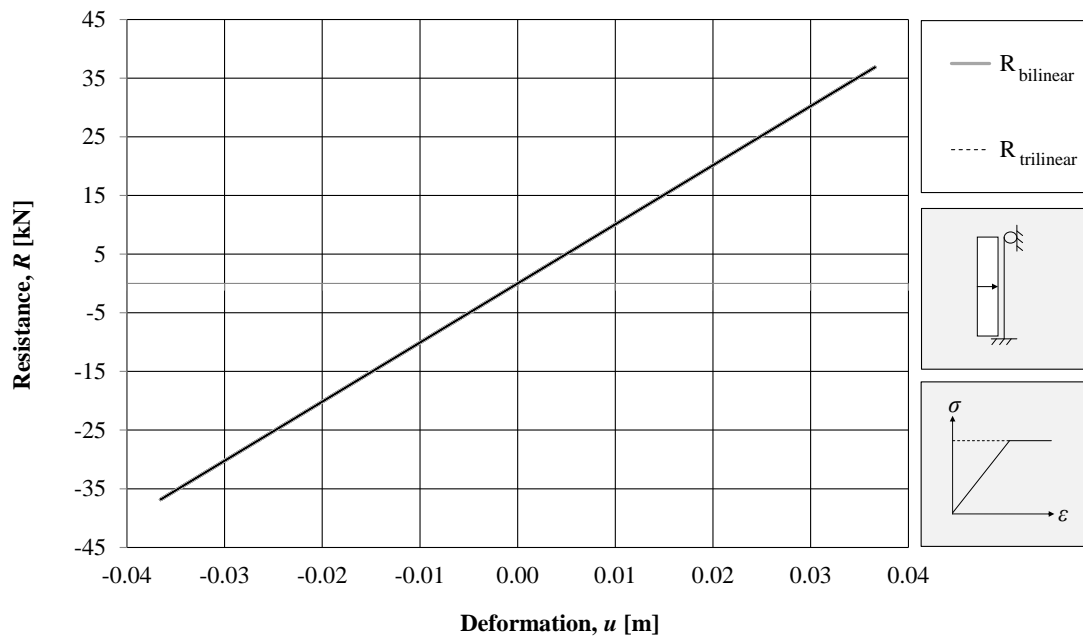


Figure 4.39 Comparison of resistance-deformation curves obtained by employing a trilinear and bilinear model for an impulse load of 20 kPa and duration of 0.025 s.

When the column is subjected to an impulse load of with a magnitude of 40 kPa and duration of 0.025 s, the resistance and deformation in the trilinear model reaches the second branch, i.e. the fixed support has yielded. At this stage the trilinear model differs from the bilinear. The work done by the structure and the area under resistance curve for the two models must be the same,  $W_t = W_b$ , given that the load is a characteristic impulse load. As a result of the different shapes of the resistance curves, the deformation for the trilinear model,  $u_t$ , is higher than for the bilinear model  $u_b$ , see Figure 4.40. This means that the deformation will be underestimated when employing the bilinear model. The stiffness at the maximum deformations is different for the two models, following that also the frequency is expected to differ.

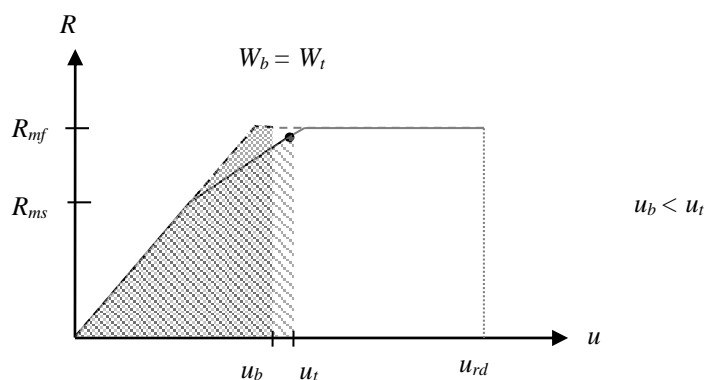


Figure 4.40 A comparison of the bilinear and trilinear response model for an impulse load with a magnitude of 40 kPa and duration of 0.025 s.

For an impulse load of 40 kPa, the resistance of the structure in the bilinear model has reached its ultimate value,  $R_{mf}$ , which can be seen in Figure 4.42. As the structure has

started to develop some plastic deformations, the resulting deformations oscillate at a higher position than its initial position, which can be seen in Figure 4.41. However, the structure simulated with a trilinear model has not reached its ultimate resistance, even though the fixed support has yielded and reached its resistance  $R_{ms}$ . The first deformation peak is higher for the trilinear model than for the bilinear in Figure 4.41, which agrees with the difference in deformations in Figure 4.40. However, the following elastic deformations are much smaller than the value reached in the first peak due to the shape of the response model.

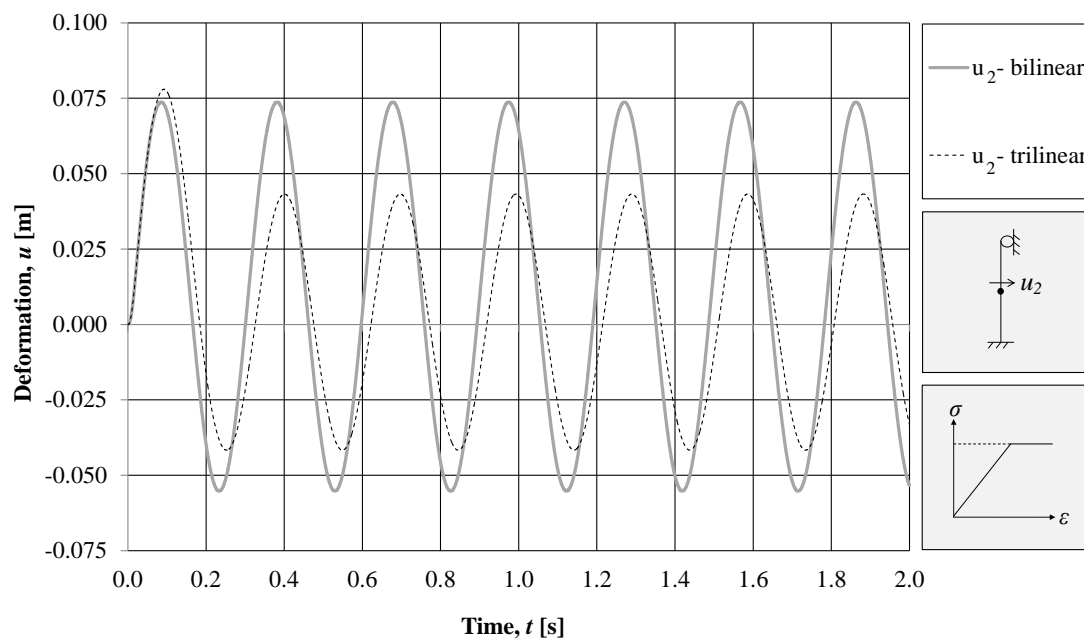


Figure 4.41 Comparison of deformations obtained by employing a trilinear and a bilinear model for an impulse load of 40 kPa and duration of 0.025 s.

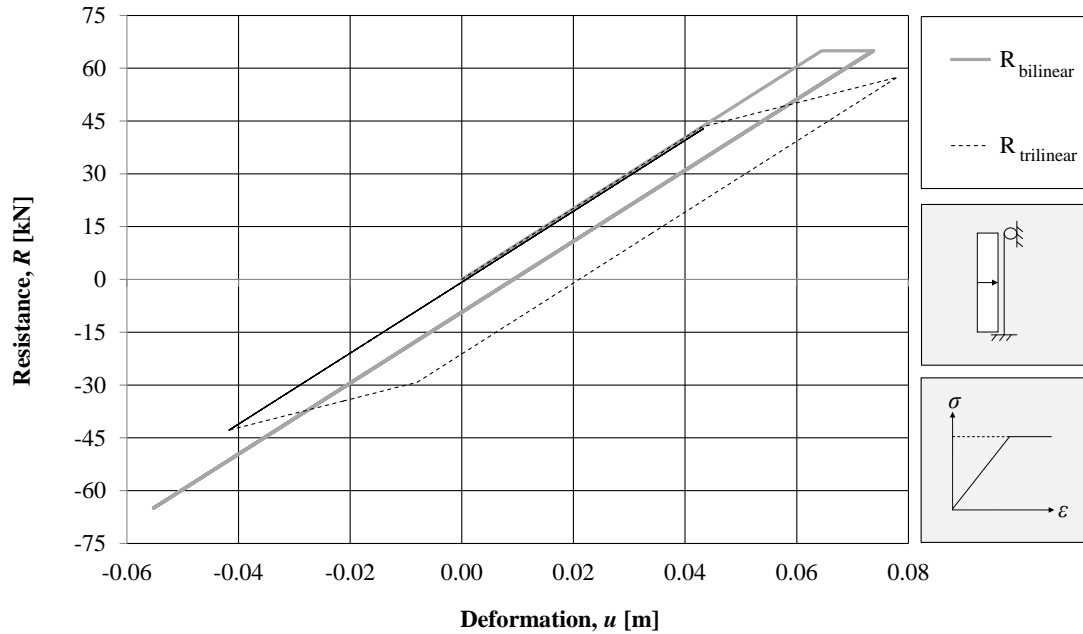


Figure 4.42 Comparison of resistance-deformation curves obtained by employing a trilinear and bilinear response model for an impulse load of 40 kPa and duration of 0.025 s.

For an impulse load of 60 kPa and duration of 0.025 s, the structure simulated with bilinear and trilinear models reaches their ultimate resistance,  $R_{mf}$ , see Figure 4.43. Similarly as for the impulse load of 40 kPa, the deformation obtained when using the bilinear model is underestimated.

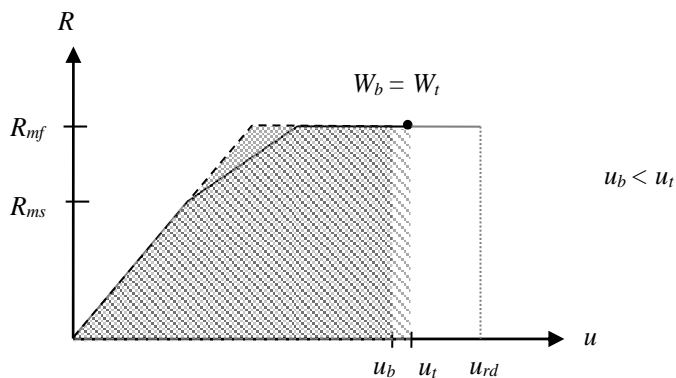


Figure 4.43 Comparison of a trilinear and bilinear response model for an impulse load of 60 kPa and duration of 0.025 s.

A comparison of deformations in time as well as the resistance–deformation curves for the two response models is presented in Figure 4.44 and Figure 4.45, respectively.

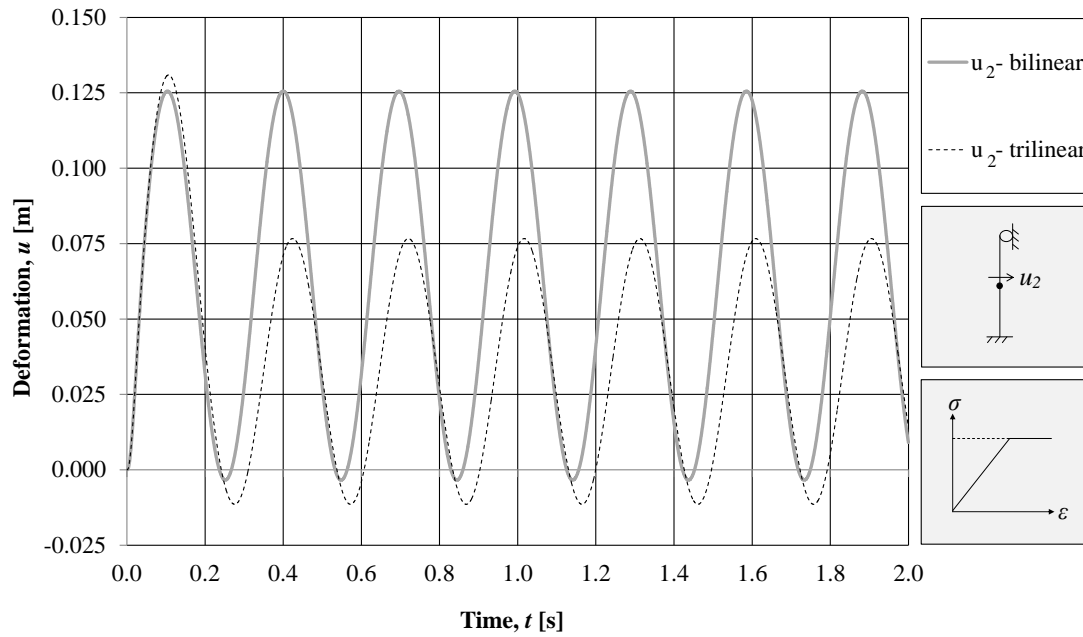


Figure 4.44 Comparison of deformation obtained by employing a trilinear and a bilinear response model for an impulse load of 60 kPa and duration of 0.025 s.

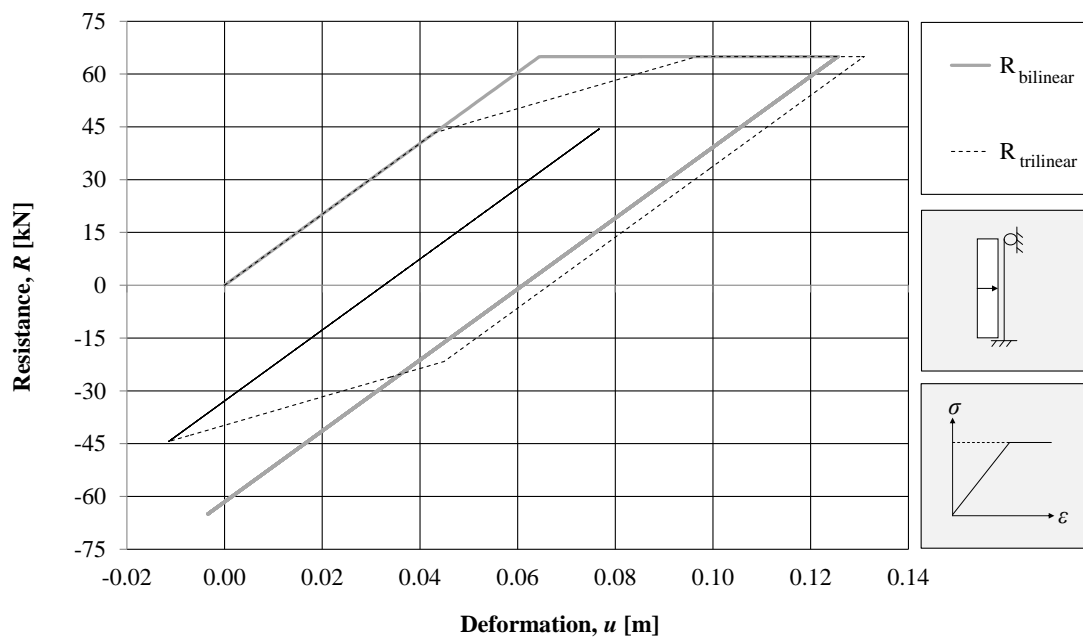


Figure 4.45 Comparison of resistance-deformation curves obtained by employing trilinear and bilinear response model for an impulse load of 60 kPa and duration of 0.025 s.

The fact that the magnitude of deformation is underestimated in the first sway when employing the bilinear model may be critical for the structure. If the deformation in the first sway exceeds the value of the ultimate plastic deformation,  $u_{rd}$ , the structure collapses. The bilinear model provides lower values of resulting deformation,  $u_b$ , due to the shape of the resistance-deformation curve which does not fully agree with the

deformation delivered by the more accurate, trilinear model,  $u_t$ . This difference is especially important for a structure provided with a low value of ultimate plastic deformation, see Figure 4.46. For the illustrated impulse load, the bilinear model indicates that the structure resists the load, while the trilinear model will lead to collapse. The difference between the area under the bilinear and trilinear response model is for this case relatively large compared to the total area of the work done by the structure.

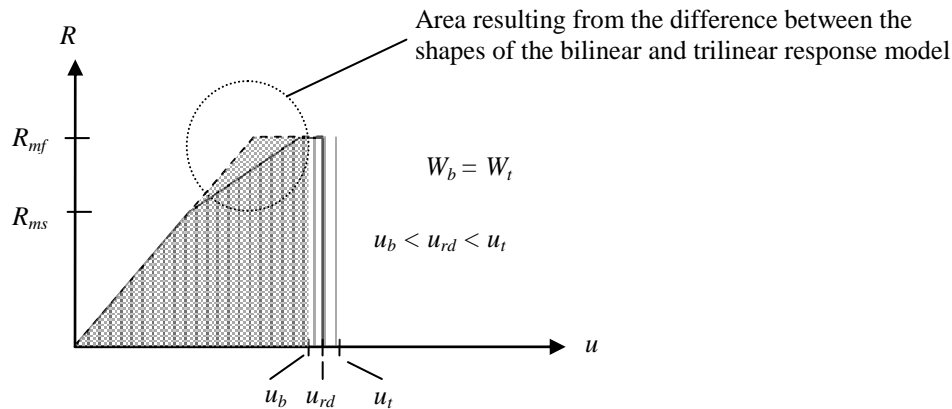


Figure 4.46 A comparison between the trilinear and bilinear model for a structure with a low value of plastic deformation capacity,  $u_{rd}$ . For the considered load, the trilinear model exceeds the critical value,  $u_{rd}$ , while the bilinear does not.

For the studied local, elasto-plastic front column the difference in obtained deformation between the trilinear and bilinear model is relatively small. Therefore the bilinear model can be considered to give an acceptable approximation of the deformation for the studied case. The concept of deformation capacity is further discussed in Section 4.7.1.4.

If the ultimate plastic deformation,  $u_{rd}$ , is large compared to the elastic deformation,  $u_{ep,el}$ , a large part of the internal energy,  $W_i$ , will be within the plastic part of the deformation,  $u_{ep,pl}$ . For this case, the bilinear model will give a satisfying approximation of the deformation.

A real structure provides a certain amount of natural damping, thus the true deformation will be a bit lower than the calculated. When the purpose of the calculations is to perform a capacity check, the simplified bilinear model can be assumed, as it is simple and easy to implement. However, in order to deliver more comprehensive understanding of the response of this statically indeterminate structure it is essential to implement the trilinear response model.

#### 4.7.1.4 Plastic deformation capacities

The trilinear structural response model of the local front column complicates the estimation of the plastic deformation capacity,  $u_{rd}$ . The plastic rotation at the fixed support begins to develop when the moment at this support,  $M_s$ , reaches the value that the section was designed for,  $M_{rd,s}$ . This is shown as stage 1 in Figure 4.47a, with corresponding plastic deformation capacity,  $u_{rd,s}$ , in Figure 4.47b. When the load is further increased, the span reaches its maximum moment capacity,  $M_{rd,f}$ . This is presented as stage 2 in Figure 4.47a. At this point the plastic rotation in the span

starts and the corresponding plastic deformation capacity is termed as  $u_{rd,f}$  in Figure 4.47b. When the fixed support has reached its limit,  $u_{rd,s}$ , failure occurs in the plastic hinge. This is shown as a sudden vertical jump in Figure 4.47b. After this, the boundary conditions and therefore the resistance of the structure correspond to a simply supported beam.

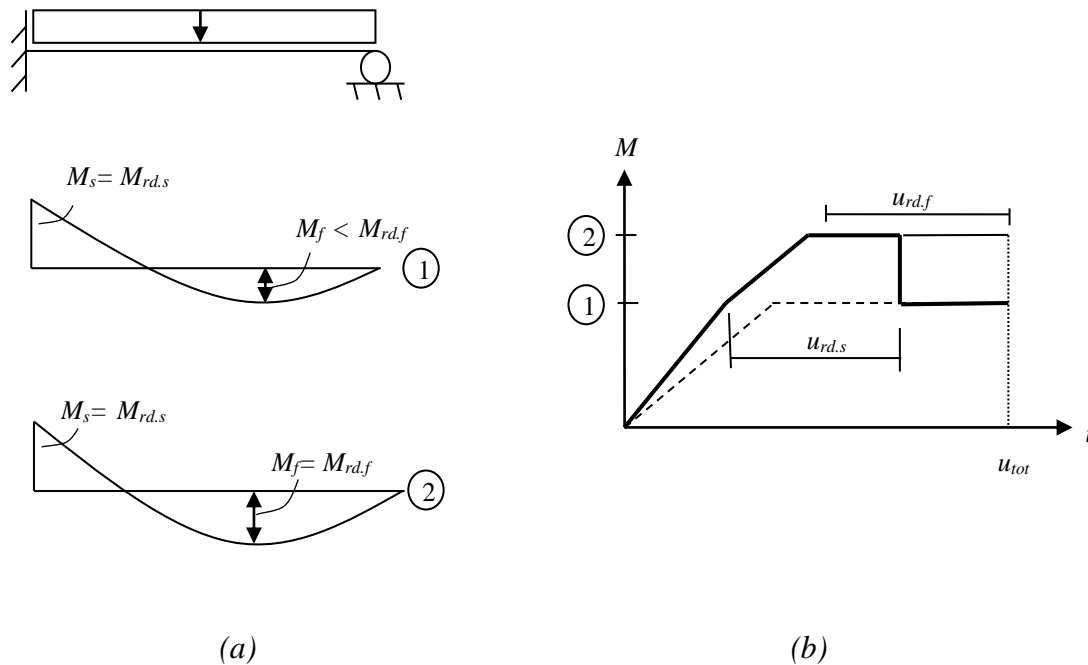


Figure 4.47 (a) Moment distribution for stage 1 and stage 2. (b) Moment-deformation curve with plastic deformation capacities. The dashed line corresponds to the response of a simply supported beam.

In this study, a simplification has been made when estimating the plastic rotation capacity. The plastic deformation capacity for the structure has been assumed to correspond to  $u_{rd,s}$  which provides results on the safe side. If a bilinear model is used,  $u_{rd,s}$  should also be used, starting from when the fixed support yields, illustrated in Figure 4.48.

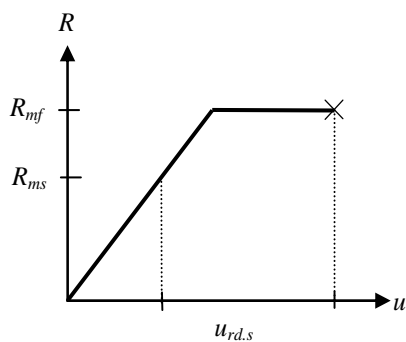


Figure 4.48 For a bilinear model,  $u_{rd,s}$  should be used, starting from when the fixed support yields.

The plastic deformation capacity  $u_{rd,s}$  is calculated from the plastic rotation capacity with regard to shear slenderness,  $\theta_{rd}$ , according to Eurocode 2 where

$$\theta_{rd} = k_{\lambda} \cdot \theta_{pl} \quad (4.19)$$

The distance between the considered maximum moment section and the adjacent zero moment section is called  $L_0$  in the calculation of the shear slenderness  $\lambda$  in equation (4.20). In order to further calculate the factor  $k_{\lambda}$ , equation (4.21),  $L_0$  is taken as  $L_I$  according to Figure 4.49.

$$\lambda = \frac{L_0}{d} \quad (4.20)$$

$$k_{\lambda} = \sqrt{\frac{\lambda}{3}} \quad (4.21)$$

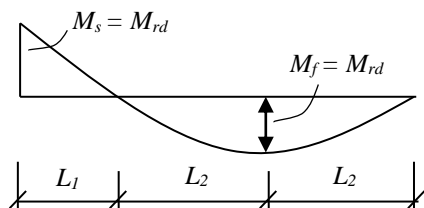


Figure 4.49 Possible choices of the distance between the considered maximum moment section and the adjacent zero moment section.

A check of the plastic deformation capacity was performed for the chosen load of 60 kPa and 0.025 s. The results are presented in Table 4.10 and the calculations can be found in Section E.3. The check showed that the front column did not possess the required plastic deformation capacity for either reinforcement of Class B or Class C. However, it can be noticed that the plastic deformation capacity was almost twice as large when reinforcement Class C was used compared to Class B.

Table 4.10 Comparison of plastic rotation capacity and maximum deformation obtained from an impulse load of 60 kPa and 0.025 s.

Reinforcement	$u_{rds}$ [m]	$u_{max}$ [m]
Class B	0.066	0.13
Class C	0.115	0.13

#### 4.7.1.5 Plastic strain

In order to better understand the local elasto-plastic response of the frame the development of plastic strain is investigated. Plastic hinges can be formed at the fixed support and in the mid span, point A and B in Figure 4.50, respectively.



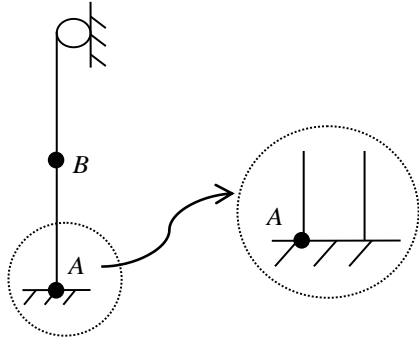


Figure 4.50 Critical sections marked with black points in the local elasto-plastic model.

The plastic strain in point A and the deformation for the local model,  $u_2$ , are plotted together in Figure 4.51. It can be noticed that there is only one main peak for the plastic strain in the interval 0 - 0.3 s. The peak is followed by an almost straight line, with insignificant changes in plastic strain. When the plastic strain is constant with time, it means that the response is elastic. An initiation of plastic strain means that a plastic hinge has been reached in point A. When the plastic strain is increasing the structure is swinging in the positive direction, and when it is decreasing it is swinging in the opposite direction. The deformation in the interval 0 – 0.3 s corresponds well with the changes in plastic strain.

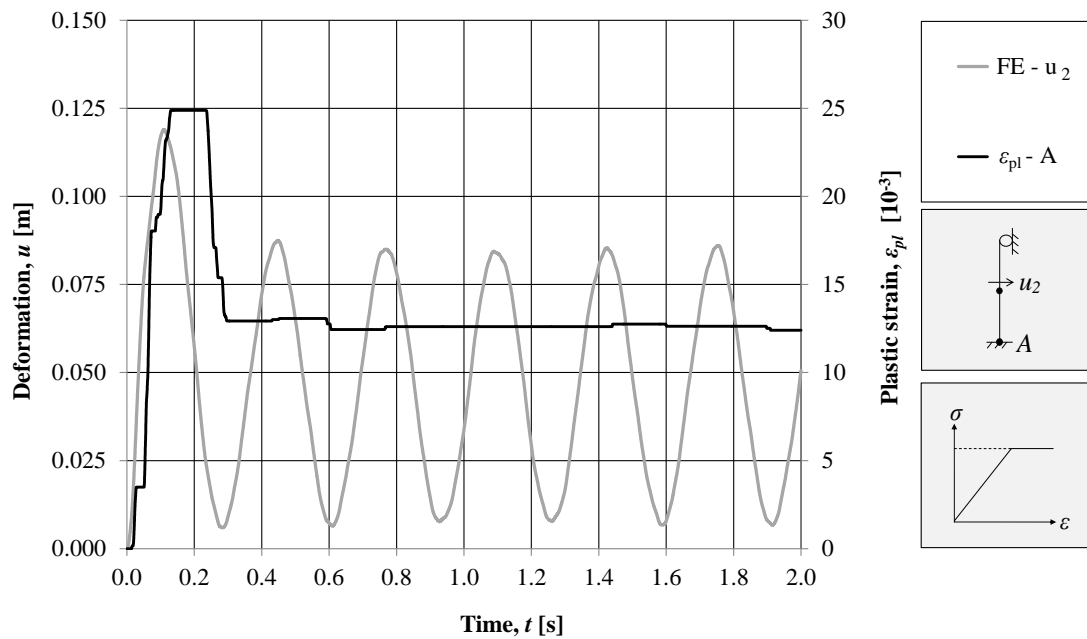


Figure 4.51 A comparison of deformation,  $u_2$ , in the local model to the plastic strain,  $\epsilon_{pl}$ , in point A.

## 4.7.2 Global elasto-plastic model

### 4.7.2.1 Response of the structure

The SDOF and FE model of the global elasto-plastic frame with corresponding material model is shown in Figure 4.52.

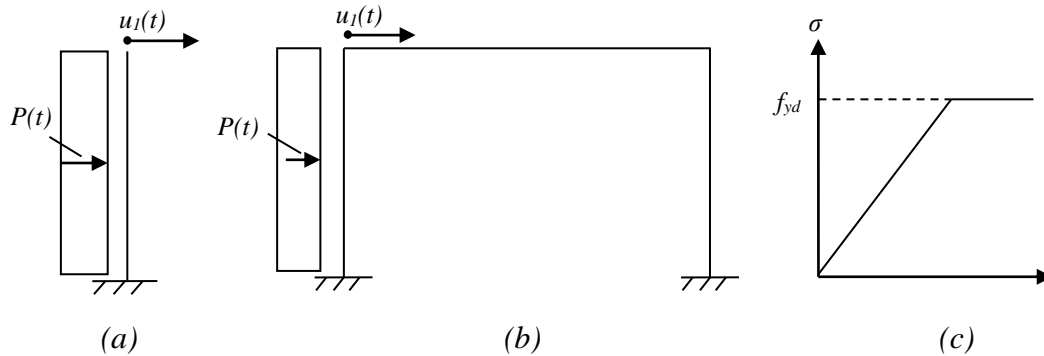


Figure 4.52 An illustration of: (a) the global SDOF model and the deformation  $u_I(t)$ ; (b) the global FE model and the deformation  $u_I(t)$  and (c) the elasto-plastic material response model.

The deformations,  $u_I$ , obtained for the global elasto-plastic model from the FE analysis and the SDOF model are presented in Figure 4.53.

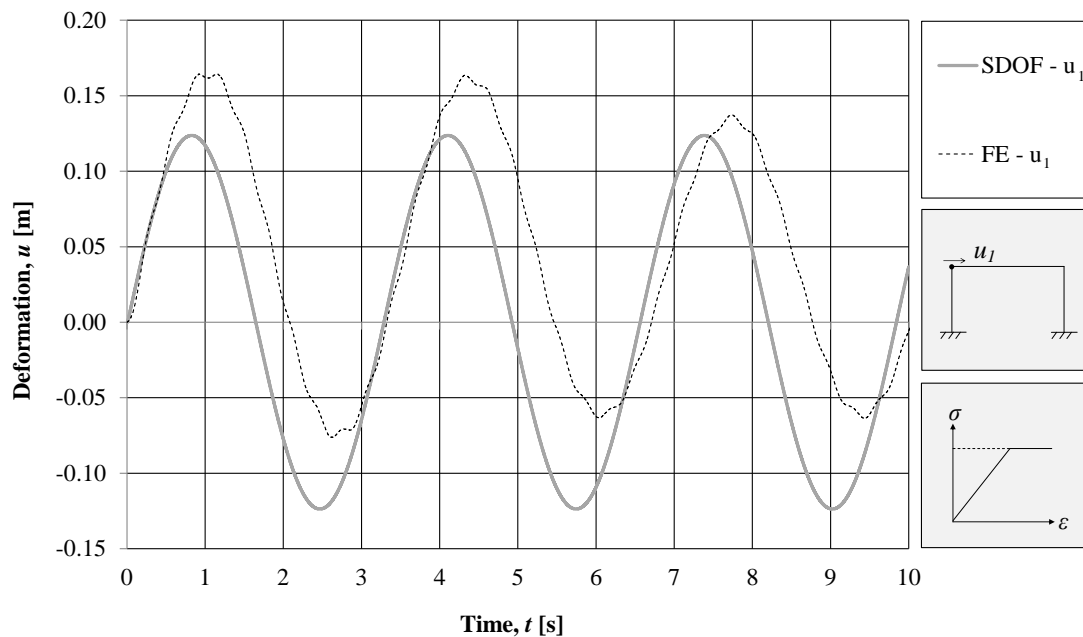


Figure 4.53 The deformations obtained in the global analysis, at the top of column in the frame subjected to impulse load for the elasto-plastic case.

It can be noticed that the FE model experiences some plastic deformation since the centre of the oscillations is above the zero axis. The value of the maximum deformation also seems to decrease with time, which can be noticed especially for the positive deformations. This phenomenon is in disagreement with the SDOF response which is completely elastic.

The static FE analysis resulted in the resistance curve shown in Figure 4.54. However, the dynamic FE analysis showed that for the maximum deformation obtained in the FE analysis the response is expected to be elastic since the first plastic hinge according to the expected resistance-deformation curve,  $R(u)$ , is not reached. An illustration of the expected resistance is shown in Figure 4.55. Nevertheless, the dynamic analysis showed that the deformation possesses some plastic parts.

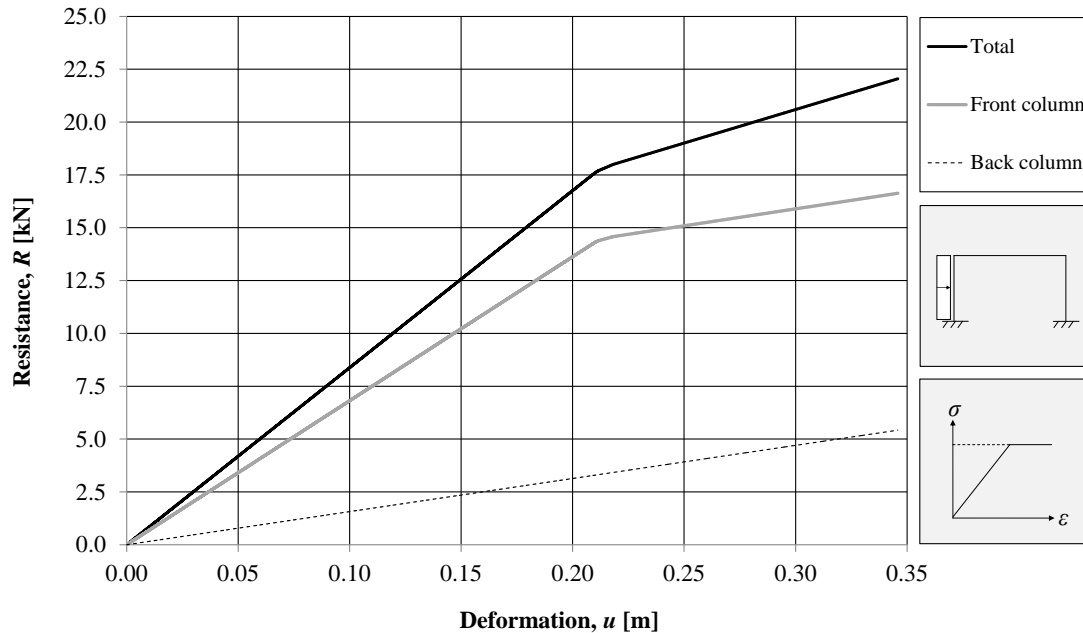


Figure 4.54 The resistance-deformation curve obtained in the static analysis of the frame.

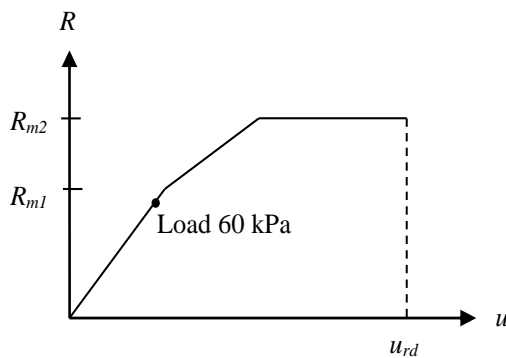


Figure 4.55 The maximum deformation reached, shown in the resistance-deformation curve for an impulse load of 60 kPa and 0.025 s. The first plastic hinge is not reached.

Since the FE analysis of the global frame shows some plastic behaviour, it seems that the static structural response model is not enough to describe the true behaviour of the global frame in a SDOF system. In order to better understand the behaviour of the global frame, the deformations at the top of the frame,  $u_1$ , and in the middle of the front column,  $u_2$ , are studied together in Figure 4.56. It can be noticed that a decrease in magnitude of  $u_1$  occurs after the oscillations in  $u_2$  have been magnified, i.e. before the intervals where some damping of the oscillations for  $u_2$  has occurred. The

behaviour is studied more closely, in relation to other parameters, in the following sections.

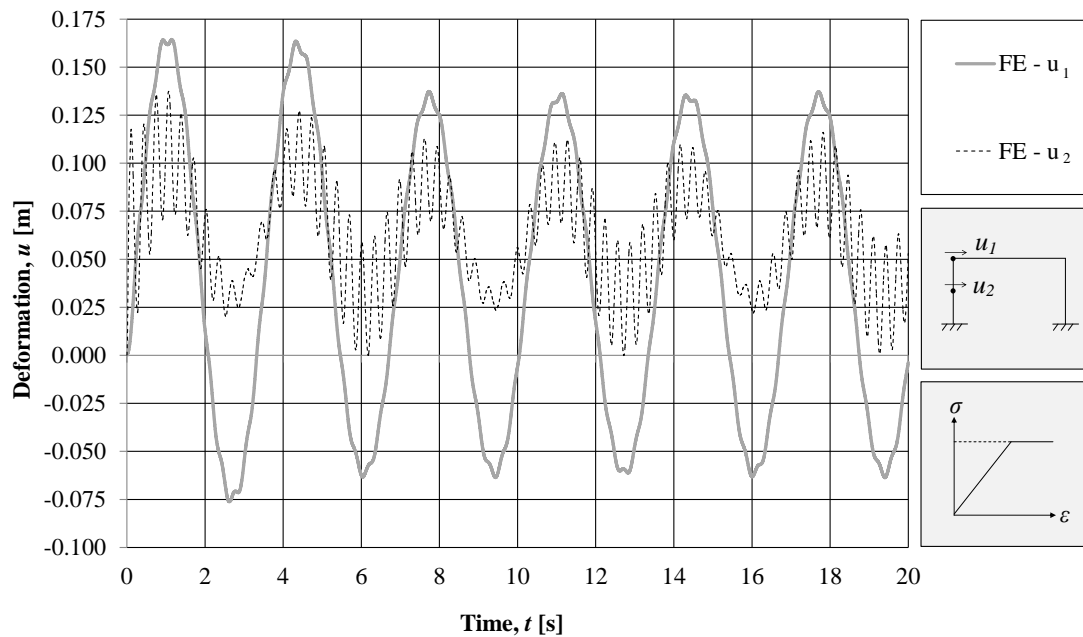


Figure 4.56 A comparison of the deformations  $u_1$  and  $u_2$ .

#### 4.7.2.2 Stress and plastic strain

In order to better understand the global response of the frame the development of plastic strain and stresses for the critical sections are further investigated. The critical sections are those that gain the largest plastic strain and where plastic hinges are formed. Thus, the sections at the supports and in the mid span of the first column are compared and analysed, see Figure 4.57. Plastic hinges can be developed in tension and compression.

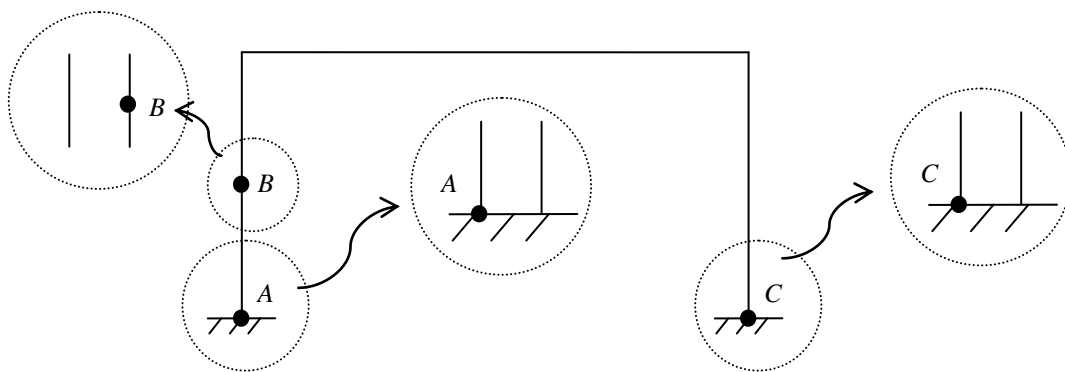


Figure 4.57 Critical sections marked with black points in the global elasto-plastic model.

A change in plastic strain means that a plastic hinge has been reached. When the plastic strain is increasing, a plastic hinge is reached in tension, and when it is decreasing it is reached in compression. When the plastic strain is constant with time, the response is elastic.

The plastic strain for the three critical sections A, B and C in Figure 4.57 are plotted together in Figure 4.58. The plastic strain at the back column, point C, is very small compared to the plastic strain in the front column, point A. The plastic strain in the mid span, point B, is only changing in magnitude at the very first time interval. This shows that point B is mostly relevant for the initial stage in the frame analysis, i.e. the local model. The main focus in this analysis is on the plastic strain at the fixed support of the front column, since it is expected to have the main influence on the behaviour of the global frame structure.

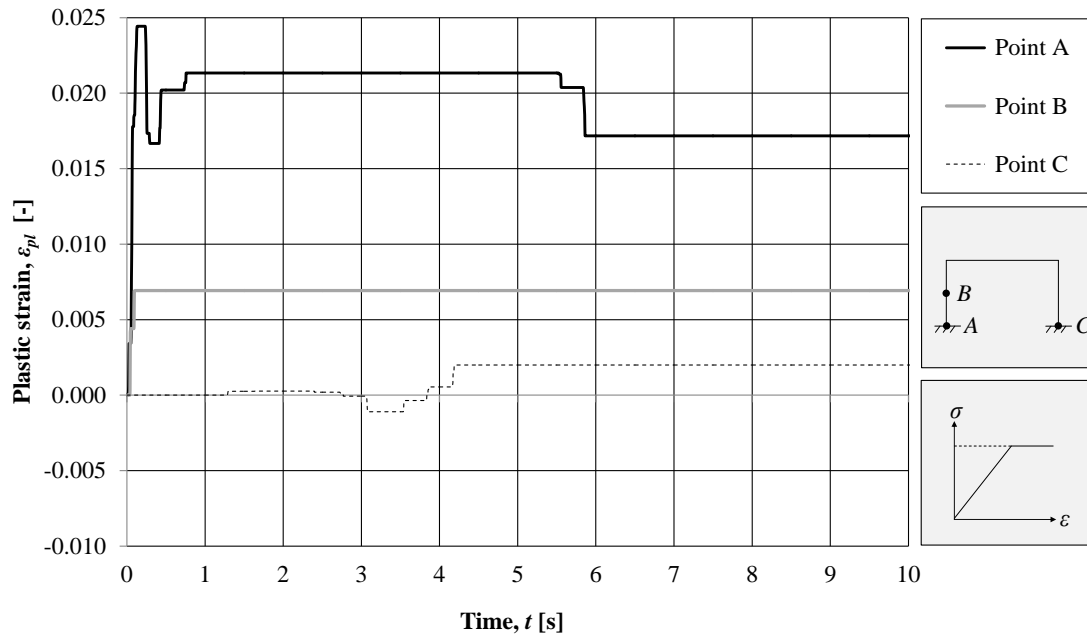


Figure 4.58 Plastic strain obtained in point A, B and C in the global FE analysis.

In Figure 4.59 the deformation from the FE analysis at the top of the front column,  $u_1$ , and in the middle of the front column,  $u_2$ , are plotted together with the plastic strain in point A.

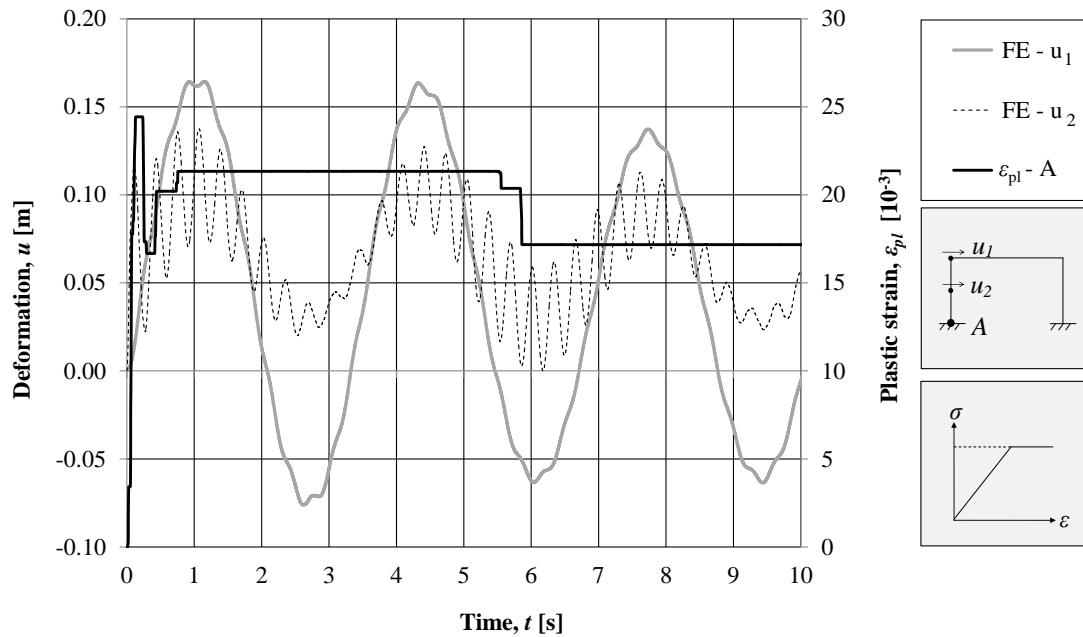


Figure 4.59 A comparison of deformations  $u_1$  and  $u_2$  to the plastic strain in point A for a time interval of 10 seconds.

Studying Figure 4.59 it can be noticed that there are some sudden changes in plastic strain around 0 to 1 seconds and 5 to 6 seconds. When analysing this time interval it is obvious that these changes coincide with the maximum deformations in the middle of the front column,  $u_2$ . The intervals are magnified in Figure 4.60 and Figure 4.61. When  $u_2$  reaches a maximum or minimum peak, the plastic strain increases or decreases simultaneously.

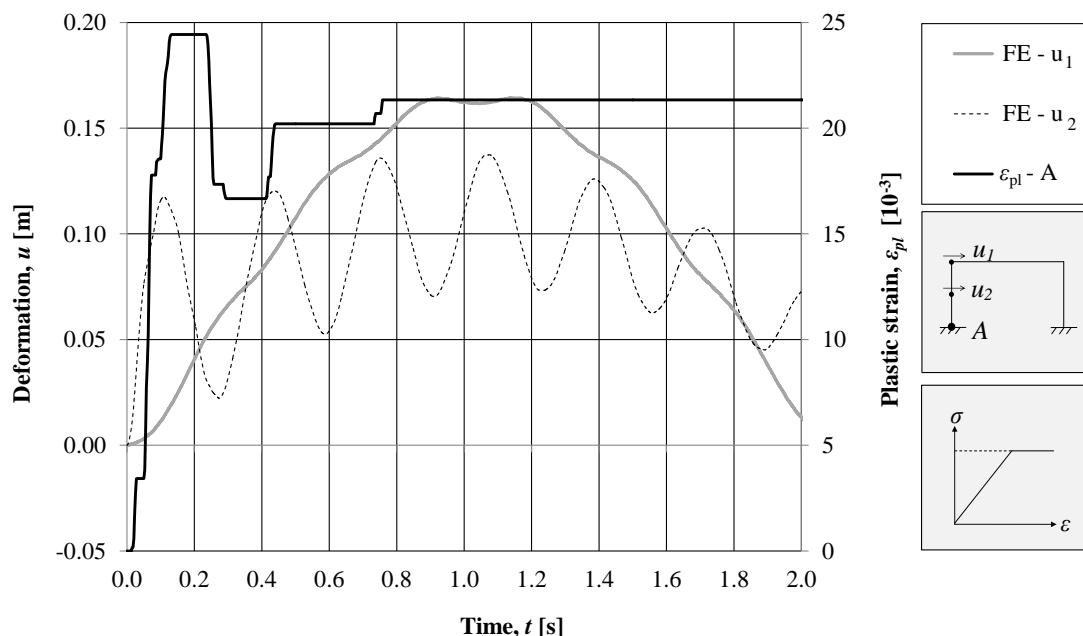


Figure 4.60 A comparison of the deformations  $u_1$  and  $u_2$  to the plastic strain in point A for a time interval of 0 to 2 seconds.

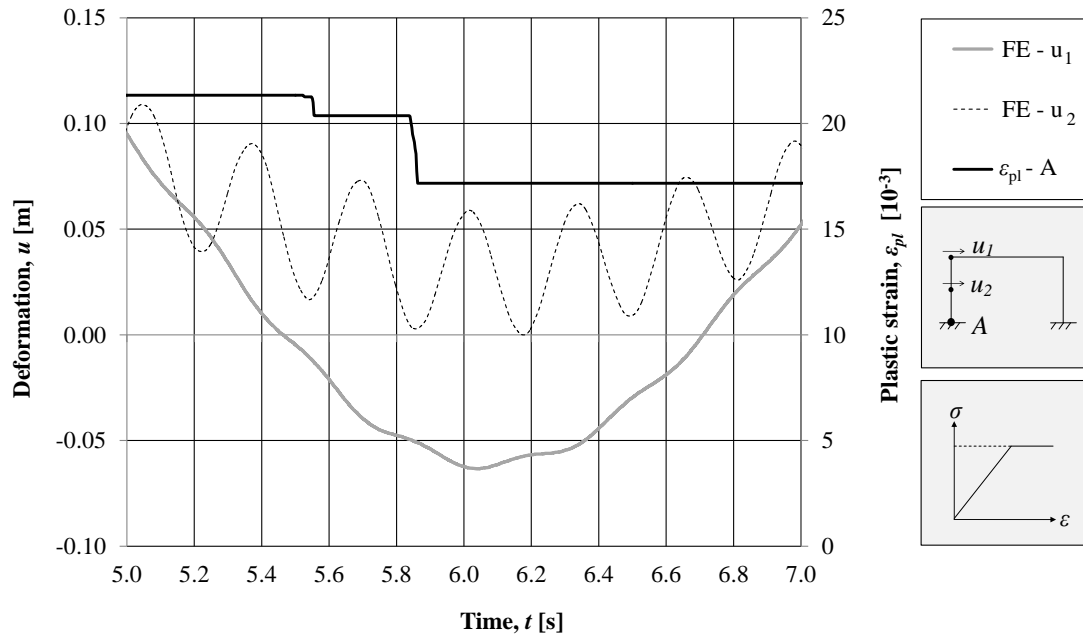


Figure 4.61 A comparison of deformations  $u_1$  and  $u_2$  to the plastic strain in point A for the time interval of 5 to 7 s.

In order to get a better understanding of the deformed shape of the frame at different points in time a comparison is made between the graphs, see Figure 4.62. The deformed shapes of the frame are shown in Table 4.11. Two of the most extreme shapes, which occur at point 1 and 7, seem to coincide with changes in plastic strain.

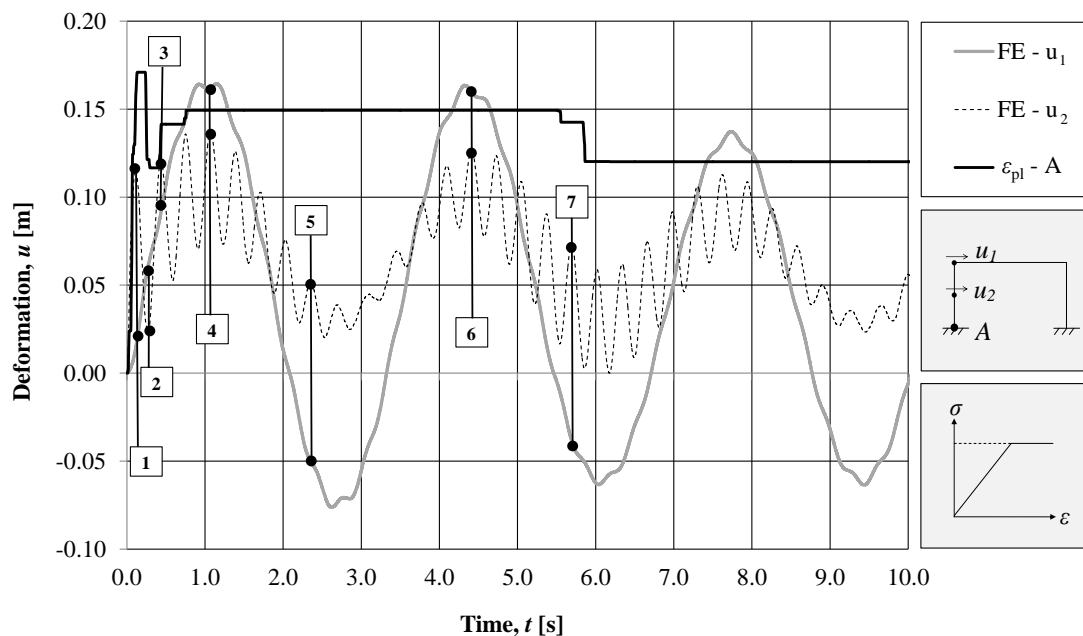




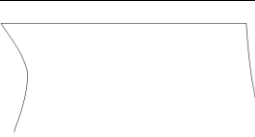




Figure 4.62 A comparison of the deformations  $u_1$  and  $u_2$  to the plastic strain in point A for a time interval of 10 seconds. The points are described in Table 4.11.

Table 4.11 The deformed shape of the global frame at the first three deformations peaks for  $u_2$  and at the stage when  $u_1$  is equal to  $u_2$ .

Point	Time [s]	Deformation [m]	Deformed shape	Description
1	0.109	$u_1 = 0.013$ $u_2 = 0.117$ $u_2 \gg u_1$		First maximum peak of $u_2$ . Plastic hinge at point A and point B is formed.
2	0.273	$u_1 = 0.062$ $u_2 = 0.022$ $u_2 < u_1$		First minimum peak of $u_2$ . Plastic hinge at point A is formed, in opposite direction.
3	0.436	$u_1 = 0.091$ $u_2 = 0.120$ $u_2 > u_1$		Second maximum peak of $u_2$ . Plastic hinge formed again at point A.
4	1.075	$u_1 = 0.162$ $u_2 = 0.137$ $u_2 < u_1$		Maximum deformation of $u_2$ and of $u_1$ occurring at the same time.
5	2.361	$u_1 = -0.051$ $u_2 = 0.052$ $u_2 > u_1$		Deformation peaks in opposite directions for $u_2$ and $u_1$ . No plastic hinge is formed.
6	4.412	$u_1 = 0.159$ $u_2 = 0.127$ $u_2 < u_1$		Deformation peaks in the same direction for both $u_2$ and of $u_1$ .
7	5.695	$u_1 = -0.038$ $u_2 = 0.073$ $u_2 > u_1$		Deformation peaks in opposite directions for $u_2$ and $u_1$ . Case is more extreme than point 5. Plastic hinge is formed at point A.



To further investigate the behaviour of the global frame model the stress and plastic strain at the fixed support as well as the deformation at the top of the frame are evaluated together. The stress versus strain at the fixed support of the front column is plotted in Figure 4.63. The colours in the figure correspond to the same period in time as the plastic strain plotted in Figure 4.64 and as in the deformations shown in Figure 4.65 and Figure 4.66.

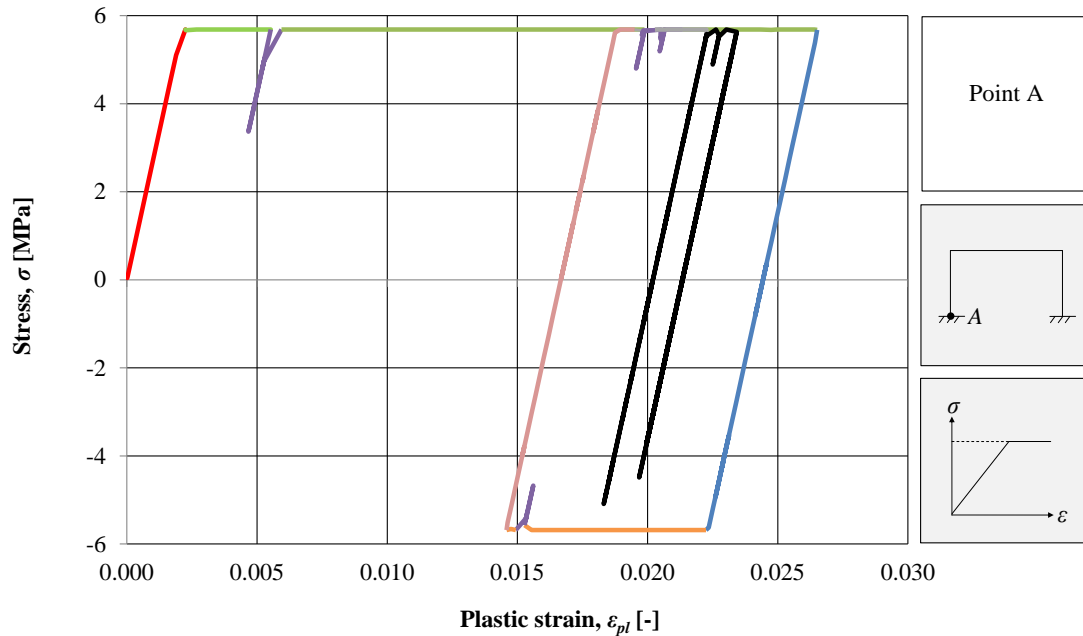


Figure 4.63 Stress-strain relationship at the fixed support for the front column.

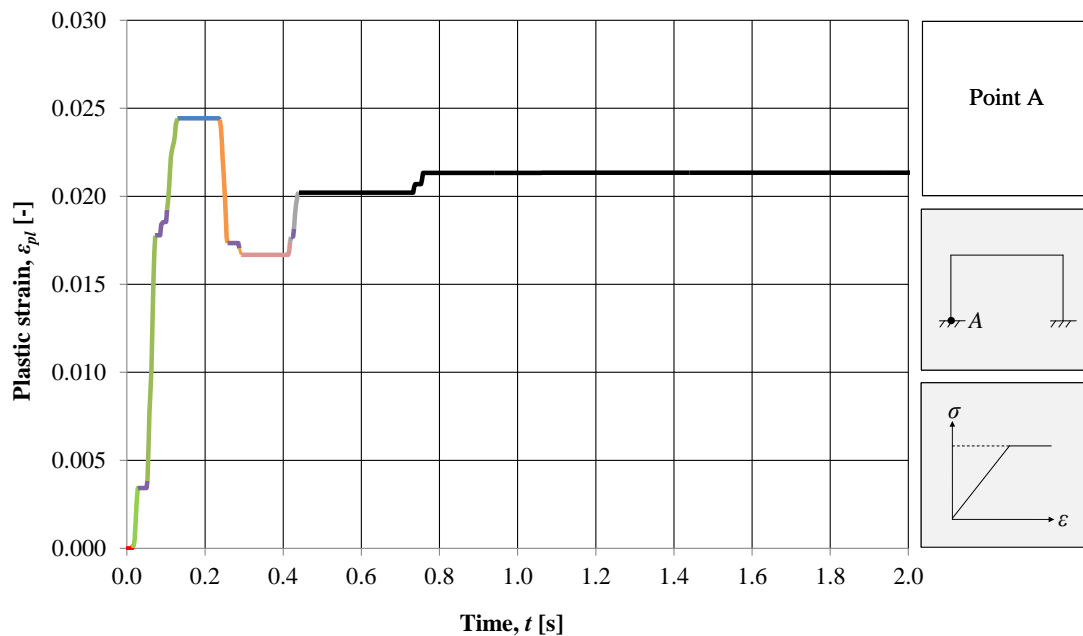


Figure 4.64 Plastic strain development over time at the fixed support for the front column.

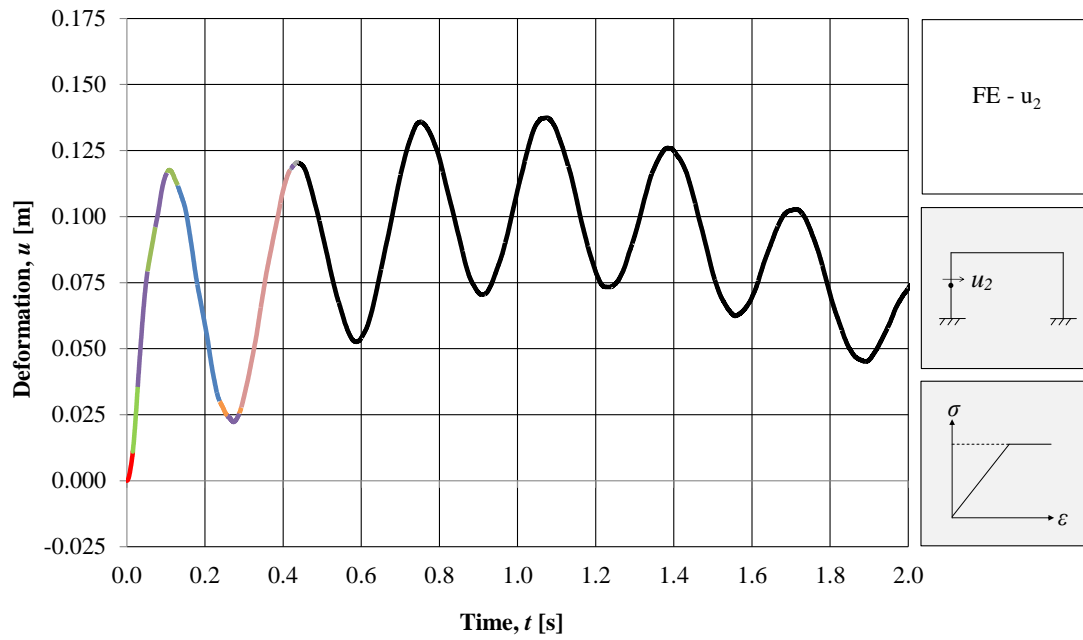


Figure 4.65 Deformation  $u_2$  over time for the global elasto-plastic model.

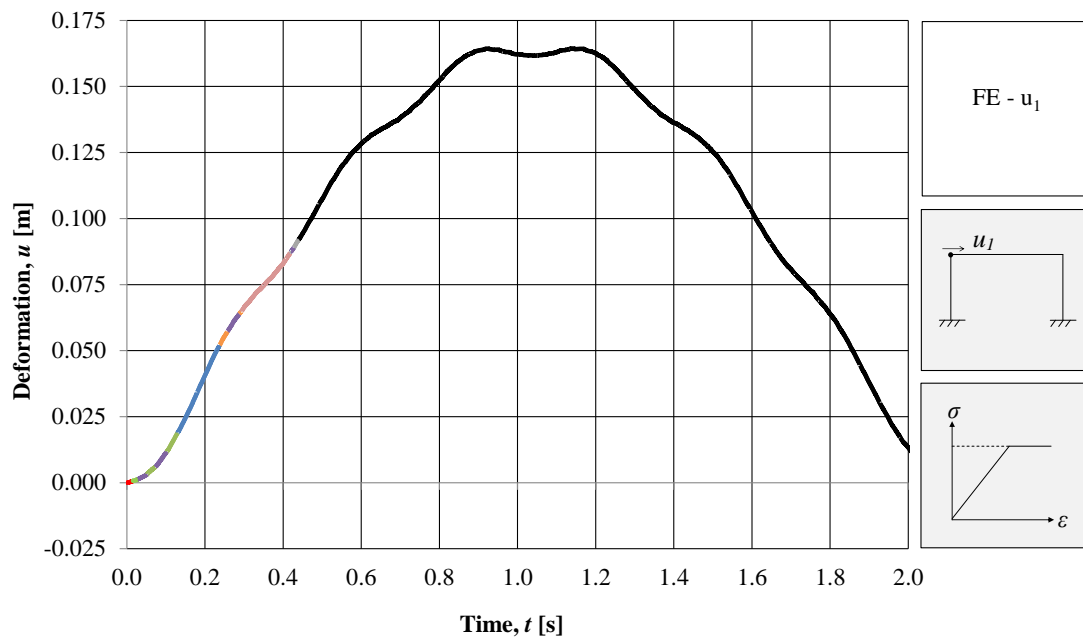


Figure 4.66 Deformation  $u_1$  over time for the global elasto-plastic model.

A further explanation of the phenomena at every colour can be found in Table 4.12.

Table 4.12 Description of the phenomena at different points in time.

Colour	Phenomenon	Plastic strain, $\epsilon_{pl}$	Stress, $\sigma$	Deformation, $u_2$
<b>Red</b>	Elastic behaviour.	Elastic behaviour, no plastic strain occurs.	Increases.	Increases.
<b>Green</b>	Plastic hinge has been formed at the fixed support.	Plastic strain increases.	Maximum stress has been reached. Stress is constant.	Increases.
<b>Blue</b>	Elastic behaviour. Maximum deformation has been reached.	Plastic strain is constant.	Starts to decrease.	Starts to decrease, i.e. swinging back.
<b>Orange</b>	Plastic hinge has been formed at the fixed support, frame is swinging in the opposite direction.	Plastic strain decreases.	The stress has reached its ultimate value in its opposite direction and is constant.	Decreases.
<b>Pink</b>	Elastic behaviour. Deformation has reached its minimum value and its first negative peak.	Plastic strain is constant.	Stress is increasing.	Starting to increase again.
<b>Grey</b>	A plastic hinge has been formed at the fixed support again.	Plastic strain increases.	Maximum value reached. Stress is constant.	Increasing.
<b>Black</b>	Mainly elastic behaviour. Small changes in plastic strain and stress when maximum stress is reached.	Constant.	Increases and decreases elastically.	Starts to decrease. Sways back and forth elastically.
<b>Purple</b>	Unevenness due to higher modes.			

The plastic strain studied so far increases and decreases when plastic hinges are formed in the different directions. This means that when the structure is swinging in the positive direction, the plastic strain increases and when it is swinging in the negative direction the plastic strain decreases. Until now, it has been assumed that the plastic hinges are formed when the maximum stress is reached without any consideration of the history of the steel. It can be questioned if the reinforcement changes properties after the plastic hinges have been formed in both directions several times. Therefore, the accumulated plastic strain,  $\varepsilon_{pl,acc}$ , is described in equation (4.20) and plotted in Figure 4.67 in order to get an understanding of the total strain the section has been exposed to. This is however not further investigated in this report.

$$\varepsilon_{pl,acc} = \sum |\varepsilon_{pl}| \quad (4.22)$$

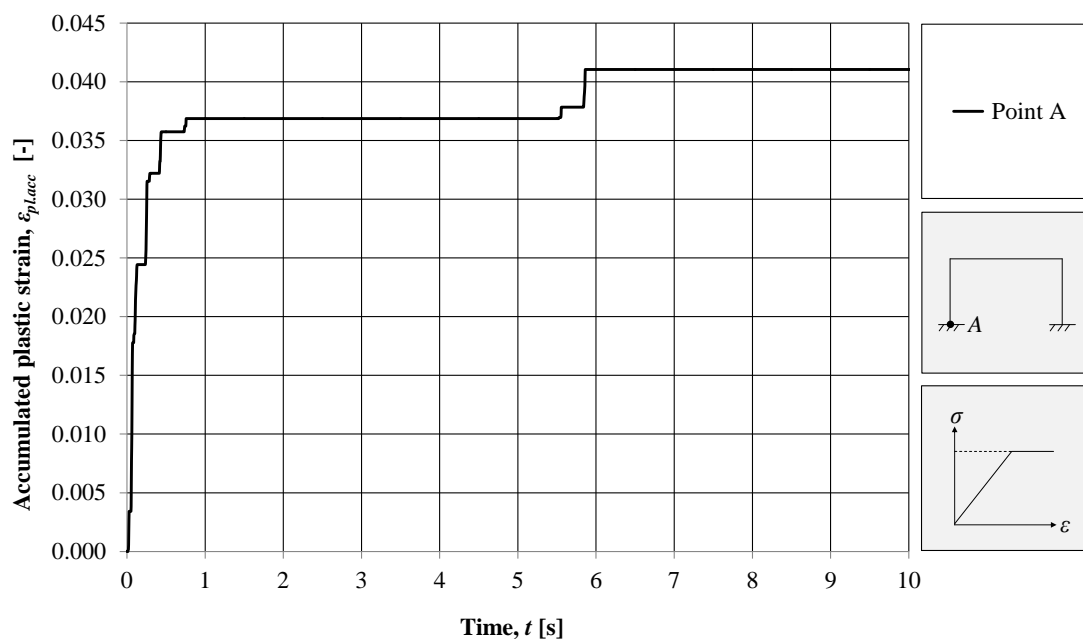


Figure 4.67 Accumulated plastic strain,  $\varepsilon_{pl,acc}$ , for point A in the global elasto-plastic model.

#### 4.7.2.3 Moment and damping

In order to investigate the structural behaviour of the frame even further, the moment at the fixed support is investigated in relation to the plastic strain. In Figure 4.68 it can be noticed that the plastic strain changes when  $M_A > M_{rd}$ , i.e. when the maximum capacity for the considered section has been reached. In reality, the moment will reach  $M_{rd}$  but never exceed it. Here, the fact that the values are larger than  $M_{rd}$  is due to the size of the elements used in ADINA.

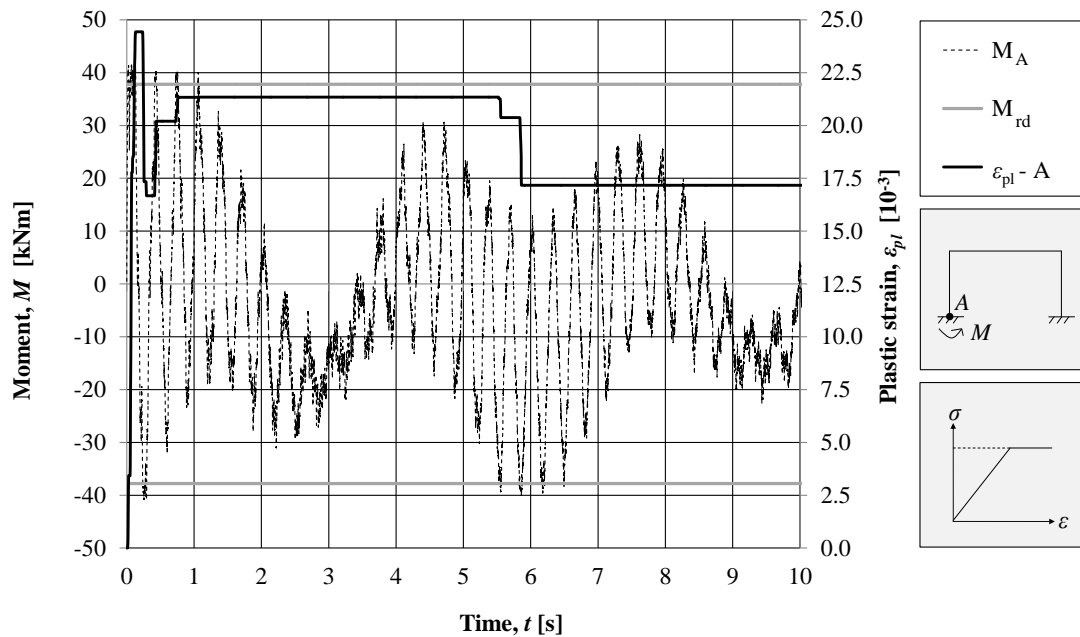


Figure 4.68 A comparison of the moment and plastic strain at the fixed support of the front column.

In reality, a structure subjected to an impulse load experiences a certain degree of natural damping. A reinforced concrete structure with considerable cracking normally has a damping of about 3 - 5 %. In order to get further information about damping, the reader is directed to Carlsson and Kristensson (2012).

Figure 4.69 and Figure 4.70 shows the moment when a modal damping of 1 % and 5 %, respectively, is implemented. For both cases it can be noticed that the moment is decreased with time and is lower than  $M_{rd}$  after the first second. Figure 4.71 illustrates the plastic strain for different percentage of damping together.

The moment within the first second still exceeds the ultimate moment resistance, even if a damping of 5 % is implemented. This shows that in reality, where a certain degree of damping will exist, the critical moments seem to occur only at the very beginning. However, this needs to be investigated further in order to not make any premature conclusions.

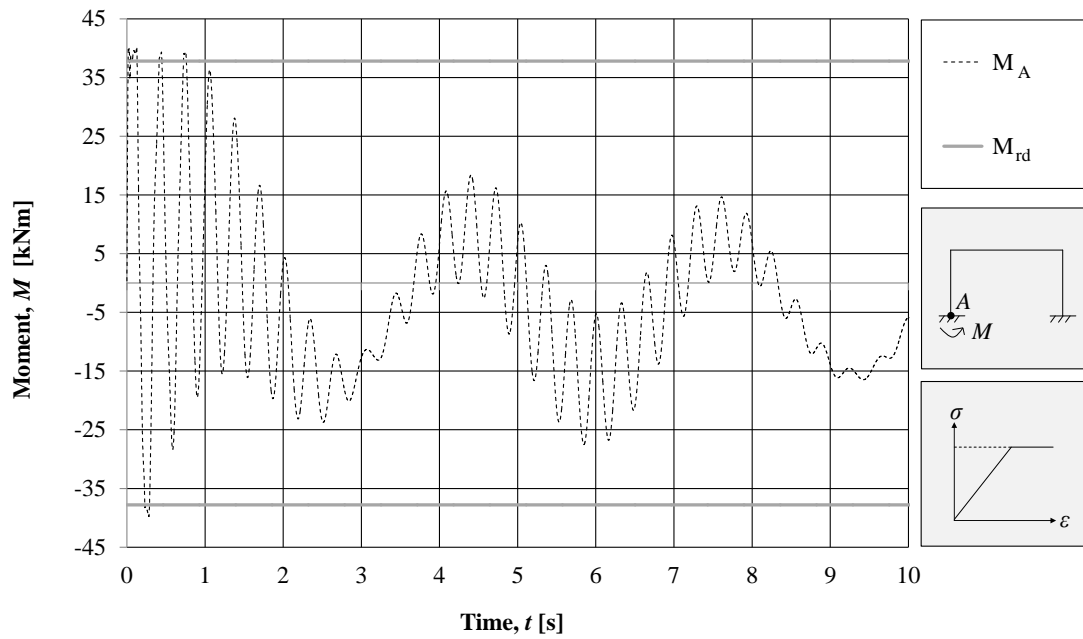


Figure 4.69 Moment at the fixed support of the front column for a modal damping of 1 %.

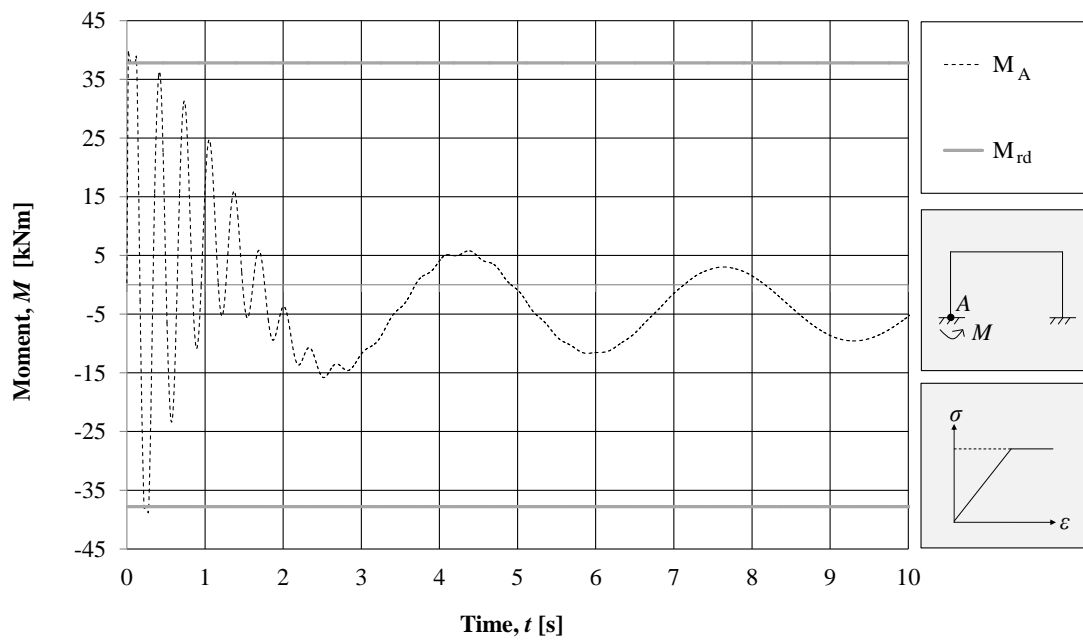


Figure 4.70 Moment at the fixed support of the front column for a modal damping of 5 %.

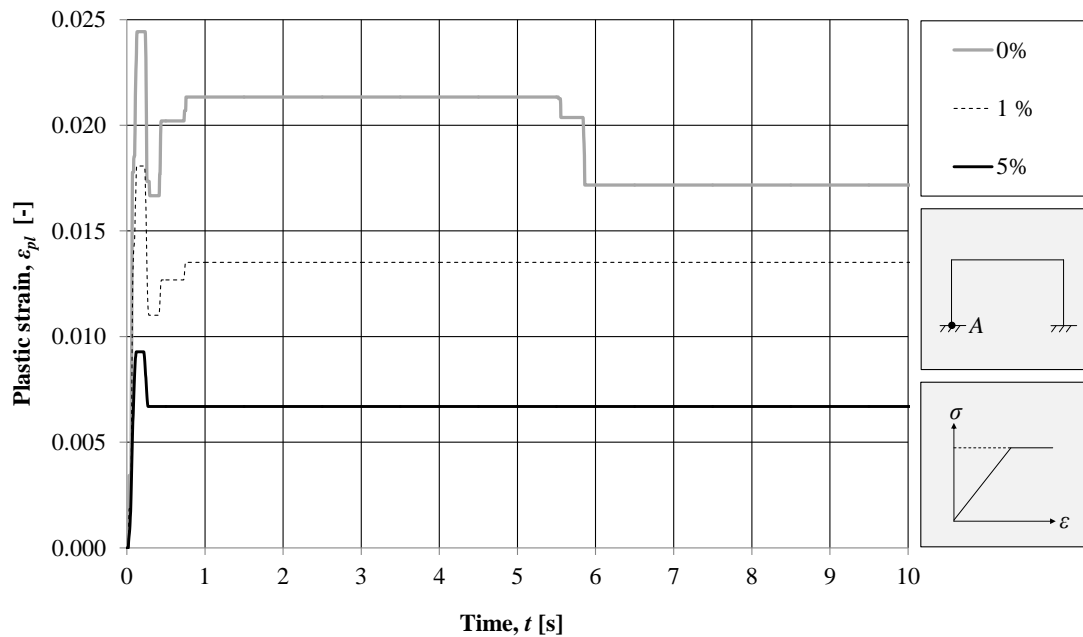


Figure 4.71 Plastic strain at the fixed support of the front column for a modal damping of 0, 1 and 5 %. The change in plastic strain at 5.5 seconds is absent when damping is applied.

### 4.7.3 Combination of the local and global elasto-plastic model

The local and global elasto-plastic SDOF models are plotted together in Figure 4.72. The frequency for the local model is, similarly as for the elastic model, much larger than for the global model.

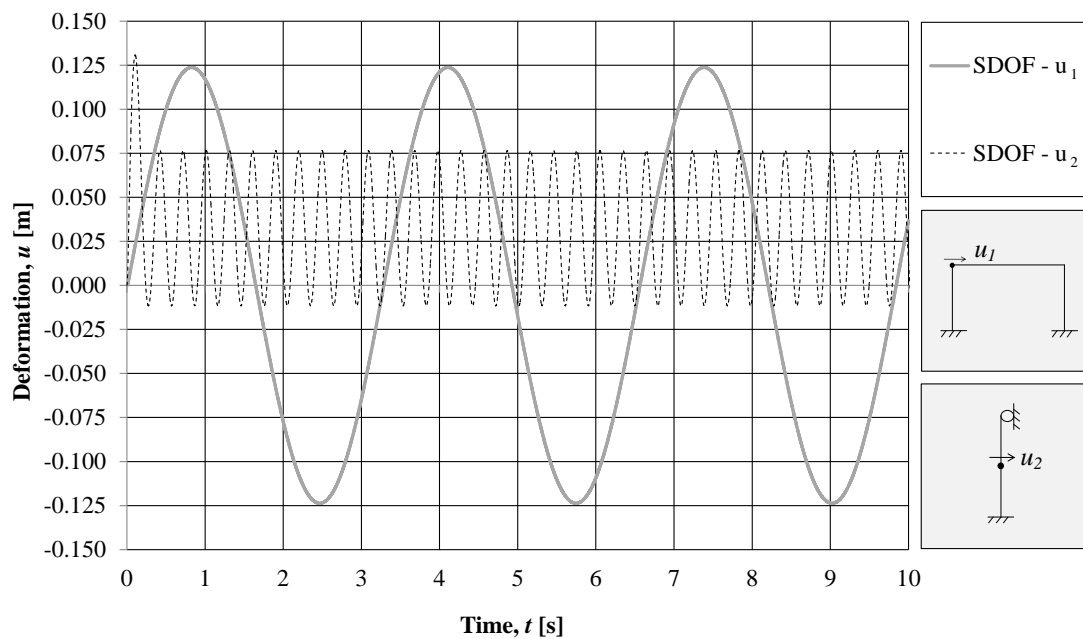


Figure 4.72 The local and global deformations obtained from the SDOF model when the frame is subjected to an impulse load of 60 kPa and 0.025 s for the elsto-plastic case.

The response in the middle of the front column when combining the global and local SDOF model is presented in Figure 4.73. The combination of the SDOF models is carried out according to Section 4.4.4. The deformations obtained in the FE analysis are shown in Figure 4.74.

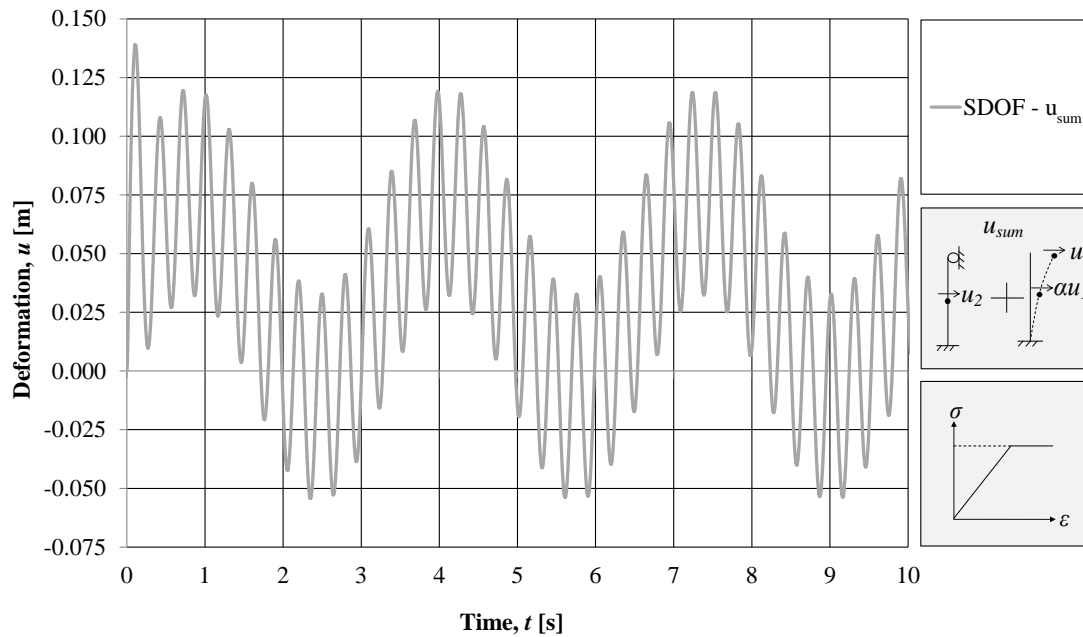


Figure 4.73 A combination of the local and global deformations due to an impulse load of 60 kPa and duration of 0.025 s for the elasto-plastic case.

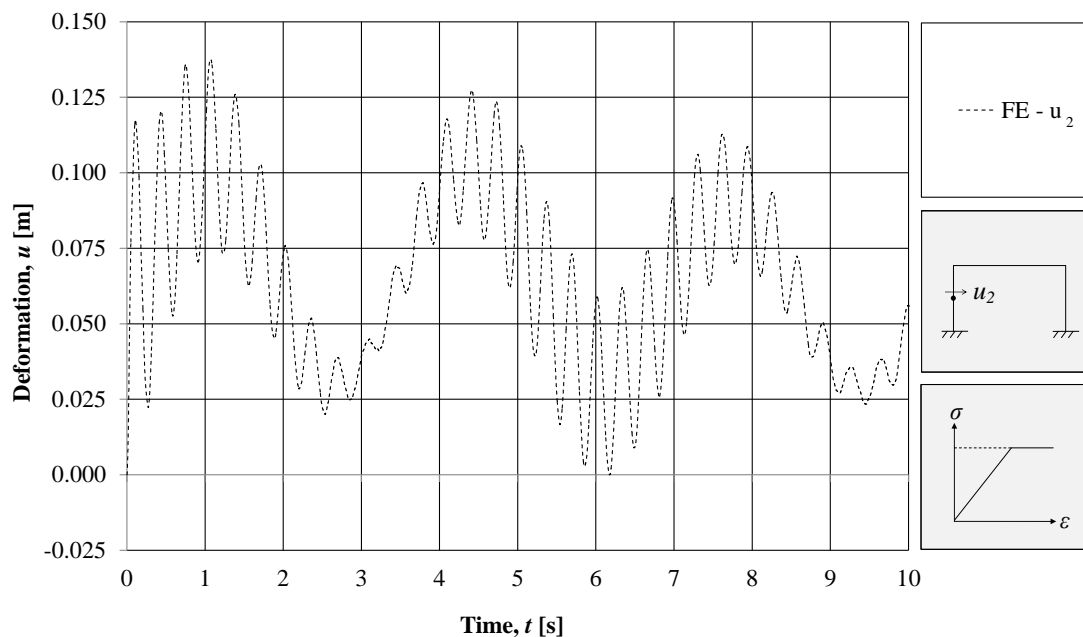


Figure 4.74 The deformations,  $u_2$ , obtained in the FE analysis for the considered impulse load of 60 kPa and duration of 0.025 s for the elasto-plastic case.

When comparing the results obtained by implementing these two methods, Figure 4.75, the magnitude of the deformations differs between the two cases. The frequency, however, seems to agree quite well. The small difference in frequency is due to the transformation factors used.



The SDOF model shows a larger magnitude in the deformations than the FE model. On the other hand, the FE model has gained a larger plastic deformation why the SDOF calculations do not provide results on the safe side. As can be seen in the elastic model in Section 4.6.3, a significant difference in deformation magnitude is obvious at certain intervals.

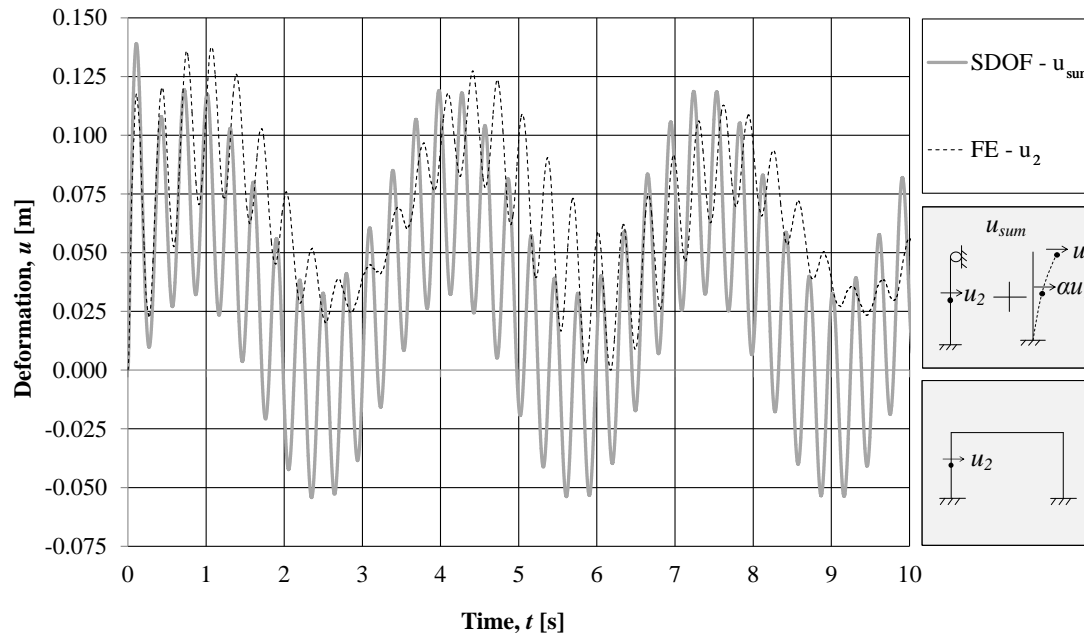


Figure 4.75 The deformations obtained from the SDOF system and FE modelling in the global analysis for the middle of the front column. Both the material response and structural response are elasto-plastic.

Since the global elasto-plastic SDOF model is still not completely corresponding to the FE analysis, this combination of the local and global elasto-plastic case will also differ. The combined SDOF model gives a rough estimation of the behaviour of the frame, but should not be trusted completely.

## 4.8 Concluding remarks

This study of the structural response of a 2D frame has brought some interesting results. For starters, the elastic local and global SDOF models agree well with the FE analysis. Thus, it can be stated that the methodology proposed in Johansson (2013) for the local and global elastic response is reliable.

The local model is proposed to primarily represent the initial stage after the loading has occurred. Since the global model has a frequency about ten times smaller than the local model, it has not had any significant deformations at the time when the local model reaches its first peak. This means that at the initial stage, the top of the local column can be approximated to be simply supported by the frame, why the local model should be appropriate at the initial stage.

The local and global elastic models give a behaviour that corresponds well with the FE analysis when combined. However, the FE analysis shows a decrease in deformation magnitude at certain intervals, a behaviour that has not been examined further since it is not considered to be critical.

The elasto-plastic case is more complicated than the elastic. The structural response model of the local frame model proved to be trilinear, even though the material model is bilinear. This is due to the fact that it can develop two plastic hinges, one at the fixed support and one in the span. The trilinear response model will, when the load is large enough, result in a higher first deformation peak.

Since a trilinear response model is more complicated than a bilinear model, a comparison between the two cases was made. It showed that the obtained deformation is roughly the same for the two models, and a bilinear response model can be used for estimations of the deformation. However, since the bilinear model provides results on the unsafe side it is recommended to use the trilinear model when the obtained deformation from the bilinear model is close to reaching the deformation capacity. For cases with a low plastic deformation capacity, it is also suggested to be more careful when choosing the response model.

The global elasto-plastic model was also proven to have a trilinear response model. However, this static response model did not fully represent the behaviour of the global frame since it showed some plastic deformations even though the response model did not indicate this. This response seems to be connected to the relationship between the local and global deformations and the corresponding shapes. However, the response of the elasto-plastic global model is not completely understood. Due to this fact, the combination of the local and global model does not correspond as well with the FE analysis as the elastic combination did.

## 5 Structural response of a 3D frame

### 5.1 Introduction and method

This chapter studies the structural response of a front column in a 3D frame structure subjected to a load applied on both the column itself and on the surrounding wall. The aim of the study is to evaluate the difference between when the total load is applied directly on the column, and when it is delayed in form of dynamic reaction from the adjacent wall. The effect of the dynamic reaction is expected to be less destructive than the direct application of the load as the magnitude of the reaction is much lower and its duration is prolonged in time. An evaluation of the simplifications used for applying the impulse load in the frame analysis, proposed in Johansson (2013), is also performed.

A SDOF model, similar to the local model in the 2D frame study in Chapter 4, is created to simulate the response of the front column. Both elastic and elasto-plastic response models are introduced. The SDOF system is solved by the use of the software Matlab R2013a and the results are compared to the response obtained in FE analyses conducted in ADINA (2011).

### 5.2 Geometry and properties

The structure analysed in this study is presented in Figure 5.1. The roof beam with supporting columns stabilizes the walls and the roof. The columns are fully fixed to the ground. The wall is supported only on the columns and transfers the load only in the horizontal direction. The front column is considered to carry the load to the ground and through the roof beam to the back column while the wall only transfers the load to the column. The analysed section of the structure is marked in Figure 5.2.

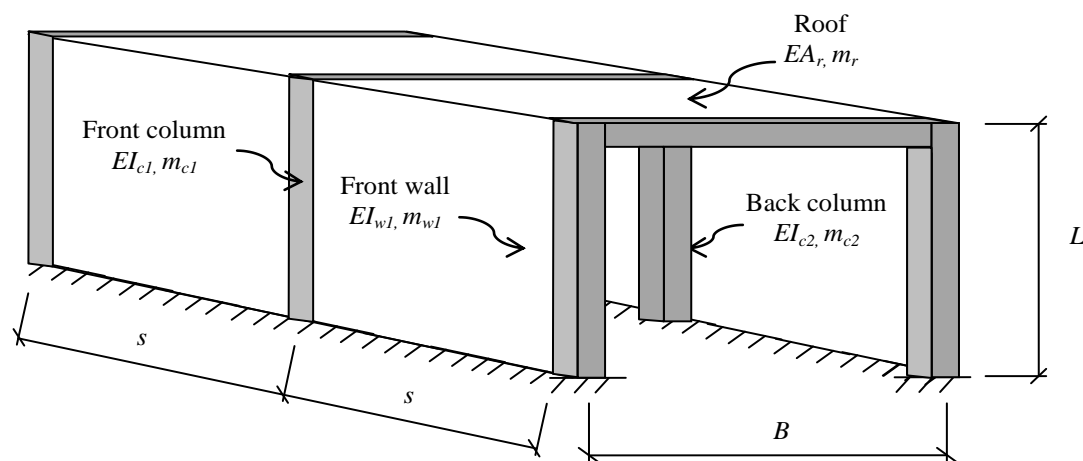


Figure 5.1 3D-illustration of the structure.

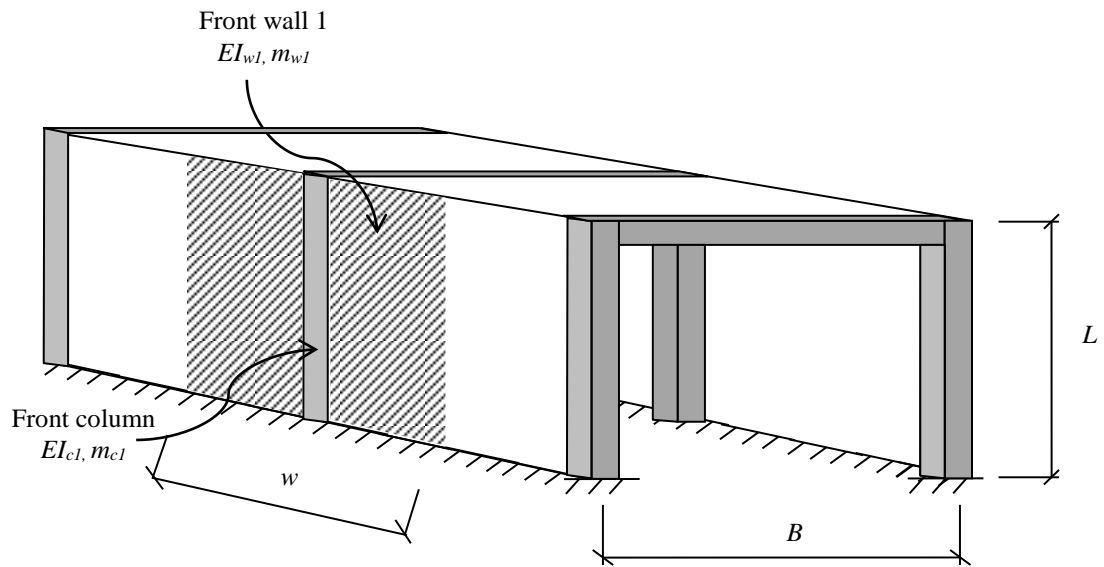


Figure 5.2 The analysed section of the structure is marked as a hatched area.

A top view of the considered section is schematically illustrated in Figure 5.3. It is assumed that the column is provided with longitudinal reinforcement, parallel to the length  $L$ , where  $A_{s,c} = 3\phi 20$ . The wall is provided with the reinforcement, where  $A_{s,w} = \phi 10$  s 150 mm, parallel to the width of considered section  $w$ . Material properties are presented in Table 5.1. The study is performed with reinforcement of Class B as well as Class C in order to compare the deformation capacities. The dimensions are presented in Table 5.2.

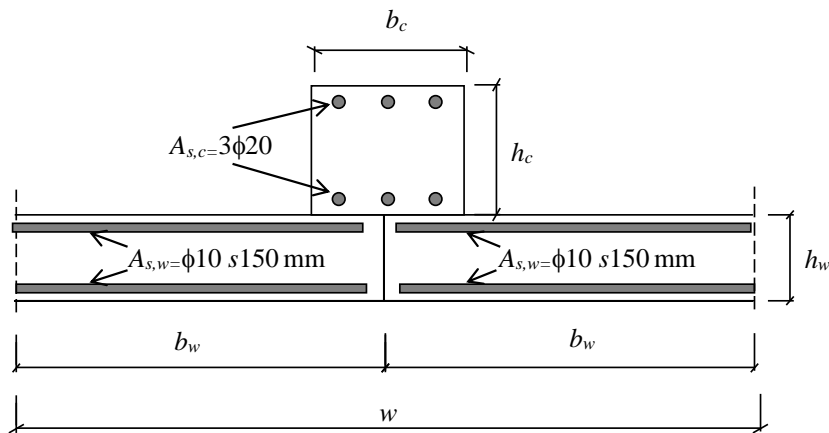


Figure 5.3 Top view of the analysed front column and wall with main dimensions and reinforcement amounts.

Table 5.1 Material properties of the frame.

Part	$E_c$ [GPa]	$f_{cd}$ [MPa]	$E_s$ [GPa]	$f_{yd}$ [MPa]
Front column	33	25	200	500
Front wall	33	25	200	500

Table 5.2 Dimensions of the structure.

Part	$b_w / b_c$ [m]	$h_w / h_c$ [m]	$w$ [m]	$s$ [m]	$B$ [m]	$L$ [m]
Wall	3.0	0.2	6.0	6.0	15.0	7.0
Column	0.5	0.6	-	-	15.0	7.0

## 5.3 Adaptation into SDOF system

### 5.3.1 SDOF model of the wall

The wall is simply supported on the columns and can therefore be described as a simply supported beam, Figure 5.4.

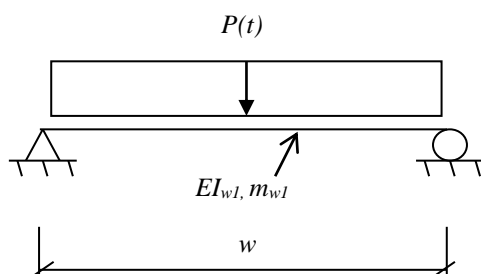


Figure 5.4 SDOF model of the wall.

The properties and dimensions of the wall are described in Section 5.2 and the load applied on it,  $P(t)$ , is described in Section 5.4.1. The input data for the SDOF system for the wall panel of 1 m width is calculated in Section F.1.1 and presented in Table 5.3. The elasto-plastic response is simulated with a bilinear resistance-deformation curve,  $R(u)$ , where the inclination of the first branch  $k_{l,w}$  corresponds the stiffness in state II. The resistance  $R_{m,w}$  corresponds to the ultimate resistance of the critical span section. When implementing the SDOF system for the elasto-plastic response, the plastic transformation factors are used.

Table 5.3 Mass, stiffness and transformation factors used for the elastic and elasto-plastic model for wall panel of 1 m width.

Model	$\kappa_{mF}$ [-]	$m_w$ [kg]	$I_w=I_{II,w}$ [ $10^{-4} \text{ m}^4$ ]	$k_{L,w}$ [kN/m]	$M_{rd,w}$ [kNm]	$R_{m,w}$ [kN]
Elastic	0.788	2 880	0.54	640	-	-
Elasto-plastic	0.667	2 880	0.54	640	37.8	50

### 5.3.2 SDOF model of the front column

The front column of the frame structure is fixed at the ground. Similarly as the front column in the 2D analysis in Chapter 4, the top support can be approximated as simply supported at the initial stage of the analysis. The SDOF model of the front column is illustrated in Figure 5.5. The model is established in agreement with the method proposed by Johansson (2013).

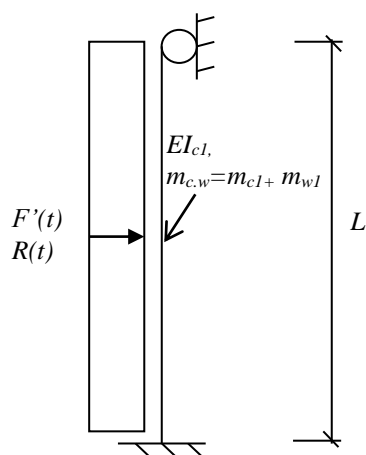


Figure 5.5 SDOF model of the front column. The mass of the model is the total mass of the column and considered wall section. The stiffness only corresponds to the stiffness of the column.

Since the wall contributes with its mass to the structure, the mass of this SDOF model is the total mass of the column and wall. However, since the wall is only transferring load between the columns it does not contribute to the stiffness of the column. Therefore, the stiffness of the SDOF model corresponds to the stiffness of the column. The structure is subjected to two load types,  $F'(t)$  and  $R(t)$ , described in Section 5.4.

The parameters of the column are established in the same manner as for the local front column described in Chapter 4. The calculations of these parameters can be found in Section F.1.2 and the values are presented in Table 5.4. The elasto-plastic response is simulated with a trilinear resistance-deformation curve,  $R(u)$ , where the stiffness  $k_{L,c}$  corresponds to the inclination of the first branch and  $k_{2,c}$  to the inclination of the second branch. Only the stiffness in state II is considered. The resistance  $R_{ms,c}$  corresponds to the ultimate resistance at the fixed support while  $R_{mf,c}$  to the ultimate resistance of the critical span section. When implementing the SDOF system for the

elasto-plastic response plastic transformation factors are used, as they provide satisfactory results, according to Andersson and Karlsson (2012).

Table 5.4 Mass, stiffness, resistance and transformation factors used for the elastic and elasto-plastic response model of the front column.

Model	$\kappa_{mF}$ [-]	$m_{c.w}$ [kg]	$I_c=I_{II.c}$ [ $10^{-4} \text{ m}^4$ ]	$k_{1.c}$ [kN/m]	$k_{2.c}$ [kN/m]	$M_{rd.c}$ [kNm]	$R_{ms.c}$ [kN]	$R_{mf.c}$ [kN]
Elastic	0.805	25 200	11	20 967	-	-	-	-
Elasto-plastic	0.667	25 200	11	20 967	8 128	211	241	361

## 5.4 Application of impulse load

### 5.4.1 Introduction

In this study the considered area, which is marked in Figure 5.6, is subjected to an impulse load with a magnitude of 60 kPa and duration of 0.025 s which is the same as in the 2D frame study. This load is referred to as External load in the following paragraphs.

The response of the front column subjected to this load is studied. The parameters of the load are described in Figure 5.7 and Table 5.5.

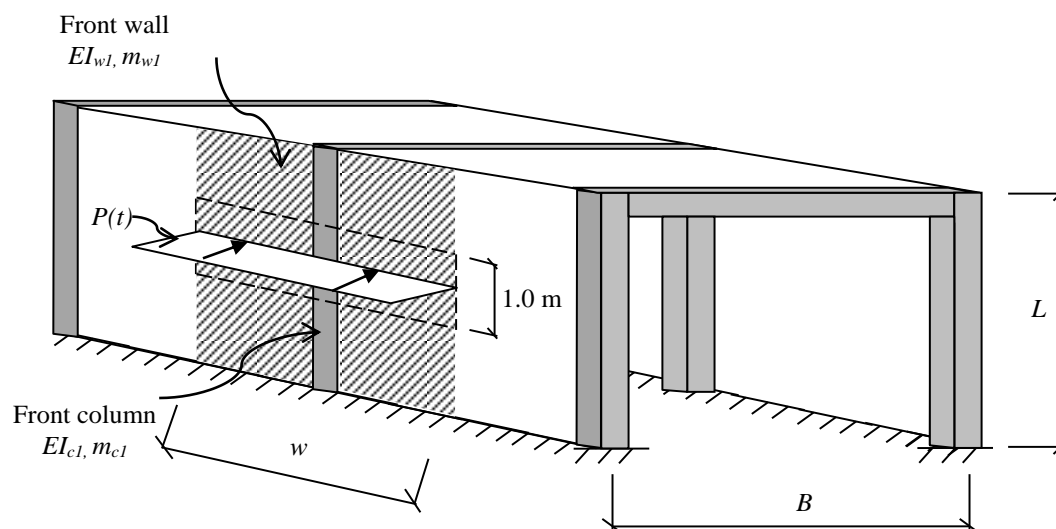


Figure 5.6 3D-illustration of how the External load,  $P(t)$ , hits the structure.  $P(t)$  is applied on the marked area.

Table 5.5 Parameters for the chosen load.

$P_{peak}$ [kN/m]	$t_{peak}$ [s]	$t_I$ [s]
60	0.00025	0.025

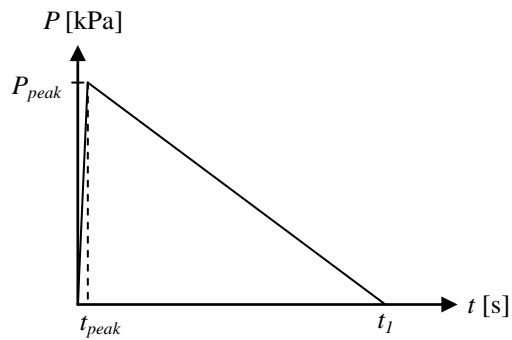


Figure 5.7 Properties of the chosen impulse load.

There are two different ways of applying the External load on the front column. The simplified version is when the total load is directly applied on the column, which is further described in Section 5.4.2. The second version, where consideration is taken to the delay due to the dynamic reaction of the walls, is described in Section 5.4.3.

### 5.4.2 Direct application of load

The simplest way of applying the load on the column is to apply the total impulse load from the considered area, marked in Figure 5.8, directly on the column.

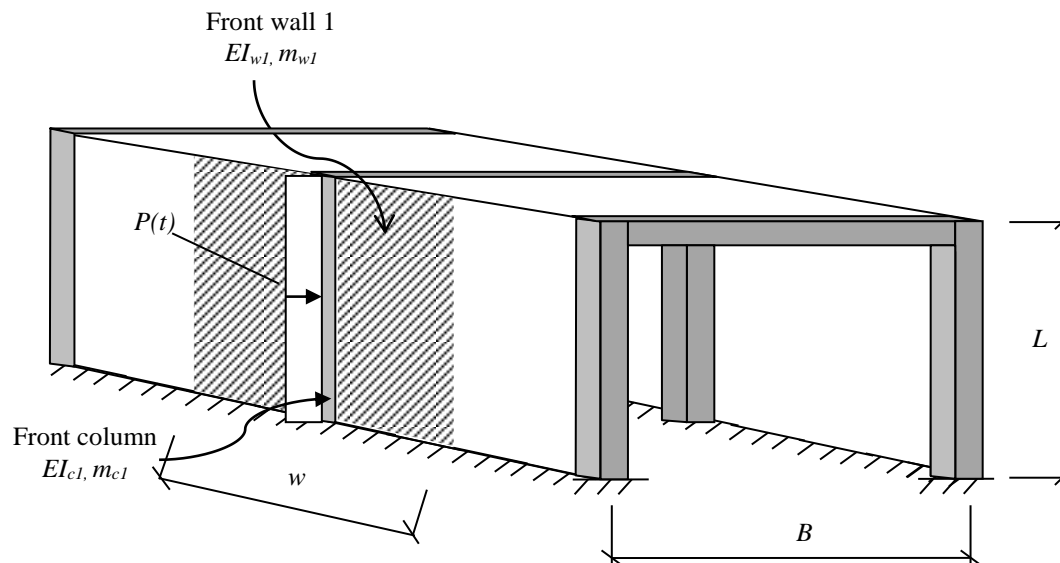


Figure 5.8 The total load from the marked area is applied on the front column at the same time.



The shape and duration of the load applied on the column will be the same as for the External load,  $P(t)$ , described in Section 5.4.1. However, the magnitude of the load will be larger since the area of where the load is applied is larger than one meter. The total load,  $F'(t)$ , applied directly on the front column is calculated according to equation (5.1) and is referred to as Direct load in this chapter.

$$F'(t) = w \cdot P(t) = 6 \cdot 60 = 360 \frac{kN}{m} \quad (5.1)$$

This calculation methodology, where the load is directly applied on the front column, is used in Johansson (2013). It is expected to provide conservative results since the load will have a higher magnitude than the load described in Section 5.4.3.

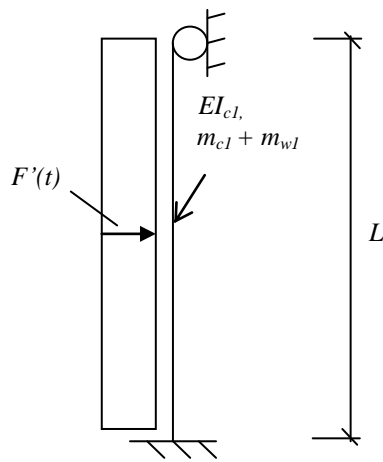


Figure 5.9 Direct application of the total impulse load,  $F'(t)$ , gathered from the marked area of the wall section.

## 5.4.3 Delayed application of load

### 5.4.3.1 Concept of delayed load

The front column is considered to carry the impulse load to the ground and through the roof beam to the back column while the wall only transfers the load to the column. When the impulse load hits the wall, the load is transferred to the column in form of support reaction. The transfer path of the load applied on the wall as well as the load direction within the column is presented in Figure 5.10.

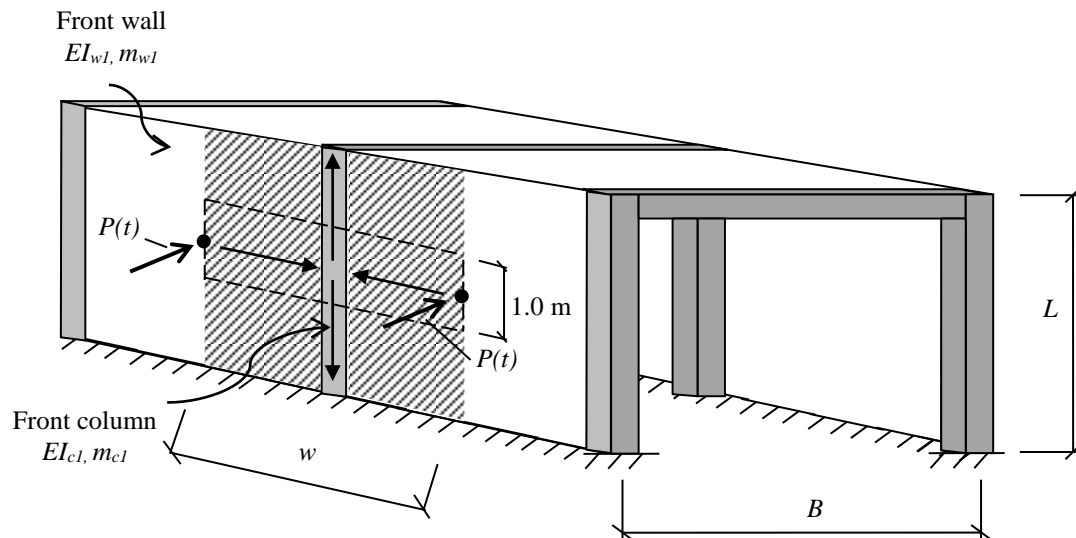


Figure 5.10 Path of the External load,  $P(t)$ , transferred through the wall to the column. The load is further transmitted to the restraints of the column, at the ground and at the top.

The dynamic reaction induced in the wall section by the External load  $P(t)$  is presented Figure 5.11a and the concept used in its estimation can be found in Section F.3. This dynamic reaction is loading the supporting column, according to Figure 5.11b. It is reasonable to expect that the effect on the structure of this dynamic reaction is less destructive than in case of the direct application of the load. The magnitude of the dynamic reaction is much lower and its duration is prolonged in time.

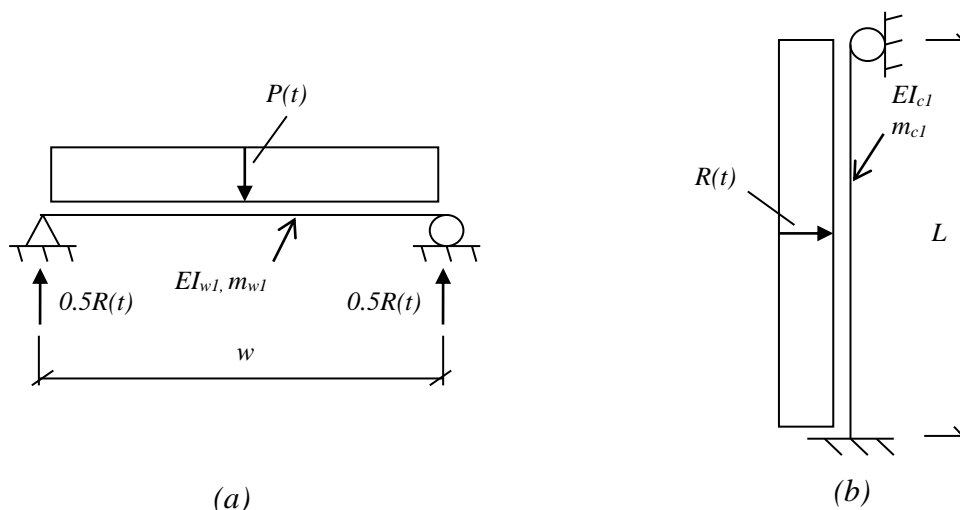


Figure 5.11 (a) The External load  $P(t)$  acting on the wall induces the dynamic reaction  $0.5 R(t)$ . (b) The dynamic reaction  $R(t)$ , from the wall sections on both sides of column, becomes the load on the column.

The dynamic reaction from the wall,  $R(t)$ , is calculated by implementing the central difference method, see Appendix D. The wall is modelled as a simply supported beam. The reaction,  $R(t)$ , is simulated for both an elastic and an elasto-plastic SDOF model of the wall. The development of the dynamic reaction and its correlation to the External load as well as the deformation and resistance is presented in Table 5.6.

It can be noticed that the maximum deformation of the wall is obtained at time  $t_{max}$  when the wall has absorbed the entire energy delivered by the External impulse load. The total impulse  $I_k$ , marked in Table 5.6a, multiplied by the area on which the impulse is acting corresponds to the marked area under the reaction-time curve in Table 5.6d. After the maximum deformation  $u_{max}$  is reached, the structure starts to oscillate elastically as it has been provided with a surplus of energy.

Table 5.6 Elastic and elasto-plastic models for: (a) the External load; (b) deformations obtained in wall; (c) resistance-deformation relationship; (d) development of resistance in time i.e. delayed load.

	Elastic response	Elasto-plastic response
(a)		
(b)		
(c)		
(d)		

The reaction  $R(t)$  in Table 5.6d will oscillate as the wall sways back and forth and therefore there are several different ways of interpreting the load from the wall which is transferred to the column. The different loads used for the elastic and elasto-plastic cases are described in Section 5.4.3.2 and 5.4.3.3, respectively.

### 5.4.3.2 Elastic reaction loads

The support reaction for the elastic model is simulated in four different ways, illustrated in Figure 5.12 and described in Table 5.7.

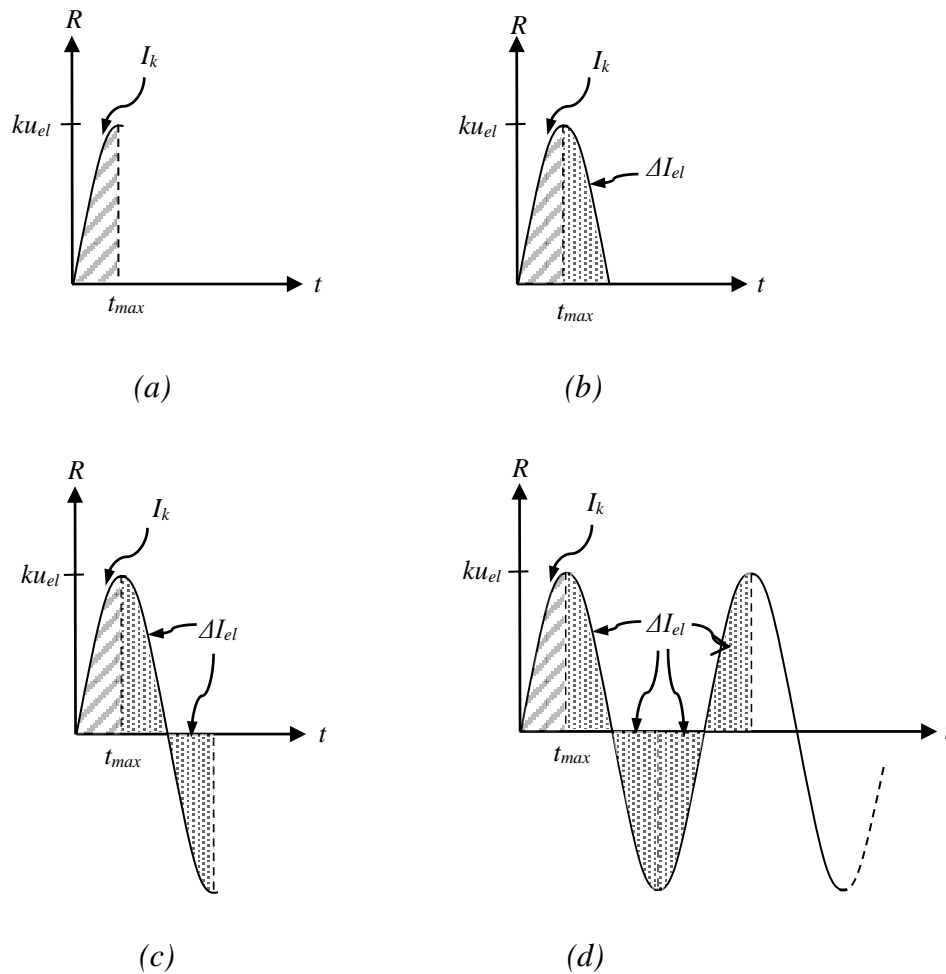


Figure 5.12 The reaction loads used in the study of the structure simulated with the elastic response curve: (a) Reaction load 1; (b) Reaction load 2; (c) Reaction load 3; (d) Reaction load 4.

Table 5.7 Description of the four different loads shown in Figure 5.12. Elastic model is used.

Reaction load	Description
Reaction load 1 Figure 5.12a	This load operates until the time $t_{max}$ when the External load, $P(t)$ , has been transmitted into the structure. This means that the Direct load, $F'(t)$ , and Reaction load 1 will contain the exact same impulse $I_k$ and are therefore comparable with regard to impulse size.
Reaction load 2 Figure 5.12b	Reaction load 2 is a continuation of Reaction load 1. For this load, the total impulse $I_k$ is increased with an extra impulse $\Delta I_{el}$ of the same magnitude as $I_k$ . Thus, this reaction load is expected to result in larger deformation.
Reaction load 3 Figure 5.12c	For Reaction load 3 an additional impulse $\Delta I_{el}$ , but with a negative sign, is added. The positive and negative additional impulse $\Delta I_{el}$ cancel out each other. Thus the total impulse transmitted into the structure corresponds to the impulse $I_k$ , which is the same as for Reaction load 1.
Reaction load 4 Figure 5.12d	Reaction load 4 is based on that the wall sways back and forth, creating an infinite oscillating reaction force. This is the most realistic interpretation of the load, except for the natural damping which would occur in reality. For Reaction load 4 the positive and negative additional impulse $\Delta I_{el}$ continues to cancel each other.

### 5.4.3.3 Elasto-plastic reaction loads

Two different reaction loads, illustrated in Figure 5.13 and described in Table 5.8, are investigated for the elasto-plastic case.

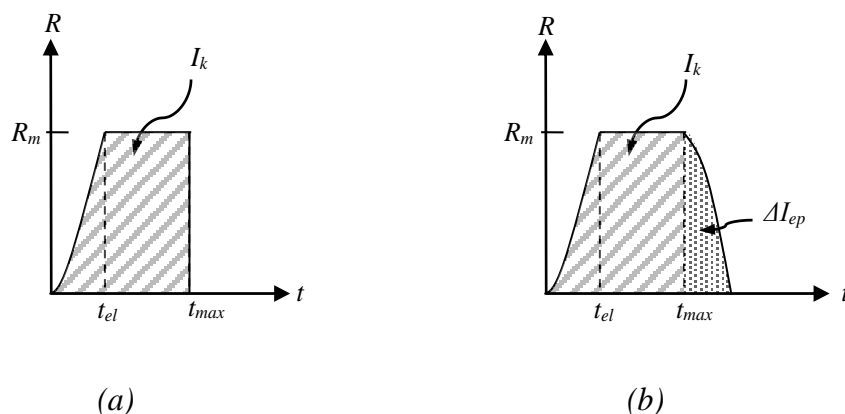


Figure 5.13 The reaction loads used in the study of the structure simulated with the elasto-plastic response curve: (a) Reaction load 5; (b) Reaction load 6.

Table 5.8 Description of the loads shown in Figure 5.13. Elasto-plastic model is used.

Reaction load	Description
Reaction load 5 Figure 5.13a	The concept of this load corresponds to Reaction load 1 for the elastic case. The load operates until the External load, $P(t)$ , has been transmitted into the structure. The size of the impulse, $I_k$ , is identical to the Direct load
Reaction load 6 Figure 5.13b	Reaction load 6 has the same concept as Reaction load 2 for the elastic case. Reaction load 5 is increased with an additional positive impulse $\Delta I_{ep}$ . Since the impulse is larger than for Reaction load 5, the effect and resulting deformation is predicted to be larger.

## 5.5 Modelling in ADINA

### 5.5.1 Introduction

The response of the considered structure is also studied with a FE analysis, where two different models are simulated in ADINA. The 2D model, further described in Section 5.5.2 corresponds to the SDOF model. The 3D model, described in Section 5.5.3, is created with both the wall and column in order to reassemble the real situation. Input files for the 3D model for elasto-plastic response can be found Section H.2.

### 5.5.2 2D model

The 2D model describes the front column. The boundary conditions, geometry and properties are identical to the SDOF model described in Section 5.3.2.

The method of modelling is the same as for the local response of the 2D frame structure, described in Section 4.5. 2D beam elements with three integration points across the height of the cross sections are used. The value of the equivalent Young's modulus  $E_{II}$  is calculated as

$$E_{II} = \frac{I_{II.c}}{I_{I.c.a}} E_I = \frac{1.1 \cdot 10^{-3}}{9.0 \cdot 10^{-3}} \cdot 33 = 4.16 \text{ GPa} \quad (5.2)$$

where  $I_{II.c}$  is the moment of inertia for the cracked section found in Table 5.4 and  $I_{I.c.a}$  is the moment of inertia for the uncracked section. The calculation of these parameters can be found in Section F.1.2.  $E_I$  is Young's modulus in state I from Table 5.1. The fictional yield limit  $f_{yd}$  is established as

$$f_{yd} = \frac{M_{rd.c}}{W_{el.c}} = \frac{211 \cdot 10^3}{(0.5 \cdot 0.6^2) / 6} = 7.03 \text{ MPa} \quad (5.3)$$

where  $M_{rd,c}$  is the moment capacity of the section which can be found in Table 5.4 and  $W_{el,c}$  is the elastic bending resistance.

The 2D model is used to confirm the correctness of the SDOF calculations. The comparison of the results from these two methods is presented in Section F.4.

### 5.5.3 3D model

The 3D model is created to better simulate the real behaviour of the analysed structure consisting of the wall, on where the load is applied, and the column. The real behaviour of the structure means that ADINA considers the speed of propagation of the impulse within the structure and the fact that it takes a certain time before the impulse applied on the wall has reached the column. Furthermore, the interaction of the wall's and column's dynamic response is included.

Both the column and the wall are modelled with their real dimensions and properties according to Section 5.2. The transfer of the load within the structure occurs in two directions while the deformation occurs in the third. Therefore it is not possible to describe the response by mean of a two dimensional space and a third direction must be introduced. The model implemented in ADINA is schematically presented in Figure 5.14. The column is modelled with mass  $m_{c1}$ , stiffness  $EI_{c1}$  while the wall is provided with mass  $m_{w1}$  and stiffness  $EI_{w1}$ . The calculations of these parameters can be found in Section F.1. The External load  $P(t)$  is applied only on the wall. The column is therefore subjected only to the support reaction,  $R(t)$ , induced by External load  $P(t)$ , transferred from the wall through the wall supports.

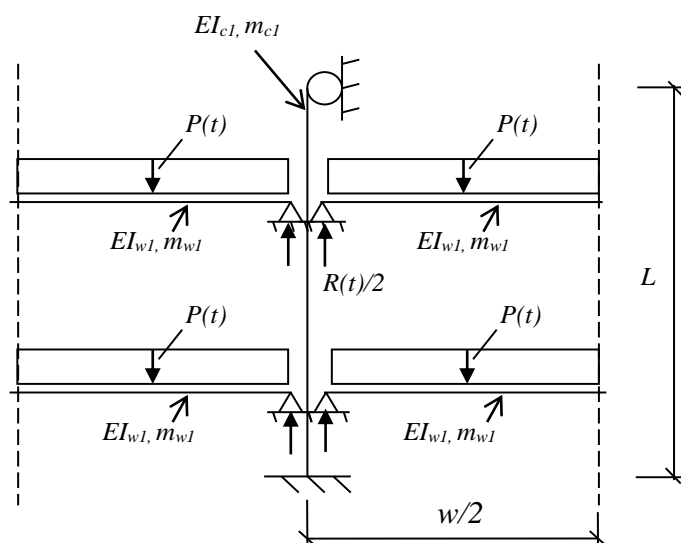


Figure 5.14 Schematic illustration of the 3D model implemented in ADINA. In the true model there are seven wall panels on each side of the column.

The response obtained in ADINA is assumed to simulate the real behaviour of the structure. However, the wall in this 3D FE model consists of 7 wall panels, resulting in seven point loads on the column instead of a uniformly distributed load. This means that the 3D FE model is an approximation of the reality, but it is assumed to reassemble the true behaviour of the structure more closely than the SDOF model and the 2D FE model.



For 3D beam elements, the Equivalent Young's modulus can be calculated in the same way as in the 2D analysis. For the wall and column, respectively, the equivalent Young's modulus is calculated as

$$E_{II} = \frac{I_{II.w}}{I_{I.w.a}} E_I = \frac{0.54 \cdot 10^{-3}}{0.64 \cdot 10^{-3}} \cdot 33 = 2.70 \text{ GPa} \quad (5.4)$$

$$E_{II} = \frac{I_{II.c}}{I_{I.c.a}} E_I = \frac{1.1 \cdot 10^{-3}}{9.0 \cdot 10^{-3}} \cdot 33 = 4.16 \text{ GPa} \quad (5.5)$$

where  $I_{II.w}$ ,  $I_{II.c}$ ,  $I_{I.w.a}$  and  $I_{I.c.a}$  are calculated in Section F.1. The values of Young's modulus in state I  $E_I$  can be found in Table 5.1.

When using 3D beam elements ADINA sets the number of integration points across the height of the section to 7 and it is not possible to choose any other option. According to Augustsson and Härenstam (2010) and Ek and Matsson (2009) the expected stress distribution for 7 integration point should be as in Figure 5.15b which differs from the theoretical distribution for a fully plasticised section, Figure 5.15a. Moreover, the yield stress obtained in ADINA, Figure 5.15c, has been proven to not agree with the expected stress distribution in Figure 5.15b. Therefore the input value of the yield stress must be modified.

The bending resistance for the fully plasticised section, Figure 5.15a, and for the section with stress distribution corresponding to the expected distribution in ADINA, Figure 5.15b, is calculated as

$$W_{pl} = \frac{1}{4} bh^2 \quad (5.6)$$

$$W'_{pl} = \frac{13}{54} bh^2 \quad (5.7)$$

where  $b$  is the width of the section and  $h$  is the height.

It can be noticed that  $W_{pl}$  is about 4 % larger than  $W'_{pl}$ . Moreover, Ek and Matsson (2009) have shown that in order to obtain the assumed value of the stress distribution as in Figure 5.15b, the input yield strength should be increased with 4.3 %. Therefore, when using the theoretical stress distribution, Figure 5.15a, the input yield strength should be increased with 8.3 %.

$$f_{yd.mod} = 1.083 f_{yd} \quad (5.8)$$

where

$$f_{yd} = \frac{M_{rd}}{W_{pl}} \quad (5.9)$$

Thus, the modified yield stress for the wall and column, respectively, to be used in ADINA in order to get the correct response is calculated as

$$f_{yd.mod.w} = 1.083 \cdot \frac{M_{rd.w}}{W_{pl.w}} = 1.083 \cdot \frac{38 \cdot 10^3 \cdot 4}{1 \cdot 0.2^2} = 4.10 \text{ MPa} \quad (5.10)$$

$$f_{yd.mod.c} = 1.083 \cdot \frac{M_{rd.c}}{W_{pl.c}} = 1.083 \cdot \frac{211 \cdot 10^3 \cdot 4}{0.5 \cdot 0.6^2} = 5.07 \text{ MPa} \quad (5.11)$$

where  $M_{rd.w}$  and  $M_{rd.c}$  is calculated in Section F.1.1 and F.1.2, respectively.

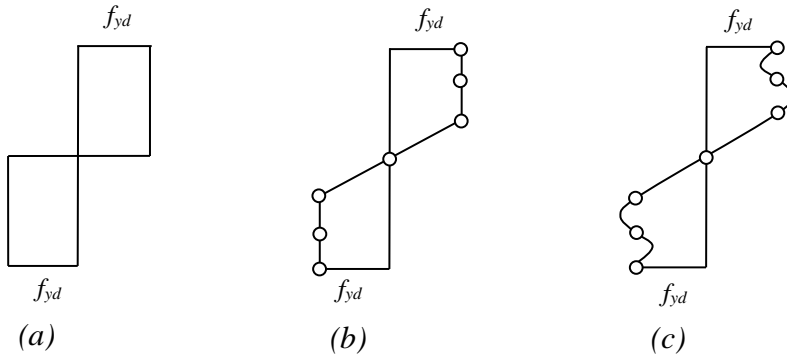


Figure 5.15. (a) Stress distribution for a fully plasticised section. (b) Assumed stress distribution for 7 integration points. (c) Stress distribution in ADINA for 3D beam elements according to Augustsson and Härenstam (2010).

The simply supported connection of the wall to the column is modelled with rigid links which is shortly described in Section 4.5.

## 5.6 Results and comparison

### 5.6.1 Elastic model

#### 5.6.1.1 Deformation obtained in SDOF and 3D FE analysis

In the SDOF model, presented in Figure 5.16a, the deformation of the column is obtained for the Direct load and for the reaction loads simulating the delayed loading. Comparison of these loads is done in Figure 5.17. The deformation,  $u(t)$ , is measured in the middle of the column. In the 3D FE analysis the delayed load corresponds to the reactions at the supports of the wall. The reactions from the wall are induced by the External load  $P(t)$  acting only on the wall.

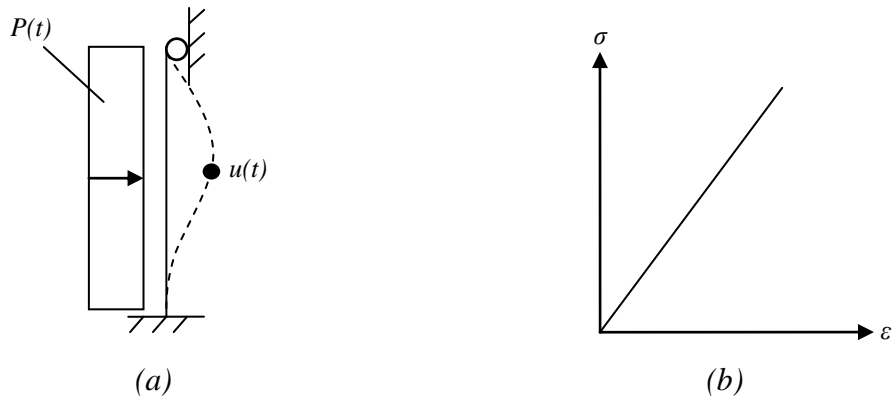


Figure 5.16 Illustration of: (a) the SDOF model of the front column and its deformation  $u(t)$ ; (b) the elastic material response model.

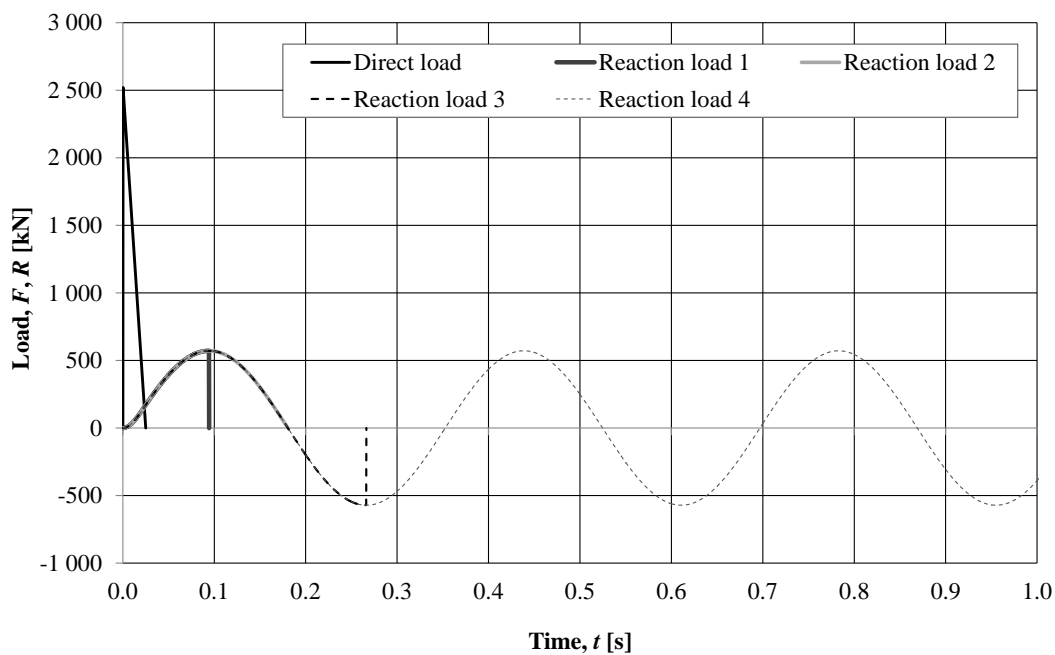


Figure 5.17 Load types used in the SDOF analysis of the structure simulated with the elastic response model. The loads are the sum of the load from the total considered area.

In Figure 5.17 the area under the Direct load curve, i.e. the impulse  $I$ , is the same as the area under the curve for Reaction load 1. The sizes of the impulses for the different loads are shown in Table 5.9 where positive and negative impulses are considered to cancel out each other.

Table 5.9 Total impulse transmitted to the structure for different loads.

Load type	$I = \int F(t) dt$ [kNs]
Direct load	32.5
Reaction load 1	32.5
Reaction load 2	65
Reaction load 3	32.5
Reaction load 4	0 - 65

The deformation obtained from the 3D FE analysis due to External load  $P(t)$  and the deformation due to the Direct load applied on the SDOF model are presented in Figure 5.18.

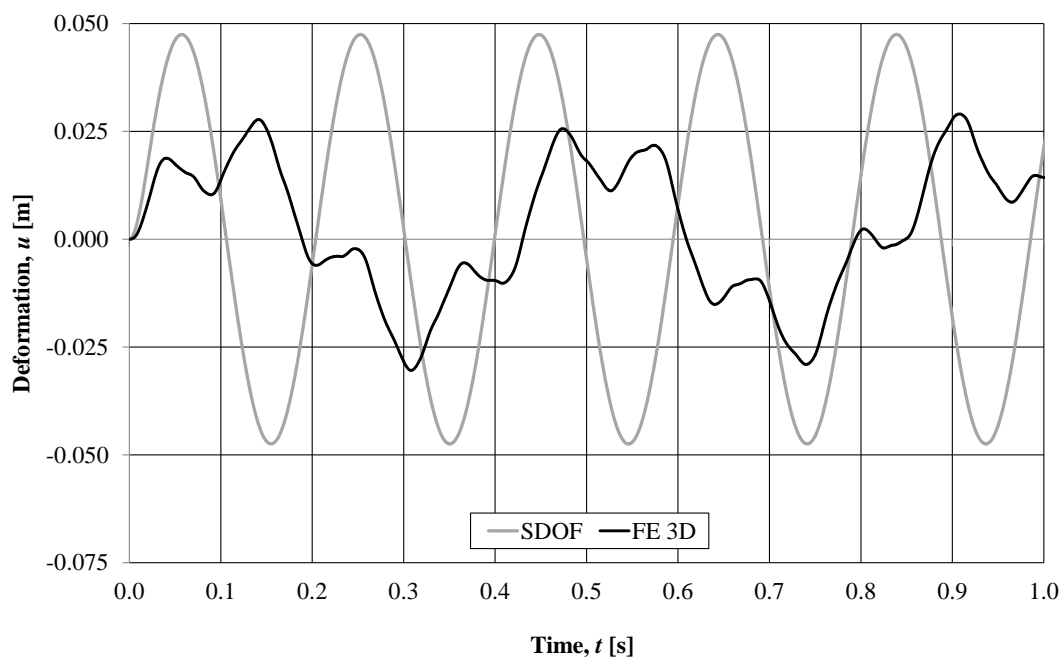


Figure 5.18 Comparison of deformation in the middle of the column obtained in the 3D FE analysis due to External load  $P(t)$  and in the SDOF analysis for the Direct load.

It can be noticed that the deformation of the column obtained in the SDOF analysis is almost twice as large as in case of the deformation from the 3D FE analysis. This shows that the simplified method of the frame structure provides results considerably on the safe side.

An FE analysis is also done where only the first bending mode is considered, which corresponds to the SDOF model. An FE analysis with only the first bending mode of the structure allows deformation of the column whereas the wall remains undeformed.

The results delivered from this FE analysis agrees well with the deformation obtained in the SDOF calculations, see Figure 5.19.

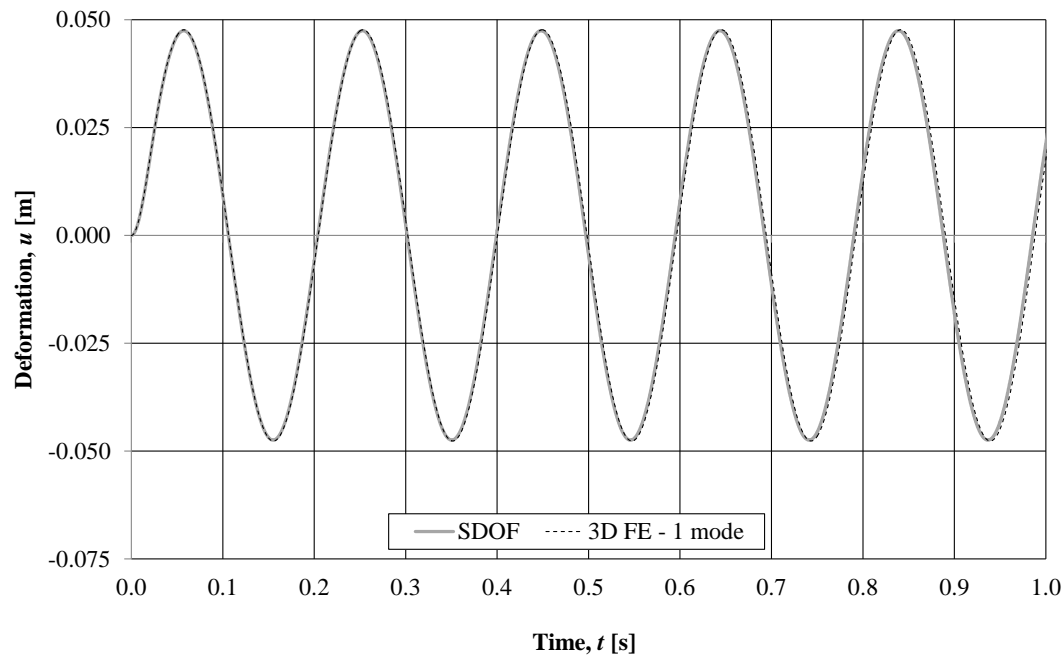


Figure 5.19 Comparison of the deformation in the middle of the column obtained in the 3D FE analysis due to External load  $P(t)$  for the first bending mode and in the SDOF calculation for the Direct load.

In addition to verifying the simplified SDOF method, which has shown to provide conservative results, a comparison of the deformation in the 3D FE analysis to the deformation obtained in SDOF for the delayed loading is also done. The reaction loads, presented in Figure 5.17 for the whole considered wall area, are created in order to simulate the true loading of the column, i.e. the reactions at the wall supports induced by the impulse load. The deformations obtained in SDOF for the studied reaction loads are compared to the results from the 3D FE analysis in Figure 5.20 and Figure 5.21.

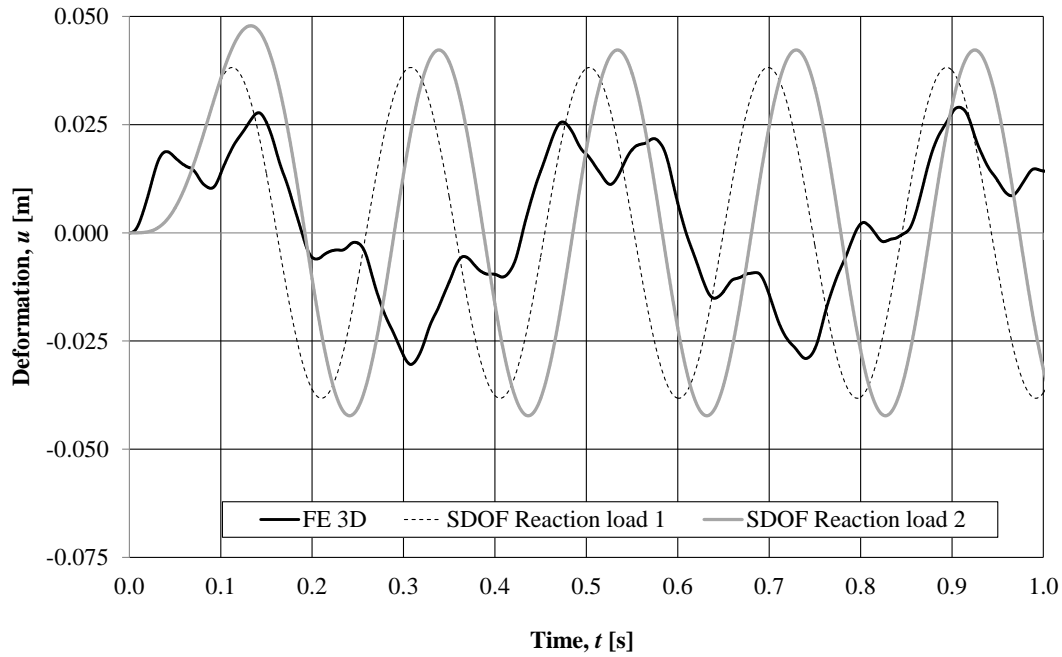


Figure 5.20 Comparison of the deformation in the middle of the column obtained in the 3D FE analysis due to External load  $P(t)$  and in the SDOF for Reaction load 1 and Reaction load 2.

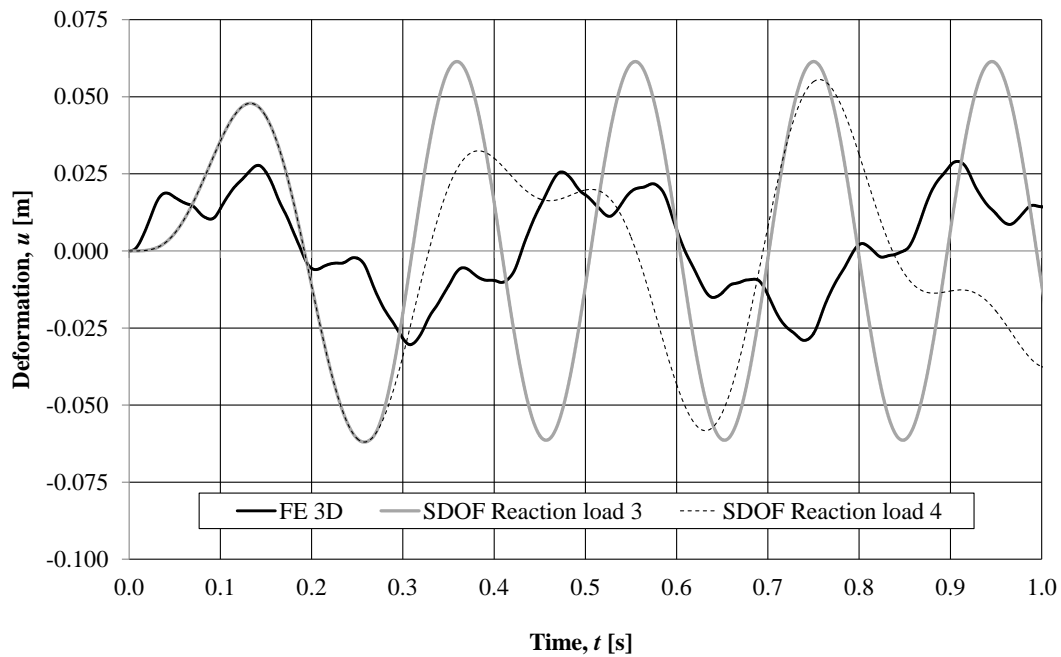


Figure 5.21 Comparison of deformation in the middle of the column obtained in the 3D FE analysis due to External load  $P(t)$  and in the SDOF for Reaction load 3 and Reaction load 4.

A summary of the maximum deformations obtained in SDOF and in the FE model can be found in Table 5.10. For each type of load, the SDOF analysis provides results on the safe side.

Table 5.10 Maximum deformation in the middle of column obtained in the FE analysis and SDOF calculations.

Load type	SDOF $u_{max}$ [m]	FE 3D $u_{max}$ [m]
Direct load	0.047	0.027
Reaction load 1	0.038	
Reaction load 2	0.047	
Reaction load 3	0.062	
Reaction load 4	0.062	

The SDOF deformations are further discussed in Section 5.6.1.2 and the reasons for the shape of the deformation curve from the 3D FE analysis are discussed in Section 5.6.1.3.

### 5.6.1.2 Discussion of the SDOF deformation

When comparing the loads used for the study of the structure, which are presented in Figure 5.17, the difference in time at which their maximum value is reached is obvious. The Direct load reaches its peak value instantaneously at  $t_{peak}$  equal to 0 ms, while the reaction loads at  $t_{peak}$  around 100 ms.

The deformation due to the Direct load, Reaction load 1 and Reaction load 2 are shown in Figure 5.22.

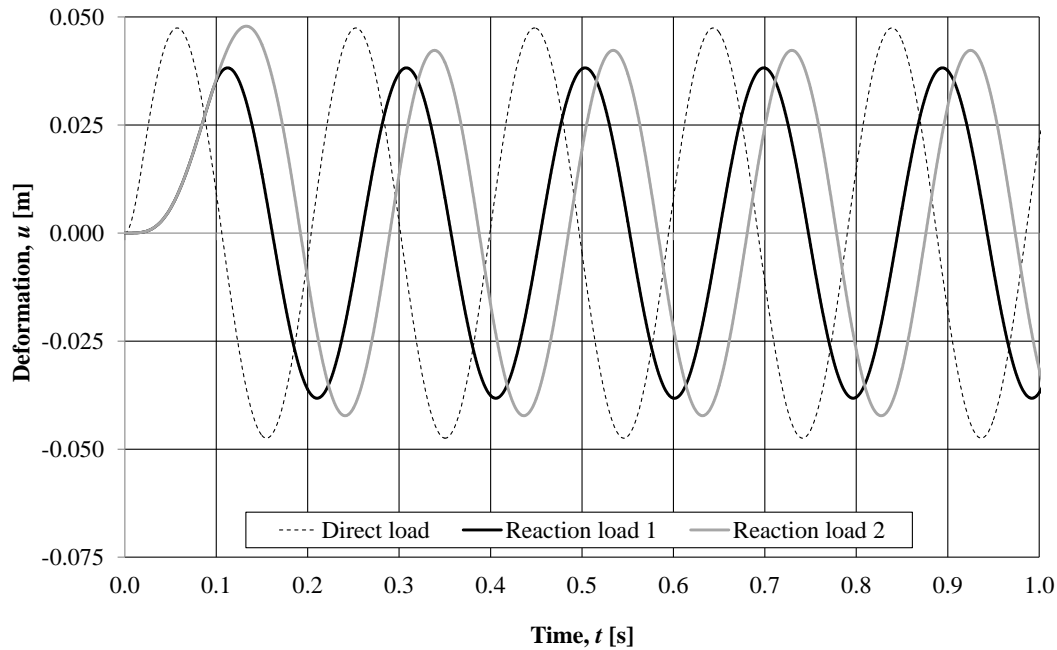


Figure 5.22 Deformation in the middle of the column obtained from the SDOF calculations for Direct load, Reaction load 1 and Reaction load 2.

A comparison of the loads and deformation for the Direct load and Reaction load 1 is shown in Figure 5.23. The Direct load and Reaction load 1 contains the same impulse, see Table 5.7. However, the duration of the Direct load is seven times shorter than the duration of Reaction load 1 while its magnitude is around four times larger. The fact that Reaction load 1 is prolonged in time enables the structure to develop a resistance against the energy transferred when the impulse hits the structure. Thus, the external work done by the Direct load is larger than the external work done by Reaction load 1. When comparing the internal work for these two cases of loading, the deformation is larger for the Direct load as the area under resistance-deformation curve for this load is also larger than for Reaction load 1, see Figure 5.24.



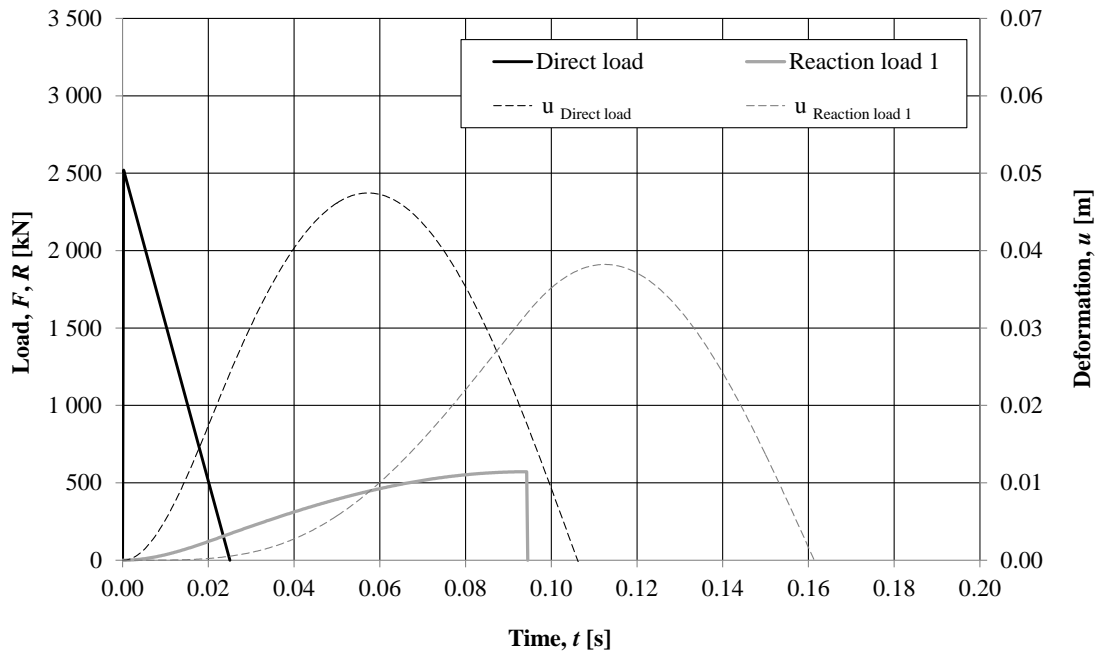


Figure 5.23 Comparison of the deformation in the middle of the column due to the Direct load and Reaction load 1.

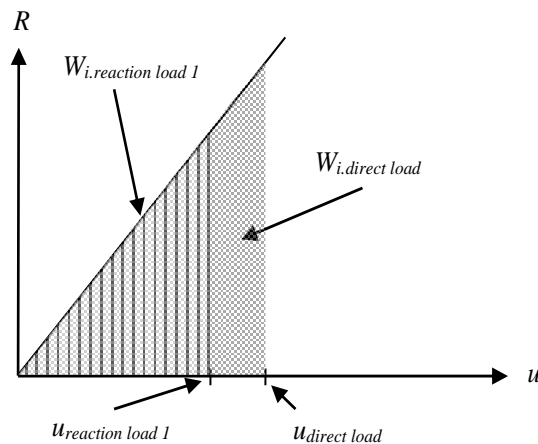


Figure 5.24 Comparison of internal work and resulting deformation for the structure subjected to the Direct load and Reaction load 1.

For Reaction load 1 all deformation peaks reaches the same magnitude, which can be seen in Figure 5.22. In this case, the load has stopped before the deformation has reached its maximum value, see Figure 5.25.

Reaction load 2 is a continuation of Reaction load 1. Both the duration and the total impulse for Reaction load 2 are twice as large as for Reaction load 1. Thus, the resulting deformation from Reaction load 2 is expected to be also larger. However, the difference in deformation for the two loads is only 0.004 m, see Figure 5.25. The external work done by Reaction load 2 is not significantly larger than for Reaction load 1. The fact that the load is prolonged in time gives the structure time to develop resistance against the kinetic energy transferred when the load hits the structure.

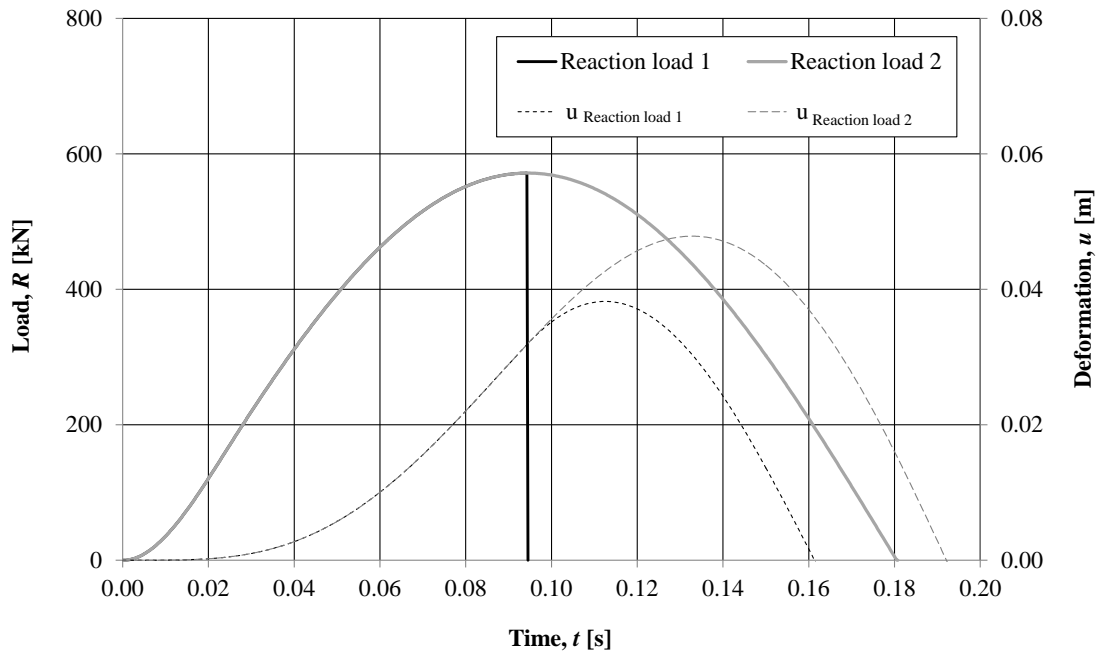


Figure 5.25 Comparison of the deformations in the middle of the column due to Reaction load 1 and Reaction load 2.

The first peak of the deformation caused by Reaction load 2 is higher than the following peaks, see Figure 5.22. This is a result of the prolonged duration of this load. At the time when the first peak occurs, the load is still acting, pushing the deformation to a higher value. This can be seen in Figure 5.26 where the development of the deformation due to the Direct load and Reaction load 2 is compared.

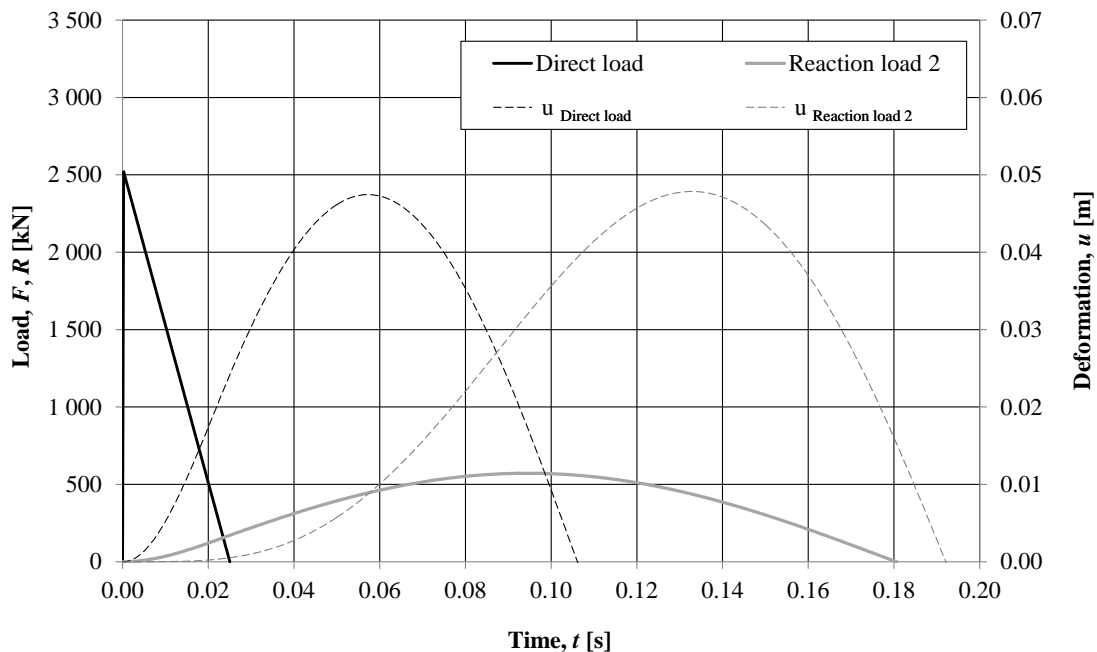


Figure 5.26 Comparison of the deformations in the middle of the column due to the Direct load and Reaction load 2.

The deformation induced by Reaction load 3 is larger than for the Direct load, see Figure 5.27. Moreover, the common assumption that the initial response is the most critical for dynamically loaded structures does not agree here.

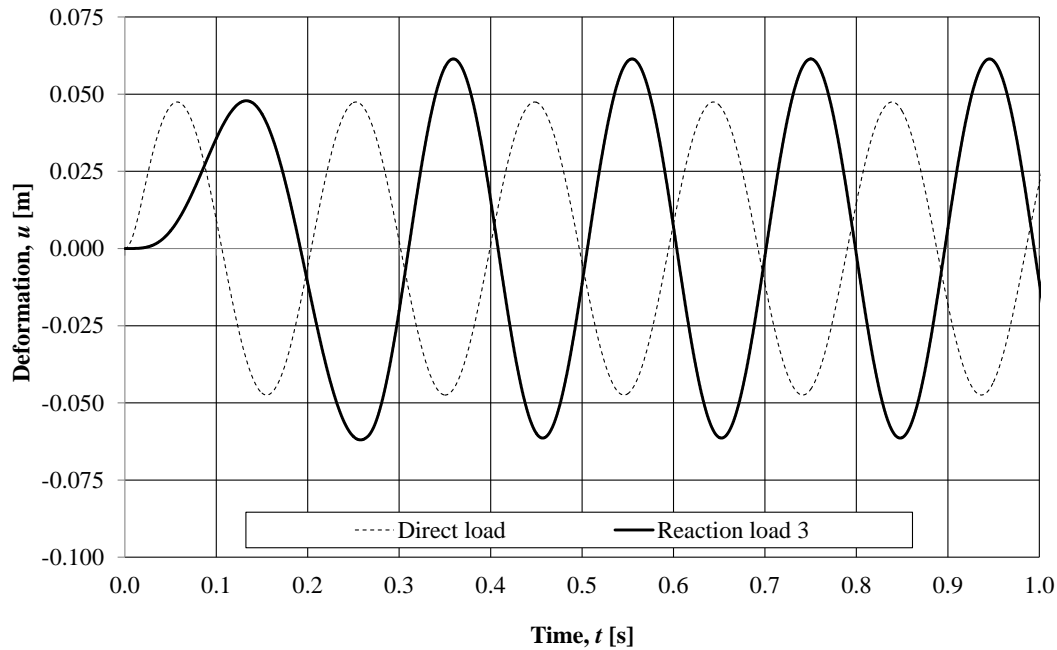


Figure 5.27 Deformation in the middle of the column due to the Direct load and Reaction load 3.

For Reaction load 3 the additional negative impulse,  $-AI_{el}$ , theoretically counterbalances the positive additional impulse,  $AI_{el}$ , in order to get a total impulse  $I_{el}$ , see Table 5.7. However, in this case the frequency of the reaction load coincides with the frequency of the structure which thus enhances the effect of the load and pushes the negative deformation to a higher value, see Figure 5.28.

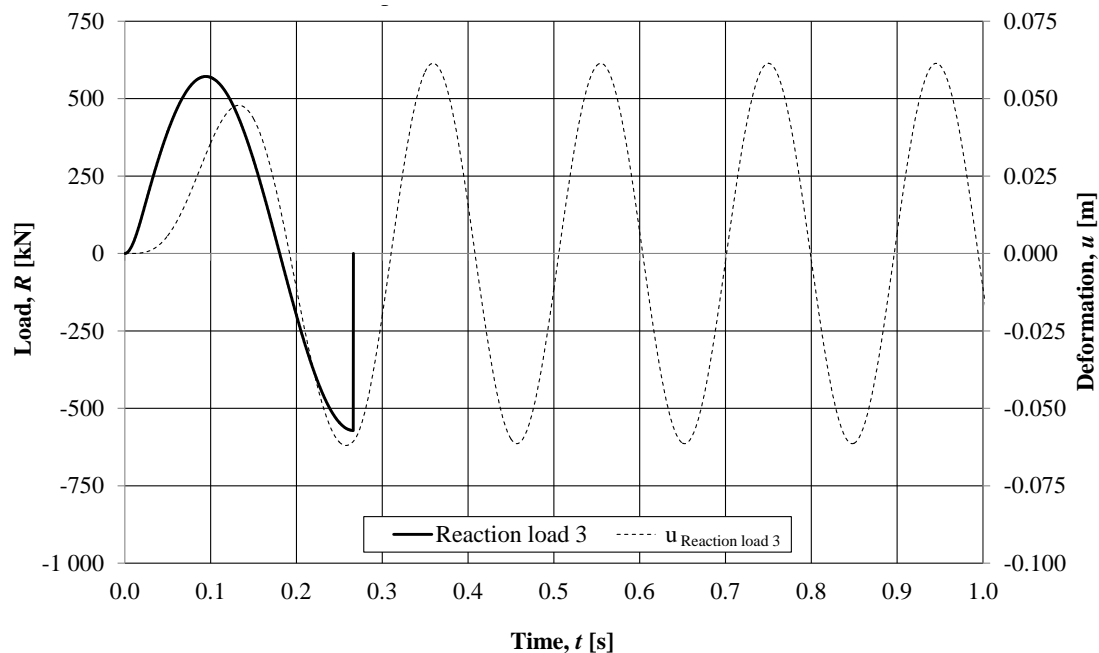


Figure 5.28 Comparison of the deformation in the middle of the column and Reaction load 3.

The deformation obtained due to Reaction load 4 is compared with the deformation caused by the Direct load in Figure 5.29. It can be noticed that the highest

deformation due to Reaction load 4 is obtained after several sways. Moreover, this deformation is larger than the maximum deformation caused by the Direct load.

These results does not agree with the common assumption for impulse loaded structures that the impulse load is the most destructive, nor that the most critical part is the initial response. However, since the structures in reality have a certain amount of damping the deformations decreases significantly with time. Therefore, the higher deformation obtained after several sways can be disregarded.

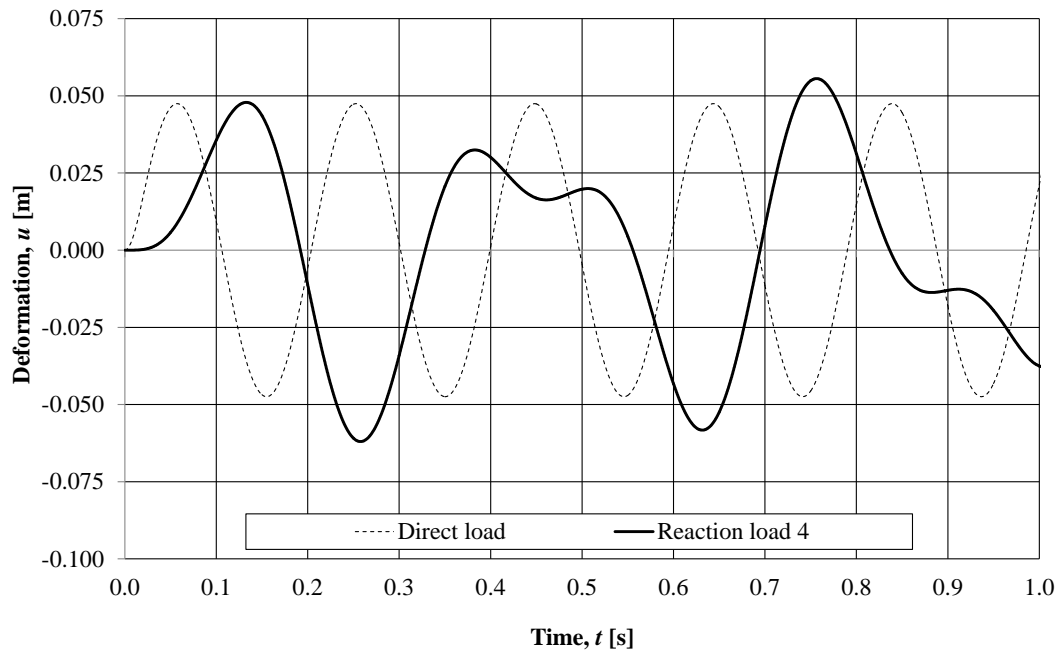


Figure 5.29 Deformation in the middle of the column due to the Direct load and to Reaction load 4.

Reaction load 4 and the resulting deformation are presented in Figure 5.30. The shape of the deformation curve is a result of how the development of deformations coincides with the frequency of the reaction load.

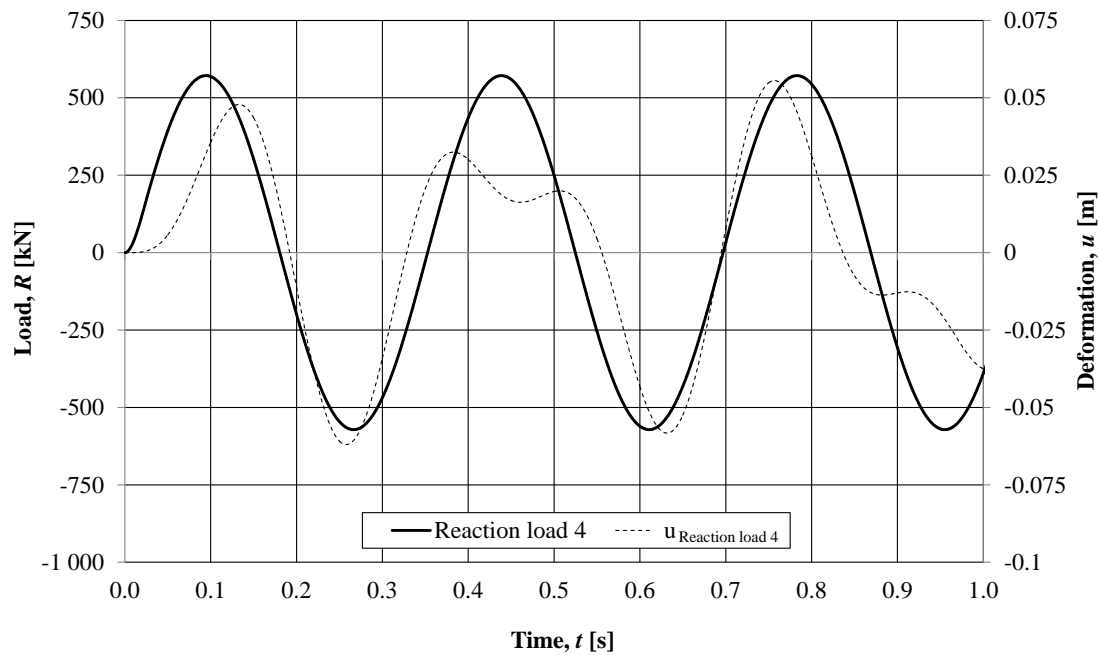


Figure 5.30 Deformation in the middle of the column due to Reaction load 4.

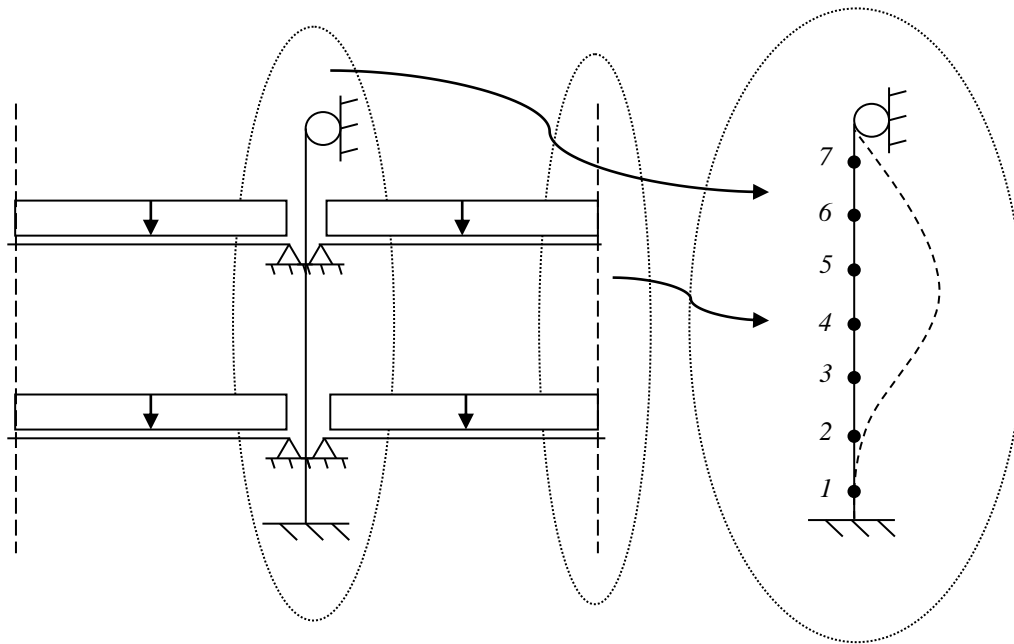
The maximum deformations obtained for different loads are presented together with the theoretical size of the impulse load in Table 5.11. It can be seen that the most critical deformation obtained in the SDOF calculations is for Reaction load 3 and 4. However, since those deformations are obtained after several sways, they might still not be the most critical in reality due to the natural damping.

Table 5.11 Maximum deformation and total impulse transmitted to the structure for different loads.

Load type	$u_{max}$ [m]	$I=\int F(t)dt$ [kNs]
Direct load	0.047	32.5
Reaction load 1	0.038	32.5
Reaction load 2	0.047	65
Reaction load 3	0.062	32.5
Reaction load 4	0.062	0 - 65

### 5.6.1.3 Structural response of wall panels in 3D FE analysis

In order to better understand the behaviour of the 3D structure, the wall panels are investigated. The points where the deformation in the middle of the wall is measured are illustrated in Figure 5.31.



*Figure 5.31 The different points along the column, for which the support reactions and the deformations in the middle of the wall, are measured.*

A comparison of the deformation obtained in the middle of the wall as well as in the middle of the column is presented in Figure 5.32. The deformations of the wall are also compared to the deformation of a simply supported beam with the same properties and dimensions as the wall panels. The best agreement of deformations for all points is at the beginning of the response i.e. within the first 0.3 seconds.

The deformation that agrees best with the simply supported beam is the deformation for the point which is closest to the fixed support, i.e. point 1. This region of the column is characterised by the highest stiffness and lowest deformation of the column and therefore the support of the wall corresponds to a simple support. The largest deformations of the wall is obtained for the panels located in the middle of the column and panels closer to the simply supported edge of the column, i.e. point 4 and 5. The deformations in these points becomes delayed while their magnitudes increase.

The deformation in the middle of the column is much smaller than in the middle of the wall. This is partly due to the difference in stiffness and boundary conditions of the wall and column as well as due to difference between the loads acting on column and wall. Since the 3D FE wall model is made of seven wall panels on each side of the column, the column is exposed to seven support reactions instead of one uniformly distributed load. Figure 5.33 shows those reactions acting on the column at the locations illustrated in Figure 5.31.

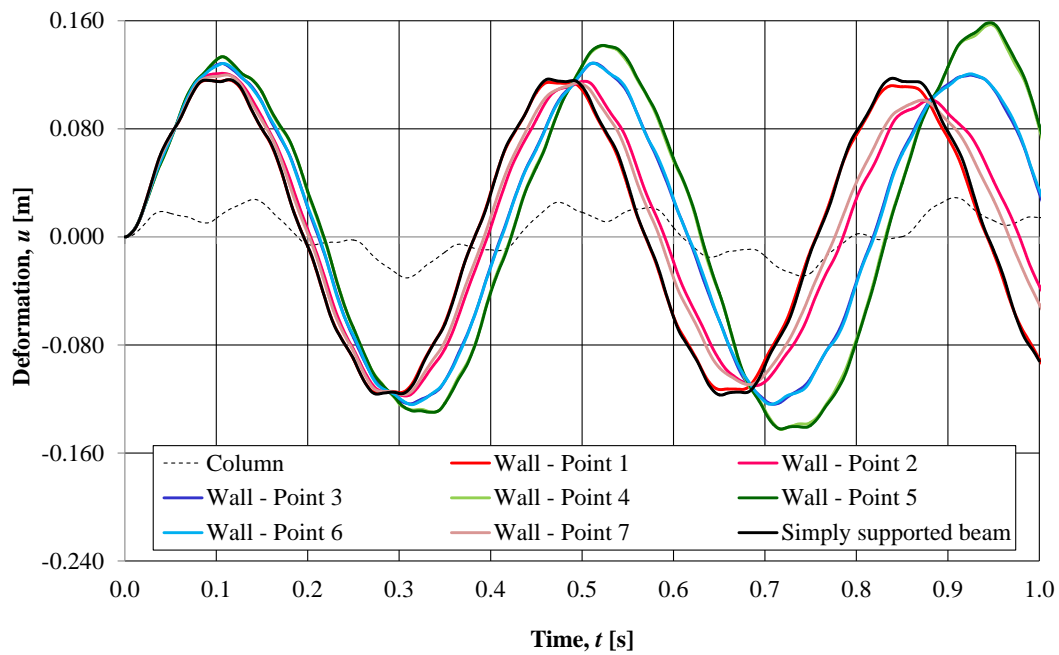


Figure 5.32 The deformations in the middle of the wall, measured in different points along the column, are compared to the deformation of a simply supported beam and to the deformation in the middle of the column.

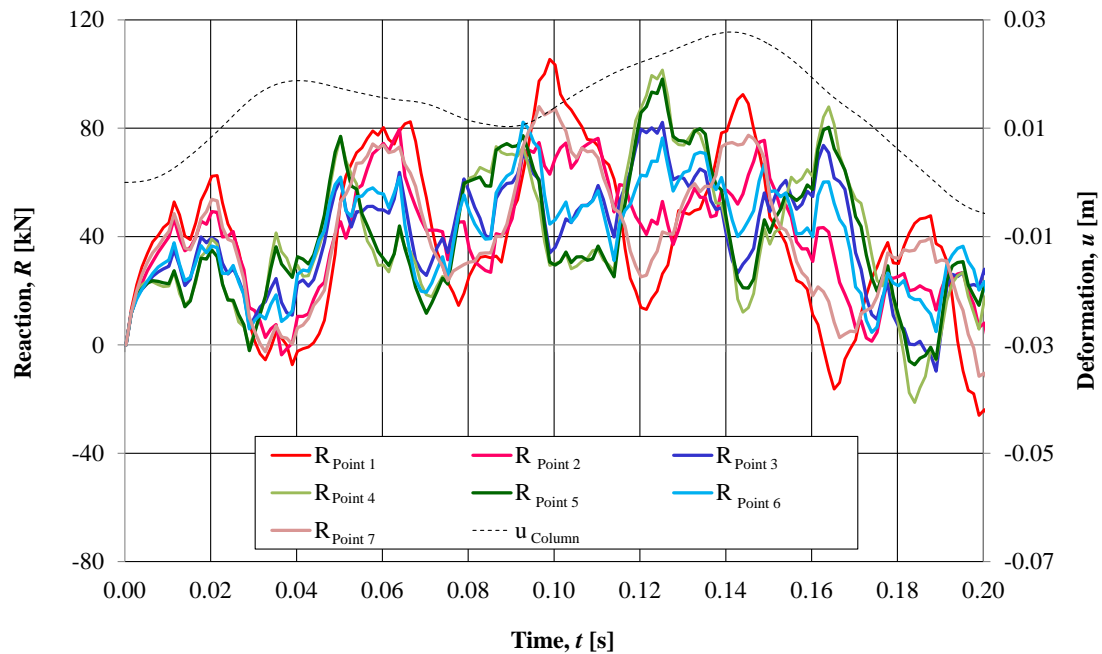


Figure 5.33 A comparison of deformation in the middle of the column and the support reactions acting on the column. The reactions are the sum from the wall panels on both sides of the column.

In Figure 5.33 it can be seen that the reaction forces transferred from the wall to the column do not coincide. For a certain time interval the load case can be illustrated as in Figure 5.34.

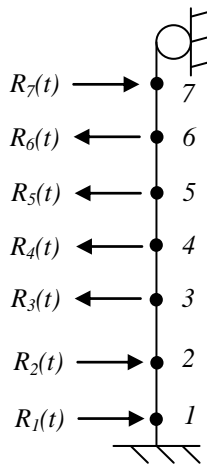


Figure 5.34 The reactions transferred from the wall to the column have different frequencies and do not coincide. At a certain time interval both the magnitude and the direction of reactions vary.

The behaviour of the reaction forces is partly a consequence of that the wall is modelled with a number of independent wall panels in ADINA. Their action corresponds to the action of the beam supported on springs. The stiffness of the springs is decided by the stiffness of the column, which varies along the length of the column, see Figure 5.35. Thus, for the different wall panels the supports are provided with different stiffnesses. For example, the stiffness of the wall panel next to the fixed edge of the column,  $k_1$ , is larger than for the wall panel in the middle of column,  $k_4$ . As a result the different wall panels have different frequency.

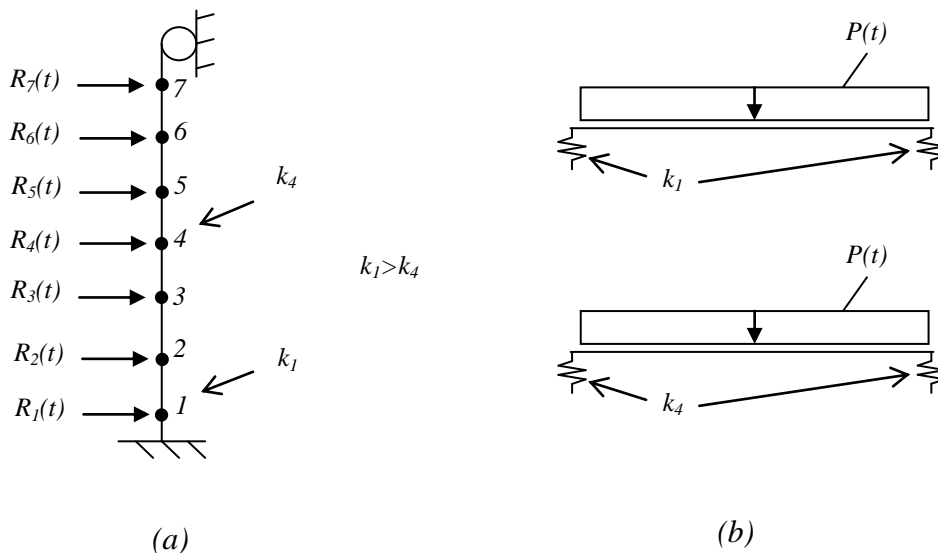


Figure 5.35 (a) The stiffness of the column supporting the wall panels differ for different regions. (b) The stiffness of the support of the wall panel is decided by the stiffness of the column at the corresponding location.



The fact that the reaction forces doesn't coincide is a probable reason for the uneven development of deformation in the middle of the column. The counteraction of the reaction forces can be considered as a sort of damping.

In order to understand the behaviour of the reaction forces better, point 1 and 4 in Figure 5.35 are investigated further. The reaction transferred from the wall panel to the column at those point during the first second is presented in Figure 5.36 and Figure 5.37. The reaction force is compared to the support reaction for a simply supported beam. The support reactions for all other points along the column can be found in Section F.5.1.

Similarly as for the deformation the best agreement with the simply supported beam is for the wall panel with its support next to the fixed support of the column, i.e. point 1. For the wall supports towards the middle of the column, the reaction is delayed due to the decreased stiffnesses in this region. The supports in the middle of the column corresponds to a spring, since it is not fixed in the vertical direction.

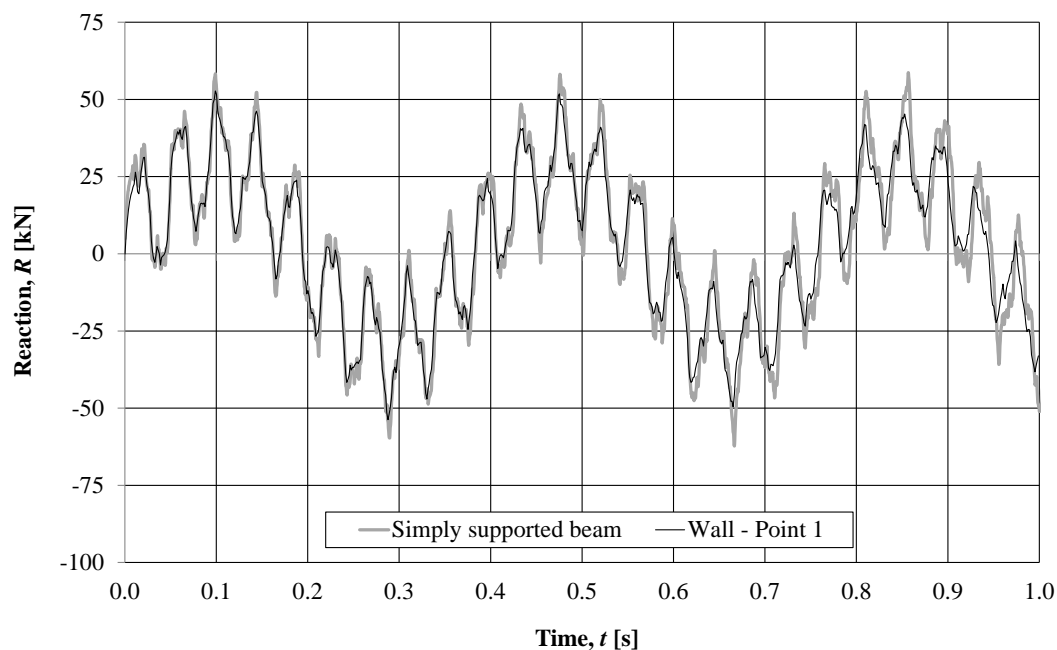


Figure 5.36 A comparison of reaction forces for a simply supported beam and the reaction transferred from the wall panel to the column at location 1.

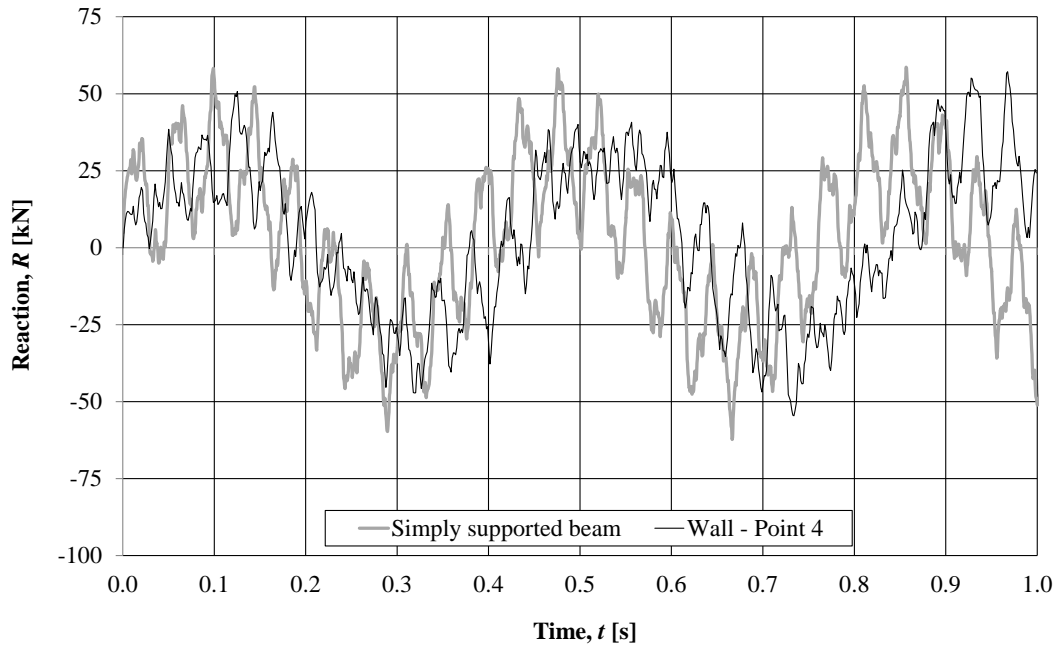


Figure 5.37 A comparison of reaction forces from a simply supported beam and the reaction transferred from the wall panel to the column at location 4.

In order to compare the delayed load in the 3D FE analysis with the delayed load from the SDOF analysis, the reactions from the wall panels are added according to equation (5.12) and plotted together with the delayed load from SDOF in Figure 5.38.

$$R_{tot}(t) = \sum_{i=1}^7 R_i(t) \quad (5.12)$$

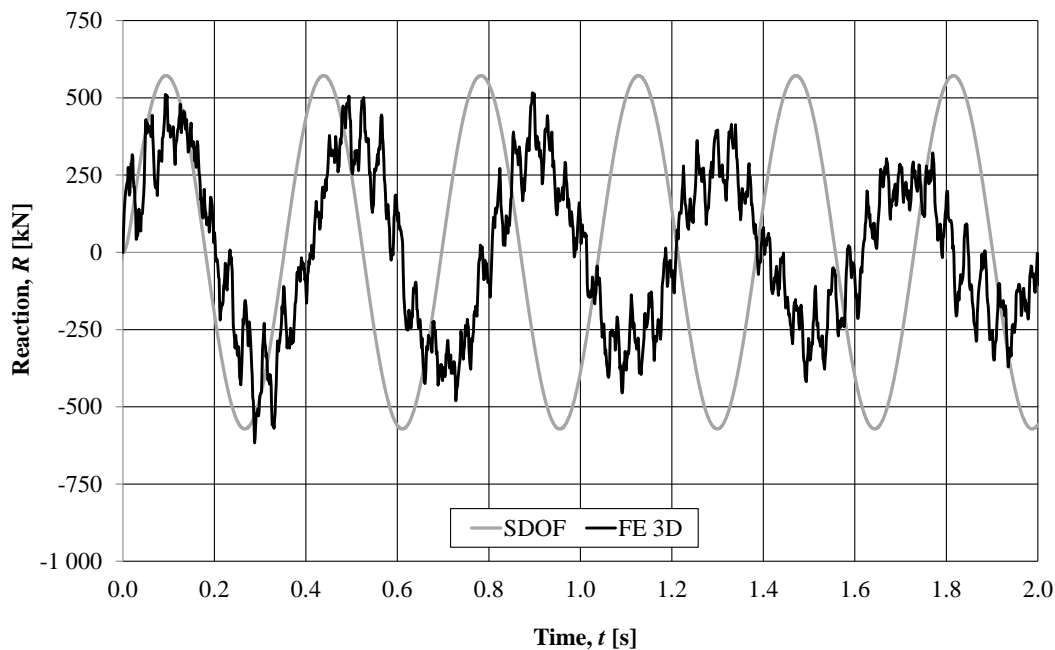


Figure 5.38 A comparison of the delayed loading in SDOF and 3D FE analysis.

It can be noticed that  $R_{tot}(t)$  from the 3D FE analysis is decreasing with time. This is caused by the fact that the vibrations of the different wall panels do not coincide, which can be considered as a sort of damping.

The magnitude of the total reaction calculated in SDOF is higher than in the 3D FE analysis, which agrees with the fact that the dynamic reaction is overestimated when it is calculated with regard to the assumption for the static load according to Andersson and Karlsson (2012). The concept of calculation the dynamic reaction can be found in Section F.3. The reactions obtained in the SDOF and 3D FE analysis, presented in Figure 5.38, agrees best at the very beginning of the response. The frequency is somewhat similar. However, the total reaction in the FE analysis becomes delayed since the supports of the wall panels in this FE analysis have different stiffnesses. However, the supports in the SDOF model of the wall are fixed in the vertical direction.

The development of the total reaction acting on the column in the FE analysis in a longer time interval is plotted in Figure 5.39. §

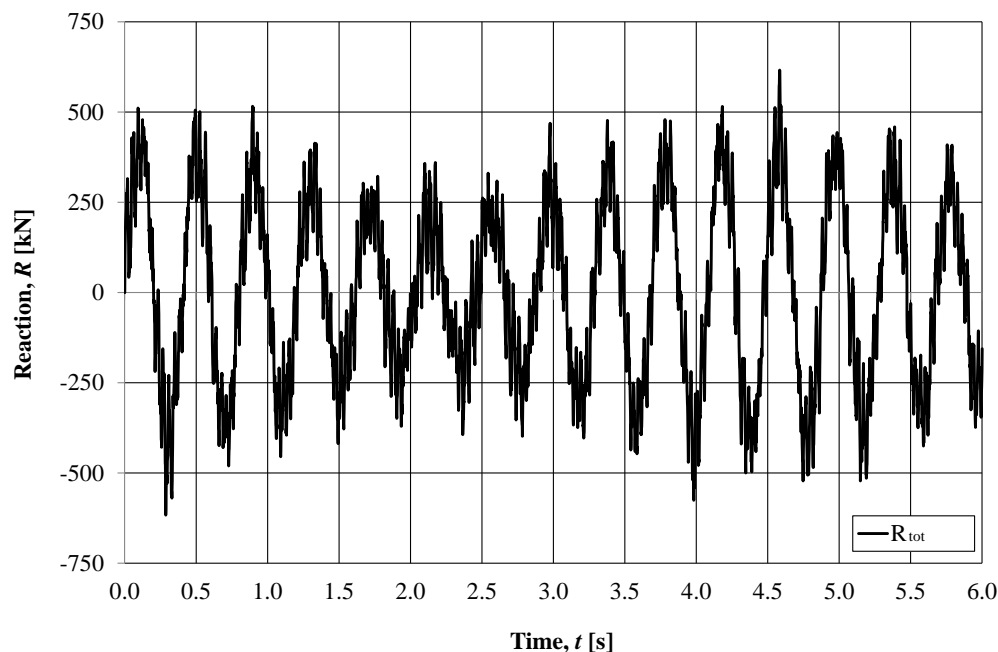


Figure 5.39 Total reaction acting on the column in the 3D FE analysis.

At around 2.5 seconds, when the total reaction reaches its lowest magnitude, the reactions at the stiffer regions of the column are working in another direction than the reactions in the regions with lower stiffness, see Figure 5.34. At around 4.5 seconds the highest magnitude of the total reaction is reached since the support reactions are working in the same direction. This effect makes the simulation of the response difficult to conduct in the SDOF system.

## 5.6.2 Elasto-plastic model

### 5.6.2.1 Deformation obtained in SDOF and FE 3D analysis

The deformation of the column in the SDOF analysis is obtained for the Direct load and for the reaction loads which simulate the delayed loading. The deformation  $u(t)$  is measured in the middle of the column, shown in Figure 5.40. In the 3D FE analysis

the delayed load corresponds to the reactions at the supports of the wall which are induced by the External load  $P(t)$  acting only on the wall. An illustration of all loads used for the study of the structure in SDOF analysis is shown in Figure 5.41.

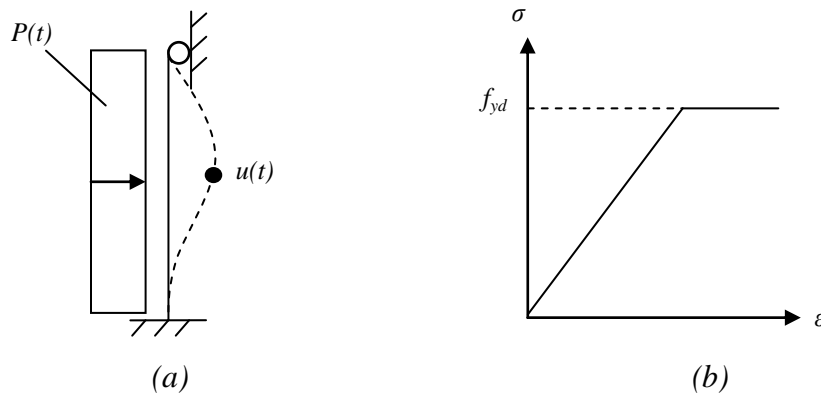


Figure 5.40 Illustration of: (a) the SDOF model of the front column and the deformation  $u(t)$ ; (b) the elasto-plastic material response model.

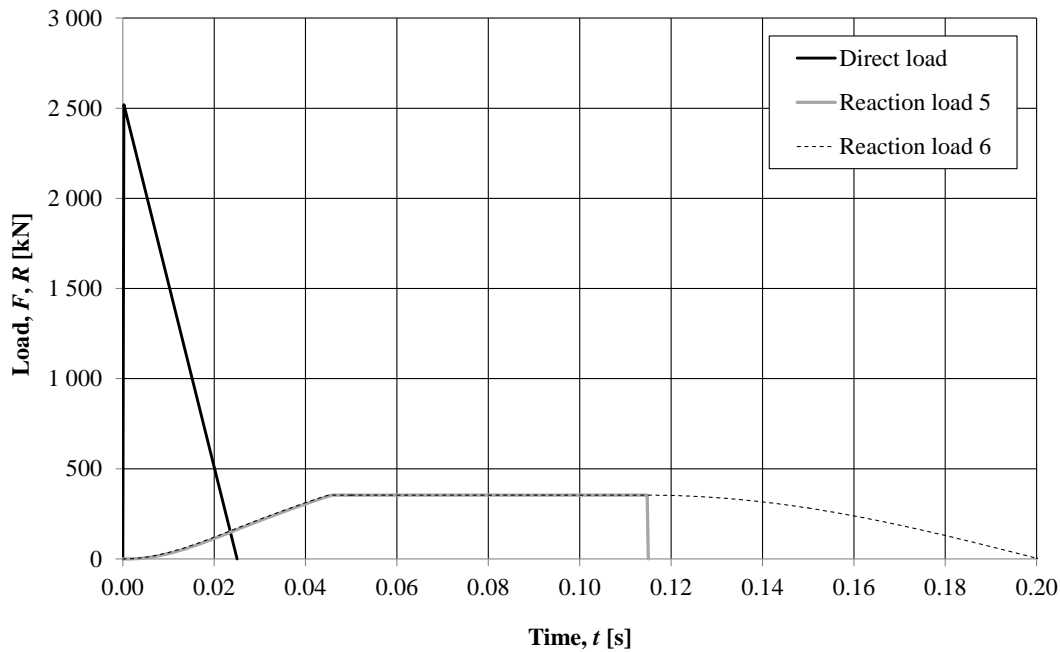


Figure 5.41 Load types used in the analysis of the structure simulated with the elasto-plastic response curve. The loads are the sum of the load from the total considered area.

When studying Figure 5.41, it can be noticed that the duration of the Direct load is shorter than the duration of the reaction loads, while its magnitude is around seven times larger. Reaction load 5 contains the same impulse as the Direct load, see Table 5.8. The area under the Direct load curve, i.e. the impulse  $I$ , is the same as the area under the curve for Reaction load 5. The sizes of the impulses for the different loads are shown in Table 5.12.

Table 5.12 Total impulse transmitted to the structure for different loads.

Load type	$I = \int F(t) dt$ [kNs]
Direct load	32.5
Reaction load 5	32.5
Reaction load 6	51.6

The deformation obtained from the 3D FE analysis due to External load  $P(t)$  and the deformation for the Direct load and the reaction loads applied on the SDOF model are presented in Figure 5.42.

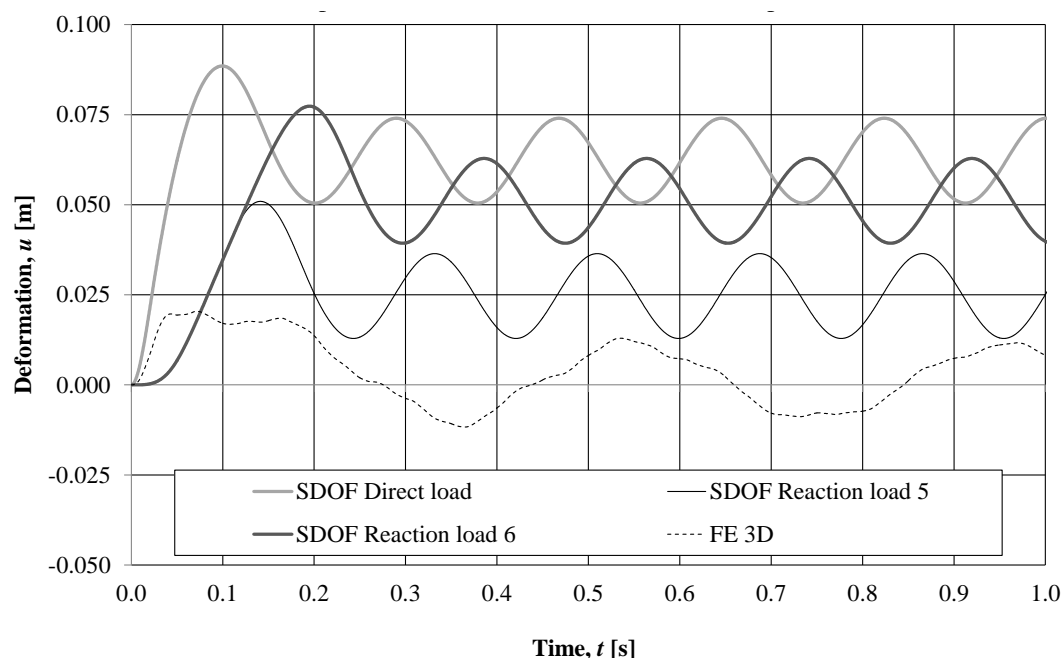


Figure 5.42 Comparison of deformation in the middle of the column obtained in the 3D FE analysis due to External load  $P(t)$  and in the SDOF for the Direct load and reaction loads.

The maximum magnitude of the deformation in the 3D FE analysis is 0.02 m, while it is almost 0.09 m in the SDOF for the Direct load. Thus, it can be stated that the method proposed by Johansson (2013) provides conservative results which are very much on the safe side.

The reaction loads implemented in SDOF provide smaller deformation than the Direct load, i.e. the results for the delayed loads are still on the safe side. The elasto-plastic reaction models are further discussed in Section 5.6.2.2. The probable reasons for the behaviour of the column in the 3D FE analysis is explained in Section 5.6.2.3. A comparison of maximum deformations in Figure 5.42 is presented in Table 5.13.

Table 5.13 Maximum deformation obtained in SDOF and FE analysis.

Load type	SDOF $u_{max}$ [m]	FE $u_{max}$ [m]
Direct load	0.088	0.020
Reaction load 5	0.051	
Reaction load 6	0.077	

### 5.6.2.2 Discussion of SDOF deformation

An illustration of all loads used for the study of the structure, simulated with the elasto-plastic response curve in SDOF, is shown in Figure 5.41. The deformation due to these loads are shown in Figure 5.43.

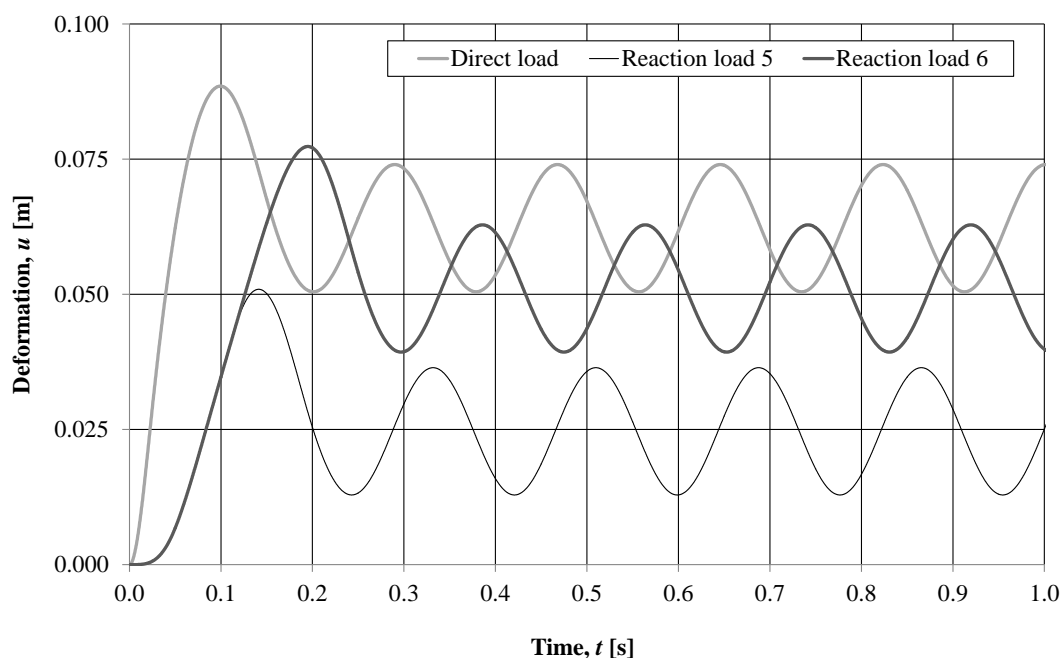


Figure 5.43 Deformation in the middle of the column for the Direct load, Reaction load 5 and Reaction load 6.

Reaction load 5 is prolonged in time compared to the Direct load, see Figure 5.41, which enables the structure to develop a resistance against the energy transferred when the impulse load hits the structure. This resistance increases with time and depends on the stiffness of the structure. Thus, the external work done by the Direct load is larger than the work done by Reaction load 5. When comparing this to the position on the resistance-deformation curve in Figure 5.44, the deformation is larger for the Direct load than for Reaction load 5 as the area under this curve, corresponding to internal work, is also larger.

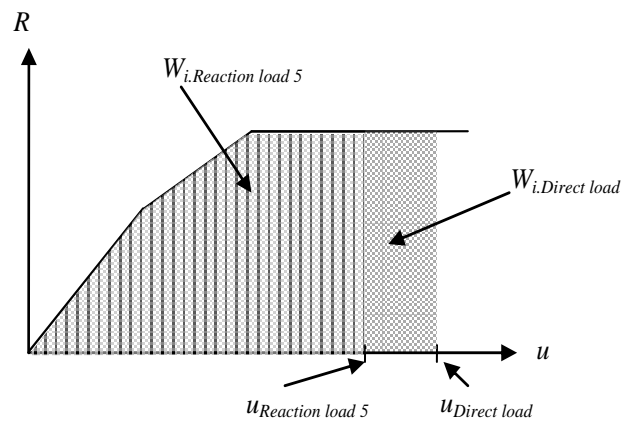


Figure 5.44 Comparison of internal work and resulting deformation for the structure with elasto-plastic response subjected to the Direct load and to Reaction load 5.

Reaction load 6 is a continuation of Reaction load 5 and since it is prolonged in time, see Figure 5.41, the impulse is almost twice as large as in case of Reaction load 5. Therefore, the internal work done by the structure subjected to Reaction load 6 and the resulting deformation is larger compared to Reaction load 5.

The maximum deformations as well as the total impulse transmitted by the studied loads are compiled in Table 5.14.

Table 5.14 Maximum deformation and total impulse transmitted to the structure for the different loads.

Load type	$u_{max}$ [m]	$I=\int F(t)dt$ [kNs]
Direct load	0.088	32.5
Reaction load 5	0.051	32.5
Reaction load 6	0.077	51.6

### 5.6.2.3 Structural response of wall panels in 3D FE analysis

The deformation obtained in the 3D FE analysis in the middle of the wall is investigated at the points illustrated in Figure 5.45.

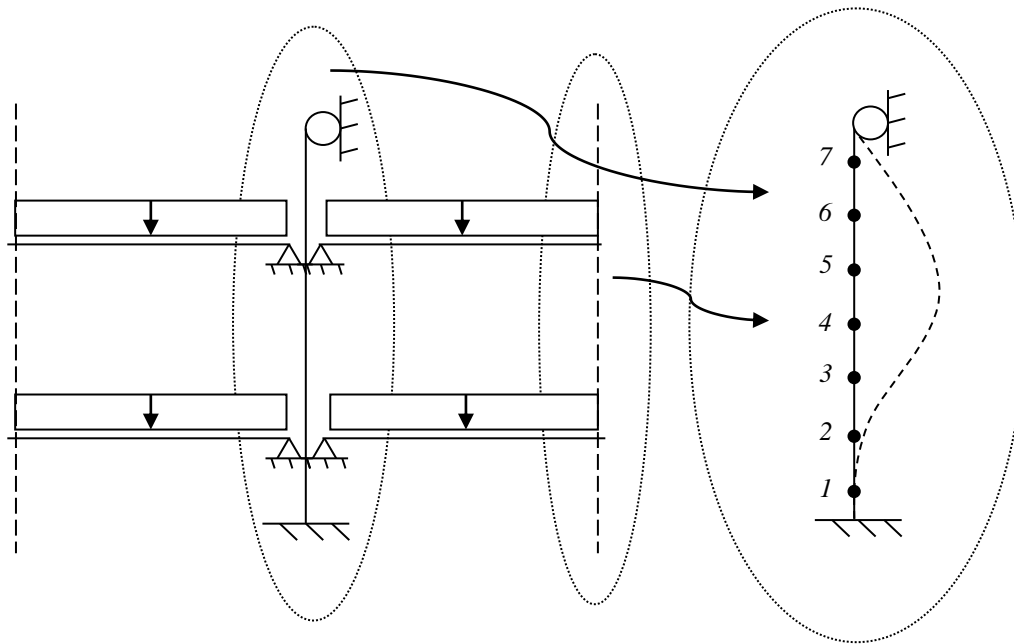


Figure 5.45 The deformations and reaction forces are measured at different points along the column.

A comparison of the deformations obtained in the middle of the wall in the different points as well as the deformation in the middle of the column are presented in Figure 5.46. The deformation in the middle of the wall is also compared to the deformation of a simply supported beam with the same properties and dimensions. In this figure, it can be noticed that at the beginning of the loading, within the first 0.2 seconds, the deformation for the wall panels which are near the supports of the column i.e. in point 1, 2 and 7 are similar to the deformation of the simply supported beam. Similarly as for the elastic model, the deformation for the wall panel closest to the fixed support of the column is most similar to the deformation of the simply supported beam since the column is stiffest there. The largest deformation of the wall is obtained for the panels in the middle of the column i.e. in point 4 and 5. Similarly as for the elastic response, the difference in the frequency and magnitude of the deformation is a result of different stiffnesses of the column in its different regions.

A comparison of the deformation in the middle of the column and the reaction forces from the different wall supports along the column is done and presented in Figure 5.47. It can be noticed that the reactions do not coincide but works against each other, as they did for the elastic model. This effect, caused by the different frequencies of the wall panels, decreases the deformation of the column.



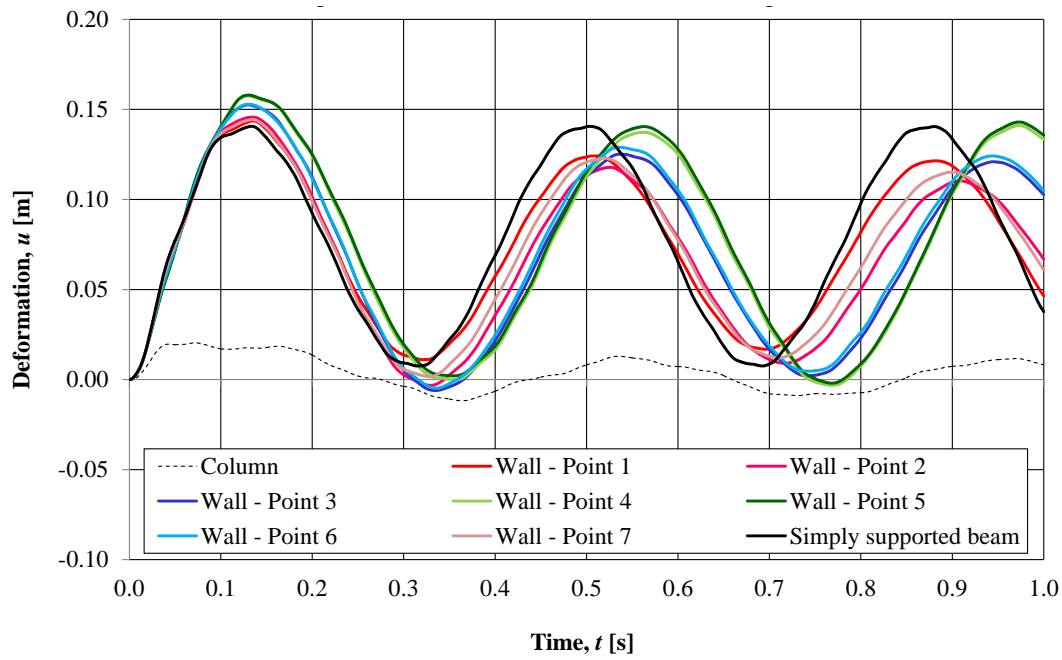


Figure 5.46 The deformation in the middle of the wall, measured in different points along the column, are compared to the deformation of a simply supported beam and to the deformation in the middle of the column.

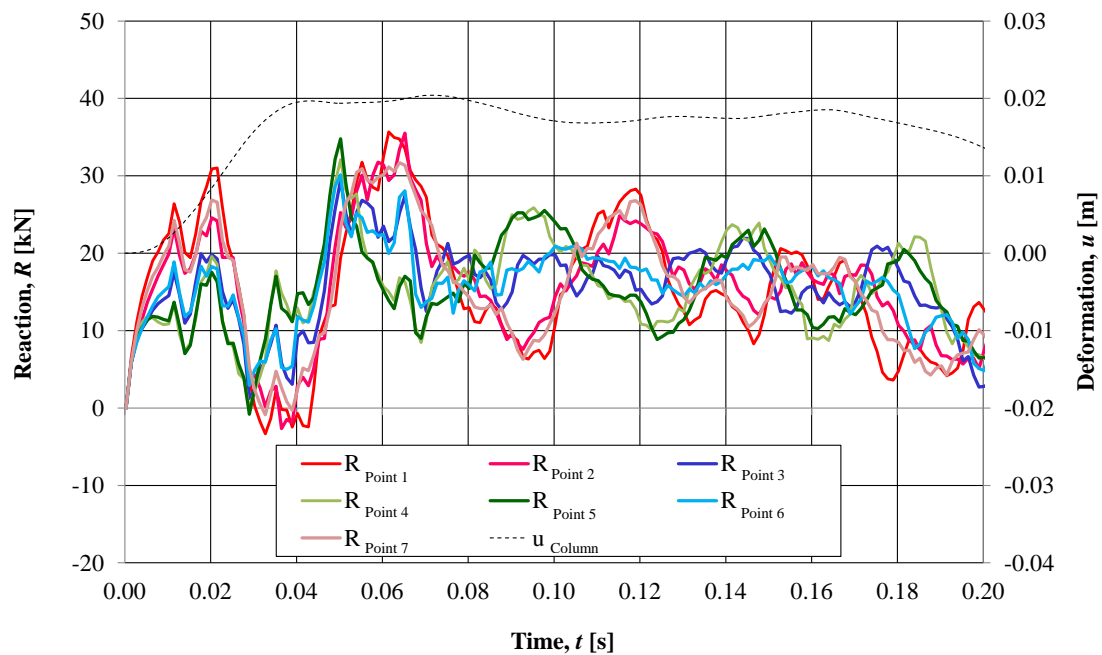


Figure 5.47 A comparison of the deformation in the middle of the column and the support reactions acting on the column. The reactions are the sum from the wall panels on both sides of the column.

The elasto-plastic reactions from the wall supports reach the maximum value at the beginning of the response and decreases after the first 0.7 seconds. The counteraction of the reactions is a possible explanation for the small deformation of the column.

In order to investigate the behaviour of the reaction forces further, point 1 and 4 are plotted against the support reaction of a simply supported beam in Figure 5.48 and

Figure 5.50, respectively. Figure 5.49 shows the reactions of point 1 for a longer time interval. The support reactions for all other points along the column can be found in Section F.5.2.

As for the elastic case the largest similarity to the simply supported beam is for the wall panel with its support next to the fixed support of the column, i.e. point 1, Figure 5.48. For the wall panels with supports towards the middle of the column, the reaction is delayed due to the stiffness of this region which differs more than in case of a simple support, Figure 5.50.

In Figure 5.49 the magnitude of the support reaction decreases from 36 kN to 15 kN. This behaviour can be compared to damping, which agrees with the general consideration of the elasto-plastic response as a source of damping. After 0.7 seconds the reaction continues with the same amplitude of oscillations and the same maximum deformation.

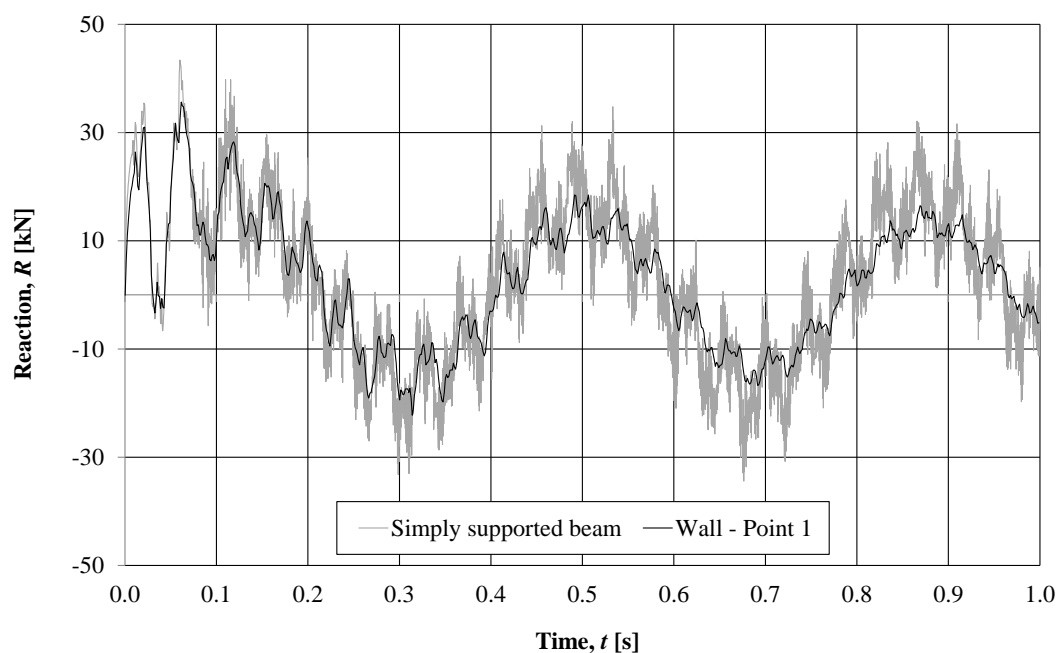


Figure 5.48 A comparison of the reactions for a simply supported beam and the reactions transferred from the wall panel to the column at point 1.

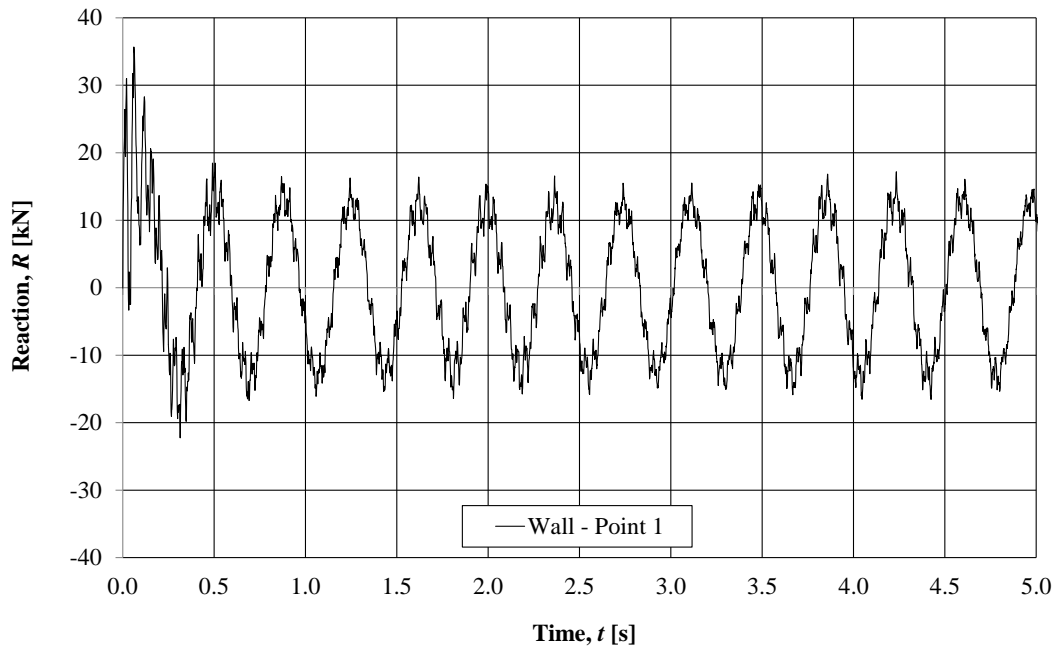


Figure 5.49 The reaction transferred from the wall panel to the column at point 1 for the first 6 seconds.

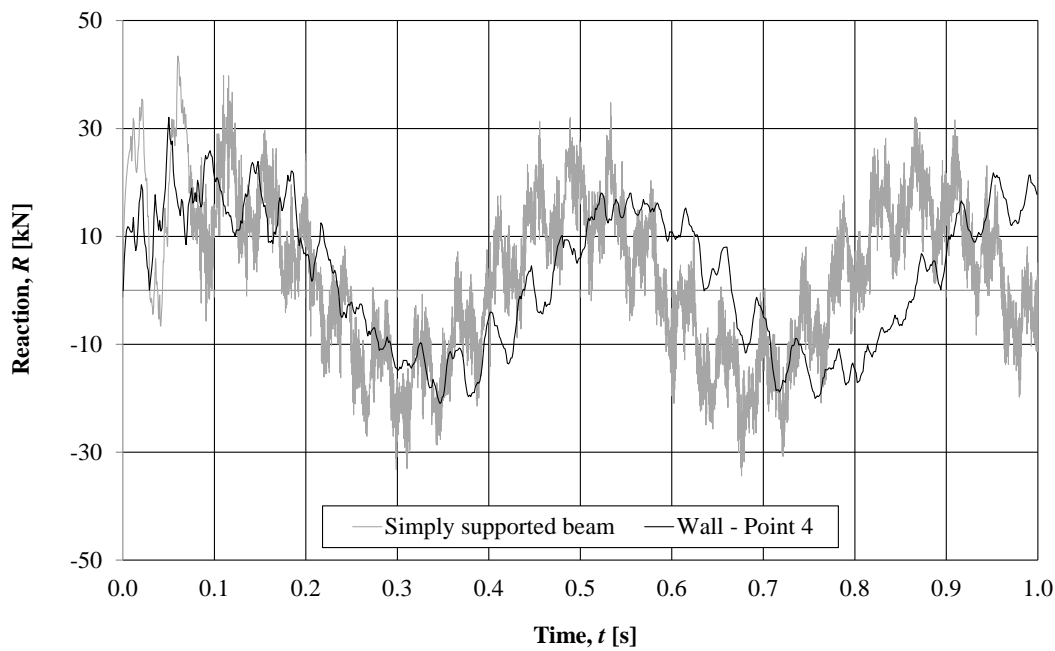


Figure 5.50 A comparison of the reactions for a simply supported beam and the reactions transferred from the wall panel to the column at point 4.

A comparison between the delayed loads obtained in the 3D FE analysis, which is calculated as the sum of all support reactions according to equation (5.12), to the assumed delayed load established in SDOF is presented in Figure 5.51.

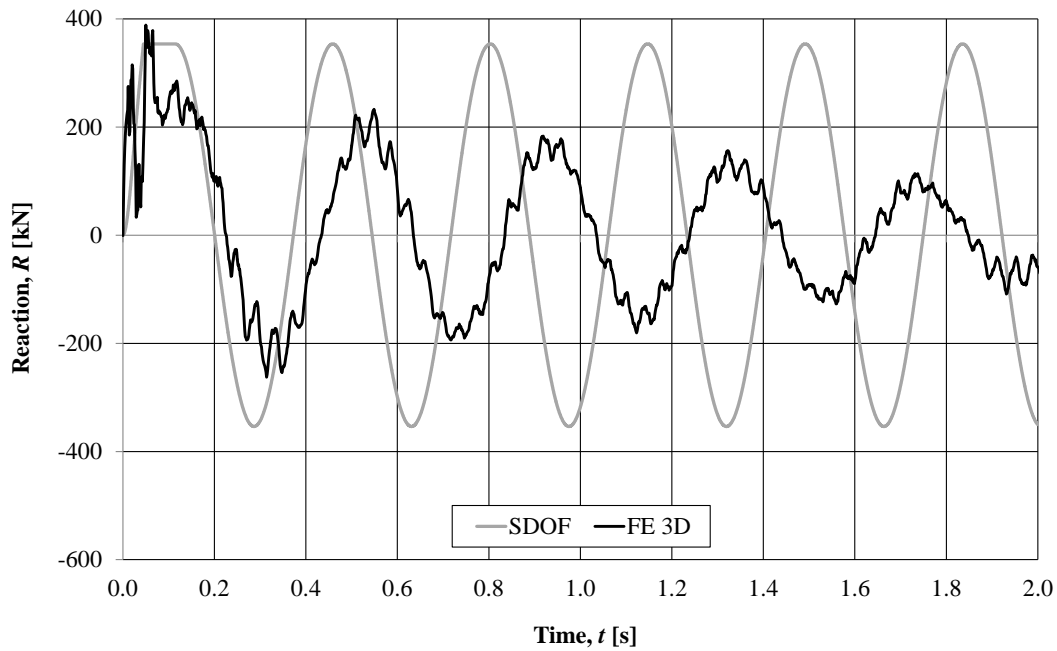


Figure 5.51 A comparison of the total delayed load in SDOF and in the 3D FE analysis.

The total reaction in SDOF is overestimated when it is calculated with regard to the assumption for the static load. This concept of calculation of the dynamic reaction can be found in Section F.3. According to Andersson and Karlsson (2012) the correct value of the dynamic reaction for a simply supported beam is not  $0.5R_m$  but  $0.39R_m$ .

The total reaction in the FE analysis  $R_{tot}$ , equation (5.12), becomes delayed and decreases due to different frequencies of the wall panels. Its development for a longer time interval is presented in Figure 5.52.

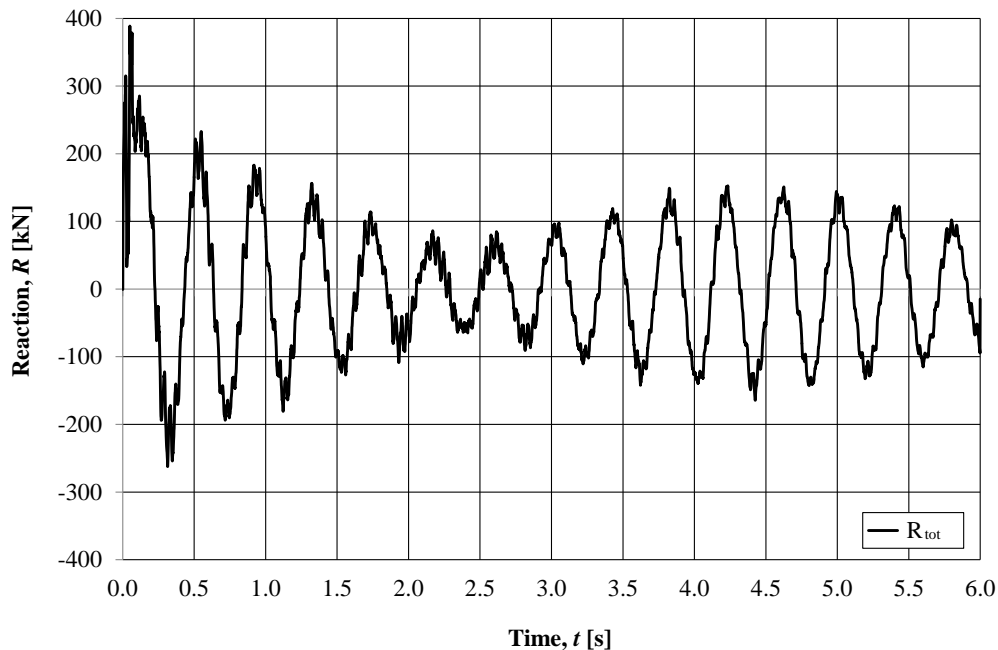


Figure 5.52 Total reaction acting on the column in the 3D FE analysis.

The shape of the total reaction in Figure 5.52 is caused by the difference in frequency of the support reactions from wall, similarly as for the elastic response. At the time 2.5 s, when the total reaction reaches the lowest magnitude, the reactions at the regions with the highest and lowest stiffness are working against each other. After this the frequency of the support reactions starts to coincide more. At the time of around 4.5 s all reactions are working in the same direction and the total reaction  $R_{tot}$  reaches higher value.

#### 5.6.2.4 Check of deformation capacity

The check of the plastic deformation capacity of the front column is presented in this section. The studied here SDOF model of the front column is similar to the model of the front column in the 2D frame analysis performed in Chapter 4. The concept of calculating the deformation capacity for a structure with a trilinear response model is described in Section 4.7.1.4. The calculations are presented in Section F.2 and the results in Table 5.15.

Table 5.15 Comparison of plastic deformation capacity and maximum deformation obtained for the different loads.

Reinf. Class	$u_{rds}$ [m]	SDOF			3D FE
		Direct load $u_{max}$ [m]	Reaction load 5 $u_{max}$ [m]	Reaction load 6 $u_{max}$ [m]	$u_{max}$ [m]
B	0.040	0.088	0.051	0.077	0.020
C	0.102	0.088	0.051	0.077	0.020

This check shows that for the Direct load, the deformation capacity is sufficient for reinforcement of Class C, but not for reinforcement of Class B. The maximum deformation due to Reaction load 5 and 6 is lower than due to the Direct load, but the deformation capacity is still not sufficient when reinforcement of Class B is used.

Since all SDOF calculations has been proven to be on the safe side, and the maximum deformation obtained in the 3D FE analysis is 0.020 m the structure would not collapse for the considered load, for both reinforcement of Class B and Class C.

#### 5.6.3 Comparison of elastic and elasto-plastic model

When comparing the deformation in the middle of the column for the elastic and elasto-plastic response, a difference in magnitude is obvious while the frequency is similar, see Figure 5.53.

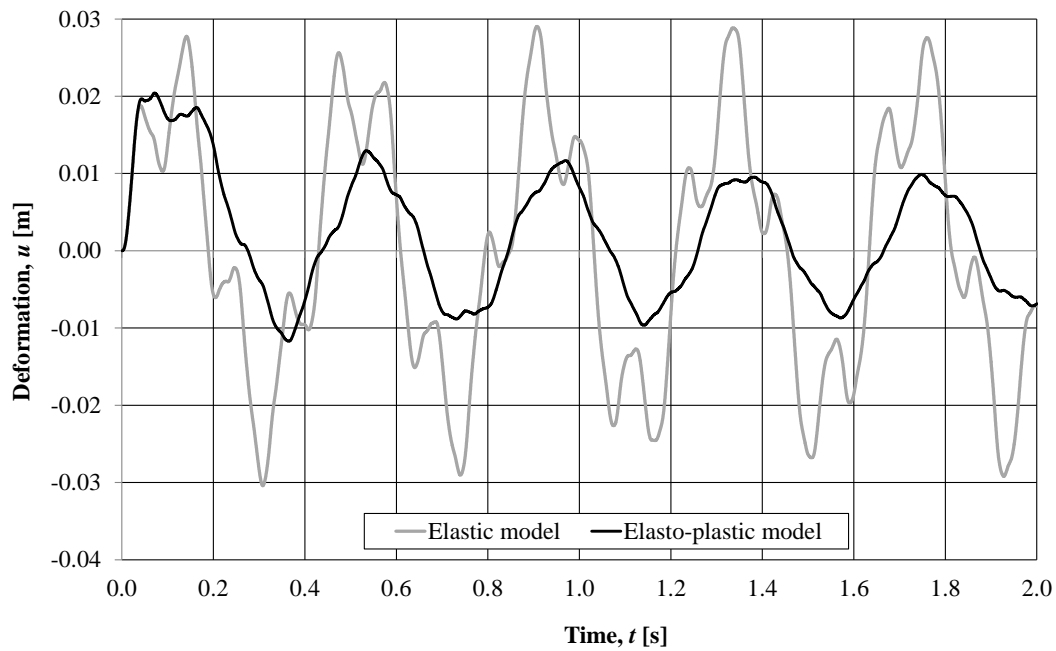


Figure 5.53 The deformation in the middle of the column for the elastic and elasto-plastic response.

The fact that the deformation for the elasto-plastic response is smaller is a result of a lower reaction load induced at the supports of the wall panels which are simulated with an elasto-plastic response curve. For both response models the frequency of deformation and the support reactions are the same. The support reactions of wall panel 1 for two models are compared in Figure 5.54.

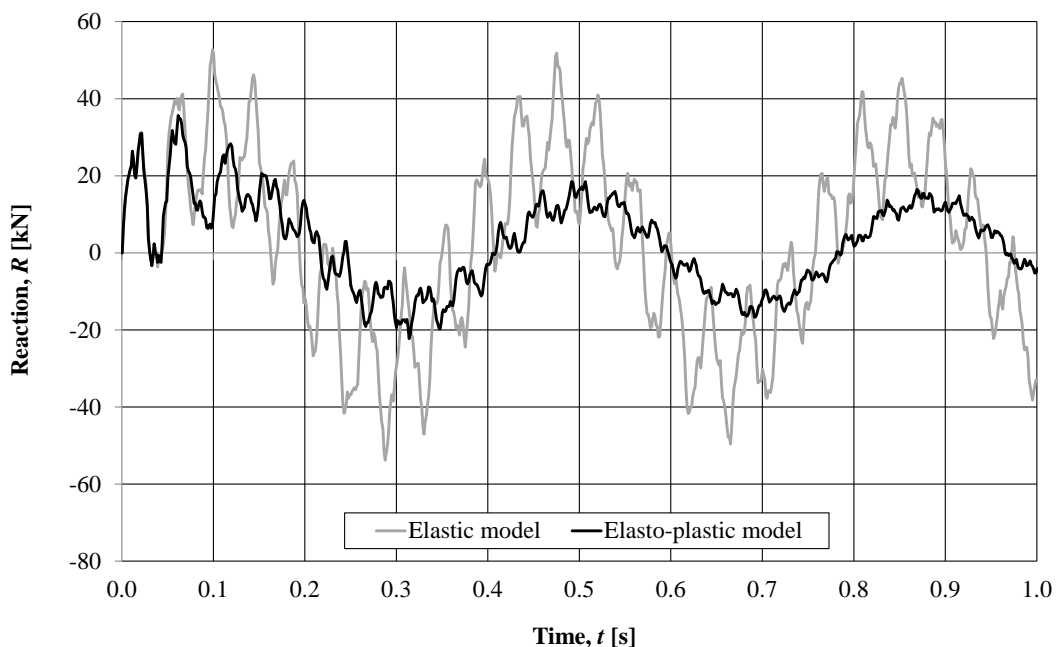


Figure 5.54 The support reaction for the wall panel at point 1, i.e. next to the fixed support of column, for the elastic and elasto-plastic response.

For the studied structure the elastic reactions are larger than the elasto-plastic. The maximum value for the elastic response is 52 kN while for the elasto-plastic response it is 35 kN. In this study the simulation of the response of the structure with the elastic model results in higher load acting on the column and thus in higher deformation. In general, however, a larger deformation is more often obtained when implementing the elasto-plastic response. The difference in magnitudes of deformation between the elastic and elasto-plastic model depends on the chosen parameters of the structure. Thus, further investigation of the influence of different parameters on the response of the studied frame is done and presented in Section 5.6.

## 5.7 Parametric study

### 5.7.1 Orientation

The results obtained in Section 5.6 are in this section compared to structures where the stiffness and internal resistance of the wall is varied for the elastic and elasto-plastic model, respectively. The other properties of the wall and column are the same as in the previous study, see Section 5.2.

This parametric study is conducted in the same manner as the previous analysis in Section 5.6. The Direct load and the dynamic reaction from the supports of the wall are simulated and applied on the column in the SDOF system. The results are verified with a 2D FE analysis, and a 3D FE analysis of the structure is performed in ADINA (2011).

In this section a selection of the results is presented and discussed. The other results such as the verification of the SDOF model with 2D FE analysis, a comparison of wall support reactions with a simply supported beam as well as a comparison of the delayed loading in SDOF and in the 3D FE analysis can be found in Appendix G.

### 5.7.2 Elastic model

#### 5.7.2.1 Parameters studied

For the elastic model only the stiffness of the wall is varied. Three different cases are considered here, see Figure 5.55. The first case is an unchanged stiffness  $k_u$  which is the same as in the previous study, see Table 5.3 and equation (F.6). The second case is stiffness  $k_d$  which corresponds to the stiffness used in the previous study decreased with factor 4. The last stiffness,  $k_i$ , is increased with factor 4 compared to  $k_u$ . The frequency for the studied cases differs with factor 2, according to Figure 5.55. Studied values of stiffnesses are compiled in Table 5.16.

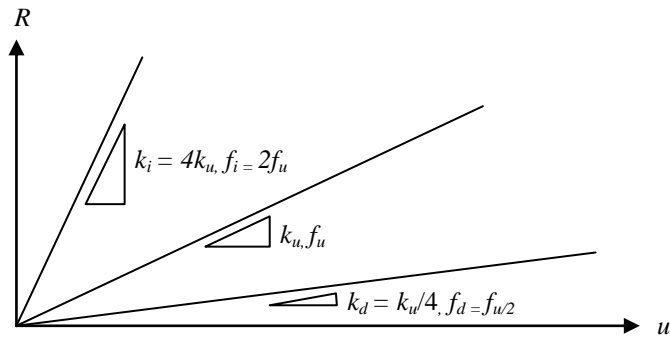


Figure 5.55 Three different stiffnesses of the wall used in the elastic response model.

Table 5.16 The values of stiffnesses for which the study is conducted.

Stiffness	Decreased $k_d$ [kN/m]	Unchanged $k_u$ [kN/m]	Increased $k_i$ [kN/m]
Wall	160	640	2560
Column	20967		

### 5.7.2.2 Loads and deformation

The studied column simulated in SDOF is subjected to the Direct load, Reaction load 1, 2 and 3.

Reaction load 1 for the different values of the stiffnesses together with the Direct load is presented in Figure 5.56.



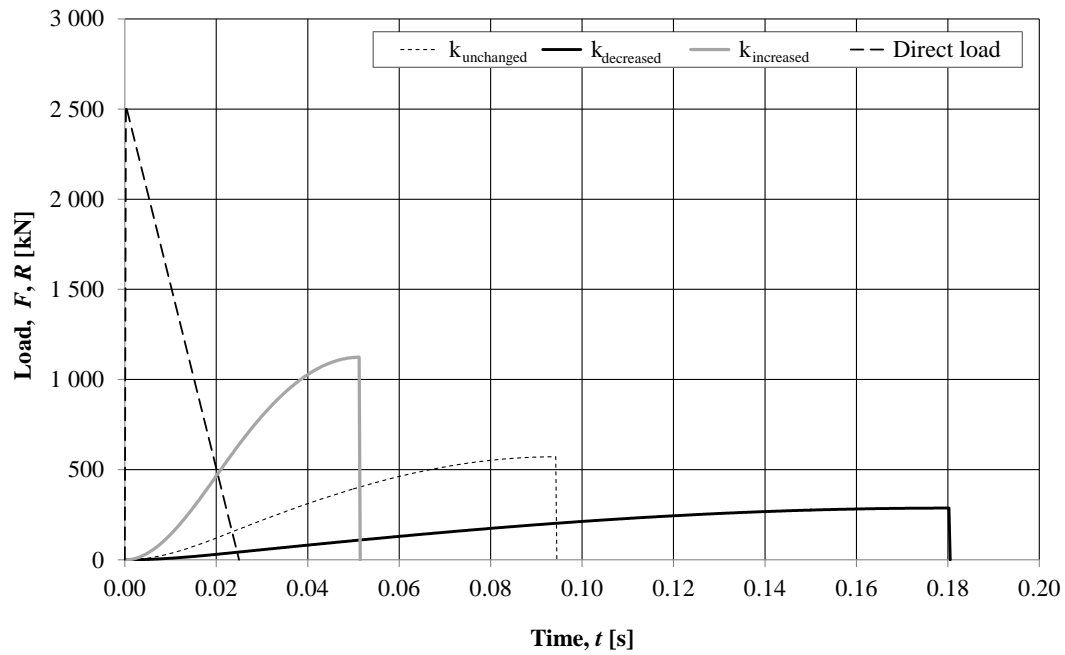


Figure 5.56 Reaction load 1 obtained in SDOF for different values of stiffnesses of the wall together with the Direct load.

The resulting deformation in the middle of the column for each case of stiffness due to Reaction load 1 is compared with the deformation obtained for the Direct load in Figure 5.57.

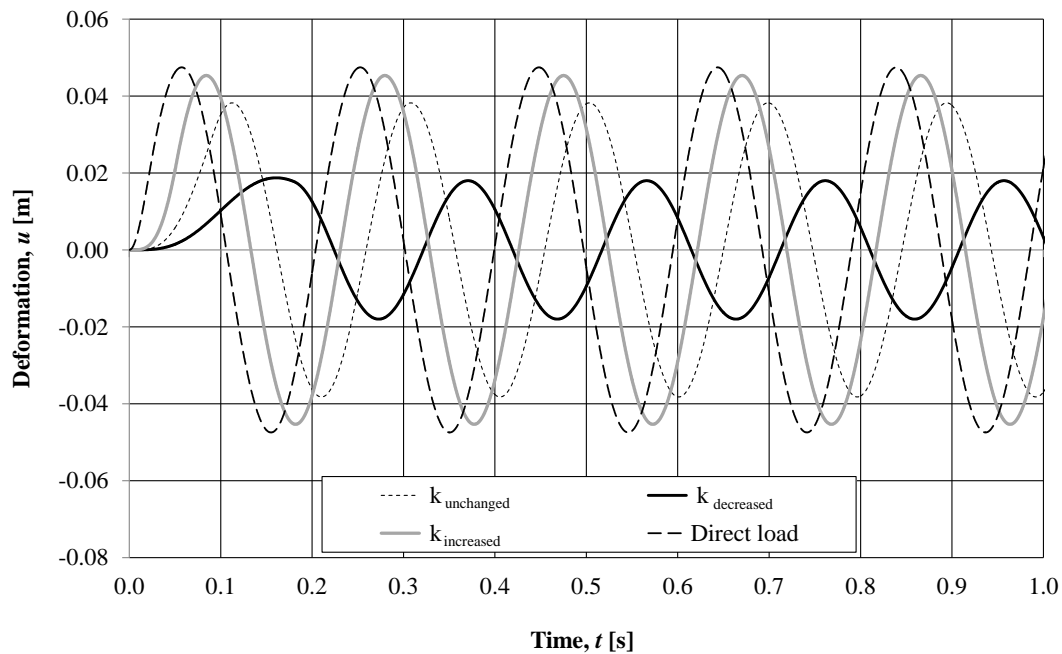


Figure 5.57 Comparison of deformation in the middle of column obtained in SDOF for different cases of Reaction load 1 together with the Direct load.

In Figure 5.57 the largest deformation is obtained for the structure subjected to the Direct load. Moreover when comparing those results with Figure 5.56, it can be noticed that an increase in stiffness leads to a higher magnitude and a shorter duration of reaction load making it more similar to the impulse load. Thus, the deformation induced by Reaction load 1 increases with increasing stiffness of the wall.

Reaction load 2 for different values of wall stiffness is shown in Figure 5.58 together with the Direct load.

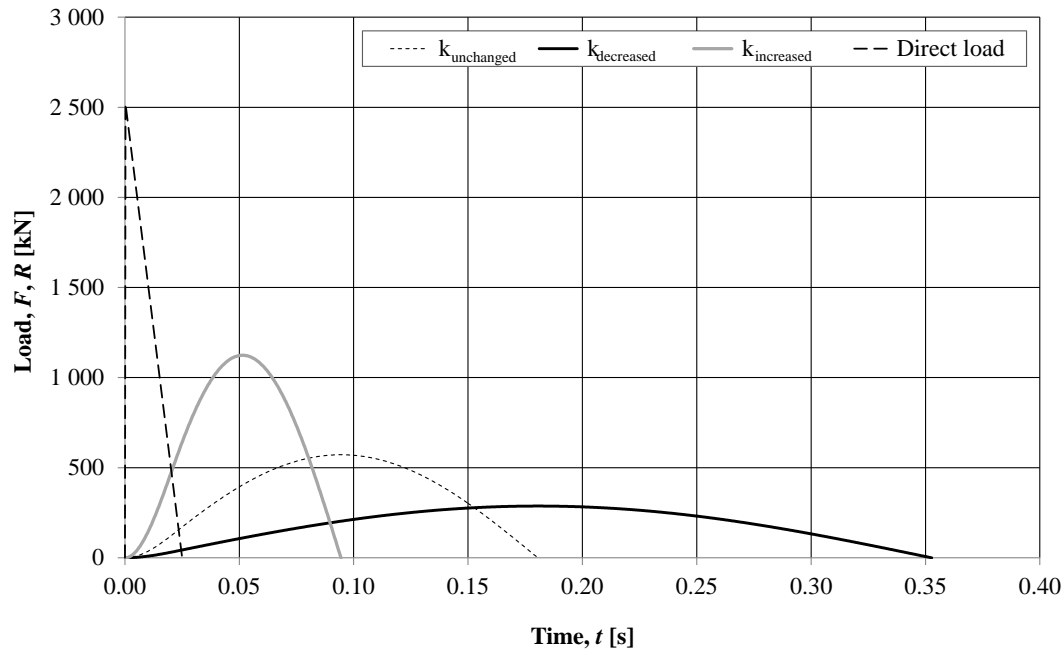


Figure 5.58 Reaction load 2 obtained in SDOF for different values of stiffnesses of the wall together with the Direct load.

The deformation due to the different loads from Reaction load 2 is compared to the deformation caused by the Direct load in Figure 5.59.

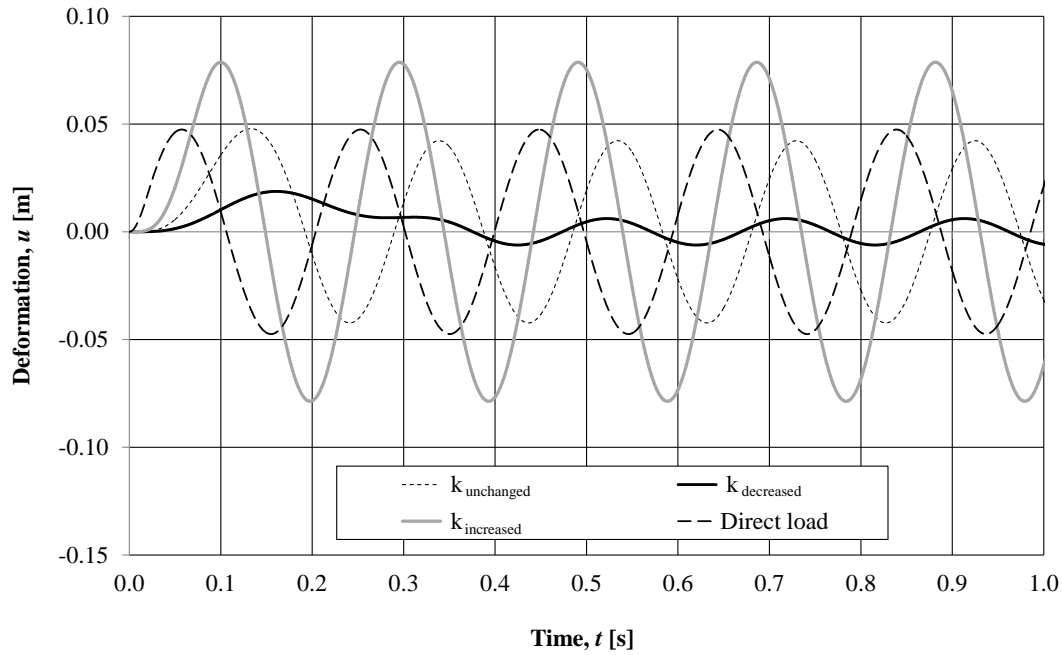


Figure 5.59 Comparison of deformation in the middle of column obtained in SDOF for different cases of Reaction load 2 together with the Direct load.

Similarly as for Reaction load 1, the largest deformation is obtained for the wall with the highest stiffness. Moreover, this deformation is larger than the deformation induced by the Direct load. As mentioned in Section 5.6, this effect is caused by the fact that Reaction load 2 is prolonged in time and increases the deformation to a higher value, see Figure 5.60.

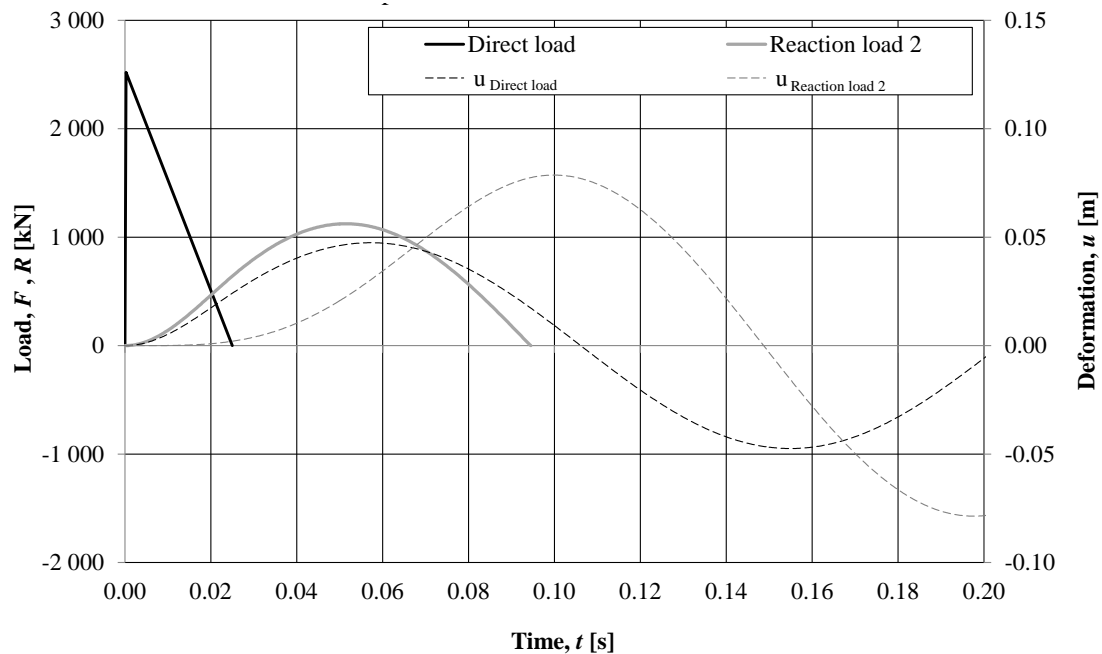


Figure 5.60 Comparison of the deformation in the middle of column and loads for the Direct load and Reaction load 2 for a case with the increased stiffness  $k_i$ . All results are obtained in SDOF.

For the wall with decreased stiffness the deformation is compared to causing it Direct load and Reaction load 2 in Figure 5.61. The elongated shape of deformation is caused by the prolonged Reaction load 2 which is still active after reaching the highest deformation and sustains the positive deformation.

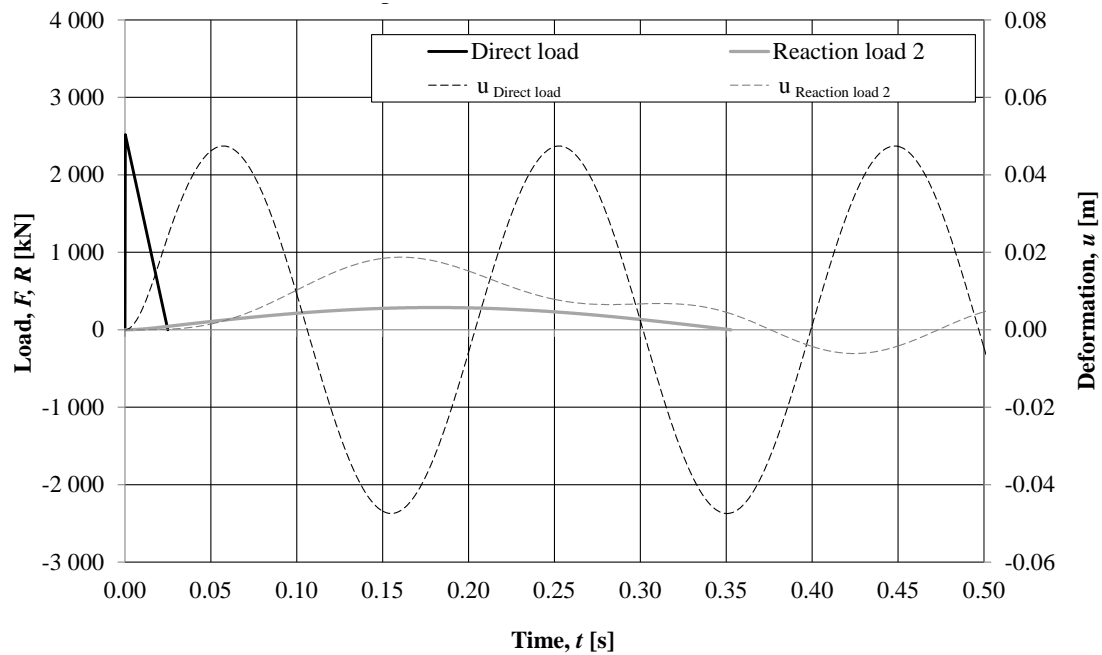


Figure 5.61 Comparison of the deformation in the middle of the column and loads for the Direct load and Reaction load 2 for a case with decreased stiffness  $k_d$ . All results are obtained in SDOF.

Reaction load 3 for different stiffnesses of the wall is illustrated in Figure 5.62 together with the Direct load. The resulting deformation for those loads is presented in Figure 5.63.

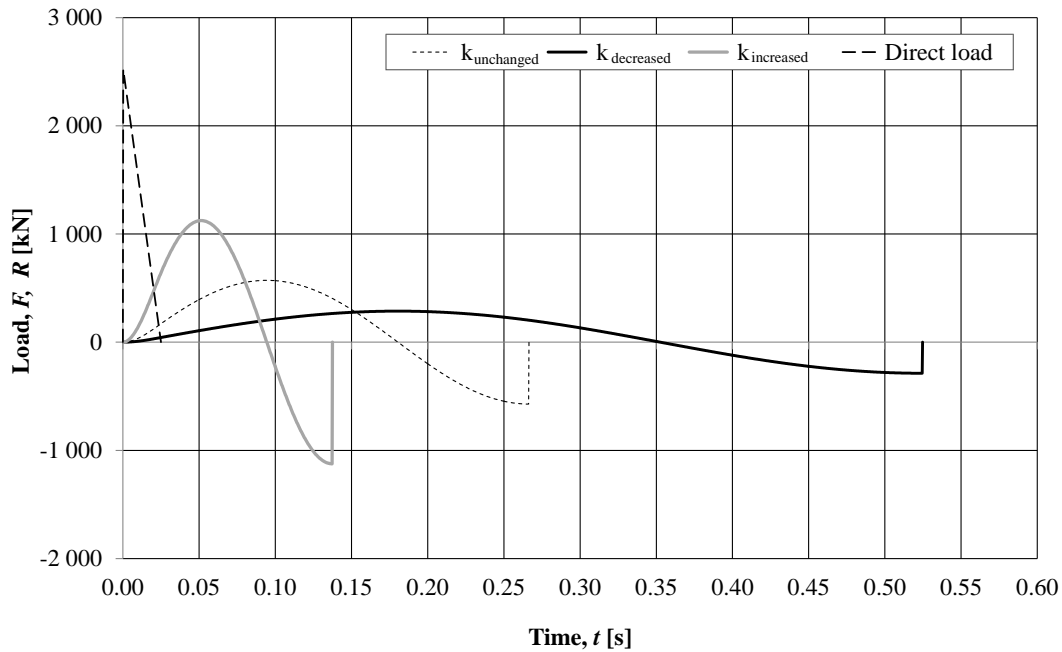


Figure 5.62 Reaction load 3 obtained in SDOF for the different values of stiffness of the wall together with the Direct load.

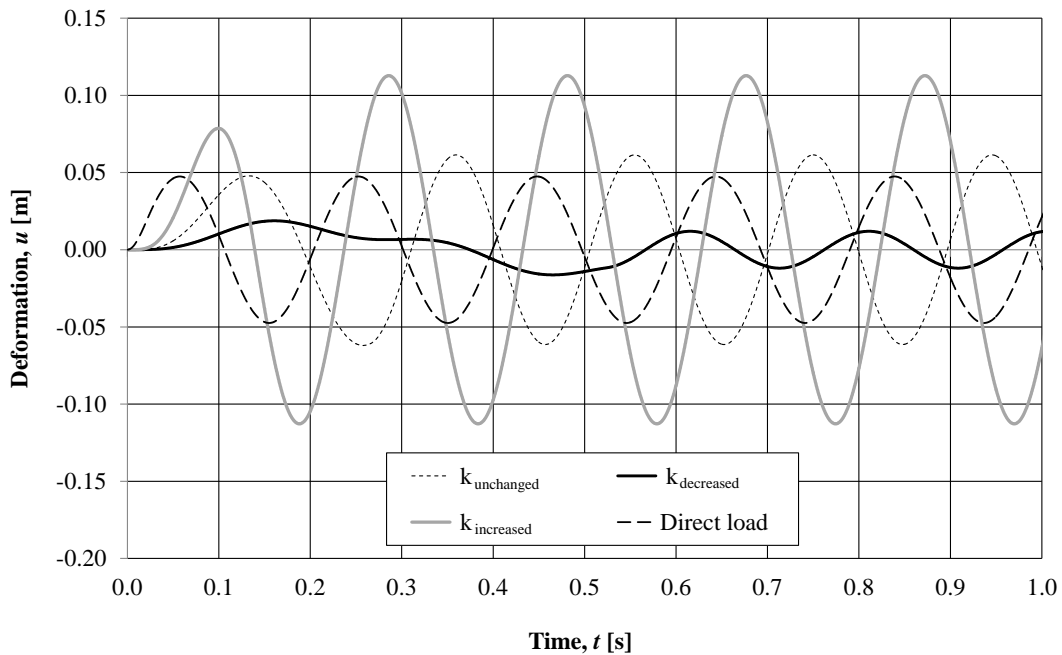


Figure 5.63 Comparison of deformation in the middle of column obtained in SDOF for different cases of Reaction load 3 together with the Direct load.

Similarly as for Reaction load 1 and 2, the largest deformation is obtained for the wall with increased stiffness. The first deformation peak is smallest due to the change of direction of the load at the time when this deformation occurs. The negative load starts to act before this deformation peak is reached. It cannot reach a higher value since it is pushed back by the load acting in the opposite direction.

In order to assess the simplified method recommended by Johansson (2013), the deformation due to the Direct load obtained in the SDOF system is compared to the deformation in the 3D FE analysis. Figure 5.64 presents this comparison for different stiffnesses of the wall introduced in the FE model.

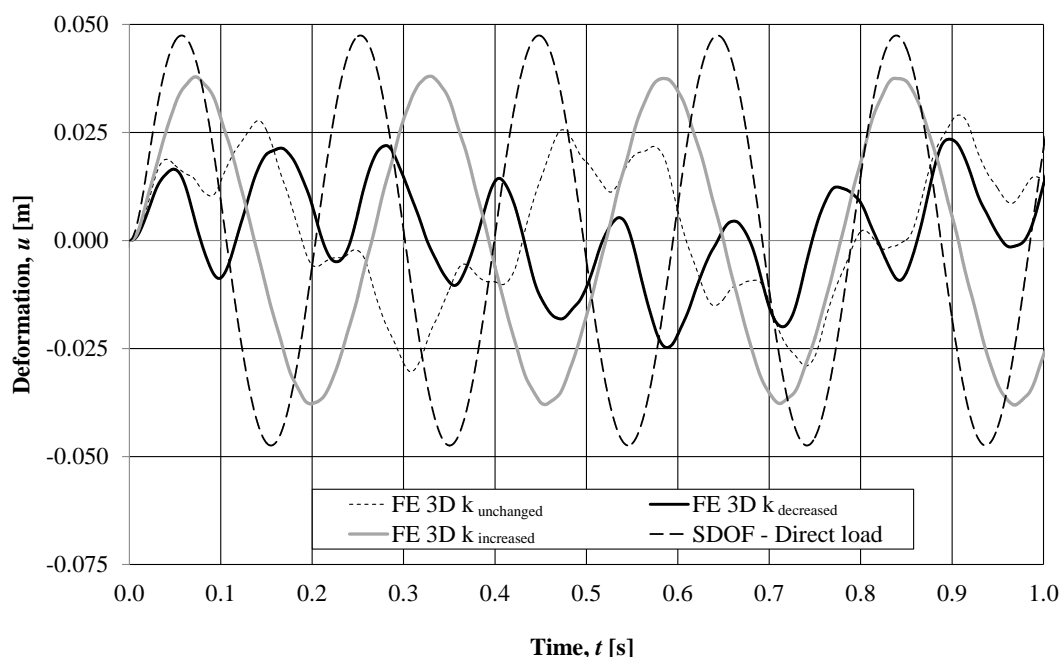


Figure 5.64 Comparison of deformation in the middle of the column obtained in the 3D FE analysis for varied stiffness of the wall to the deformation obtained in SDOF, caused by the Direct load.

The simplified method, i.e. the Direct load, provides results on the safe side for all three stiffnesses of the wall. The maximum deformations obtained for the Direct load in SDOF and for the different stiffnesses in the 3D FE analysis is presented in Table 5.17. Increased stiffness of the wall in the FE analysis leads to increased deformation of the column.

Table 5.17 Maximum deformation of the column obtained in SDOF for the Direct load is compared to the deformation from the 3D FE analysis for the different cases of stiffnesses of the wall.

	SDOF Direct load All cases of $k$	3D FE Increased stiffness of wall, $k_i$	3D FE Unchanged stiffness of wall, $k_u$	3D FE Decreased stiffness of wall, $k_d$
$u_{max}$ [m]	0.047	0.037	0.026	0.020

### 5.7.2.1 Investigation of wall panels in FE model

The support reactions and deformations for the wall panels are measured along the column in points illustrated in Figure 5.65. The deformation in the middle of the column is plotted against the support reactions for point 1 and 4 for the decreased and increased stiffness of the wall in Figure 5.66 and Figure 5.67, respectively. The support reactions in all points along the column compared to the support reactions from a simply supported beam are shown in Section G.4.

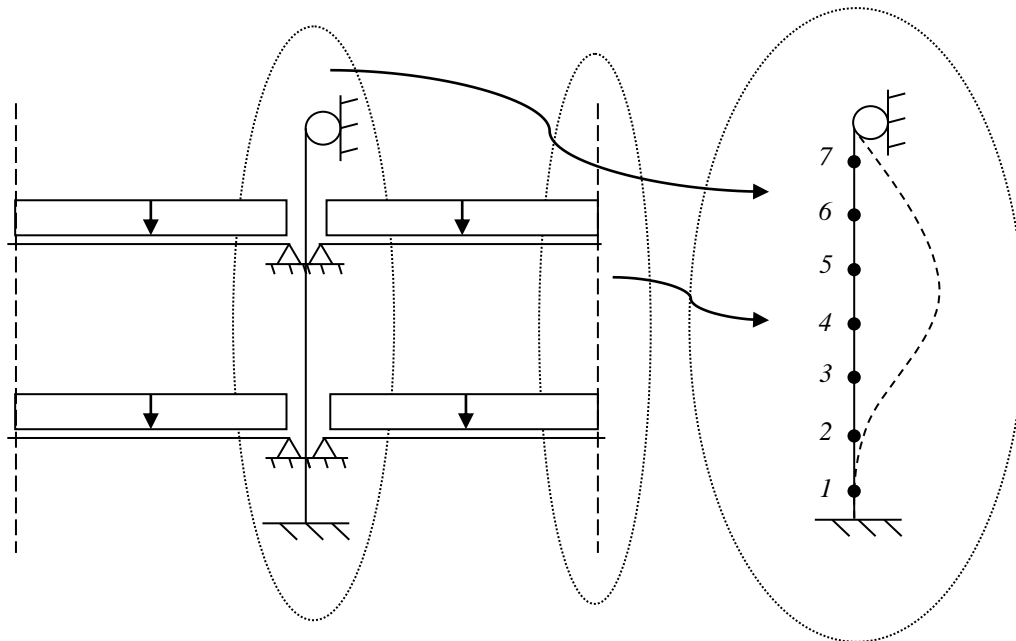


Figure 5.65 The different points along the column, for which the support reactions and the deformations, in the middle of the wall, are measured.

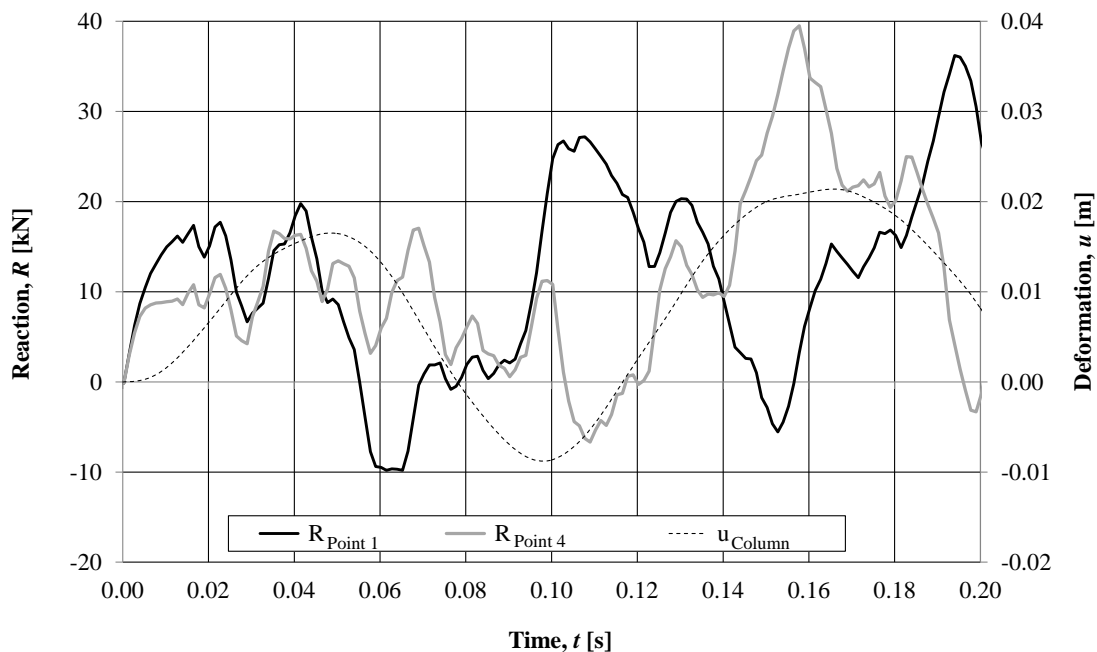


Figure 5.66 Comparison of the deformation in the middle of the column and the support reactions from wall panels at point 1 and 4 for the case with decreased stiffness of the wall.

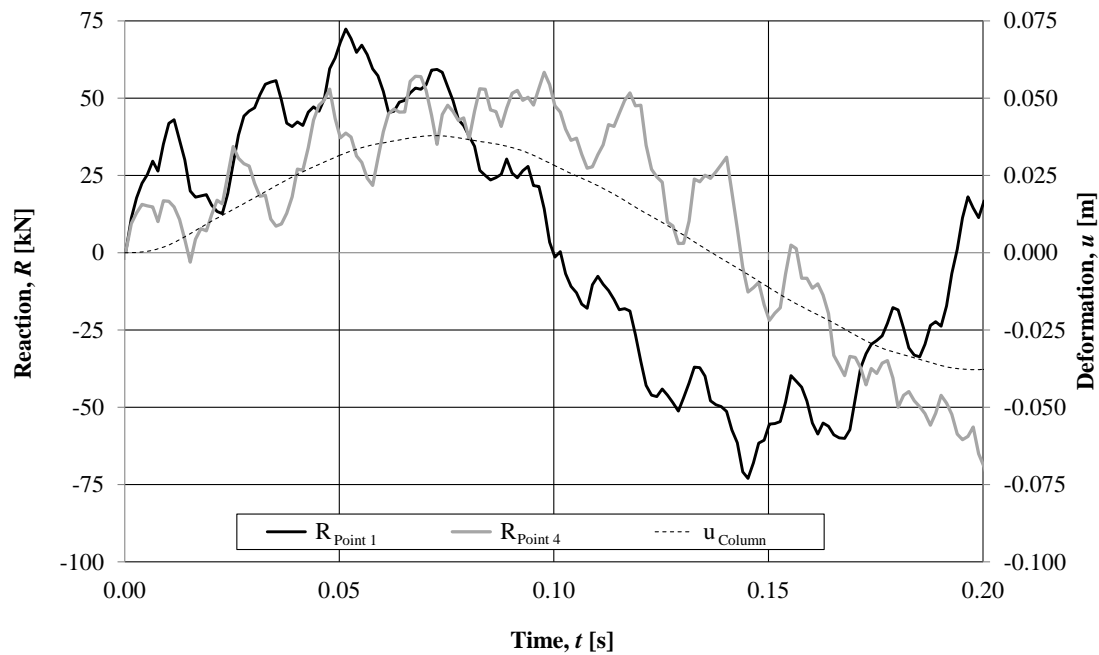


Figure 5.67 Comparison of the deformation in the middle of the column and the support reactions from wall panels at point 1 and 4 for the case with increased stiffness of the wall.

Comparing Figure 5.66 and Figure 5.67 it is obvious that the amplitude of sways in the deformation curve of the column is strongly influenced by the magnitude of the support reactions which is larger for the wall with increased stiffness.

The deformations in the middle of wall for point 1 and 4, for the decreased and increased stiffness of wall, is also measured and presented in Figure 5.68 and Figure 5.69.



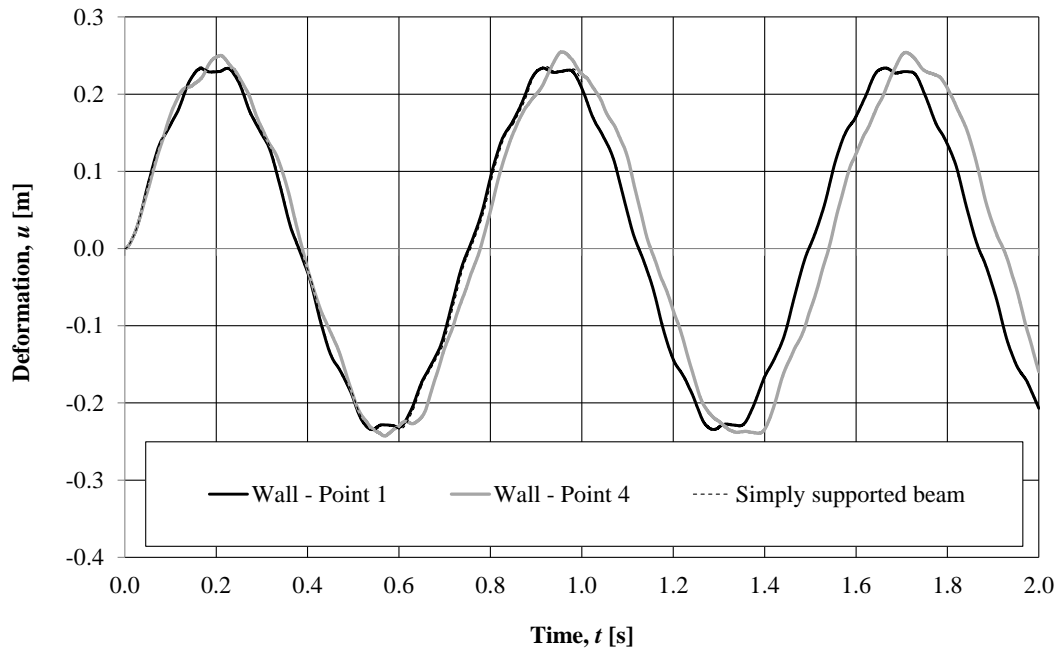


Figure 5.68 The deformation in the middle of the wall with decreased stiffness  $k_d$  measured for point 1 and 4 compared to the deformation of a simply supported beam.

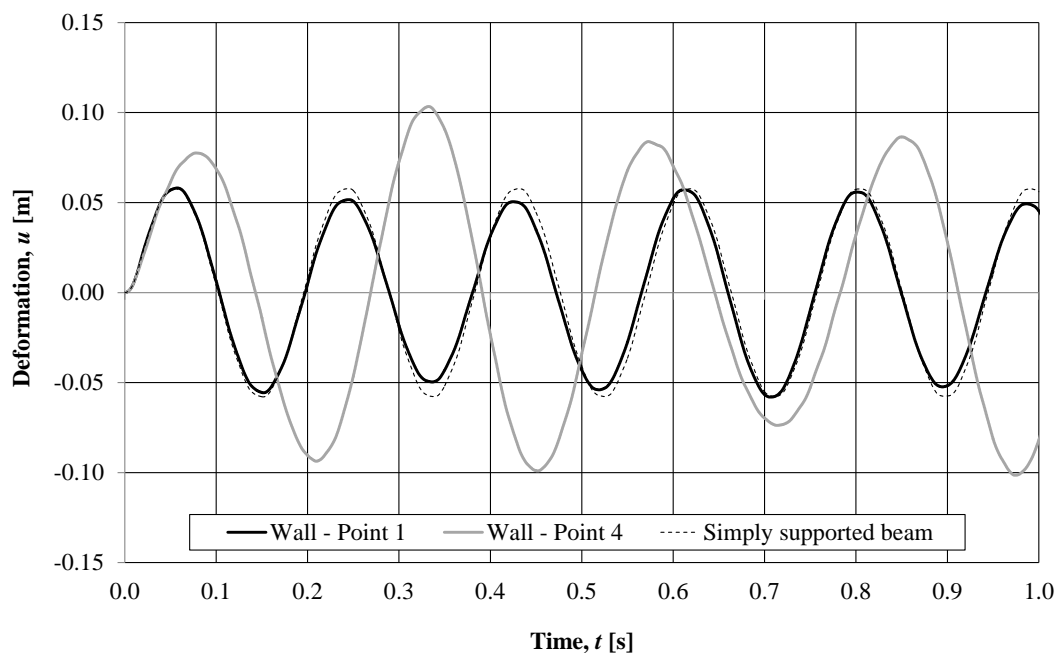


Figure 5.69 The deformation in the middle of the wall with increased stiffness  $k_i$ , measured for point 1 and 4 are compared to the deformation of a simply supported beam.

It can be noticed that for the wall with decreased stiffness the frequency of the support reactions and deformation in the middle of the wall in the studied points along the column are relatively similar to each other, compare Figure 5.66 and Figure 5.68. This indicates that the response of the wall panels with such properties can be compared to the response of a simply supported beam. Thus, the fact that the stiffness

of the column varies along its length is not so important when dealing with a structure where the stiffness of the wall is considerably decreased.

For the wall with increased stiffness, on the other hand, the fact that the stiffness of the column varies has a considerable influence on the reaction at the wall supports as well as on the deformation in the middle of the wall, compare Figure 5.67 and Figure 5.69. This indicates that the wall with increased stiffness can be compared to a beam supported on springs, which stiffness corresponds to the stiffness of the column in the points along its length. In summary, the stiffness of the column becomes an important parameter for a structure with a wall panel provided with higher stiffness.

### **5.7.2.2 Influence of stiffness**

For the elastic model, the stiffness of the wall has been varied according to Section 5.7.2.1. The column simulated in SDOF has been subjected to the Direct load, Reaction load 1, 2 and 3 according to Figure 5.56, Figure 5.58 and Figure 5.62, respectively. For each case of reaction load the resulting deformation of the column has been compared to the deformation caused by application of the Direct load, see Figure 5.57, Figure 5.59, Figure 5.60, Figure 5.61 and Figure 5.63. The deformation obtained from the Direct load in the SDOF calculations has been compared to the deformation obtained in the 3D FE analysis, Figure 5.64. The support reactions and deformation for wall panel 1 and 4 according to Figure 5.65, for the decreased and increased stiffness of the wall, have been also compared.

A conclusion that can be drawn is that if the stiffness of the wall is decreased, the wall can be related to the behaviour of a simply supported beam. If the stiffness of the wall is increased, the response of the wall corresponds to the response of a beam supported on springs where the stiffness of the springs corresponds to the stiffness of the column in different regions along its length. This is illustrated in Figure 5.70.

A structure with an infinitively stiff wall is briefly mentioned in Section 5.6.1.1, where the results from the analysis of the first bending mode of the 3D FE model are presented. The first bending mode only allows for deformation of the column, and hence, the wall stays undeformed. Thus, the behaviour of the wall corresponds to the behaviour of an infinitively stiff element. The deformation of the column in such case corresponds the deformation obtained when the column is subjected to the Direct load. This means that the load applied on the wall is instantaneously transferred from the wall to the column. The wall does not deflect but rather translates in the direction of the load application, i.e. the deformation for each point along every wall panel is the same.

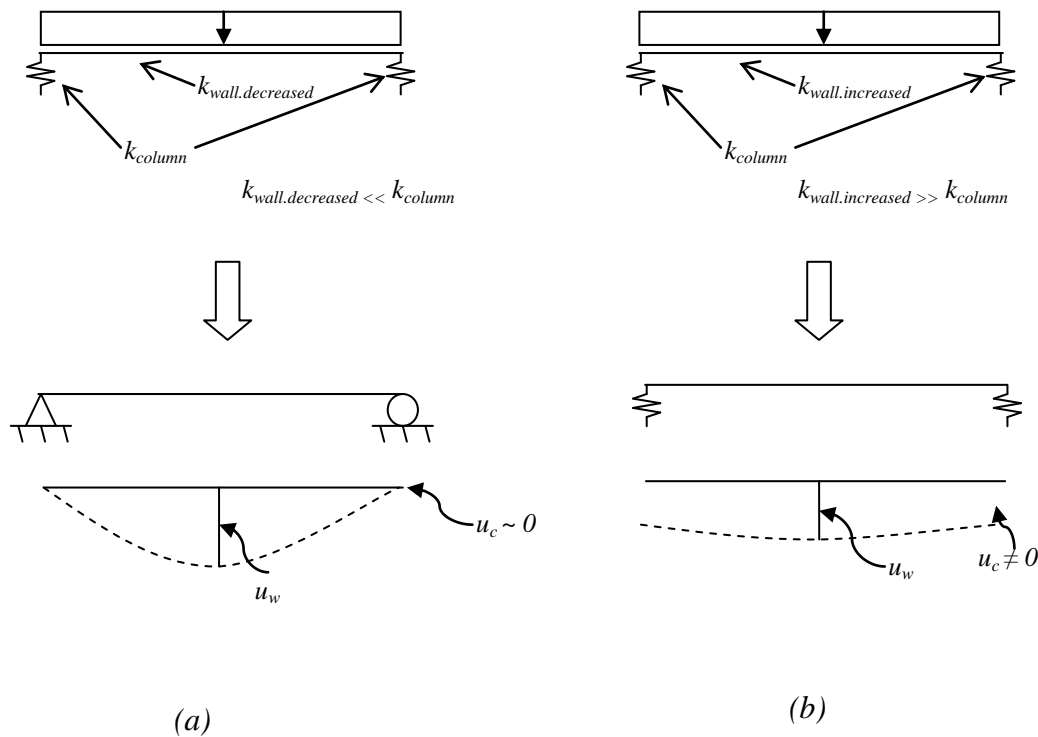


Figure 5.70 (a) When the stiffness of the wall is decreased, the behaviour of the structure becomes similar to the behaviour of a simply supported beam. (b) When the stiffness of the wall is increased, the response corresponds to the response of a beam supported on springs.

In summary, different responses are obtained depending on the stiffness of the wall. Thus, the stiffness of the wall has proved to be an important parameter which considerably influences the response of the column. The Direct load application in SDOF is on the safe side compared to the 3D FE analysis for all stiffnesses of the wall.

### 5.7.3 Elasto-plastic model

#### 5.7.3.1 Parameters studied

For the elasto-plastic model, only the internal resistance of the wall is varied while the stiffness is unchanged and corresponds to the stiffness of the wall in the previous study,  $k_u$ , see Table 5.3. The first internal resistance used in the parametric analysis is the unchanged resistance,  $R_{m,u}$ , which is the same as in the previous study. It is calculated according to equation (F.10) with the dimensions and properties as shown in Figure 5.3, Table 5.1 and Table 5.2. The other resistances used corresponds to the resistance from the previous study,  $R_{m,u}$ , decreased and increased with a factor 2, resulting in  $R_{m,d}$  and  $R_{m,i}$ , respectively. The studied cases for the elasto-plastic model are presented in Figure 5.71. In Table 5.18 the values of the internal resistance of the wall for which the study is conducted are presented.

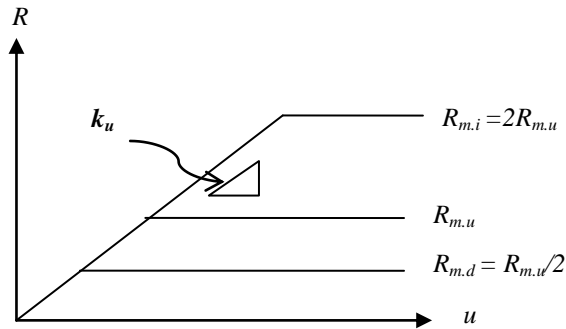


Figure 5.71 Studied cases of the elasto-plastic response model adapted for the wall in a frame structure. Only the internal resistance is varied. The stiffness is the same for all cases.

Table 5.18 The studied values of internal resistance of one wall panel.

Internal resistance of wall panel	$R_{m,d}$	$R_{m,u}$	$R_{m,i}$
	[kN]	[kN]	[kN]
	25	50	100

### 5.7.3.2 Loads and deformation

For the elasto-plastic model the column simulated in SDOF is subjected to the Direct load, Reaction load 5 and 6, according to Figure 5.41.

Reaction load 5 obtained for the studied values of resistances is presented in Figure 5.72 together with the Direct load.

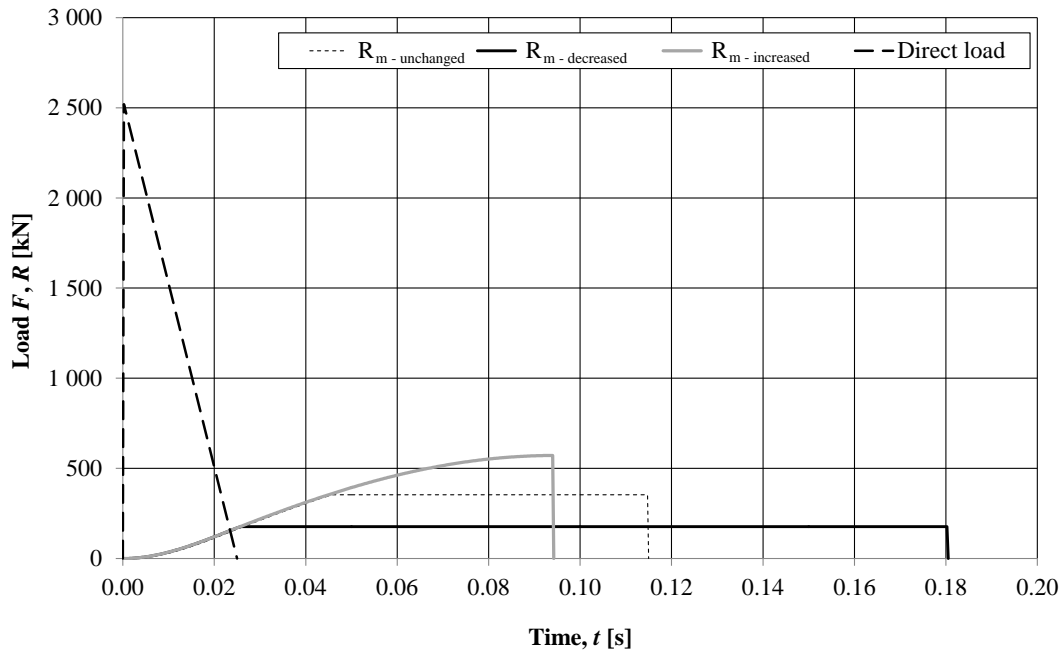


Figure 5.72 Reaction load 5 obtained in SDOF for different values of internal resistance of the wall together with the Direct load.

For each case of Reaction load 5 the resulting deformation of the column is compared to the deformation caused by the application of the Direct load in Figure 5.73.

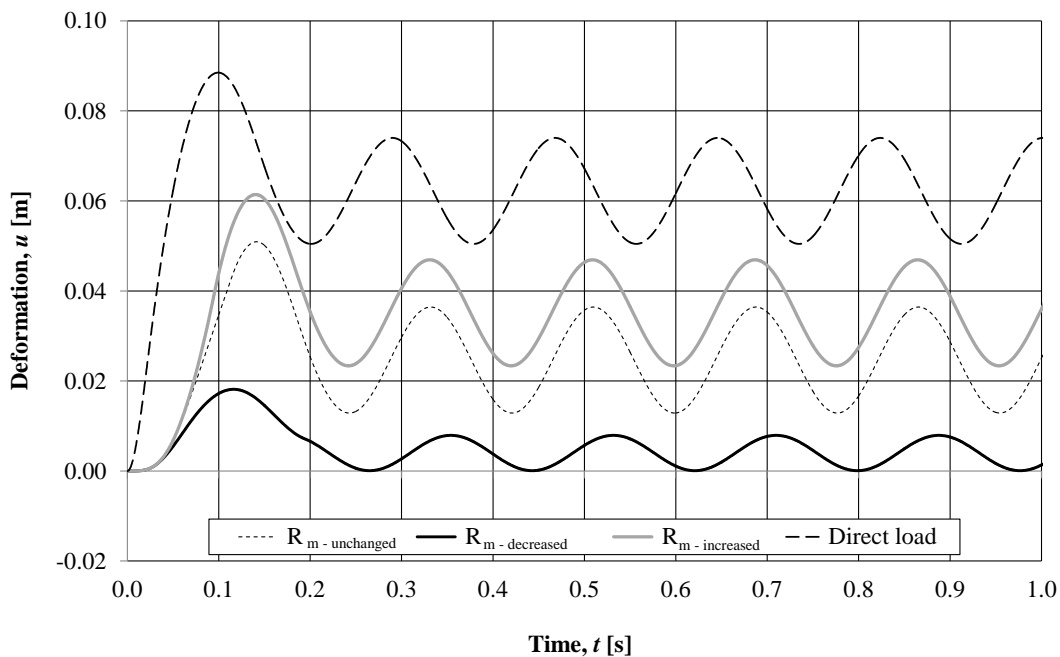


Figure 5.73 Comparison of the deformation in the middle of the column obtained in SDOF for the different cases of Reaction load 5 in Figure 5.72 and the deformation caused by the Direct load.

The largest deformation is obtained for the Direct load. For Reaction load 5, the simplified method for the analytical calculations of the deformation of the frame, proposed in Johansson (2013), provides results on the safe side. The magnitudes of deformation for analysed cases are presented in Table 5.19. Similarly as when the

stiffness of the wall was varied, an increase in the internal resistance leads to an increase in deformation, which is explained in following paragraphs.

Table 5.19 Maximum deformation of the column obtained for the Direct load and for Reaction load 5 in SDOF.

	Direct load	Reaction load 5		
	All cases of $R_m$	Increased $R_m$ , $R_{m,i}$	Unchanged $R_m$ , $R_{m,u}$	Decreased $R_m$ , $R_{m,d}$
$u_{max}$ [m]	0.088	0.061	0.050	0.018

For Reaction load 5 the magnitude of the impulse  $I$  is the same for each case of internal resistance, see Figure 5.74. As the stiffness  $k_u$  is also the same, the maximum value of resistance  $R_i$  reached for the case with increased resistance  $R_{m,i}$  is higher than for the case with decreased resistance  $R_{m,u}$ , compare Figure 5.74a to Figure 5.74b. Thus, the reaction acting on the column and the corresponding deformation of the column for a case with increased internal resistance is also higher.

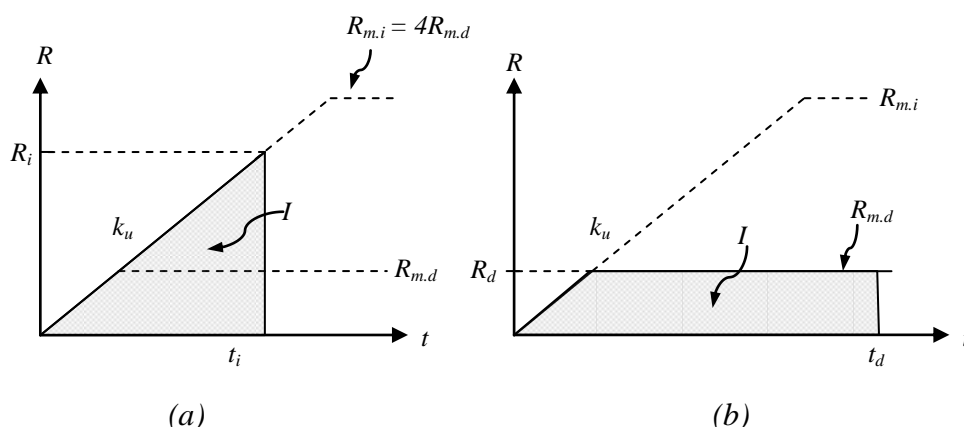


Figure 5.74 The maximum value of reaction for Reaction load 5 in case of a wall with: (a) increased resistance; (b) decreased resistance.

Moreover the duration of Reaction load 5 for a case with increased resistance,  $t_i$ , is shorter than for the case with decreased resistance,  $t_u$ . Thus, the effect of the support reaction for the case with increased resistance is more similar to the effect of the Direct load.

Reaction load 6 for the considered magnitudes of internal resistance is presented in Figure 5.75. For the case when the wall has an increased resistance  $R_{m,i}$ , Reaction load 6 corresponds to the elastic model. The chosen impulse is not big enough for the resistance of wall to reach the limiting value  $R_{m,i}$ . Instead, after absorbing all energy transferred from the impulse, the reaction load starts to decrease before reaching  $R_{m,i}$ . This effect is further explained in following paragraphs.

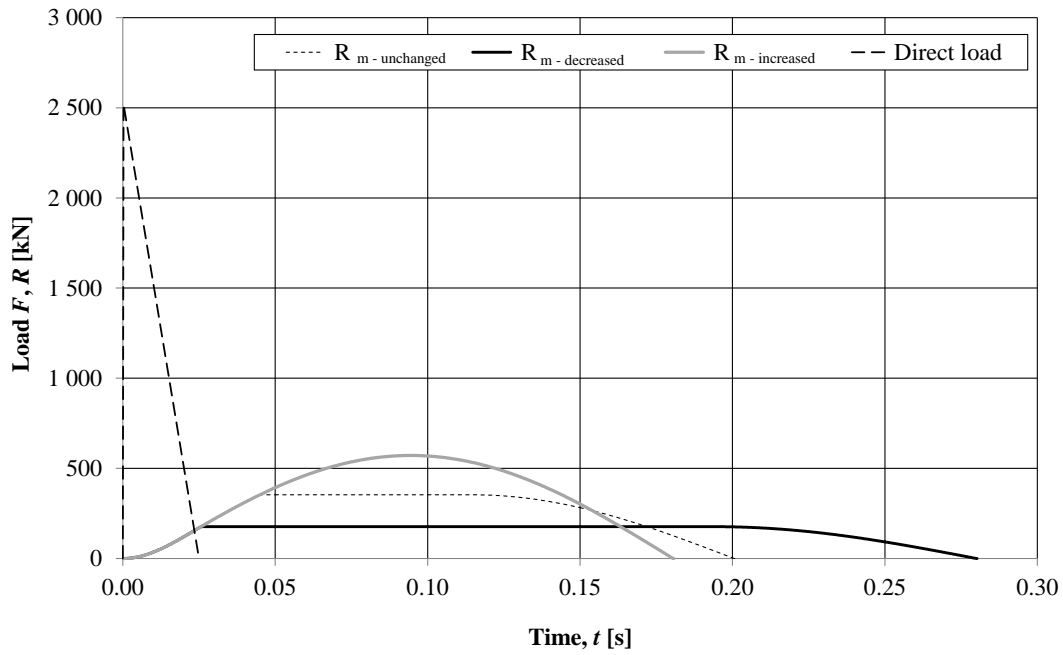


Figure 5.75 Reaction load 6 obtained in SDOF for different values of internal resistance of the wall together with the Direct load.

The deformation of the column caused by Reaction load 6 for the different cases of internal resistance are compared to the deformation caused by the direct application of the impulse load in Figure 5.76. The magnitudes are compiled in Table 5.20.

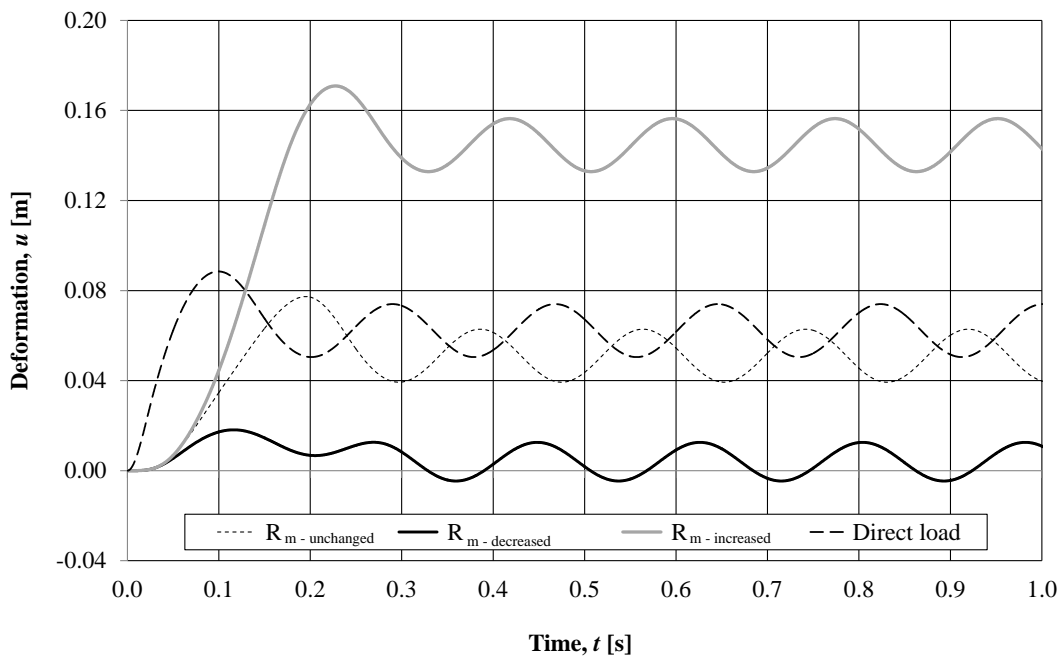


Figure 5.76 Comparison of the deformations in the middle of column, obtained in SDOF for the different cases of Reaction load 6 together with the deformation caused by the Direct load.

Table 5.20 Maximum deformation of the column obtained for the Direct load and for Reaction load 6 in SDOF.

	Direct load	Reaction load 6		
	All cases of $R_m$	Increased $R_m$ , $R_{m,i}$	Unchanged $R_m$ , $R_{m,u}$	Decreased $R_m$ , $R_{m,d}$
$u_{max}$ [m]	0.088	0.170	0.077	0.018

Here, it can be noticed that the case with increased resistance results in a larger deformation of the column than the Direct load. For this case of Reaction load 6 the position on the curves describing the development of the reaction in time is illustrated Figure 5.77.

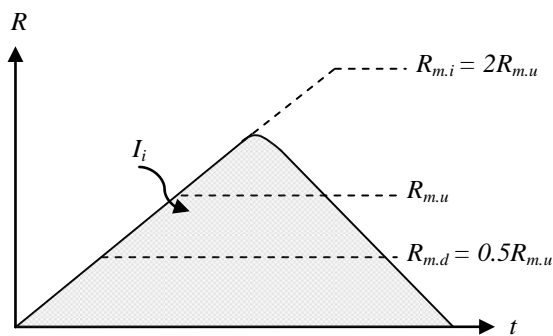


Figure 5.77 Development of the support reaction of the wall with increased internal resistance,  $R_{m,i}$ , for Reaction load 6.

As can be seen in Figure 5.77, the considered reaction does not reach the value of the resistance of the wall,  $R_{m,i}$ , as the chosen impulse magnitude for the Direct load  $I_k$  (see Table 5.8) is not large enough. In this case the response is completely elastic. Thus, the total impulse for this reaction load,  $I_i$ , is twice as large as for the Direct load,  $I_k$ .

For the wall provided with internal resistance  $R_{m,u}$  the Reaction load 6 reaches the value of the internal resistance of the wall, see Figure 5.78.

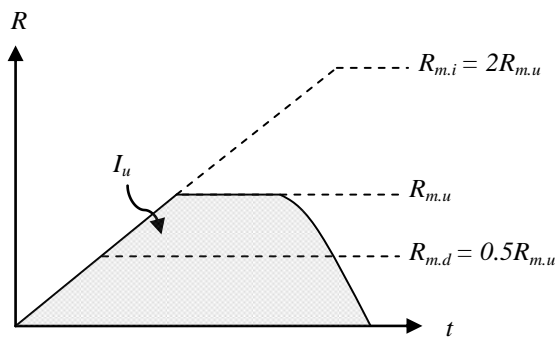


Figure 5.78 Development of the support reactions coming of the wall with internal resistance as in the previous study,  $R_{m,u}$ , for Reaction load 6.



The deformation obtained from the Direct load in SDOF is compared to the deformation obtained in the 3D FE analysis in Figure 5.79. The maximum deformation obtained for the different cases is presented in Table 5.21.

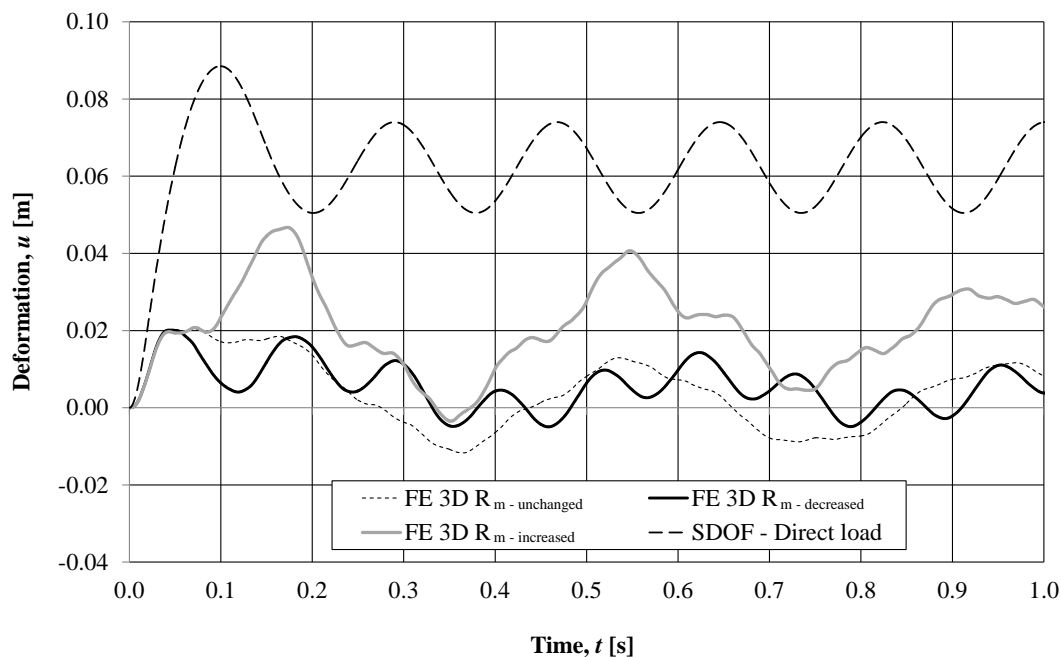


Figure 5.79 Comparison of deformations in the middle of the column obtained in SDOF for the Direct load and the deformation from the FE 3D analysis for the different cases of internal resistance of the wall.

Studying Figure 5.79 and Table 5.21 it is obvious that the simplified method, i.e. the Direct load, provides results on the safe side and the deformation of the column increases with increasing internal resistance of the wall.

Table 5.21 Maximum deformation of the column obtained in SDOF for the Direct load the deformation from the 3D FE analysis for the different cases of internal resistance of the wall according to Figure 5.71.

	SDOF Direct load All cases of $R_m$	FE 3D Increased $R_m$ , $R_{m,i}$	FE 3D Unchanged $R_m$ , $R_{m,u}$	FE 3D Decreased $R_m$ , $R_{m,d}$
$u_{max}$ [m]	0.088	0.046	0.020	0.019

### 5.7.3.3 Investigation of wall panels in FE model

The support reactions and deformation for the wall panels are measured along the column in points illustrated in Figure 5.80. The deformation in the middle of the column is plotted against the wall support reactions for point 1 and 4 for the decreased and increased resistance in Figure 5.81 and Figure 5.82, respectively. The support reactions in all points along the column compared to the support reactions for a

simply supported beam are shown in Section G.4.2. The deformation in the middle of the wall for point 1 and 4 for the decreased and increased resistance of the wall are compared to the deformation of a simply supported beam in Figure 5.83 and Figure 5.84, respectively.

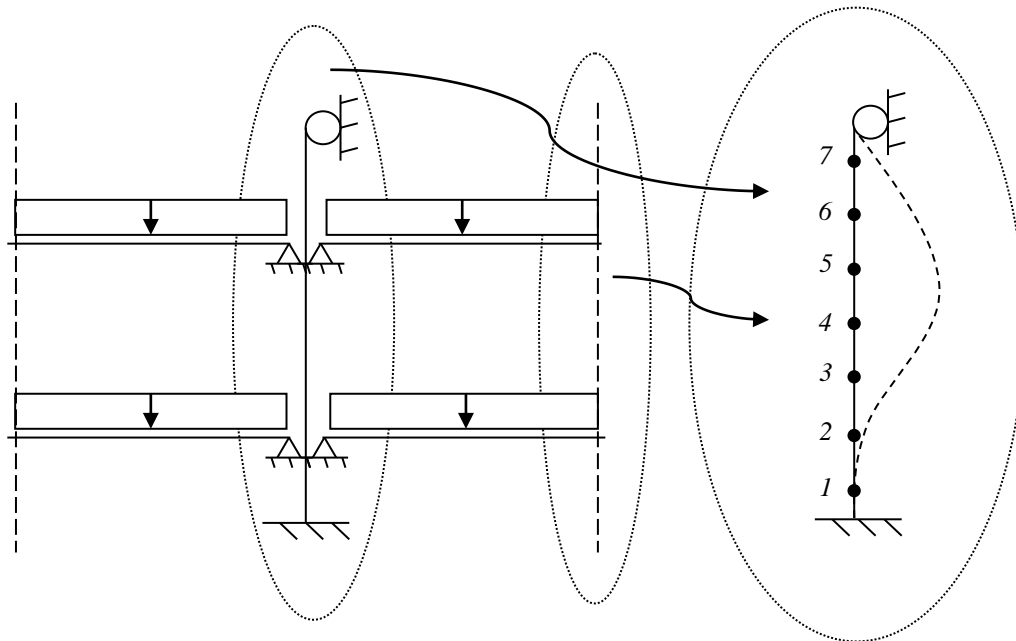


Figure 5.80 The different points along the column, for which the support reactions and the deformations, in the middle of the wall, are measured.

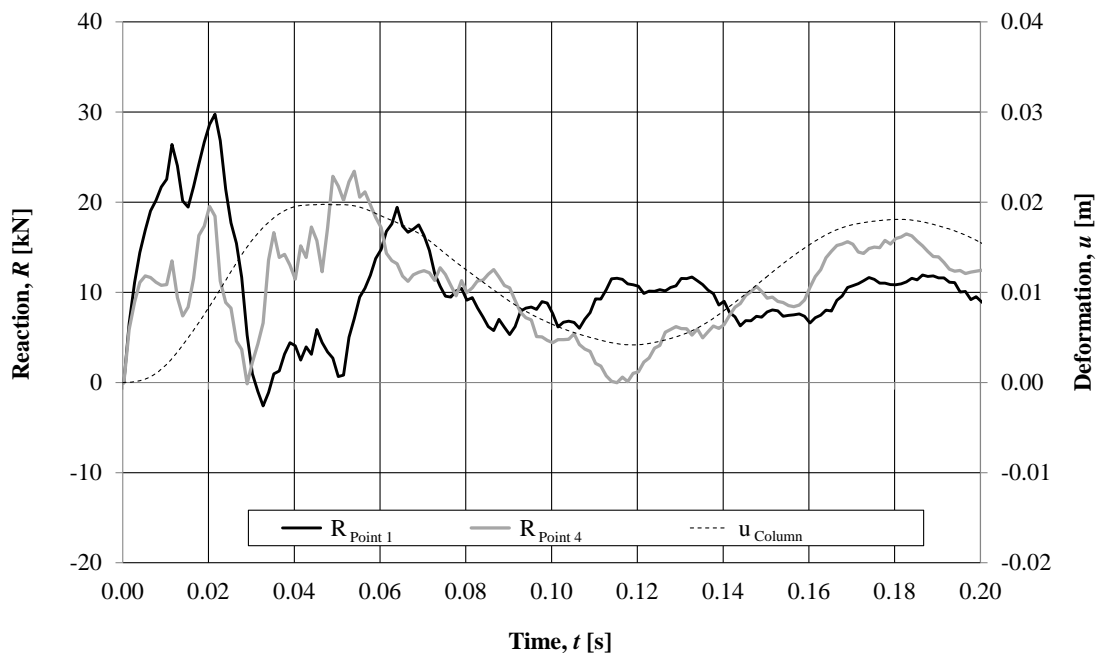


Figure 5.81 Comparison of the deformation in the middle of the column and the support reactions from one wall panel in point 1 and 4 for the case with decreased internal resistance of the wall.

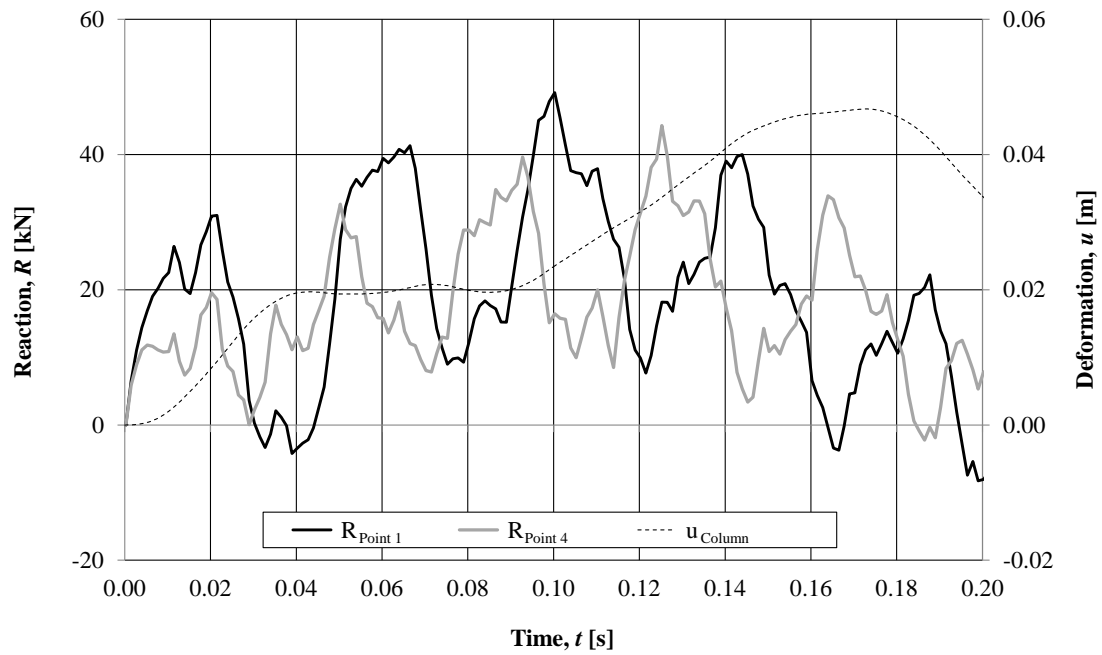


Figure 5.82 Comparison of the deformation in the middle of the column and the support reactions from one wall panel in point 1 and 4 for the case with increased internal resistance of the wall.

Comparing Figure 5.81 and Figure 5.82 it is evident that the amplitude of sways in the deformation curve of the column is strongly influenced by the magnitude of the support reactions which is larger for the wall with increased resistance.

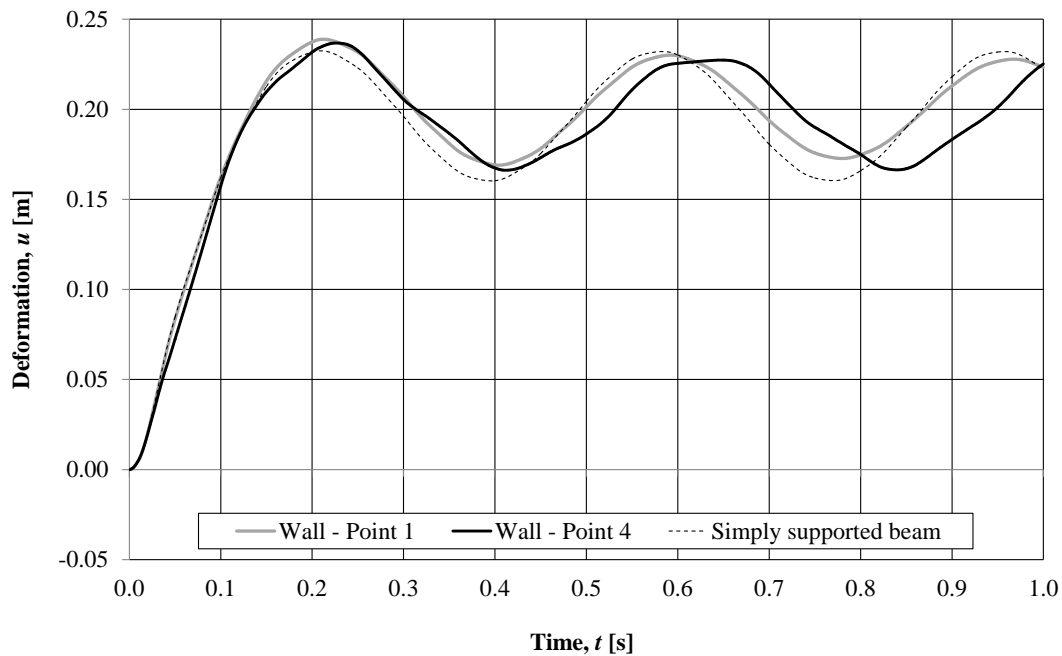


Figure 5.83 The deformation in the middle of the wall with decreased internal resistance, measured in point 1 and 4, compared to the deformation of a simply supported beam.

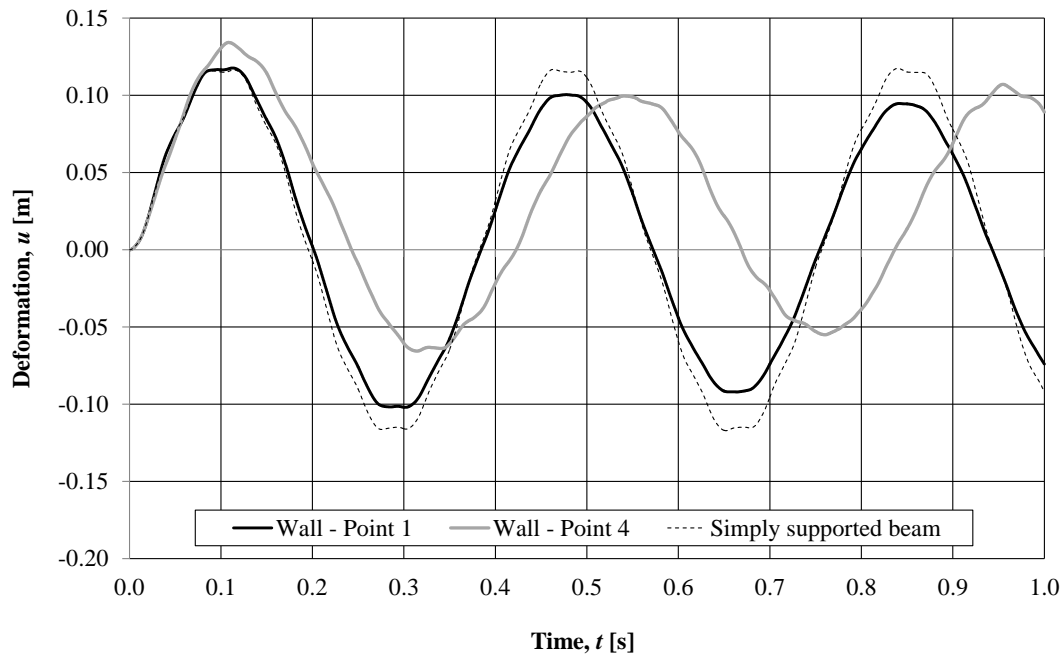


Figure 5.84 The deformation in the middle of the wall with increased internal resistance, measured in point 1 and 4, compared to the deformation of a simply supported beam.

It can be noticed that wall panels with decreased internal resistance show elasto-plastic behaviour and the frequencies are quite similar. When the internal resistance is very low, the reaction forces and deformations of the wall behave more similar to each other. The wall panels with increased internal resistance have elastic behaviour since the internal resistance is not reached (see Figure 5.77) and thus the frequencies are quite different.

#### 5.7.3.4 Influence of internal resistance

For the elasto-plastic model, the internal resistance of the wall is varied according to Section 5.7.3.1. The column simulated in SDOF has been subjected to the Direct load, Reaction load 5 and 6, according to Figure 5.41. For each case of Reaction load the resulting deformation of the column has been compared to the deformation caused by application of the Direct load, see Figure 5.73 and Figure 5.76. The deformation obtained from the Direct load in SDOF has been compared to the deformation obtained in the 3D FE analysis, Figure 5.79. The deformation and support reactions for the wall panel 1 and 4, according to Figure 5.80, for the decreased and increased resistance of the wall, have also been compared.

It is clear that the deformation of the column as well as the reaction forces from the wall panels increases with increasing internal resistance of the wall.

When the internal resistance of the wall is decreased, the simplified method in SDOF always provides results on the safe side. For the case when the internal resistance of the wall panels is increased, the simplified method is on the safe side for all cases except for Reaction load 6, see Figure 5.76. However, Reaction load 6 can be considered to be excessive since the impulse of the load is twice as large as the impulse of the External load applied on the structure, see Figure 5.77. Moreover, the deformation from 3D FE analysis, which is considered to provide the most realistic

results, are lower than in SDOF when the Direct load is applied. Therefore, the simplified method can be considered to be on the safe side.

When the wall panels have decreased internal resistance, the internal resistance is reached and the panels have elasto-plastic behaviour. For the case of wall panel with resistance  $R_{m,i}$ , the internal resistance is not reached why the panels have elastic behaviour for the considered load, see Figure 5.77.

## 5.8 Concluding remarks

The aim of this study was to evaluate the concept of load application in the simplified method of the frame analysis proposed by Johansson (2013). Both this method, when applying a direct load, as well as applying the load due to dynamic reaction of the wall, on the column, has been implemented in the SDOF system. The results from the analytical method have been compared with a 3D FE analysis. Finally, a parametric study is carried out in order to provide a more comprehensive understanding of the response of the studied structure subjected to impulse load.

One main conclusion from this study is that when comparing the SDOF analysis and the 3D FE analysis, for each type of load studied, the SDOF analysis provides results on the safe side.

When comparing the results obtained in SDOF for the different loads for the elastic model, the direct load did not result in the largest deformation. This was due to the fact that the frequency of the reaction loads coincided with the frequency of the deformation, which increased the deformation further. The largest deformation was obtained for the reactions prolonged in time which can be considered as critical. However, as the largest deformation occurs further in time it can be disregarded with consideration to the natural damping effect.

For the elasto-plastic response the direct application of load provided results much on the safe side compared to the 3D analysis. Substituting this load for the dynamic reaction still provided conservative results but the difference to the response of the 3D FE analysis was decreased.

The plastic deformation capacity check showed that for the SDOF simulations, the structure did not possess the capacity to withstand the different loads if reinforcement of Class B was used. If Class C was used, the structure did possess the capacity to withstand the Direct load and the first part of the delayed load, but not when it was extended. The 3D FE analysis showed that the structure would not collapse for reinforcement of Class B nor Class C, proving that the SDOF calculations are well on the safe side.

When adapting the support reactions of a simply supported beam in the analytical method, it is obvious that they cannot be fully simulated using a SDOF model. This is due to the fact that the support of the wall panels is the column, which stiffness corresponds to a spring and not a fixed support. Because of this the true behaviour of the structure is very complicated to create in the SDOF model.

The 3D FE analysis also showed that the shape of the deformation curve for the column does not act as in a 2D FE analysis. This issue has been proved to be strongly influenced by the difference in frequencies of the different support reactions from the wall panels. The divergence of the frequencies in reaction loads decreases the effect of the load on the column and makes the simulation of the response difficult to

conduct in the analytical method. It should be remembered that this method of analysis should be simple and fast to implement. Simultaneously it should provide good results with an acceptable margin of safety. The analytical method has not provided satisfactory results in this study. The obtained differences with regard to the FE analysis are large and even though they are on the safe side they cannot be fully accepted. Further investigations of the 3D response are recommended.

The 3D FE model was built of several wall panels instead of one wall, which created seven point loads along the column instead of one uniformly distributed load. In reality, these wall panels would be connected as one and it is not studied if the reaction forces in the different support points would counteract in the way they did in this analysis, creating an uneven behaviour of the column.

It is worth to mention that the different response models provided different values of deformation of the column. For the simplified method conducted in SDOF the difference between the deformation of the column simulated with the elastic and elasto-plastic response model is about 50 %. This is due to the fact that the internal resistance in the elasto-plastic case forces the reaction from the wall panels to have a lower magnitude and a longer duration, which is less destructive for the column.

The parametric study proved that for high values of stiffness and internal resistance of the wall the deformation of the wall is small. However the deformation of the column is larger than for the case with low stiffness and low internal resistance of the wall. Thus, the proper choice of wall parameters becomes a critical issue as it affects the response of the column which is the load bearing element in the considered structure.

A conclusion that can be drawn is that if the stiffness of the wall is decreased, the wall can be related to the behaviour of a simply supported beam. If the stiffness of the wall is increased, the response of the wall corresponds to the response of a beam supported on springs.

Moreover, when comparing the results from the simplified method to the deformation obtained in the 3D FE analysis, the analytical method proposed by Johansson (2013) provides results on the safe side for all cases studied. However, when the parameters for which the study is done are further increased the difference between the results from the analytical and numerical method decreases.

## 6 Conclusions

### 6.1 Final comments

#### 6.1.1 Parametric beam study

A parametric beam study was carried out in order to investigate the important parameters for the concrete sections with reinforcement at both sides subjected to impulse load. The influence of including the top reinforcement in the calculations was also evaluated. It was proven that for most cases it could be considered conservative to neglect the top reinforcement when calculating the internal work. However, for a certain interval the internal energy was higher for a case without top reinforcement than for a case with top reinforcement due to decrease in the plastic rotation capacity curve in Eurocode 2. Within these intervals the conservative way would be to consider the top reinforcement. However, if the top reinforcement did not yield it did not influence the internal resistance in a significant way and could then be disregarded.

A study of different interpretations of the distance to the reinforcement from the top of the beam,  $d$ , depending on the neutral axis was also carried out for calculations of the plastic deformation capacity. However, the conclusion is to follow the simplest way of interpreting  $d$ , which is only considering the bottom reinforcement. For the studied cases, this provided results on the safe side for most cases.

#### 6.1.2 Structural response of a 2D frame

A single degree of freedom system, SDOF system, was used in order to simulate a 2D frame where the front column was presented by a local SDOF model and the whole frame was modelled with a global SDOF model. The response from the elastic local and global model agreed well with the FE analysis. Thus it can be stated that a SDOF system can be used in order to describe the linear elastic response of both the local and global model. The local and global elastic models proved to provide results, in the middle of the front column, that corresponded well with the FE analysis when combined.

The elasto-plastic models were to be more complicated than the elastic. The structural response model of the local frame model proved to be trilinear, even though the material response model was bilinear, resulting in a higher first deformation peak. The trilinear response model is due to the fact that the structure can develop two plastic hinges, one at the fixed support and one in the span. A comparison between the bilinear and trilinear structural response models showed that the obtained deformation was roughly the same for the two models, and a bilinear response model is not on the safe side, but can be used for estimations of the deformation. For cases with a low plastic deformation capacity, it is suggested to be more careful when choosing a simplified response model.

The global elasto-plastic model also proved to have a trilinear static response model in the SDOF system. However, this static response model did not fully represent the behaviour of the global frame since it showed some plastic deformation even though the response obtained in the SDOF model was limited to elastic behaviour. The response of the global model seemed to be affected by the local model and therefore, it became complicated to describe in SDOF. An interaction between the local and

global model is the probable reason for the behaviour in the 3D FE model. However, this is not captured by the simplified models used in this study and to capture the behaviour a more complex model is needed in order to describe the interaction of additional modes of the frame. A complete understanding of this behaviour has not been found and further investigations are needed in order to improve the understanding.

### **6.1.3 Structural response of a 3D frame**

The 3D behaviour of the front wall and front column of the frame has been investigated where the wall was modelled as seven wall panels on each side of the front column. A comparison was done between a simplified SDOF model, when the total load was applied on the front column at the same time, and when the load application was delayed due to the dynamic reaction of the wall. The approximated method of simulating the 3D effect in the SDOF calculations was to first calculate a load from a SDOF analysis simulating the response of the wall. The delayed load was modelled by a 3D FE model with a column supporting the wall panels.

When comparing the SDOF analyses and the 3D FE analyses, for each type of load studied, the SDOF analyses always provided results on the safe side. The simplified method can be considered to be on the safe side, but since the difference can be quite large compared to the FE model it can be concluded that there is room for improvement.

The reaction loads with an impulse bigger than the direct load have proven not to correspond better to the 3D FE analysis. Therefore the delayed load in SDOF is recommended to be modelled with the same impulse as the external load.

Applying the load through the wall to the column in form of dynamic reaction, instead of directly applying it on the column can have a favourable effect on the response of the column. A less stiff wall induced less stress in the column down to a certain level depending on the relationship between the stiffness and capacity of the column and wall. A wall with a low stiffness and internal resistance provided a lower load on the column.

## **6.2 Further investigations**

The knowledge of reinforced concrete structures subjected to impulse load is limited. Consequently, there are several investigations that can be carried out in order to get a deeper knowledge within this subject, focusing on frame structures.

In the 2D frame study, the global elasto-plastic case was not fully understood why further studies are recommended. The static response model did not completely correspond with the dynamic results obtained in the FE analysis why further investigations are recommended. Considering the interaction between the local and global elasto-plastic models it is suggested that further investigations are carried out to better predict the true behaviour of the frame. To study the interaction between the local and global analysis a two degrees of freedom system is probably required.

Carlsson and Kristensson (2012) found a transformation factor for damping in the central difference method for a simply supported beam. For a frame structure, this transformation factor would differ from a simply supported beam and also would



differ for the local and global models. A future study is recommended in order to find these transformation factors and to explain the theoretical background of how to determine them.

In this Master's Thesis it has been assumed that the plastic hinges are formed when the maximum stress is reached without any consideration to the history of the reinforcement. It can be questioned if the reinforcement changes properties after the plastic hinges have been formed in both directions several times. This is a subject which has not been further investigated in this Master's Thesis.

In the 3D FE analysis, the 3D FE model was built of several wall panels instead of one wall model. This created seven point loads along the column instead of one uniformly distributed load. In reality, these wall panels would be connected and it is not sure if the reaction forces at the different wall supports would counteract in the same way as in this analysis. Therefore, this FE model cannot be considered to simulate the true behavior of the structure. Further studies of the 3D structure are desirable to provide a deeper understand the resulting response and to capture it with a more simple model.

## 7 References

- ADINA (2011): *Theory and Modelling Guide*, Vol 1: ADINA Solids & Structures Report ARD 10-8, ADINA R & D, Inc., Watertown, MA. USA.
- Al-Emrani, M. Engstöm, B. Johansson, M. Johansson. P. (2011): *Bärande konstruktioner*. Report 2011:11, Chalmers University of Technology, Division of Structural Engineering, Göteborg, Sweden.
- Andersson S. och Karlsson H. (2012): *Structural Response of Reinforced Concrete Beams Subjected to Explosions*. Division of Structural Engineering, Concrete Structures, Chalmers University of Technology, Master's Thesis 2012:103, Göteborg, Sweden.
- Augustsson R. och Härenstam M. (2010): *Design of reinforced concrete slab with regard to explosions*. Division of Structural Engineering, Concrete Structures, Chalmers University of Technology, Master's Thesis 2010:38, Göteborg, Sweden.
- Bathe K-J. (1996): *Finite Element procedures*. Prentice Hall, New Jersey, USA.
- Biggs J.M. (1964): *Introduction to Structural Dynamics*. McGraw-Hill Inc., New York, USA.
- Carlsson M. och Kristensson R. (2012): *Structural Response With Regard to Explosions - Mode Superposition, Damping and Curtailment*. Division of Construction Sciences, Structural Mechanics, Lund University of Technology, Report TVSM - 5185, Göteborg, Sweden.
- CEN (2004): Eurocode 2: Design of concrete Structures – Part 1-1: General rules and rules for buildings. European Committee for Standardization, Brussels, Belgium.
- Engström B. (2011): *Design and analysis of continuous beams and columns*, Report 2007:3, Edition 2011. Division of Structural Engineering, Concrete Structures, Chalmers University of Technology, Göteborg, Sweden.
- Fortifikationsverket (2011): *FortSkydd. Bilaga till Fortifikationsverkets Konstruktionsregler FKR 2011*. Dnr 4535/2011, Försvarsmakten
- Johansson M. och Laine L. (2007): *Bebyggelsens motståndsförmåga mot extrem dynamisk belastning*, Delrapport 1: *Last av luftstöt våg*. Räddningsverket, Rapport B54-232/07, Karlstad.
- Johansson M. och Laine L. (2012a): *Bebyggelsens motståndsförmåga mot extrem dynamisk belastning*, Delrapport 3: *Kapacitet hos byggnader*. MSB, Rapport MSB 0142-10, Sverige.
- Johansson, M. (2013), Ph. D., Reinertsen Sverige AB, Sweden.
- Johansson M. (2013): *Stållram*. Myndigheten för samhällsskydd och beredskap (MSB), MSB:s dokumentserie för beräkning av impulsbelastad konstruktion, Dokument B05-102, Karlstad.
- Lundh H. (2005): *Hållfasthetslära*. Kungliga Tekniska Högskolan, Stockholm, Sweden
- MATLAB. Version R 2013 a.

Nyström U. (2006): *Design with regard to explosions*. Division of Structural Engineering, Concrete Structures, Chalmers University of Technology, Master's Thesis 2006:14, Göteborg, Sweden.

MSB (2009): *Skyddsrumregler SR 09*. Myndighete för samhällsskydd och beredskap (MSB), författad av Ekengren B., Beställningsnummer: B54-141/09, Karlstad, Sweden.

## APPENDIX A Hand Calculations

### A.1 Introduction

In order to fast get a result of the maximum values, hand calculations can be used instead of numerical SDOF calculations or FE analyses. The hand calculations are not time dependent. The equations used are stated in following sections.

### A.2 Deformations

The maximum deformations for the elastic, plastic and elasto-plastic case are calculated as

$$u_{el} = \frac{I_k}{\sqrt{km}} = \frac{I_k}{m\omega} \quad (7.1)$$

$$u_{pl} = \frac{I_k^2}{2mR_m} \quad (7.2)$$

$$u_{ep} = u_{ep,el} + u_{ep,pl} = \frac{R_m}{2k} + \frac{I_k^2}{2mR_m} \quad (7.3)$$

where  $I_k$  is the characteristic impulse load,  $m$  is the mass,  $k$  is the stiffness,  $\omega$  is the angular frequency and  $R_m$  is the resistance. The transformation factors used to create the equivalent mass and stiffness are found in Table 2.4 and Table 2.5.

### A.3 Stiffness and moment of inertia

The stiffness for a simply supported beam is calculated as

$$k = \frac{384EI}{5L^3} \quad (7.4)$$

where  $E$  is the Young's modulus and  $L$  is the length. The moment of inertia,  $I$ , is for the elastic case is calculated in different ways depending on if the section is cracked or not. For an uncracked rectangular cross section, state I, the moment of inertia is calculated as

$$I_I = \frac{bh^3}{12} + bh \cdot \left(\frac{h}{2} - x_{cg}\right)^2 + (\alpha - 1) \cdot A_s' \cdot (d' - x_{cg})^2 + (\alpha - 1) \cdot A_s \cdot (d - x_{cg})^2 \quad (7.5)$$

where  $b$  is the width,  $h$  is the height and  $x_{cg}$  is the distance from the top of the beam to the centre of gravity of the cross section. The notations  $A_s'$  and  $A_s$  represents the area of the top and bottom reinforcement and  $d'$  and  $d$  is the distance from the top of the beam to the top and bottom reinforcement, respectively. The parameters used for calculating the moment of inertia of the uncracked beam are shown in Figure 7.1.

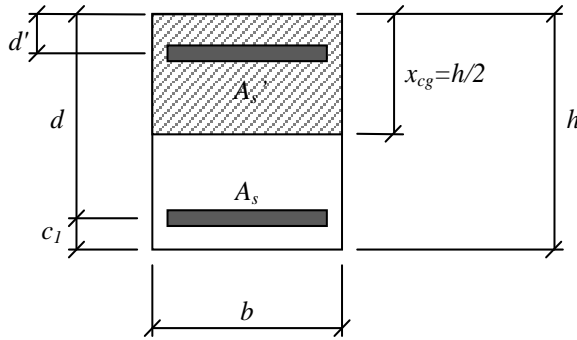


Figure 7.1 Model illustrating the parameters of the beam.

The factor  $\alpha$  is the relation between the Young's modulus of steel  $E_s$  and concrete  $E_c$  calculated as

$$\alpha = \frac{E_s}{E_c} \quad (7.6)$$

For a case where the cross section is symmetric, the centre of gravity,  $x_{cg}$ , is calculated as

$$x_{cg} = \frac{h}{2} \quad (7.7)$$

For a case where the cross section is cracked, state II, equation (7.8) is used to calculate the moment of inertia:

$$I_{II} = \frac{bx_{II}^3}{3} + \alpha A_s' (x_{II} - d') + \alpha A_s (d - x_{II})^2 \quad (7.8)$$

where  $x_{II}$  is the distance from the top of the beam to the neutral axis. For a cracked beam the neutral axis and the centre of gravity doesn't coincide like it does for the uncracked section. In a case where no axial forces are acting on the beam, the neutral axis is calculated, using area equilibrium, as

$$\frac{bx_{II}^2}{2} + (\alpha - 1) \cdot A_s' (x_{II} - d') = \alpha A_s (d - x_{II}) \quad (7.9)$$

## A.4 Moment resistance

### A.4.1 Main concept

For a plastic case, the maximum resistance needs to be calculated in order to calculate the displacement. For a simply supported beam with a uniformly distributed load, the maximum resistance,  $R_m$ , is calculated as

$$R_m = \frac{8M_{rd}}{L} \quad (7.10)$$

where  $L$  is the length. The resisting moment,  $M_{rd}$ , is calculated by force and moment equilibrium from Figure 7.2. The calculations depend on if the section has top reinforcement or not and if the reinforcement yielding or not. The different calculations are presented in Section A.4.2 and A.4.3.

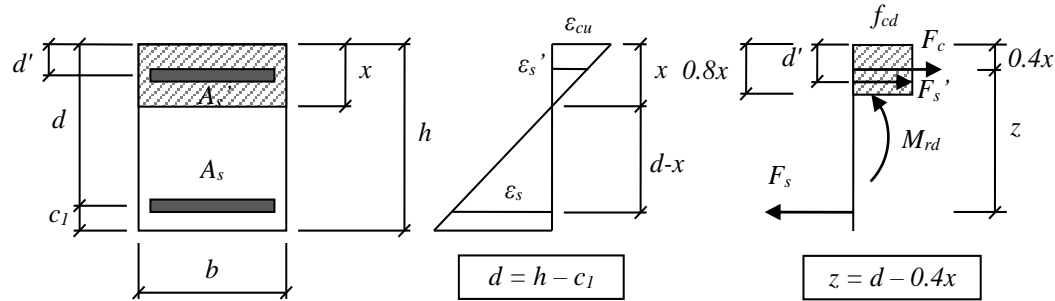


Figure 7.2 Concrete beam with top and bottom reinforcement.

The design values for steel,  $f_{yd}$ , and concrete strength,  $f_{cd}$ , are calculated as

$$f_{cd} = \frac{f_{ck}}{1.2} \quad (7.11)$$

$$f_{yd} = \frac{f_{yk}}{1.0} \quad (7.12)$$

where  $f_{ck}$  is the characteristic concrete strength and  $f_{yk}$  is the characteristic yield strength. The relation between the steel yield strength,  $f_{yd}$ , and the modulus of elasticity of steel,  $E_s$ , is noted by  $\varepsilon_{sy}$  and calculated as

$$\varepsilon_{sy} = \frac{f_{yd}}{E_s} \quad (7.13)$$

#### A.4.2 Section without top reinforcement

For a case without top reinforcement, the neutral axis,  $x_{III}$ , when the ultimate concrete strain is reached is calculated using equation (7.14) assuming that the bottom reinforcement is yielding.

$$x_{III} = \frac{A_s \cdot f_{yd}}{0.8 \cdot f_{cd} \cdot b} \quad (7.14)$$

To check if the reinforcement is yielding or not, a control of the strain at the level of bottom reinforcement,  $\varepsilon_s$ , is done as

$$\varepsilon_s = \frac{d - x_{III}}{x_{III}} \cdot \varepsilon_{cu} \geq \varepsilon_{sy} \quad (7.15)$$

where  $\varepsilon_{cu}$  is the ultimate concrete strain.

For a case when the bottom reinforcement is not yielding, a new position of the neutral axis,  $x_{III}$ , is calculated by solving

$$f_{cd} \cdot 0.8 \cdot x_{III} \cdot b - \frac{d - x_{III}}{x_{III}} \cdot A_s \cdot \varepsilon_{cu} \cdot E_s = 0 \quad (7.16)$$

Now, the moment capacity,  $M_{rd}$ , can be calculated by moment equilibrium around the bottom reinforcement:

$$M_{rd} = f_{cd} \cdot 0.8 \cdot x_{III} \cdot b \cdot (d - 0.4 \cdot x_{III}) \quad (7.17)$$

### A.4.3 Section with top reinforcement

For a case with top reinforcement, the neutral axis is first calculated assuming only yielding at the bottom reinforcement. The neutral axis,  $x_{III}$ , is then decided from

$$f_{cd} \cdot 0.8 \cdot x_{III} \cdot b - A_s \cdot f_{yd} + A_s' \cdot \varepsilon_{cu} \cdot \frac{d' - x_{III}}{x_{III}} \cdot E_s = 0 \quad (7.18)$$

To check if the top reinforcement is yielding or not, the strain at the top reinforcement is calculated using equation (7.19) and compared with the steel yield strain  $\varepsilon_{sy}$ :

$$\varepsilon_s' = \frac{d' - x_{III}}{x_{III}} \cdot \varepsilon_{cu} \quad (7.19)$$

If the top reinforcement is not yielding,  $\varepsilon_s' < \varepsilon_{sy}$ , the moment resistance is found as

$$M_{rd} = f_{cd} \cdot 0.8 \cdot x_{III} \cdot b \cdot (d - 0.4 \cdot x_{III}) - A_s' \cdot \varepsilon_{cu} \cdot \frac{d' - x_{III}}{x_{III}} \cdot E_s \cdot (d - d') \quad (7.20)$$

However, if the top reinforcement is yielding,  $\varepsilon_s' \geq \varepsilon_{sy}$ , a new neutral axis,  $x_{III}$ , is estimated from

$$f_{cd} \cdot 0.8 \cdot x_{III} \cdot b - A_s' \cdot f_{yd} - A_s f_{yd} = 0 \quad (7.21)$$

The moment resistance for this case is

$$M_{rd} = f_{cd} \cdot 0.8 \cdot x_{III} \cdot b \cdot (d - 0.4 \cdot x_{III}) - A_s' \cdot f_{yd} \cdot (d - d') \quad (7.22)$$

According to Eurocode 2, the contribution to the moment capacity of the compressive reinforcement can only be taken into account if stirrups with minimum allowable spacing are provided.

## A.5 Maximum deformation capacity

The maximum deformation can be calculated by multiplying the plastic rotation capacity with regard to shear slenderness,  $\theta_{rd}$ , with the distance between a point with zero moment and a point where a plastic hinge has occurred,  $L_0$ . For a simply supported beam this is shown in Figure 7.3.

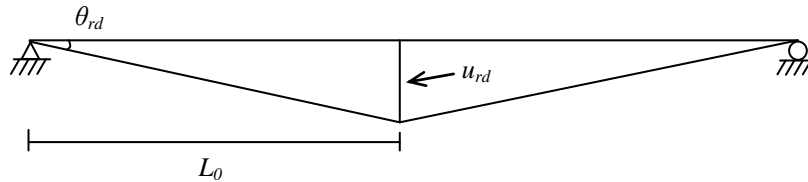


Figure 7.3 Plastic rotation capacity and distance to the plastic hinge in the middle of the span for a simply supported beam.

The maximum deformation,  $u_{rd}$ , can be then calculated as

$$u_{rd} = \theta_{rd} \cdot L_0 = k_{\lambda} \cdot \theta_{pl} \cdot L_0 \quad (7.23)$$

The plastic rotation,  $\theta_{pl}$ , is received from a graph, Figure 7.4, according to Eurocode 2, CEN (2004).

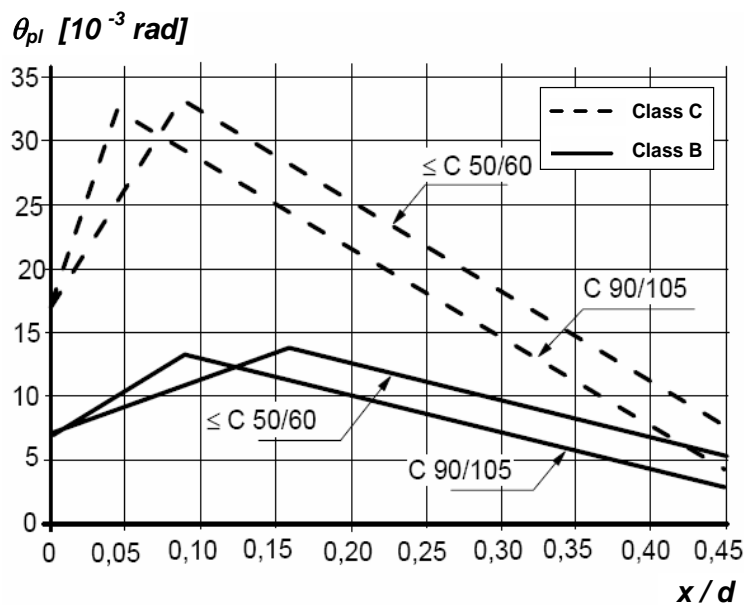


Figure 7.4. Diagram for evaluating the plastic rotation capacity according to Eurocode 2, CEN (2004).

Since the graph doesn't contain exact values, an interpretation of the graph used for the analyses conducted in this Master's Thesis is the following for reinforcement of Class B,  $\le C 50/60$ .

$$\text{For } 0 \leq \frac{x}{d} \leq 0.159$$



$$\theta_{pl} = \left( 7 + \frac{7}{0.159} \cdot \frac{x}{d} \right) \cdot 10^{-3} \quad (7.24)$$

For  $0.159 < \frac{x}{d} \leq 0.45$

$$\theta_{pl} = \left( 13.7 - \frac{8.5}{0.291} \cdot \left( \frac{x}{d} - 0.159 \right) \right) \cdot 10^{-3} \quad (7.25)$$

For reinforcement of Class C,  $\leq C 50/60$ , the interpretation of the graph is as follows.

For  $0 \leq \frac{x}{d} \leq 0.085$

$$\theta_{pl} = \left( 16.7 + \frac{16.6}{0.085} \cdot \frac{x}{d} \right) \cdot 10^{-3} \quad (7.26)$$

For  $0.085 < \frac{x}{d} \leq 0.45$

$$\theta_{pl} = \left( 33.3 - \frac{25.9}{0.365} \cdot \left( \frac{x}{d} - 0.085 \right) \right) \cdot 10^{-3} \quad (7.27)$$

$\theta_{pl}$  is multiplied by a factor  $k_\lambda$  calculated as

$$k_\lambda = \sqrt{\frac{\lambda}{3}} \quad (7.28)$$

where

$$\lambda = \frac{L_0}{d} \quad (7.29)$$

## A.6 Internal and external work

The internal energy  $W_i$  can be calculated as the area under the graph describing the relationship between the static load and the deformation. For an elastic case the internal energy is expressed as

$$W_{i.el} = \frac{k \cdot u_{el}^2}{2} \quad (7.30)$$

where  $k$  is the stiffness and  $u_{el}$  is the elastic deformation. For the plastic case the internal energy can be calculated as

$$W_{i,pl} = R_m \cdot u_{pl} \quad (7.31)$$

For a characteristic impulse  $I_k$  where  $R_m$  is the internal resistance and  $u_{pl}$  is the plastic deformation the external energy can be calculated as

$$W_e = \frac{I_k^2}{2 \cdot m} \quad (7.32)$$

where  $I_k$  is the characteristic impulse load and  $m$  is the mass.

## A.7 Equivalent static load

In order to approximate a load that is easier to relate to for most engineers, a dynamic load can be translated into an equivalent static load. The size of the equivalent static load in an elastic case,  $Q_{el}$ , is

$$Q_{el} = k \cdot u_{el} \quad (7.33)$$

where the stiffness  $k$  and the deformation  $u_{el}$  is depending on if the structure is in state I or II, i.e. if it is uncracked or cracked.

For a plastic case the equivalent static load,  $Q_{pl}$ , is equal to the maximum resistance  $R_m$

$$Q_{pl} = R_m \quad (7.34)$$

From the equivalent static loads, the resulting moment,  $M_{rd}$ , and shear,  $V_{rd}$ , can for a simply supported beam be calculated as

$$M_{rd} = \frac{Q \cdot L}{8} \quad (7.35)$$

$$V_{rd} = \frac{Q}{2} \quad (7.36)$$

# APPENDIX B Additional graphs for Parametric beam study

## B.1 Introduction

A compilation of the graphs from the parametric beam study, discussed in Section 3, is presented in Section B.2 to Section B.13. The parametric beam study was performed for two cases of calculating the effective depth  $d$ , called Case 1 and Case 2, which are further described in Section B.1.1 and B.1.2, respectively.

### B.1.1 Case 1

Case 1 is when the effective depth  $d$  is calculated as the distance from the centre of the bottom reinforcement to the top edge of the beam, not depending on the position of the neutral axis, as shown in Figure 3.2.

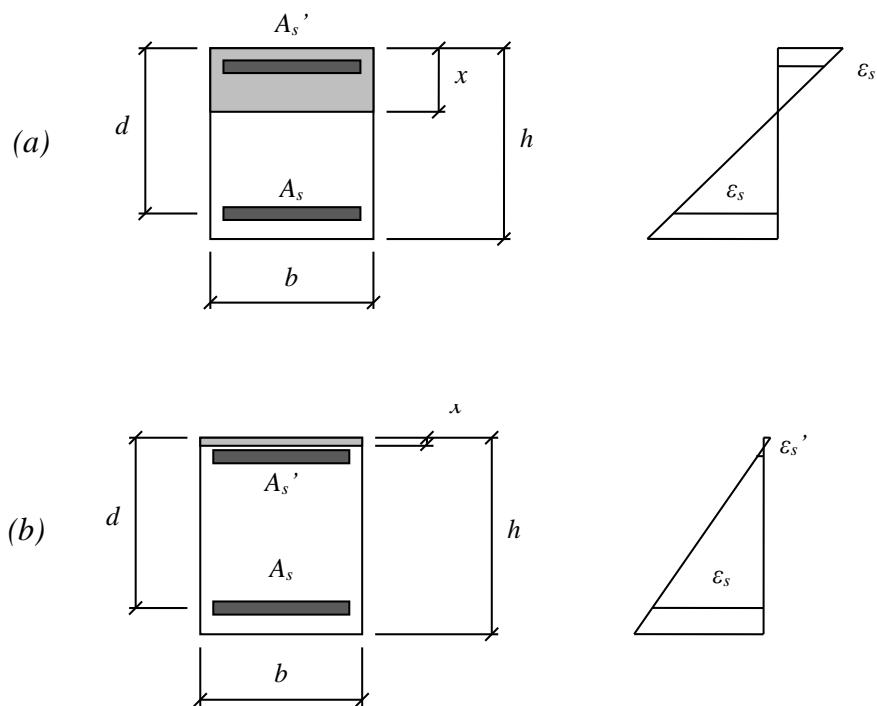


Figure B.1 Effective depth according to Case 1. Neutral axis is located: (a) below top reinforcement layer, and (b) above.

### B.1.2 Case 2

Case 2 considers the location of neutral axis when calculating the effective depth,  $d$ , which is calculated as the distance from the centre of the bottom reinforcement to the top edge of the beam when the neutral axis is below the top reinforcement. However, if the neutral axis is located above the top reinforcement,  $d$  is the distance from the top edge to the centre of gravity of the uncracked cross section, see Figure 3.3.

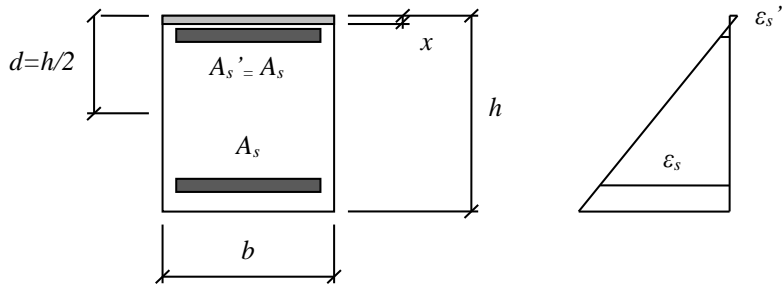


Figure B.2 Calculation of effective depth for Case 2 when the neutral axis is located above the centre of gravity of the top reinforcement.

## B.2 Resistance versus deformation for Case 1

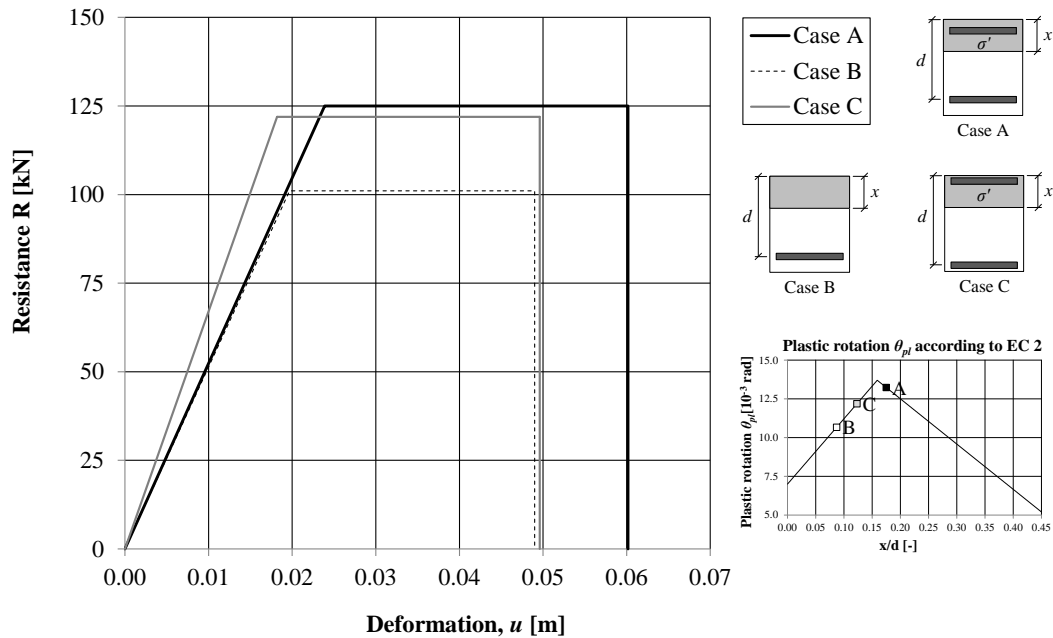


Figure B.3 Internal resistance, ultimate deflection and position on the plastic rotation capacity graph (Eurocode 2) for a section with a height of 200 mm and reinforcement  $\phi 10$  s 150.

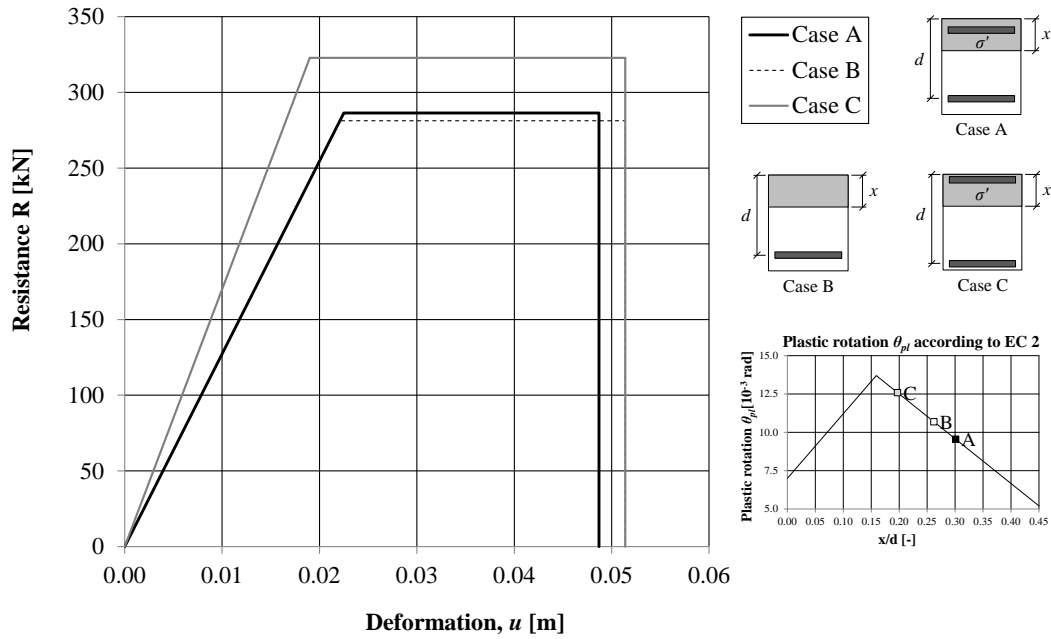


Figure B.4 Internal resistance, ultimate deflection and position on the plastic rotation capacity graph (Eurocode 2) for a section with a height of 200 mm and reinforcement  $\phi 20$  s 200.

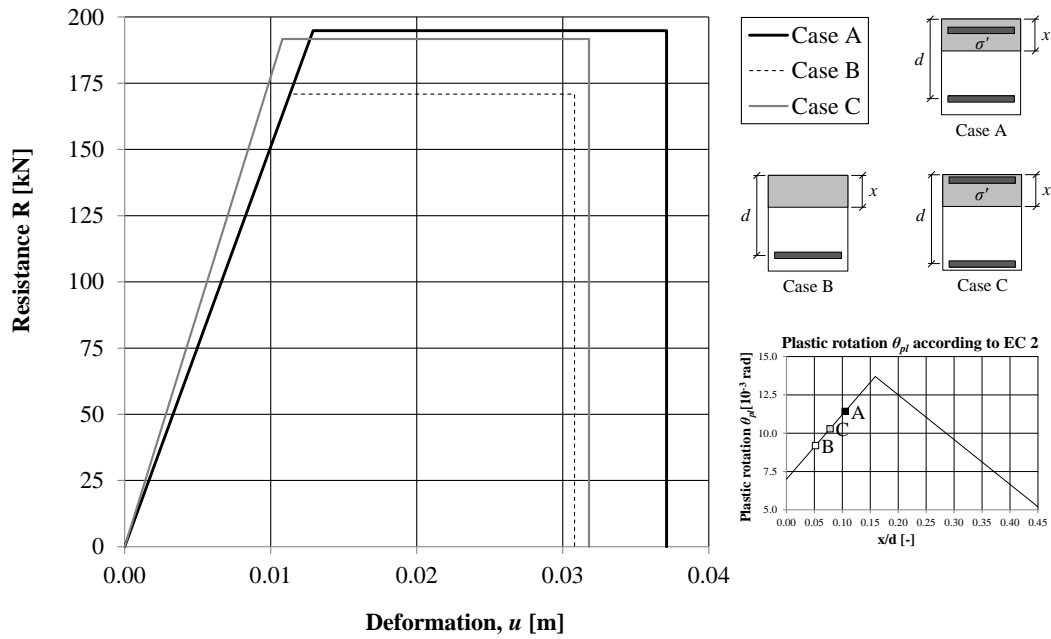


Figure B.5 Internal resistance, ultimate deflection and position in the plastic rotation capacity graph (Eurocode 2) for a section with a height of 300 mm and reinforcement  $\phi 10$  s 150.

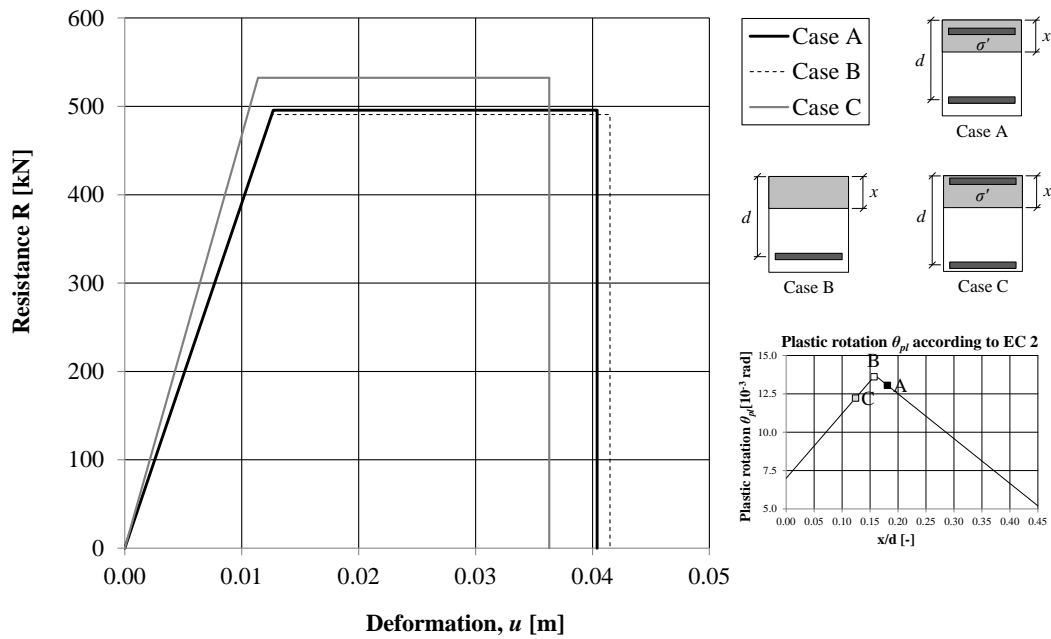


Figure B.6 Internal resistance, ultimate deflection and position in the plastic rotation capacity graph (Eurocode 2) for a section with a height of 300 mm and reinforcement  $\phi 20$  s 200.

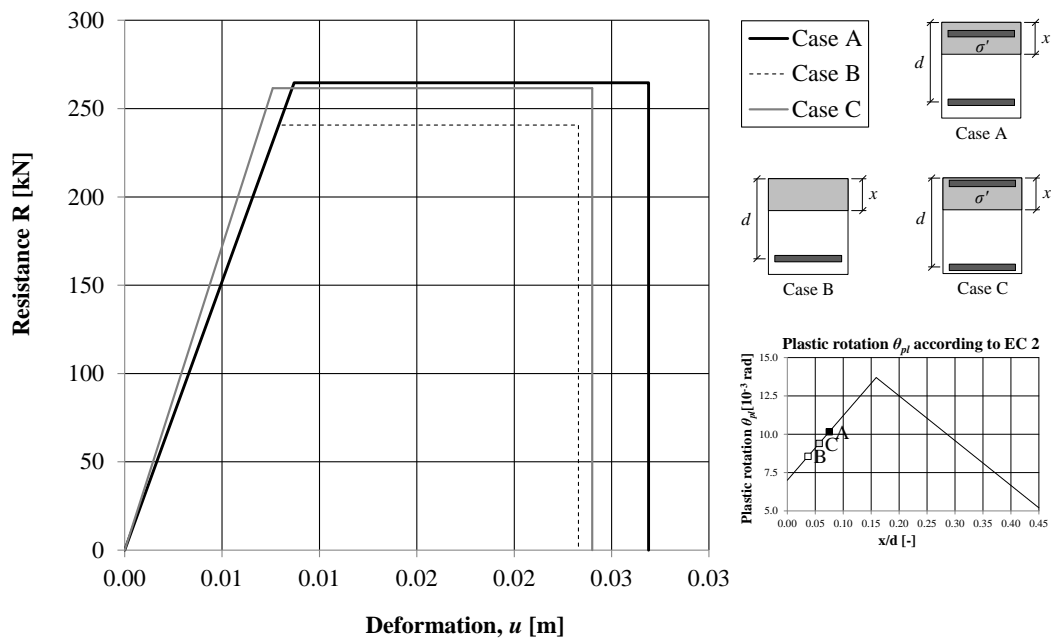


Figure B.7 Internal resistance, ultimate deflection and position in the plastic rotation capacity graph (Eurocode 2) for a section with a height of 400 mm and reinforcement  $\phi 10$  s 150.

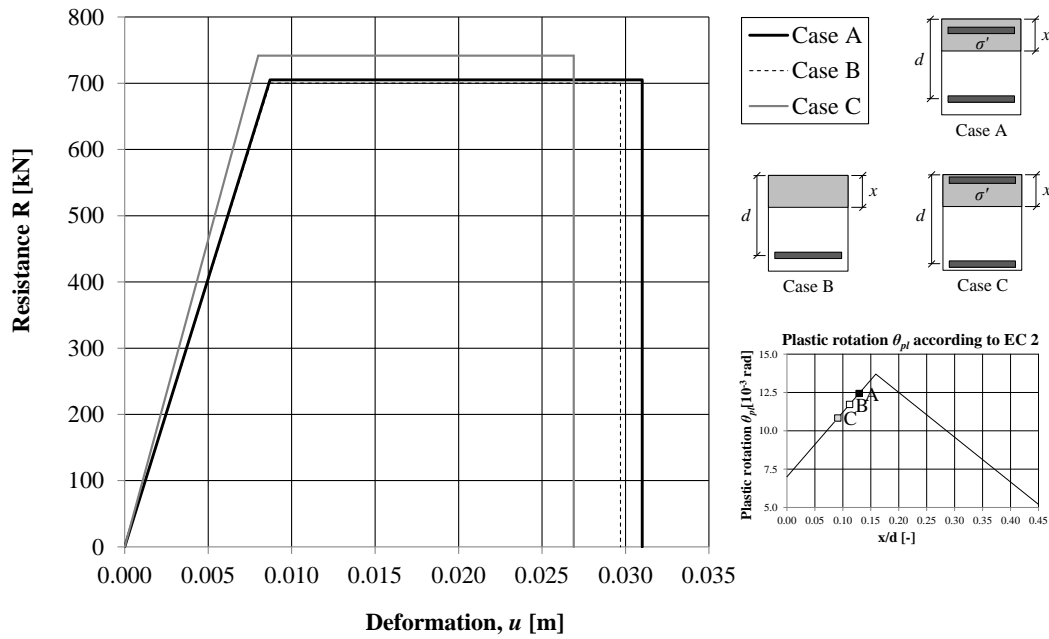


Figure B.8 Internal resistance, ultimate deflection and position in the plastic rotation capacity graph (Eurocode 2) for a section with a height of 400 mm and reinforcement  $\phi 20$  s 200.

### B.3 Plastic rotation capacity for Case 1

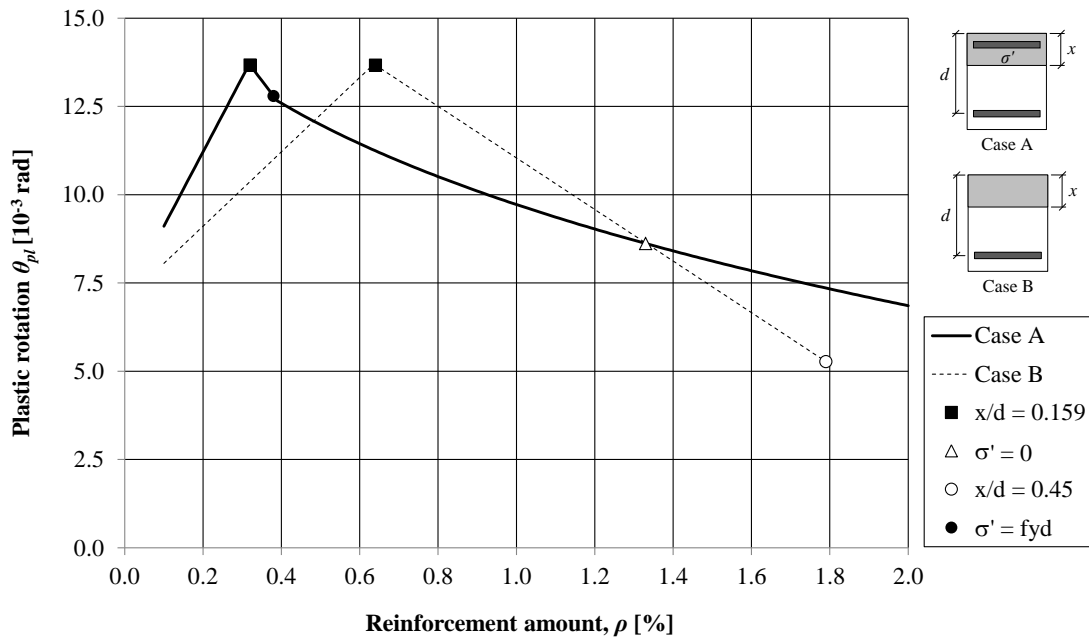


Figure B.9 Plastic rotation capacity  $\theta_{pl}$  vs. reinforcement amount  $\rho$  for a section with a height of 200 mm.

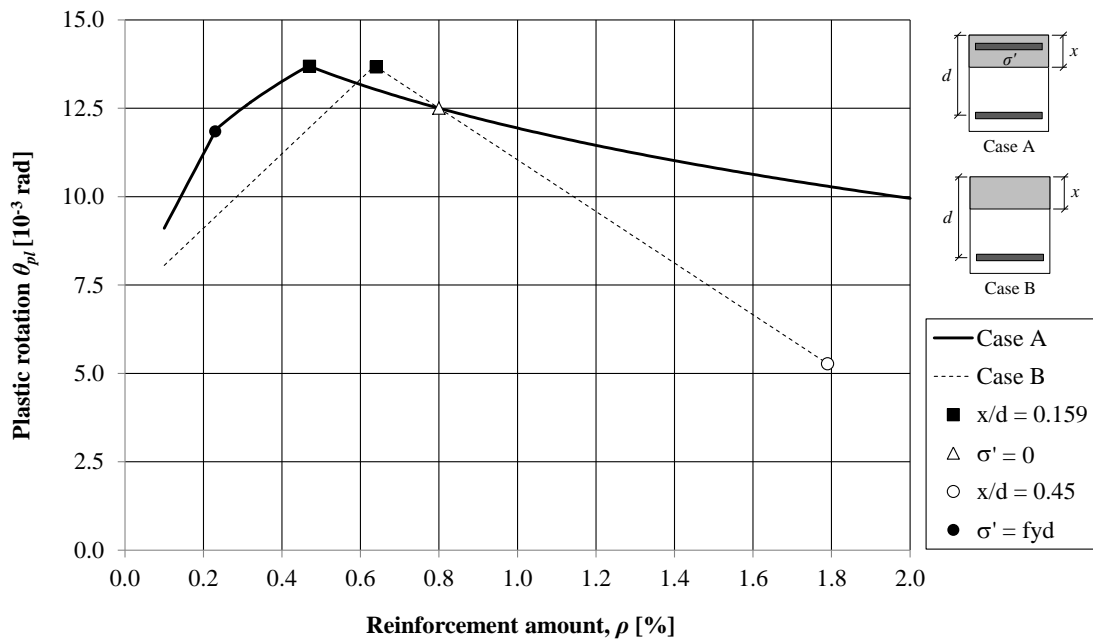


Figure B.10 Plastic rotation capacity  $\theta_{pl}$  vs. reinforcement amount  $\rho$  for a section with a height of 300 mm.

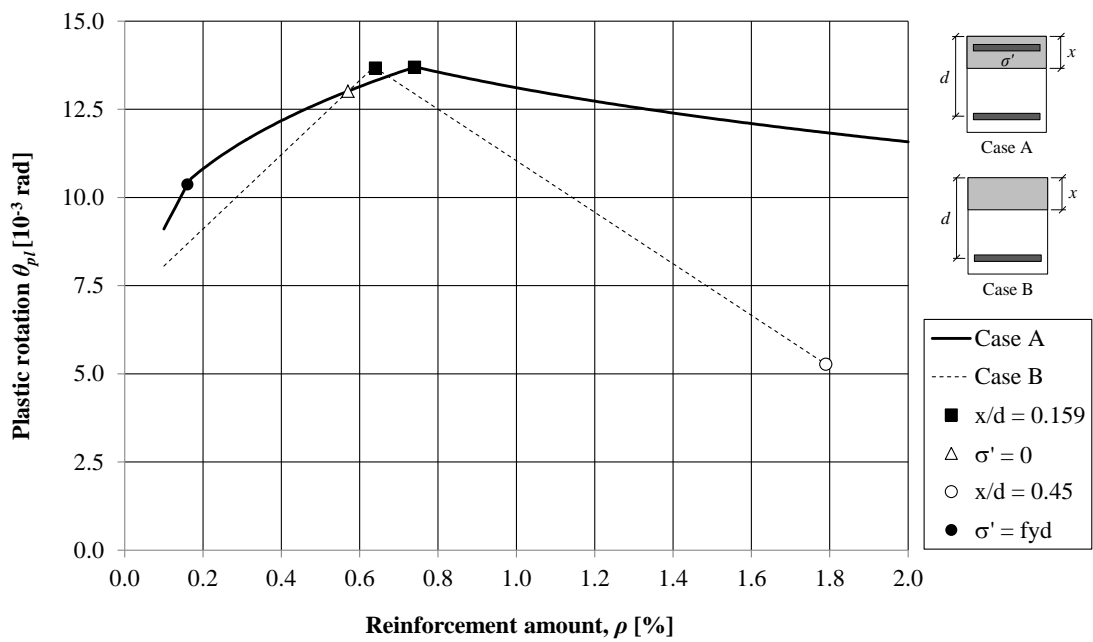


Figure B.11 Plastic rotation capacity  $\theta_{pl}$  vs. reinforcement amount  $\rho$  for a section with a height of 400 mm.



## B.4 Internal work for Case 1

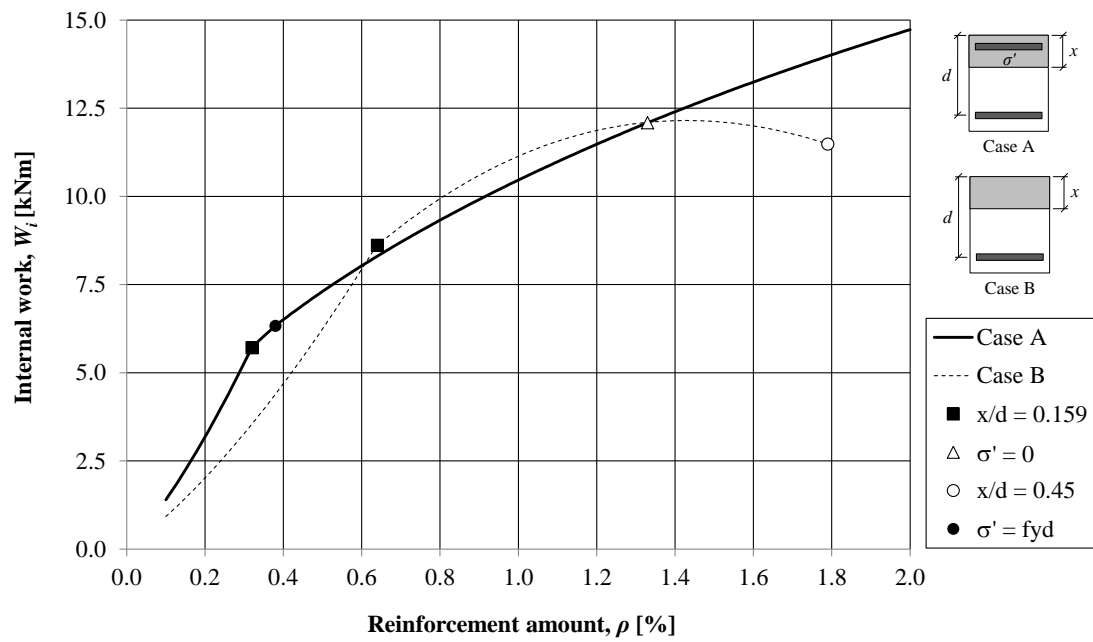


Figure B.12 Internal work vs. reinforcement amount  $\rho$  for a section with a height of 200 mm.

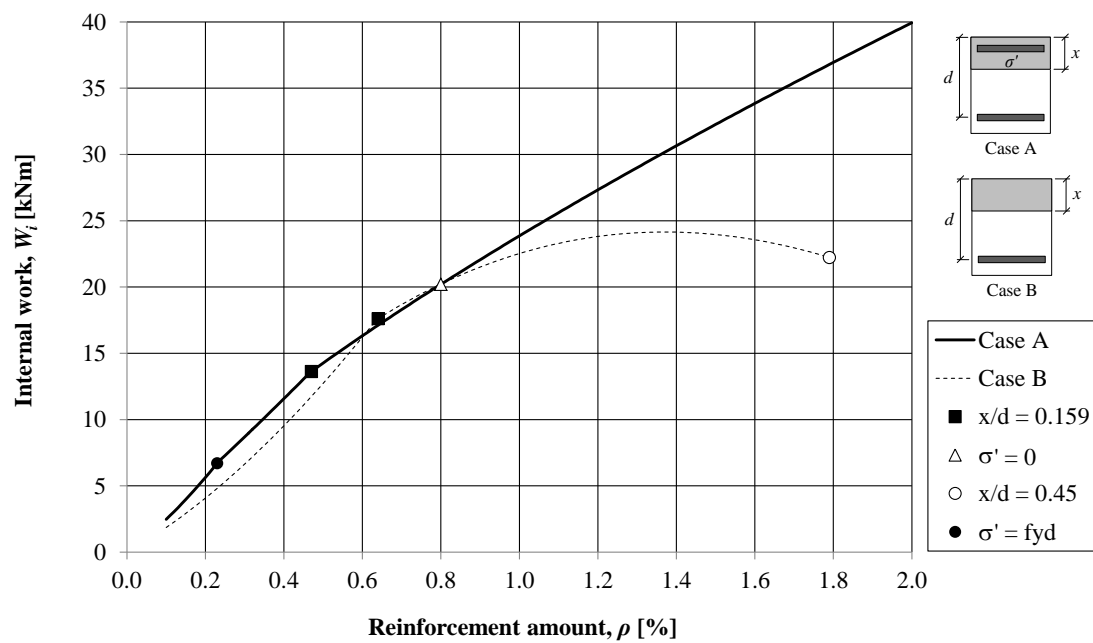


Figure B.13 Internal work vs. reinforcement amount  $\rho$  for a section with a height of 300 mm.

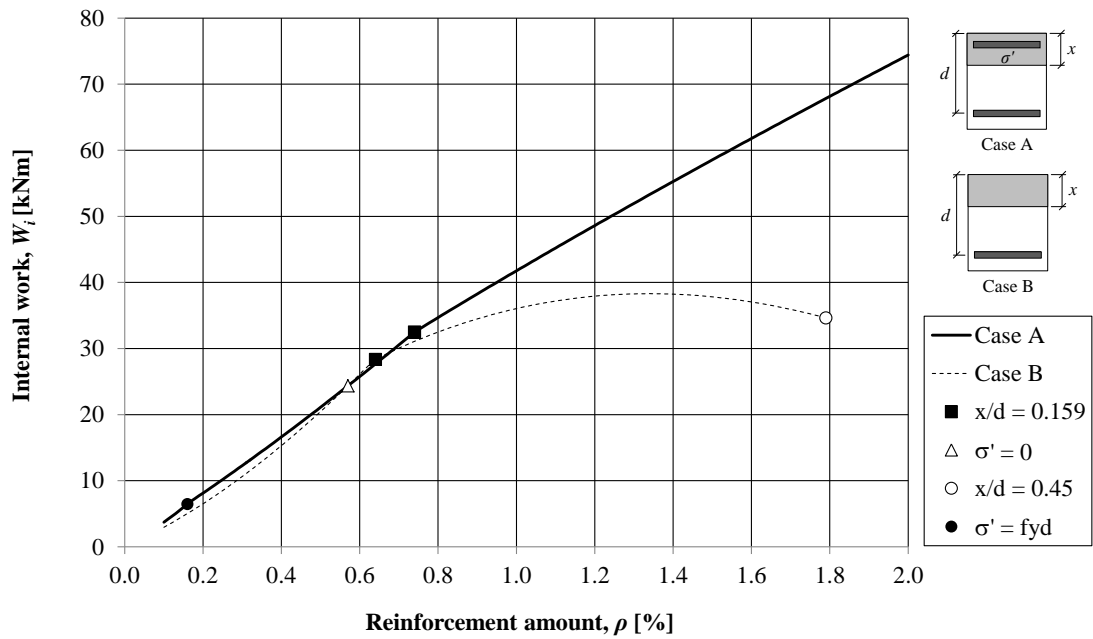


Figure B.14 Internal work vs. reinforcement amount  $\rho$  for a section with a height of 400 mm.

## B.5 Internal resistance for Case 1

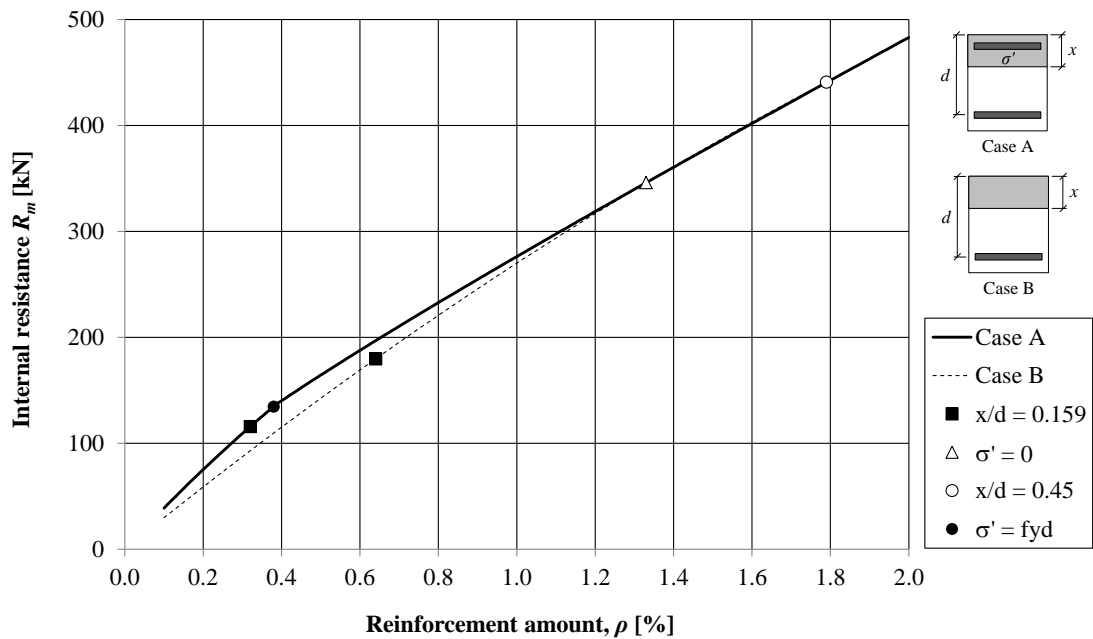


Figure B.15 Internal resistance vs. reinforcement amount  $\rho$  for a section with a height of 200 mm.

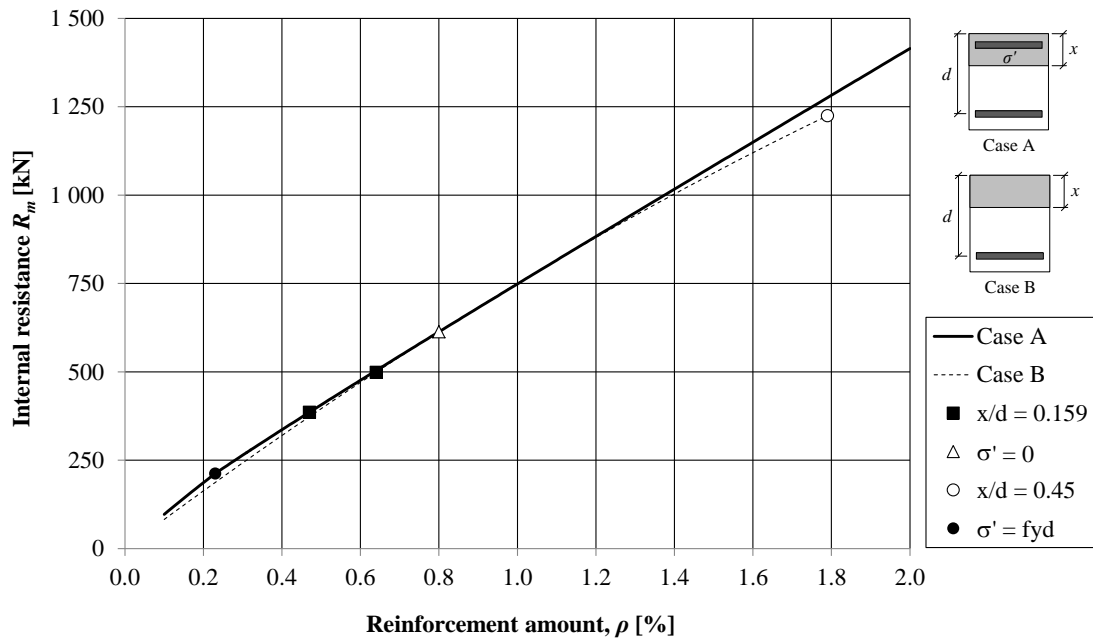


Figure B.16 Internal resistance vs. reinforcement amount  $\rho$  for a section with a height of 300 mm.

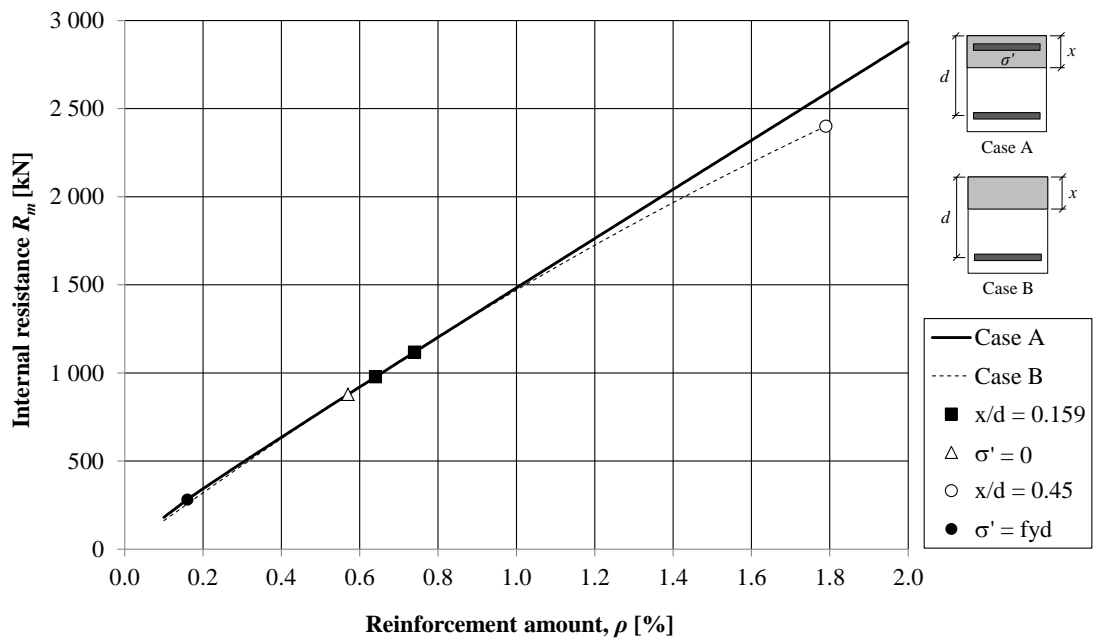


Figure B.17 Internal resistance vs. reinforcement amount  $\rho$  for a section with a height of 400 mm.

## B.6 Maximum plastic deformation for Case 1

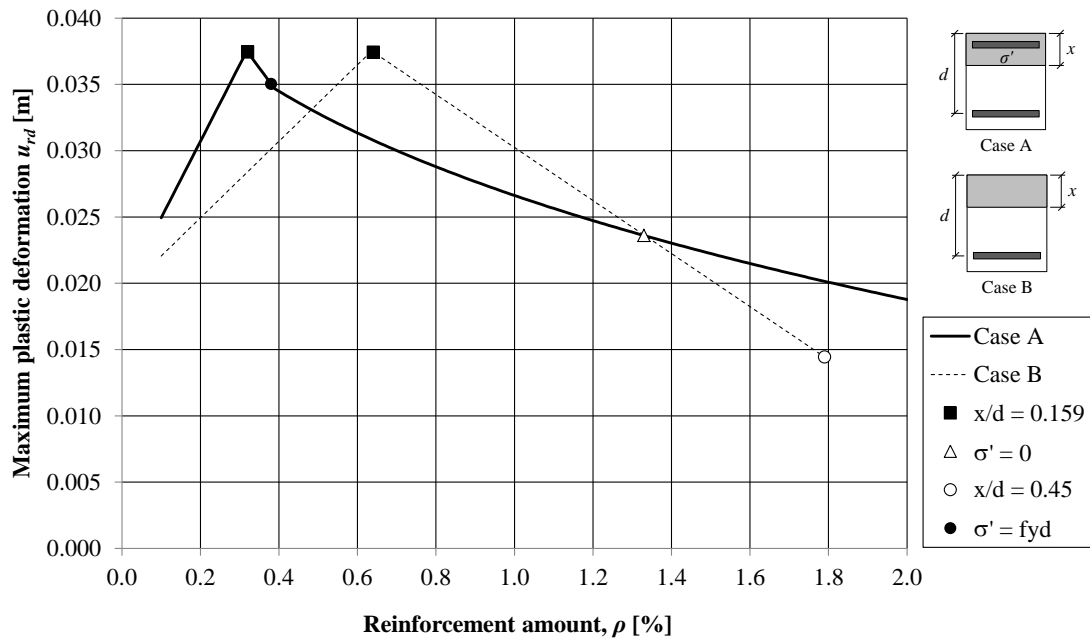


Figure B.18 Maximum plastic deformation vs. reinforcement amount  $\rho$  for a section with a height of 200 mm.

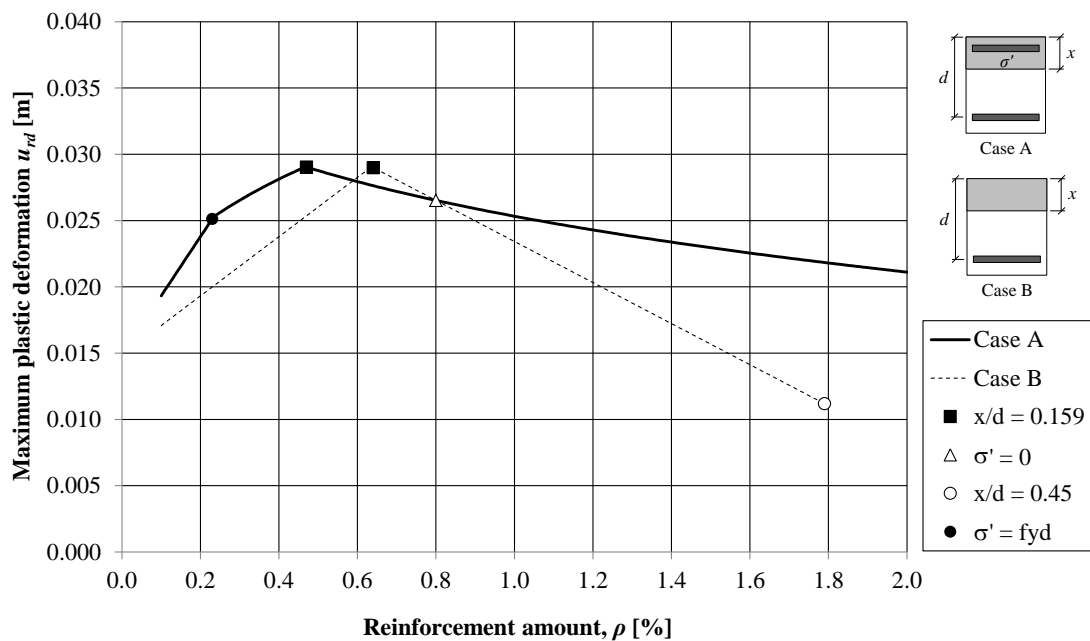


Figure B.19 Maximum plastic deformation vs. reinforcement amount  $\rho$  for a section with a height of 300 mm.

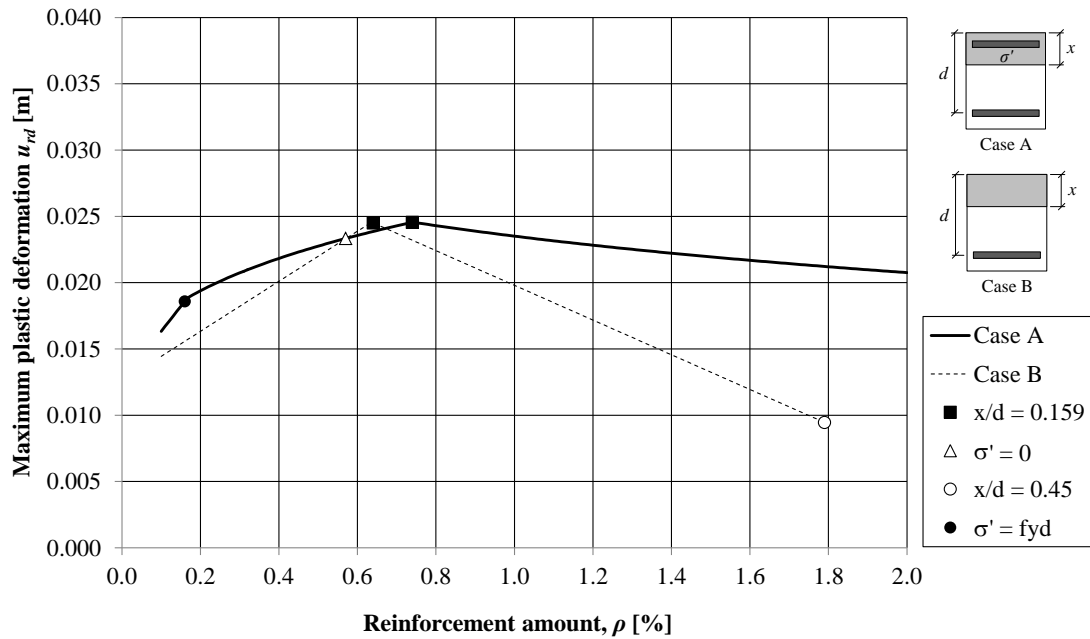


Figure B.20 Maximum plastic deformation vs. reinforcement amount  $\rho$  for a section with a height of 400 mm.

## B.7 Sections with and without top reinforcement for Case 1

In this section, the cases with top reinforcement, Case A, are compared with the ones without top reinforcement, Case B, as described in equation (B.1) to (B.3). The ratio,  $\gamma$ , varies with the reinforcement amount  $\rho$  and a compilation of the results are presented in Figure 3.22 to Figure B.29. The effective depth,  $d$ , is calculated according to Case 1 which is described in Section B.1.1.

$$\gamma_{R_m} = \frac{R_{m,A}}{R_{m,B}} \quad (\text{B.1})$$

where  $R_{m,A}$  is the internal resistance for Case A and  $R_{m,B}$  is the internal resistance for Case B.

$$\gamma_{u_{rd}} = \frac{u_{rd,A}}{u_{rd,B}} \quad (\text{B.2})$$

where  $u_{rd,A}$  is the ultimate plastic deformation for Case A and  $u_{rd,B}$  is the ultimate plastic deformation for Case B.

$$\gamma_{W_i} = \frac{W_{i,A}}{W_{i,B}} \quad (\text{B.3})$$

where  $W_{i,A}$  is the internal work for Case A and  $W_{i,B}$  is the internal work for Case B.

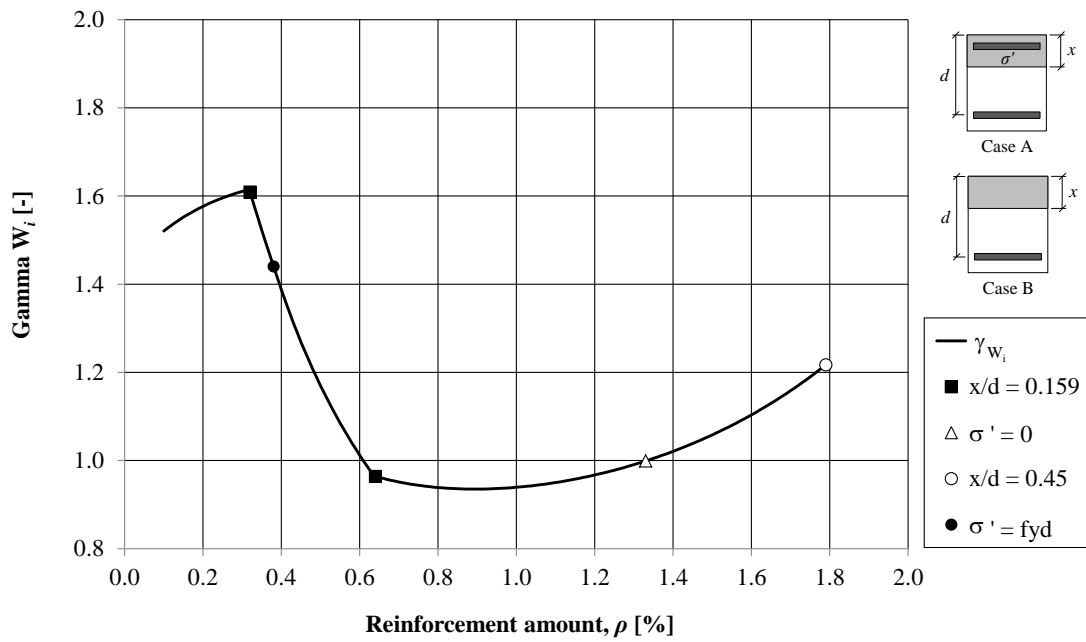


Figure B.21 Ratio of internal work,  $\gamma_{W_i}$ , vs. reinforcement amount  $\rho$ . The section has a height of 200 mm.

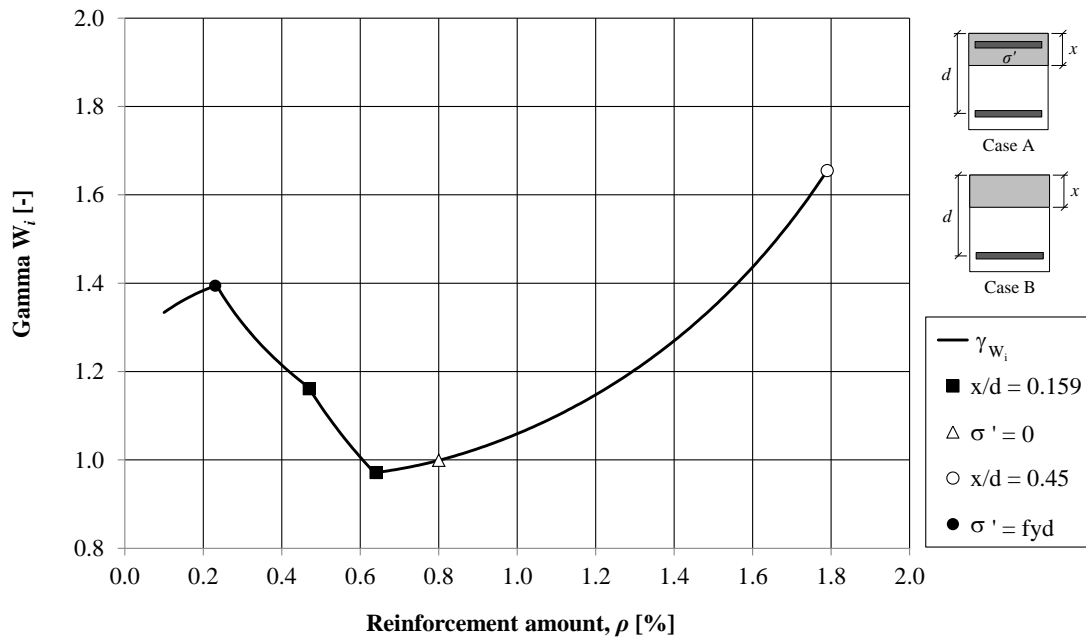


Figure B.22 Ratio of internal work,  $\gamma_{W_i}$ , vs. reinforcement amount  $\rho$ . The section has a height of 300 mm.

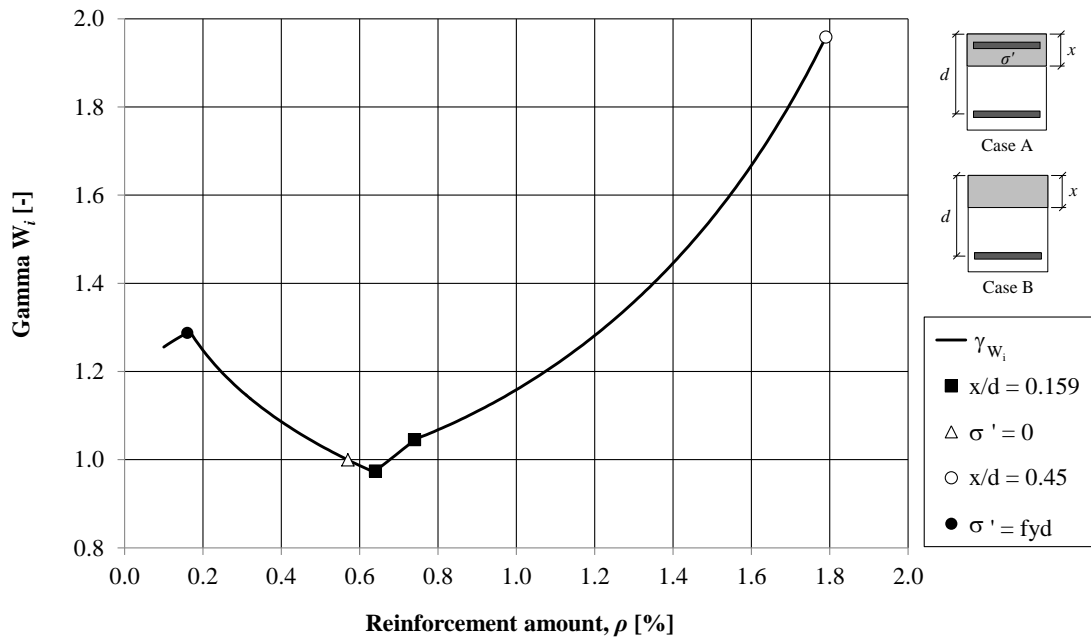


Figure B.23 Ratio of internal work,  $\Gamma_{W_i}$ , vs. reinforcement amount  $\rho$ . The section has a height of 400 mm.

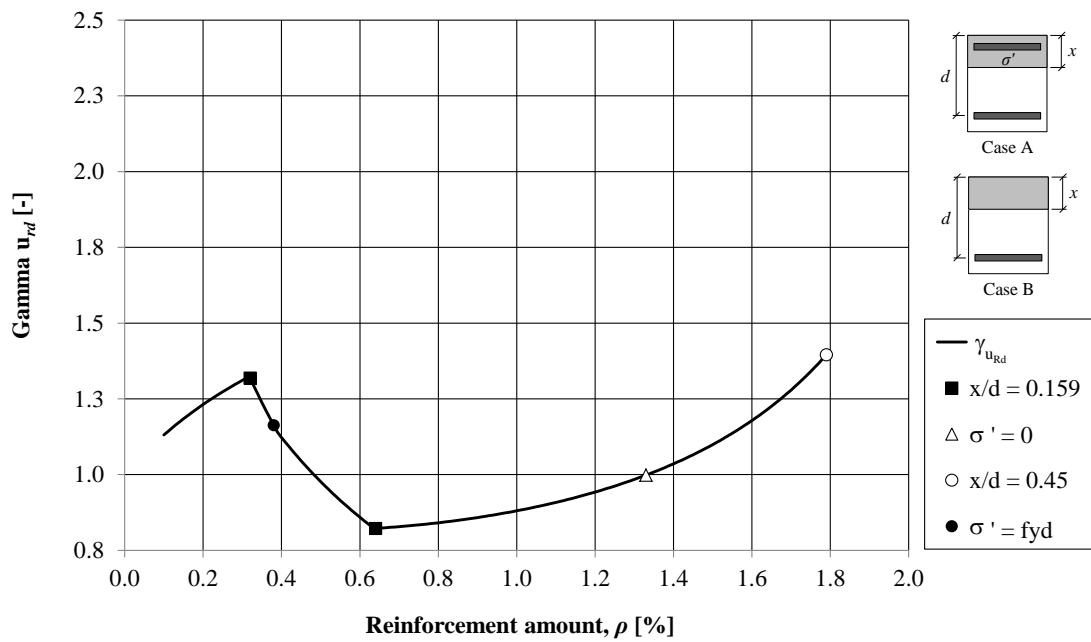


Figure B.24 Ratio of ultimate plastic deformation,  $\Gamma_{u_{rd}}$ , vs. reinforcement amount  $\rho$ . The section has a height of 200 mm.

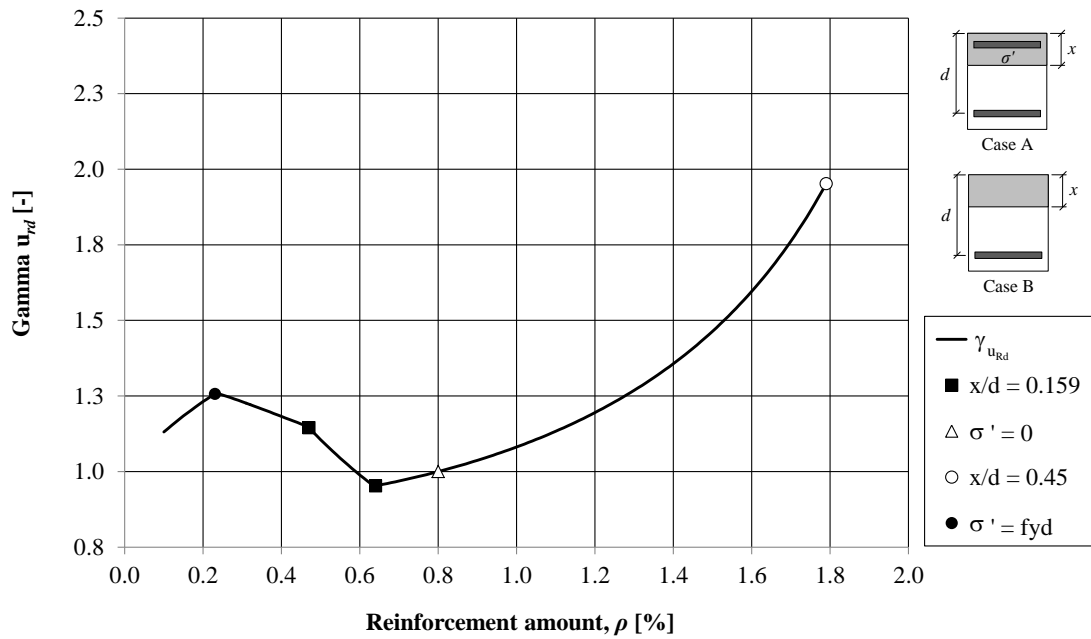


Figure B.25 Ratio of ultimate plastic deformation,  $\Gamma_{u_{Rd}}$ , vs. reinforcement amount  $\rho$ . The section has a height of 300 mm.

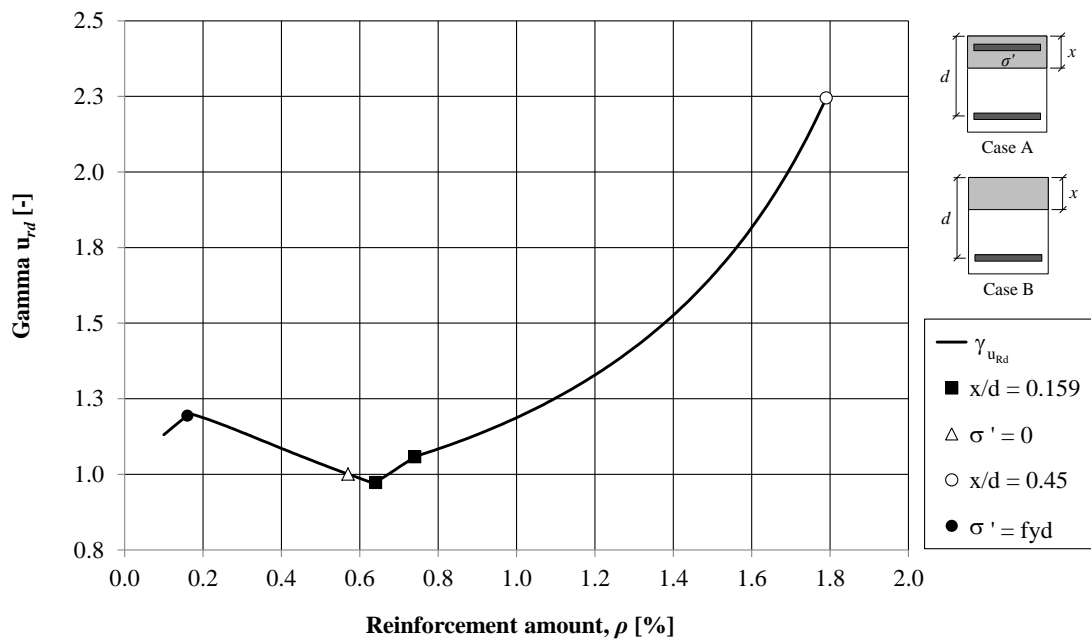


Figure B.26 Ratio of ultimate plastic deformation,  $\Gamma_{u_{Rd}}$ , vs. reinforcement amount  $\rho$ . The section has a height of 400 mm.



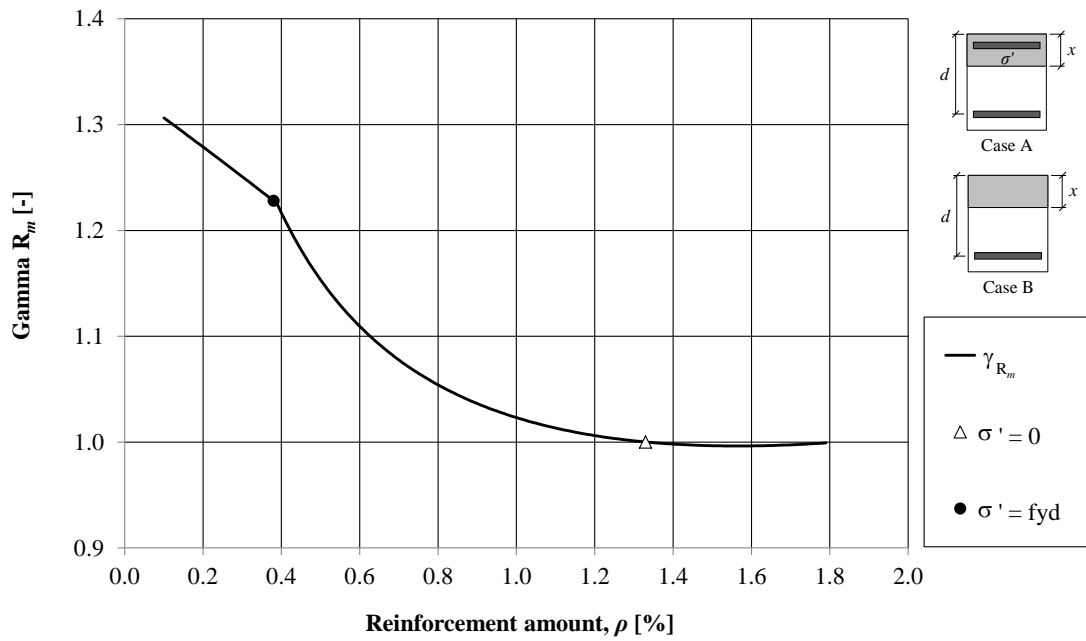


Figure B.27 Ratio of internal resistance,  $\Gamma_{R_m}$ , vs. reinforcement amount  $\rho$  for a section with a height of 200 mm.

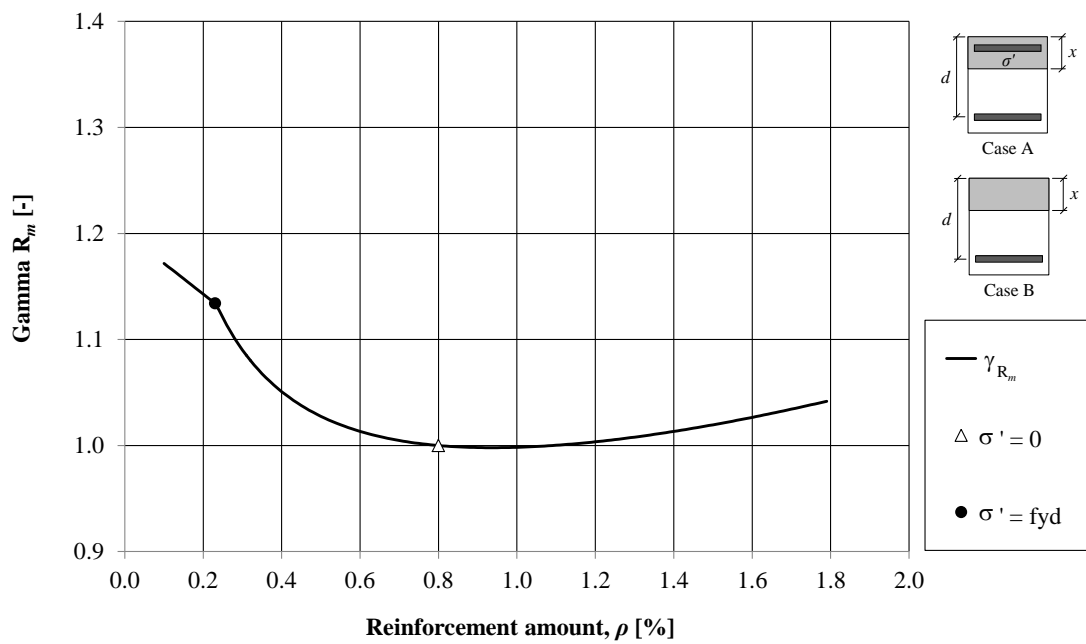


Figure B.28 Ratio of internal resistance,  $\Gamma_{R_m}$ , vs. reinforcement amount  $\rho$  for a section with a height of 300 mm.

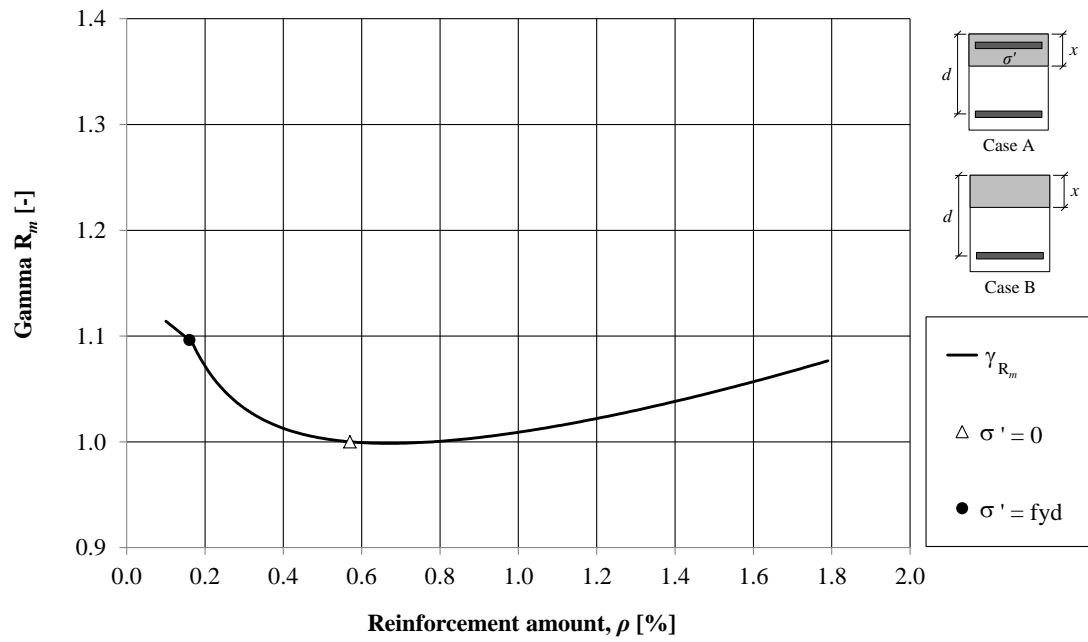


Figure B.29 Ratio of internal resistance,  $\Gamma_{R_m}$ , vs. reinforcement amount  $\rho$  for a section with a height of 400 mm.

## B.8 Resistance versus deformation for Case 2

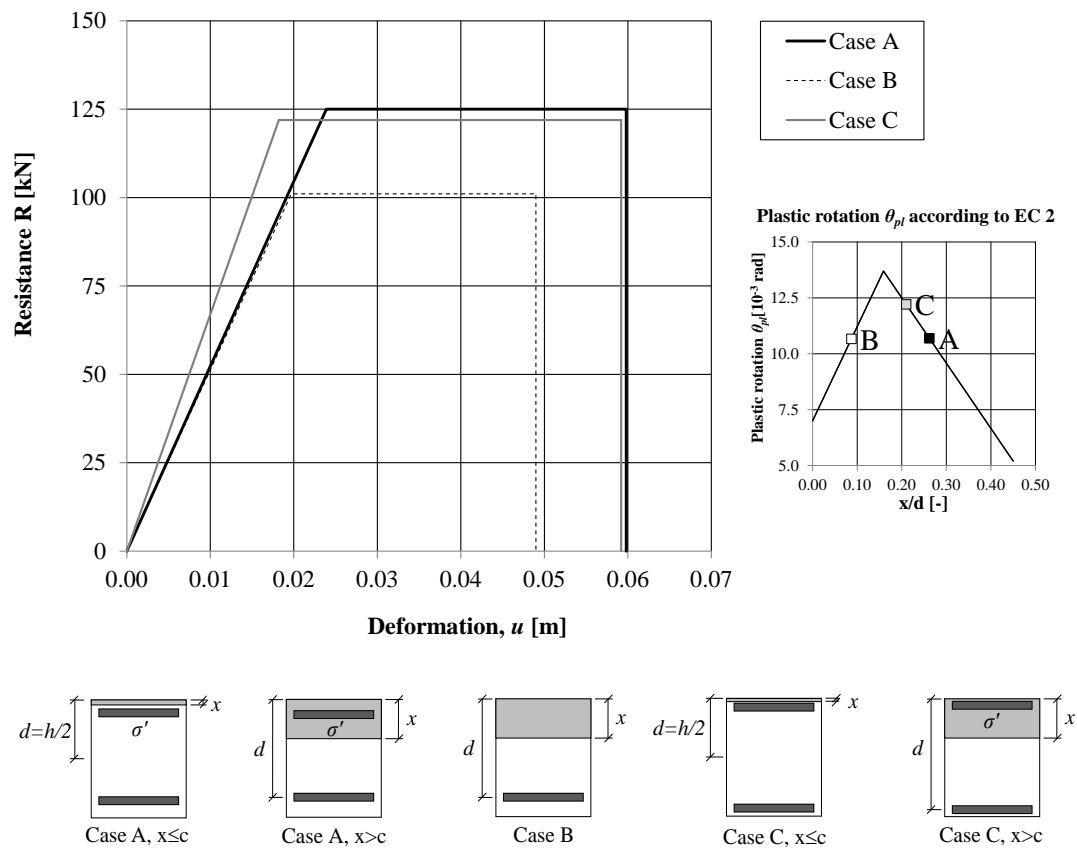


Figure B.30 Internal resistance, ultimate deflection and position in the plastic rotation capacity graph (Eurocode 2) for a section with a height of 200 mm and reinforcement  $\phi 10$  s 150.

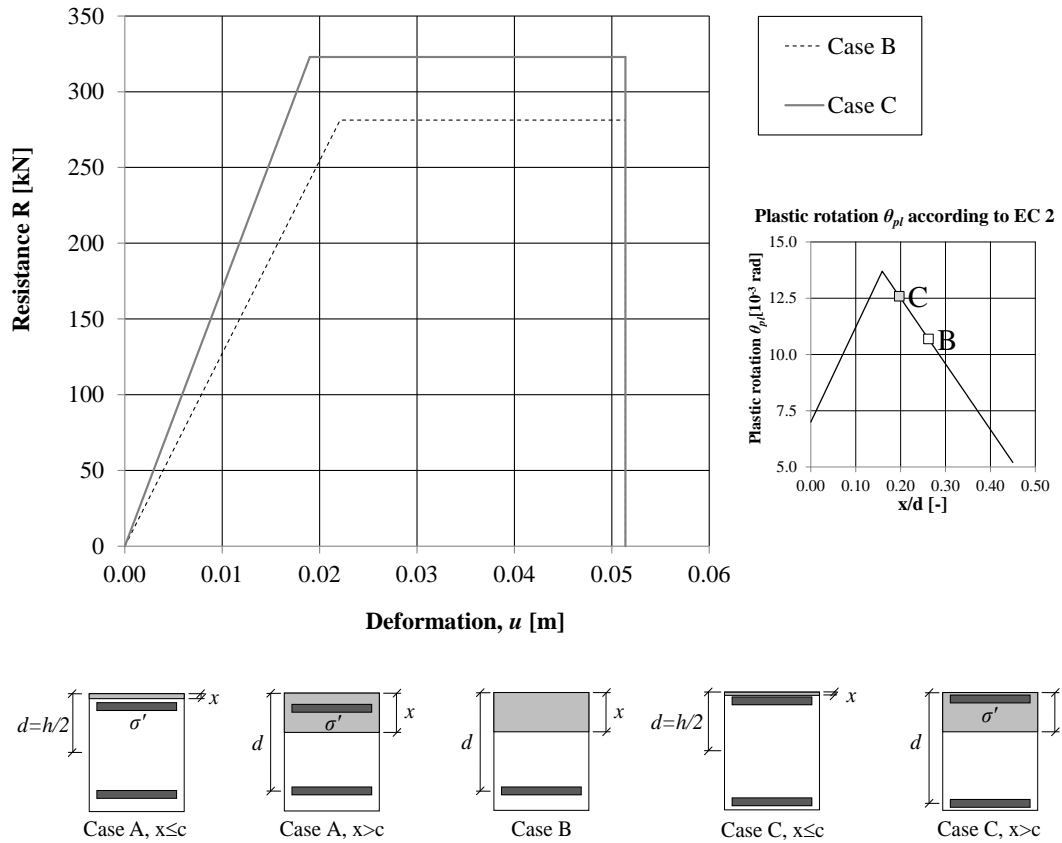


Figure B.31 Internal resistance, ultimate deflection and position in the plastic rotation capacity graph (Eurocode 2) for a section with a height of 200 mm and reinforcement  $\phi 20$  s 200.

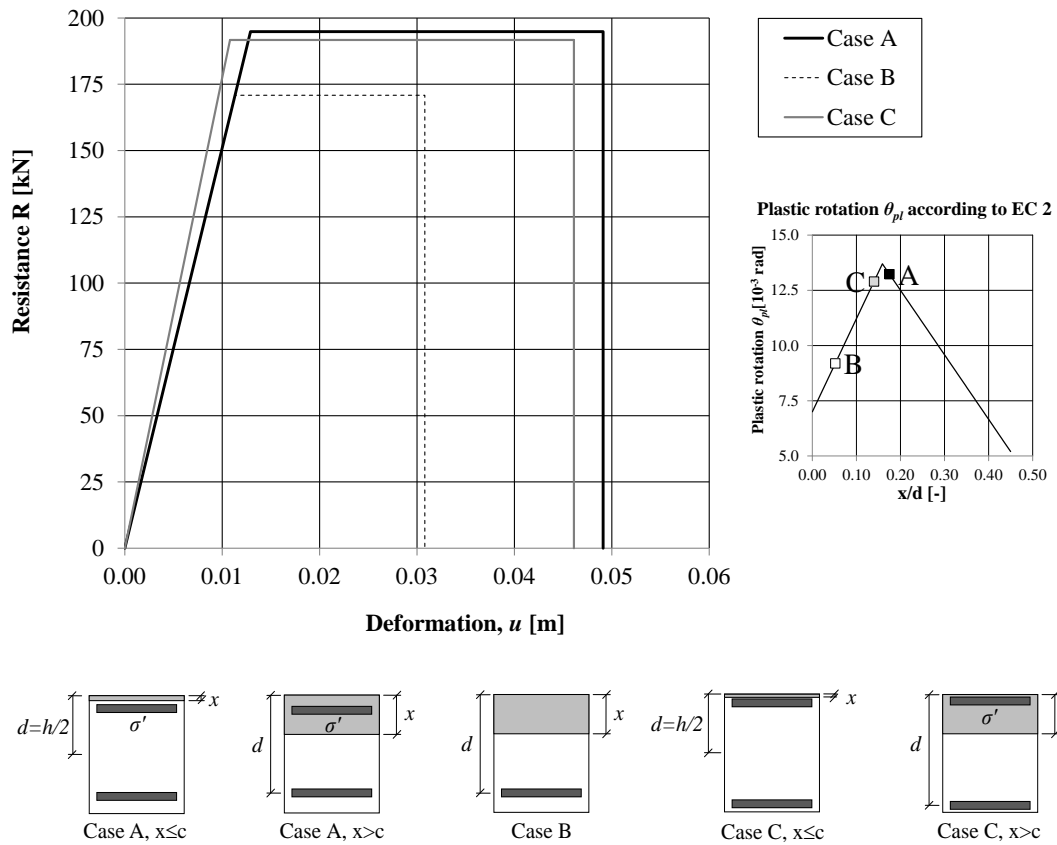


Figure B.32 Internal resistance, ultimate deflection and position in the plastic rotation capacity graph (Eurocode 2) for a section with a height of 300 mm and reinforcement  $\phi 10$  s 150.

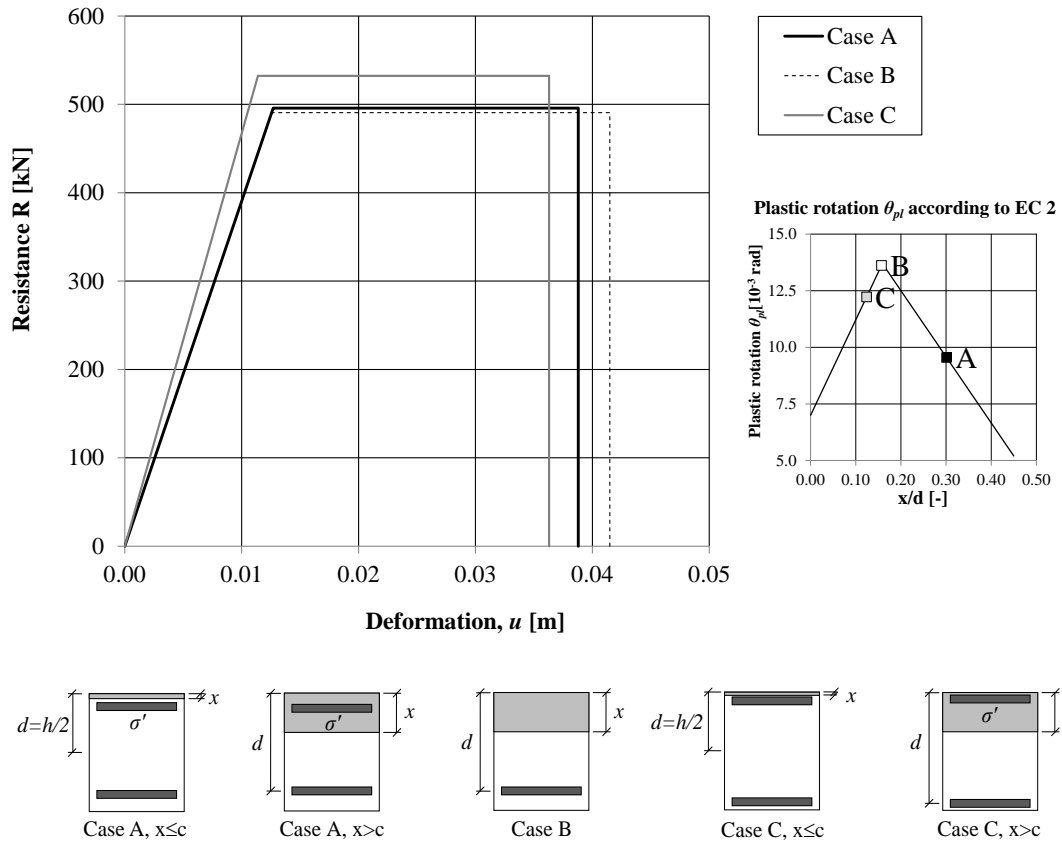


Figure B.33 Internal resistance, ultimate deflection and position in the plastic rotation capacity graph (Eurocode 2) for section with a height of 300 mm and reinforcement  $\phi 20$  s 200.

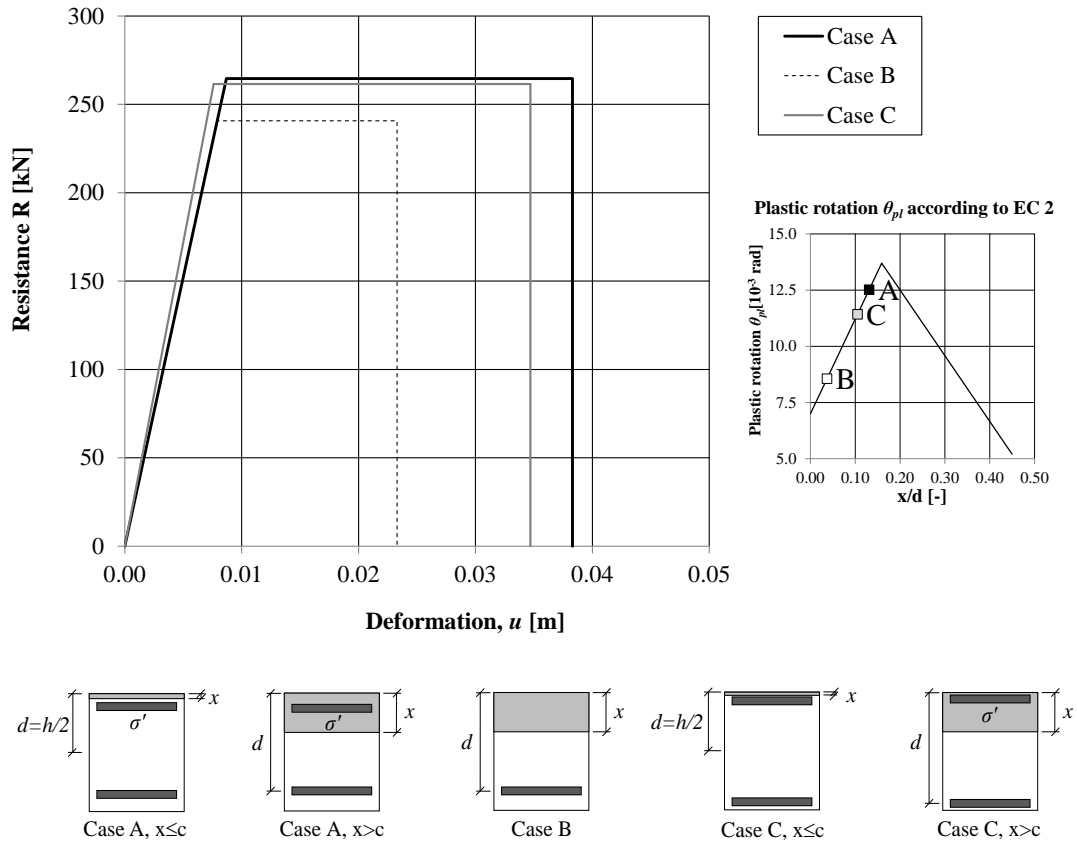


Figure B.34 Internal resistance, ultimate deflection and position in the plastic rotation graph capacity (Eurocode 2) for a section with a height of 400 mm and reinforcement  $\phi 10$  s 150.

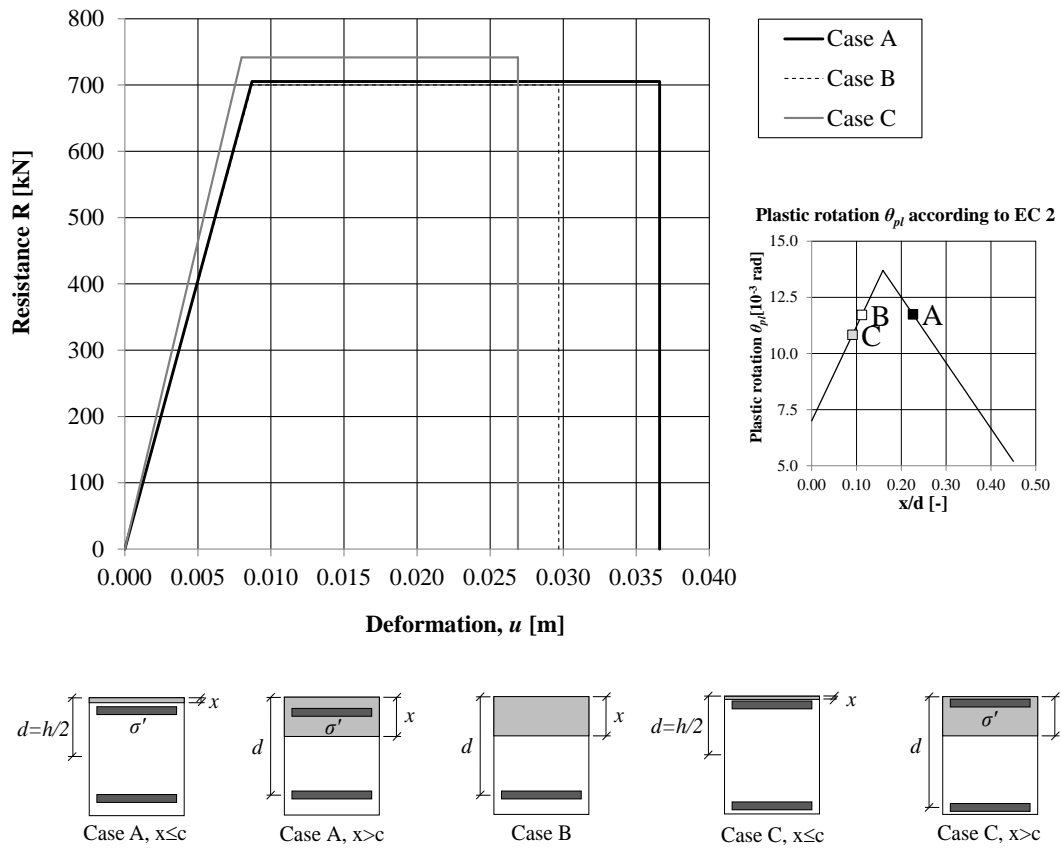


Figure B.35 Internal resistance, ultimate deflection and position in the plastic rotation capacity graph (Eurocode 2) for a section with a height of 400 mm and reinforcement  $\phi 20$  s 200.



## B.9 Plastic rotation capacity for Case 2

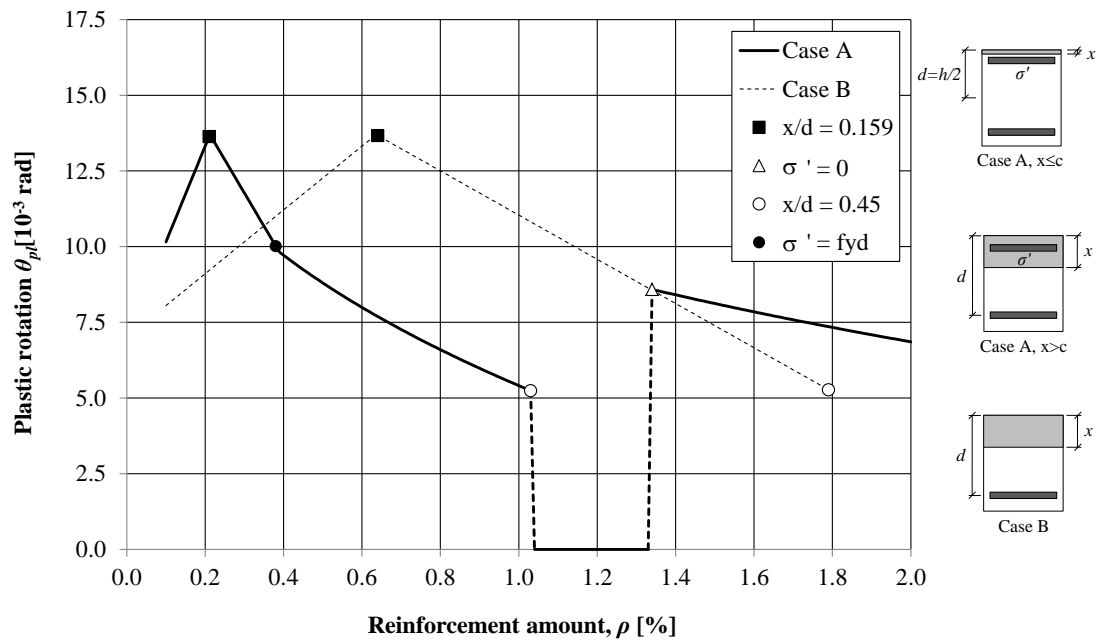


Figure B.36 Plastic rotation capacity  $\theta_{pl}$  vs. reinforcement amount  $\rho$  for a section with a height of 200 mm.

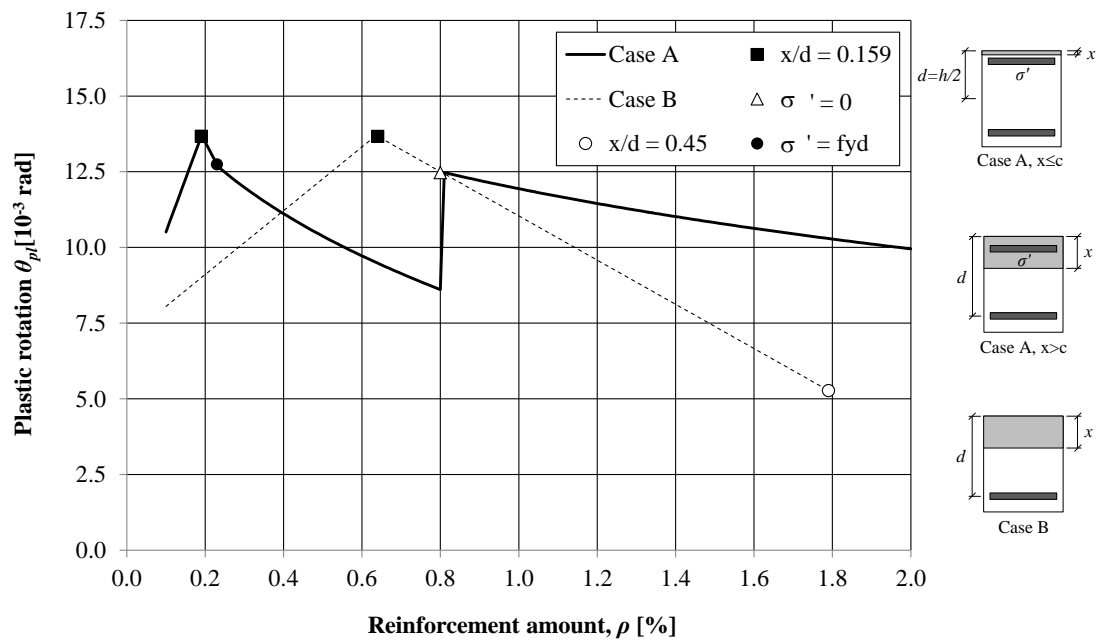


Figure B.37 Plastic rotation capacity  $\theta_{pl}$  vs. reinforcement amount  $\rho$  for a section with a height of 300 mm.

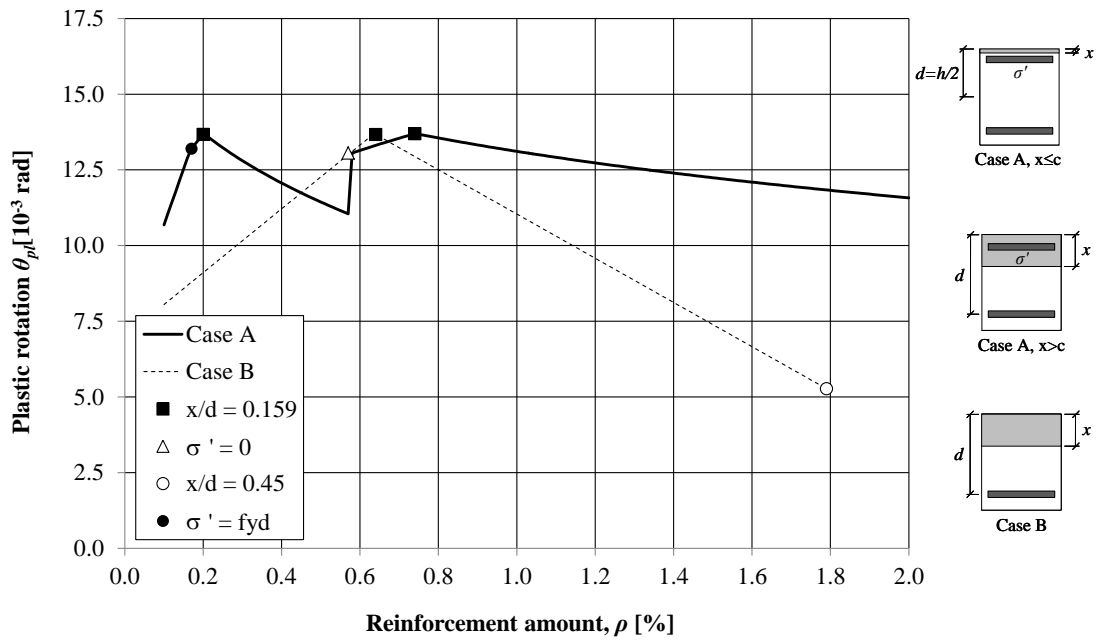


Figure B.38 Plastic rotation capacity  $\theta_{pl}$  vs. reinforcement amount  $\rho$  for a section with a height of 400 mm.

## B.10 Internal work for Case 2

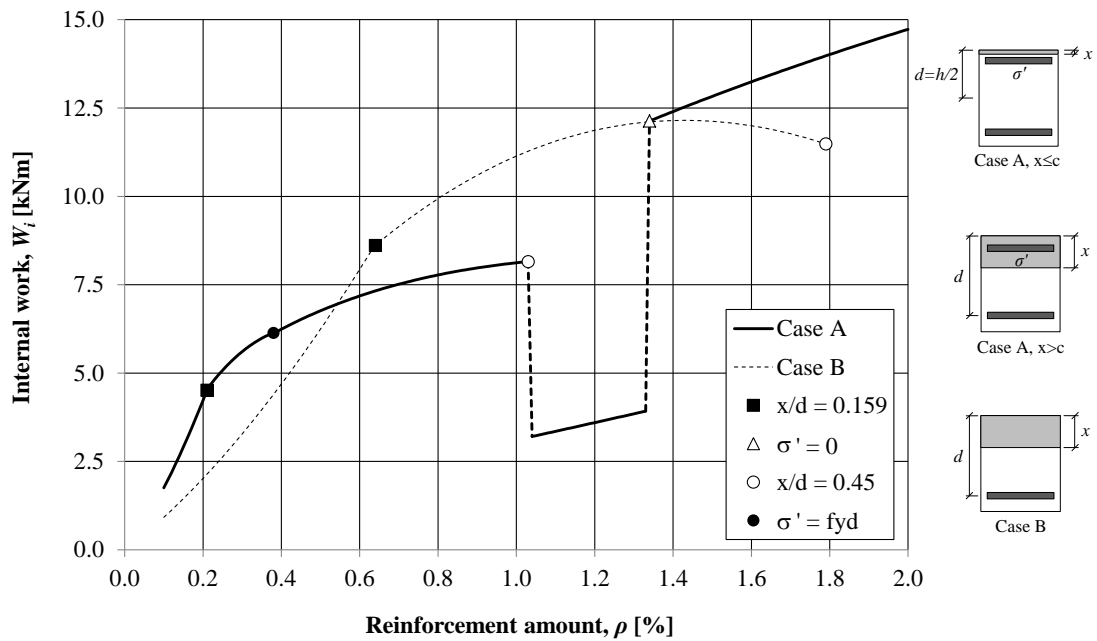


Figure B.39 Internal work  $W_i$  vs. reinforcement amount  $\rho$  for a section with a height of 200 mm.

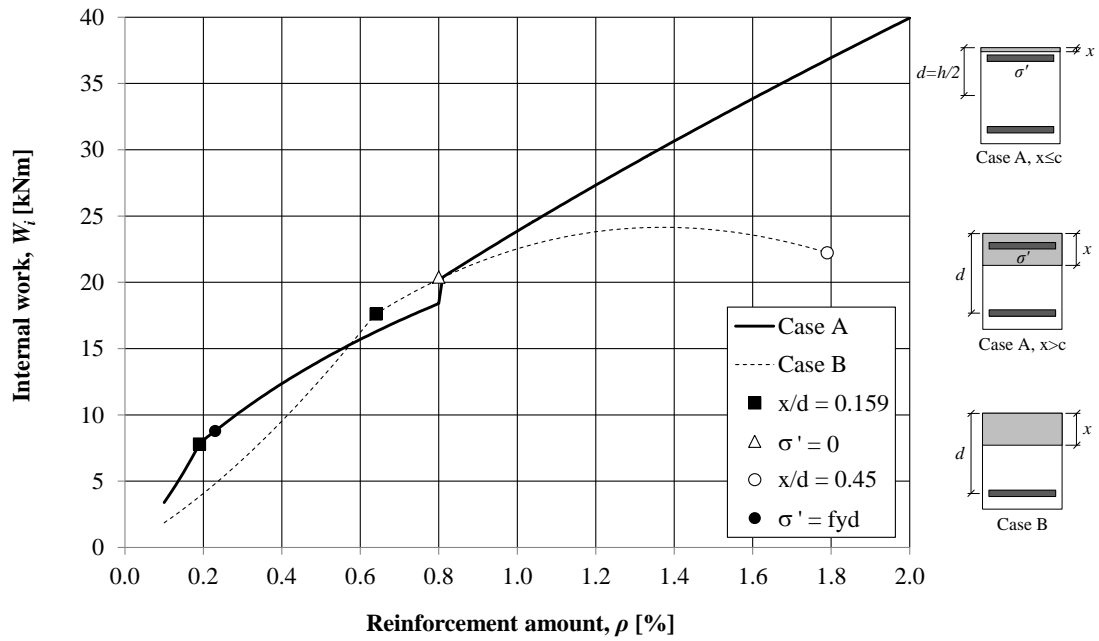


Figure B.40 Internal work  $W_i$  vs. reinforcement amount  $\rho$  for a section with a height of 300 mm.

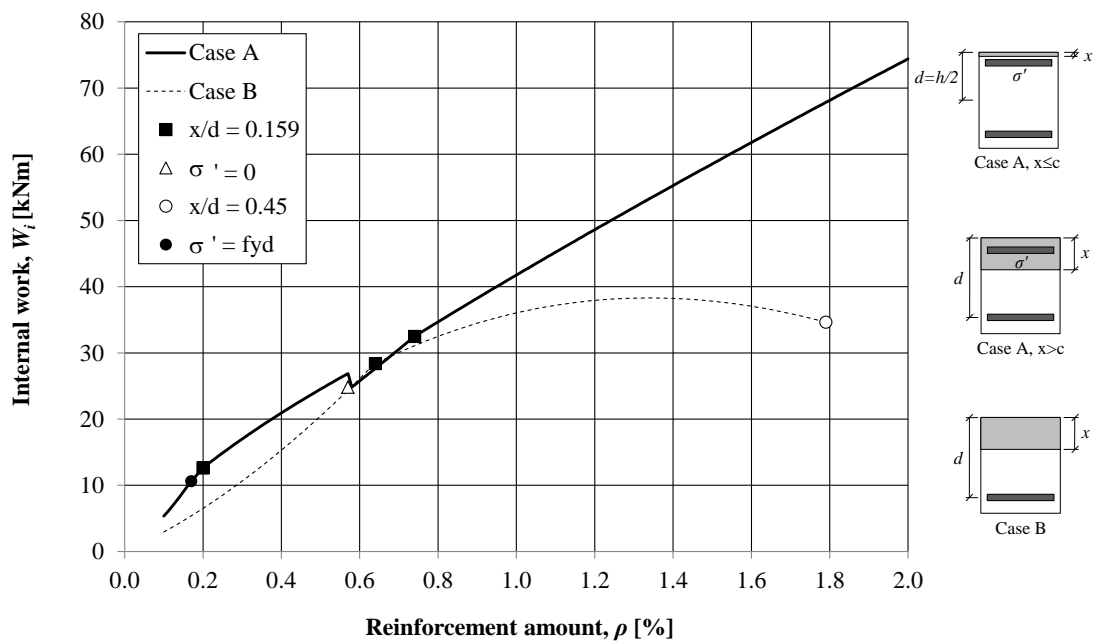


Figure B.41 Internal work  $W_i$  vs. reinforcement amount  $\rho$  for a section with a height of 400 mm.

## B.11 Internal resistance for Case 2

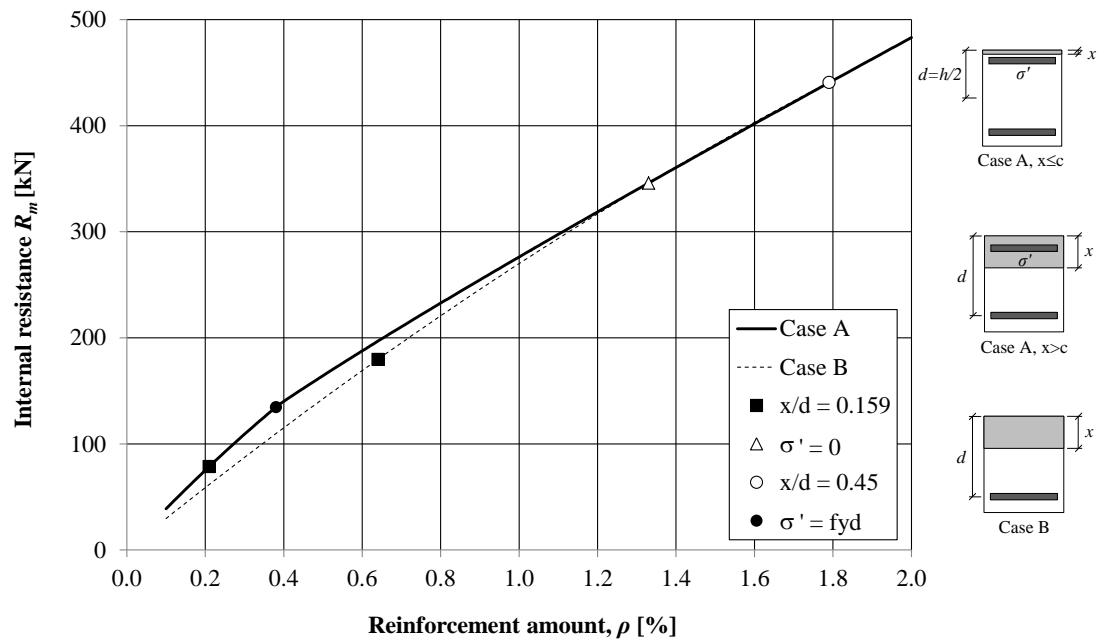


Figure B.42 Internal resistance  $R_m$  vs. reinforcement amount  $\rho$  for a section with a height of 200 mm.

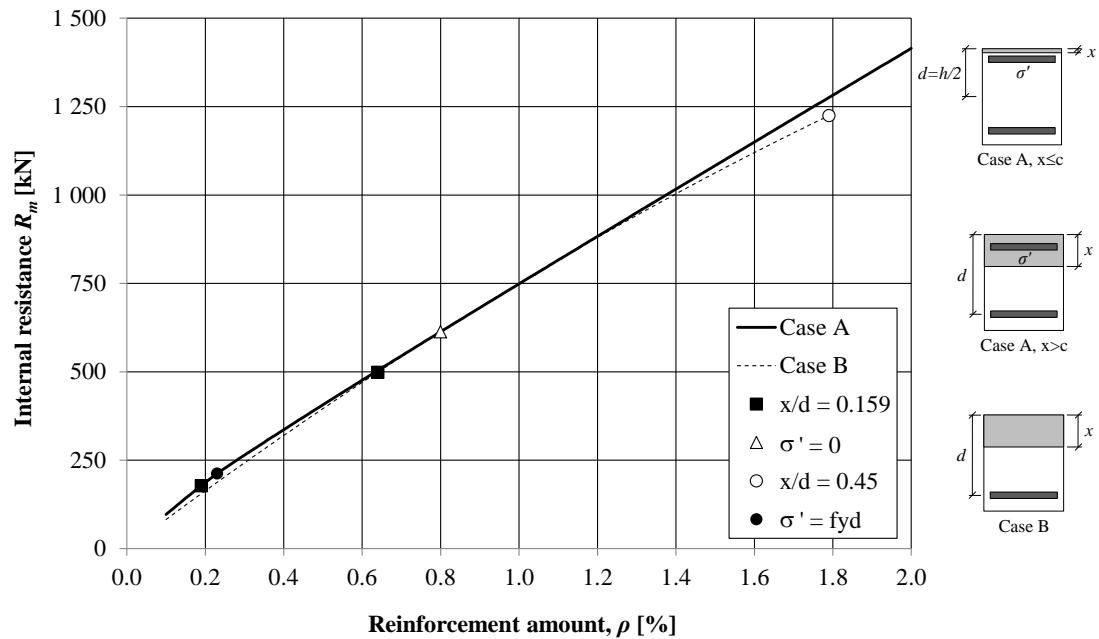


Figure B.43 Internal resistance  $R_m$  vs. reinforcement amount  $\rho$  for a section with a height of 300 mm.

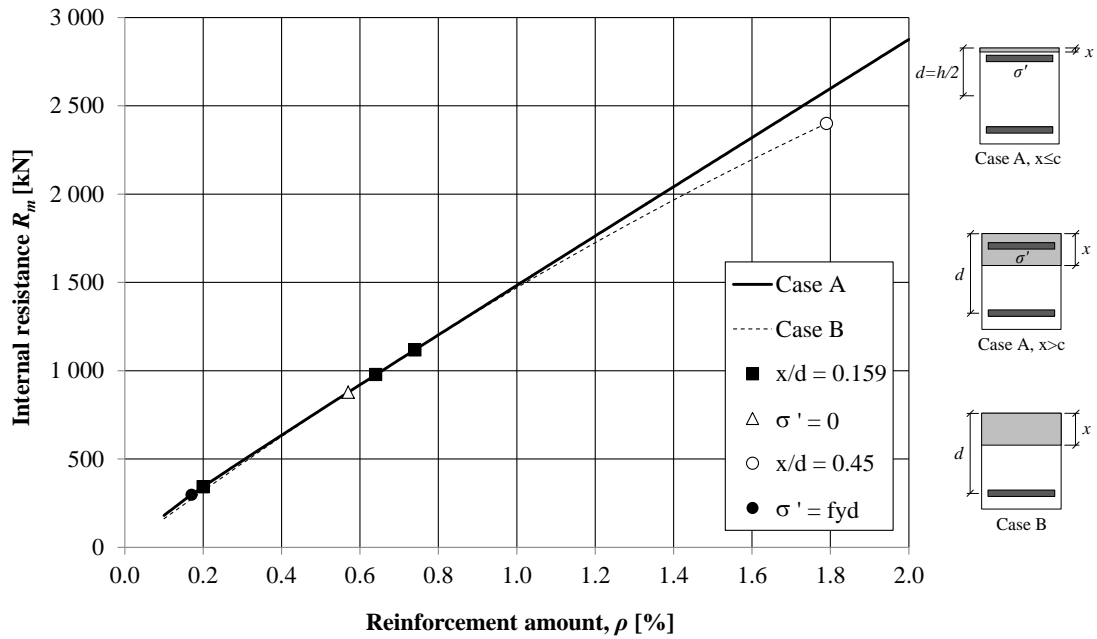


Figure B.44 Internal resistance  $R_m$  vs. reinforcement amount  $\rho$  for a section with a height of 400 mm.

## B.12 Maximum plastic deformation for Case 2

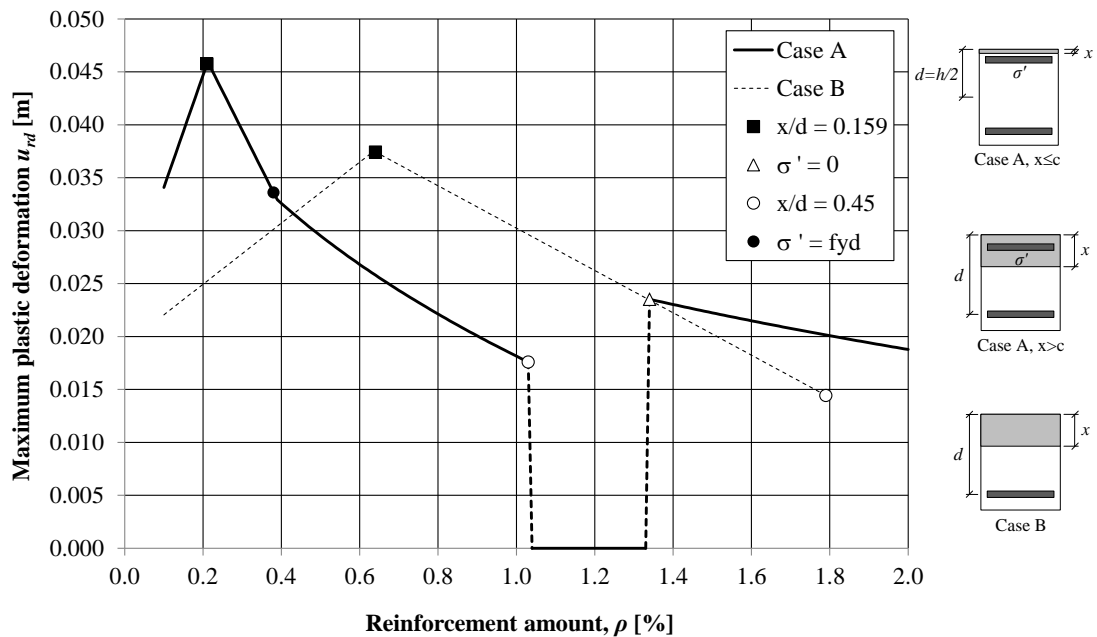


Figure B.45 Maximum plastic deformation  $u_{rd}$  vs. reinforcement amount  $\rho$  for a section with a height of 200 mm.

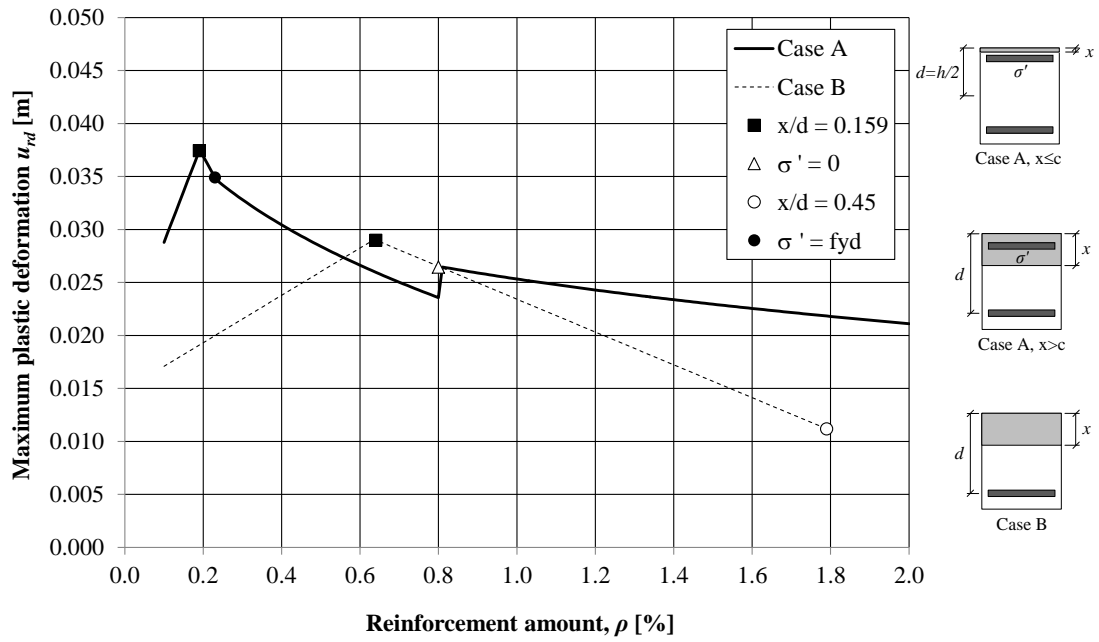


Figure B.46 Maximum plastic deformation  $u_{rd}$  vs. reinforcement amount  $\rho$  for a section with a height of 300 mm.

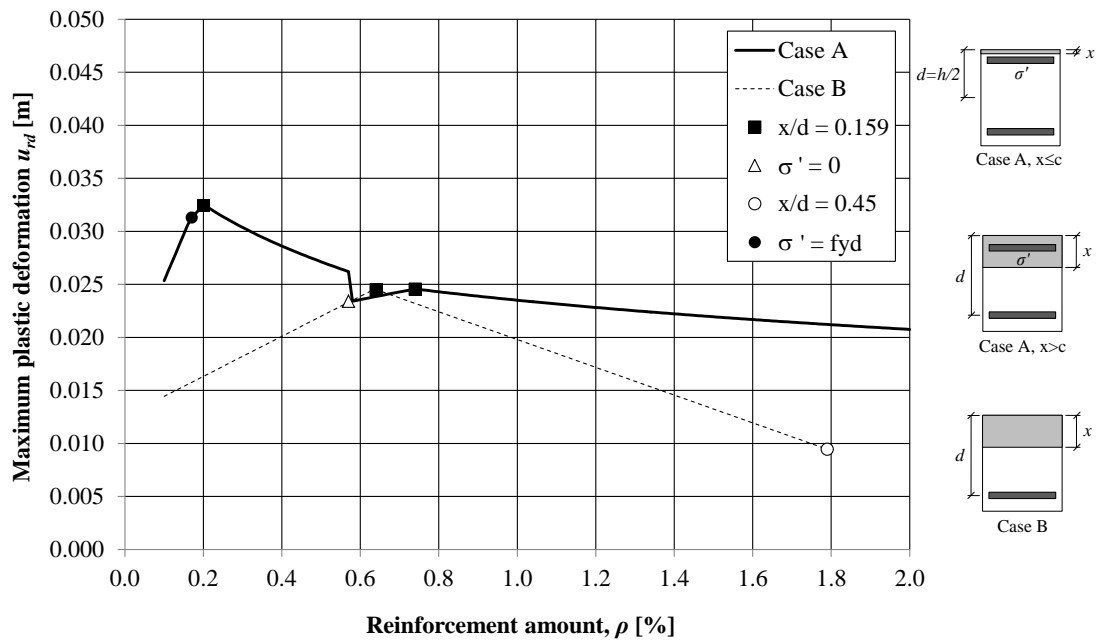


Figure B.47 Maximum plastic deformation  $u_{rd}$  vs. reinforcement amount  $\rho$  for a section with a height of 400 mm.

## B.13 Sections with and without top reinforcement for Case 2

The ratios,  $\gamma$ , plotted in this section are described in Section B.7.

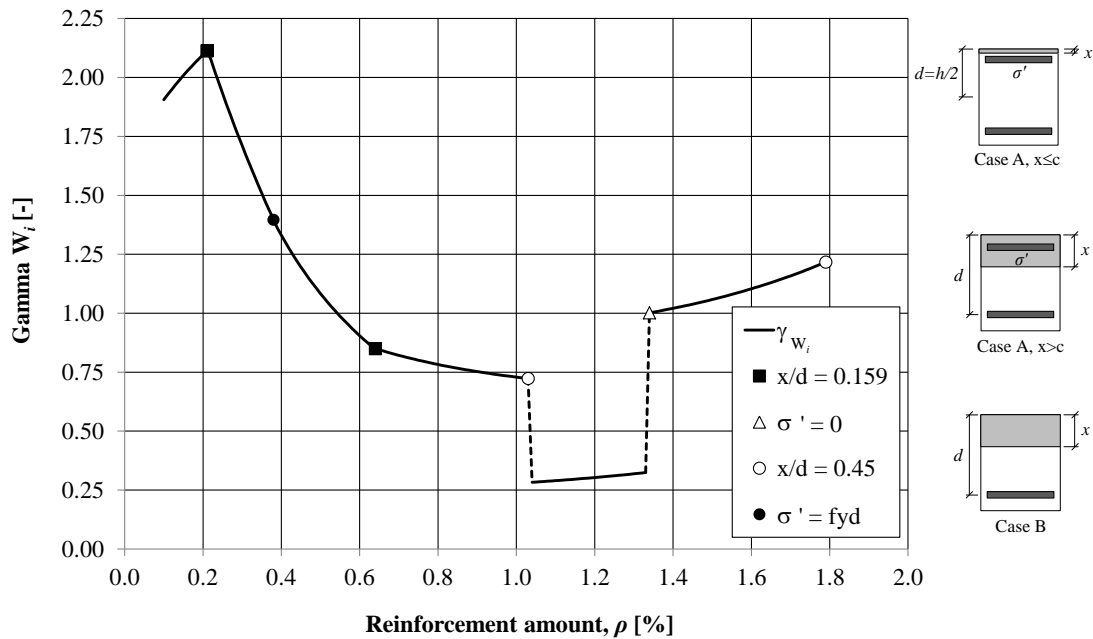


Figure B.48 Ratio of internal work,  $\Gamma W_i$ , vs. reinforcement amount  $\rho$ . The section has a height of 200 mm.

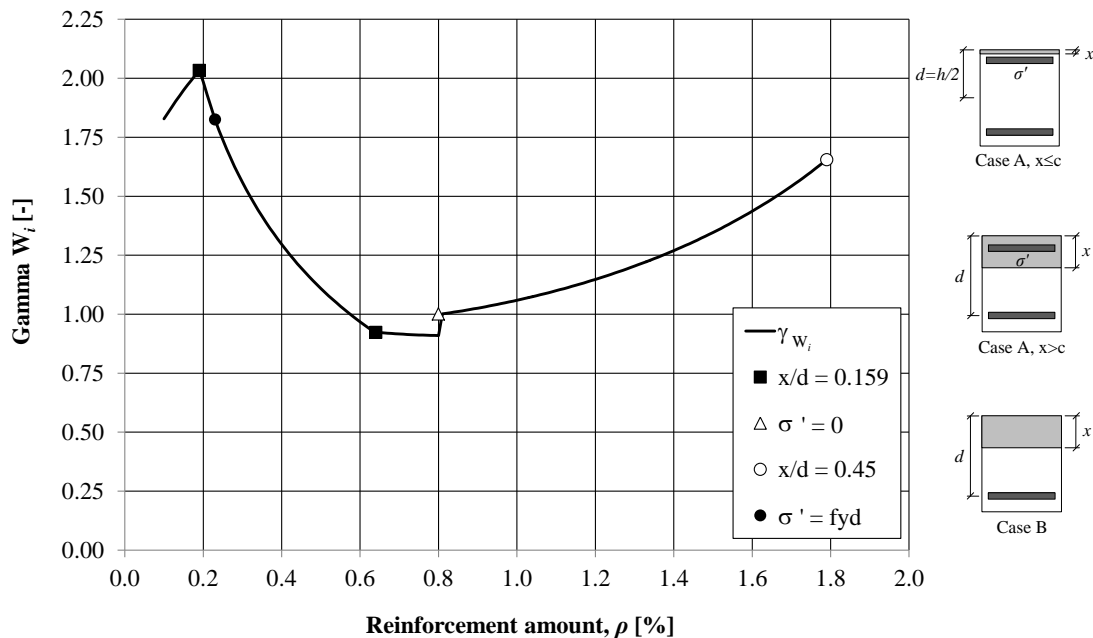


Figure B.49 Ratio of internal work,  $\Gamma W_i$ , vs. reinforcement amount  $\rho$ . The section has a height of 300 mm.

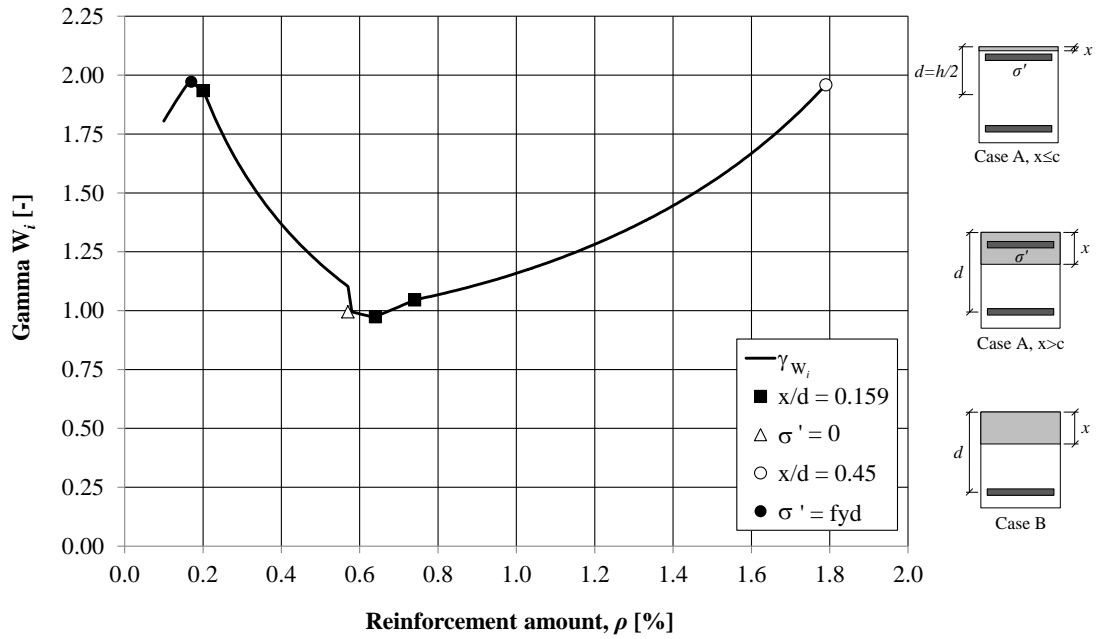


Figure B.50 Ratio of internal work,  $\Gamma W_i$ , vs. reinforcement amount  $\rho$ . The section has a height of 400 mm.

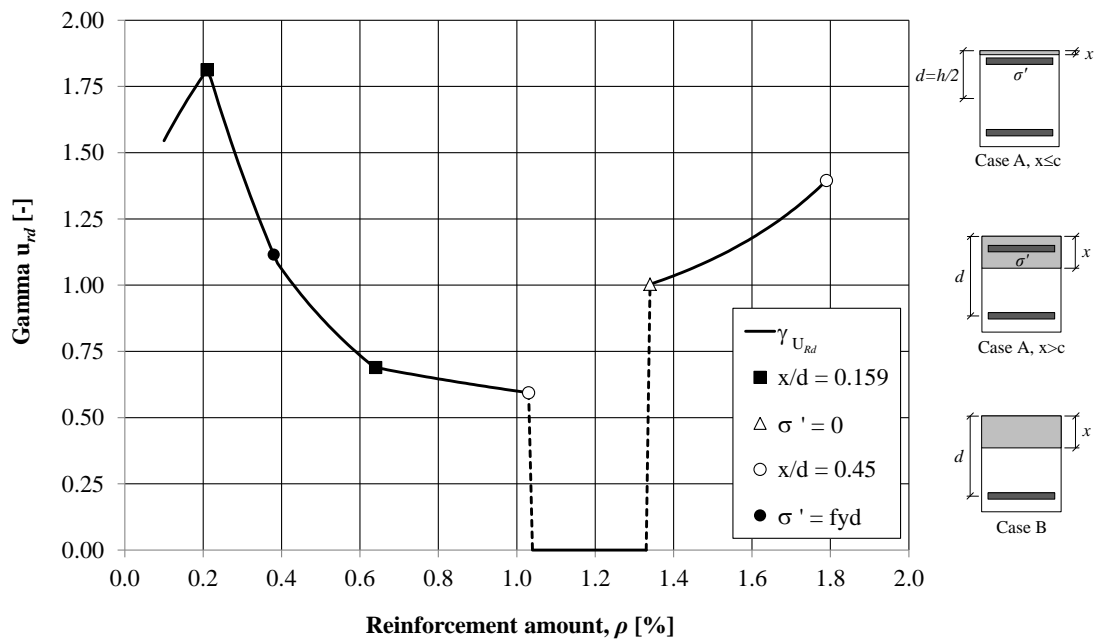


Figure B.51 Ratio of ultimate plastic deformation,  $\Gamma u_{rd}$ , vs. reinforcement amount  $\rho$ . The section has a height of 200 mm.



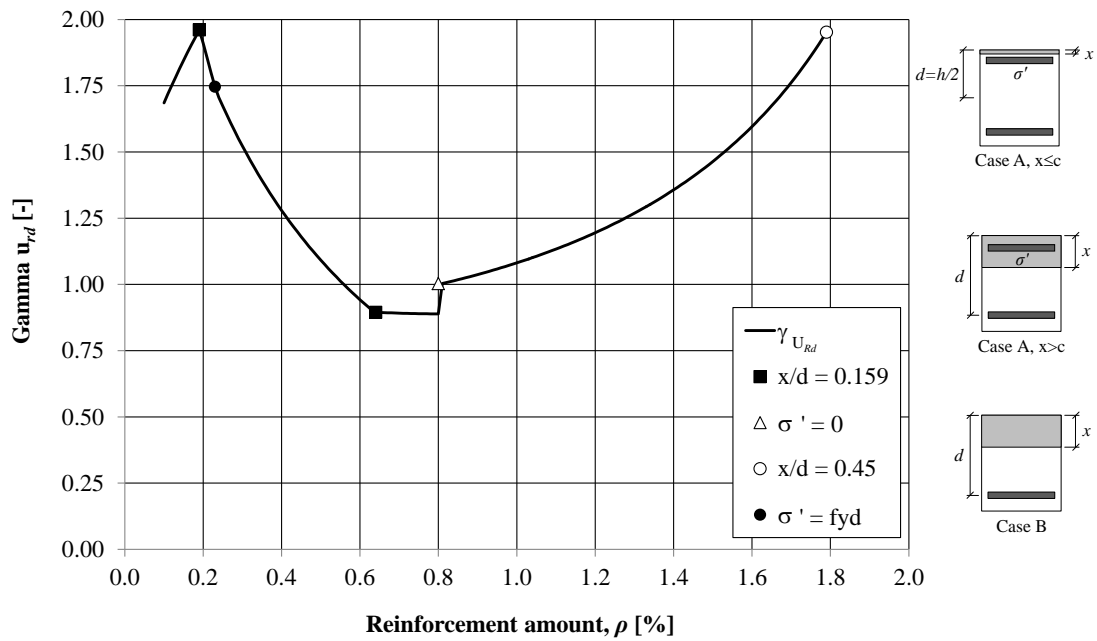


Figure B.52 Ratio of ultimate plastic deformation,  $\Gamma_{U_{Rd}}$ , vs. reinforcement amount  $\rho$ . The section has a height of 300 mm.

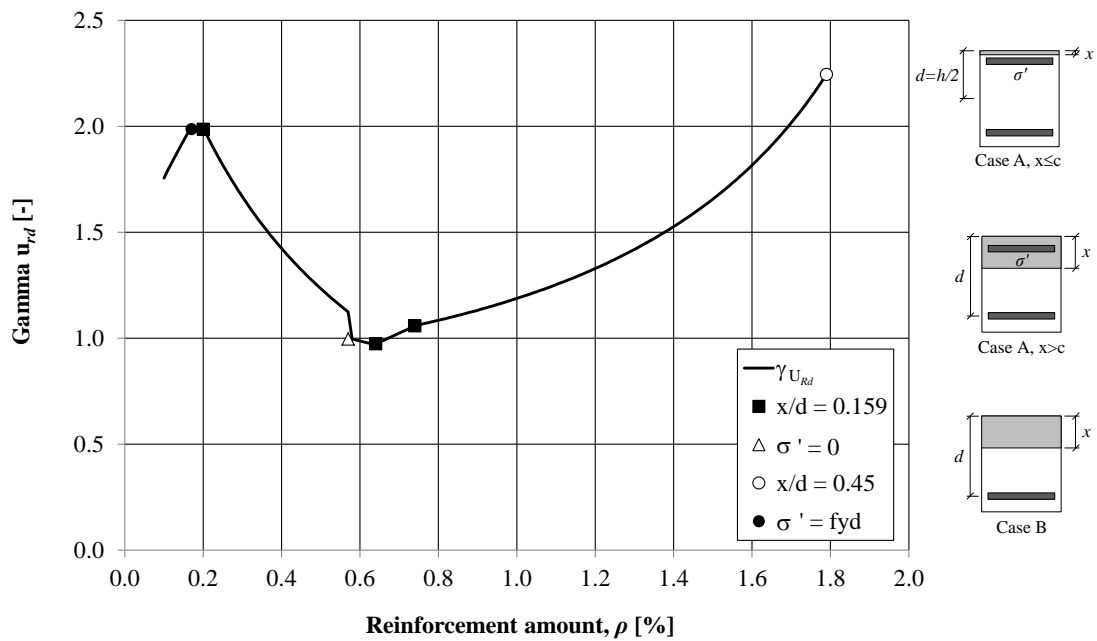


Figure B.53 Ratio of ultimate plastic deformation,  $\Gamma_{U_{Rd}}$ , vs. reinforcement amount  $\rho$ . The section has a height of 400 mm.

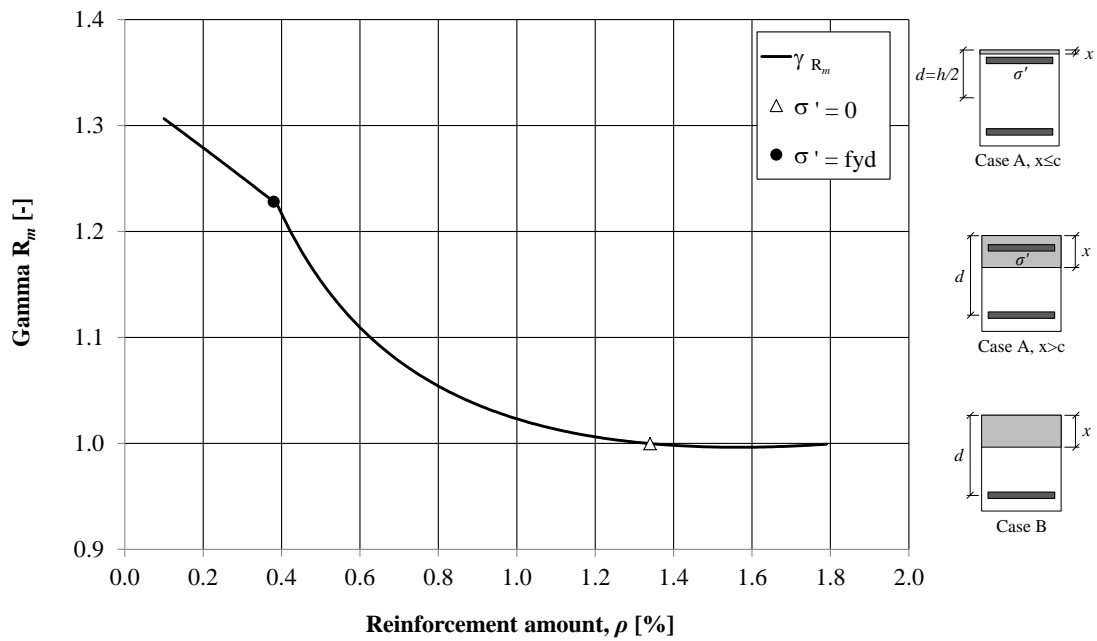


Figure B.54 Ratio of internal resistance,  $\gamma_{R_m}$ , vs. reinforcement amount  $\rho$  for a section with a height of 200 mm.

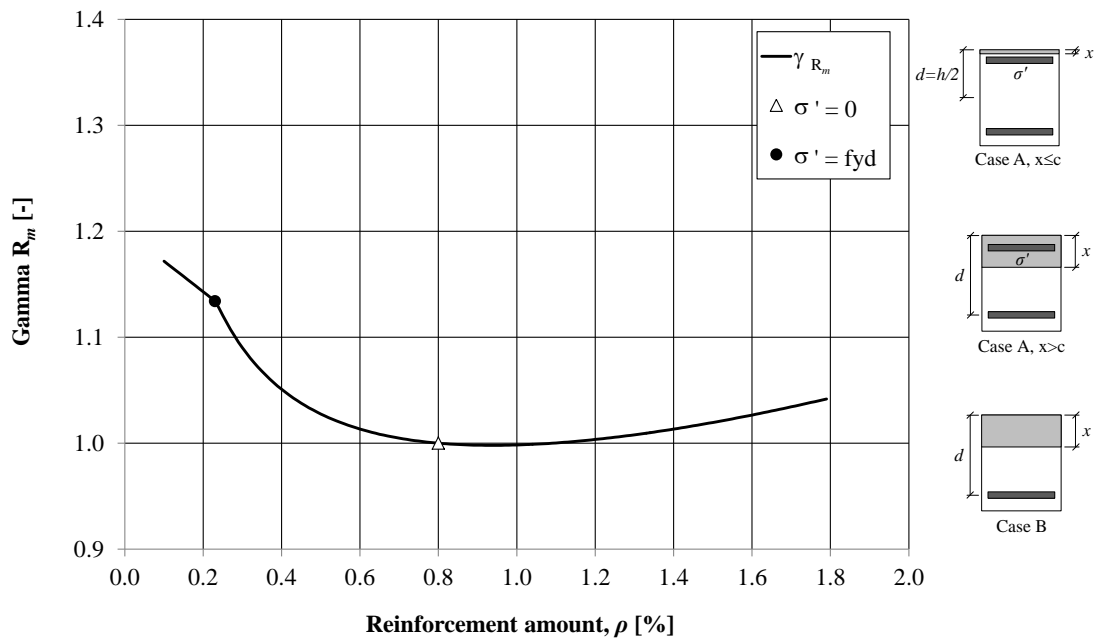


Figure B.55 Ratio of internal resistance,  $\gamma_{R_m}$ , vs. reinforcement amount  $\rho$  for a section with a height of 300 mm.

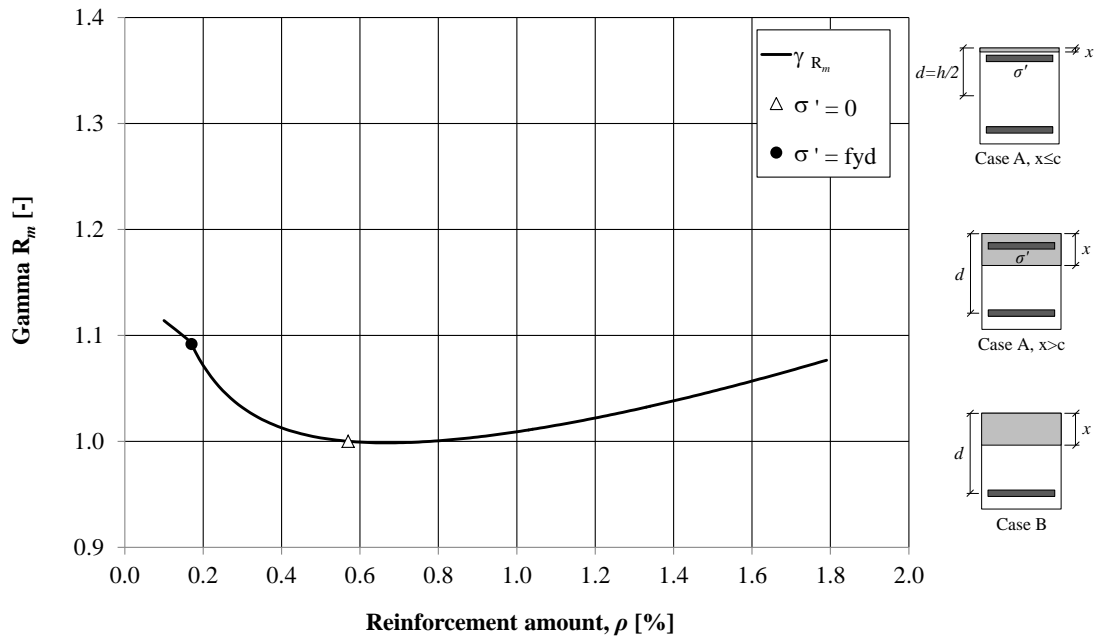


Figure B.56 Ratio of internal resistance,  $\Gamma R_m$ , vs. reinforcement amount  $\rho$  for a section with a height of 400 mm.

# APPENDIX C Trilinear structural response models

## C.1 Introduction

The object of this study is the beam shown in Figure C.1. The critical sections which influences the response of this structure are presented in Figure C.1a. Point  $s$  in Figure C.1b defines the section at the fixed support and Point  $f$  defines the midsection, for which the maximum stresses are analysed.

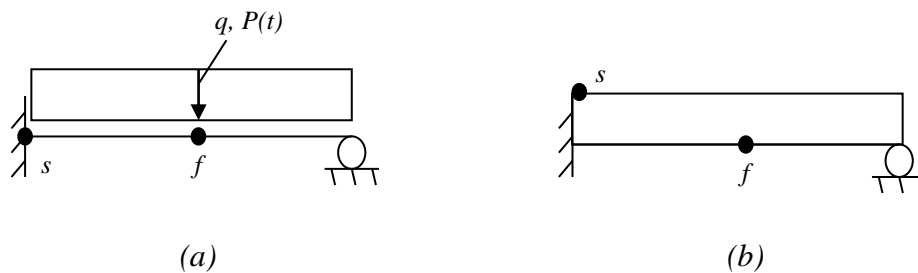


Figure C.1 (a) Critical sections in the studied beam. (b) Positions, within the sections, where the maximum stresses occur.

## C.2 Ultimate moments and resistances for the local frame model

The resistance of the span and the critical support section can be established by superimposing the moment diagrams for separate load cases. For a beam fixed at both supports, the moment distribution in ultimate limit state, when the plastic hinges at both considered sections has been formed, is presented in Figure C.2.

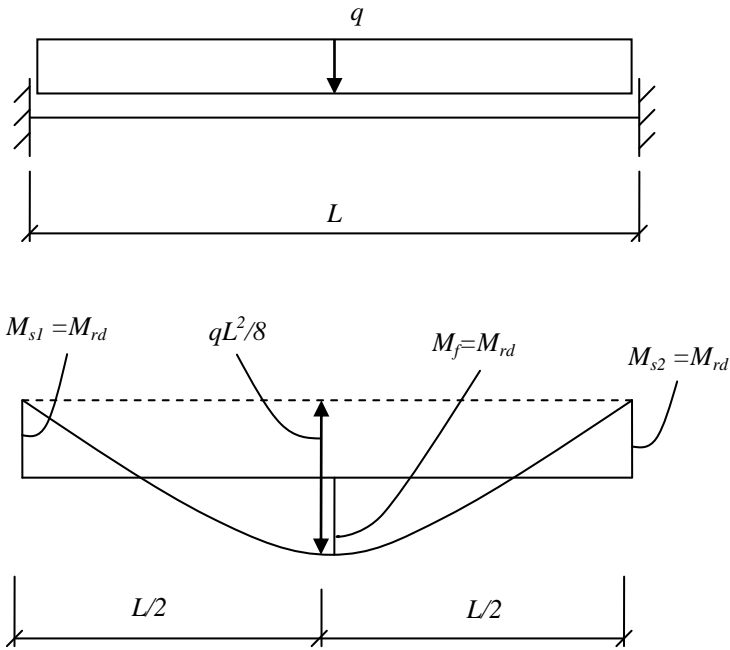


Figure C.2 Superimposing the moment diagrams for separate load cases.

This can be described as

$$\frac{q \cdot L^2}{8} = M_f + \frac{1}{2}(M_{s1} + M_{s2}) \quad (\text{C.1})$$

In the local model of the frame studied in Chapter 4, the column is described as a structure with one fixed edge and one simply supported. In this case

$$M_{s2} = 0 \quad (\text{C.2})$$

and the equation (C.1) can approximately be written as

$$\frac{q \cdot L^2}{8} = M_f + \frac{1}{2}M_{s1} \quad (\text{C.3})$$

Both critical sections, at the fixed support and in the span, are provided with the same amount of reinforcement and as the calculations are made in ultimate limit state, both sections will reach the moment capacity they were designed for,  $M_{rd}$ . Thus,

$$M_f = M_{s1} = M_{rd} \quad (\text{C.4})$$

When the beam is subjected to increasing load, the section at the fixed support first reaches its ultimate capacity for the load  $q_s$ . The ultimate moment it can withstand is

$$M_{s1} = \frac{q_s \cdot L^2}{8} \quad (\text{C.5})$$

When the load is further increased to  $q_f$ , the ultimate moment which the section in the span can withstand when the plastic hinge at the fixed support and in the span is created and the collapse mechanism forms is calculated from equation (C.3) as

$$\frac{q_f \cdot L^2}{8} = \frac{3}{2} M_{rd} \quad (C.6)$$

$$M_f = \frac{q_f \cdot L^2}{12} \quad (C.7)$$

Knowing the ultimate moment for both sections,  $M_s$  and  $M_f$ , the maximum resistance for the section at the fixed support is established as

$$R_{ms} = \frac{8 \cdot M_{rd}}{L} \quad (C.8)$$

and for the critical section in the span as

$$R_{mf} = \frac{12 \cdot M_{rd}}{L} \quad (C.9)$$

### C.3 Structure subjected to impulse load

The general model for the response of a statically indeterminate structure subjected to impulse load is developed by simulating the loading and is presented in Figure C.3.

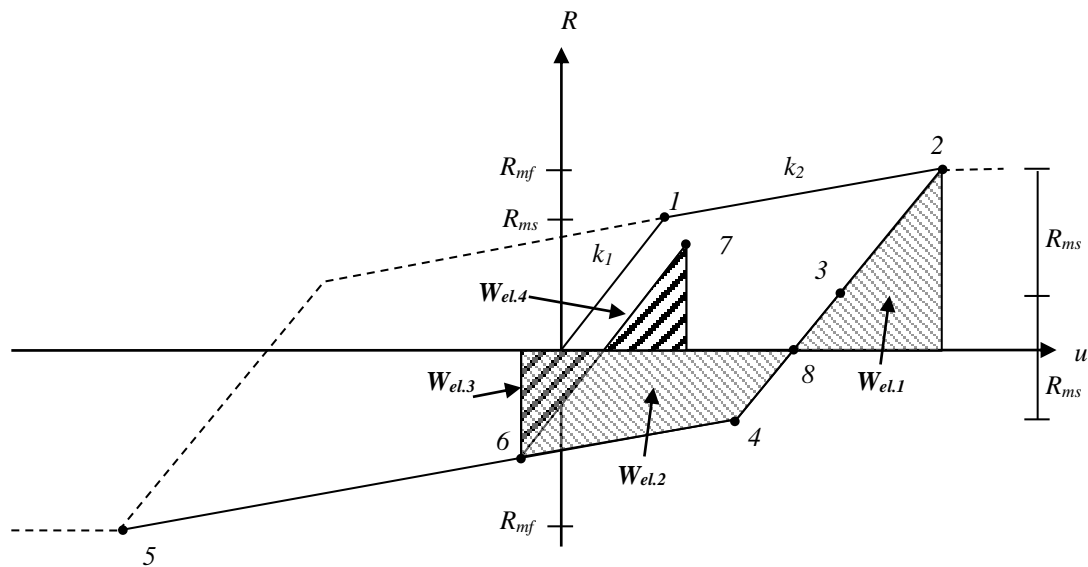


Figure C.3 The response model, representing the response of an impulse loaded statically indeterminate structure for the elasto-plastic case.

In this model, resistance  $R_{ms}$  and  $R_{mf}$  corresponds to the resistance for which yielding at section  $s$  and section  $f$  in Figure C.1 begins. The notations  $k_1$  and  $k_2$  represents the

stiffnesses of the beam before reaching the ultimate resistance at the fixed support,  $R_{ms}$ , and in the span,  $R_{mf}$ , respectively.

When the load is applied, the resistance and deformation increases. The studied model represents a case where the structure starts to sway back when its ultimate resistance is reached (at point 2) and then starts to sway dynamically. For the load direction presented in Figure C.1a, the beam deforms downwards which is indicated as positive deformation.

A description of the response model in Figure C.3 is presented in Table C.1 while the development of the stress and strain for both critical sections is illustrated in Figure C.4.

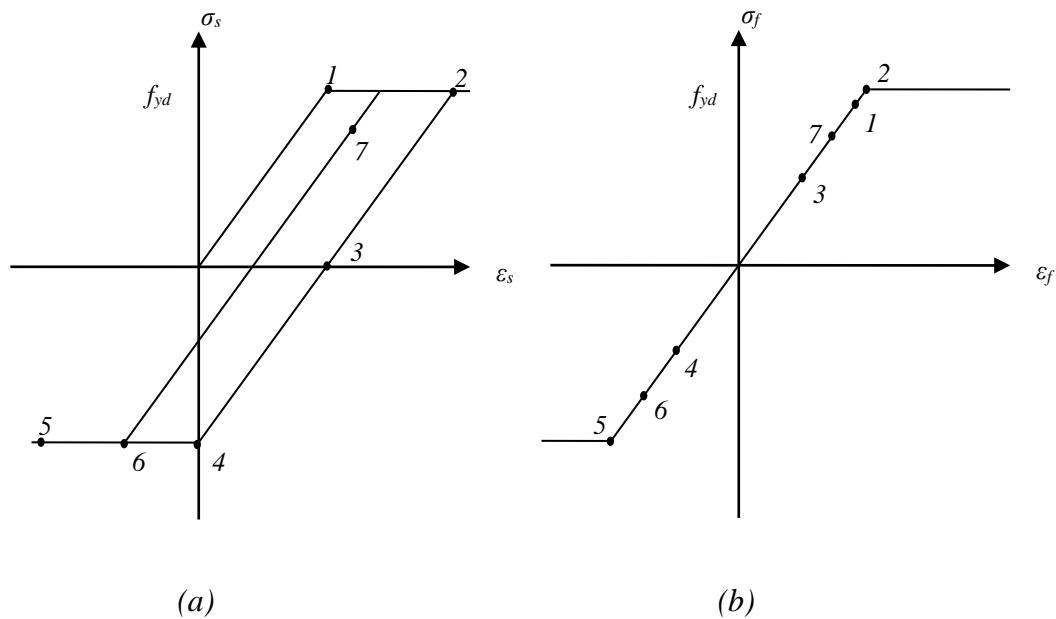


Figure C.4 Development of stresses for (a) section s and (b) section f.

Table C.1 Course of events when the structure shown in Figure C.1 is hit by an impulse load  $P(t)$ . The numbered points can be seen in Figure C.3 and Figure C.4.

Point	Description
1	To start with, the structure yields in section $s$ , which is described as point 1 in Figure C.3 and Figure C.4. The obtained stresses for section $s$ and $f$ are positive tensile stresses. When the structure reaches point 1, a decrease in stiffness, from $k_1$ to $k_2$ , occurs. The stiffness $k_1$ corresponds to the stiffness of a beam which is fixed at one support and simply supported at the other. Stiffness $k_2$ represents the stiffness of a simply supported beam.
2	When the load is further increased, yielding in section $f$ occurs and point 2 is reached. If the load had been further increased, a plastic plateau would have been developed, which is described with a dashed line in Figure C.3. At point 2 the structure starts to sway back since the total external work has been taken by the internal work of the structure. From this point the structure starts to sway dynamically without any external load. At first, the structure follows the elastic stiffness $k_1$ which is a consequence of the changed direction.
3	Point 3 defines when the stresses at section $s$ reach zero, see Figure C.4a. After passing this point the stresses in the section increases, but in the other direction, i.e. the stresses at section $s$ becomes compressive instead of tensile.
4	When section A begins to yield again point 4 is reached, and as a consequence the stiffness is again decreased to $k_2$ .
5	Point 5 indicates when yielding occurs in the span again. However, for this impulse loaded structure, point 5 is never reached since the structure starts to sway back before this happens. This phenomenon is due to the fact that the structure deforms depending on the elastic energy which is illustrated as the area below the graph in Figure C.3.
6	When the areas $W_{el.1}$ and $W_{el.2}$ are equal, the structure changes direction and starts to sway in the positive direction again.
7	After point 6 the structure starts to oscillate elastically between point 6 and 7 since the work $W_{el.3}$ and $W_{el.4}$ are equal. The stiffness of these oscillations is $k_1$ .
8	At point 8 in Figure C.3 the structure only possesses kinetic energy and the potential energy is zero.



## C.4 Structure subjected to a static load

When the local frame model, a beam with one edge simply supported and one edge fully fixed, is subjected to a static load the areas under the resistance-deformation curve does not necessarily have to match as for an impulse loaded structure.

If the static load is increasing, the resistance, deformation or both will increase depending on the position on the resistance-deformation curve and vice versa. Figure C.5 illustrates the response curve of a structure where the deformation is increasing up to point 3, decreasing to point 5 and increasing again to point 7. The response of the structure is further described in Table C.2.

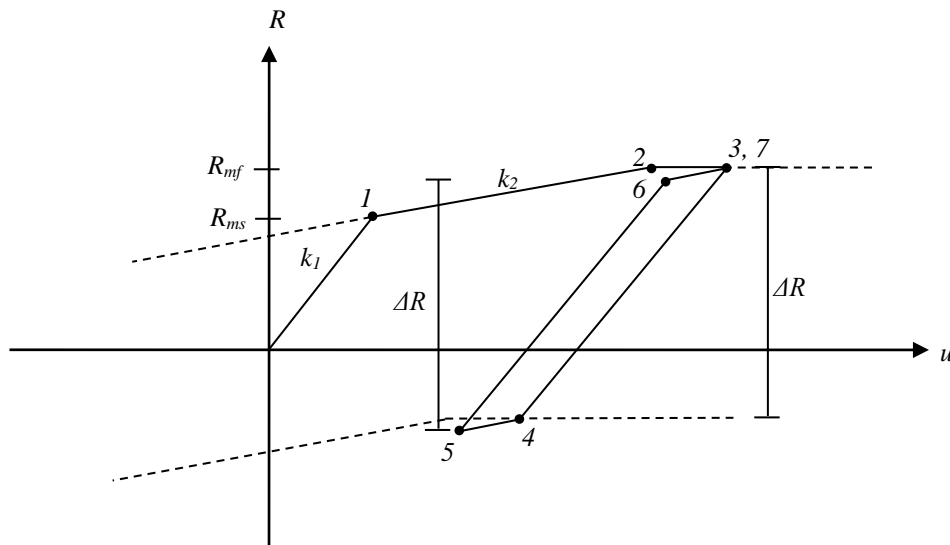


Figure C.5 The response model of a statically loaded structure where the deformation is increasing from point 1 to 3, decreasing from point 3 to 5 and increasing again between point 5 and 7.

The course of events is described in Table C.2.

Table C.2 Course of events for the structure subjected to a static load  $q$ . The numbered points are shown in Figure C.5.

Point	Description	Deformation
1	The structure yields at the fixed support, point 1, and the stiffness is decreased from $k_1$ to $k_2$ .	Increases
2	The structure yields at the span, point 2, and a plastic plateau is developed. Here, the static load is constant but the deformation is increasing.	Increases
3	At point 3 the deformation starts to decrease and the resistance decreases with a stiffness $k_1$ .	Starts to decrease
4	At point 4 the resistance has decreased with the amount $\Delta R$ , corresponding to two times the resistance $R_{ms}$ . The section yields at the fixed support in the opposite direction.	Decreases
5	At point 5 the static load starts to increase again and the resistance is increasing with a stiffness of $k_1$ .	Starts to increase
6	The resistance increases from point 5, with a stiffness of $k_1$ , until the amount $\Delta R$ is reached and a plastic hinge at the fixed support is developed at point 6.	Increasing
7	The resistance increases with the stiffness $k_2$ until the plastic plateau is reached and the section yields in the span at point 7.	Increasing

The development of the resistance and deformation for the structure described in Figure C.6 is explained in Table C.3. In this case the deformation increases up to point 2 where it starts to decrease until point 5. From point 5 to point 8 the deformation is increasing.

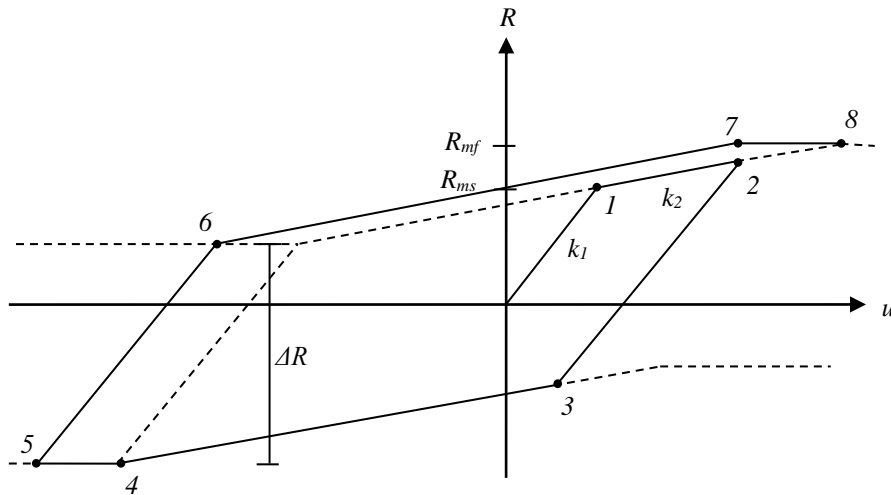


Figure C.6 The response model of a statically loaded structure where the deformation is increasing from point 1 to 2, decreasing from point 2 to 5 and increasing again between point 5 and 8.

Table C.3 Course of events for the local front column subjected to a static load  $q$ . The numbered points are shown in Figure C.6.

Point	Description	Deformation
1	The structure yields at the fixed support, point 1, and the stiffness is decreased from $k_1$ to $k_2$ .	Increases
2	The static load starts to decrease and therefore the resistance starts to decrease before the span has yielded. The resistance decreases with a stiffness of $k_1$ .	Starts to decrease
3	At point 3 the fixed support yields in the opposite direction and the stiffness is changed from $k_1$ to $k_2$ .	Decreases
4	At point 4 the span yields and a plastic plateau starts to develop. At this point the static load is constant.	Decreases
5	At point 5 the static load starts to increase again and the resistance is increasing with a stiffness $k_1$ .	Starts to increase
6	The resistance increases from point 5, with a stiffness $k_1$ , until the amount $\Delta R$ is reached and a plastic hinge at the fixed support is developed at point 6 where the stiffness is changed to $k_2$ .	Increasing
7	The resistance increases with the stiffness $k_2$ until the plastic plateau is reached and the section yields in the span at point 7.	Increasing
8	As the load increases further the deformation increases and the resistance is constant on the plastic plateau.	Increasing

## APPENDIX D Central difference method

### D.1 Introduction

The central difference method, described in equation (D.1), is an explicit calculation method which can be used for approximating the solution of the equation of motion at a certain time  $t$ .

$$m\ddot{u} + c\dot{u} + ku = F(t) \quad (\text{D.1})$$

where  $m$  is the mass,  $\ddot{u}$  is the acceleration,  $c$  is the damping,  $\dot{u}$  is the velocity,  $k$  is the stiffness,  $u$  is the displacement and  $F(t)$  is the external force.

### D.2 Calculation method

The calculation method uses the displacements at time  $t$  and  $t - \Delta t$ ,  $u_t$  and  $u_{t-\Delta t}$ , in order to find the displacement at time  $t + \Delta t$ ,  $u_{t+\Delta t}$ , as shown in Figure D.1. Equation (D.1) can be written as

$$m\ddot{u}_t + c\dot{u}_t + ku_t = F(t) \quad (\text{D.2})$$

where the index  $t$  implies the time. The mass  $m$ , stiffness  $k$  and damping  $c$  are constant in time, i.e.  $m = m_t$ ,  $c = c_t$  and  $k = k_t$ .

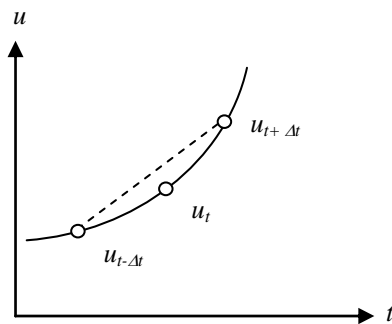


Figure D.1 In the central difference method,  $u_{t-\Delta t}$  and  $u_t$  is used to find the solution of  $u_{t+\Delta t}$  (Andersson and Karlsson (2012)).

The acceleration  $\ddot{u}$  at time  $t$  can be written as

$$\ddot{u}_t = \frac{1}{\Delta t^2} (u_{t+\Delta t} - 2u_t + u_{t-\Delta t}) \quad (\text{D.3})$$

The velocity  $\dot{u}$  at time  $t$  is

$$\dot{u}_t = \frac{1}{2\Delta t} (u_{t+\Delta t} - u_{t-\Delta t}) \quad (\text{D.4})$$

Inserting equation (D.3) and (D.4) into equation (D.2) gives the following equation for the displacement at time  $t + \Delta t$ :

$$u_{t+\Delta t} = \left( \frac{m_t}{\Delta t^2} + \frac{c_t}{2\Delta t} \right)^{-1} \left( F(t) - R(u_t) + \frac{2m_t u_t}{\Delta t^2} - \left[ \frac{m_t}{\Delta t^2} - \frac{c_t}{2\Delta t} \right] u_{t-\Delta t} \right) \quad (\text{D.5})$$

where  $R(u_t)$  depends on the material model and structural response model, which are further described in Section D.3.

To calculate the deformation at time  $t + \Delta t$ , information is needed about the deformation at both time  $t$  and  $t - \Delta t$ . To solve this, a start value is required and the deformation at time  $-\Delta t$ ,  $u_{-\Delta t}$ , can be calculated as

$$u_{-\Delta t} = u_0 - \Delta t \dot{u}_0 + \frac{\Delta t^2}{2} \ddot{u}_0 \quad (\text{D.6})$$

When using the central difference method to solve the equation of motion, a constant time step,  $\Delta t$ , is used. For the method to be stable, the time step must be smaller than a certain critical time step.

$$\Delta t \leq \Delta t_{cr} \quad (\text{D.7})$$

where

$$\Delta t_{cr} = \frac{2}{\omega} = 2\sqrt{\frac{m}{k}} \quad (\text{D.8})$$

To increase the accuracy, especially for a SDOF system, it can be wise to use an even smaller time step,  $\Delta t_1$ , according to

$$\Delta t_1 \leq \begin{cases} \Delta t_{cr} \\ t_1 \\ 100 \end{cases} \quad (\text{D.9})$$

where  $t_1$  is the duration of the load.

## D.3 Response models

### D.3.1 Introduction

When calculating the deformation according to the central difference method in this Master's Thesis, Matlab is used. The resistances used in the calculations are estimated differently depending on if the response model is elastic or elasto-plastic. For the elasto-plastic model a distinction must be done depending on if the model can develop

one or two plastic hinges, i.e. if it is bilinear or trilinear. The different response models are explained in Section D.3.2 to D.3.4.

### D.3.2 Elastic response model

For the elastic response model, the resistance  $R_t$  in equation (D.5) can be written as

$$R_t = ku_t \quad (\text{D.10})$$

where  $k$  is the stiffness and  $u_t$  is the deformation.

### D.3.3 Bilinear elasto-plastic response model

A bilinear elasto-plastic response model is illustrated in Figure D.2 where

$$u_l = R_m / k \quad (\text{D.11})$$

and where  $R_m$  the maximum resistance.

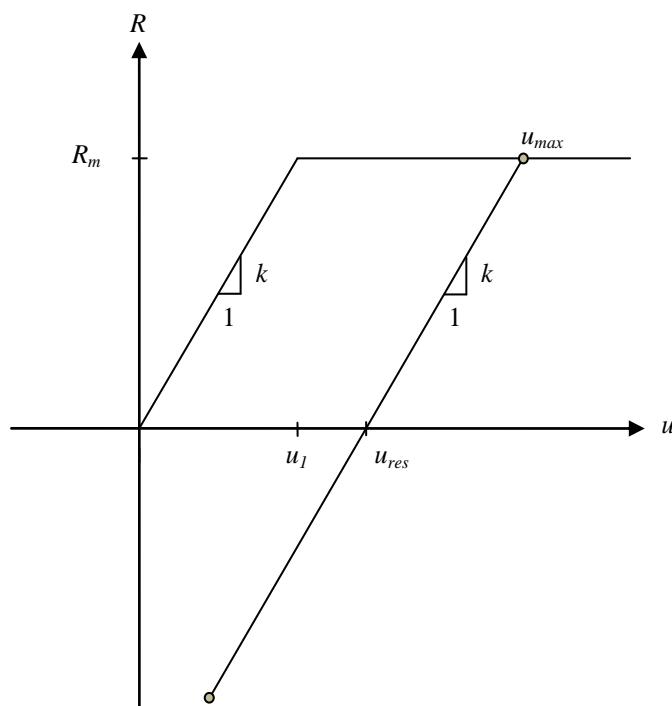


Figure D.2 Resistance-deformation curve for a bilinear elasto-plastic model.

For  $0 \leq ku_t < R_m$

$$R_t = ku_t \quad (\text{D.12})$$

For  $ku_t \geq R_m$

$$R_t = R_m \quad (\text{D.13})$$

When the deformation starts to decrease, the maximum deformation is reached and the resistance goes back to the elastic mode, though with a plastic deformation. When  $u_{t+\Delta t} < u_t$  the resistance is changed to

$$R_t = k(u_t - u_{res}) \quad (\text{D.14})$$

where the residual plastic deformation,  $u_{res}$ , can be calculated as

$$u_{res} = u_{\max} - \frac{R_m}{k} \quad (\text{D.15})$$

### D.3.4 Trilinear elasto-plastic response model

A trilinear elasto-plastic model is illustrated in Figure D.3 where  $u_1$  and  $u_2$  are the deformations for the corresponding resistances  $R_{m1}$  and  $R_{m2}$  where the first and second plastic hinges is reached. The deformations  $u_1$  and  $u_2$  can be calculated as

$$u_1 = \frac{R_{m1}}{k_1} \quad (\text{D.16})$$

and

$$u_2 = u_1 + (R_{m2} - R_{m1})/k_2 \quad (\text{D.17})$$

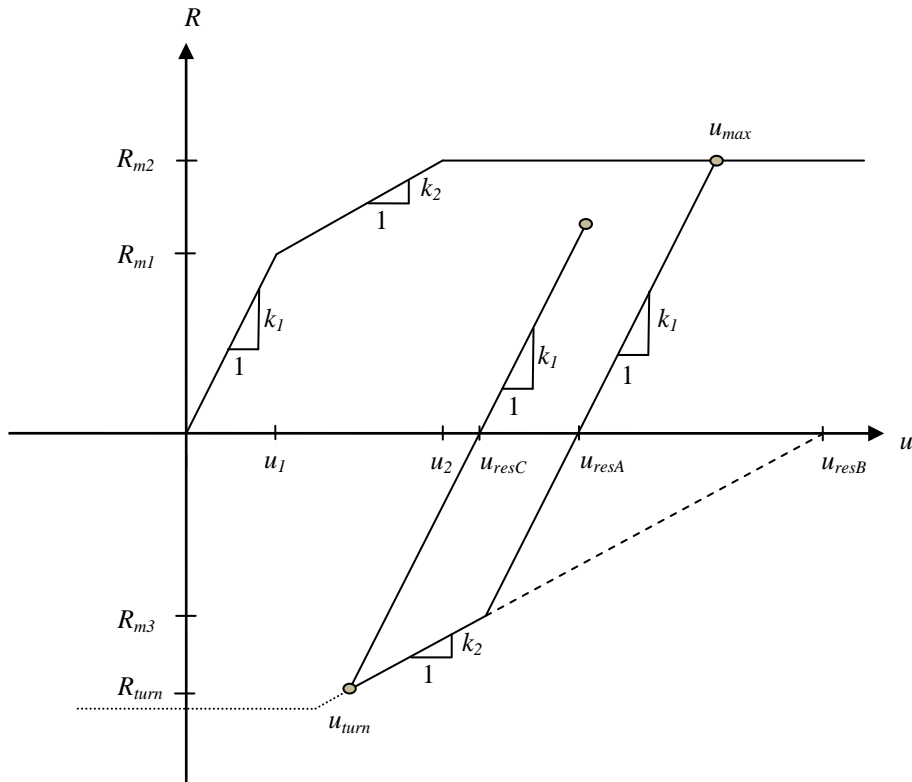


Figure D.3 Resistance-deformation curve for a trilinear elasto-plastic model.

For  $0 \leq k_1 u_t < R_{m1}$

$$R_t = k_1 u_t \quad (\text{D.18})$$

For  $R_{m1} \leq (R_{m1} + k_2(u_t - u_1)) < R_{m2}$

$$R_t = (R_{m1} + k_2(u_t - u_1)) \quad (\text{D.19})$$

For  $R_{m1} + k_2(u_t - u_1) \geq R_{m2}$

$$R_t = R_{m2} \quad (\text{D.20})$$

When  $u_{t+\Delta t} < u_t$  the resistance is changed to

$$R_t = k_1(u_t - u_{resA}) \quad (\text{D.21})$$

where the residual plastic deformation,  $u_{resA}$  can be calculated as

$$u_{resA} = u_{max} - R_{m2} / k_1 \quad (\text{D.22})$$



where the index  $max$  indicates the time at which the maximum deformation is reached.

Now, when the resistance passes a certain value,  $R_{m3}$ , calculated in equation (D.23) the stiffness changes to  $k_2$ .

$$R_{m3} = R_{m2} - 2R_{m1} \quad (D.23)$$

When  $R_t \leq R_{m3}$  the resistance changes to

$$R_t = k_2(u_t - u_{resB}) \quad (D.24)$$

where

$$u_{resB} = u_{max} - R_{m3} / k_2 + 2R_{m1} / k_1 \quad (D.25)$$

When the deformation starts to increase again, at  $u_{turn}$ , a new residual plastic deformation,  $u_{resC}$ , can be calculated as

$$u_{resC} = u_{turn} - R_{turn} / k_1 \quad (D.26)$$

The resistance have now found equilibrium and will oscillate with the resistance

$$R_t = k_1(u_t - u_{res3}) \quad (D.27)$$

## APPENDIX E Hand calculations for 2D frame

### E.1 Input data

The cross section of the front and back column as well as of the roof beam is presented in Figure E.1. Additional dimensions and the reinforcement amount are presented in Figure E.2 and Table E.1. The boundary conditions and load type for the local and global response model are presented in Figure E.2a and b, respectively, while the material parameters are presented in Table E.2. The design values of concrete and reinforcement strength,  $f_{cd}$  and  $f_{yd}$ , are calculated according to equation (7.11) and (7.12). Following the recommendation from Chapter 3 the top reinforcement is not introduced in the calculation of sectional stiffness and moment resistance. The general equations are presented in Appendix A.

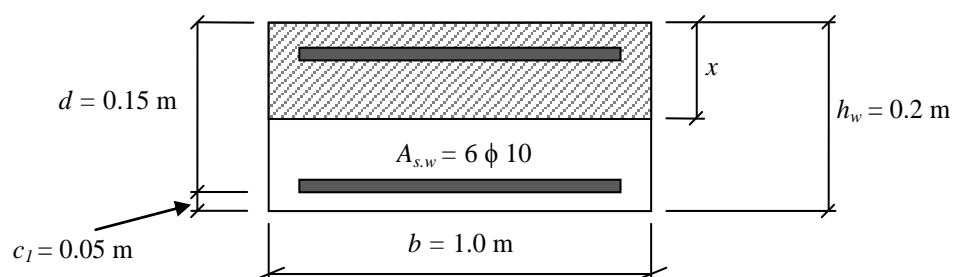


Figure E.1 Model illustrating the cross section of the 2D frame.

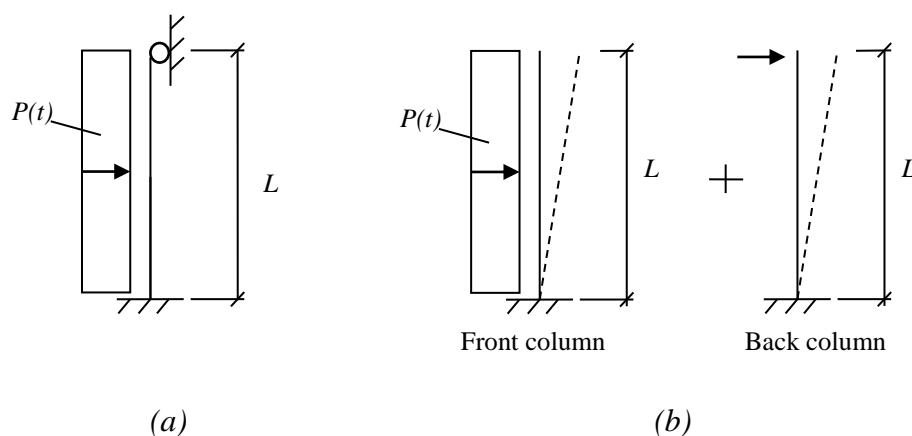


Figure E.2 (a) Local response model; (b) global response model.

Table E.1 Additional parameters of the frame.

Length of the column, $L$ [m]	Length of the roof beam, $B$ [m]	Reinforcement amount, $A_s$ [ $10^{-4} \text{ m}^4$ ]
7.0	15.0	5.3

Table E.2 Material parameters of the frame.

$E_c$ [GPa]	$f_{cd}$ [MPa]	$E_s$ [GPa]	$f_{yd}$ [MPa]	$\rho$ [kg/m <sup>3</sup> ]
33	25	200	500	2 400

The factor  $\alpha$ , i.e. the ratio between  $E_s$  and  $E_c$ , for the considered section, calculated according to equation (7.6), is

$$\alpha = \frac{200}{33} = 6.06 \quad (\text{E.1})$$

The moment of inertia for the uncracked section, without consideration to the reinforcement, is established according to

$$I_{I.a} = \frac{bh^3}{12} = \frac{1 \cdot 0.2^3}{12} = 0.64 \cdot 10^{-4} \text{ m}^{-4} \quad (\text{E.2})$$

For a case where the cross section is cracked, state II, and where no axial forces are acting on the section, the distance from the top of the cross section to the neutral axis,  $x_{II}$ , is calculated according to equation (7.9). Thus, for the cross section of the 2D frame the distance to the neutral axis,  $x_{II}$ , is calculated as

$$\frac{0.2 \cdot x_{II}^2}{2} = 6.06 \cdot 5.24 \cdot 10^{-4} \cdot (0.15 - x_{II}) \quad (\text{E.3})$$

resulting in 0.028 m.

In order to calculate the moment of inertia of the section in state II, equation (7.8) is used, which for the 2D frame results in

$$I_{II} = \frac{0.2 \cdot 0.028^3}{3} + 6.06 \cdot 5.24 \cdot 10^{-4} \cdot (0.15 - 0.028)^2 = 0.54 \cdot 10^{-4} \text{ m}^{-4} \quad (\text{E.4})$$

The inclination of the first and second branch in the elasto-plastic response curve,  $k_1$  and  $k_2$ , for local SDOF model with boundary conditions and load type as in Figure E.2a is calculated as

$$k_1 = \frac{192 \cdot E_c \cdot I_{II}}{L^3} = \frac{192 \cdot 33 \cdot 10^9 \cdot 0.54 \cdot 10^{-4}}{7^3} = 1007.6 \text{ kN/m} \quad (\text{E.5})$$

$$k_2 = \frac{384 \cdot E_c \cdot I_{II}}{5 \cdot L^3} = \frac{384 \cdot 33 \cdot 10^9 \cdot 0.54 \cdot 10^{-4}}{5 \cdot 7^3} = 403.0 \text{ kN/m} \quad (\text{E.6})$$

In the global model the stiffnesses for the front and back column, illustrated in Figure E.2b, is established as

$$k_{l.fr} = \frac{8 \cdot E_c \cdot I_{II}}{L^3} = \frac{8 \cdot 33 \cdot 10^9 \cdot 0.54 \cdot 10^{-4}}{7^3} = 41.9 \text{ kN/m} \quad (\text{E.7})$$

$$k_{l.ba} = \frac{3 \cdot E_c \cdot I_{II}}{L^3} = \frac{3 \cdot 33 \cdot 10^9 \cdot 0.54 \cdot 10^{-4}}{7^3} = 15.7 \text{ kN/m} \quad (\text{E.8})$$

The neutral axis for when the ultimate concrete strain is reached, state III, is calculated using equation (7.14) assuming that the bottom reinforcement is yielding. For the 2D frame this results in

$$x_{III} = \frac{5.24 \cdot 10^{-4} \cdot 500 \cdot 10^6}{0.8 \cdot 25 \cdot 10^6 \cdot 1} = 0.013 \text{ m} \quad (\text{E.9})$$

The yielding strain,  $\varepsilon_{sy}$ , for the reinforcement is calculated according to equation (7.13). Thus for the considered section it is

$$\varepsilon_{sy} = \frac{500 \cdot 10^6}{200 \cdot 10^9} = 2.5 \cdot 10^{-3} \quad (\text{E.10})$$

A control of the strain at the bottom reinforcement,  $\varepsilon_s$ , is made according to equation (7.15) where the ultimate concrete strain  $\varepsilon_{cu} = 0.0035$ .

$$\varepsilon_s = \frac{0.15 - 0.013}{0.013} \cdot 3.5 \cdot 10^{-3} = 36.8 \cdot 10^{-3} > 2.5 \cdot 10^{-3} \quad (\text{E.11})$$

The moment capacity,  $M_{rd}$ , is calculated according to equation (7.17) and for the 2D frame it is

$$M_{rd} = 25 \cdot 10^6 \cdot 0.8 \cdot 0.013 \cdot 1 \cdot (0.15 - 0.4 \cdot 0.013) = 37.8 \text{ kNm} \quad (\text{E.12})$$

For the local model the resistance  $R_{ms}$  corresponds to the ultimate resistance at the fixed support and the resistance  $R_{mf}$  corresponds to the ultimate resistance of the critical span section. These are calculated according to equation (E.30) and (E.31) resulting in

$$R_{ms} = \frac{8 \cdot M_{rd}}{L} = \frac{8 \cdot 37.8}{7} = 43.3 \text{ kN} \quad (\text{E.13})$$

$$R_{mf} = \frac{12 \cdot M_{rd}}{L} = \frac{12 \cdot 37.8}{7} = 64.8 \text{ kN} \quad (\text{E.14})$$

The mass of the front and back column is

$$m = b \cdot h \cdot L \cdot \rho = 1.0 \cdot 0.2 \cdot 7.0 \cdot 2400 = 3360 \text{ kg} \quad (\text{E.15})$$

The mass of the roof beam is

$$m = b \cdot h \cdot B \cdot \rho = 1.0 \cdot 0.2 \cdot 15.0 \cdot 2400 = 7200 \text{ kg} \quad (\text{E.16})$$

## E.2 Global and local elastic frame models

### E.2.1 Deformation

The elastic deformation of the structure, subjected to characteristic impulse load, is calculated from the condition of work equilibrium which is explained in Section 2.7.5. The parameters used in this section are calculated in Section E.1 and the values for the local and global model are presented in Table E.3 and Table E.4, respectively.

Table E.3 Mass, stiffness and transformation factors used for the local elastic model.

Part	$m$ [kg]	$\kappa_m$ [-]	$k_I$ [kN/m]	$\kappa_{mF}$ [-]
Front column (1)	3 360	0.486	1 007.6	0.805

Table E.4 Mass, stiffness and transformation factors used for the global elastic model.

Part	$\kappa_m$ [-]	$m$ [kg]	$\kappa_k = \kappa_F$ [-]	$I_{II}$ [ $10^{-4} \text{ m}^4$ ]	$k_I$ [kN/m]
Front column (1)	0.257	3 360	0.400	0.54	41.9
Back column (2)	0.236	3 360	1.000	0.54	15.7
Roof beam (3)	1.000	7 200	0	0.54	0

The resulting deformation,  $u_{el}$ , is described as

$$u_{el} = \frac{I_k}{m\omega} \quad (\text{E.17})$$

where  $I_k$  is the characteristic load,  $m$  the mass and  $\omega$  the angular frequency, calculated as

$$\omega = \sqrt{\frac{k}{m}} \quad (\text{E.18})$$

For the studied structure, the angular frequency for the local and global system, respectively is

$$\omega_{el.1} = \sqrt{\frac{1007.6 \cdot 10^3}{3360 \cdot 0.805}} = 19.3 \text{ rad/s} \quad (\text{E.19})$$

$$\omega_{el,gl} = \sqrt{\frac{(41.9 \cdot 0.4 + 15.7 \cdot 1 + 0) \cdot 10^3}{3360 \cdot 0.257 + 3360 \cdot 0.236 + 7200 \cdot 1}} = 1.92 \text{ rad/s} \quad (\text{E.20})$$

The total impulse load acting on the considered area of the structure is established as

$$I = i \cdot A = \frac{P_{peak} \cdot t_1}{2} \cdot b \cdot L = \frac{60 \cdot 10^3 \cdot 0.025}{2} \cdot 1 \cdot 7 = 5250 \text{ Ns} \quad (\text{E.21})$$

The elastic deformation for the local and global model is

$$u_{el,l} = \frac{I_k}{m\omega} = \frac{5250}{3360 \cdot 0.805 \cdot 19.3} = 0.10 \text{ m} \quad (\text{E.22})$$

$$u_{el,gl} = \frac{I_k}{m\omega} = \frac{5250}{(3360 \cdot 0.257 + 3360 \cdot 0.236 + 7200 \cdot 1) \cdot 1.92} = 0.12 \text{ m} \quad (\text{E.23})$$

This definition of deformation is established with regard to a characteristic impulse load. In order to get the correct value of the deformation for the chosen impulse load the deformation should be modified, see Section 2.7.6.

Thus, the frequency of the dynamic loaded structure,  $f$ , and its periodicity,  $T$  must be established accordingly

$$f = \frac{\omega}{2\pi} \quad (\text{E.24})$$

$$T = \frac{1}{f} \quad (\text{E.25})$$

For the local and global model this gives

$$f_{el,l} = 3.07 \text{ Hz} \quad (\text{E.26})$$

$$f_{el,gl} = 0.30 \text{ Hz} \quad (\text{E.27})$$

$$T_{el,l} = 0.32 \text{ s} \quad (\text{E.28})$$

$$T_{el,gl} = 3.28 \text{ s} \quad (\text{E.29})$$

The ratio of the periodicity,  $T$ , to the duration of the load,  $t_l$ , for the local and global model, respectively is

$$\frac{T_{el,l}}{t_1} = \frac{0.32}{0.025} = 12.8 \quad (\text{E.30})$$

$$\frac{T_{el,gl}}{t_1} = \frac{3.28}{0.025} = 131.2 \quad (\text{E.31})$$

For  $n = 1$ , which corresponds to a triangular load, and for the calculated relations of  $T$  to  $t_1$ , the impulse factors  $\gamma_I$ , according to Section 2.7.6.2 are

$$\gamma_{I,l} = 1.0 \quad (\text{E.32})$$

$$\gamma_{I,gl} = 1.0 \quad (\text{E.33})$$

This means that the chosen load, with a peak value of 60 kPa and a duration of 0.025 s, corresponds to a characteristic impulse load. Therefore the magnitudes of the calculated deformations are realistic and do not need to be modified.

### E.3 Local elasto-plastic frame model

#### E.3.1 Deformation

The parameters used in this section are calculated in Section E.1 and are presented in Table E.5.

*Table E.5 Mass, stiffness and transformation factors used for the local elasto-plastic model.*

Part	$m$ [kg]	$\kappa_m$ [-]	$k_1$ [kN/m]	$k_2$ [kN/m]	$\kappa_k = \kappa_F$ [-]	$M_{rd}$ [kNm]	$R_{ms}$ [kN]	$R_{mf}$ [kN]
Front column (1)	3 360	0.333	1 007.6	403.0	0.500	37.8	43.3	64.9

The elasto-plastic deformation of the structure,  $u_{ep}$ , is described as

$$u_{ep} = u_{ep,el} + u_{ep,pl} = \frac{R_m}{2k} + \frac{I_k^2}{2mR_m} \quad (\text{E.34})$$

where  $u_{ep,el}$  and  $u_{ep,pl}$  are the elastic and plastic parts of the elasto-plastic deformation.  $R_m$  is the maximum resistance,  $I_k$  is the characteristic load and  $m$  and  $k$  is the mass and stiffness, respectively.

The total impulse acting on the considered area of the structure has a magnitude of 5250 Ns according to equation (E.21).

The deformations  $u_1$  and  $u_2$  is

$$u_1 = \frac{R_{ms}}{k_1} = 42.9 \text{ mm} \quad (\text{E.35})$$

$$u_2 = u_1 + \frac{R_{mf} - R_{ms}}{k_2} = 96.5 \text{ mm} \quad (\text{E.36})$$

Since the stiffness in equation (E.34) is meant for a bilinear case, two stiffnesses are used in these hand calculations. The first stiffness is taken as the stiffness for a beam with one fixed edge and one simply supported,  $k_1$ . The second stiffness is taken as the secant stiffness,  $k_3$ , according to Figure E.3. The stiffness that would give the correct results should lie in between these values.

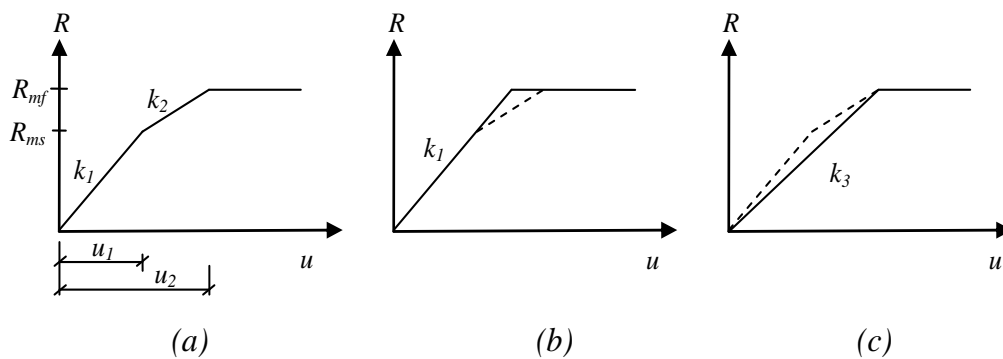


Figure E.3 (a) Stiffness of the elasto-plastic local front column (b) Simplified bilinear case with stiffness  $k_1$  (c) Simplified bilinear case with stiffness  $k_3$ .

The stiffness  $k_3$  is calculated as follows

$$k_3 = \frac{R_{mf}}{u_2} = 671 \frac{\text{kN}}{\text{m}} \quad (\text{E.37})$$

Now the deformations can be calculated. Deformation for stiffness  $k_1$  respective stiffness  $k_3$ , estimated according to equation (E.34) is

$$u_{ep1} = \frac{0.5 \cdot 64.8 \cdot 10^3}{2 \cdot 0.5 \cdot 1007.6 \cdot 10^3} + \frac{(0.5 \cdot 5250)^2}{2 \cdot 0.333 \cdot 3360 \cdot 0.5 \cdot 64.8 \cdot 10^3} = 0.127 \text{ m} \quad (\text{E.38})$$

$$u_{ep3} = \frac{0.5 \cdot 64.8 \cdot 10^3}{2 \cdot 0.5 \cdot 671 \cdot 10^3} + \frac{(0.5 \cdot 5250)^2}{2 \cdot 0.333 \cdot 3360 \cdot 0.5 \cdot 64.8 \cdot 10^3} = 0.143 \text{ m} \quad (\text{E.39})$$



### E.3.2 Plastic deformation capacity

The calculation of the plastic deformation capacity for the local elasto-plastic frame model is presented in this section. The concept of calculating the required deformation capacity for a trilinear model is described in Section E.3.1 and the hand calculation method is presented in Section A.5. Parameters and dimensions of the studied frame are presented in Section E.1. Properties of the chosen impulse load can be found in Section 4.3.

In order to calculate the distance from the simply supported edge to where the maximum moment is,  $L_0$ , the reaction force at the simply supported edge,  $R_1$ , and the equivalent static load,  $q_1$ , is calculated as

$$q_1 = P_{peak} \cdot b = 60 \frac{\text{kN}}{\text{m}} \quad (\text{E.40})$$

$$R_1 = \frac{q_1 \cdot L}{2} - \frac{M_{rd}}{L} = \left( \frac{60 \cdot 10^3 \cdot 7}{2} - \frac{37.8 \cdot 10^3}{7} \right) N = 205 \text{ kN} \quad (\text{E.41})$$

$L_0$  can now be calculated as

$$L_0 = L - \frac{2 \cdot R_1}{q_1} = \left( 7 - \frac{2 \cdot 205 \cdot 10^3}{60 \cdot 10^3} \right) \text{m} = 0.18 \text{ m} \quad (\text{E.42})$$

The shear slenderness  $\lambda$  and the factor for allowed plastic rotation capacity,  $k_\lambda$ , is

$$\lambda = \frac{L_0}{d} = \frac{0.18}{0.15} = 1.20 \quad (\text{E.43})$$

$$k_\lambda = \sqrt{\frac{\lambda}{3}} = 0.63 \quad (\text{E.44})$$

The plastic rotation capacity,  $\theta_{pl}$ , for reinforcement of Class B and Class C is calculated according to Section A.5 which for the local frame gives

$$\theta_{plB} = 10.7 \cdot 10^{-3} \text{ rad} \quad (\text{E.45})$$

$$\theta_{plC} = 33.1 \cdot 10^{-3} \text{ rad} \quad (\text{E.46})$$

The modified values of the plastic rotation capacities with regard to shear slenderness,  $\theta_{rd}$ , can now be calculated as

$$\theta_{rdB} = \theta_{plB} \cdot k_\lambda = 6.8 \cdot 10^{-3} \text{ rad} \quad (\text{E.47})$$

$$\theta_{rdC} = \theta_{plC} \cdot k_\lambda = 21.0 \cdot 10^{-3} \text{ rad} \quad (\text{E.48})$$

The plastic deformation capacities,  $u_{rd}$ , can be calculated as

$$u_{rdB} = \theta_{rdB} \cdot \frac{R_1}{q_1} = 23.1 \text{ mm} \quad (\text{E.49})$$

$$u_{rdC} = \theta_{rdC} \cdot \frac{R_1}{q_1} = 71.6 \text{ mm} \quad (\text{E.50})$$

The total deformation capacity,  $u_{rd,tot}$ , is the sum of the elastic deformation,  $u_1$ , and the plastic deformation capacity,  $u_{rd}$ , and is calculated as

$$u_{rdB,tot} = u_{rdB} + u_1 = (23.1 + 42.9) \text{ mm} = 66.0 \text{ mm} \quad (\text{E.51})$$

$$u_{rdC,tot} = u_{rdC} + u_1 = (71.6 + 42.9) \text{ mm} = 114.5 \text{ mm} \quad (\text{E.52})$$

where the elastic deformation  $u_1$  is calculated in equation (E.35).

## APPENDIX F Study of 3D structure

### F.1 Input data

#### F.1.1 Wall

The cross section of the wall panels is presented in Figure F.1. Additional dimensions and the reinforcement amount are presented in Table 5.2 and the material parameters are presented in Table F.2. The design values of the concrete and reinforcement strength,  $f_{cd}$  and  $f_{yd}$ , are calculated according to equation (7.11) and (7.12). Following the recommendation from Chapter 3 the top reinforcement is not introduced in the calculation of the sectional stiffness and moment resistance.

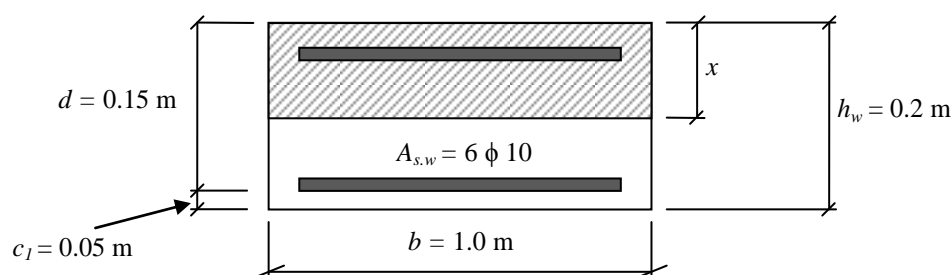


Figure F.1 Model illustrating the cross section of a wall panel with a width of 1 m.

Table F.1 Additional parameters of the wall panel.

Part	Length of wall panel, $w$ [m]	Reinforcement amount, $A_{s,w}$ [ $10^{-4} \text{ m}^4$ ]
Wall	6.0	5.3

Table F.2 Material parameters

Part	$E_c$ [GPa]	$f_{cd}$ [MPa]	$E_s$ [GPa]	$f_{yd}$ [MPa]	$\rho$ [kg/m <sup>3</sup> ]
Front wall	33	25	200	500	2 400

The factor  $\alpha$ , i.e. the ratio between  $E_s$  and  $E_c$ , is calculated according to equation (7.6), which for the wall panel is

$$\alpha = \frac{200}{33} = 6.06 \quad (\text{F.1})$$

The moment of inertia for the uncracked section, state I, without any consideration to the reinforcement is calculated as

$$I_{I.w.a} = \frac{bh_w^3}{12} = \frac{1 \cdot 0.2^3}{12} = 0.64 \cdot 10^{-4} \text{ m}^{-4} \quad (\text{F.2})$$

For a case where the cross section is cracked, state II, and where no axial forces are acting on the section, the distance to the neutral axis  $x_{II}$  is calculated according to equation (7.9). Thus, for the considered section the location of the neutral axis is calculated as

$$\frac{0.2 \cdot x_{II}^2}{2} = 6.06 \cdot 5.24 \cdot 10^{-4} \cdot (0.15 - x_{II}) \quad (\text{F.3})$$

$$\rightarrow x_{II} = 0.028 \text{ m} \quad (\text{F.4})$$

In order to calculate the moment of inertia of the section in state II, equation (7.8) is used which for the wall panels becomes

$$I_{II.w} = \frac{0.2 \cdot 0.028^3}{3} + 6.06 \cdot 5.24 \cdot 10^{-4} \cdot (0.15 - 0.028)^2 = 0.54 \cdot 10^{-4} \text{ m}^{-4} \quad (\text{F.5})$$

The stiffness for a simply supported wall panel in state II is calculated using equation (7.4), resulting in

$$k_{1.w} = \frac{384 \cdot 33 \cdot 10^9 \cdot 0.54 \cdot 10^{-4}}{5 \cdot 6^3} = 640 \text{ kN/m} \quad (\text{F.6})$$

The neutral axis when the ultimate concrete strain is reached (state III) is calculated using equation (7.14) where the bottom reinforcement is assumed to reach yielding. For the wall panels  $x_{III}$  is calculated as

$$x_{III} = \frac{5.24 \cdot 10^{-4} \cdot 500 \cdot 10^6}{0.8 \cdot 25 \cdot 10^6 \cdot 1} = 0.013 \text{ m} \quad (\text{F.7})$$

Yielding strain,  $\varepsilon_{sy}$ , for reinforcement is calculated according to equation (7.13) and for the studied section it is

$$\varepsilon_{sy} = \frac{500 \cdot 10^6}{200 \cdot 10^9} = 2.5 \cdot 10^{-3} \quad (\text{F.8})$$

A control of the strain at the bottom reinforcement,  $\varepsilon_s$ , is made according to equation (7.15) where the ultimate concrete strain,  $\varepsilon_{cu}$ , is 0.0035.

$$\varepsilon_s = \frac{0.15 - 0.013}{0.013} \cdot 3.5 \cdot 10^{-3} = 36.8 \cdot 10^{-3} > 2.5 \cdot 10^{-3} \quad (\text{F.9})$$

The moment capacity for the wall,  $M_{rd.w}$ , is calculated according to equation (7.17):

$$M_{rd.w} = 25 \cdot 10^6 \cdot 0.8 \cdot 0.013 \cdot 1 \cdot (0.15 - 0.4 \cdot 0.013) = 37.8 \text{ kNm} \quad (\text{F.10})$$

The maximum resistance for a simply supported wall panel with a uniformly distributed load, is established using equation (7.10), and calculated as

$$R_{m,w} = \frac{8 \cdot 37.8}{6} = 50.4 \text{ kN} \quad (\text{F.11})$$

The mass of the wall panel is

$$m_w = b \cdot h_w \cdot w \cdot \rho = 1.0 \cdot 0.2 \cdot 6.0 \cdot 2400 = 2880 \text{ kg} \quad (\text{F.12})$$

## F.1.2 Front Column

The cross section of the front column is presented in Figure F.3. Additional dimensions and the reinforcement amount are shown in Table F.3 and the material parameters can be found in Table F.4. The design values of the concrete and reinforcement strength,  $f_{cd}$  and  $f_{yd}$ , are calculated according to equation (7.11) and (7.12).

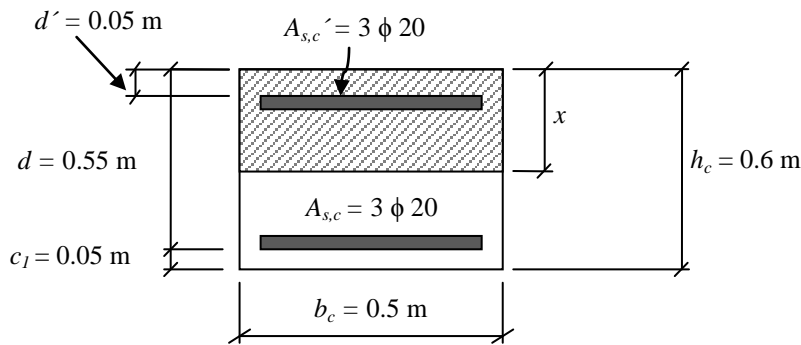


Figure F.2 Model illustrating the cross section of the front column.

Table F.3 Additional parameters of the front column.

Part	Length, $L$ [m]	Reinforcement amount, $A_{s,c} = A_{s,c'}$ [ $10^{-4} \text{ m}^4$ ]
Column	7.0	7.8

Table F.4 Material parameters of the front column

Part	$E_c$ [GPa]	$f_{cd}$ [MPa]	$E_s$ [GPa]	$f_{yd}$ [MPa]	$\rho$ [ $\text{kg/m}^3$ ]
Front column	33	25	200	500	2 400

The factor  $\alpha$  for the column, calculated according to equation (7.6), is

$$\alpha = \frac{200}{33} = 6.06 \quad (\text{F.13})$$

The moment of inertia for state I without consideration to the reinforcement is established as

$$I_{I.c.a} = \frac{b_c h_c^3}{12} = \frac{0.5 \cdot 0.6^3}{12} = 90 \cdot 10^{-4} \text{ m}^4 \quad (\text{F.14})$$

For a case where the cross section is cracked, state II, and where no axial forces are acting on the section, the distance to the neutral axis  $x_{II}$  is calculated according to equation (7.9). Thus, for the considered section the location of the neutral axis is found as

$$\frac{0.5 \cdot x_{II}^2}{2} + (6.06 - 1)7.85 \cdot 10^{-4} (x_{II} - 0.05) = 6.06 \cdot 7.85 \cdot 10^{-4} (0.55 - x_{II}) \quad (\text{F.15})$$

$$\rightarrow x_{II} = 0.09 \text{ m} \quad (\text{F.16})$$

In order to calculate the moment of inertia of the section in state II, equation (7.8) is used and  $I_{II.c}$  is calculated as

$$I_{II.c} = \frac{0.5 \cdot 0.09^3}{3} + 6.06 \cdot 7.85 \cdot 10^{-4} \cdot (0.55 - 0.9)^2 + 6.06 \cdot 7.85 \cdot 10^{-4} \cdot (0.09 - 0.05)^2 = 11.0 \cdot 10^{-4} \text{ m}^4 \quad (\text{F.17})$$

The stiffness of the column before and after the plastic hinge at the fixed support is reached,  $k_{1.c}$  and  $k_{2.c}$ , respectively, is calculated as

$$k_{1.c} = \frac{192 \cdot E_c \cdot I_{II.c}}{L^3} = \frac{192 \cdot 33 \cdot 10^9 \cdot 11.0 \cdot 10^{-4}}{7^3} = 20967 \text{ kN/m} \quad (\text{F.18})$$

$$k_{2.c} = \frac{384 \cdot E_c \cdot I_{II.c}}{L^3} = \frac{384 \cdot 33 \cdot 10^9 \cdot 11.0 \cdot 10^{-4}}{5 \cdot 7^3} = 8128 \text{ kN/m} \quad (\text{F.19})$$

The neutral axis when the ultimate concrete strain is reached, in state III, is calculated using equation (7.18). Assuming that the bottom reinforcement is yielding and that the ultimate concrete strain  $\varepsilon_{cu} = 0.0035$  the neutral axis,  $x_{III}$ , can be calculated as

$$25 \cdot 10^6 \cdot 0.8 \cdot x_{III} \cdot 0.5 - 7.85 \cdot 10^{-4} \cdot 500 \cdot 10^6 + 7.85 \cdot 10^{-4} \cdot 0.0035 \cdot \frac{0.05 - x_{III}}{x_{III}} \cdot 200 \cdot 10^9 = 0 \quad (\text{F.20})$$

$$\rightarrow x_{III} = 0.045 \text{ m} \quad (\text{F.21})$$

A yielding strain for the reinforcement is calculated according to equation (7.13) and for the column it is

$$\varepsilon_{sy} = \frac{500 \cdot 10^6}{200 \cdot 10^9} = 2.5 \cdot 10^{-3} \quad (\text{F.22})$$

A control of the strain at the top reinforcement,  $\varepsilon_s'$ , is made according to equation (7.18) as

$$\varepsilon_s' = \frac{0.05 - 0.045}{0.045} \cdot 3.5 \cdot 10^{-3} = 0.39 \cdot 10^{-3} < 2.5 \cdot 10^{-3} \quad (\text{F.23})$$

The moment capacity of the front column,  $M_{rd,c}$ , is calculated according to equation (7.20). Thus

$$\begin{aligned} M_{rd,c} &= 25 \cdot 10^6 \cdot 0.8 \cdot 0.045 \cdot 0.5 \cdot (0.55 - 0.4 \cdot 0.045) \\ &\quad - 7.85 \cdot 10^{-4} \cdot 0.0035 \cdot \frac{0.05 - 0.045}{0.045} \cdot 200 \cdot 10^9 \cdot (0.55 - 0.05) = 211 \text{ kNm} \end{aligned} \quad (\text{F.24})$$

The resistance  $R_{ms,c}$ , which corresponds to the ultimate resistance at the fixed support, and  $R_{mf,c}$ , which corresponds to the ultimate resistance of the critical span section, are calculated accordingly

$$R_{ms,c} = \frac{8 \cdot M_{rd,c}}{L} = \frac{8 \cdot 211}{7} = 241.1 \text{ kN} \quad (\text{F.25})$$

$$R_{mf,c} = \frac{12 \cdot M_{rd,c}}{L} = \frac{12 \cdot 211}{7} = 361.7 \text{ kN} \quad (\text{F.26})$$

The mass of the column including the mass of the wall, used in SDOF and the 2D FE analysis, is

$$m_{c,w} = (7 \cdot 1.0 \cdot 0.2 \cdot 6.0 + 7 \cdot 0.5 \cdot 0.6) \cdot 2400 = 25200 \text{ kg} \quad (\text{F.27})$$

The mass of only the column, used in the 3D FE analysis, is

$$m_c = 7 \cdot 0.5 \cdot 0.6 \cdot 2400 = 5040 \text{ kg} \quad (\text{F.28})$$

## F.2 Plastic deformation capacity of the front column

The calculation of the plastic deformation capacity for the elasto-plastic model of the front column in the 3D study is presented in this section. The concept of calculating the required deformation capacity for a trilinear model is described in Section E.3.1 and the hand calculation method is presented in Section A.5. Parameters and dimensions of the front column are presented in Section F.1.2 and properties of the chosen impulse load can be found in Section 4.3.

The deformation  $u_I$  according to equation (E.35) and Figure E.3 is calculated as

$$u_1 = \frac{R_{ms.c}}{k_{1.c}} = \frac{241.1}{20967} = 11.5 \text{ mm} \quad (\text{F.29})$$

In order to calculate the distance from the simply supported edge to where the maximum moment is,  $L_0$ , the reaction force at the simply supported edge,  $R_1$ , and the equivalent static load,  $q_1$ , needs to be calculated.

$$q_1 = P_{peak} \cdot b_c = 30 \frac{\text{kN}}{\text{m}} \quad (\text{F.30})$$

$$R_1 = \frac{q_1 \cdot L}{2} - \frac{M_{rd.c}}{L} = 74.8 \text{ kN} \quad (\text{F.31})$$

$L_0$  can now be calculated as

$$L_0 = L - \frac{2 \cdot R_1}{q_1} = 2.0 \text{ m} \quad (\text{F.32})$$

The shear slenderness  $\lambda$  and the factor for allowed plastic rotation capacity  $k_\lambda$  is

$$\lambda = \frac{L_0}{d} = 3.6 \quad (\text{F.33})$$

$$k_\lambda = \sqrt{\frac{\lambda}{3}} = 1.1 \quad (\text{F.34})$$

The plastic rotation capacity,  $\theta_{pl}$ , for reinforcement of Class B and Class C is calculated according to Section A.5. For the front column it is calculated as

$$\theta_{plB} = 10.5 \cdot 10^{-3} \text{ rad} \quad (\text{F.35})$$

$$\theta_{plC} = 32.7 \cdot 10^{-3} \text{ rad} \quad (\text{F.36})$$

The modified values of the plastic rotation capacities,  $\theta_{rd}$ , can now be calculated as

$$\theta_{rdB} = \theta_{plB} \cdot k_\lambda = 11.5 \cdot 10^{-3} \text{ rad} \quad (\text{F.37})$$

$$\theta_{rdC} = \theta_{plC} \cdot k_\lambda = 36.1 \cdot 10^{-3} \text{ rad} \quad (\text{F.38})$$

The plastic deformation capacities,  $u_{rd}$ , can now be calculated as

$$u_{rdB} = \theta_{rdB} \cdot \frac{R_1}{q_1} = 28.8 \text{ mm} \quad (\text{F.39})$$



$$u_{rdC} = \theta_{rdC} \cdot \frac{R_1}{q_1} = 90.1 \text{ mm} \quad (\text{F.40})$$

The total deformation capacity is the sum of the elastic deformation, where  $u_1$  is calculated in equation (E.35), and the plastic deformation capacity

$$u_{rdB.tot} = u_{rdB} + u_1 = (28.8 + 11.5) \text{ mm} = 40.3 \text{ mm} \quad (\text{F.41})$$

$$u_{rdC.tot} = u_{rdC} + u_1 = (90.1 + 11.5) \text{ mm} = 101.6 \text{ mm} \quad (\text{F.42})$$

### F.3 Hand calculations of the dynamic reaction from the wall

An approximation of the size of the dynamic reaction is found by using the equivalent static load, see Section 2.8. For the elastic and plastic response the equivalent static load  $Q$  is expressed as

$$Q_{el} = I_k \omega \quad (\text{F.43})$$

$$Q_{pl} = \frac{I_k^2}{2m u_{pl}} \quad (\text{F.44})$$

where  $I_k$  is the characteristic load,  $m$  is the mass,  $\omega$  is the angular frequency and  $u_{pl}$  is the plastic deformation.

The equivalent static load provides a value of the maximum deformation of the structure and corresponds to the ultimate resistance. For the elastic and elasto-plastic response it can be described as

$$Q_{el} = k u_{el} \quad (\text{F.45})$$

$$Q_{ep} = R_m \quad (\text{F.46})$$

where

$$R_m = k u_{ep,el} \quad (\text{F.47})$$

and where  $u_{ep,el}$  is the elastic deformation in the elasto-plastic response model according to Figure 2.16.

By applying the equivalent static load on the wall the dynamic reaction is calculated for the elastic and elasto-plastic model as

$$R_{el} = \frac{Q_{el}}{2} = \frac{k u_{el}}{2} \quad (\text{F.48})$$

$$R_{ep} = \frac{Q_{ep}}{2} = \frac{R_m}{2} \quad (\text{F.49})$$

## F.4 Verification of the SDOF models

### F.4.1 Elastic model

The accuracy of the SDOF model is verified with the response obtained in a 2D FE analysis. For all types of loads the deformation obtained in the SDOF calculations agrees with the results from the 2D FE analysis, see Figure F.3 to Figure F.7. A simple check of the frequency for the two methods is also done and presented below. Parameters of the column can be found in Section F.1.2.

For the elastic response the angular frequency,  $\omega$ , of the structure is estimated to be

$$\omega = \sqrt{\frac{k_{1.c}}{m_{c.w}}} = \sqrt{\frac{20967 \cdot 10^3}{25200 \cdot 0.805}} = 32.1 \text{ rad/s} \quad (\text{F.50})$$

The frequency and periodicity is established as

$$f = \frac{\omega}{2\pi} = \frac{32.14}{2\pi} = 5.1 \text{ Hz} \quad (\text{F.51})$$

$$T = \frac{1}{f} = \frac{1}{5.11} = 0.195 \text{ s} \quad (\text{F.52})$$

A frequency of 5.1 corresponds well to the frequency obtained in the 2D FE analysis which is 5.09. The accuracy is obvious when comparing the shapes of the deformation curves from the SDOF calculations and the FE analysis, shown in Figure F.3 to Figure F.7.

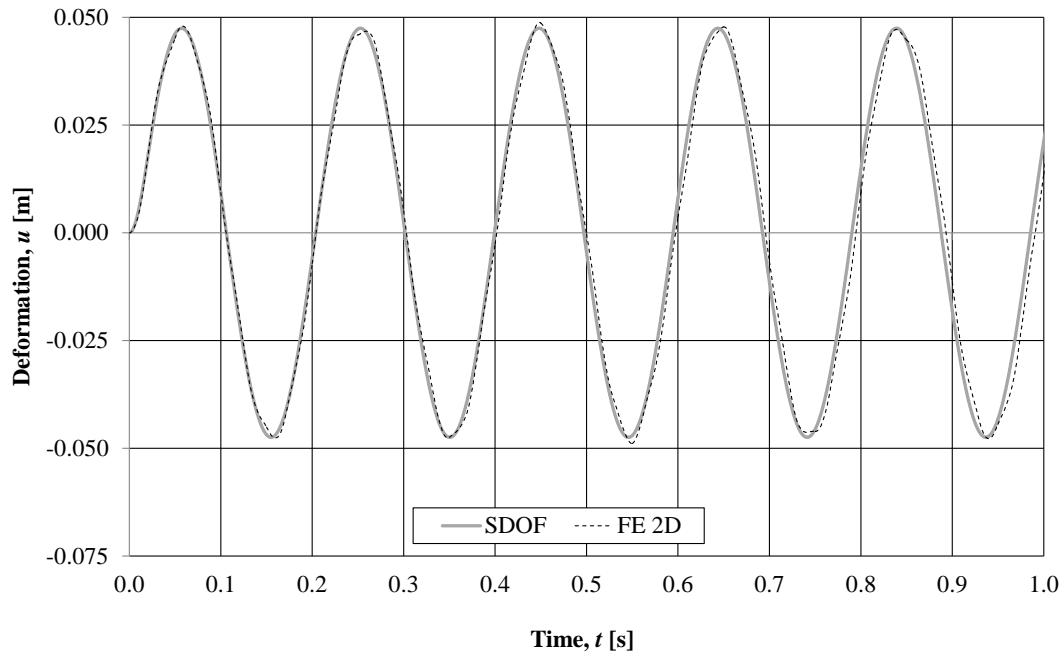


Figure F.3 The accuracy of the SDOF calculations is verified with results from the 2D FE analysis for the Direct load.

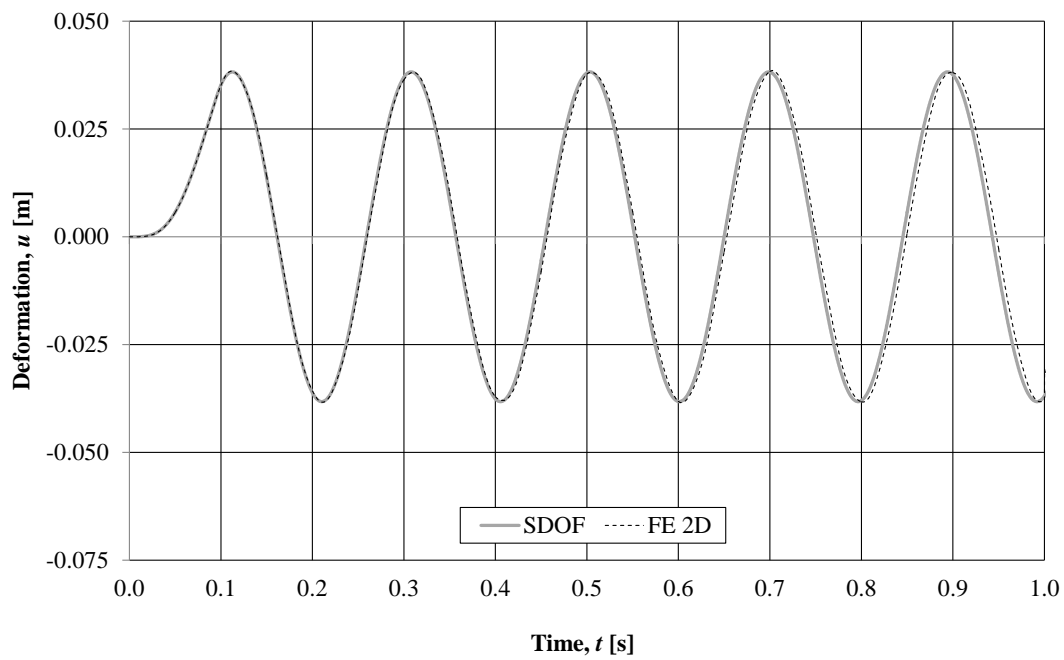


Figure F.4 The accuracy of the SDOF calculations is verified with results from the 2D FE analysis for Reaction load 1.

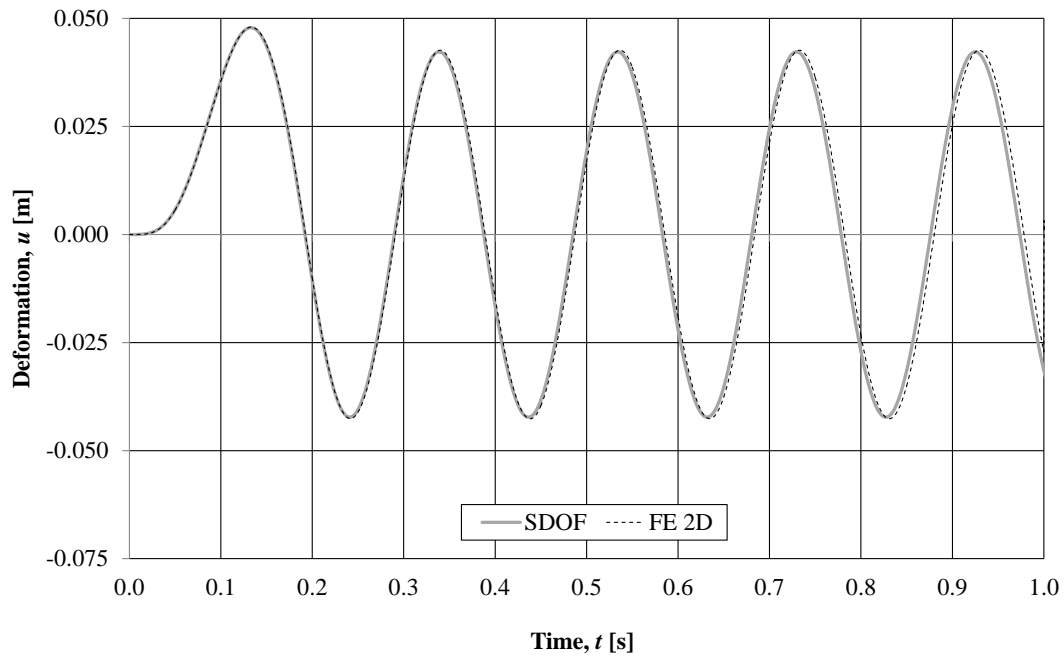


Figure F.5 The accuracy of the SDOF calculations is verified with the results from the 2D FE analysis for Reaction load 2.

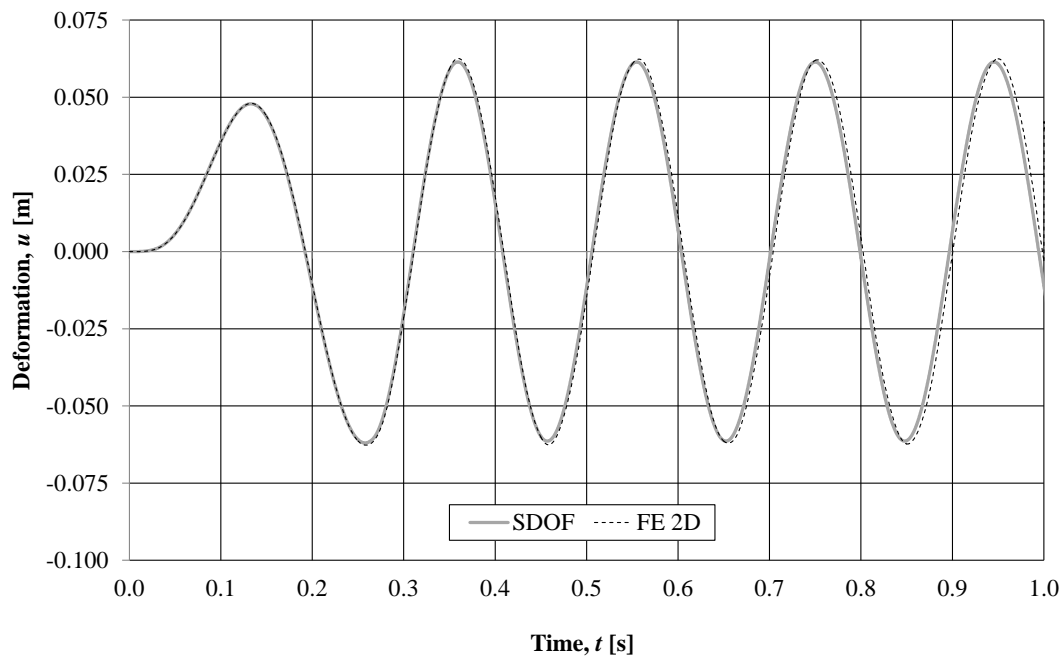


Figure F.6 The accuracy of the SDOF calculations is verified with the results from the 2D FE analysis for Reaction load 3.

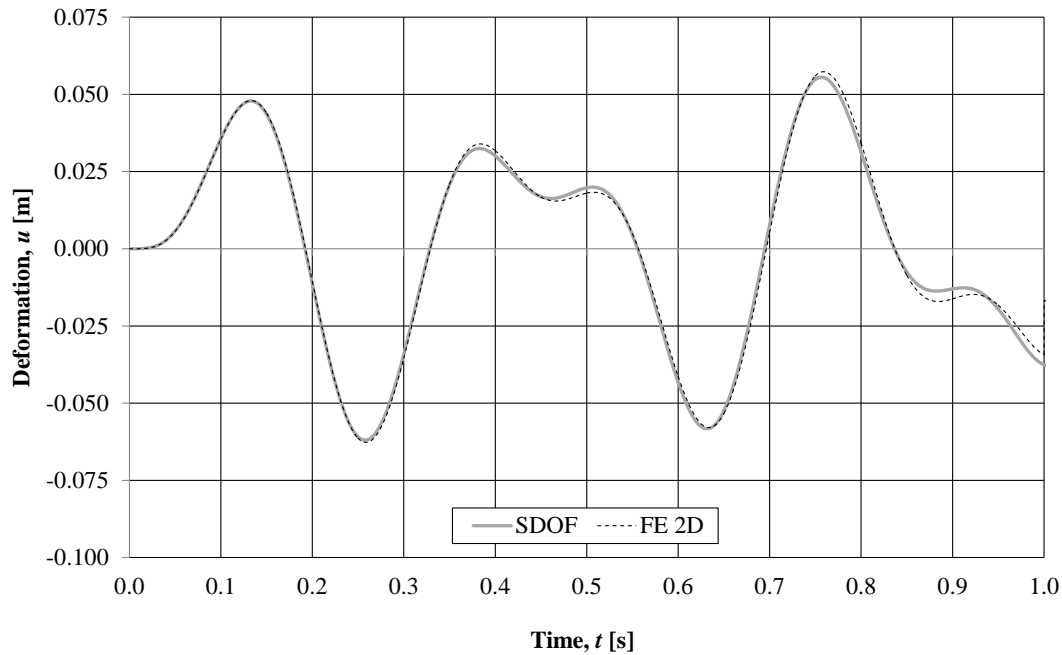


Figure F.7 The accuracy of the SDOF calculations is verified with the results from the 2D FE analysis for Reaction load 4.

#### F.4.2 Elasto-plastic model

The response obtained in the SDOF calculations is verified with the response of the same structure in the 2D FE analysis, see Figure F.8. It can be noticed that there are some divergences between the results from the two methods, both in magnitude and in frequency. A possible reason for the differences is the transformations factors applied in the SDOF system, which are plastic for the elasto-plastic calculations. Despite the fact that the structure is modelled with the elasto-plastic response curve, only the plastic transformations factors are used.

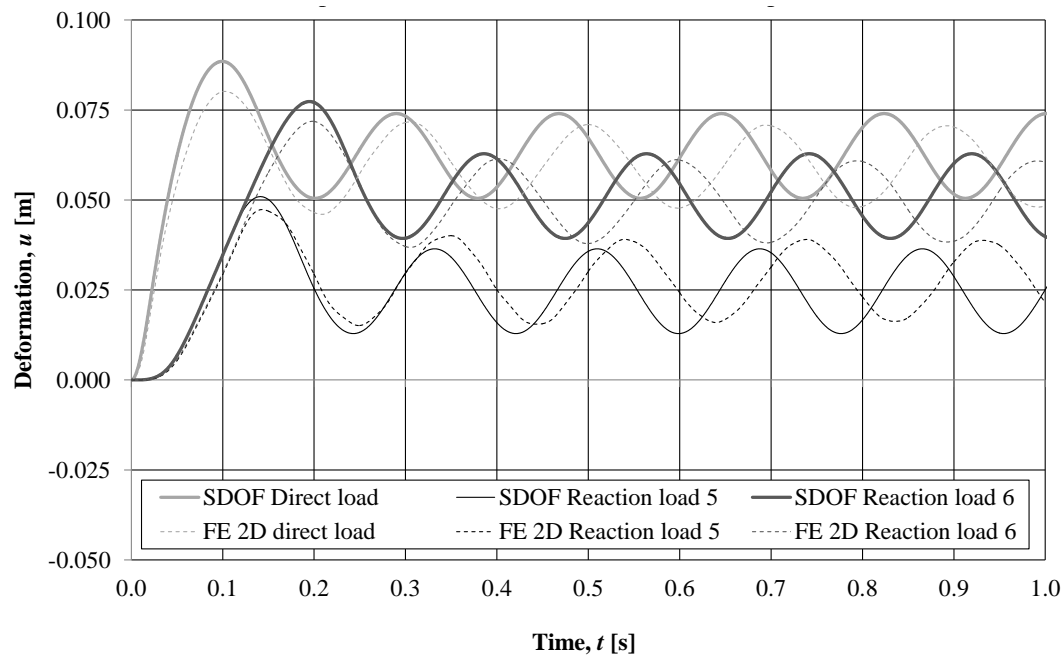


Figure F.8 The accuracy of the SDOF calculations is verified with the results from the 2D FE analysis.

## F.5 Support reactions in 3D FE analysis

### F.5.1 Elastic response

The reaction forces transferred from the wall panels to the column during the first second are presented in Figure F.10 to Figure F.16. The locations along the column are chosen according to Figure 5.45. The reactions are compared to the reaction from a simply supported beam with the same dimensions and parameters as the wall.

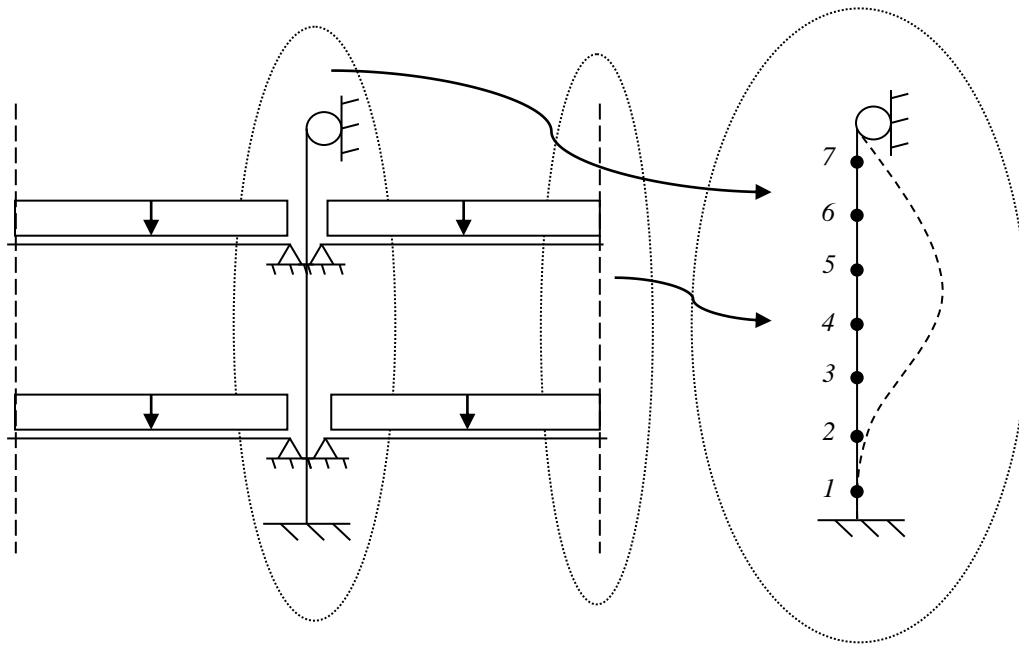


Figure F.9 The deformations and reaction forces are measured at different points along the column.

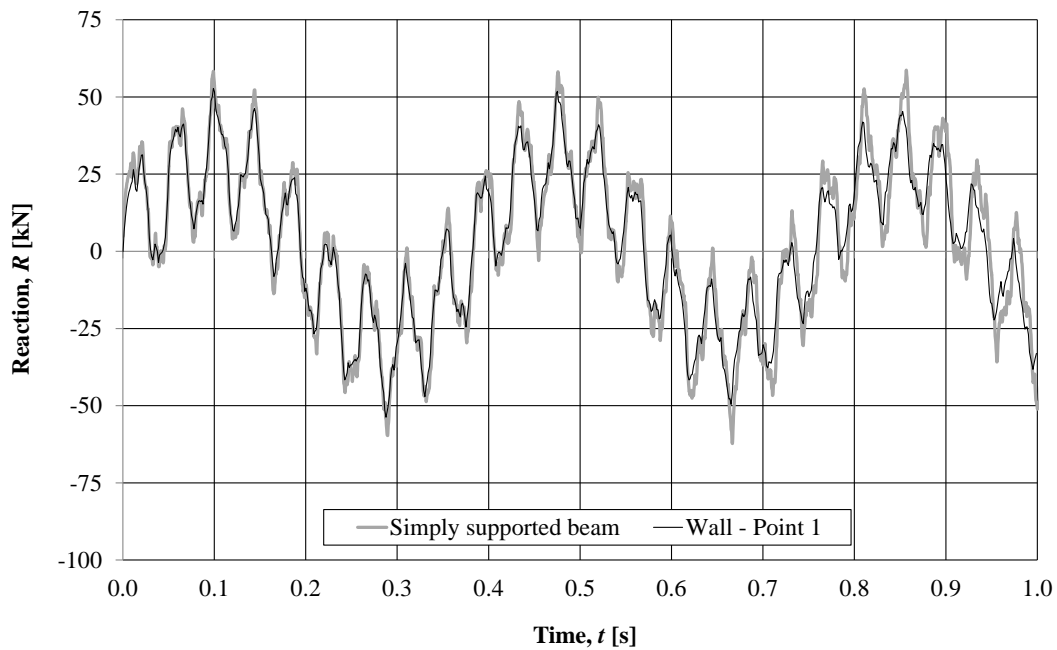


Figure F.10 A comparison of the reaction forces from a simply supported beam and the reaction transferred from the wall panel to the column at Point 1.

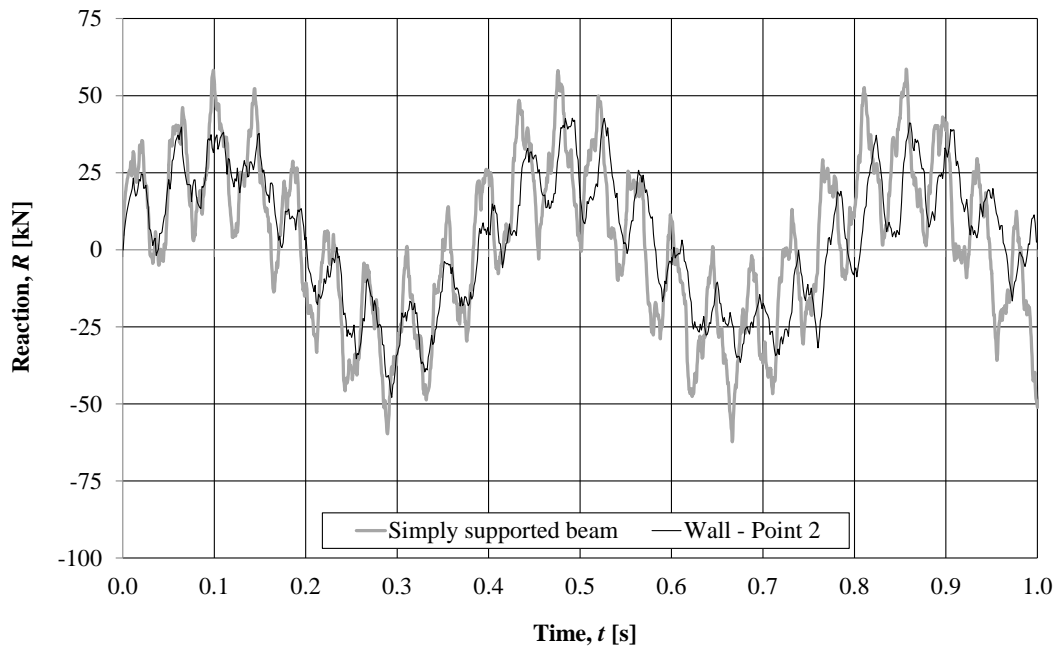


Figure F.11 A comparison of the reaction forces from a simply supported beam and the reaction transferred from the wall panel to the column at Point 2.

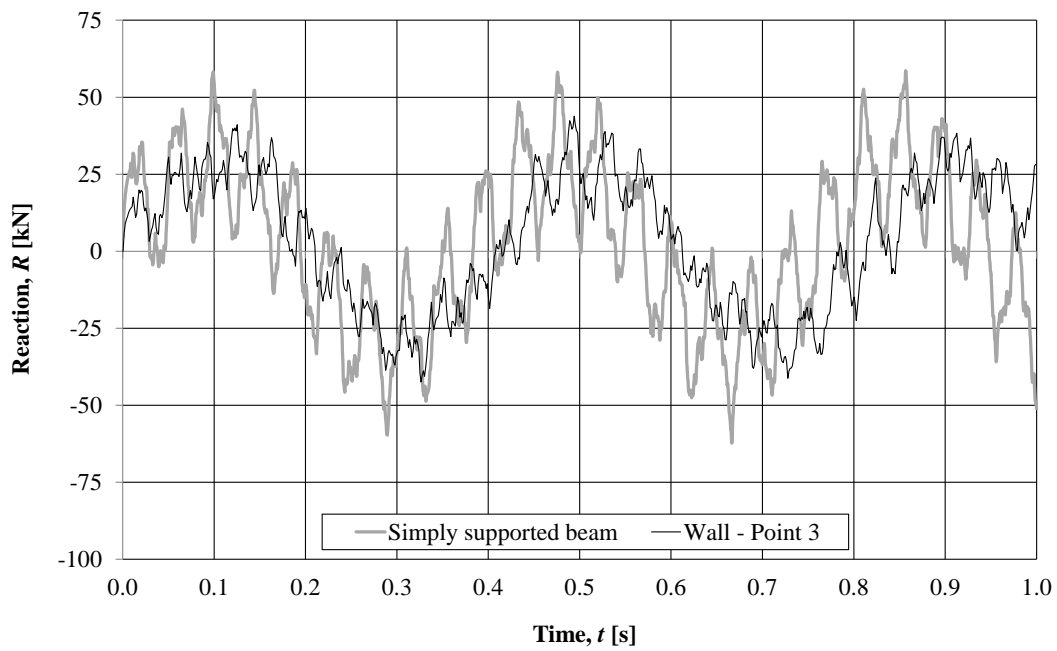


Figure F.12 A comparison of the reaction forces from a simply supported beam and the reaction transferred from the wall panel to the column at Point 3.



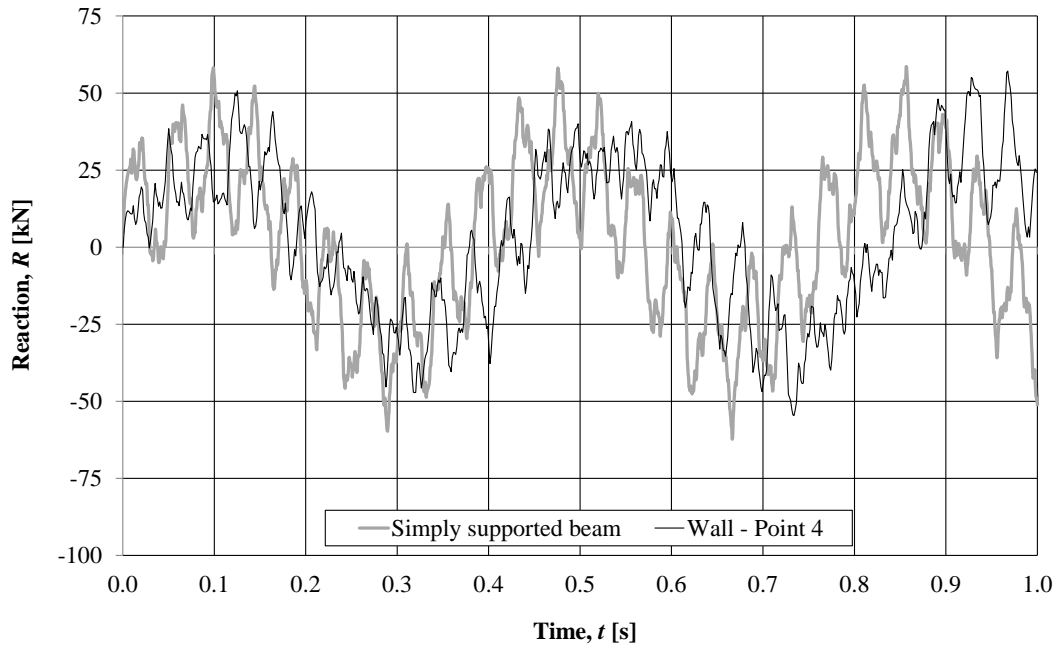


Figure F.13 A comparison of the reaction forces from a simply supported beam and the reaction transferred from the wall panel to the column at Point 4.

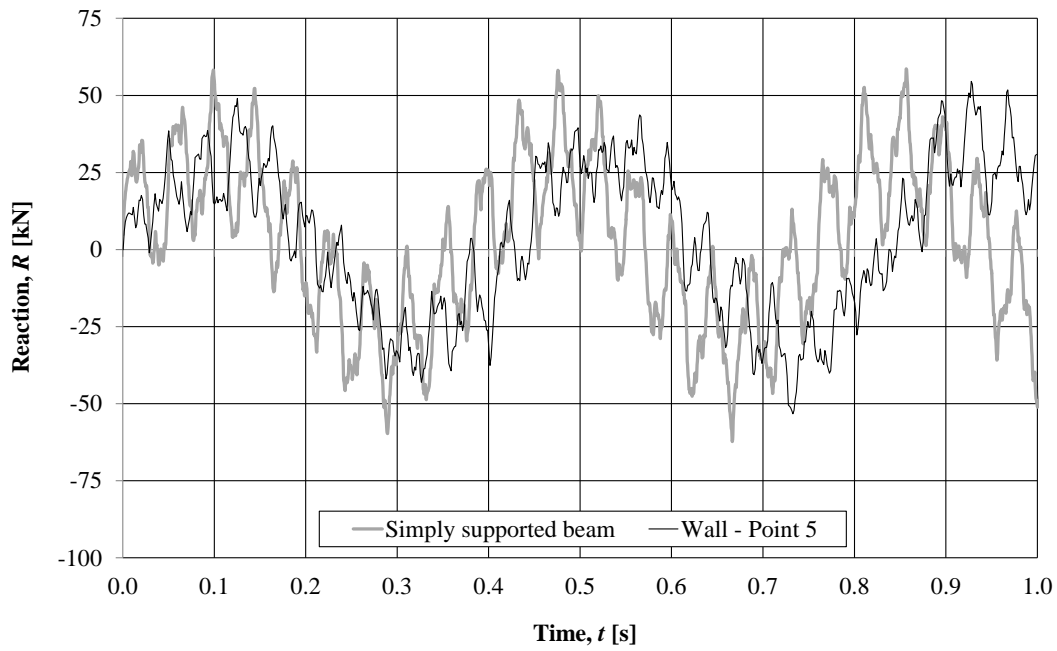


Figure F.14 A comparison of the reaction forces from a simply supported beam and the reaction transferred from the wall panel to the column at Point 5.

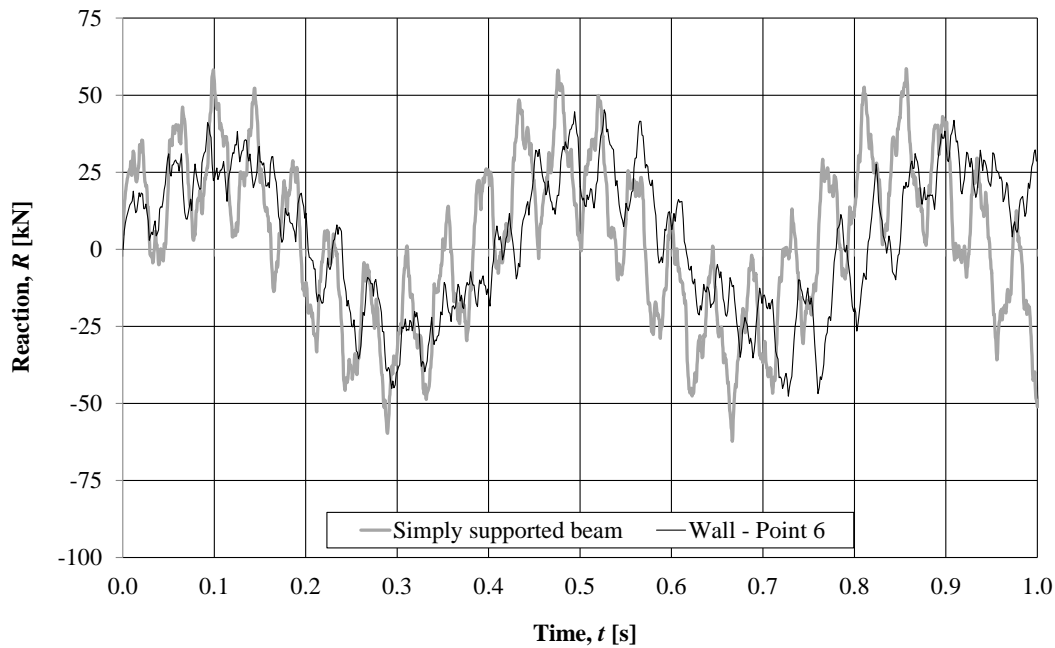


Figure F.15 A comparison of the reaction forces from a simply supported beam and the reaction transferred from the wall panel to the column at Point 6.

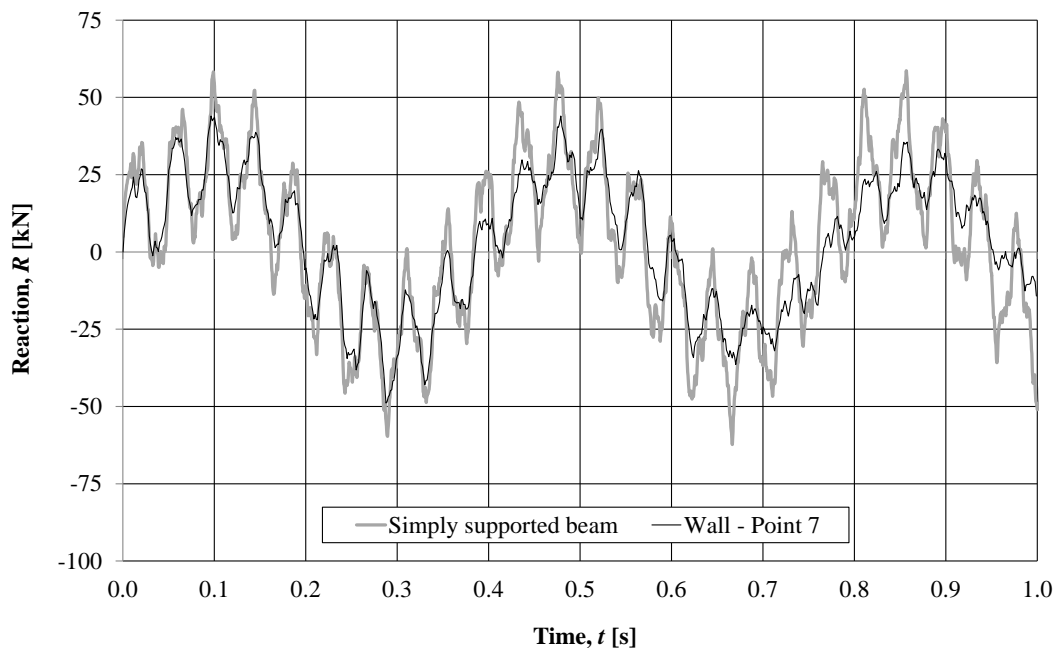


Figure F.16 A comparison of the reaction forces from a simply supported beam and the reaction transferred from the wall panel to the column at Point 7.

## F.5.2 Elasto-plastic response

The reactions that are induced at the wall supports and transferred to the column are presented in Figure F.17 to Figure F.23. The studied points along the column are illustrated in Figure 5.45. The reactions are compared to the reaction from a simply supported beam with the same dimensions and parameters as the wall in a frame structure.

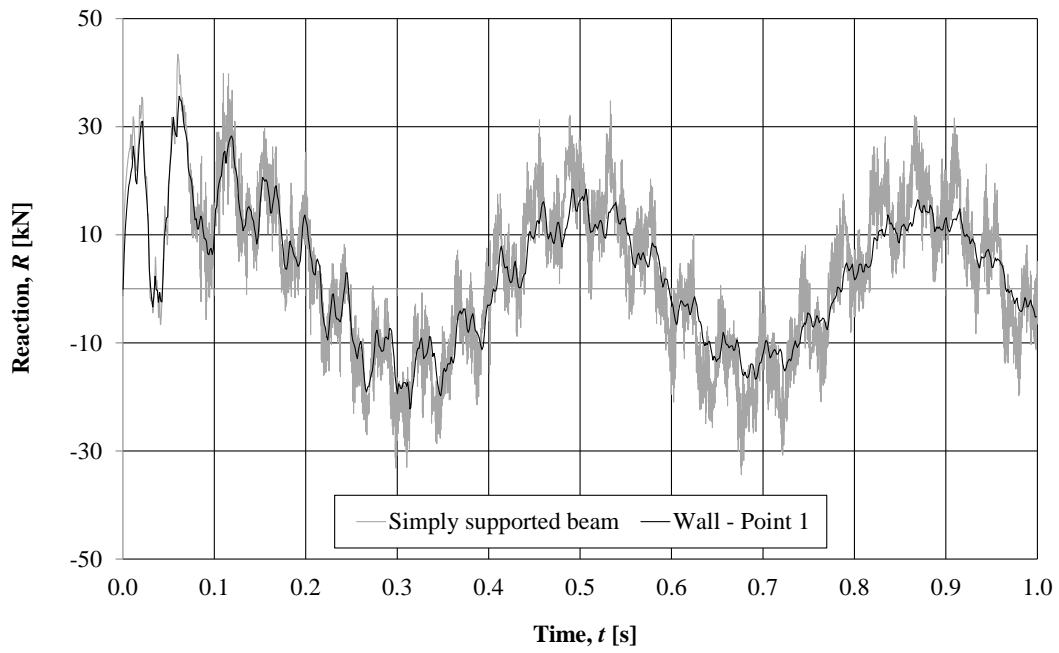


Figure F.17 A comparison of reaction forces from a simply supported beam and the reaction transferred from the wall panel to the column at Point 1.

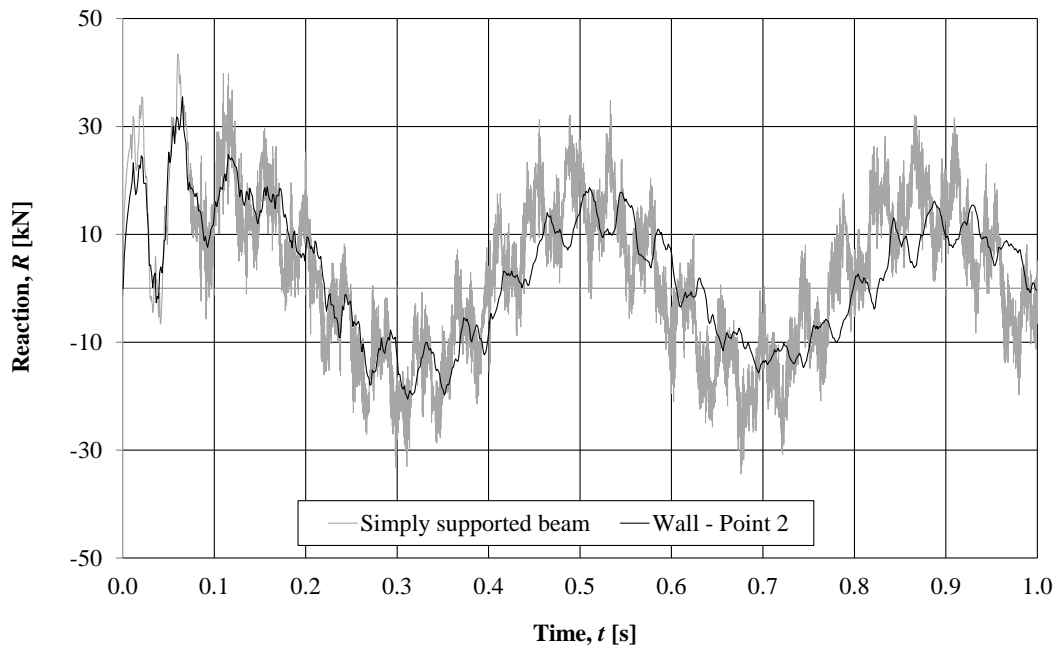


Figure F.18 A comparison of reaction forces from a simply supported beam and the reaction transferred from the wall panel to the column at Point 2.

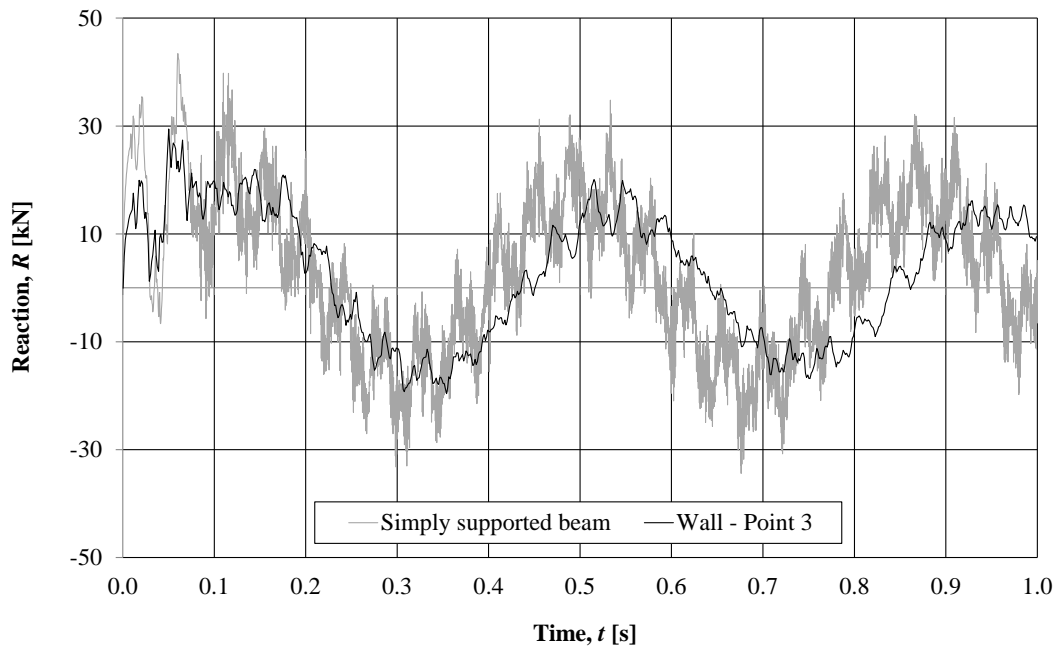


Figure F.19 A comparison of reaction forces from a simply supported beam and the reaction transferred from the wall panel to the column at Point 3.

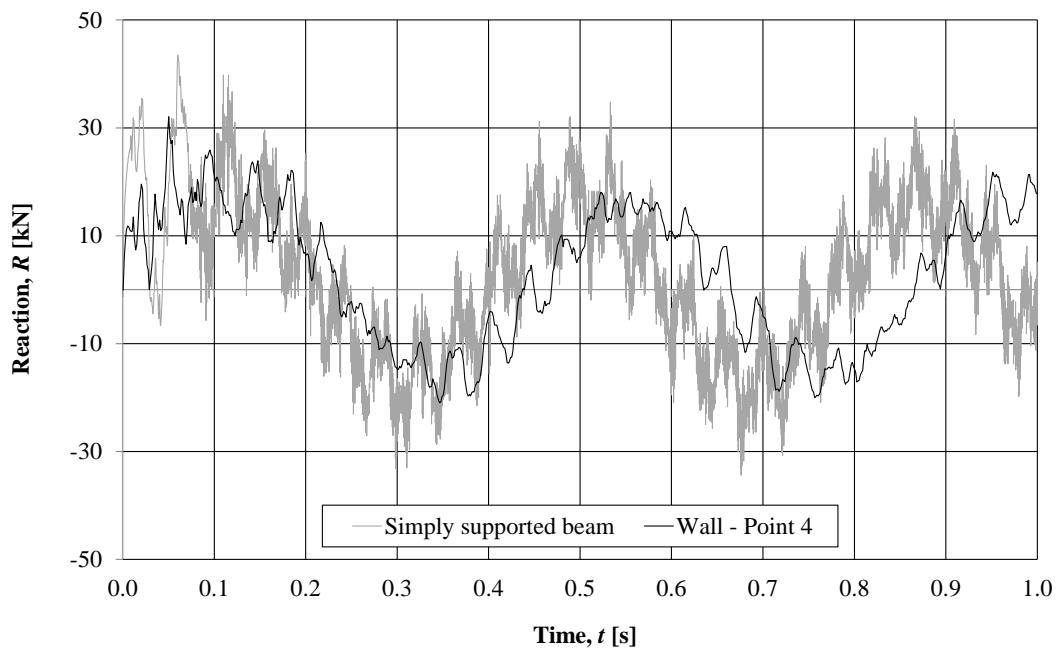


Figure F.20 A comparison of reaction forces from a simply supported beam and the reaction transferred from the wall panel to the column at Point 4.

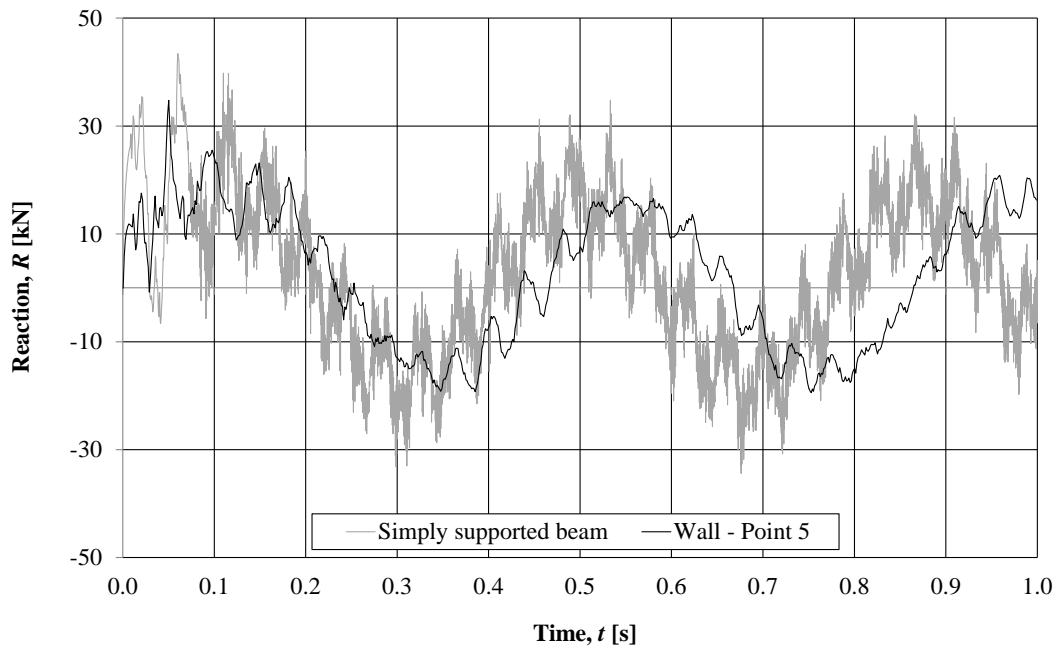


Figure F.21 A comparison of reaction forces from a simply supported beam and the reaction transferred from the wall panel to the column at Point 5.

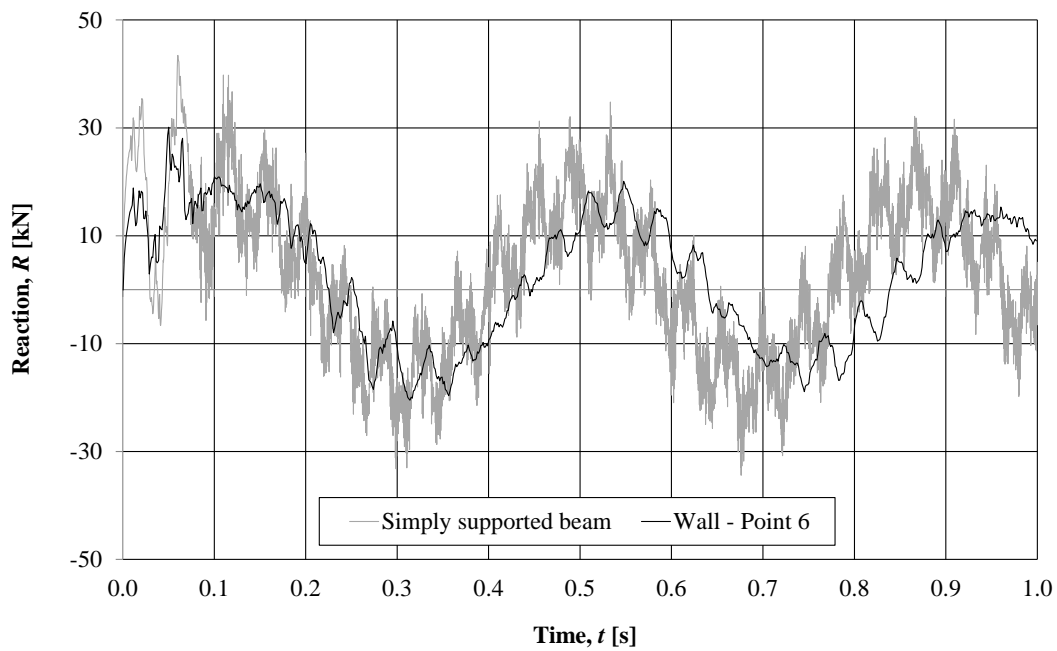


Figure F.22 A comparison of reaction forces from a simply supported beam and the reaction transferred from the wall panel to the column at Point 6.

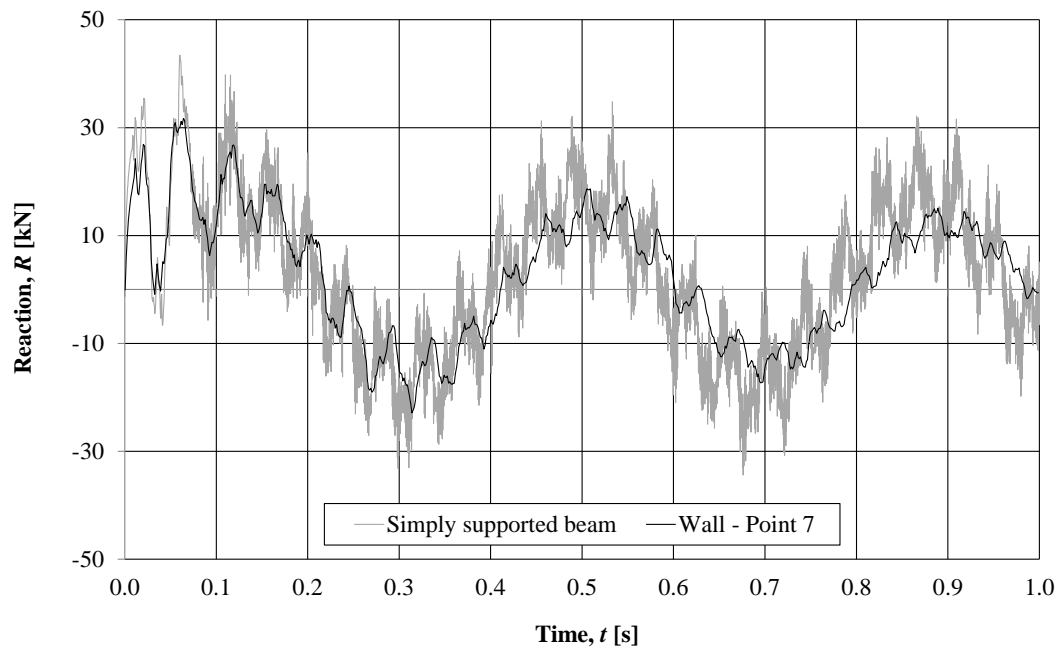


Figure F.23 A comparison of reaction forces from a simply supported beam and the reaction transferred from the wall panel to the column at Point 7.

## **APPENDIX G      Parametric study of 3D structure**

### **G.1    Orientation**

In this appendix additional graphs are presented for the parametric study of the 3D structure where the stiffness and internal resistance is varied for the elastic and elasto-plastic case, respectively. The results of the case with unchanged stiffness,  $k_u$ , and unchanged internal resistance,  $R_{m,u}$ , are presented calculated according to equation (F.6) and (F.11), respectively.

For the elastic model, two cases of stiffnesses of the wall are considered. The first one is stiffness  $k_d$  which corresponds to the stiffness used in the previous study decreased with a factor 4. The second case is stiffness  $k_i$  which is 4 times larger than  $k_u$ . The values of these parameters can be found in Table 5.16 and Figure 5.55.

For the elastio-plastic model, two cases of resistance of the wall are considered here which corresponds to the resistance from the previous study decreased and increased with a factor 2,  $R_{m,d}$  and  $R_{m,i}$ , respectively. The values of these parameters can be found in Table 5.18 and Figure 5.71.

### **G.2    Verification of SDOF model**

#### **G.2.1    Elastic response**

##### **G.2.1.1    Decreased stiffness of the wall**

The accuracy of the SDOF model is verified with the response obtained in the 2D FE analysis, see Figure G.1 to Figure G.4. For all types of loads the deformation obtained in the SDOF calculations agrees well with the results from 2D FE analysis.

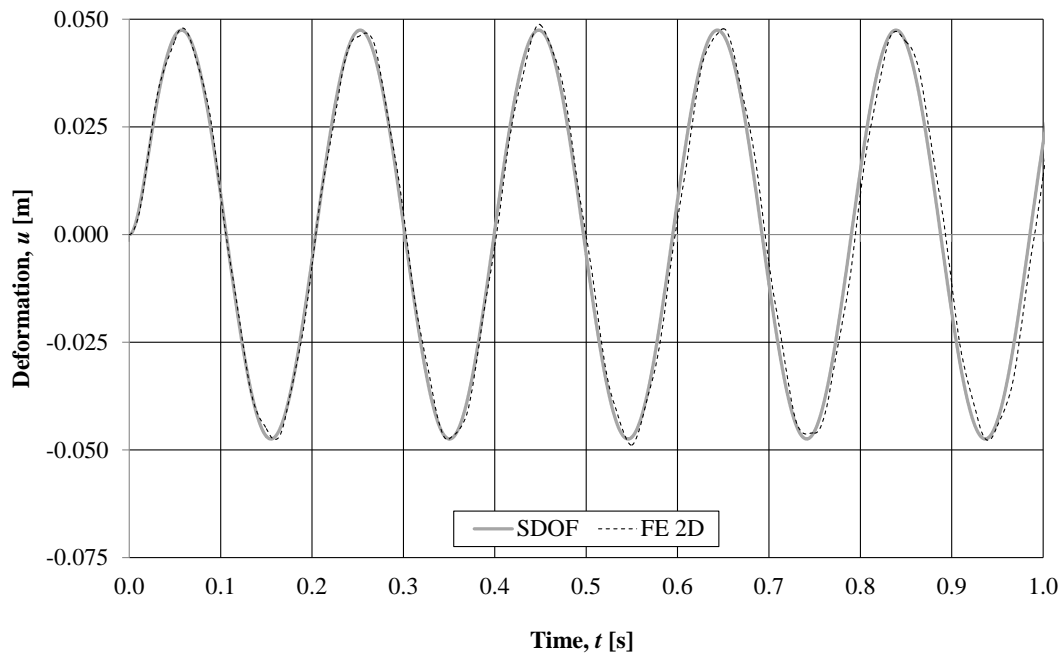


Figure G.1 The accuracy of the SDOF calculations is verified with results from the 2D FE analysis for the Direct load.

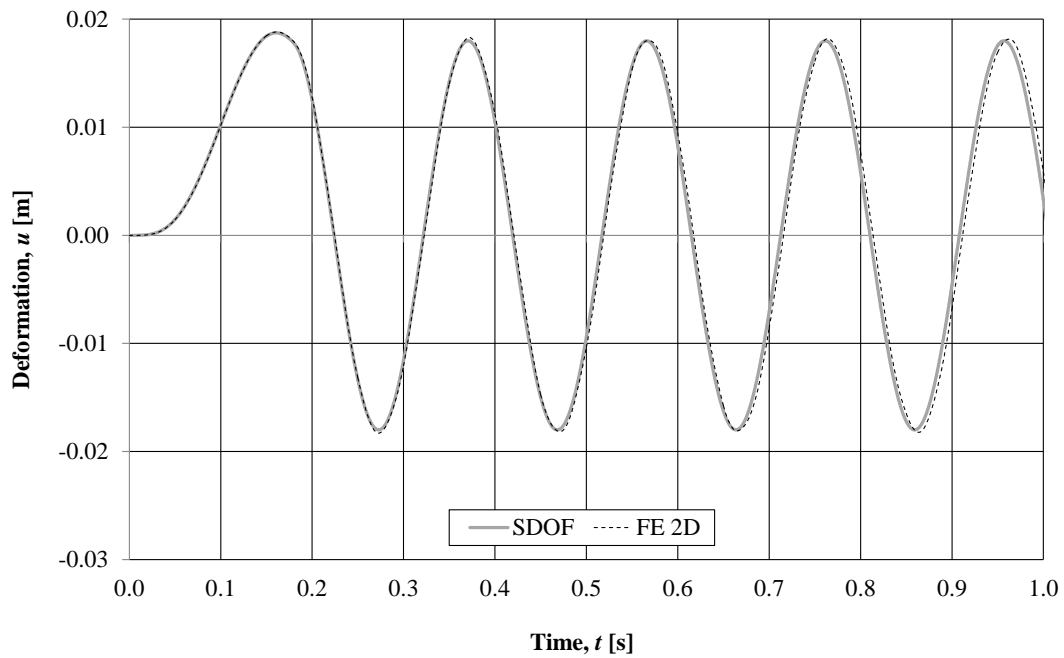


Figure G.2 The accuracy of the SDOF calculations is verified with results from the 2D FE analysis for Reaction load 1.



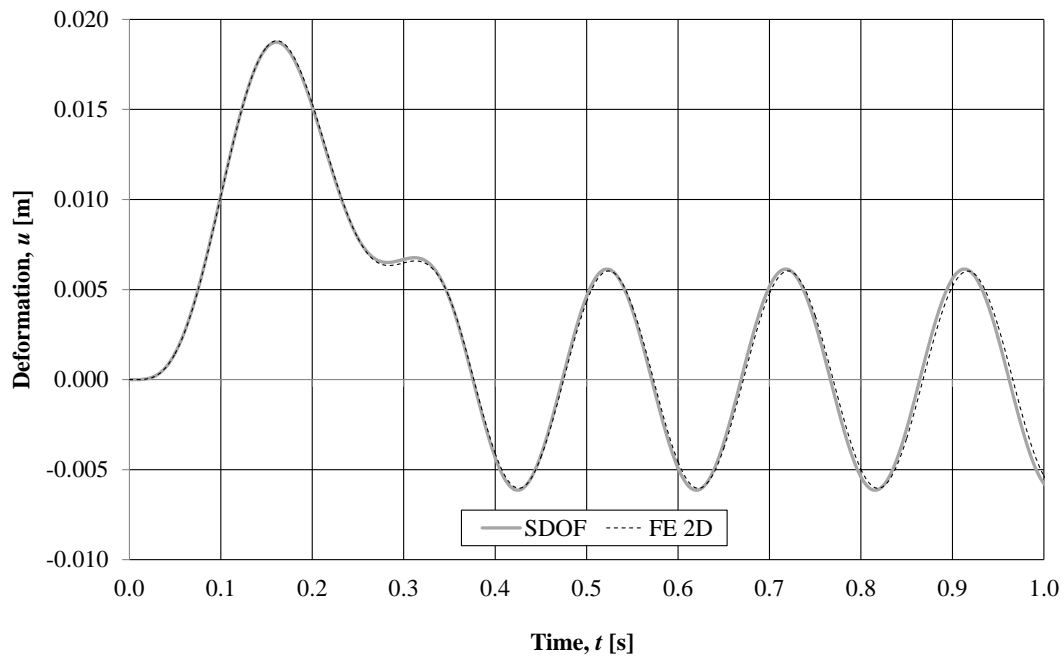


Figure G.3 The accuracy of the SDOF calculations is verified with results from the 2D FE analysis for Reaction load 2.

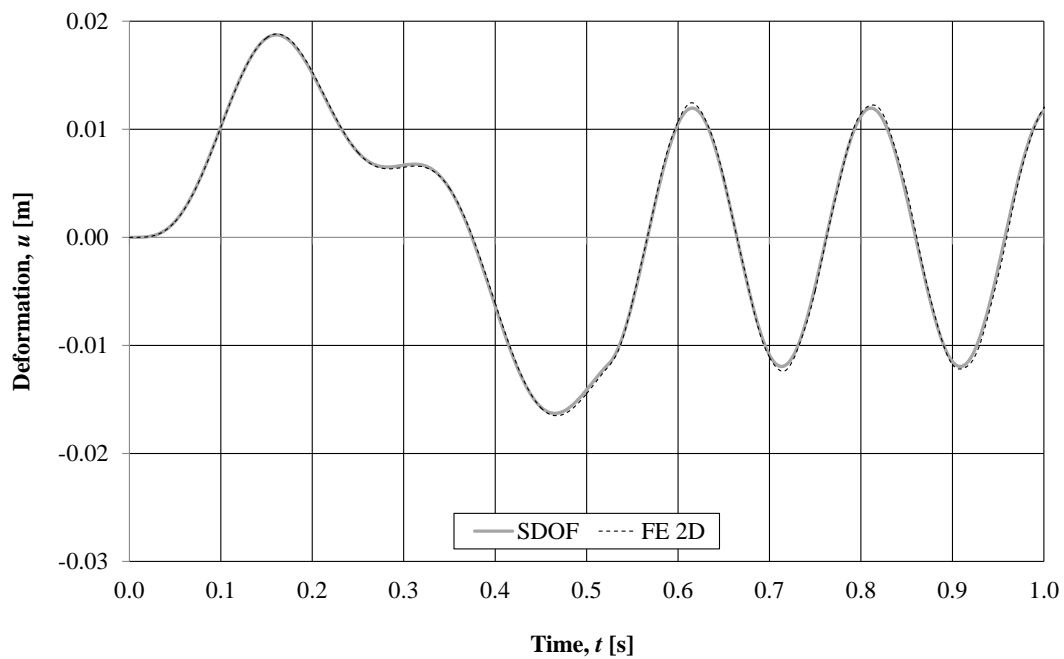


Figure G.4 The accuracy of the SDOF calculations is verified with results from the 2D FE analysis for Reaction load 3.

### G.2.1.2 Increased stiffness of the wall

The SDOF model is verified with the response obtained in the 2D FE analysis, see Figure G.5 to Figure G.8. For all types of loads the deformation obtained in the SDOF calculations agrees well with the results from 2D FE analysis.

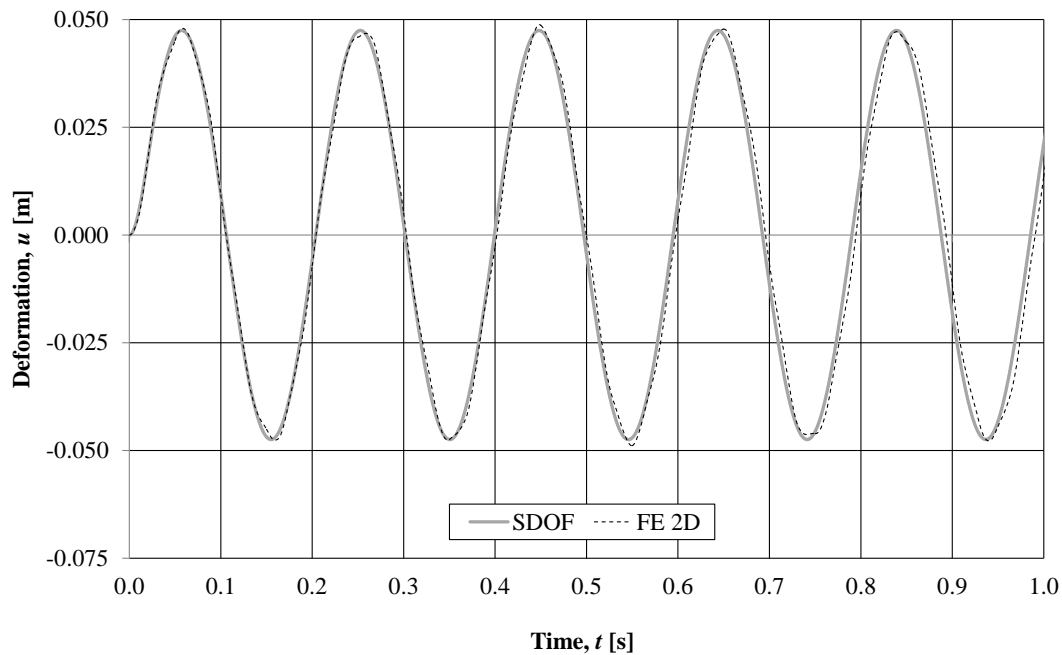


Figure G.5 The accuracy of the SDOF calculations is verified with results from the 2D FE analysis for the Direct load.

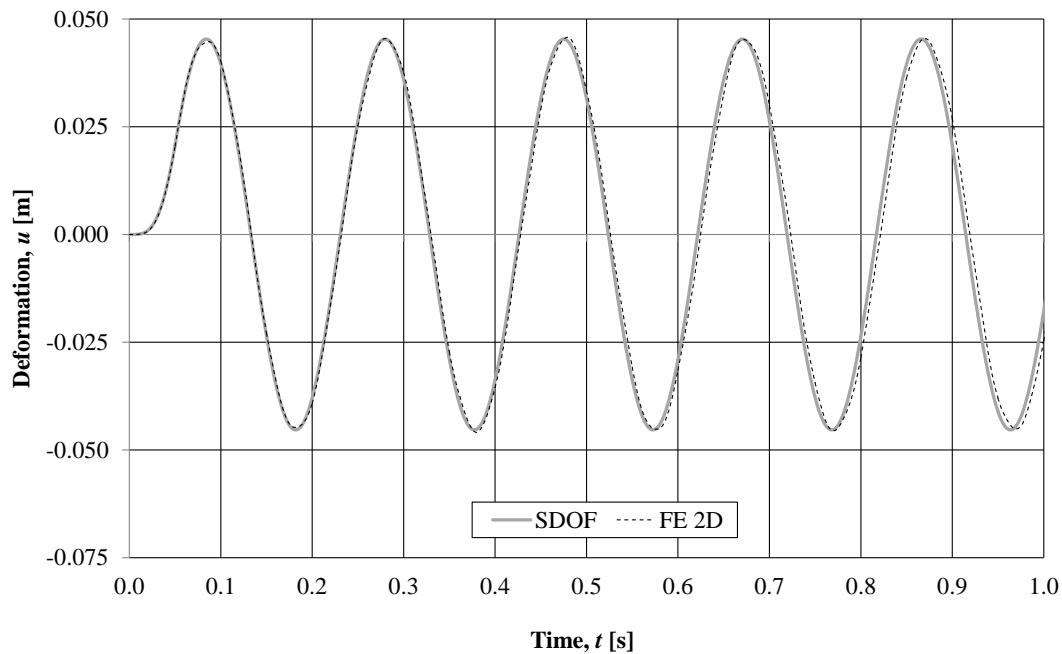


Figure G.6 The accuracy of the SDOF calculations is verified with results from the 2D FE analysis for Reaction load 1.

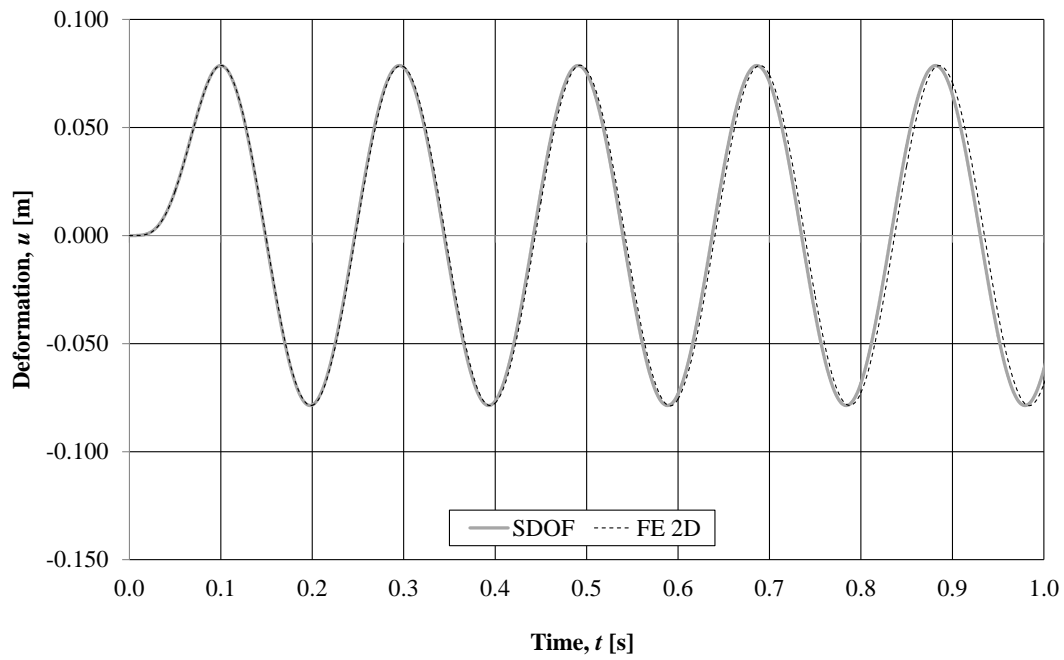


Figure G.7 The accuracy of the SDOF calculations is verified with results from the 2D FE analysis for Reaction load 2.

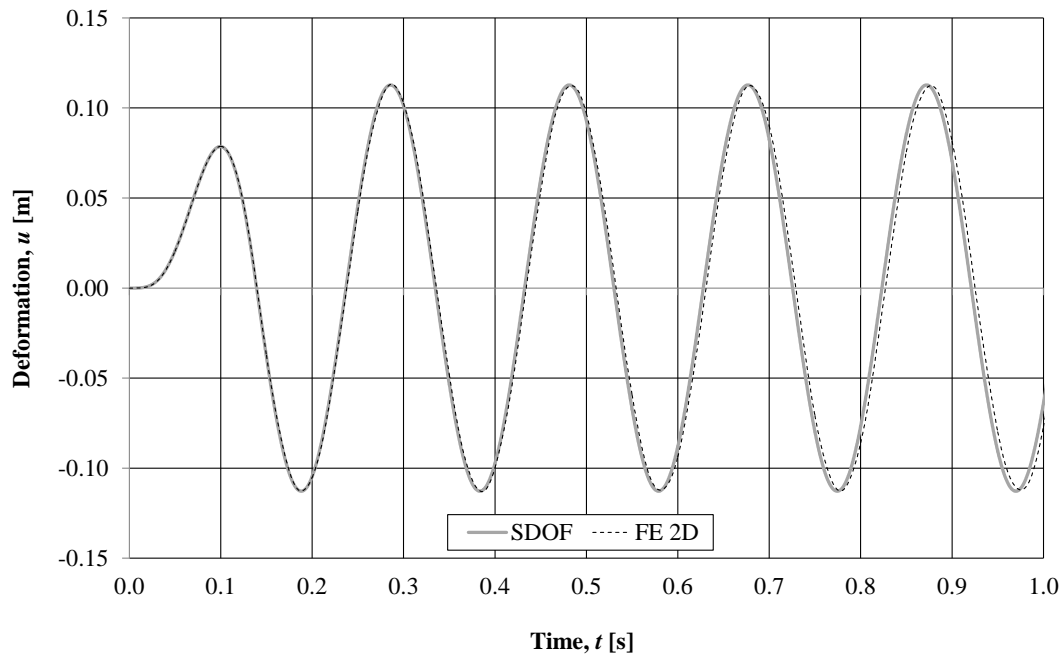


Figure G.8 The accuracy of the SDOF calculations is verified with results from the 2D FE analysis for Reaction load 3.

## G.2.2 Elasto-plastic response

### G.2.2.1 Decreased internal resistance of the wall

The SDOF model is verified with the response obtained in the 2D FE analysis, see Figure G.9. For all types of loads the deformation obtained in the SDOF calculations is similar to the results from the 2D FE analysis. However, the elasto-plastic results do not correspond as well as the elastic results.

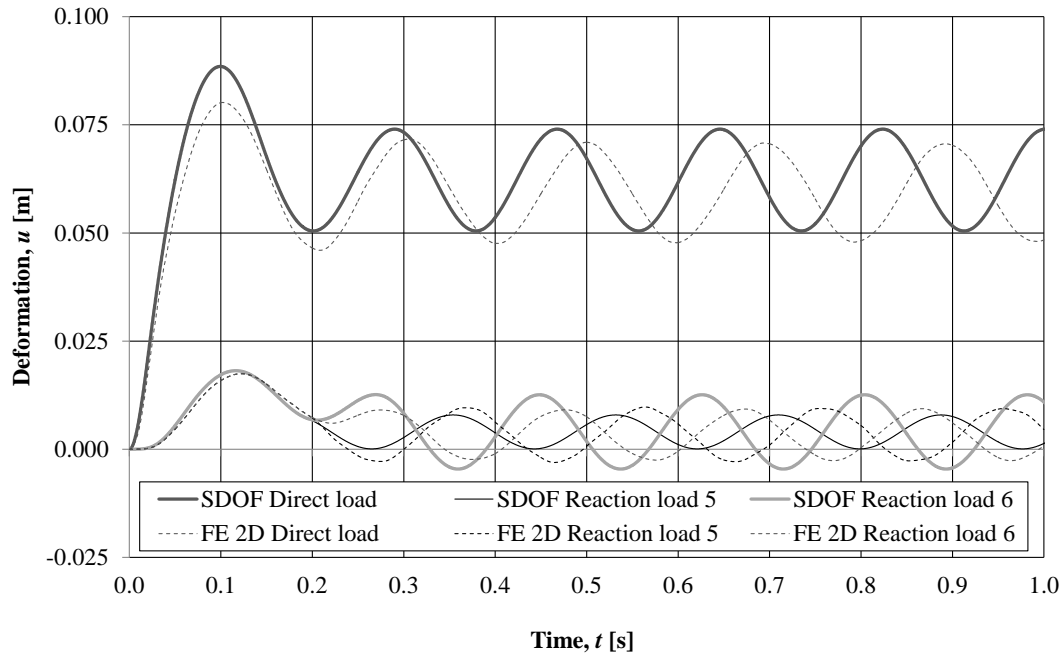


Figure G.9 The accuracy of the SDOF calculations is verified with the results from the 2D FE analysis for the Direct load, Reaction load 5 and Reaction load 6.

### G.2.2.2 Increased internal resistance of the wall

The SDOF model is verified with the response obtained in the 2D FE analysis, see Figure G.10. For all types of loads the deformation obtained in the SDOF calculations is similar to the results from the 2D FE analysis. However, the elasto-plastic results do not correspond as well as the elastic.

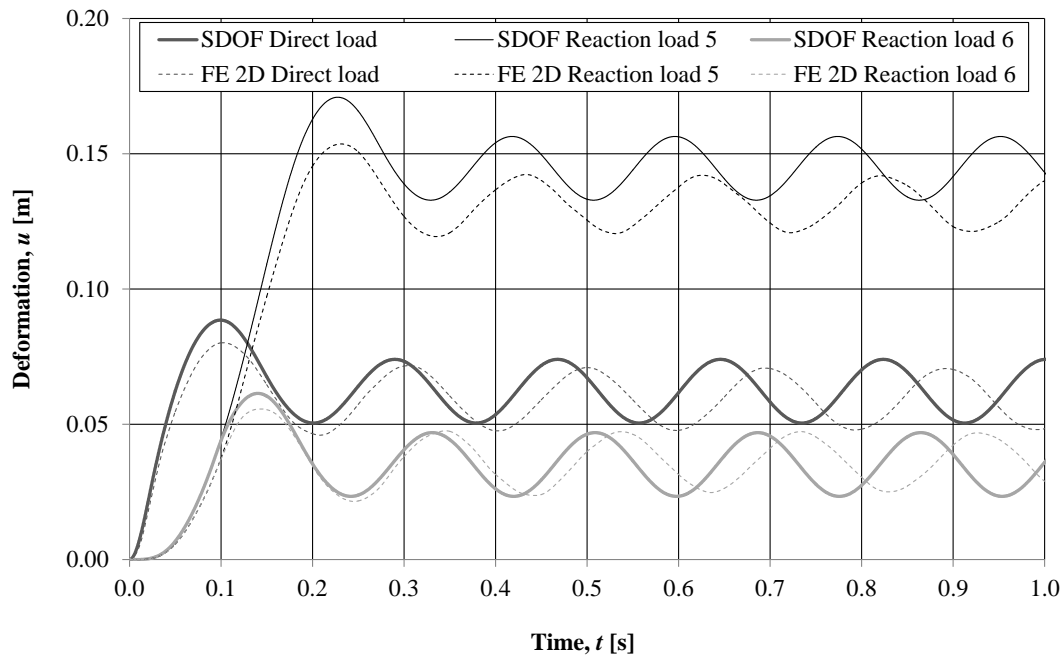


Figure G.10 The accuracy of the SDOF calculations is verified with the results from the 2D FE analysis for the Direct load, Reaction load 5 and Reaction load 6.

### G.3 Comparison of deformation in SDOF and 3D FE analysis

#### G.3.1 Elastic response

##### G.3.1.1 Decreased stiffness of the wall

The deformation of the column for the different loads in the SDOF model is compared to the deformations of the 3D FE model, see Figure G.11 to Figure G.14.

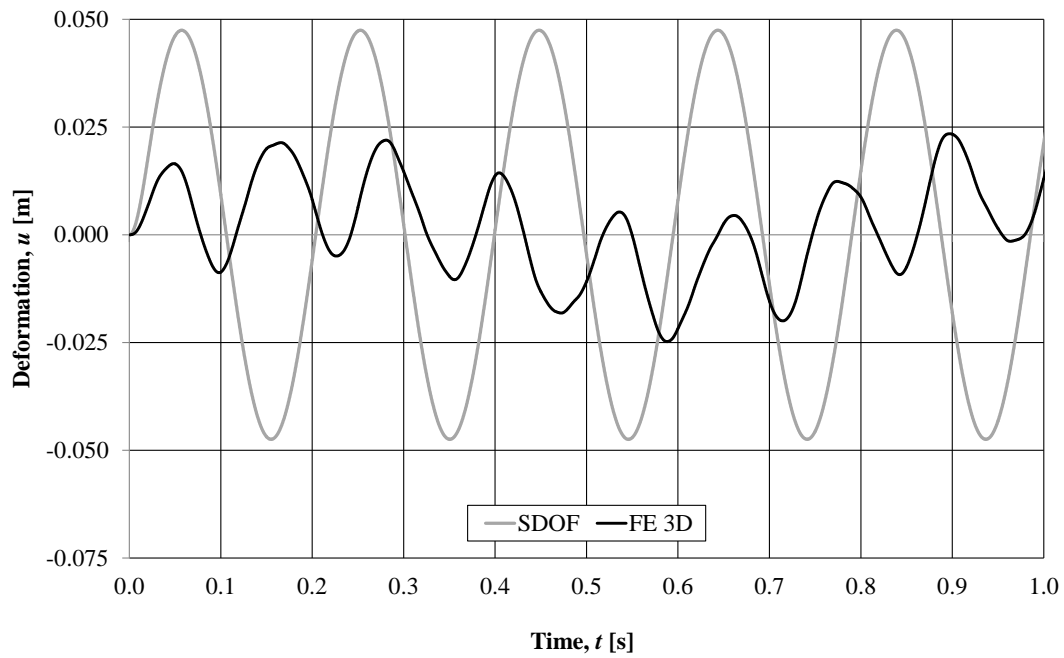


Figure G.11 Comparison of the deformation in the middle of the column obtained in the 3D FE analysis and in the SDOF analysis for the Direct load.

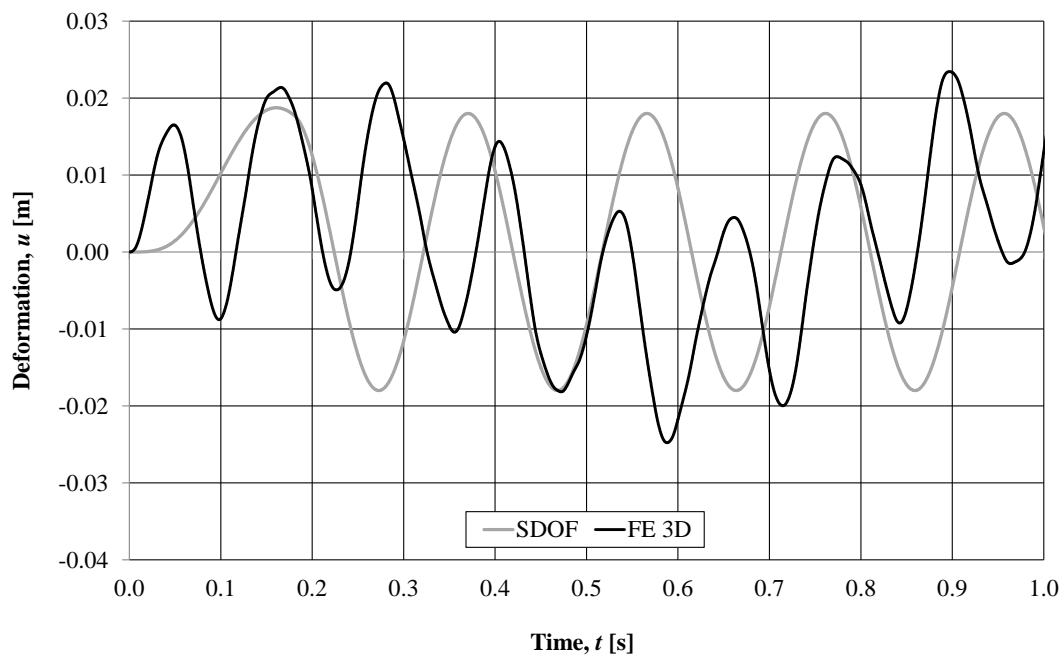


Figure G.12 Comparison of the deformation in the middle of the column obtained in the 3D FE analysis and in the SDOF calculations for Reaction load 1.

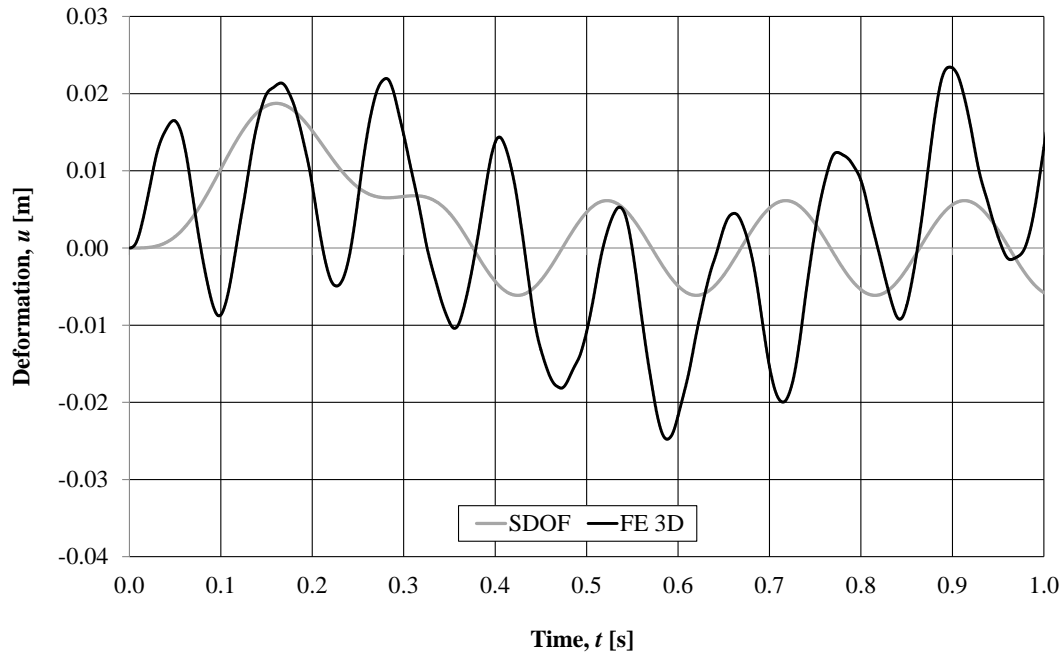


Figure G.13 Comparison of the deformation in the middle of the column obtained in the 3D FE analysis and in the SDOF calculations for Reaction load 2.

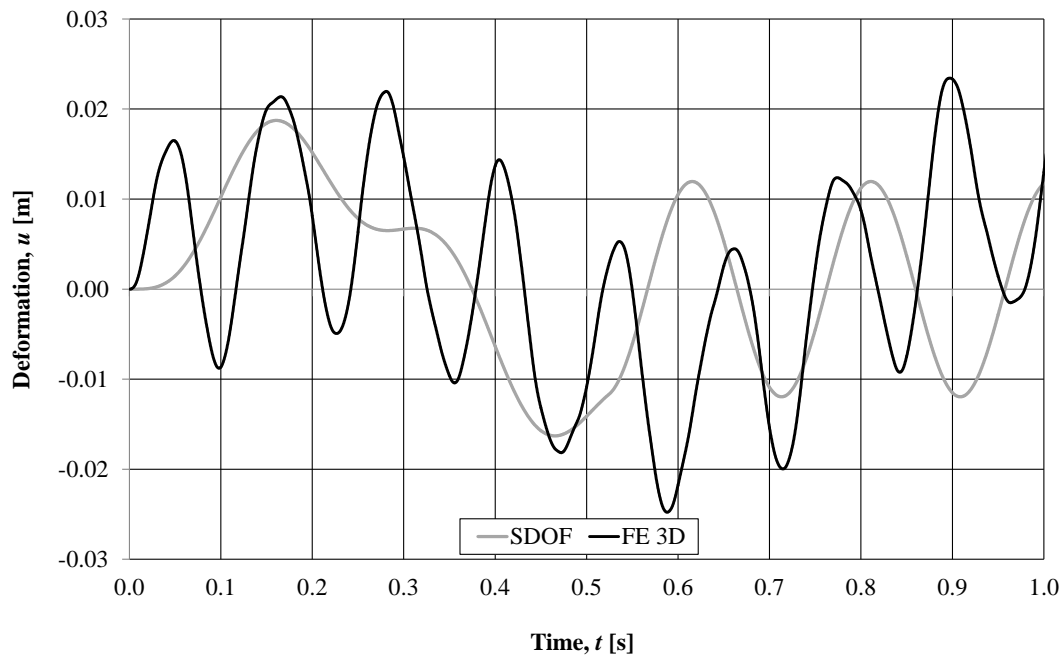


Figure G.14 Comparison of the deformation in the middle of the column obtained in the 3D FE analysis and in the SDOF calculations for Reaction load 3.

### G.3.1.2 Increased stiffness of the wall

The deformation of the column for the different loads in the SDOF calculations is compared to the deformations of the 3D FE model.

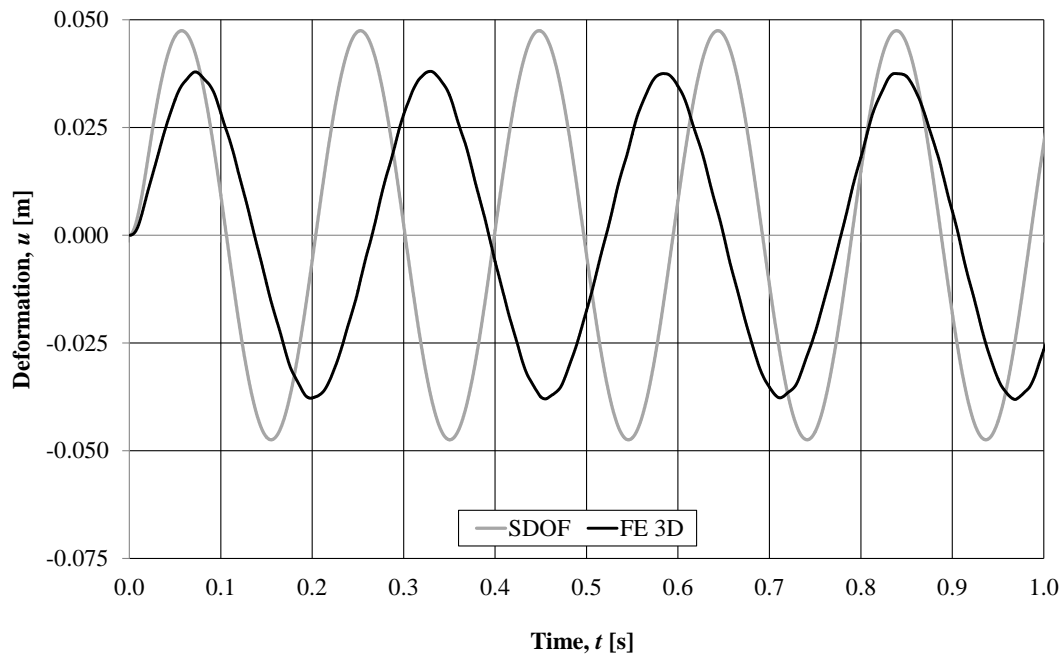


Figure G.15 Comparison of the deformation in the middle of the column obtained in the 3D FE analysis and in the SDOF analysis for the Direct load.

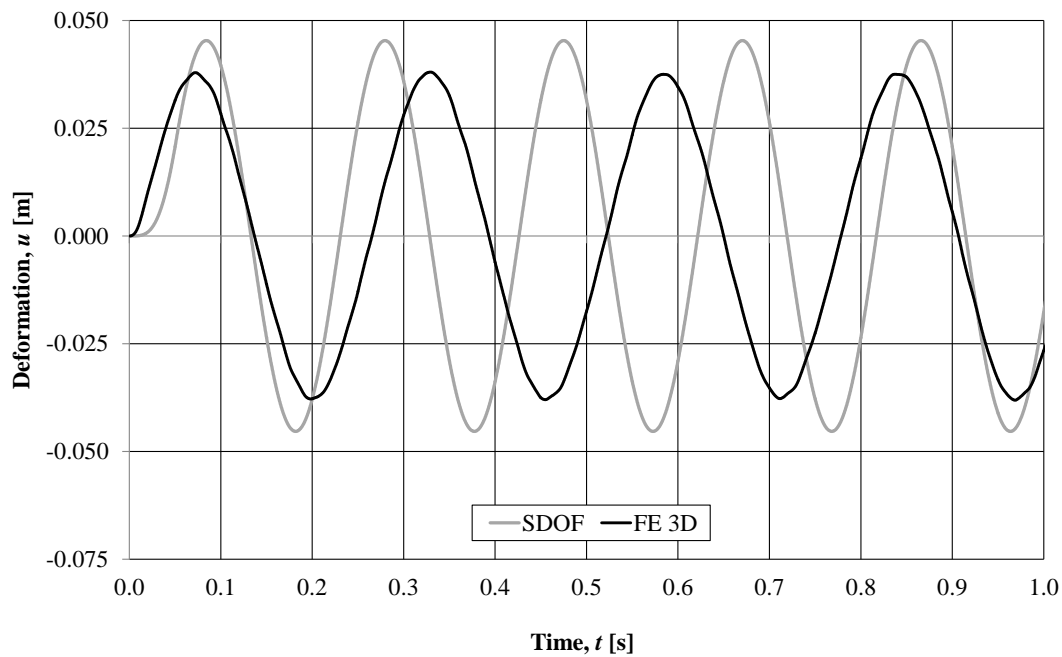


Figure G.16 Comparison of the deformation in the middle of the column obtained in the 3D FE analysis and in the SDOF calculations for Reaction load 1.



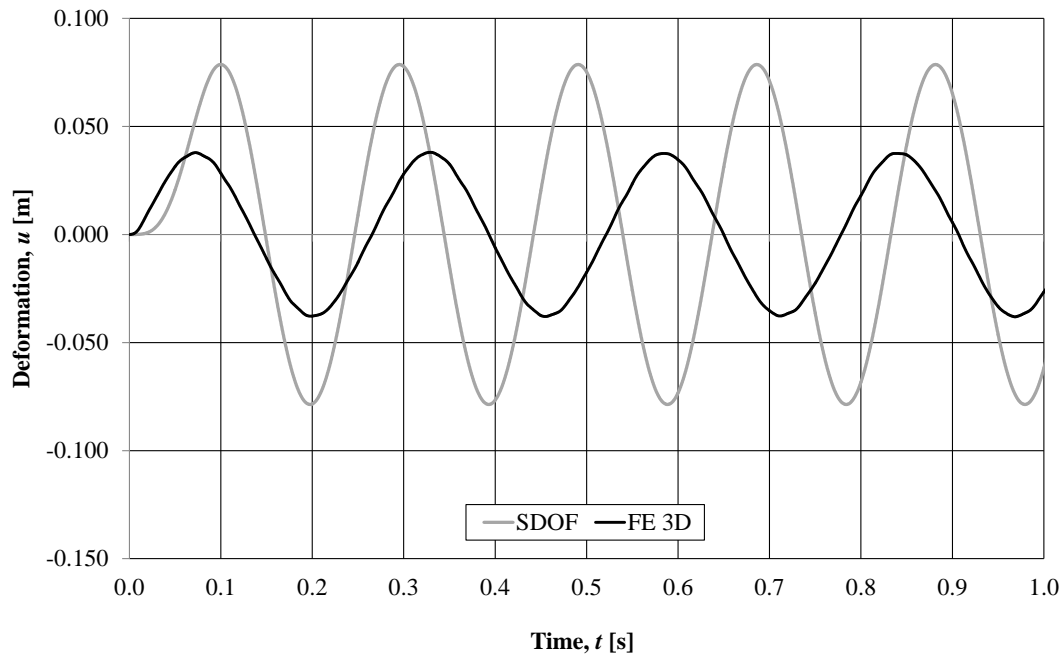


Figure G.17 Comparison of the deformation in the middle of the column obtained in the 3D FE analysis and in the SDOF calculations for Reaction load 2.

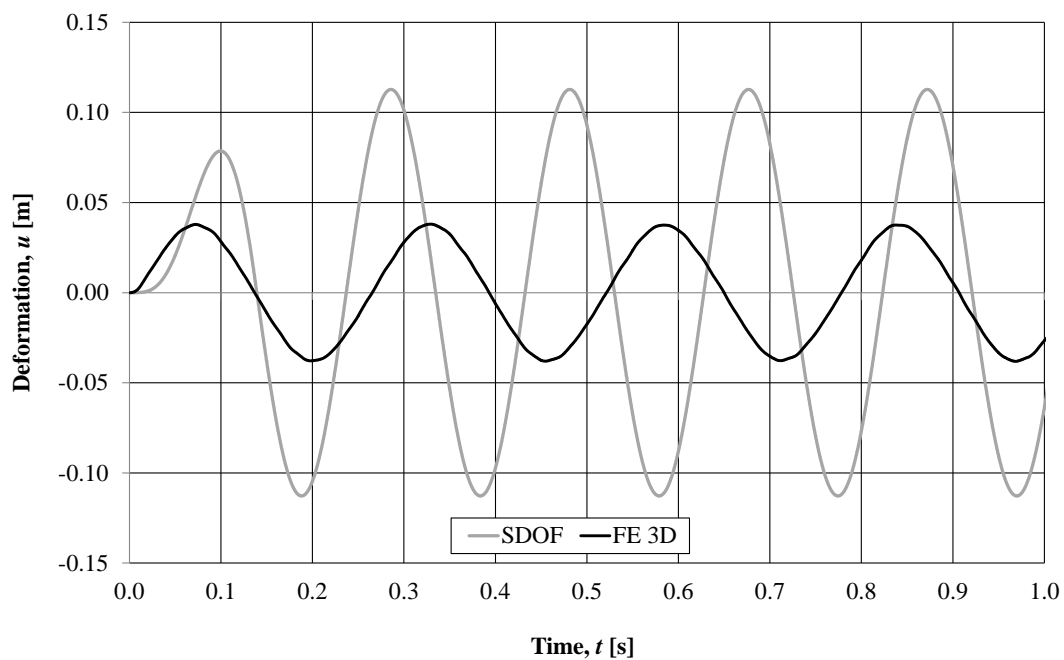


Figure G.18 Comparison of the deformation in the middle of the column obtained in the 3D FE analysis and in the SDOF calculations for Reaction load 3.

## G.3.2 Elasto-plastic response

### G.3.2.1 Decreased internal resistance of the wall

The deformation of the column for the different loads in the SDOF calculations is compared to the deformation of the 3D FE model, see Figure G.19 to Figure G.20.

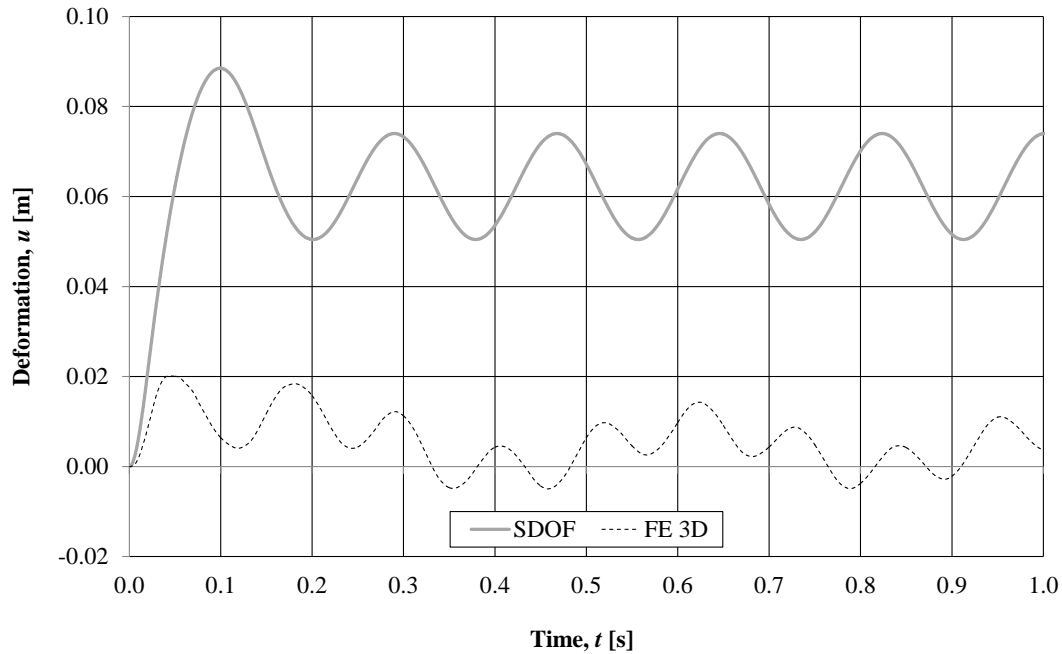


Figure G.19 Comparison of the deformation in the middle of the column obtained in the 3D FE analysis and in the SDOF analysis for the Direct load.

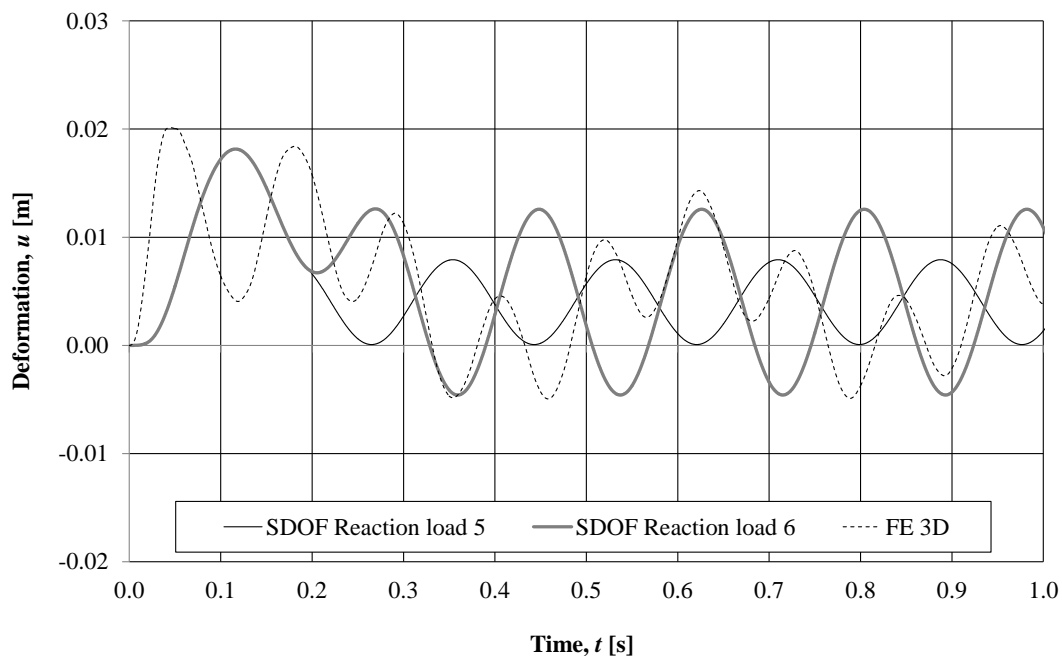


Figure G.20 Comparison of the deformation in the middle of the column obtained in the 3D FE analysis and in the SDOF analysis for Reaction load 5 and 6.

### G.3.2.2 Increased internal resistance of the wall

The deformation of the column for the different SDOF loads are compared to the deformation of the 3D FE model, see Figure G.21 to Figure G.22.

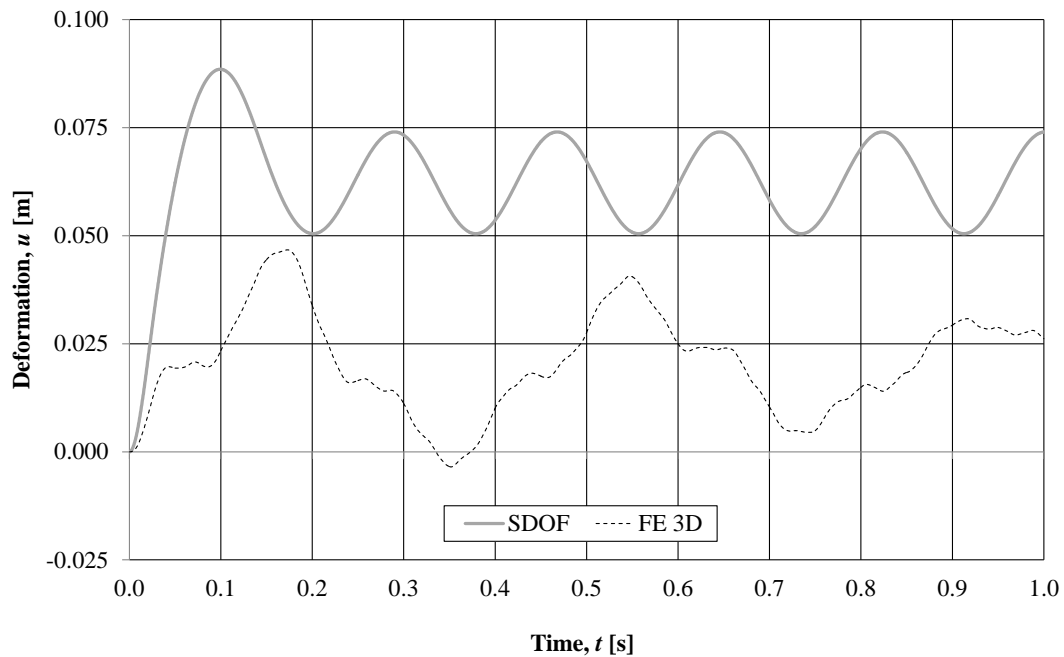


Figure G.21 Comparison of the deformation in the middle of the column obtained in the 3D FE analysis and in the SDOF analysis for the Direct load.

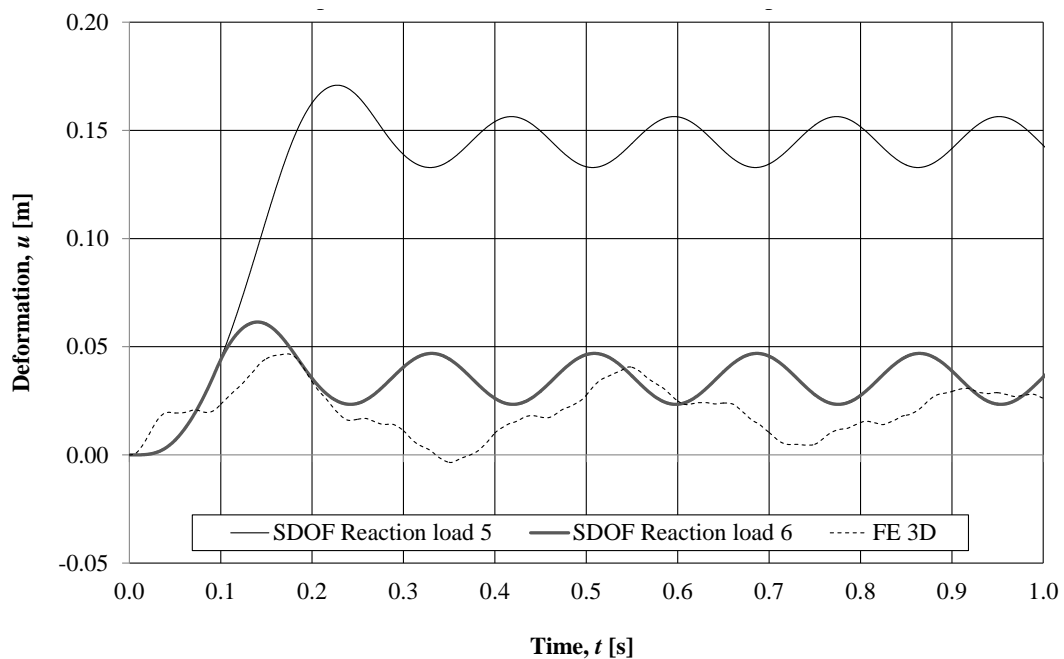


Figure G.22 Comparison of the deformation in the middle of the column obtained in the 3D FE analysis and in the SDOF analysis for Reaction load 5 and 6.

## G.4 Reaction loads

### G.4.1 Elastic response

#### G.4.1.1 Decreased stiffness of the wall

The reaction forces in the different points along the column are compared to a simply supported beam, see Figure G.23 to Figure G.29.

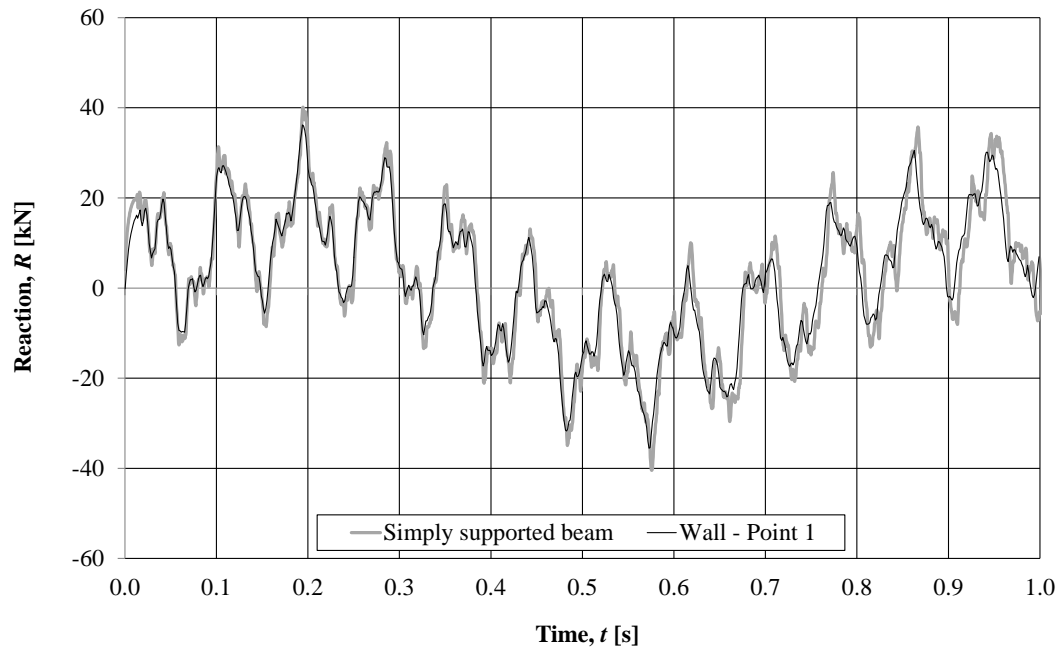


*Figure G.23 A comparison of the reaction forces from a simply supported beam and the reaction forces transferred from the wall panel to the column in point 1.*

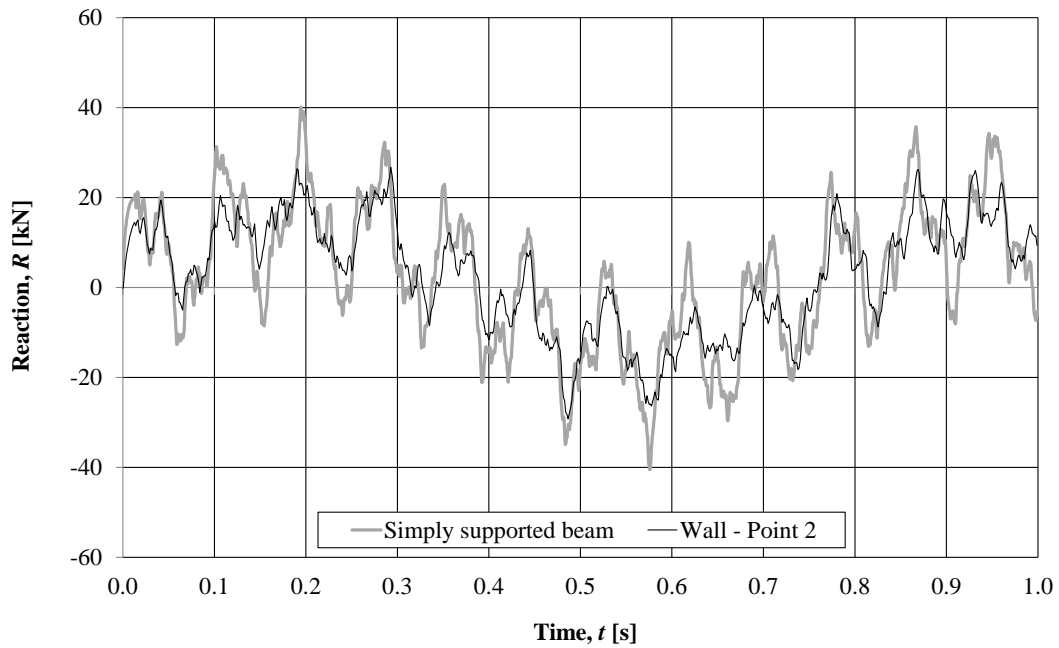


Figure G.24 A comparison of the reaction forces from a simply supported beam and the reaction forces transferred from the wall panel to the column in point 2.

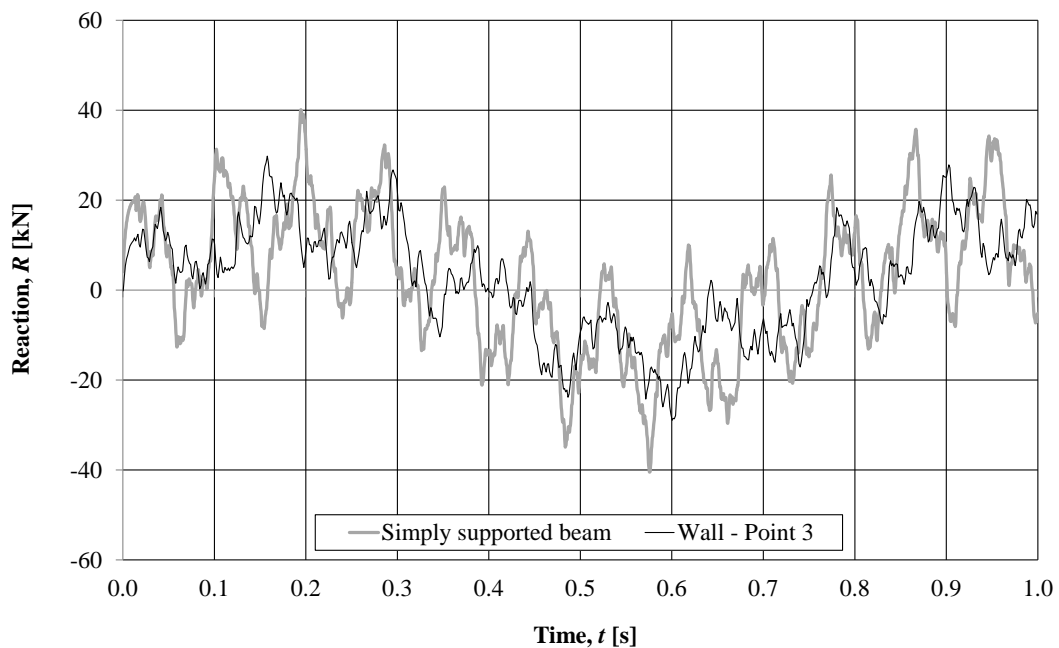


Figure G.25 A comparison of the reaction forces from a simply supported beam and the reaction forces transferred from the wall panel to the column in point 3.

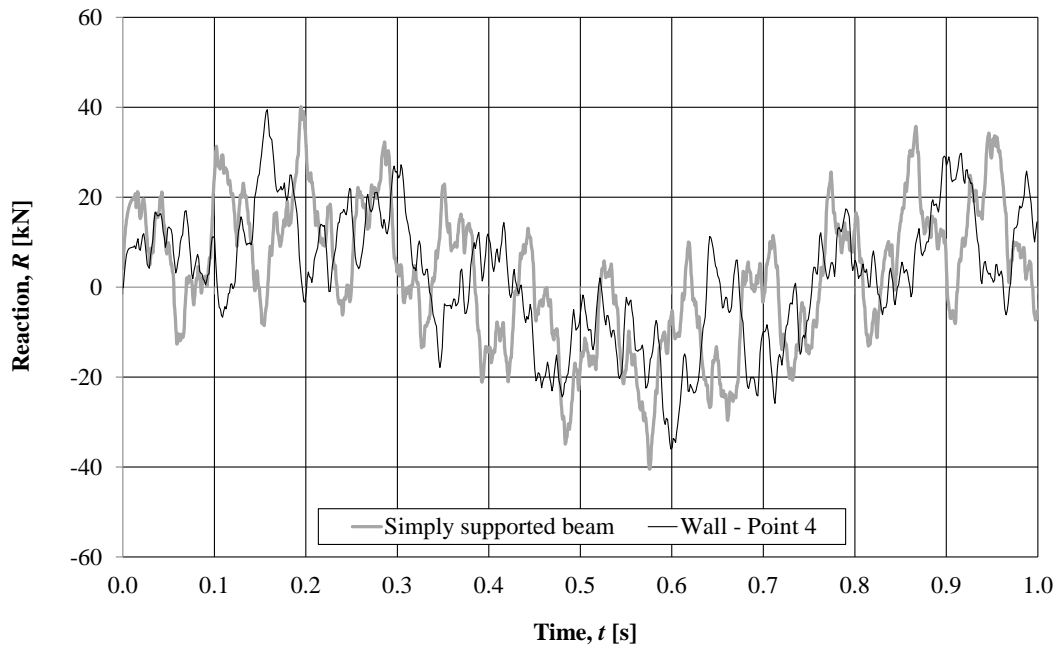


Figure G.26 A comparison of the reaction forces from a simply supported beam and the reaction forces transferred from the wall panel to the column in point 4.

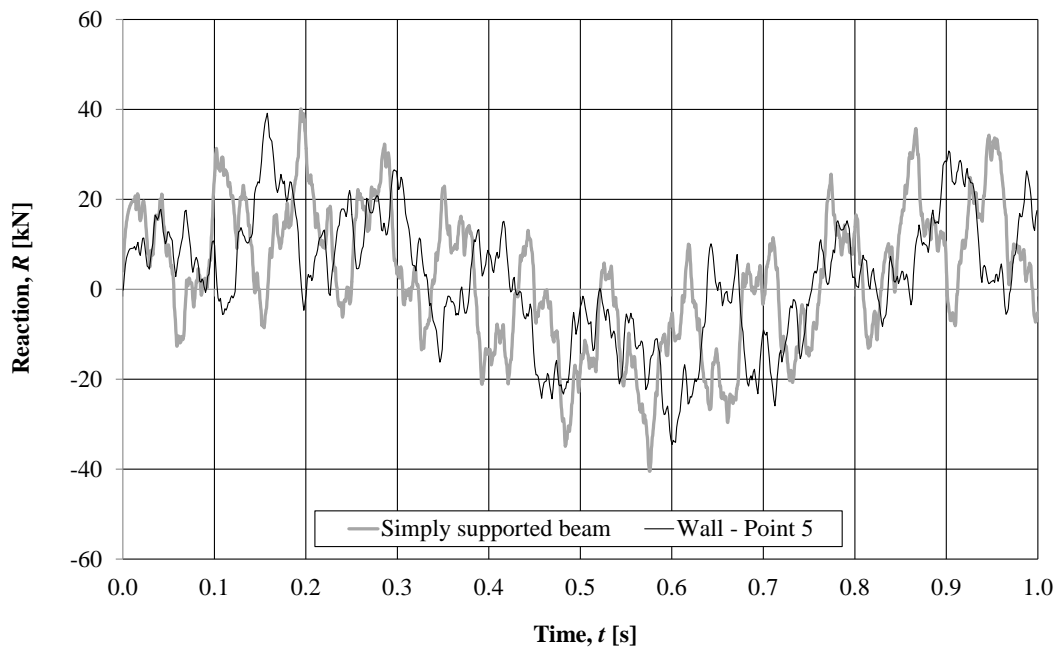


Figure G.27 A comparison of the reaction forces from a simply supported beam and the reaction forces transferred from the wall panel to the column in point 5.

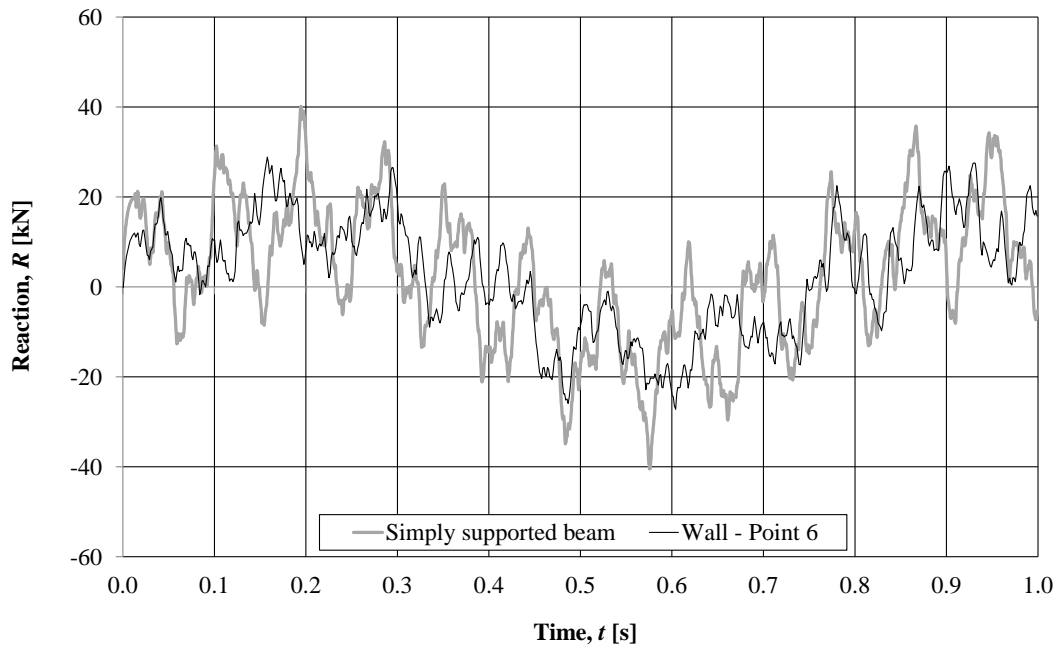


Figure G.28 A comparison of the reaction forces from a simply supported beam and the reaction forces transferred from the wall panel to the column in point 6.

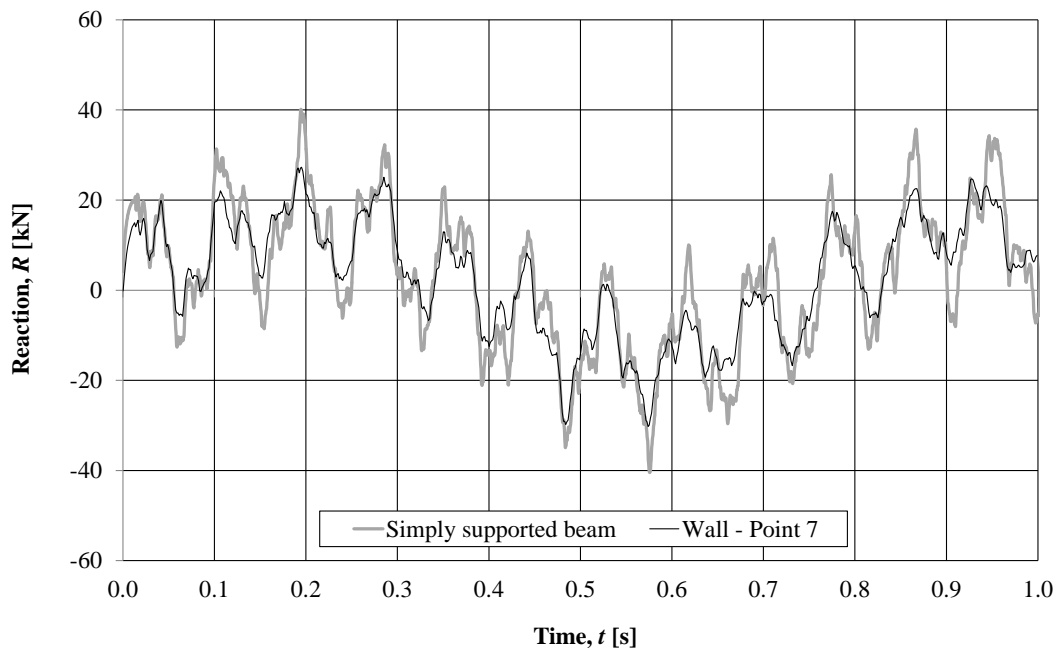


Figure G.29 A comparison of the reaction forces from a simply supported beam and the reaction forces transferred from the wall panel to the column in point 7.

#### G.4.1.2 Increased stiffness of the wall

The reaction forces in the different points along the column are compared to a simply supported beam in Figure G.30 to Figure G.36.

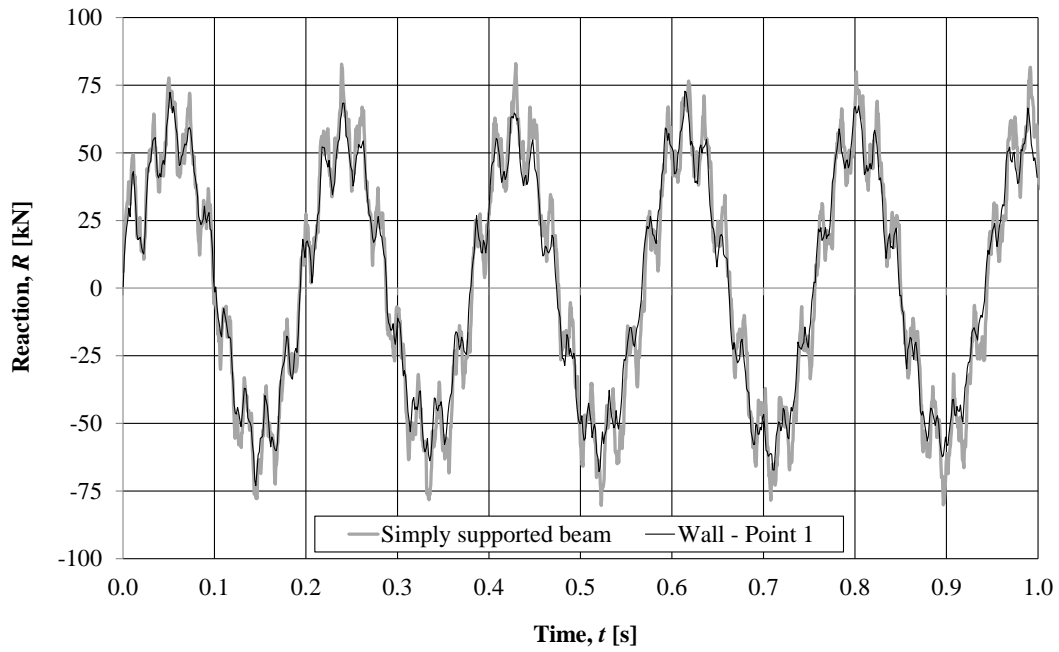


Figure G.30 A comparison of the reaction forces from a simply supported beam and the reaction forces transferred from the wall panel to the column in point 1.

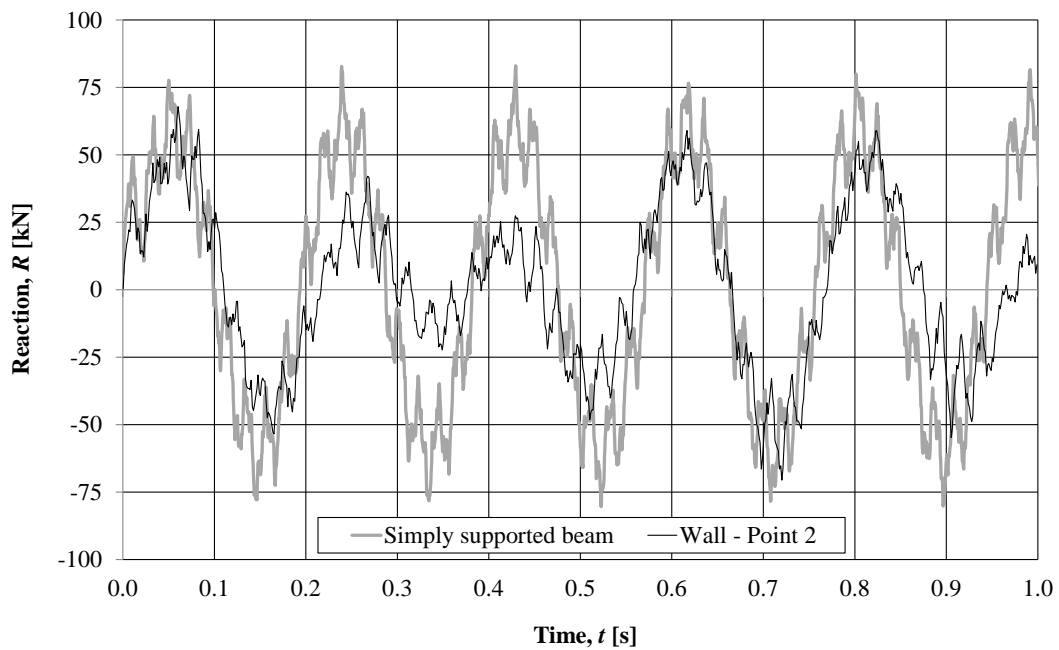


Figure G.31 A comparison of the reaction forces from a simply supported beam and the reaction forces transferred from the wall panel to the column in point 2.



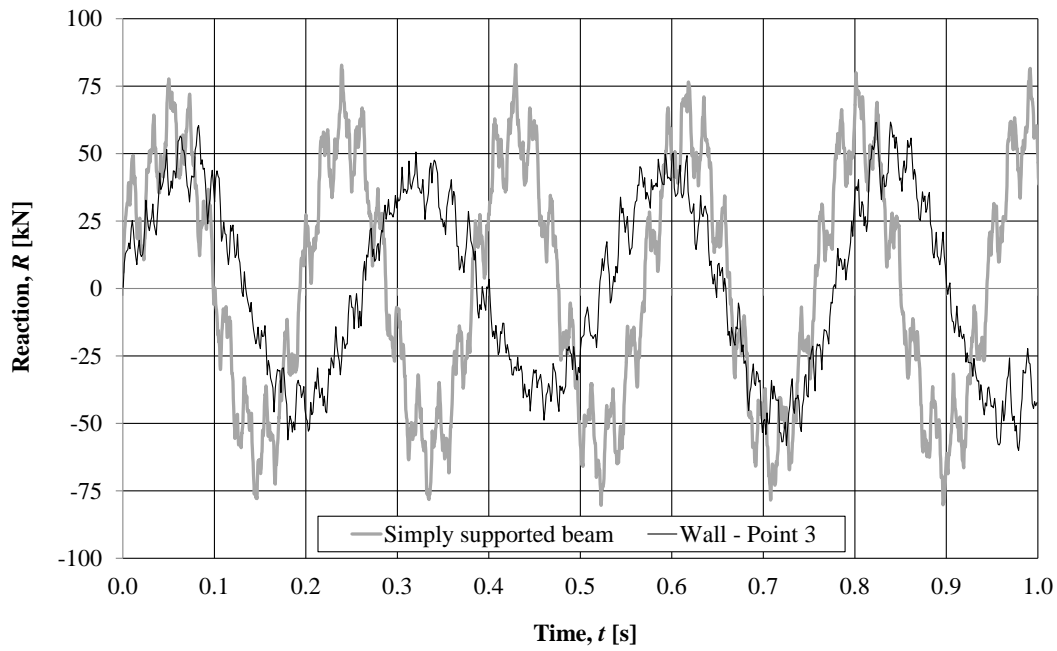


Figure G.32 A comparison of the reaction forces from a simply supported beam and the reaction forces transferred from the wall panel to the column in point 3.

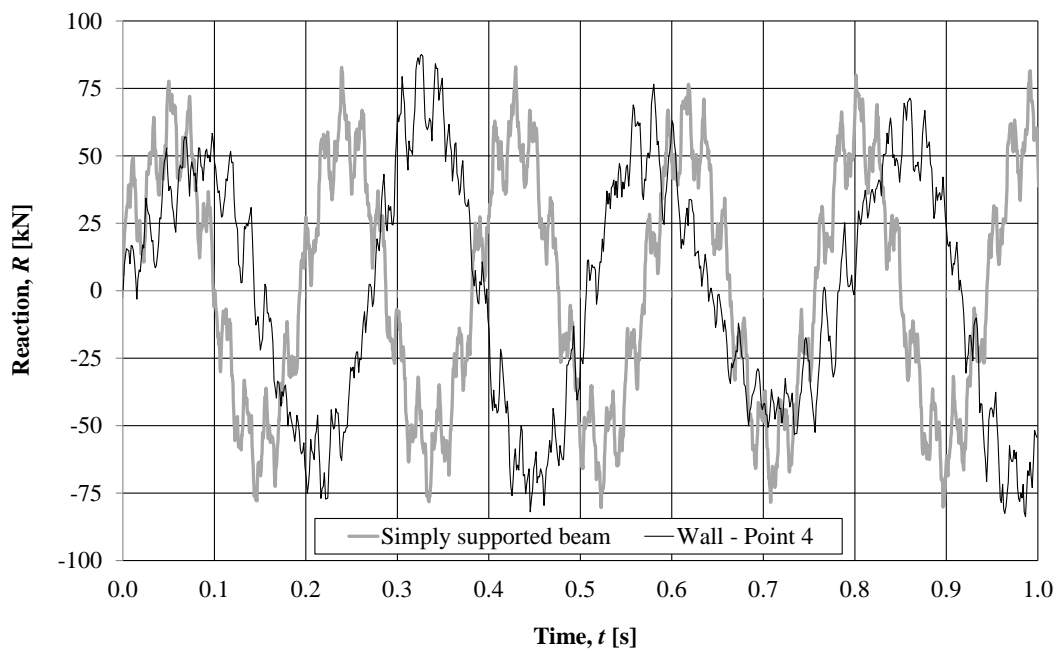


Figure G.33 A comparison of the reaction forces from a simply supported beam and the reaction forces transferred from the wall panel to the column in point 4.

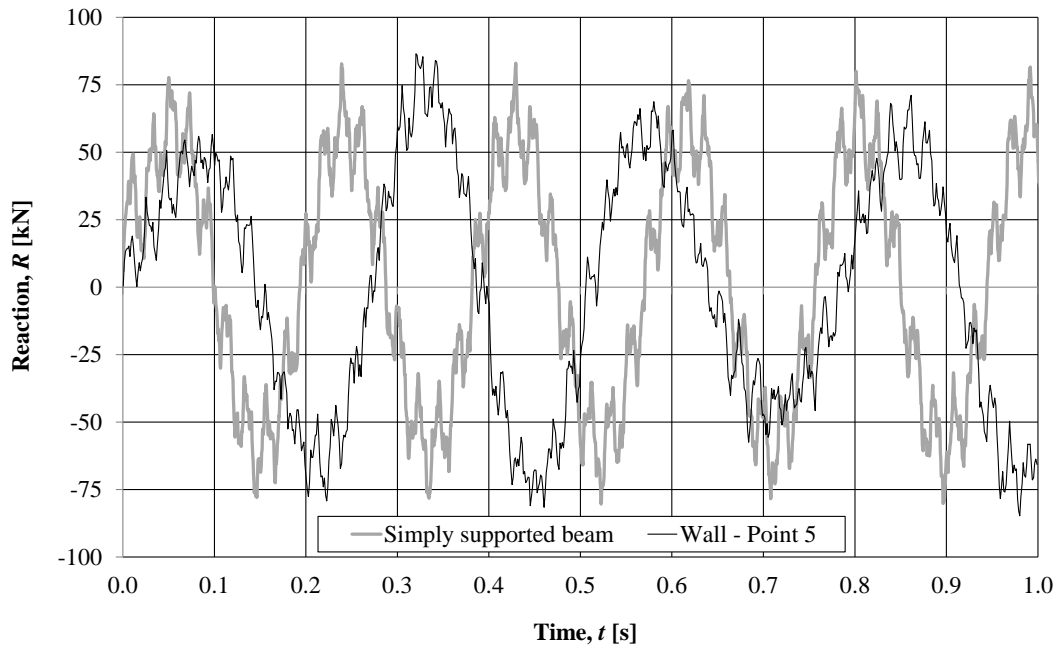


Figure G.34 A comparison of the reaction forces from a simply supported beam and the reaction forces transferred from the wall panel to the column in point 5.

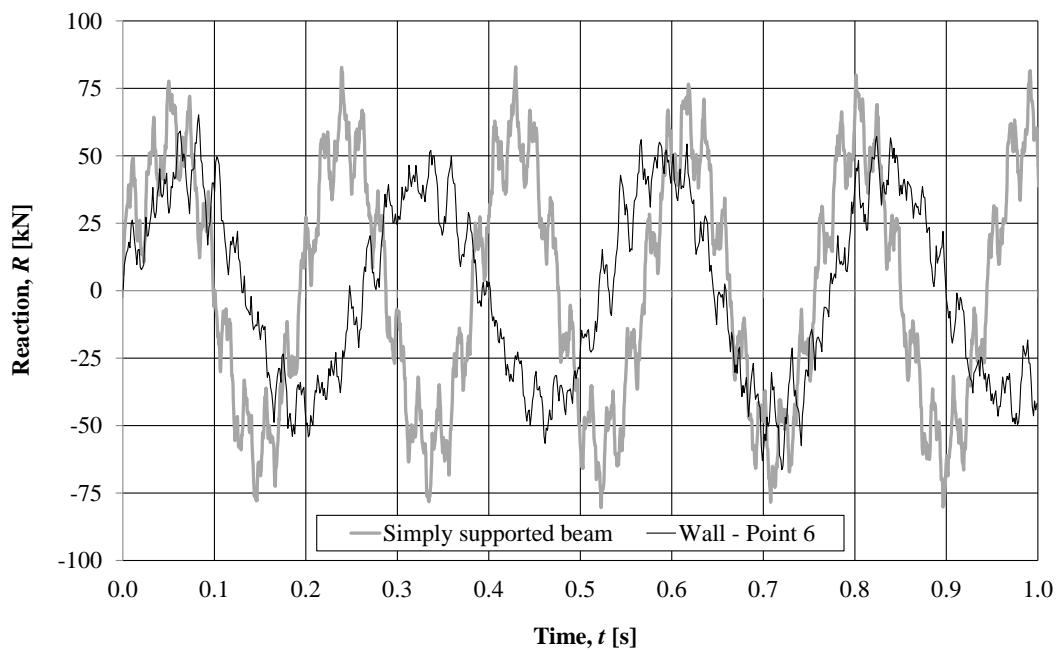


Figure G.35 A comparison of the reaction forces from a simply supported beam and the reaction forces transferred from the wall panel to the column in point 6.

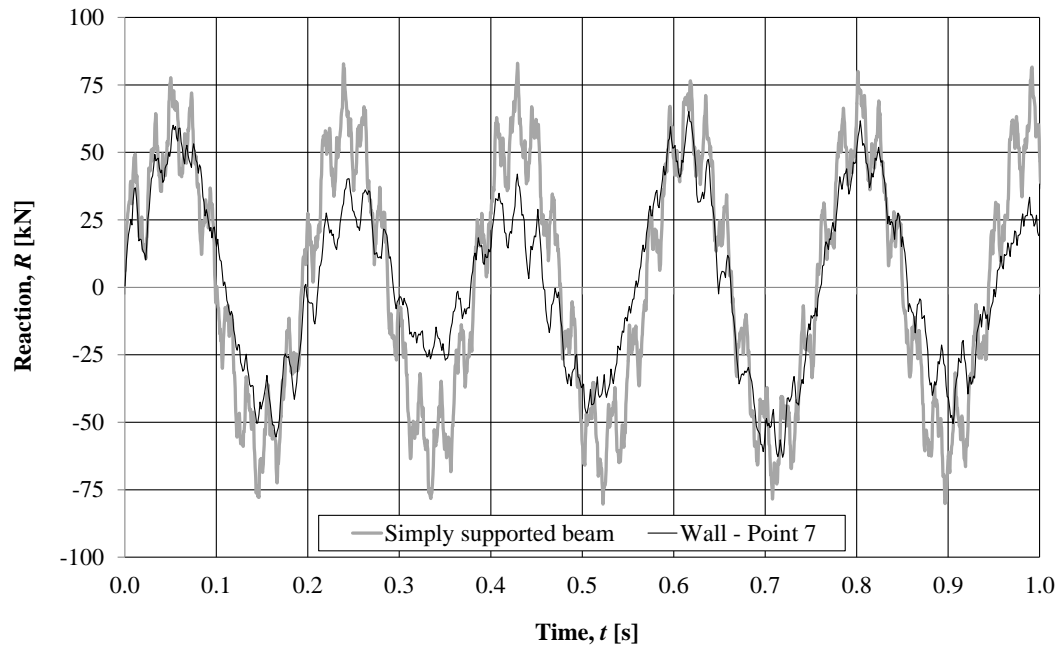


Figure G.36 A comparison of the reaction forces from a simply supported beam and the reaction forces transferred from the wall panel to the column in point 7.

## G.4.2 Elasto-plastic response

### G.4.2.1 Decreased internal resistance of the wall

The reaction forces in the different points along the column are compared to a simply supported beam in Figure G.37 to Figure G.43.

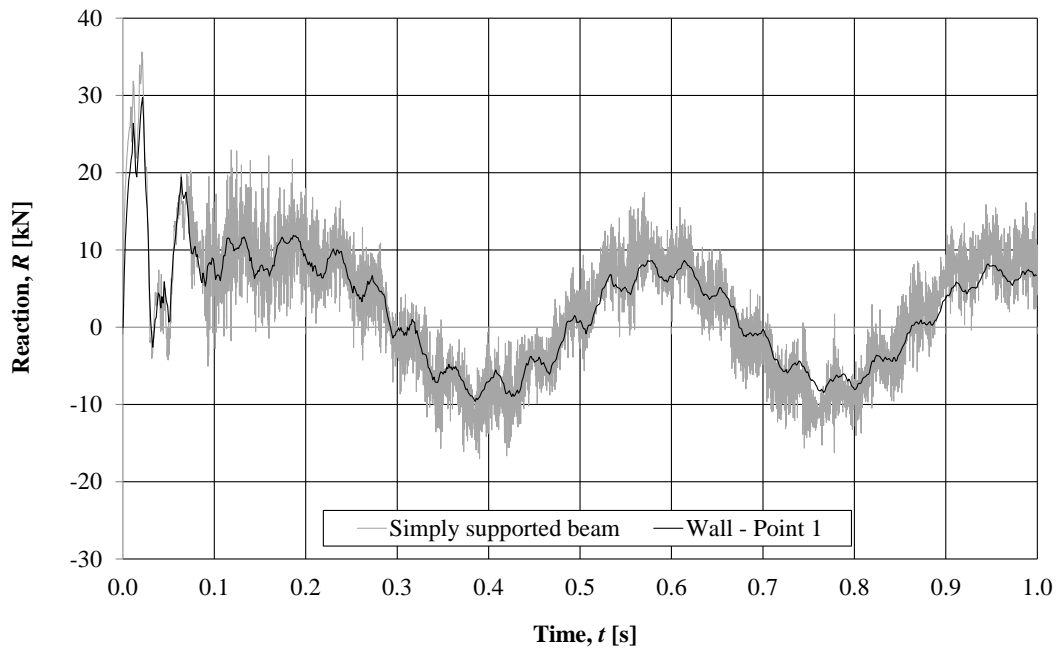


Figure G.37 A comparison of the reaction forces from a simply supported beam and the reaction forces transferred from the wall panel to the column in point 1.

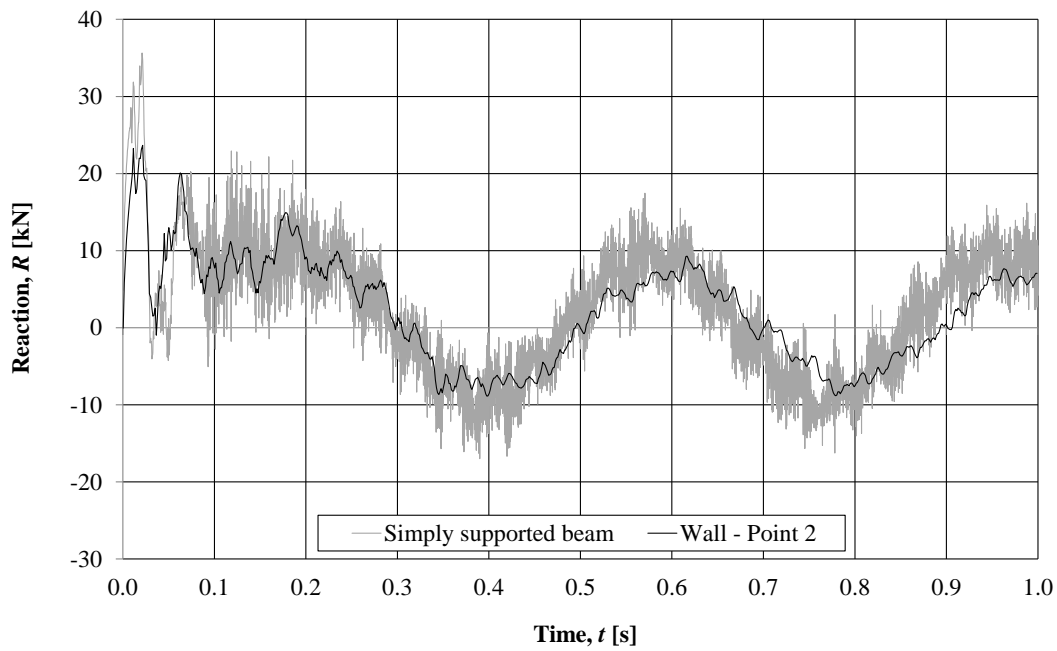


Figure G.38 A comparison of the reaction forces from a simply supported beam and the reaction forces transferred from the wall panel to the column in point 2.

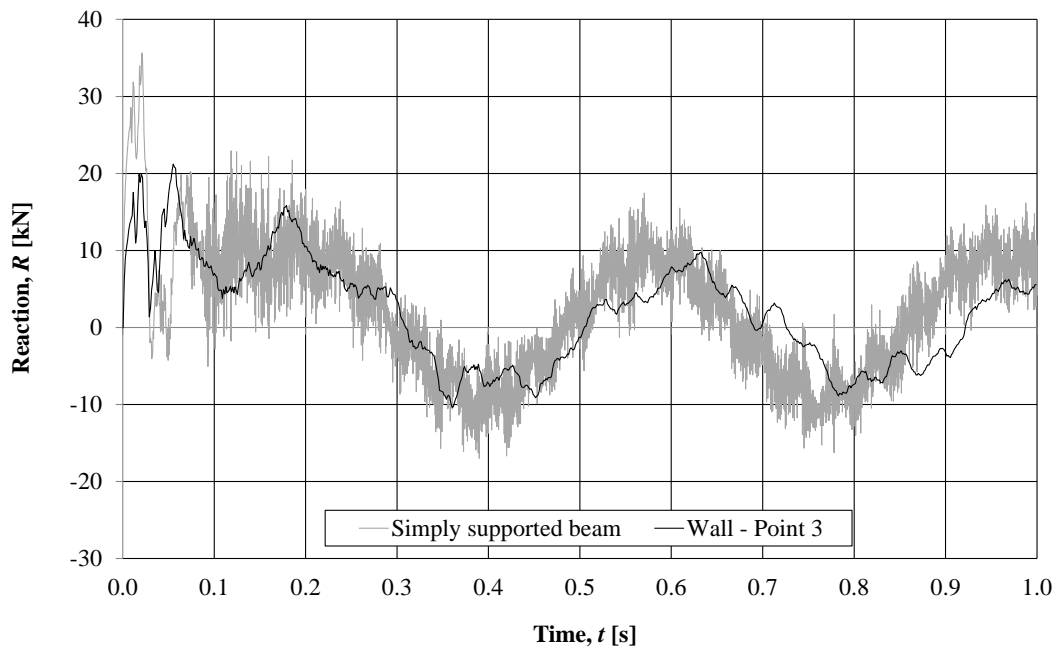


Figure G.39 A comparison of the reaction forces from a simply supported beam and the reaction forces transferred from the wall panel to the column in point 3.

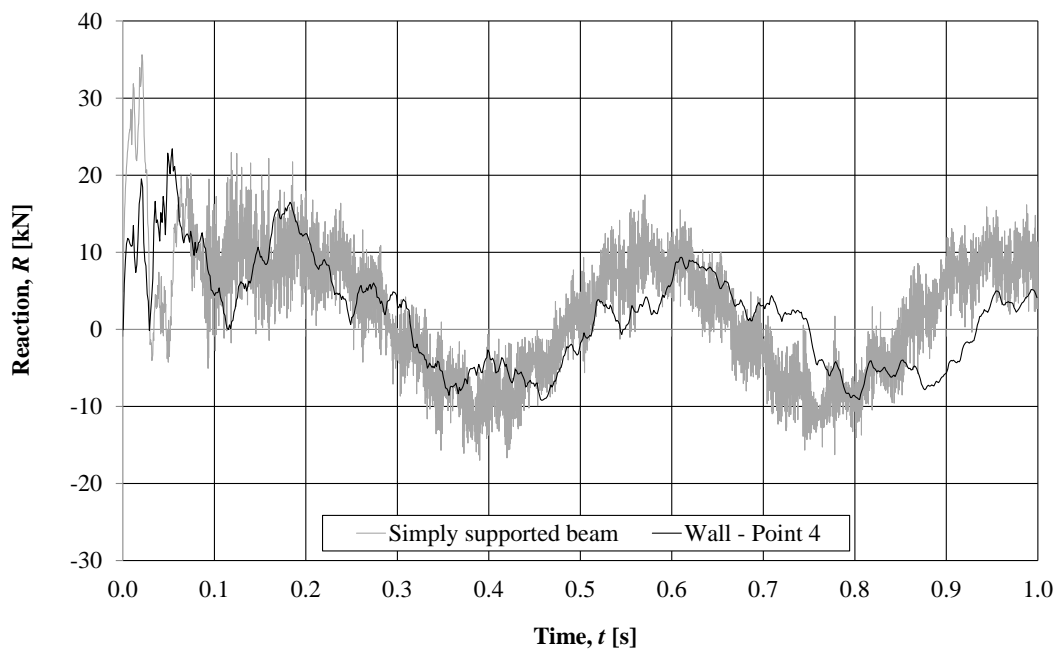


Figure G.40 A comparison of the reaction forces from a simply supported beam and the reaction forces transferred from the wall panel to the column in point 4.

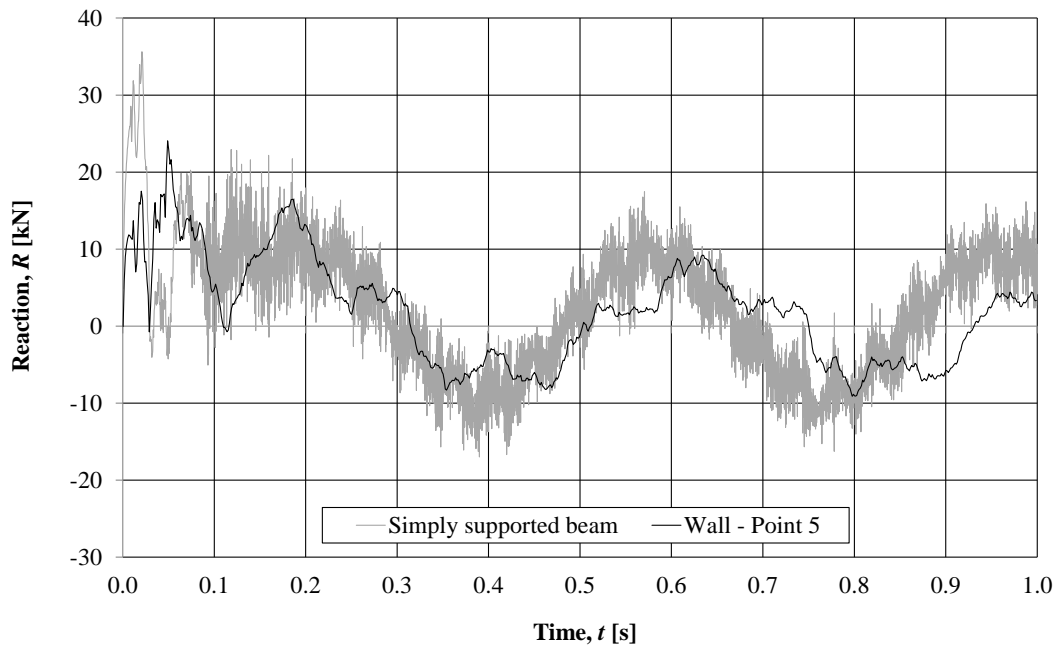


Figure G.41 A comparison of the reaction forces from a simply supported beam and the reaction forces transferred from the wall panel to the column in point 5.

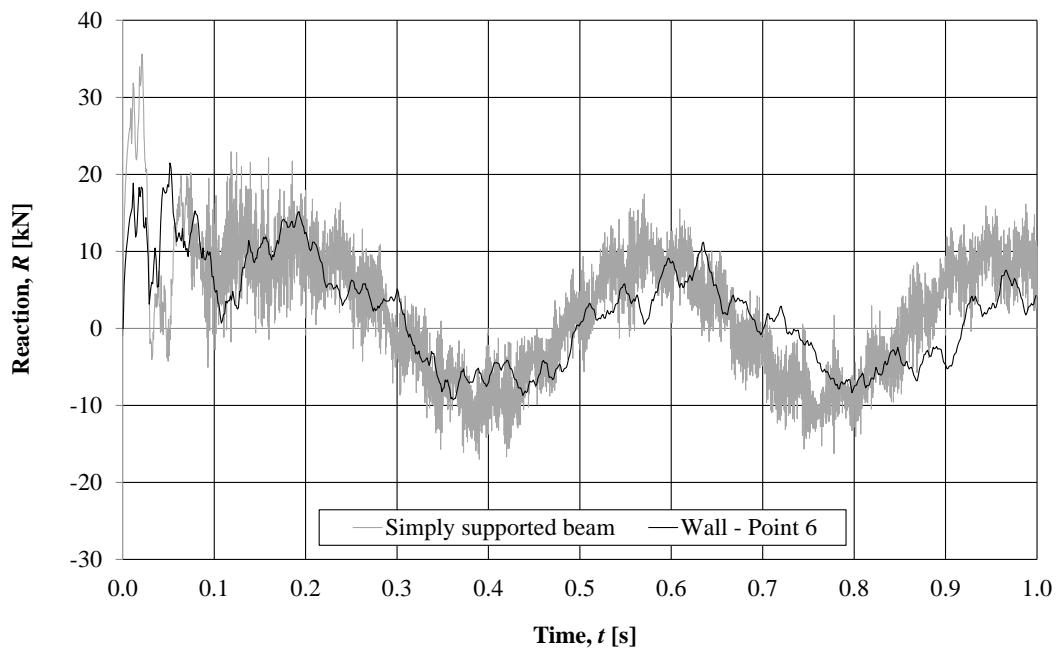


Figure G.42 A comparison of the reaction forces from a simply supported beam and the reaction forces transferred from the wall panel to the column in point 6.

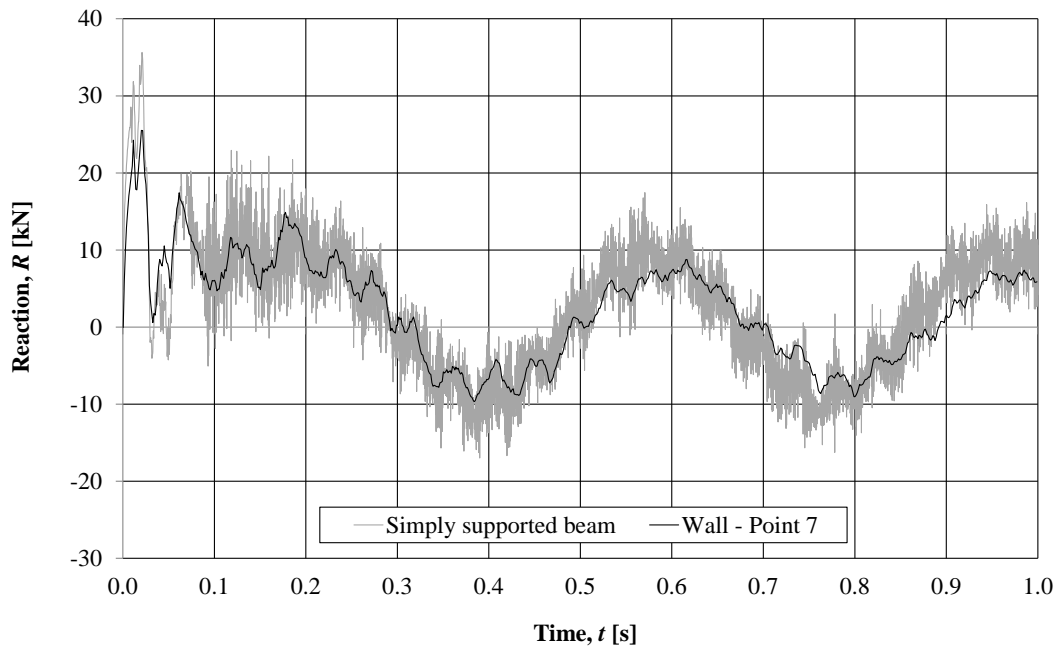


Figure G.43 A comparison of the reaction forces from a simply supported beam and the reaction forces transferred from the wall panel to the column in point 7.

#### G.4.2.2 Increased internal resistance of the wall

The reaction forces in the different points along the column are compared to a simply supported beam in Figure G.44 to Figure G.50.

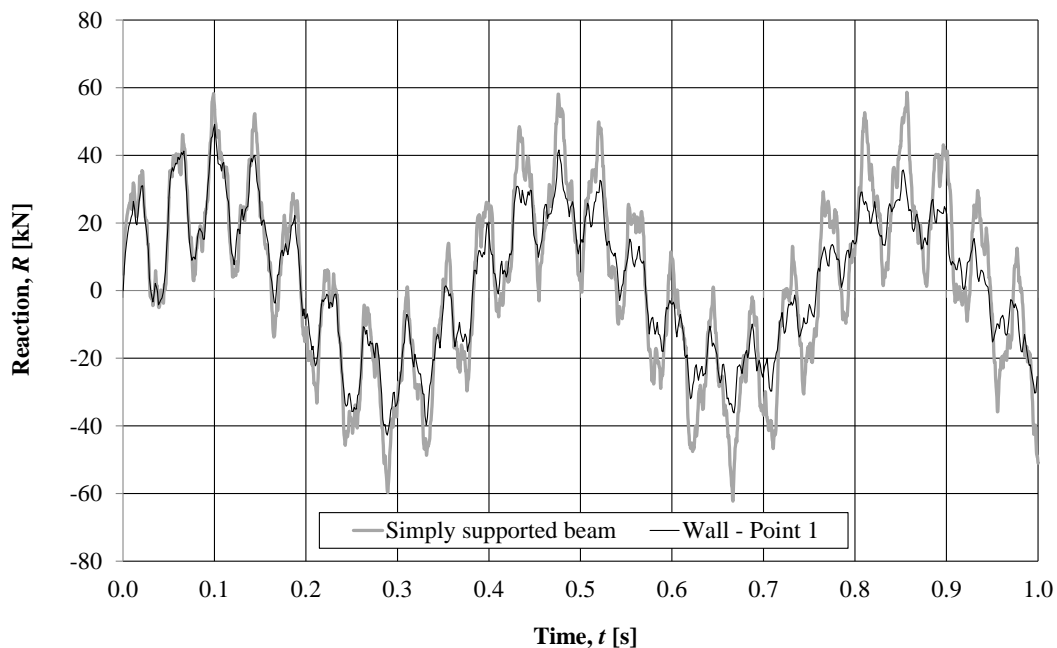


Figure G.44 A comparison of the reaction forces from a simply supported beam and the reaction forces transferred from the wall panel to the column in point 1.

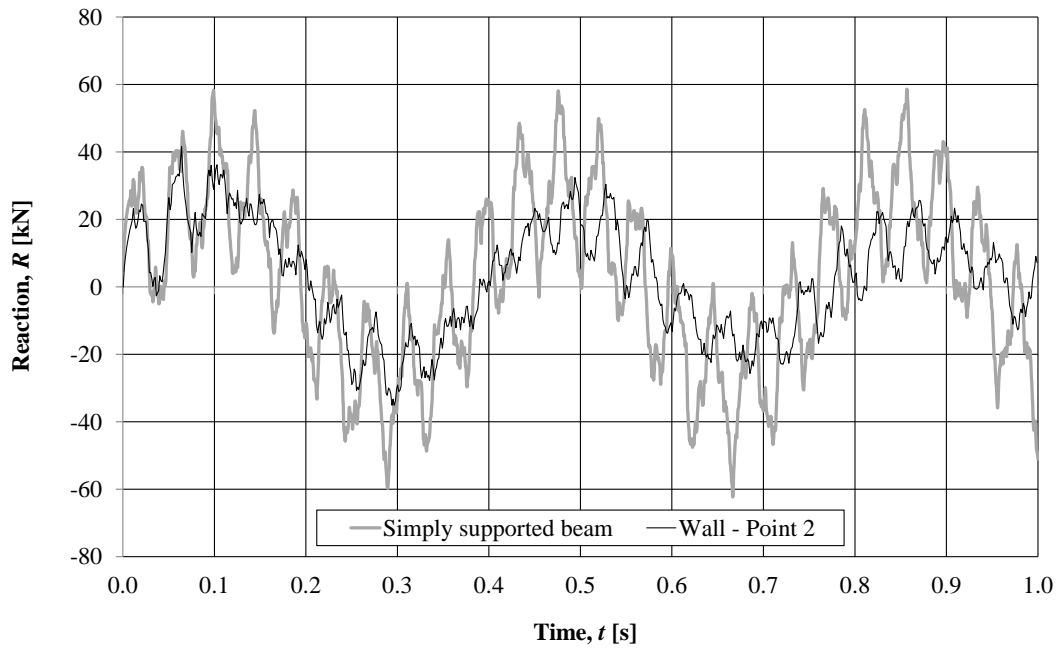


Figure G.45 A comparison of the reaction forces from a simply supported beam and the reaction forces transferred from the wall panel to the column in point 2.

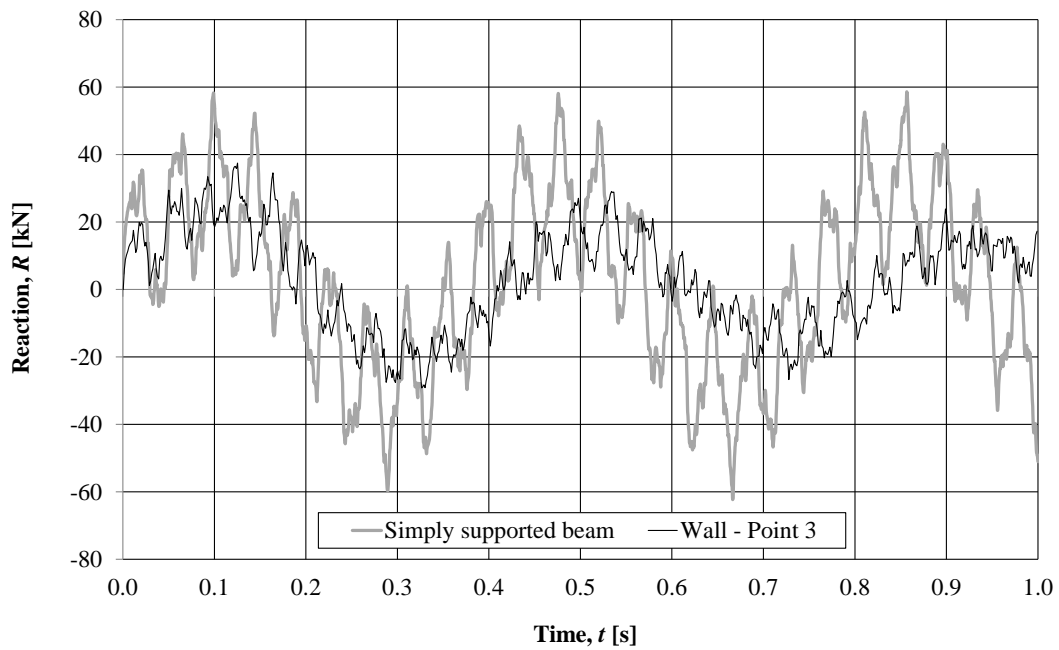


Figure G.46 A comparison of the reaction forces from a simply supported beam and the reaction forces transferred from the wall panel to the column in point 3.



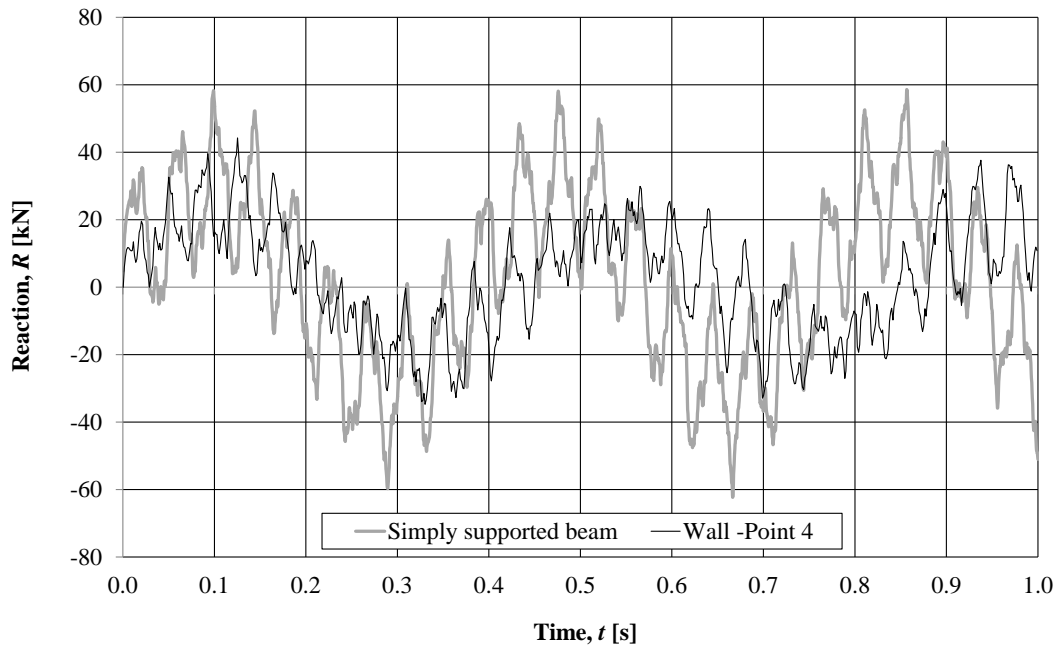


Figure G.47 A comparison of the reaction forces from a simply supported beam and the reaction forces transferred from the wall panel to the column in point 4.

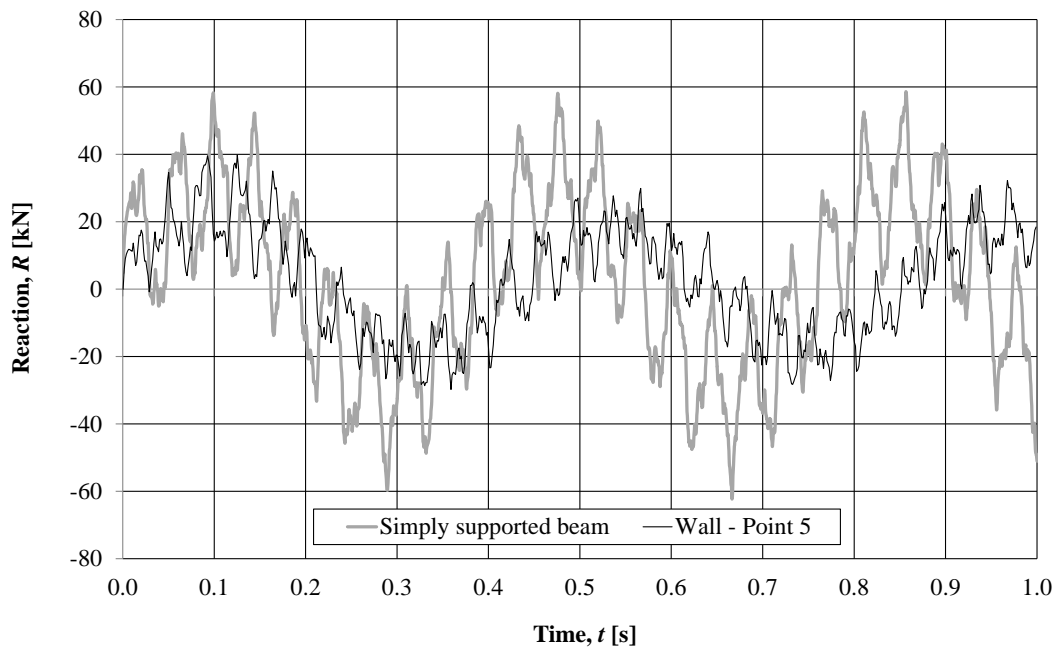


Figure G.48 A comparison of the reaction forces from a simply supported beam and the reaction forces transferred from the wall panel to the column in point 5.

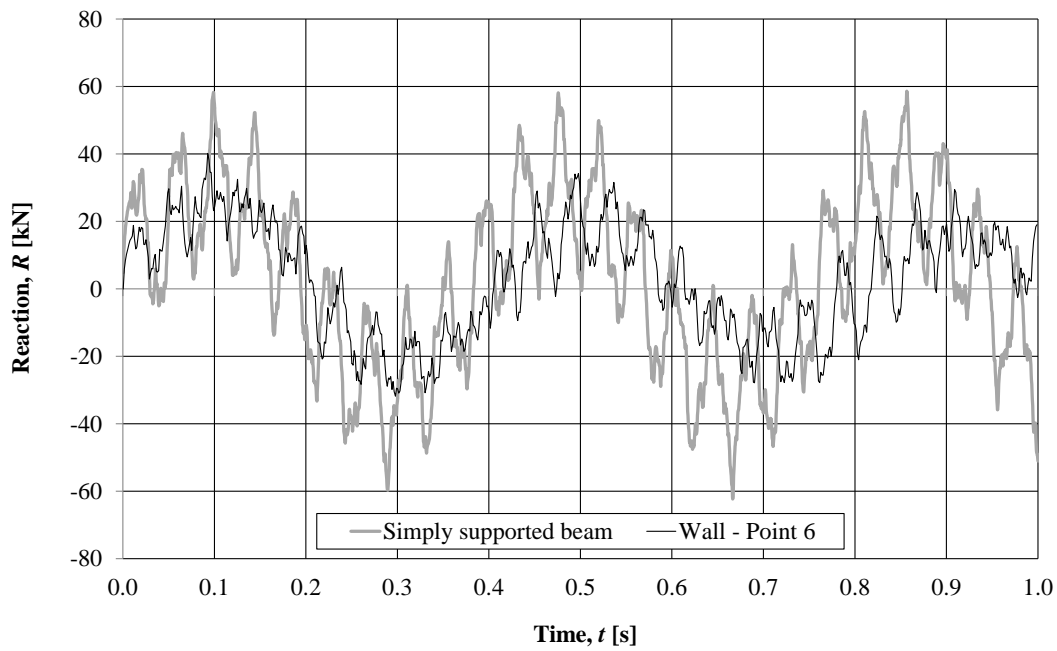


Figure G.49 A comparison of the reaction forces from a simply supported beam and the reaction forces transferred from the wall panel to the column in point 6.

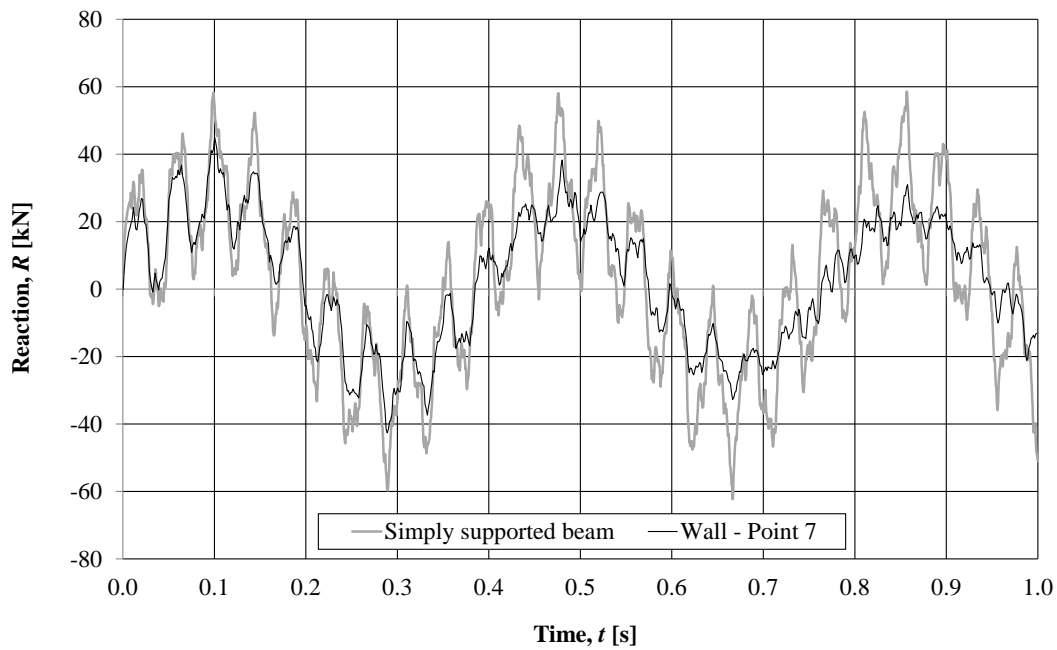


Figure G.50 A comparison of the reaction forces from a simply supported beam and the reaction forces transferred from the wall panel to the column in point 7.

## G.5 Comparison of delayed load in SDOF and 3D FE analysis

### G.5.1 Elastic response

#### G.5.1.1 Decreased stiffness of the wall

In the 3D FE analysis the delayed load is calculated as the sum of all support reactions acting on the column. Here, it is compared to the total delayed load simulated in SDOF in Figure G.51.

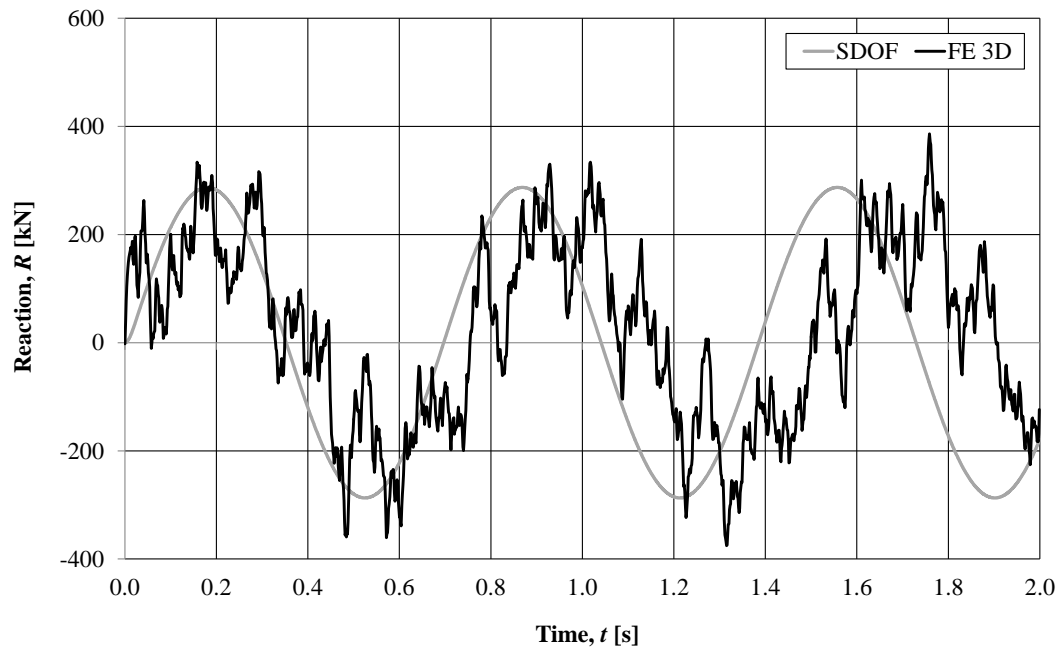


Figure G.51 A comparison of the delayed load in SDOF and in the 3D FE analysis.

#### G.5.1.2 Increased stiffness of the wall

In the 3D FE analysis the delayed load is calculated as the sum of all support reactions acting on the column. Here, it is compared to the total delayed load simulated in SDOF in Figure G.52.

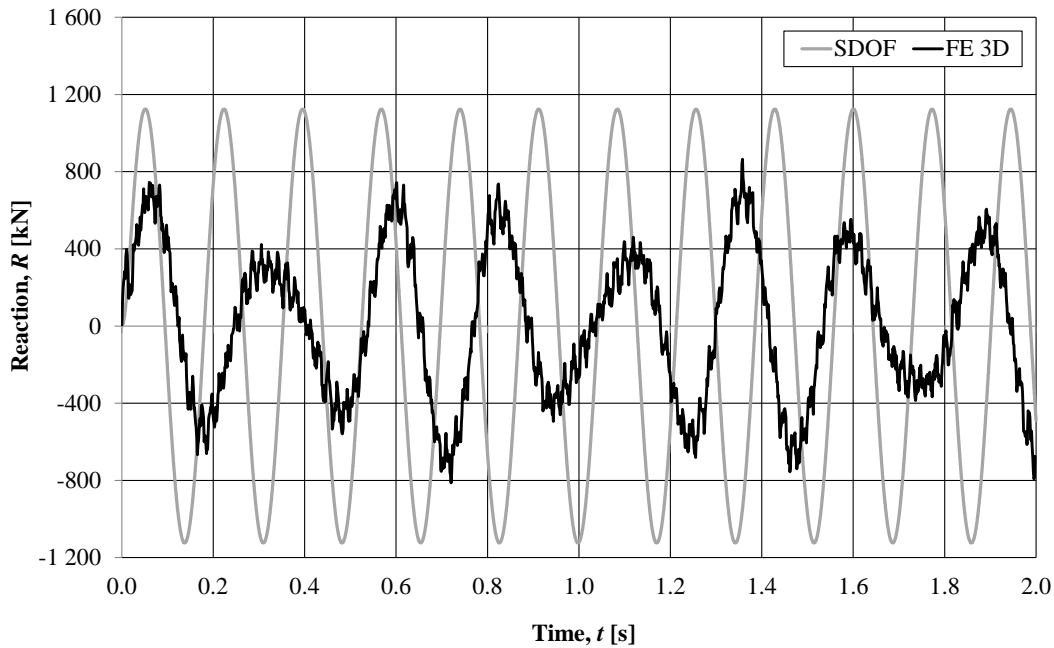


Figure G.52 A comparison of the delayed loading in SDOF and in the 3D FE analysis.

## G.5.2 Elasto-plastic response

### G.5.2.1 Decreased internal resistance of the wall

In the 3D FE analysis the delayed load is calculated as the sum of all support reactions acting on the column. Here, it is compared to the total delayed load simulated in SDOF in Figure G.53.

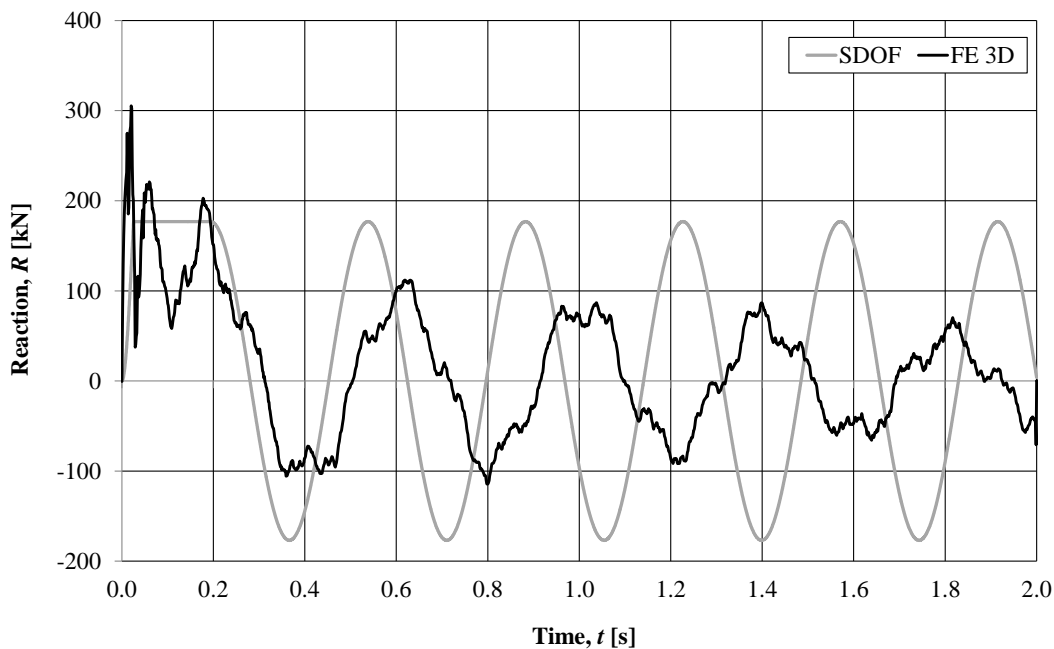


Figure G.53 A comparison of the delayed loading in SDOF and in the 3D FE analysis.

### G.5.2.2 Increased internal resistance of the wall

In the 3D FE analysis the delayed load is calculated as the sum of all support reactions acting on the column. Here, it is compared to the total delayed load simulated in SDOF in Figure G.54.

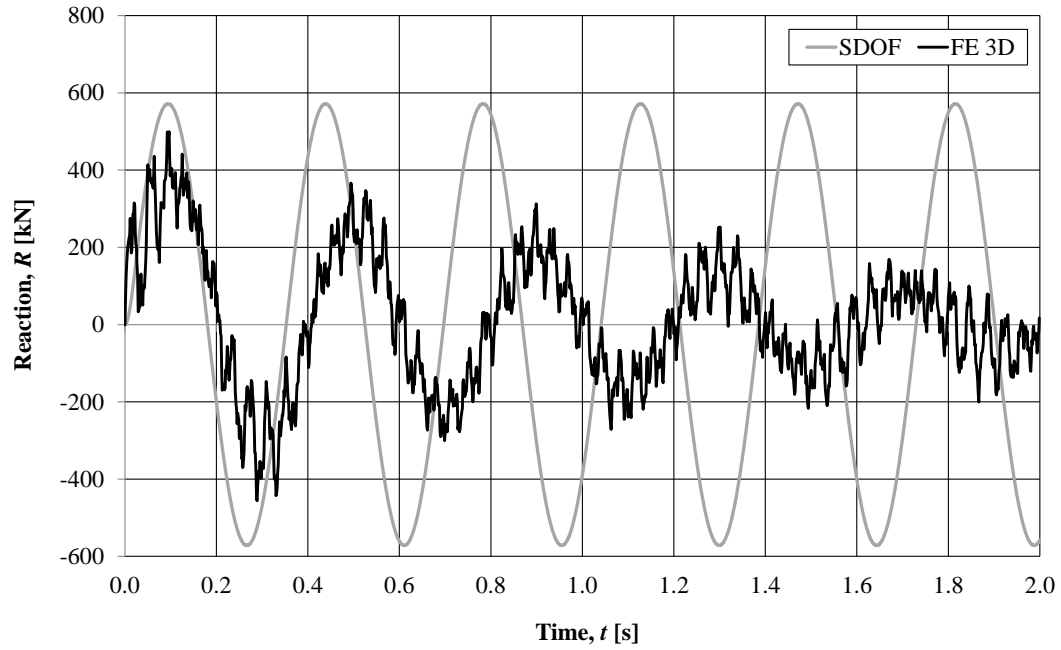


Figure G.54 A comparison of the delayed loading in SDOF and in the 3D FE analysis.

# APPENDIX H Indata files for ADINA

## H.1 2D Frame with elasto-plastic material model

DATABASE NEW SAVE=NO PROMPT=NO  
FEPROGRAM ADINA  
CONTROL FILEVERSION=V88

\*\*\*\*\* ANALYSIS TYPE \*\*\*\*\*

MASTER'S ANALYSIS=DYNAMIC-DIRECT-INTEGRATION MODEX=EXECUTE,  
TSTART=0 IDOF=1110 OVALIZAT=NONE,  
FLUIDPOT=AUTOMATIC CYCLICPA=1 IPOSIT=STOP REACTION=YES,  
INITIALS=NO FSINTERA=NO IRINT=DEFAULT CMASS=NO,  
SHELLNDO=AUTOMATIC AUTOMATI=OFF SOLVER=SPARSE,  
CONTACT=CONSTRAINT-FUNCTION TRELEASE=0,  
RESTART=NO FRACTURE=NO LOAD-CAS=NO LOAD-PEN=NO SINGULAR=YES,  
STIFFNES=0.0001 MAP-OUTP=NONE MAP-FORM=NO,  
NODAL-DE=" POROUS-C=NO ADAPTIVE=0 ZOOM-LAB=1 AXIS-CYC=0,  
PERIODIC=NO VECTOR-S=GEOMETRY EPSI-FIR=NO STABILIZ=NO,  
STABFACT=1E-10 RESULTS=PORTHOLE FEFCORR=NO,  
BOLTSTEP=1 EXTEND-S=YES CONVERT=NO DEGEN=YES TMC-MODE=NO,  
ENSIGHT=NO IRSTEPS=1 INITIALT=NO TEMP-INT=NO ESINTERA=NO,  
OP2GEOM=NO

\*

ANALYSIS DYNAMIC-DIRECT-INTEGRATION METHOD=NEWMARK,  
DELTA=0.5 ALPHA=0.25,  
THETA=1.4 TIMESTEP=TOTALTIME NCRSTEP=1,  
CRSTEP=0 MASS-SCA=1,  
DTMIN1=0 DTMIN2=0,  
GAMMA=0.5

\*\*\*\*\* GEOMETRY \*\*\*\*\*

COORDINATES POINT SYSTEM=0

@CLEAR

1 0 0 0  
2 0 7 0  
3 0 7.01 0  
4 15 7.01 0  
5 15 7 0  
6 15 0 0  
7 0 8 0  
8 16 0 0

@

\*

LINE STRAIGHT NAME=1 P1=1 P2=2  
LINE STRAIGHT NAME=2 P1=3 P2=4  
LINE STRAIGHT NAME=3 P1=5 P2=6

\*

CROSS-SECTIO RECTANGULAR NAME=1 WIDTH=0.2,  
HEIGHT=1 SC=0 TC=0,  
TORFAC=1 SSHEARF=0,  
TSHEARF=0 ISHEAR=NO SQUARE=NO

\*\*\*\*\* MATERIAL \*\*\*\*\*

MATERIAL PLASTIC-BILINEAR NAME=1 HARDENIN=ISOTROPIC,  
E=2.7001E+09 NU=0,  
YIELD=5684900 ET=100 EPA=0,

STRAINRA=0      DENSITY=2400      ALPHA=0,  
TREF=0          DEPENDEN=NO      TRANSITI=0.0001,  
EP-STRAI=0      BCURVE=0          BVALUE=0,  
XM-INF=0        XM0=0,  
ETA=0            MDESCRIP='NONE'

\*\*\*\*\* BOUNDARY CONDITIONS \*\*\*\*\*

FIXBOUNDARY POINTS FIXITY=ALL

@CLEAR

1 'ALL'

6 'ALL'

@

\*

RIGIDLINK    NAME=1    SLAVETYP=POINT    SLAVENAM=2    MASTER'STY=POINT  
MASTER'SNA=3,

DISPLACE=DEFAULT OPTION=0 SLAVEBOD=0 MASTER'SBO=0 DOF=ALL,

DOFSI=123

\*

RIGIDLINK    NAME=2    SLAVETYP=POINT    SLAVENAM=4    MASTER'STY=POINT  
MASTER'SNA=5,

DISPLACE=DEFAULT OPTION=0 SLAVEBOD=0 MASTER'SBO=0 DOF=ALL,

DOFSI=123

\*

RIGIDLINK    NAME=1    SLAVETYP=POINT    SLAVENAM=3    MASTER'STY=POINT  
MASTER'SNA=2,

DISPLACE=DEFAULT OPTION=0 SLAVEBOD=0 MASTER'SBO=0 DOF=ALL,

DOFSI=123

\*\*\*\*\* ELEMENTS \*\*\*\*\*

SUBDIVIDE MODEL MODE=DIVISIONS SIZE=0 NDIV=30,

PROGRESS=GEOMETRIC MINCUR=1

\*

EGROUP BEAM NAME=1 SUBTYPE=TWO-D DISPLACE=DEFAULT MATERIAL=1 RINT=5,

SINT=3 TINT=DEFAULT RESULTS=STRESSES INITIALS=NONE CMASS=DEFAULT,

RIGIDEND=NONE MOMENT-C=NO RIGIDITY=0 MULTIPLY=1000000,

RUPTURE=ADINA OPTION=NONE BOLT-TOL=0 DESCRIPT=,

'NONE' SECTION=1 PRINT=DEFAULT SAVE=DEFAULT TBIRTH=0,

TDEATH=0 SPOINT=4 BOLTFORC=0,

BOLTNCUR=0 TMC-MATE=1 BOLT-NUM=0 BOLT-LOA=0,

WARP=NO

\*

GLINE NODES=2 AUXPOINT=8 NCOINCID=ENDS NCENDS=12,

NCTOLERA=1E-05 SUBSTRUC=0 GROUP=1 MIDNODES=CURVED,

XO=0 YO=0 ZO=0,

XYZOSYST=SKEW

@CLEAR

1

3

@

\*

EGROUP BEAM NAME=2 SUBTYPE=TWO-D DISPLACE=DEFAULT MATERIAL=1 RINT=5,

SINT=3 TINT=DEFAULT RESULTS=STRESSES INITIALS=NONE CMASS=DEFAULT,

RIGIDEND=NONE MOMENT-C=NO RIGIDITY=0 MULTIPLY=1000000,

RUPTURE=ADINA OPTION=NONE BOLT-TOL=0 DESCRIPT=,

'NONE' SECTION=1 PRINT=DEFAULT SAVE=DEFAULT TBIRTH=0,

TDEATH=0 SPOINT=4 BOLTFORC=0,

BOLTNCUR=0 TMC-MATE=1 BOLT-NUM=0 BOLT-LOA=0,

WARP=NO

```

*
GLINE NODES=2 AUXPOINT=7 NCOINCID=ENDS NCENDS=12,
NCTOLERA=1E-05 SUBSTRUC=0 GROUP=2 MIDNODES=CURVED,
XO=0 YO=0 ZO=0,
XYZOSYST=SKEW
@CLEAR
2
@

***** DYNAMIC LOAD *****

LOAD LINE NAME=1 MAGNITUD=-60000
*
APPLY-LOAD BODY=0
@CLEAR
1 'LINE' 1 'LINE' 1 0 1 0 0 -1 8 0 0 'NO',
0 0 1 0 'MID'
@
*
TIMEFUNCTION NAME=1 IFLIB=1 FPAR1=0,
FPAR2=0          FPAR3=0,
FPAR4=0          FPAR5=0,
FPAR6=0
@CLEAR
0          0
0.00025   1
0.025     0
2          0
@
*
TIMESTEP NAME=LOAD
@CLEAR
8000 0.00025
@

```

## H.2 3D Frame with elasto-plastic material model

```

DATABASE NEW SAVE=NO PROMPT=NO
FEPROGRAM ADINA
CONTROL FILEVERSION=V88
*
FEPROGRAM PROGRAM=ADINA
*
***** ANALYSIS TYPE *****
*
MASTER'S ANALYSIS=DYNAMIC-DIRECT-INTEGRATION MODEX=EXECUTE,
TSTART=0 IDOF=0 OVALIZAT=NONE FLUIDPOT=AUTOMATIC,
CYCLICPA=1 IPOSIT=STOP REACTION=YES INITIALS=NO FSINTERA=NO,
IRINT=DEFAULT CMASS=NO SHELLNDO=AUTOMATIC AUTOMATI=OFF,
SOLVER=SPARSE CONTACT=-CONSTRAINT-FUNCTION,
TRELEASE=0.0000000000000000 RESTART=-NO FRACTURE=NO LOAD-CAS=NO,
LOAD-PEN=NO SINGULAR=YES STIFFNES=0.000100000000000000,
MAP-OUTP=NONE MAP-FORM=NO NODAL-DE=" POROUS-C=NO ADAPTIVE=0,
ZOOM-LAB=1 AXIS-CYC=0 PERIODIC=NO VECTOR-S=GEOMETRY EPSI-FIR=NO,
STABILIZ=NO STABFACT=1.0000000000000000E-10 RESULTS=PORTHOLE,
FEFCORR=NO BOLTSTEP=1 EXTEND-S=YES CONVERT=-NO DEGEN=YES,
TMC-MODE=NO ENSIGHT=-NO IRSTEPS=1 INITIALT=NO TEMP-INT=NO,
ESINTERA=NO OP2GEOM=NO
*
ANALYSIS DYNAMIC-DIRECT-INTEGRATION METHOD=NEWMARK,

```



DELTA=0.5      ALPHA=0.25,  
THETA=1.4      TIMESTEP=TOTALTIME NCRSTEP=1,  
CRSTEP=0      MASS-SCA=1,  
DTMIN1=0      DTMIN2=0,  
GAMMA=0.5

\*\*\*\*\* GEOMETRY \*\*\*\*\*

COORDINATES POINT SYSTEM=0

@CLEAR

1	0	0	0
2	7	0	0
3	0	1	0
4	0.5	0	0.01
5	0.5	0	3
6	0.5	0	-3
7	0.5	0	-0.01
9	0	0	3
10	0.5	1	3
11	0.25	0	0
12	0.5	0	0
13	0.75	0	0
14	1	0	0
15	1.25	0	0
16	1.5	0	0
17	1.75	0	0
18	2	0	0
19	2.25	0	0
20	2.5	0	0
21	2.75	0	0
22	3	0	0
23	3.25	0	0
24	3.5	0	0
25	3.75	0	0
26	4	0	0
27	4.25	0	0
28	4.5	0	0
29	4.75	0	0
30	5	0	0
31	5.25	0	0
32	5.5	0	0
33	5.75	0	0
34	6	0	0
35	6.25	0	0
36	6.5	0	0
37	6.75	0	0
38	7	0	0
39	1.5	0	0.01
40	1.5	0	3
41	1.5	0	-0.01
42	1.5	0	-3
43	2.5	0	0.01
44	2.5	0	3
45	2.5	0	-0.01
46	2.5	0	-3
47	3.5	0	0.01
48	3.5	0	3
49	3.5	0	-0.01
50	3.5	0	-3
51	4.5	0	0.01

52 4.5 0 3 0  
 53 4.5 0 -0.01 0  
 54 4.5 0 -3 0  
 55 5.5 0 0.01 0  
 56 5.5 0 3 0  
 57 5.5 0 -0.01 0  
 58 5.5 0 -3 0  
 59 6.5 0 0.01 0  
 60 6.5 0 3 0  
 61 6.5 0 -0.01 0  
 62 6.5 0 -3 0  
 63 1.5 1 3 0  
 64 2.5 1 3 0  
 65 3.5 1 3 0  
 66 4.5 1 3 0  
 67 5.5 1 3 0  
 68 6.5 1 3 0

@

\*

LINE STRAIGHT NAME=1 P1=1 P2=2

\*

LINE STRAIGHT NAME=2 P1=5 P2=4

\*

LINE STRAIGHT NAME=3 P1=7 P2=6

\*

LINE STRAIGHT NAME=4 P1=39 P2=40

\*

LINE STRAIGHT NAME=5 P1=41 P2=42

\*

LINE STRAIGHT NAME=6 P1=43 P2=44

\*

LINE STRAIGHT NAME=7 P1=45 P2=46

\*

LINE STRAIGHT NAME=8 P1=47 P2=48

\*

LINE STRAIGHT NAME=9 P1=49 P2=50

\*

LINE STRAIGHT NAME=10 P1=51 P2=52

\*

LINE STRAIGHT NAME=11 P1=53 P2=54

\*

LINE STRAIGHT NAME=12 P1=55 P2=56

\*

LINE STRAIGHT NAME=13 P1=57 P2=58

\*

LINE STRAIGHT NAME=14 P1=59 P2=60

\*

LINE STRAIGHT NAME=15 P1=61 P2=62

\*

CROSS-SECTIO RECTANGULAR NAME=1 WIDTH=0.6,

HEIGHT=0.5 SC=0 TC=0,

TORFAC=1 SSHEARF=0,

TSHEARF=0 ISHEAR=NO SQUARE=NO

\*

CROSS-SECTIO RECTANGULAR NAME=2 WIDTH=1,

HEIGHT=0.2 SC=0 TC=0,

TORFAC=1 SSHEARF=0,

TSHEARF=0 ISHEAR=NO SQUARE=NO

\*\*\*\*\* MATERIAL \*\*\*\*\*

MATERIAL PLASTIC-BILINEAR NAME=1 HARDENIN=ISOTROPIC,  
E=2.7001E+09 NU=0,  
YIELD=4101600 ET=100 EPA=0,  
STRAINRA=0 DENSITY=2400 ALPHA=0,  
TREF=0 DEPENDEN=NO TRANSITI=0.0001,  
EP-STRAI=0 BCURVE=0 BVALUE=0,  
XM-INF=0 XM0=0,  
ETA=0 MDESCRIP='wall'

\*

MATERIAL PLASTIC-BILINEAR NAME=2 HARDENIN=ISOTROPIC,  
E=4.1619E+09 NU=0,  
YIELD=5069100 ET=100 EPA=0,  
STRAINRA=0 DENSITY=2400 ALPHA=0,  
TREF=0 DEPENDEN=NO TRANSITI=0.0001,  
EP-STRAI=0 BCURVE=0 BVALUE=0,  
XM-INF=0 XM0=0,  
ETA=0 MDESCRIP='column'

\*\*\*\*\* BOUNDARY CONDITIONS \*\*\*\*\*

FIXITY NAME=2  
@CLEAR  
'Y-TRANSLATION'  
'OVALIZATION'

@

\*

FIXITY NAME=5  
@CLEAR  
'X-TRANSLATION'  
'Z-TRANSLATION'  
'X-ROTATION'  
'Y-ROTATION'  
'Z-ROTATION'  
'OVALIZATION'

@

\*

FIXBOUNDARY POINTS FIXITY=ALL

@CLEAR

1 'ALL'

2 '2'

5 '5'

6 '5'

40 '5'

44 '5'

48 '5'

52 '5'

56 '5'

60 '5'

62 '5'

58 '5'

54 '5'

50 '5'

46 '5'

42 '5'

@

\*

RIGIDLINK NAME=1 SLAVETYP=POINT SLAVENAM=4 MASTER'STY=POINT  
MASTER'SNA=12,

DISPLACE=DEFAULT OPTION=0 SLAVEBOD=0 MASTER'SBO=0 DOF=ALL,  
DOFSI=123  
\*

RIGIDLINK NAME=2 SLAVETYP=POINT SLAVENAM=7 MASTER'STY=POINT  
MASTER'SNA=12,  
DISPLACE=DEFAULT OPTION=0 SLAVEBOD=0 MASTER'SBO=0 DOF=ALL,  
DOFSI=123  
\*

RIGIDLINK NAME=3 SLAVETYP=POINT SLAVENAM=41 MASTER'STY=POINT,  
MASTER'SNA=16 DISPLACE=DEFAULT OPTION=0 SLAVEBOD=0 MASTER'SBO=0,  
DOF=ALL DOFSI=123  
\*

RIGIDLINK NAME=4 SLAVETYP=POINT SLAVENAM=39 MASTER'STY=POINT,  
MASTER'SNA=16 DISPLACE=DEFAULT OPTION=0 SLAVEBOD=0 MASTER'SBO=0,  
DOF=ALL DOFSI=123  
\*

RIGIDLINK NAME=5 SLAVETYP=POINT SLAVENAM=43 MASTER'STY=POINT,  
MASTER'SNA=20 DISPLACE=DEFAULT OPTION=0 SLAVEBOD=0 MASTER'SBO=0,  
DOF=ALL DOFSI=123  
\*

RIGIDLINK NAME=6 SLAVETYP=POINT SLAVENAM=45 MASTER'STY=POINT,  
MASTER'SNA=20 DISPLACE=DEFAULT OPTION=0 SLAVEBOD=0 MASTER'SBO=0,  
DOF=ALL DOFSI=123  
\*

RIGIDLINK NAME=7 SLAVETYP=POINT SLAVENAM=47 MASTER'STY=POINT,  
MASTER'SNA=24 DISPLACE=DEFAULT OPTION=0 SLAVEBOD=0 MASTER'SBO=0,  
DOF=ALL DOFSI=123  
\*

RIGIDLINK NAME=8 SLAVETYP=POINT SLAVENAM=49 MASTER'STY=POINT,  
MASTER'SNA=24 DISPLACE=DEFAULT OPTION=0 SLAVEBOD=0 MASTER'SBO=0,  
DOF=ALL DOFSI=123  
\*

RIGIDLINK NAME=9 SLAVETYP=POINT SLAVENAM=51 MASTER'STY=POINT,  
MASTER'SNA=28 DISPLACE=DEFAULT OPTION=0 SLAVEBOD=0 MASTER'SBO=0,  
DOF=ALL DOFSI=123  
\*

RIGIDLINK NAME=10 SLAVETYP=POINT SLAVENAM=53 MASTER'STY=POINT,  
MASTER'SNA=28 DISPLACE=DEFAULT OPTION=0 SLAVEBOD=0 MASTER'SBO=0,  
DOF=ALL DOFSI=123  
\*

RIGIDLINK NAME=11 SLAVETYP=POINT SLAVENAM=55 MASTER'STY=POINT,  
MASTER'SNA=32 DISPLACE=DEFAULT OPTION=0 SLAVEBOD=0 MASTER'SBO=0,  
DOF=ALL DOFSI=123  
\*

RIGIDLINK NAME=12 SLAVETYP=POINT SLAVENAM=57 MASTER'STY=POINT,  
MASTER'SNA=32 DISPLACE=DEFAULT OPTION=0 SLAVEBOD=0 MASTER'SBO=0,  
DOF=ALL DOFSI=123  
\*

RIGIDLINK NAME=13 SLAVETYP=POINT SLAVENAM=59 MASTER'STY=POINT,  
MASTER'SNA=36 DISPLACE=DEFAULT OPTION=0 SLAVEBOD=0 MASTER'SBO=0,  
DOF=ALL DOFSI=123  
\*

RIGIDLINK NAME=14 SLAVETYP=POINT SLAVENAM=61 MASTER'STY=POINT,  
MASTER'SNA=36 DISPLACE=DEFAULT OPTION=0 SLAVEBOD=0 MASTER'SBO=0,  
DOF=ALL DOFSI=123

\*\*\*\*\* ELEMENTS \*\*\*\*\*

EGROUP BEAM NAME=1 SUBTYPE=THREE-D DISPLACE=DEFAULT MATERIAL=2 RINT=5,  
SINT=DEFAULT TINT=DEFAULT RESULTS=FORCES INITIALS=NONE,

CMASS=DEFAULT RIGIDEND=NONE MOMENT-C=NO RIGIDITY=0,  
 MULTIPLY=1000000 RUPTURE=ADINA OPTION=NONE,  
 BOLT-TOL=0 DESCRIPT='column' SECTION=1,  
 PRINT=DEFAULT SAVE=DEFAULT TBIRTH=0,  
 TDEATH=0 SPOINT=4 BOLTFORC=0,  
 BOLTNCUR=0 TMC-MATE=1 BOLT-NUM=0 BOLT-LOA=0,  
 WARP=NO  
 \*  
 EGROUP BEAM NAME=2 SUBTYPE=THREE-D DISPLACE=DEFAULT MATERIAL=1 RINT=5,  
 SINT=DEFAULT TINT=DEFAULT RESULTS=FORCES INITIALS=NONE,  
 CMASS=DEFAULT RIGIDEND=NONE MOMENT-C=NO RIGIDITY=0,  
 MULTIPLY=1000000 RUPTURE=ADINA OPTION=NONE,  
 BOLT-TOL=0 DESCRIPT='wall' SECTION=2,  
 PRINT=DEFAULT SAVE=DEFAULT TBIRTH=0,  
 TDEATH=0 SPOINT=4 BOLTFORC=0,  
 BOLTNCUR=0 TMC-MATE=1 BOLT-NUM=0 BOLT-LOA=0,  
 WARP=NO  
 \*  
 SUBDIVIDE LINE NAME=1 MODE=LENGTH SIZE=0.25  
 \*  
 GLINE NODES=2 AUXPOINT=3 NCOINCID=ENDS NCENDS=12,  
 NCTOLERA=1E-05 SUBSTRUC=0 GROUP=1 MIDNODES=CURVED,  
 XO=0 YO=0 ZO=0,  
 XYZOSYST=SKEW  
 @CLEAR  
 1  
 @  
 \*  
 SUBDIVIDE LINE NAME=2 MODE=DIVISIONS NDIV=12 RATIO=1,  
 PROGRESS=GEOMETRIC CBIAS=NO  
 \*  
 SUBDIVIDE LINE NAME=3 MODE=DIVISIONS NDIV=12 RATIO=1,  
 PROGRESS=GEOMETRIC CBIAS=NO  
 \*  
 SUBDIVIDE LINE NAME=4 MODE=DIVISIONS NDIV=12 RATIO=1,  
 PROGRESS=GEOMETRIC CBIAS=NO  
 \*  
 SUBDIVIDE LINE NAME=5 MODE=DIVISIONS NDIV=12 RATIO=1,  
 PROGRESS=GEOMETRIC CBIAS=NO  
 \*  
 SUBDIVIDE LINE NAME=6 MODE=DIVISIONS NDIV=12 RATIO=1,  
 PROGRESS=GEOMETRIC CBIAS=NO  
 \*  
 SUBDIVIDE LINE NAME=7 MODE=DIVISIONS NDIV=12 RATIO=1,  
 PROGRESS=GEOMETRIC CBIAS=NO  
 \*  
 SUBDIVIDE LINE NAME=8 MODE=DIVISIONS NDIV=12 RATIO=1,  
 PROGRESS=GEOMETRIC CBIAS=NO  
 \*  
 SUBDIVIDE LINE NAME=9 MODE=DIVISIONS NDIV=12 RATIO=1,  
 PROGRESS=GEOMETRIC CBIAS=NO  
 \*  
 SUBDIVIDE LINE NAME=10 MODE=DIVISIONS NDIV=12 RATIO=1,  
 PROGRESS=GEOMETRIC CBIAS=NO  
 \*  
 SUBDIVIDE LINE NAME=11 MODE=DIVISIONS NDIV=12 RATIO=1,  
 PROGRESS=GEOMETRIC CBIAS=NO  
 \*  
 SUBDIVIDE LINE NAME=12 MODE=DIVISIONS NDIV=12 RATIO=1,  
 PROGRESS=GEOMETRIC CBIAS=NO

```

*
SUBDIVIDE LINE NAME=13 MODE=DIVISIONS NDIV=12 RATIO=1,
PROGRESS=GEOMETRIC CBIAS=NO
*
SUBDIVIDE LINE NAME=14 MODE=DIVISIONS NDIV=12 RATIO=1,
PROGRESS=GEOMETRIC CBIAS=NO
*
SUBDIVIDE LINE NAME=15 MODE=DIVISIONS NDIV=12 RATIO=1,
PROGRESS=GEOMETRIC CBIAS=NO
*
GLINE NODES=2 AUXPOINT=9 NCOINCID=ENDS NCENDS=12,
NCTOLERA=1E-05 SUBSTRUC=0 GROUP=2 MIDNODES=CURVED,
XO=0 YO=0 ZO=0,
XYZOSYST=SKEW
@CLEAR
2
3
4
5
6
7
8
9
10
11
12
13
14
15
@

***** DYNAMIC LOAD *****

LOAD LINE NAME=1 MAGNITUD=-60000.0000000000
*
APPLY-LOAD BODY=0
@CLEAR
1 'LINE' 1 'LINE' 3 0 1 0 0 -1 10 0 0 'NO',
0 0 1 0 'MID'
2 'LINE' 1 'LINE' 2 0 1 0 0 -1 10 0 0 'NO',
0 0 1 0 'MID'
3 'LINE' 1 'LINE' 4 0 1 0 0 -1 63 0 0 'NO',
0 0 1 0 'MID'
4 'LINE' 1 'LINE' 5 0 1 0 0 -1 63 0 0 'NO',
0 0 1 0 'MID'
5 'LINE' 1 'LINE' 6 0 1 0 0 -1 64 0 0 'NO',
0 0 1 0 'MID'
6 'LINE' 1 'LINE' 7 0 1 0 0 -1 64 0 0 'NO',
0 0 1 0 'MID'
7 'LINE' 1 'LINE' 8 0 1 0 0 -1 65 0 0 'NO',
0 0 1 0 'MID'
8 'LINE' 1 'LINE' 9 0 1 0 0 -1 65 0 0 'NO',
0 0 1 0 'MID'
9 'LINE' 1 'LINE' 10 0 1 0 0 -1 66 0 0 'NO',
0 0 1 0 'MID'
10 'LINE' 1 'LINE' 11 0 1 0 0 -1 66 0 0 'NO',
0 0 1 0 'MID'
11 'LINE' 1 'LINE' 12 0 1 0 0 -1 67 0 0 'NO',
0 0 1 0 'MID'
12 'LINE' 1 'LINE' 13 0 1 0 0 -1 67 0 0 'NO',

```

```
0 0 1 0 'MID'  
13 'LINE' 1 'LINE' 14 0 1 0 0 -1 68 0 0 'NO',  
0 0 1 0 'MID'  
14 'LINE' 1 'LINE' 15 0 1 0 0 -1 68 0 0 'NO',  
0 0 1 0 'MID'  
@  
*  
TIMEFUNCTION NAME=1 IFLIB=1 FPAR1=0,  
FPAR2=0 FPAR3=0,  
FPAR4=0 FPAR5=0,  
FPAR6=0  
@CLEAR  
0      0  
0.00025  1  
0.025    0  
2        0  
@  
*  
TIMESTEP NAME=LOAD  
@CLEAR  
8000 0.00025  
@  
*
```